

I. Functionalization and Investigation of Highly Efficient Hosts for Use in Macromolecular Self-Assemblies and II. The Design and Synthesis of ROMP Imidazolium Systems for Use as Mechanical Actuators

Terry Leon Price Jr.

Dissertation submitted to the faculty of the Virginia Polytechnic Institute and State University in
partial fulfillment of the requirements for the degree of

Doctor of Philosophy

In

Chemistry

Harry W. Gibson

James M. Tanko

Richard D. Gandour

S. Richard Turner

May 25, 2016

Blacksburg, Virginia

Keywords: host/guest, ionomer, polymer, imidazolium, paraquat, cryptand, pseudorotaxane

Terry L. Price Jr. Copyright 2016

I. Functionalization and Investigation of Highly Efficient Hosts for Use in Macromolecular Self-Assemblies and II. The Design and Synthesis of ROMP Imidazolium Systems for Use as Mechanical Actuators

Terry Leon Price Jr.

ABSTRACT

Recent advancements in supramolecular chemistry have given a wealth of strongly binding host-guest combinations. However, the deployment of these systems into meaningful constructs has been hindered due to difficulty of synthesis or to the lack of functionality in one or both components. Systems caught in this trap were the pyridyl cryptands of dibenzo-30-crown-10 and bis(*m*-phenylene)-32-crown-10 paired with paraquat. Exceptionally high association constants in the range of 10^5 to 10^6 have been observed for these systems, but their applications have been hindered.

Easing the implementation of pyridyl cryptands based on dibenzo-30-crown-10 was made a priority. An efficient method for the synthesis of pyridyl cryptands based on dibenzo-30-crown-10 and bis(*m*-phenylene)-32-crown-10 made use of the salt pyridinium bis(trifluoromethane)sulfonamide (TFSI) as a template. Optimization of the pyridinium TFSI template allowed for cyclization yields as high as 89%, as well as without the use of a syringe pump. Addressing the concern of functionality, for pyridyl cryptands, chelidamic acid was targeted as a way to build in functionality. Using a chelidamic isopropyl ester, 20 new chelidamic precursors of varying functionality were synthesized. The chelidamic derivatives fell into six groups: potential covalent monomers, initiators, chain terminators, leaving groups, aryl halides and host-guest monomers.

In an attempt to boost the association constants of pyridyl cryptands based on dibenzo-30-crown-10 with paraquat, alterations to the paraquat guest were explored. It was found that the association constants could be increased by nearly an order of magnitude. Tweaks to the paraquat included changing the counterion to TFSI, methyl groups to benzyl and allowing for access to more nonpolar solvents that were previously inaccessible, such as solvent change from DCM to acetone.

Two new biscryptands and two new bisparaquat TFSI monomers were synthesized. Using these monomers supramolecular polymers were synthesized and characterized. Fibers of these polymers drawn from concentrated solutions were found to be flexible and one such polymer solution was found to have an upper log / log specific viscosity–concentration slope of 3.55, which is the theoretical maximum. Additionally, a biscryptand was used to produce a chain extended polymer.

Using a fundamental understanding of host-guest chemistry, work was conducted on the synthesis of norbornene monomers and polymers with pendant imidazolium tethered by ethyleneoxy linkages to aid in the stabilization of the imidazolium cation. Through the use of ethyleneoxy linkages, the free anion content and conductivity was increased. Imidazolium monomer and polymer conductivities ranged up to nearly 10^{-4} S/cm. Furthermore, it was determined that as long as the ethyleneoxy spacer between the norbornene and imidazolium was two units or greater, similar properties were obtained for both the monomer and corresponding polymer. Expanding the work further, the imidazolium monomers were incorporated as a soft segment into a triblock copolymer to produce a single direction mechanical actuator.

I. Functionalization and Investigation of Highly Efficient Hosts for Use in Macromolecular Self-Assemblies and II. The Design and Synthesis of ROMP Imidazolium Systems for Use as Mechanical Actuators

Terry Leon Price, Jr.

ABSTRACT (General audience)

The research reported herein relates to two areas: 1) the development and application of systems involving two molecular components with very strong affinities for one another, and 2) design, preparation and testing of materials for use in electromechanical actuators for robotics.

Work on the two component systems included improved synthetic methods, structural alterations to increase the affinity of components for one another, and their use to self-assemble large, linear polymeric arrays with the mechanical properties of plastics, i. e., materials capable of film and fiber production with attendant novel properties.

The development of electromechanical actuators was achieved through production of a new class of ionic polymers in which the positive charges are associated with the polymer molecule and are immobile. When an electric field is placed across films of the polymers, the negatively charged anions, which are not attached to the polymer molecule and hence are mobile, are displaced toward the positive electrode, causing the film to bend, i. e., undergo actuation. For this work, advancements were made in methods of synthesis of these new materials and fundamental understanding of the structural requirements for optimal ionic conductivity and hence actuation.

Dedication

I dedicate this to my family and friends who have seen me through this process. I give special thanks to my wife Michelle Price who has been by my side since I began at Virginia Tech and my daughter Rachel Price who has been an inspiration. Additionally, I would like to thank my grandmother Audrey Goins, grandfather Samuel Goins, father Terry Price, and mother Kim Price, all of whom have pushed me onward in my life.

Acknowledgements

Many individuals have kindly contributed in various ways to this work; their contributions are appreciated and listed in no particular order. Conductivity measurements were conducted by U Hyeok Choi and Ren Xie under the direction of Dr. Ralph Colby at Penn State. Computational experiments were conducted by Dr. Richard Gandour at Virginia Tech. Light microscopy was carried out at Virginia Tech by Dr. Michelle Price. Actuation testing was conducted by Dong Wang at Virginia Tech under the direction of Dr. Randy Heflin. Priceless DSC advice and melt pressing attempts were provided by Dr. Bruce Orler. SAX was provided by Mingqiang Zhang under the direction of Prof. Robert Moore at Virginia Tech. From the Gibson group, both Minjae Lee and Zhenbin Niu provided valuable synthetic precursors and Daniel Schoonover provided instrumentation advice. Additionally, all Gibson group members have provided valuable advice over the years. A special acknowledgment is also owed to my advisor Dr. Harry Gibson and committee members Dr. James M. Tanko, Dr. Richard D. Gandour and Dr. S. Richard Turner, all of whom have guided this work. This work has been generously funded by the NSF (DMR 0704076, CHE-1106899, CHE- 1507553) and by the Army Research Lab as part of a Ionic Liquids in Electro-Active Devices (ILEAD) MURI grant (Army Research Office grant number W911NF-07-1-0452).

Table of Contents

<u>Chapter 1: Host – Guest Introduction</u>	<u>1</u>
<u>References</u>	<u>24</u>
<u>Chapter 2: New Hosts</u>	
<u>Introduction</u>	<u>27</u>
<u>Results and Discussion</u>	<u>29</u>
<u>Conclusion</u>	<u>39</u>
<u>Experimental</u>	<u>40</u>
<u>References</u>	<u>43</u>
<u>Chapter 3: Cryptand Templatation</u>	
<u>Introduction</u>	<u>45</u>
<u>Results and Discussion</u>	<u>47</u>
<u>Conclusion</u>	<u>59</u>
<u>Experimental</u>	<u>59</u>
<u>References</u>	<u>63</u>
<u>Chapter 4: New Guests</u>	
<u>Introduction</u>	<u>64</u>
<u>Results and Discussion</u>	<u>65</u>
<u>Conclusion</u>	<u>83</u>
<u>Experimental</u>	<u>84</u>
<u>References</u>	<u>91</u>
<u>Chapter 5: Chelidamic Acid Derivatives</u>	
<u>Introduction</u>	<u>93</u>

<u>Results and Discussion</u>	<u>94</u>	
<u>Conclusion</u>	<u>103</u>	
<u>Experimental</u>	<u>104</u>	
<u>References</u>	<u>119</u>	
 <u>Chapter 6: Cryptand Functionalization</u>		
<u>Introduction</u>	<u>121</u>	
<u>Results and Discussion</u>	<u>122</u>	
<u>Conclusion</u>	<u>126</u>	
<u>Experimental</u>	<u>127</u>	
<u>References</u>	<u>130</u>	
 <u>Chapter 7: Biscryptands</u>		
<u>Introduction</u>	<u>131</u>	
<u>Results and Discussion</u>	<u>132</u>	
<u>Conclusion</u>	<u>139</u>	
<u>Experimental</u>	<u>140</u>	
<u>References</u>	<u>145</u>	
 <u>Chapter 8: Supramolecular Polymers</u>		
<u>Introduction</u>	<u>147</u>	
<u>Results and Discussion</u>	<u>150</u>	
<u>Conclusion</u>	<u>166</u>	
<u>Experimental</u>	<u>167</u>	
<u>References</u>	<u>169</u>	
 <u>Chapter 9: Ionic Liquids and Mechanical Actuators</u>		<u>170</u>

References	177
Chapter 10: Norbornene TFSI Monomers	
Introduction	179
Results and Discussion	181
Conclusion	210
Experimental	210
References	230
Chapter 11: Norbornene TFSI Polymers	
Introduction	231
Results and Discussion	232
Conclusion	242
Experimental	243
References	247
Chapter 12: Norbornene TFSI Triblock Polymers	
Introduction	248
Results and Discussion	249
Conclusion	259
Experimental	259
References	261
Chapter 13: Other Norbornene Salts	
Introduction	263
Results and Discussion	264
Conclusion	270

Experimental	270
References	275
Chapter 14: Conclusions and Future Work	
Conclusions	277
Future Work	279
References	287
Appendix	288

List of Figures

Chapter 1: Host – Guest Introduction

Figure 1.1.	Host-Guest association.....	2
Figure 1.2.	Example crown ethers along with the general structures for dialkylammoniums and paraquats.....	4
Figure 1.3.	Structures supporting Table 1.1.....	6
Figure 1.4.	Cartoon depicting pseudocryptands.....	7
Figure 1.5.	Reversible threading between a host and guest to form a pseudorotaxane....	9
Figure 1.6.	The formation of a rotaxane by addition of a large bulky group and the formation of a catenane by a difunctional molecule at high dilutions.....	9
Figure 1.7.	Different types of polymeric structures which employ supramolecular chemistry.....	16
Figure 1.8.	Cartoon showing the formation of two types of supramolecular polymers, poly[2] and poly[3]pseudorotaxanes.....	18
Figure 1.9.	Star Polymer from host-guest moieties by Gibson and coworkers.....	20

Chapter 2: New Hosts

Figure 2.1.	Cartoon depicting pseudocryptands.....	28
Figure 2.2.	500 MHz ¹ H NMR Job Plot titration of 3a with diquat in acetone- <i>d</i> ₆ at room temperature; H ₁ used for analysis.....	31
Figure 2.3.	Scatter plot of enthalpies vs. entropies for 3a – 3c determined at 25 °C in acetone, values taken from Table 2.1.....	32

- Figure 2.4. Top: 500 MHz ^1H NMR spectrum of a 1:1 mixture (15 mM) of **3a** and diquat PF_6 taken in acetone- d_6 . Bottom: 2D NOESY of a 1:1 mixture of **3a** and diquat PF_6 taken in acetone- d_6 ; peaks of interest are highlighted and a possible 3D structure is shown.....34
- Figure 2.5. Top: 500 MHz ^1H NMR spectrum of a 1:1 mixture (15 mM) of **3b** and diquat PF_6 taken in acetone- d_6 . Bottom: 2D NOESY of a 1:1 mixture of **3b** and diquat PF_6 taken in acetone- d_6 ; peaks of interest are highlighted and a possible 3D structure is shown.....35
- Figure 2.6. Top: 500 MHz ^1H NMR of a 1:1 mixture (15 mM) of **3c** and diquat PF_6 taken in acetone- d_6 . Bottom: 2D NOESY of a 1:1 mixture of **3c** and diquat PF_6 taken in acetone- d_6 , peaks of interest are highlighted and a possible 3D structure is shown..
.....36
- Figure 2.7. X-ray crystallography of **3b** • DQ PF_6 grown by slow vapor diffusion of ether into acetone (crystal structure contains a reasonable amount of disorder, counterions, solvent, artifacts, and non-guest hydrogens have been removed for clarity): a) side view; b) top down view; c) hydrogen bonding to the m-ethyleneoxy chain; d) hydrogen bonding to the p-ethyleneoxy chain; e) hydrogen bonding at the ester; f) structures **3b** and diquat. Hydrogen-bond parameters: C---O distances (Å), C-H---O distances (Å), C-H ---O angles (deg) A: 3.455, 2.887, 117.29; B: 3.088, 2.405, 128.55; C: 3.605, 2.843, 137.98; D: 3.072, 2.093, 170.35; E: 3.031, 2.541, 110.42; F: 3.117, 2.458, 123.64; G: 3.320, 2.451, 146.20; H: 3.340, 2.447, 149.74; I: 3.421, 2.739, 126.35; J: 3.278, 2.808, 109.76; K: 3.619, 2.722, 150.96; L: 3.281, 2.399, 154.19; M: 2.954, 2.230, 132.31; N: 3.679, 3.170, 113.52; O: 3.445, 2.470,

173.75; P: 3.265, 2.470, 141.24. X-ray crystallography was performed and solved by Dr. Carla Slebodnick.....37

Chapter 3: Cryptand Templatation

- Figure 3.1. Sample host progression to cryptands.....46
- Figure 3.2. Paraquat H⁺PF₆ conversion to pyridinium PF₆ in the presence of pyridine...50
- Figure 3.3. Crystal structure of **5** • **11** grown by slow solvent evaporation of an equimolar chloroform solution; hydrogens of **5** have been removed for clarity; a) side view; b) top view; c) hydrogen bonding involving chloroform, water and TFSI; d) hydrogen bonding involving the 3-substituted ethyleneoxy chain (chloroform, water, and TFSI removed for clarity); e) planes of stacked aromatic rings shown with centroids of stacked rings and plane inclinations indicated; f) structures **5** and **11**. Hydrogen-bond parameters: C---O distances (Å), C-H---O distances (Å), C-H---O angles (deg) A: 3.633, 2.969, 124.71; B: 3.282, 2.289, 172.28; C: 3.503, 2.589, 161.71; D: 2.660, 1.793, 167.73; E: 2.901, 2.097, 169.41; F: 2.861, 2.060, 170.62; G: 3.205, 2.663, 116.72; H: 3.315, 2.415, 157.98. Face-to-face π -stacking parameters: centroid-centroid distance (Å): I: 3.972; J: 3.801; ring plane/ring plane inclinations (deg): i: 12.74°; ii: 0.18°. X-ray crystallography was performed and solved by Dr. Carla Slebodnick.....54
- Figure 3.4. Proposed preorganization of diol **2** to a “taco complex” brought about by the pyridinium ion.....55
- Figure 3.5. Job plot of **11** with **12**, obtained via ¹H NMR in CDCl₃ at room temperature using signal H_a of **11**. Give total concentration of components.....58

Chapter 4: New Guests

- Figure 4.1. Pyridyl cryptands **1a** and **1b**, alongside functionalized pyridyl cryptand **2**. 64
- Figure 4.2. ITC titrations: top, **1a** • **4b** in DCM at 25 °C; bottom, **1b** • **4b** in DCM at 25 °C. 69
- Figure 4.3. Scatter plot of enthalpies vs. entropies for **1a** and **1b** determined at 25 °C in acetone or DCM, values taken from Table 4.3. 72
- Figure 4.4. Crystal structure of **1a** • **3b** grown from a chloroform:acetone 1:1 (v:v) mixture by liquid-liquid diffusion of diethyl ether; non-paraquat hydrogen atoms and impurities have been removed for clarity; a) top view; b) side view; c) hydrogen bonding to the p-ethyleneoxy chain (counterions removed for clarity); d) hydrogen bonding to the m-ethyleneoxy chain (counter ions removed for clarity); e) hydrogen bonding to acetone (solvent), pyridine and ester group (counterions removed for clarity); f) planes of stacked aromatic rings shown with centroids of stacked rings and plane inclinations indicated; g) structures **1a** and **3b**. Hydrogen-bond parameters: C---O distances (Å), C-H---O distances (Å), C-H --- O angles (deg) A: 3.291, 2.560, 133.96; B: 3.818, 3.116, 129.64; C: 3.284, 2.339, 161.30; D: 3.403, 2.783, 121.72; E: 3.601, 2.826, 136.44; F: 3.264, 2.332, 156.38; G: 3.370, 2.828, 115.61; H: 3.866, 3.024, 144.66; I: 3.004, 2.327, 127.76; J: 3.140, 2.607, 115.86; K: 3.275, 2.426, 148.72; L: 3.248, 2.692, 117.95; M: 3.435, 3.066, 104.95. Face-to-face π -stacking parameters: centroid-centroid distance (Å): N) 3.586; O) 3.782; ring plane/ring plane inclinations (deg): i) 7.68°; ii) 1.63°. X-ray crystallography was performed and solved by Dr. Carla Slebodnick. 74

Figure 4.5. ITC titration of **2** • **4b** in DCM at 25 °C.76

Figure 4.6. Incomplete crystal structure of **2** • **4b** grown by liquid-liquid diffusion of pentane into a 1:1 v:v mixture of dichloromethane : acetone (missing one two TFSI counter ions); hydrogens which do not belong to the guest or host hydrogens not believed to be hydrogen bonding are removed for clarity; a) side view; b) top view with cryptand–cryptand hydrogen bonding; c) zoom showing TFSI hydrogen bonding to cryptand; d) structures **4b** and **2**; e) zoom showing TFSI and water hydrogen bonding to paraquat; f) hydrogen bonding with m-ethyleneoxy chain (Second complex along with all non-guest hydrogens, TFSI, and water atoms removed for clarity); g) hydrogen bonding with p-ethyleneoxy chain (Second complex along with all non-guest hydrogens, TFSI, and water atoms removed for clarity); h) hydrogen bonding at the pyridyl arm (Second complex along with all non-guest hydrogens, TFSI, and water atoms removed for clarity); hydrogen-bond parameters: C---O distances (Å), C-H---O distances (Å), C-H ---O angles (deg) A: 3.417, 2.532, 154.80; B: 3.758, 2.855, 158.91; C: 3.566, 2.717, 144.13; D: 3.793, 3.020, 135.71; E: 3.260, 2.428, 146.08; F: 3.414, 2.616, 141.89; G: 3.149, 2.745, 104.97; H: 3.295, 2.597, 127.53; I: 3.418, 2.515, 158.62; J: 3.368, 2.467, 158.21; K: 3.430, 2.529, 158.30; L: 3.104, 2.469, 124.18; M: 3.239, 2.261, 169.92; N: 3.502, 2.693, 143.32; O: 3.145, 2.803, 102.23; P: 3.493, 2.745, 136.13; Q: 3.110, 2.573, 115.97; R: 3.141, 2.208, 166.30; S: 3.554, 3.050, 112.89; T: 3.300, 2.833, 111.26; U: 3.790, 3.092, 131.53; V: 3.183, 2.276, 159.36; W: 3.059, 2.496, 117.87. Face-to-face π -stacking parameters: centroid-centroid distance (Å): X: 4.501; Y: 3.696; Z: 4.497; AA: 3.713; ring plane/ring plane

inclinations (deg): i: 7.90°; ii: 1.10°; iii: 3.97°; iv: 3.65°. X-ray crystallography was performed and solved by Dr. Carla Slebodnick.	79
Figure 4.7. Paraquat acidic aliphatic protons.	81

[Chapter 5: Chelidamic Acid Derivatives](#)

Figure 5.1. ¹ H NMR spectrum (500 MHz, CDCl ₃ , 23 °C) of crude reaction mixture of 12 with p-vinylbenzyl chloride after removal of unreacted chloride. O-alkylated peaks contain an arrow and dash above them; approximately 80% O-alkylation (14) and 20% N-alkylation (15).	98
--	----

[Chapter 6: Cryptand Functionalization](#)

Figure 6.1. Generic reaction for dibenzo-30-crown-10- and bis(m-phenylene)-32crown-10 based-pyridyl cryptand synthesis.	122
--	-----

[Chapter 7: Biscryptands](#)

Figure 7.1. Uses for a Ditopic Host.	131
Figure 7.2. ITC titration of 2 with dimethyl paraquat PF ₆ in acetone at 25 °C; error is indicated in parenthesis.	135
Figure 7.3. ITC titration of 17 with dibenzyl paraquat TFSI in DCM at 25 °C.	138
Figure 7.4. Niu's cooperative system: host 18 and guest 19	138

[Chapter 8: Supramolecular Polymers](#)

Figure 8.1. Association and disassociation of a supramolecular polymer.	147
--	-----

Figure 8.2.	DP vs K_a at 1M.....	148
Figure 8.3.	Cartoon depicting the intended chain extension technique employed within.....	150
Figure 8.4.	Biscryptands VII 16 and VII 17	151
Figure 8.5.	Supramolecular polymer P3 cast on glass and laid on top of text to show clarity.....	155
Figure 8.6.	A) P3 fiber color image taken on a black background, B) P3 fiber differential interference contrast image at 10x magnification, C) P3 fiber differential interference contrast image at 40x magnification, D) P3 fiber differential interference contrast image at 60x magnification.....	157
Figure 8.7.	Viscosity plot of P3	158
Figure 8.8.	DLS data for P3 and P4	160
Figure 8.9.	DSC overlay of monomer VII 17 , monomer IV 9 , and polymer P3 using a scan rate of 5 °C / min, all traces are second heating.....	162
Figure 8.10.	TGA overlay of polymers P1–P5 using a heating rate of 20 °C / min under nitrogen.....	163
Figure 8.11.	Viscosity plot of 2 and P6 in chloroform at 25 °C.....	166

[Chapter 9: Ionic Liquids and Mechanical Actuators](#)

Figure 9.1.	Generic structure of the imidazolium cation and TFSI counter ion.....	170
Figure 9.2.	Multiple vs. single direction actuation. Top contains an ionic liquid swollen polymer, both cation and anion are mobile (dual direction actuation is observed);	

	bottom contains the cation embedded into the polymer, only the anion is mobile (single direction actuation is observed).	173
Figure 9.3.	Target monomer architecture.	175
Figure 9.4.	Phase morphologies for AB and ABA block copolymers. A monomers are shown as orange ovals while B monomers are shown as light blue ovals. Figure has been adapted from literature sources.	176

Chapter 10: Norbornene TFSI Monomers

Figure 10.1.	General structure of last generation imidazolium acrylate monomers (not shelf stable).	180
Figure 10.2.	General imidazolium TFSI monomer structure.	181
Figure 10.3.	A) Observed <i>endo</i> vs <i>exo</i> NOESY correlations for norbornenes; B) partial NOESY spectrum of 8s taken in CDCl ₃ at room temperature.	187
Figure 10.4.	Partial ¹ H NMR (500 MHz) spectra of 8c at 8.8 mM taken in: a) CDCl ₃ , b) CD ₂ Cl ₂ , c) acetone- <i>d</i> ₆ , d) acetonitrile- <i>d</i> ₃ , e) methanol- <i>d</i> ₄ , f) DMSO- <i>d</i> ₆ .	192
Figure 10.5.	¹ H NMR peak ratios of H ₁ for 8c observed in Figure 10.4 compared to corresponding solvent dielectric constants.	194
Figure 10.6.	Partial ¹ H NMR spectrum of 8t , 600 mHz, CDCl ₃ A) 25 °C; B) -26 °C.	195
Figure 10.7.	Partial ¹³ C NMR of 8c at 126 mHz: A) solvent CD ₂ Cl ₂ and B) solvent DMSO- <i>d</i> ₆ .	196
Figure 10.8.	Compounds used to show intermolecular interactions between the imidazolium cation and ethyleneoxy units.	196

Figure 10.9. ^1H NMR (500 MHz) results from dimethyl imidazolium TFSI solvent experiments: A) ether, B) glyme, C) diglyme, D) triglyme, E) tetraglyme. ...	198
Figure 10.10. Figure 10.9 H_1 chemical peak shift vs oxygen content of solvent, fit to a logarithmic trend line.	199
Figure 10.11. 2D NOESY NMR of 8d taken in acetone- d_6	200
Figure 10.12. Imidazolium tail group 2-D NOESY correlation summary for 8d in acetone- d_6	201
Figure 10.13. ^1H NMR spectrum (500 MHz) for 8r in DMSO- d_6 at room temperature.	204
Figure 10.14. ^{13}C NMR spectrum (126 MHz) for 8r in DMSO- d_6 at room temperature.	205
Figure 10.15. Molecules used for computational modeling to explore the optimal spatial orientation of ester groups in norbornene monomers.	206
Figure 10.16. 2D NOESY (500 mHz) of 8r in CDCl_3 at room temperature, degassed using argon.	207
Figure 10.17. i) ^1H NMR (500 MHz) spectrum of 8r in CDCl_3 at room temperature; ii) 1D NOESY irradiated peak N; iii) 1D NOESY irradiated peak O; iv) 1D NOESY irradiated peak P.	208
Figure 10.18. 1D and 2D NOESY summary of 8r	209

[Chapter 11: Norbornene TFSI Polymers](#)

Figure 11.1. ^1H NMR spectrum (500 MHz, CD_2Cl_2 , room temp) of 1d indicating DP = 25. Initiator hydrogens are indicated in red (integral 1.20) and imidazolium hydrogens are indicated in green and blue (integrals 29.96, 30.27 and 29.24).	234
---	-----

Figure 11.2.	Partial ^1H NMR spectra (500 MHz) taken during the polymerization of monomer X 8i at 25 °C in CD_2Cl_2 .	236
Figure 11.3.	a) Consumption of monomer X 8i in the ROMP experiment of Figure 11.2 as determined by ^1H NMR, b) graph of $\ln[\text{monomer}]$ vs time (pseudo-first order plot).	236
Figure 11.4.	^1H NMR spectrum (500 MHz, CDCl_3 , room temp) of 2d indicating the loss of olefinic backbone hydrogens. Olefinic hydrogens are indicated in red (integral 0.23) and imidazolium hydrogens are indicated in green (integral 1.00).	241

[Chapter 12: Norbornene TFSI Triblock Polymers](#)

Figure 12.1.	Hard segment monomers chosen for investigation.	250
Figure 12.2.	3a and 3b visually compared to soft and hard segment homopolymers and monomers.	252
Figure 12.3.	Overlay of 3a starting and ending position with arrow showing actuation.	254
Figure 12.4.	Curvature diagram for 3a (actuation).	254
Figure 12.5.	Imidazolium diblock copolymer by Scalfani et al.	255
Figure 12.6.	SAXS data for 3a .	256
Figure 12.7.	3a thermally annealed at 170 °C for 12h and 202 °C for 24 h in nitrogen.	257

[Chapter 13: Other Norbornene Salts](#)

Figure 13.1.	Imidazolium TFSI monomer architecture alongside two new systems: imidazolium/new anions and paraquat/TFSI.	263
--------------	--	-----

Figure 13.2. Partial ^1H NMR spectra taken in acetone- d_6 at room temperature of **10** (5.9 mM) and a mixture of **10** and 30-crown-10 (5.9 mM each component).....269

[Chapter 14: Conclusions and Future Work](#)

Figure 14.1. Generic structure of an arm that may assist in the binding of a guest.....284

Figure 14.2. Large commercially available counterions.....287

List of Schemes

Chapter 1: Host – Guest Introduction

Scheme 1.1.	The conversion of Dibenzo-30-crown-10 into cryptand 2 via acid chloride.....	3
Scheme 1.2.	Synthesis of [2]catenane by phenanthroline templation.....	11
Scheme 1.3.	Molecular muscle by Stoddart and coworkers.....	21
Scheme 1.4.	Current synthetic method for the synthesis of non-functionalized cryptand.....	23
Scheme 1.5.	Synthesis of chelidamic acid.....	24

Chapter 2: New Hosts

Scheme 2.1.	Synthesis of pyridyl esters of dibenzo-30-crown-10: pseudocryptands 3a–3c	29
-------------	--	----

Chapter 3: Cryptand Templatation

Scheme 3.1.	Synthesis of 9	48
Scheme 3.2.	Synthesis of 5	51
Scheme 3.3.	Synthesis of 6 and 13	52

Chapter 4: New Guests

Scheme 4.1.	Synthesis of benzylic bisparaquat TFSI monomer 7 and methyl bisparaquat TFSI monomer 9	80
Scheme 4.2.	Variation of benzylic halide and functionality.....	81

Scheme 4.3.	Synthesis of fluorinated guests: paraquat TFSI 13 .	82
-------------	--	----

Chapter 5: Chelidamic Acid Derivatives

Scheme 5.1.	Typical route to pyridyl cryptands.	93
Scheme 5.2.	Synthesis of Chelidamic Acid.	94
Scheme 5.3.	Initial chelidamic acid derivatives.	95
Scheme 5.4.	Tautomers of 2 .	97
Scheme 5.5.	N- vs. O-alkylation in the synthesis of styrene chelidamic acid derivative 17 .	97
Scheme 5.6.	Versatility of 13 as a feedstock chemical for chelidamic derivatives.	99
Scheme 5.7.	ROMP quenching via aldehyde and ethylvinyl ether.	101
Scheme 5.8.	Difunctional A-A monomer precursors.	103

Chapter 6: Cryptand Functionalization

Scheme 6.1.	Synthesis of functionalized cryptands 5 and 6 .	124
Scheme 6.2.	Synthesis of aryl bromide cryptand 8 .	125
Scheme 6.3.	Synthesis of cryptand 10 .	126

Chapter 7: Biscryptands

Scheme 7.1.	Synthesis of Ullmann coupled cryptand 2 .	133
Scheme 7.2.	Synthesis of 4 via Ullmann coupling.	134
Scheme 7.3.	Synthesis of biscryptand 6 .	135
Scheme 7.4.	Synthesis of biscryptands 16 and 17 .	136

[Chapter 8: Supramolecular Polymers](#)

Scheme 8.1. Bisparaquats.....	152
Scheme 8.2. Supramolecular polymers P1 – P5 along with their pictures. Films were cast via slow solvent evaporation using the following solvent systems and substrates: P1 (chloroform / acetonitrile, 1/1 v/v on Teflon); P2 (1,2-dichloroethane on silicon); P3 (o-dichlorobenzene on glass); P4 (1,2-dichloroethane on Teflon); P5 (chloroform / acetonitrile, 1/1 v/v on glass).....	154
Scheme 8.3. Synthesis of chain extended polystyrene paraquat.....	165

[Chapter 10: Norbornene TFSI Monomers](#)

Scheme 10.1. Synthesis of norbornene monomers.....	182
Scheme 10.2. Synthesis of imidazole precursors.....	183
Scheme 10.3. Imidazolium monomer synthesis.....	184

[Chapter 11: Norbornene TFSI Polymers](#)

Scheme 11.1. Synthesis of imidazolium polymers 1a – 1f	232
Scheme 11.2. Synthesis of reduced polymers 2d and 2f	240

[Chapter 12: Norbornene TFSI Triblock Polymers](#)

Scheme 12.1. Synthesis of triblocks 3a and 3b	251
Scheme 12.2. Attempted synthesis of triblock copolymer 4	258

[Chapter 13: Other Norbornene Salts](#)

Scheme 13.1. Synthesis of new monomers 4b , 4c , 8b and 8c	265
Scheme 13.2. Synthesis of paraquat TFSI norbornene monomer 10 and proposed complexation with 30-crown-10.....	267

[Chapter 14: Conclusions and Future Work](#)

Scheme 14.1. Proposed switchable supramolecular polymer employing a difunctional pyridinium and biscryptand VIII 17	281
Scheme 14.2. Proposed switchable crosslink.....	282
Scheme 14.3. Proposed workable unit.....	283
Scheme 14.4. Proposed synthesis for a tricyptand.....	285

List of Equations

[Chapter 8: Supramolecular Polymers](#)

Equation 8.1. Full equation for DP estimate.....148

Equation 8.2. Simplified DP estimate equation.....148

List of Tables

Chapter 1: Host – Guest Introduction

Table 1.1.	Association constants, K_a , of selected crowns and cryptands in acetone.....	5
------------	---	---

Chapter 2: New Hosts

Table 2.1.	ITC results for 3a–3c with diquat and paraquat obtained in acetone at 25 °C via ITC.....	29
Table 2.2.	K_a values for 4a – 4c with paraquat 6 and diquat.....	33

Chapter 3: Cryptand Templatation

Table 3.1.	Association constant summary of hosts 1 – 6 with 7 . Values were obtained from literature sources for 1•7 , 2•7 , 3•7 , 4•7 , 5•7 and 6•7 . Association constants obtained in acetone at room temperature.....	46
Table 3.2.	Initial templatation experiments for the synthesis of 9	50
Table 3.3.	Association constants of hosts 1 , 2 , 5 , 6 , 12 and 13 with guest 11 in DCM at 25 °C; error is indicated in parenthesis.....	52
Table 3.4.	Templatation optimization of the synthesis of 5 ; concentrations in mM.....	56

Chapter 4: New Guests

Table 4.1.	Paraquat compounds.....	66
Table 4.2.	Paraquat solubilities (mM) at 25 °C.....	67

Table 4.3.	Association constants of hosts 1a and 1b with guests 3a , 3b , 4a and 4b at 25 oC; errors indicated in parenthesis. Values for 1a • 3a (lit.) and 1b • 3a (lit.) were obtained from published sources.	70
Table 4.4.	ITC results for 13 with 1a obtained at 25 °C.....	83

[Chapter 8: Supramolecular Polymers](#)

Table 8.1.	T _g and 5% wt loss comparison of polymers P1 - P5	161
------------	---	-----

[Chapter 10: Norbornene TFSI Monomers](#)

Table 10.1.	T _g (°C) values of NB[(EO) _x Im(EO) _y CH ₃] ₂ TFSI.....	189
Table 10.2.	NB[(EO) _x Im(EO) _y CH ₃] ₂ TFSI conductivity values (S/cm) at 25 °C.....	189

[Chapter 11: Norbornene TFSI Polymers](#)

Table 11.1.	Molecular weights (Da) and T _g values (°C) for Polymers 1a–1f and Chapter 10 Monomers X 8	238
Table 11.2.	Ionic Conductivities (S/cm) of 1a–1f and Chapter 10 monomers X 8 at 25 °C.....	239
Table 11.3.	T _{gs} and conductivities (25 °C) of hydrogenated polymers 2d and 2f compared to their unsaturated precursors 2d and 2f	242

[Chapter 12: Norbornene TFSI Triblock Polymers](#)

Table 12.1.	Properties summary of ABA block copolymers 3a and 3b	253
-------------	--	-----

Chapter 13: Other Norbornene Salts

Table 13.1.	T _g and Conductivity values for 4a – 4c and 8a – 8c	266
Table 13.2.	Conductivity comparison of 8a and 11	269

Appendix

Table A.1.	Crystal data and structure refinement for cs2219.....	289
Table A.2.	Bond lengths [Å] and angles [°] for cs2219.....	290
Table A.3.	Hydrogen bonds for cs2219 [Å and °].....	294
Table A.4.	Crystal data and structure refinement for cs2173.....	295
Table A.5.	Bond lengths [Å] and angles [°] for cs2173.....	296
Table A.6.	Hydrogen bonds for cs2173 [Å and °].....	304
Table A.7.	Crystal data and structure refinement for cs2237.....	305
Table A.8.	Bond lengths [Å] and angles [°] for cs2237.....	306
Table A.9.	Crystal data and structure refinement for cs2231.....	310
Table A.10.	Bond lengths [Å] and angles [°] for cs2231.....	311
Table A.11.	Hydrogen bonds for cs2231 [Å and °].....	318

Chapter 1

Host–Guest Introduction

1. Supramolecular chemistry

On the atomic level, many different types of bonds and attractive forces exist between atoms and complexes. Even within a given classification such as covalent bonds, a spectrum is present ranging from a perfectly covalent bond (such as dihydrogen) to a polar covalent bond (found in methane) and eventually the classification changes to ionic bonds once the electronegativities are adequately separated. Supramolecular chemistry has the same type of spectrum, since the term itself can be used to describe any type of attractive force between atoms or molecules that are not covalent.^{1,2} This leads to forces such as ionic bonds (salt complexes), metal ligands, lone pair interactions, hydrogen bonding, dipole-dipole interactions, charge transfer, hydrophobic-hydrophilic interactions, van der Waals forces, etc. falling within the realm of supramolecular chemistry. The term supramolecular chemistry, however, must be used judiciously since some structures that are comprised of noncovalent interactions, such as with some rotaxanes, are not chemical bonds per se, but instead mechanical bonds. Rotaxanes are defined as molecules that are sterically interlocked with one another, typically via electrostatic interaction between the molecules. If the electrostatic interaction is disrupted in a subsequent reaction, then the complex is not supramolecular, but instead, considered as a mechanically interlocked molecule (MIM).³

Supramolecular interactions in host-guest chemistry may be broken into two parts when considering a bi- or multi-molecular system: a host (H) that provides some type of an environment for interaction(s); and a guest (G) which can fit the environment and be stabilized

by noncovalent interactions. Of particular interest here and the focus of this review is the supramolecular chemistry of crown ethers and their corresponding cryptands. In this instance of host-guest chemistry, the host would be either a crown ether or cryptand and the guest would typically be an ammonium or pyridinium salt. The host-guest complex would result from association of the two components. **Figure 1.1** provides an example of this.

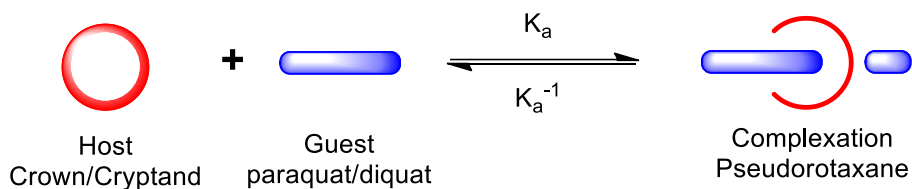


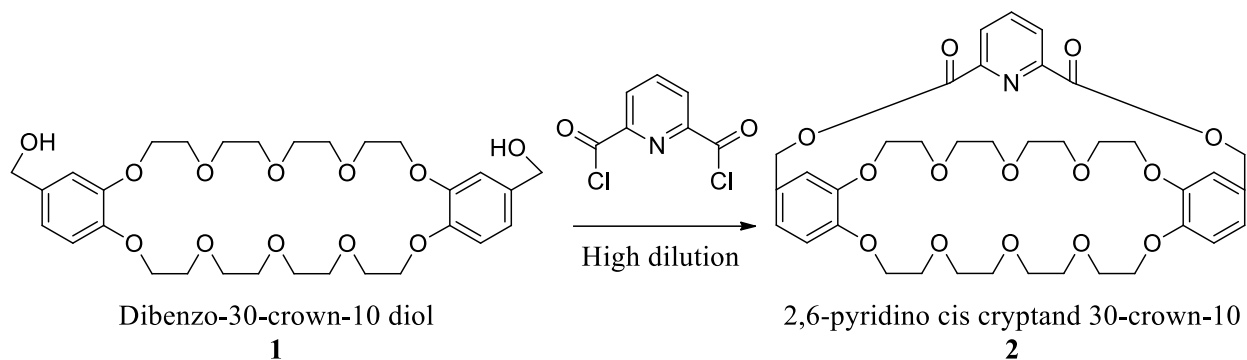
Figure 1.1. Host–Guest association.

1.1 Hosts

For host-guest chemistry, the host molecule is generally larger than the guest, providing an opening into which the guest can fit, thus allowing for some form of noncovalent interaction to hold the complex together, most commonly through hydrogen bonding (as with ammonium salts) or charge transfer (as with paraquat). Very often, the host is some type of electron rich macrocycle. Many types of crown macrocycles exist such as aza-crown ethers^{4,5} and crown thioethers,^{6,7} but the hosts of interest to this review are crown ethers and their corresponding cryptands. A cryptand is composed of a ring system that contains a third bridge to form a crypt-like structure. Synthetically the structures are synthesized by using a ring system as precursor, which is reacted with an additional molecule, such as a pyridine linkage, to form the bridge in the macrocycle. The first cryptands were reported 1968^{8,9} and 1969.¹⁰ The 1968 report by Simmons and Park described a cryptand containing an aliphatic ring with two nitrogen atoms

that were used for the production of another aliphatic bridge.^{8,9} The 1969 report by Dietrich, Lehn, and Sauvage was analogous, except that it contained ethyleneoxy linkages instead of aliphatic linkages.¹⁰ Of particular interest here are cyclics and cryptands that contain ethyleneoxy units, because the oxygen atoms can often aid in the binding of guest molecules.^{11,12}

Scheme 1.1 shows an example of a reaction used for the formation of cryptand **2**.



Scheme 1.1. The conversion of *cis*(4,4′)-Di(hydroxymethylbenzo)-30-crown-10 into cryptand **2** via 2,6-dicarboxypyridine diacid chloride.

Crown ether macrocycles are cyclic compounds that contain ether linkages; this produces an electron rich cavity which can function as a host for both metallic and organic cations. Initial crown ether complexations were reported with metals; however, organic cations have since rapidly gained in popularity.¹³ A large variety of crown ethers may be produced, ranging from entirely aliphatic cyclic ether rings to rings containing aromatic groups and substituents as well as variations in ring size. The substitution of aromatic groups into the ring system over the simple aliphatic groups allows for ease of functionalization of the crown, while also providing a more rigid structure.

The ring size dictates the nomenclature of the crown and in many ways is the most important factor with regards to guest complexation. Crown ethers are named by placing a

number before and after crown, the first number tells how many atoms make up the ring system and the second tells how many oxygens are present, for example 24-crown-8 represents a macrocycle of 24 atoms with 8 oxygens. Depending upon the size of the macrocycle, different guests better fit in the cavity and give higher association constants than others. For example 24-crown-8 has a higher association constant with dialkylammonium salts than paraquat salts with the same counterion in the identical solvent.^{14,15}

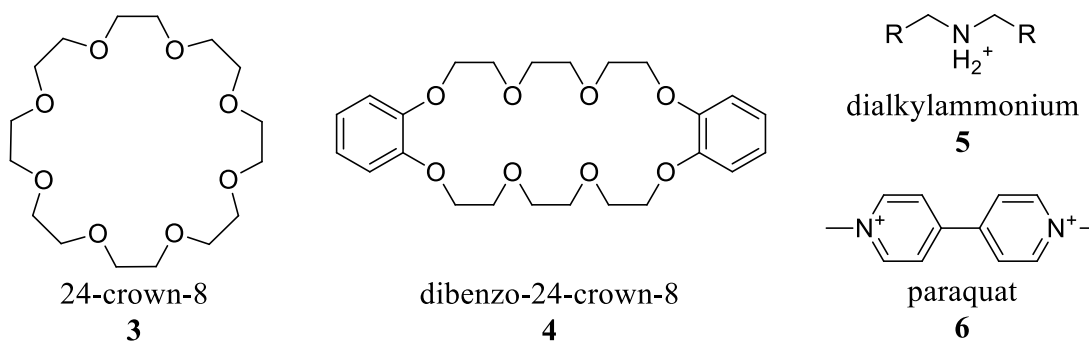


Figure 1.2. Example crown ethers along with the general structures for dialkylammoniums and paraquats.

Although smaller crown ethers have been much better characterized (likely due to their chemistry with metal cations)¹⁶⁻¹⁸ those of pressing interest here are crown ethers of sizes 24, 30, and 32 atoms and specifically those macrocycles which contain functional groups available for further modification. Macrocycles of these sizes provide adequate association constants with the organic cations dialkylammonium, paraquat, and diquat, all of which can be functionalized.

The desire for relatively high association constants between hosts and guests has brought about a shift from the use of crown ethers to their analogous cryptands; consider the trends for association constants in **Table 1.1**.

Table 1.1. Association constants, K_a (M^{-1} at 25 °C), of selected crowns and cryptands in acetone unless noted.

	dibenzylammonium PF ₆ salt (5 , R = CH ₂ C ₆ H ₅) unless noted	Paraquat PF ₆ salt (6) unless noted	Diquat PF ₆ salt (8) unless noted
Crown			
dibenzo-24-crown-8 (4) ¹⁹⁻²²	360 ^a	106 ^a	2.0 x 10 ^{2 a}
dibenzo-30-crown-10 ²³⁻²⁵	~1 x 10 ^{2 a, i}	Unobservable ^c	1.8 x 10 ^{4 a}
<i>cis</i> (4,4')-di(hydroxymethylbenzo)-30-crown-10 (1) ²⁶	N/A	1.1 x 10 ^{3 a}	5.0 x 10 ^{4 a}
<i>trans</i> -bis(hydroxymethylbenzo)-30-crown-10 ²⁶	N/A	1.7 x 10 ^{3 a}	3.3 x 10 ^{4 a}
bis(<i>m</i> -phenylene)-32-crown-10 ^{27,28}	5 ^{a, d}	393 ^{a, f}	390 ^a
bis(<i>m</i> -phenylene)-32-crown-10 diol (9) ²⁹⁻³¹	9.5 x 10 ^{2 a, g}	1.2 x 10 ^{3 a}	2.8 x 10 ^{3 a}
Cryptand			
2,6-pyridino cryptand of <i>cis</i> -dibenzo-24-crown-8 ³²	Weak	1 x 10 ^{4 a, e}	N/A
2,6-pyridino cryptand of <i>trans</i> -dibenzo-24-crown-8 ³²	Weak	1.4 x 10 ^{4 a, e}	N/A
ether cryptand of bis(<i>m</i> -phenylene)-32-crown-10 (7) ^{33,34}	N/A	6.1 x 10 ^{4 a}	2.0 x 10 ^{4 a}
2,6-pyridino cryptand of <i>cis</i> dibenzo-30-crown-10 (2) ³⁵	N/A	1 x 10 ^{5 b}	1.8 x 10 ^{6 b}
2,6-pyridino cryptand of bis(<i>m</i> -phenylene)-32-crown-10 (10) ^{34,36}	N/A	5 x 10 ^{6 a}	3.3 x 10 ^{5 a}
^a K_a obtained via NMR titration. ^b K_a obtained via ITC. ^c Interaction measured via electrodes. ^d value taken in CD ₃ CN. ^e <i>N,N'</i> -bis(β -hydroxyethyl)-4,4'-bipyridinium PF ₆ used as guest in study. ^f value taken in CDCl ₃ /CD ₃ CN. ^g value taken in 2.5:1 acetone- <i>d</i> ₆ :CDCl ₃ with guest <i>N,N'</i> -dibenzyl- <i>m</i> -xylylenediammonium PF ₆ . ^h NMR titration in 2:3 v:v CD ₃ CN:CDCl ₃ suggested a weak interaction (no value reported). ⁱ NMR titration in 1:1 v:v CD ₃ CN:CDCl ₃ and dibenzylammonium R = CH ₂ C ₆ H ₄ C(CH ₃) ₃			

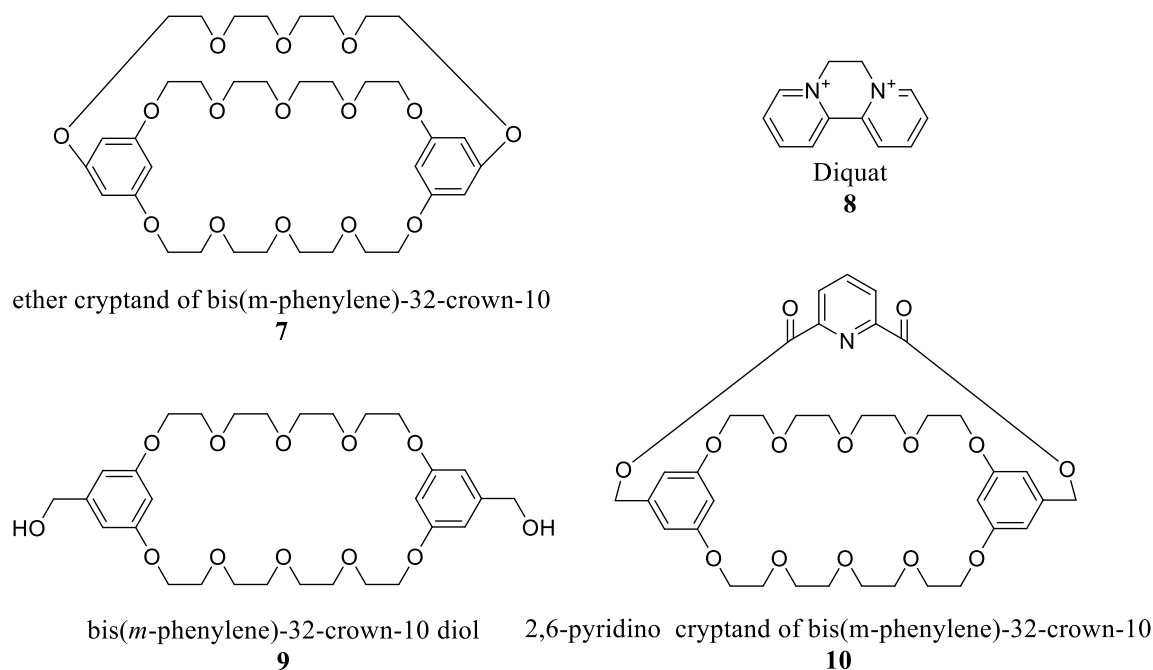


Figure 1.3. Structures supporting **Table 1.1.**

Although in nearly every case the cryptand is far superior to the crown ether, currently the synthetic schemes for these compounds are far more difficult than the syntheses of crown ethers and the yields are much lower, which greatly hinders their use. In many ways, the use of cryptands is limited by their availability, an obstacle which will be overcome with the development of novel synthetic pathways presented within this dissertation in Chapter 3.

In regards to complexation, most cryptands are superior to their crown ether counterparts; this is due to the increased electron density that is provided by the third bridge as well as a more fixed geometry, pre-organization. In the case of dibenzo-30-crown-10 versus its pyridine cryptand, the addition of the third arm increases the association constant with paraquat in acetone from $1.1 \times 10^3 \text{ M}^{-1}$ to $1 \times 10^5 \text{ M}^{-1}$. Threading has not been observed via crystal structures in the dibenzo-30-crown-10 system; instead the host wraps around the paraquat to give a taco-like complex. Threading becomes an issue when considering the complexation of crown ethers with

paraquat, since the taco complex cannot be converted into a rotaxane and the two components are not mechanically interlocked.

Strictly in terms of binding, neglecting arguments such as potential rotaxane formation, an attractive alternative to cryptands exists. Conceptually the idea is to produce a ring system that contains a side arm capable of aiding in binding, **Figure 1.4**; early workers termed these types of hosts “lariat ethers”.³⁷⁻⁴⁴ If the correct side arm is chosen, the compound behaves like a cryptand to give what is known as a pseudocryptand.^{28,37,45-48} **Figure 1.4** provides cartoons of both single and double armed pseudocryptands.^{37-41,45-47} The benefits of pseudocryptands over cryptands primarily resides in simplified synthetic routes and the potential to control whether the arms are participating in the binding event.

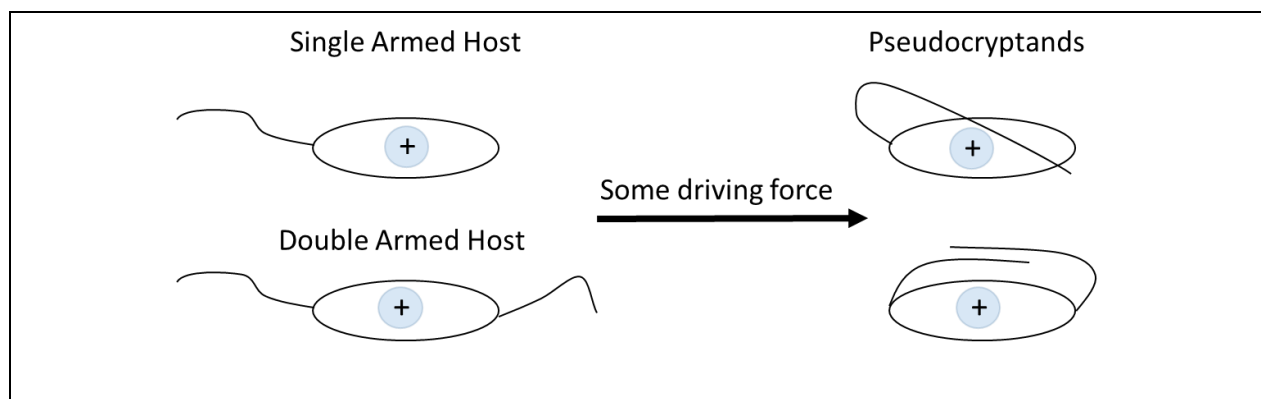


Figure 1.4. Cartoon depicting pseudocryptands.

1.2 Guests

Guest molecules complexing with crown ethers or cryptands are usually some type of cation (inorganic or organic), although due to the ease of functionality, organic cations are most commonly used in these systems. Three of the most studied and used cations with crowns are:

dialkylammonium salts (**5**) for 24-crown-8 systems, and paraquat salts (**6**) along with diquat salts (**8**) for dibenzo-30-crown-10 and bis(*m*-phenylene)-32-crown-10. All of these salts have primarily used the PF₆⁻ counterion, although complexations with other counterions^{49,50} have been reported. The rationale for using PF₆⁻ as the counterion is increased solubility in organic solvents. With paraquat, the PF₆ anion provides solubility in solvents with dielectric constants as low as acetone. Alternative counterions and their solubilities will be explored further in Chapter 4; it will be demonstrated that a better suited counter ion does exist.

1.3 Types of complexation

When a host and guest form a threaded complex, the complex may be characterized as one of three classes depending upon structure and reversibility. First, if the complex is reversible and an association constant defines the extent of complexation, then the resulting complex is classified as a pseudorotaxane. Secondly, if the complex is locked into place by addition of a large bulky group to prevent decomplexation, then the complex is considered to be a rotaxane. Finally, if the guest is converted to a macrocycle, resulting in interlocked macrocycles, the complex is termed a catenane.

1.3.1 Pseudorotaxanes

In relation to crown ethers and cryptands, pseudorotaxanes are formed when a crown is mixed with a guest molecule such as paraquat and allowed to associate in solution. The complex is free to associate and dissociate; an example is provided in **Figure 1.5**. Typically smaller crowns such as dibenzo-24-crown-8 form pseudorotaxanes with dialkylammonium salts,⁵¹ and

larger crowns or cryptands such as dibenzo-30-crown-10 will form pseudorotaxanes with guest molecules such as paraquat or diquat salts.^{26,35}

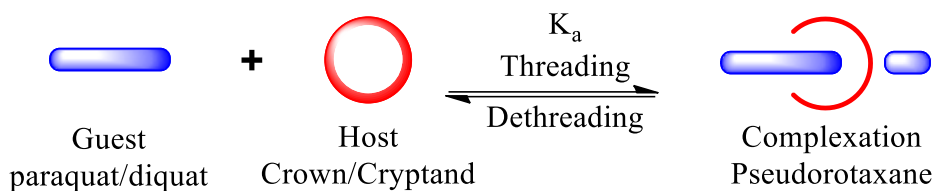


Figure 1.5. Reversible threading between a host and guest to form a pseudorotaxane.

Pseudorotaxanes serve as templates for producing rotaxanes⁵²⁻⁵⁵ and catenanes.^{56,57} Rotaxanes may be formed by adding large blocking groups to the guest molecule to prevent dethreading. Catenanes are formed through one of two methods. First a pseudorotaxane could be sufficiently diluted and reacted in such a way to produce cyclic species. Secondly, multiple host molecules can be used to complex a single guest; this results in an intertwined complex that can undergo cyclization to produce a catenane. **Figure 1.6** shows the formation of rotaxanes and catenanes.

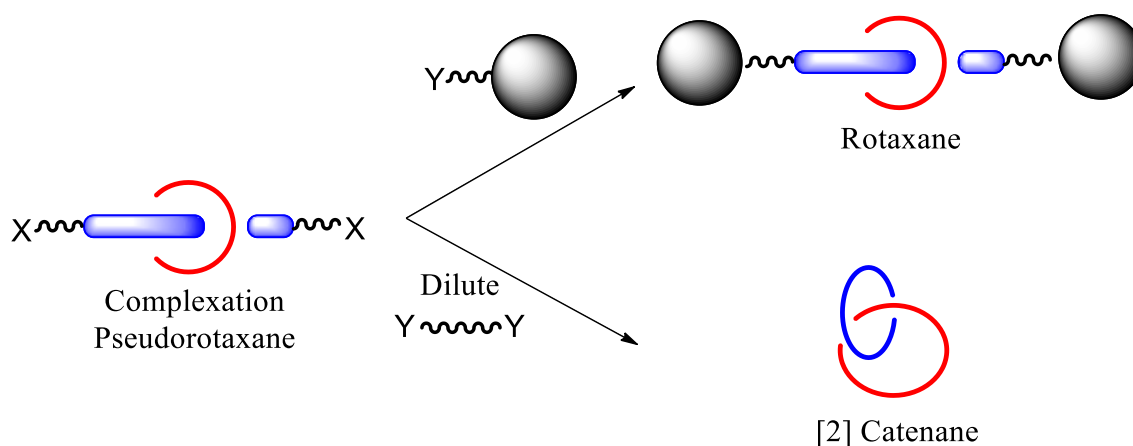


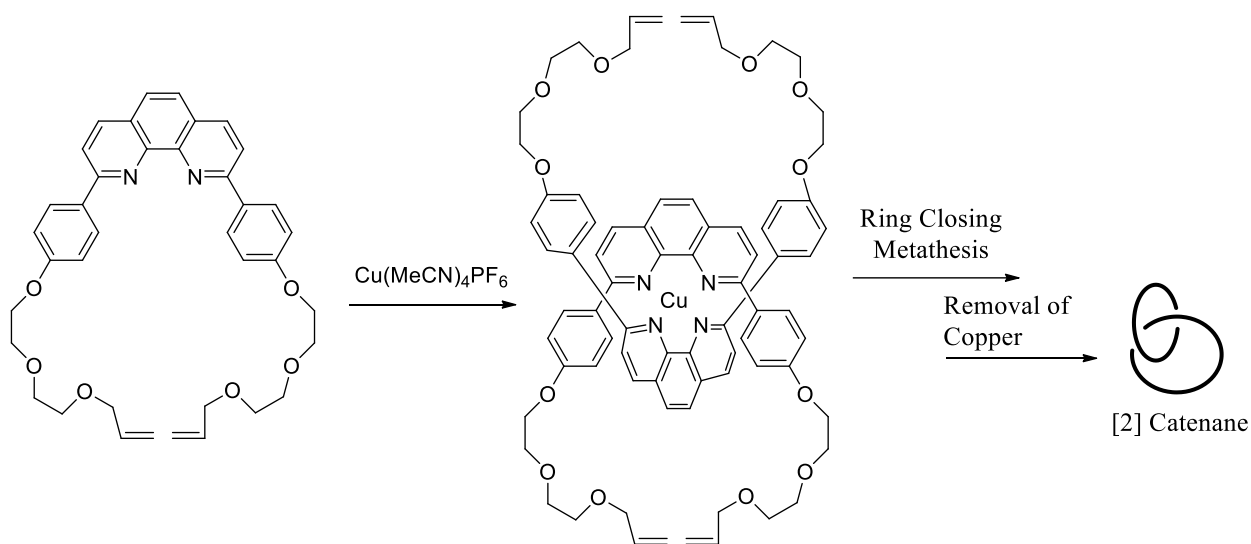
Figure 1.6. The formation of a rotaxane by addition of large bulky end groups and the formation of a catenane by cyclization with a difunctional molecule at high dilution.

1.3.2 Rotaxanes

Rotaxanes can be formed through one of three methods: pseudorotaxane precursors, slippage, or statistical methods. As previously stated the most common method for preparation is by adding large “blocking groups” to a pseudorotaxane to sterically hinder disassociation. The slippage method uses thermal energy to bring about the formation of a rotaxane from a host and sterically hindered guest.^{58,59} When ample thermal energy is supplied, the guest inserts itself into the host to bring about the formation of a rotaxane. One potential drawback of this method is that under certain conditions, such as solvent, time, and/or temperature, the rotaxane may de-thread. Rotaxanes may also be formed through a statistical method, such as when a polymer is forming. In this method, if macrocycles are present there is a probability that the polymer will insert itself through the macrocycle. After the rotaxane has been formed, the structure is locked in place mechanically and is no longer dependent upon an association constant to hold the structure together; this leads to a decreased importance of the association constant and removes reversibility.

1.3.3 Catenanes

Catenanes are interlocked rings, which can be formed from pseudorotaxanes by cyclization. **Scheme 1.2** shows a conventional method for the formation of [2]catenanes which uses phenanthroline templated with copper, followed by a ring closure and removal of copper.⁵⁷ Currently, the maximum amount of interlocked rings in a reported catenane is seven, leaving a wealth of constructs to be discovered.⁶⁰



Scheme 1.2. Synthesis of [2]catenane by phenanthroline templation

1.4 Driving force for complexation

The degree of complexation between a host and guest is controlled by several factors. The association constant can be changed due to factors such as solvent, pH, ionic strength, and temperature. The solvent is a most important and influential.⁶¹ Considering that the host is rich in electron density and the guest is a cation, polar solvents solubilize the guest and its counterion, whereas a non-polar solvent will tend to drive the guest molecule into the electron rich cavity of the host. However, the use of highly non-polar solvents (such as hexanes) is often not possible due to lack of solubility of the salt. Depending upon the guest, pH can also play a very valuable role in complexation, such as is the case for dialkylammonium salt complexes. In this situation, as the pH rises, the ammonium ion will be converted into an amine and complexation will be lost.^{14,15}

2. Characterization of complexation

The numerical value placed on the interaction between a host and guest is described as an equilibrium constant (K_a) and referred to as an association constant. Association constants may be determined by either using a type of spectroscopy or isothermal titration calorimetry (ITC), each having its own advantages and disadvantages. One of the largest problems encountered while obtaining association values is solubility; with regards to crown ether complexes, the more non-polar the solvent, the higher the association constant, and conversely, if the solvent is too non-polar the cation will be insoluble in solution.

2.1 Spectroscopy

Spectroscopic methods acceptable for determining association constants include NMR,⁶² UV-Vis,⁶³ and luminescence. The requirement for using a spectroscopic method is that there must be an observable change in the spectrum in the form of a peak shift or new peak (complexed versus uncomplexed). For these methods, data is obtained by analyzing a spectrum of a pure compound alongside varying ratios of host to guest. Peak shifts or changes in chromophore intensities are then plotted to find association constants. Since every molecule of host is not complexed two plots / equations must be assessed: one for the stoichiometry of complexed to uncomplexed species (such as a Job plot) and the other to obtain the association constant (such as a Scatchard plot). Association constants obtained in this way are generally acceptable up to approximately 10^4 , although higher values may be obtained through competitive studies.

Additionally, it should be noted that by NMR the equilibrium can be fast or slow exchanging relative to the NMR time scale at a given temperature. If a proton peak is shifted from its original location fast exchange is occurring. However, if the peak splits in to two, slow exchange is occurring. In a fast exchange system, the extent of complexation is indicated by the

percentage change of the chemical shift. In a slow exchange system, the extent of complexation is indicated by the relative areas of the two peaks.

Scatchard plots graph the percentage of complexed species divided by free species versus (the same) complexed species to give a line which (when the stoichiometry is 1:1 or statistical) has a slope and y-intercept equal to the association constant (K_a). These data are obtained by monitoring chemical shift values in the NMR spectrum. The change in chemical shift value corresponds to the percentage difference between the uncomplexed and fully complexed system peaks. The uncomplexed peaks are defined by the spectra of the pure materials and the maximum change can be defined by a system containing a large excess of either the host or guest. The difference in these chemical shifts defines the maximum range of change. The percentage of that change corresponds to the percentage of complexed species in systems with different molar ratios. Although they give no indication as to binding stoichiometry, Scatchard plots do explain to some extent how binding is occurring. For example, in a 2:1 system, cooperative, statistical, and anti-cooperative binding are witnessed when the plot appears arc-shaped, linear, or trough-shaped, respectively.

In addition to Scatchard plots (or any other data transformation), the binding stoichiometry must be determined to fully characterize the association constant of a system. Typically, for fast exchanging systems this is achieved through the use of a Job plot. Job plots are constructed by selecting a specific peak in the host or guest NMR spectrum and then monitoring the change in its chemical shift. This change in chemical shift is divided by the initial concentration of the host or guest and plotted against the mole fraction of host or guest, respectively. Even though K_a cannot be obtained by the Job plot, the determination of the

systems stoichiometry is a necessary complement to any method of K_a determination. In slow exchange systems stoichiometry can be determined by simple integration.

2.2 Isothermal Titration Calorimetry (ITC)

ITC is a method used for obtaining association constants in supramolecular systems through performing calorimetric titrations. By titrating a host into a guest solution (or guest to host), mixing between the two species occurs and heat is either transferred into or out of the system. The ITC instrument records this heat change for every point as the titration is underway and the data is used to provide ΔH directly, while association constants and the Gibbs free energy equation can be solved by back calculating from the data provided by the ITC.³⁵ The use of ITC in obtaining an association constant is generally acceptable for systems with values between 10^2 to 10^9 M^{-1} . Additionally, when using the ITC, care and discretion must be used since the data do not correlate directly to the host–guest system (such as specific NMR peak would) but instead to the solution as a whole.

The utility of NMR titrations and other spectroscopic methods is in the characterization of systems with low association constants. In regards to spectroscopic techniques the limit of detection is notable, given that it is dependent upon the instrument used for analysis, allowing for host–guest concentrations as low as 10^{-8} to be analyzed with UV–Vis. ITC however offers numerous advantages over spectroscopic methods such as: not requiring special solvents, extensive data, direct determination of ΔH at constant temperature, leading to determination of ΔS , applicable to higher K_a , and rapid analyses.

2.3 What classifies as a “good” K_a

Concerning the question of what classifies as a good association constant, the term can be considered relative. Depending upon the desired application of the motifs, association constants such as those of crown ethers may be acceptable (the range of $10-10^3 \text{ M}^{-1}$) for applications such as chain extensions, construction of star polymers, crosslinking, or for the formation of pseudorotaxanes and rotaxanes to change solubility or properties. However, for those systems which are exceptionally dependent upon the association constant, such as supramolecular polymers, higher association constants such as those of cryptands are required (10^4 M^{-1} or greater).

3. Supramolecular chemistry in relation to polymers

Supramolecular chemistry may be used to incorporate pseudorotaxane, rotaxane, or catenane complexes into polymeric structures in many ways. The various types of polymeric complexes are shown in **Figure 1.7**, and although no pseudorotaxanes are shown, each rotaxane structure corresponds to its analogous pseudorotaxane. Complexation in poly[3]rotaxanes, poly[2]rotaxanes and polycatenenes is found in the backbone of the polymer and crucial for holding the repeat unit of the polymer together. In main chain and side chain polyrotaxanes, the backbone of the polymer is held together through covalent bonds and complexation is not essential to maintaining a polymeric structure.

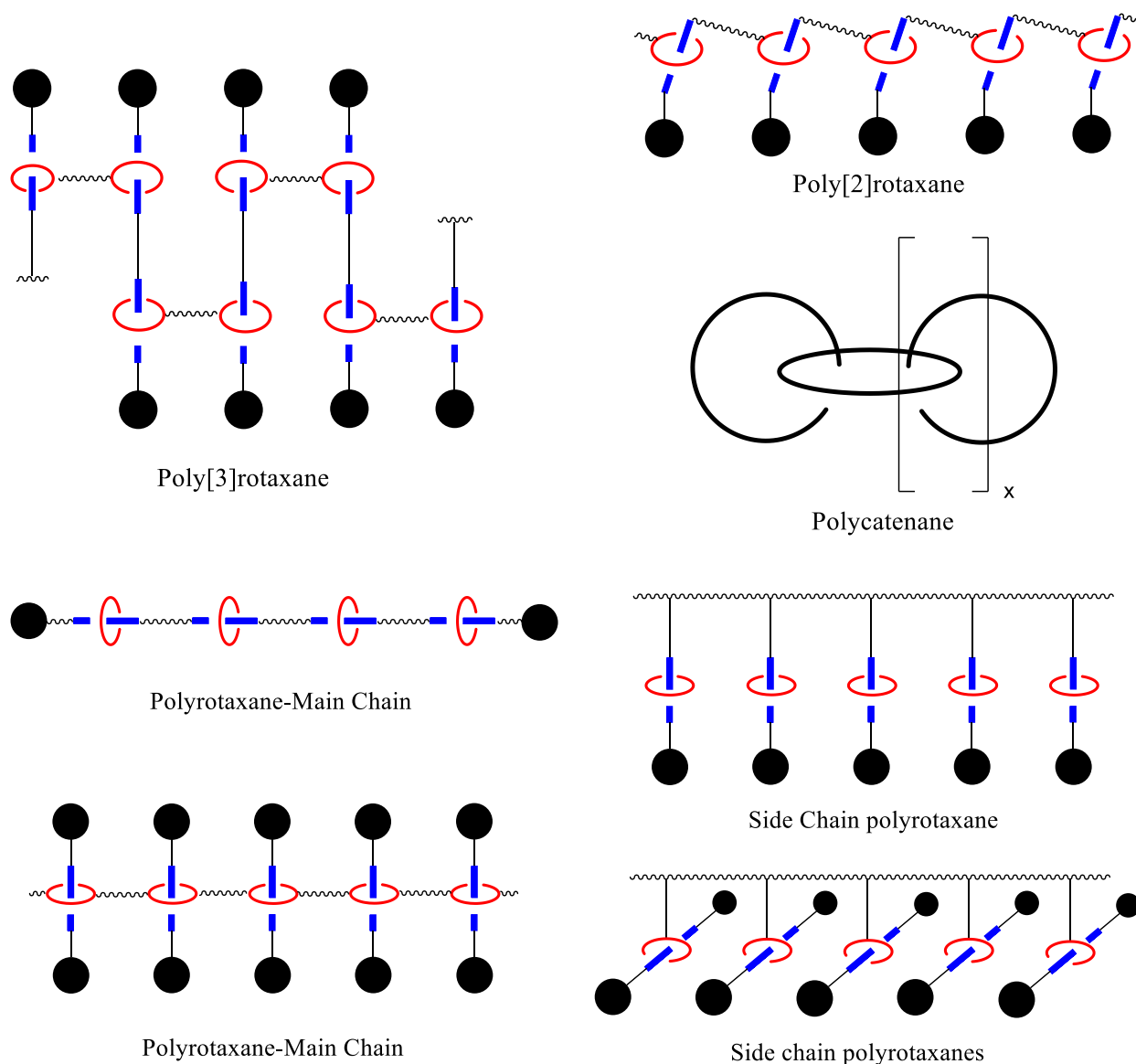


Figure 1.7. Different types of polymeric structures which employ supramolecular chemistry.

3.1. Poly[2] and [3] rotaxanes and pseudorotaxanes as well as polycatenanes

One of the most interesting branches of polymeric supramolecular chemistry is that of supramolecular polymers, which contains poly[2]rotaxanes, poly[3]rotaxanes and the corresponding pseudorotaxanes. Polymers from this class are formed through the noncovalent linking of small molecules to bring about a polymeric structure, poly[2] being a linkage of a

single small molecule or oligomer and poly[3] being a linkage between two small molecules or oligomers. Pseudorotaxanes are held together by intermolecular forces; therefore, complexation is an equilibrium process and must be treated as such. With regards to the rotaxanes, the molecules are sterically held in place and the structures are better defined. In each situation the polymers are developed in the same way in which a step growth polymerization is carried out, molecules link together in random arrays to form oligomers then eventually polymers.

The synthesis of a step growth molecule can be achieved through the use of either an A–B or A–A / B–B system where A will react with B. Supramolecular polymers are similar to covalently bound polymers in this sense, supramolecular polymers can be synthesized as either an A–B or A–A / B–B system in which A is a host and B a guest. To form poly[2]s a small molecule or oligomer must be made to be heterobifunctional with both a host and guest moiety, A-B. The host and guest moieties then align host to guest in the same manner as a step-growth reaction would align head to tail to form a polymeric structure; this is a poly[2]pseudorotaxane. Poly[2]rotaxanes are then formed by either reacting the small molecules of the pseudorotaxane with a blocking group or by producing monomer rotaxanes followed by polymerization. Poly[3]s are formed from a heteroditopic host and guest moiety incorporated into a small molecule or oligomer, A–A / B–B; as with poly[2]s the molecules then align via a step growth reaction to form a polymer. Once association has occurred between the heteroditopic hosts and guests, the poly[3]pseudorotaxane is formed and can be converted into a rotaxane by the addition of a blocking group. Polycatanenes are under-developed compounds synthetically, and because no high molecular weight polymers have to-date been reported, this class will not be further discussed.

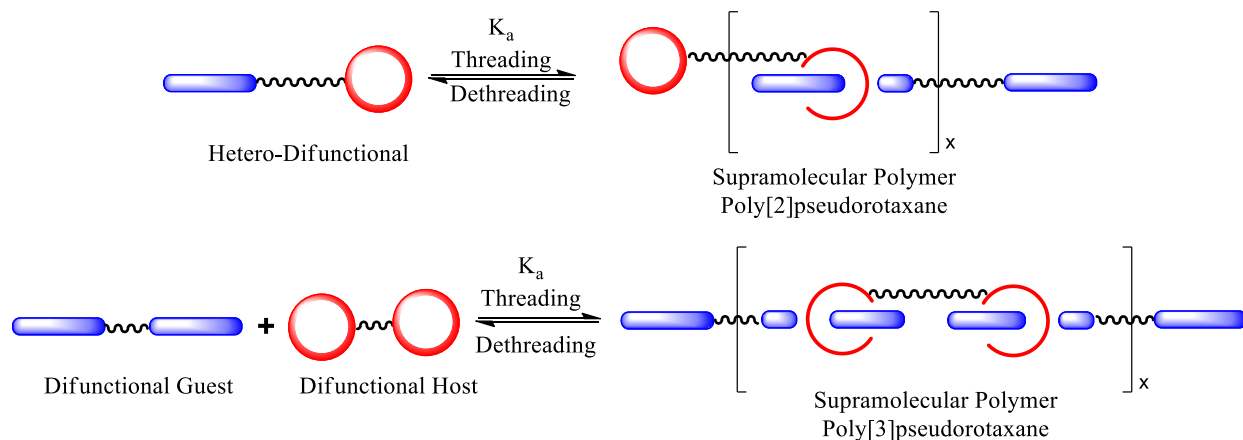


Figure 1.8. Cartoon showing the formation of two types of supramolecular polymers, poly[2]- and poly[3]pseudorotaxanes.

3.2 Main chain and side chain rotaxanes and pseudorotaxanes

In addition to supramolecular polymers and polymers that end in either a host or guest moiety, polymerization may be carried out on host and guest molecules to produce main chain rotaxanes and pseudorotaxanes. This makes it possible to form two types of main chain rotaxanes/pseudorotaxanes in which the backbone may be composed of either the host or guest. Synthetically, forming the rotaxane may be done either before or after polymerization; however, pseudorotaxane formation is generally done after polymerization. Several advantages exist for polymers of this type, such as after complexation, the solubility of the polymer can change drastically from that of the uncomplexed polymer, either improving or lowering solubility depending upon the groups added and solvent.¹³ By controlling complexation through some means such as solvent,⁶⁴ concentration,^{64,65} acidity,^{66,67} temperature,^{64,67} light,⁶⁵ etc., the polymer may be made to be stimuli responsive. Through selective choice of the complexing species, mechanical properties may also be enhanced through means such as adding crosslinking or

branching.¹³ Additionally, given that the rotaxane/pseudorotaxane joint is dynamic in nature, some polymers have the potential to exhibit self-healing properties.⁶⁷

3.5 Polymers ending in a host or guest

Polymers ending in either a host or guest provide means to couple the polymer to its complementary moiety. By the addition of a host or guest end to a polymer chain, association between the moieties can bring about the formation of block copolymers, star polymers, chain extensions, and dendronized polymers.

4. Applications of supramolecular chemistry

Although supramolecular chemistry is a relatively new field, applications have already begun to emerge from it and have received enough attention that it was awarded a Nobel Prize in 1987. The Nobel Prize was awarded to Donald J. Cram,⁶⁸ Jean-Marie Lehn,⁶⁹ and Charles J. Pedersen⁷⁰ for their work in supramolecular chemistry with crown ethers and cryptands. Concerning crown ethers, applications have begun to emerge in the way of combinatorial libraries, molecular sensors, polymer chain extenders, crosslinking, and molecular muscles.

Work conducted by Gibson and coworkers provides examples of host-guest end terminated or initiated polymers, which are used for chain extensions. These chain extenders have proven noteworthy and efficient in producing star polymers⁷¹ such as seen in **Figure 1.9**.⁶² The complex in **Figure 1.9** was the first report of a tri-armed pseudorotaxane; this was accomplished through the use of a dialkylammonium guest and dibenzo-24-crown-8 host. The average association constant for this system was $25 \times 10^2 \text{ M}^{-1}$.

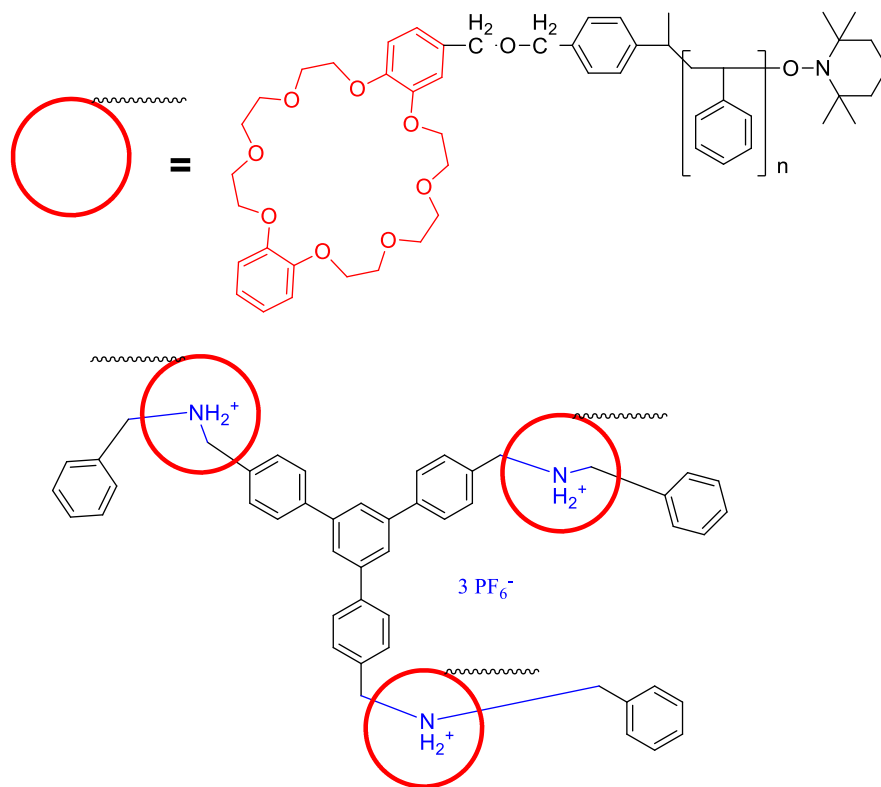
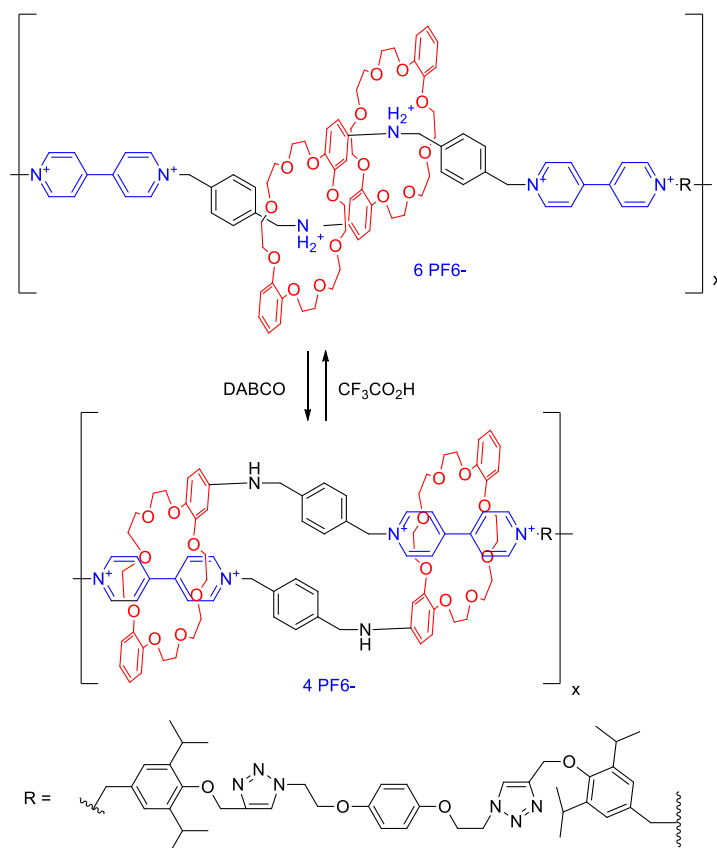


Figure 1.9. Star Polymer from host-guest moieties by Gibson and coworkers.³⁴

When correctly constructed, crown ether complexes can have the ability to function as molecular muscles. As an example of this, consider the crown ether system developed by Stoddart and coworkers, **Scheme 1.3**, a daisy chain (poly[2]rotaxane) composed of DB24C8 (dibenzo-24-crown-8) with paraquat and a dialkylammonium guests built into the polymer backbone.^{14,15} The DB24C8 within the system has a preference to associate with the dialkylammonium; however, in its absence it will associate with the paraquat. The dialkylammonium (**Scheme 1.3**) may be deprotonated by base to convert the group into a neutral species and thereby eliminate complexation, while simultaneously shifting complexation to the paraquat. Additionally, through the addition of an acid, the dialkylamine may be reprotonated,

causing complexation to revert to its previous state. This leads to the polymer functioning as a molecular muscle controlled by external stimuli.



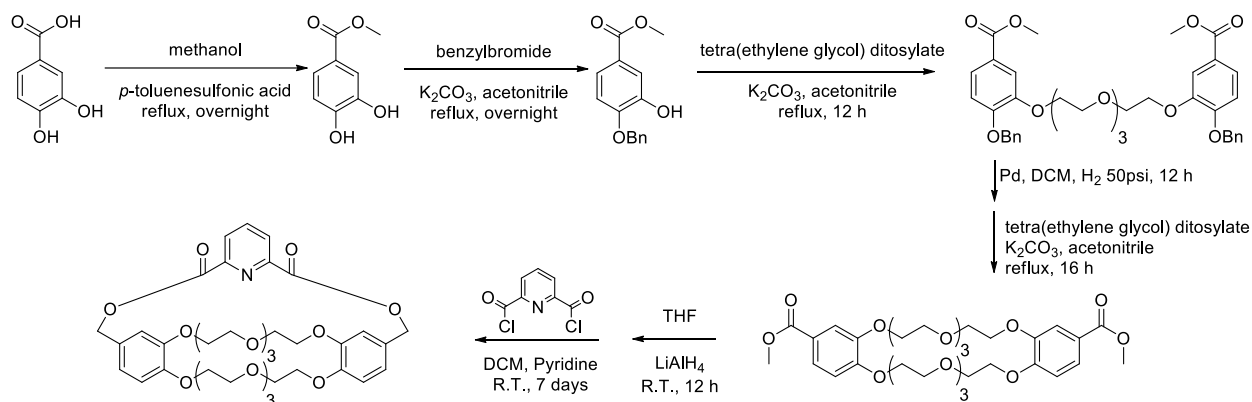
Scheme 1.3. Molecular muscle by Stoddart and coworkers^{9,10}

5. Research objectives

With any host-guest system, preliminary work begins with a search for an appropriate host-guest pair, either by analysis of known systems or a synthetic search for new pairs. The Gibson group in the past has targeted crown ethers and cryptands for complexations with alkylammonium and pyridinium salts, laying the ground work for synthetic routes for the production of crown ethers, and an understanding of how these complexations occur by analysis

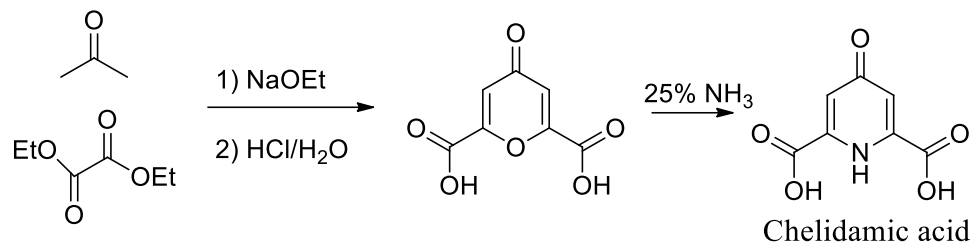
of X-ray crystal structures. Chapters 2 and 4 of this dissertation will focus on the development of new hosts and guests, respectively.

Of particular interest, regarding host–guest systems, are the pyridyl cryptand host group and the guest group of paraquats. Crown ethers have been shown to complex paraquat in the range of 10^2 M^{-1} in acetone, while affording two possibilities for complexation, either by threading or folding of the crown ether around the paraquat to form a taco-like complex. The analogous cryptands, however, give complexations in the range of $10^5\text{--}10^6 \text{ M}^{-1}$ in acetone and give complexations by threading alone, making them advantageous to use over crown ethers. Gibson et al. have provided an adequate high yielding regioselective route to produce pure disubstituted dibenzo crown ethers through templation,⁵¹ while work by Pederson et al. have provided a route to the synthesis of 2,6-pyridino cryptand of *cis* dibenzo-30-crown-10 (**Scheme 1.4**).¹⁹ Additionally the work by Pederson et al. showed the benefits of using a cryptand over its crown ether counterpart, such as the increased binding constant and only threading occurring during complexation.³⁵ Problems with the pyridyl cryptand, however, remained with functionalizing the cryptand, so that it may be further used to produce a system of interest, and determining how to appropriately scale the reaction and or reduce the time required to produce it. The method for producing the cryptand required an excess of six days and was limited to pseudo-high dilution conditions. This prompted one of our goals: the synthesis of a functionalized cryptand, which may be easily modified in high yields to provide a range of cryptands, the targets being derivatives of the 2,6-pyridino cryptand of *cis* dibenzo-30-crown-10.



Scheme 1.4. Previous method for the synthesis of non-functionalized cryptand

Chapter 3 focuses on relieving the burden of cryptand synthesis by developing a templation method for cryptand synthesis which allows for an easier scale up and reduction in overall reaction time. To bring about a solution to cryptand functionalization, we focused on the 4-position of its pyridine ring. One possibility for functionalizing the pyridine arm is to begin with chelidamic acid, seen in **Scheme 1.5**, and convert the OH into some other easily functionalized group. It should be noted that the chelidamic acid as its benzyl ether was reported by Pederson¹⁹ to not provide a suitable pathway due to hydrogenolysis of the ester linkages upon attempted deprotection. Horvath et al. provide a high-yielding synthetic route to chelidamic acid, seen in **Scheme 1.5**,⁷² allowing Chapter 5 of this dissertation to focus on its derivatives. Chapter 6 and 7 then employ the derivatives of Chapter 5 to produce functionalized cryptands. Chapter 6 explores singly functionalized cryptands while Chapter 7 concentrates on the synthesis of dicryptands. Chapter 8 builds upon the work of all previous chapters to prepare supramolecular structures, polypseudorotaxanes and polymer chain extension through the use of supramolecular motifs.



Scheme 1.5. Synthesis of chelidamic acid.⁴⁰

References

- (1) Steed, J. W.; Atwood, J. L. *Supramolecular Chemistry*; Second edition ed.; Wiley, 2009.
- (2) Lehn, J.-M. *Supramolecular Chemistry: Concepts and Perspectives*; 1 ed., 1995.
- (3) Coti, K. K.; Belowich, M. E.; Liong, M.; Ambrogio, M. W.; Lau, Y. A.; Khatib, H. A.; Zink, J. I.; Khashab, N. M.; Stoddart, J. F. *Nanoscale* **2009**, *1*, 16-39.
- (4) Krakowiak, K. E.; Bradshaw, J. S.; Zamecka-Krakowiak, D. J. *Chem. Rev.* **1989**, *89*, 929-972.
- (5) Richman, J. E.; Atkins, T. J. *J. Am. Chem. Soc.* **1974**, *96*, 2268-2270.
- (6) Cooper, S. R. *Acc. Chem. Res.* **1988**, *21*, 141-146.
- (7) Hansen, T. K.; Joergensen, T.; Stein, P. C.; Becher, J. *J. Org. Chem.* **1992**, *57*, 6403-6409.
- (8) Park, C. H.; Simmons, H. E. *J. Am. Chem. Soc.* **1968**, *90*, 2429-2431.
- (9) Simmons, H. E.; Park, C. H. *J. Am. Chem. Soc.* **1968**, *90*, 2428-2429.
- (10) Dietrich, B.; Lehn, J. M.; Sauvage, J. P. *Tetrahedron Lett.* **1969**, *10*, 2885-2888.
- (11) Zhang, M.; Yan, X.; Huang, F.; Niu, Z.; Gibson, H. W. *Acc. Chem. Res.* **2014**, *47*, 1995-2005.
- (12) Begel, S.; Puchta, R.; van Eldik, R. *Beilstein J. Org. Chem.* **2013**, *9*, 1252-1268.
- (13) Huang, F.; Gibson, H. W. *Prog. Polym. Sci.* **2005**, *30*, 982-1018.
- (14) Hmadeh, M.; Fang, L.; Trabolsi, A.; Elhabiri, M.; Albrecht-Gary, A.-M.; Stoddart, J. F. *J. Mater. Chem.* **2010**, *20*, 3422-3430.
- (15) Fang, L.; Hmadeh, M.; Wu, J.; Olson, M. A.; Spruell, J. M.; Trabolsi, A.; Yang, Y.-W.; Elhabiri, M.; Albrecht-Gary, A.-M.; Stoddart, J. F. *J. Am. Chem. Soc.* **2009**, *131*, 7126-7134.
- (16) Izatt, R. M.; Bradshaw, J. S.; Nielsen, S. A.; Lamb, J. D.; Christensen, J. J.; Sen, D. *Chem. Rev.* **1985**, *85*, 271-339.
- (17) Izatt, R. M.; Pawlak, K.; Bradshaw, J. S.; Bruening, R. L. *Chem. Rev.* **1991**, *91*, 1721-2085.
- (18) Izatt, R. M.; Pawlak, K.; Bradshaw, J. S.; Bruening, R. L. *Chem. Rev.* **1995**, *95*, 2529-2586.
- (19) Cao, J.; Fyfe, M. C. T.; Stoddart, J. F.; Cousins, G. R. L.; Glink, P. T. *J. Org. Chem.* **2000**, *65*, 1937-1946.
- (20) Ashton, P. R.; Chrystal, E. J. T.; Glink, P. T.; Menzer, S.; Schiavo, C.; Spencer, N.; Stoddart, J. F.; Tasker, P. A.; White, A. J. P.; Williams, D. J. *Chem. Eur. J.* **1996**, *2*, 709-728.

- (21) Li, S.; Huang, F.; Slobodnick, C.; Ashraf-khorassani, M.; Gibson, H. W. *Chinese J. Chem.* **2009**, *27*, 1777-1781.
- (22) Huang, F.; Jones, J. W.; Slobodnick, C.; Gibson, H. W. *J. Am. Chem. Soc.* **2003**, *125*, 14458-14464.
- (23) Moody, G. J.; Owusu, R. K.; Thomas, J. D. R. *Analyst* **1987**, *112*, 121-127.
- (24) Colquhoun, H. M.; Goodings, E. P.; Maud, J. M.; Stoddart, J. F.; Williams, D. J.; Wolstenholme, J. B. *J. Chem. Soc., Chem. Commun.* **1983**, 1140-1142.
- (25) Tokunaga, Y.; Yoshioka, M.; Nakamura, T.; Goda, T.; Nakata, R.; Kakuchi, S.; Shimomura, Y. *Bull. Chem. Soc. Jpn.* **2007**, *80*, 1377-1382.
- (26) He, C.; Shi, Z.; Zhou, Q.; Li, S.; Li, N.; Huang, F. *J. Org. Chem.* **2008**, *73*, 5872-5880.
- (27) Bryant, W. S.; Guzei, I. A.; Rheingold, A. L.; Merola, J. S.; Gibson, H. W. *J. Org. Chem.* **1998**, *63*, 7634-7639.
- (28) Niu, Z.; Slobodnick, C.; Schoonover, D.; Azurmendi, H.; Harich, K.; Gibson, H. W. *Org. Lett.* **2011**, *13*, 3992-3995.
- (29) Bryant, W. S.; Jones, J. W.; Mason, P. E.; Guzei, I.; Rheingold, A. L.; Fronczek, F. R.; Nagvekar, D. S.; Gibson, H. W. *Org. Lett.* **1999**, *1*, 1001-1004.
- (30) Huang, F.; Zakharov, L. N.; Rheingold, A. L.; Jones, J. W.; Gibson, H. W. *Chem. Commun.* **2003**, 2122-2123.
- (31) Huang, F.; Slobodnick, C.; Switek, K. A.; Gibson, H. W. *Tetrahedron* **2007**, *63*, 2829-2839.
- (32) Gibson, H. W.; Wang, H.; Slobodnick, C.; Merola, J.; Kassel, W. S.; Rheingold, A. L. *J. Org. Chem.* **2007**, *72*, 3381-3393.
- (33) Bryant, W. S.; Jones, J. W.; Mason, P. E.; Guzei, I.; Rheingold, A. L.; Fronczek, F. R.; Nagvekar, D. S.; Gibson, H. W. *Org. Lett.* **1999**, *1*, 1001-1004.
- (34) Huang, F.; Slobodnick, C.; Switek, K. A.; Gibson, H. W. *Chem. Comm.* **2006**, 1929-1931.
- (35) Pederson, A. M. P.; Ward, E. M.; Schoonover, D. V.; Slobodnick, C.; Gibson, H. W. *J. Org. Chem.* **2008**, *73*, 9094-9101.
- (36) Huang, F.; Switek, K. A.; Zakharov, L. N.; Fronczek, F. R.; Slobodnick, C.; Lam, M.; Golen, J. A.; Bryant, W. S.; Mason, P. E.; Rheingold, A. L.; Ashraf-Khorassani, M.; Gibson, H. W. *J. Org. Chem.* **2005**, *70*, 3231-3241.
- (37) Arnold, K. A.; Echegoyen, L.; Fronczek, F. R.; Gandour, R. D.; Gatto, V. J.; White, B. D.; Gokel, G. W. *J. Am. Chem. Soc.* **1987**, *109*, 3716-3721.
- (38) Miller, S. R.; Cleary, T. P.; Trafton, J. E.; Smeraglia, C.; Gandour, R. D.; Fronczek, F. R.; Gokel, G. W. *J. Chem. Soc., Chem. Commun.* **1989**, 608-610.
- (39) Gandour, R. D.; Fronczek, F. R.; Gatto, V. J.; Minganti, C.; Schultz, R. A.; White, B. D.; Arnold, K. A.; Mazzocchi, D.; Miller, S. R.; Gokel, G. W. *J. Am. Chem. Soc.* **1986**, *108*, 4078-4088.
- (40) Fronczek, F. R.; Gatto, V. J.; Schultz, R. A.; Jungk, S. J.; Colucci, W. J.; Gandour, R. D.; Gokel, G. W. *J. Am. Chem. Soc.* **1983**, *105*, 6717-6718.
- (41) Gokel, G. W. *Chem. Soc. Rev.* **1992**, *21*, 39-47.
- (42) Gokel, G. W.; Barbour, L. J.; De Wall, S. L.; Meadows, E. S. *Coordin. Chem. Rev.* **2001**, *222*, 127-154.
- (43) Gokel, G. W.; Barbour, L. J.; Ferdani, R.; Hu, J. *Acc. Chem. Res.* **2002**, *35*, 878-886.
- (44) Abbas, A. A.; Elwahy, A. H. M. *J. Heterocycl. Chem.* **2009**, *46*, 1035-1079.

- (45) Jones, J. W.; Zakharov, L. N.; Rheingold, A. L.; Gibson, H. W. *J. Amer. Chem. Soc.* **2002**, *124*, 13378-13379.
- (46) Nabeshima, T. *Bull. Chem. Soc. Jpn.* **2010**, *83*, 969-991.
- (47) Niu, Z.; Price Jr, T. L.; Slebodnick, C.; Gibson, H. W. *Tetrahedron Lett.* **2016**, *57*, 60-63.
- (48) Niu, Z.; Slebodnick, C.; Gibson, H. W. *Org. Lett.* **2011**, *13*, 4616-4619.
- (49) South, C. R.; Leung, K. C. F.; Lanari, D.; Stoddart, J. F.; Weck, M. *Macromolecules* **2006**, *39*, 3738-3744.
- (50) Heo, G. S.; Bartsch, R. A. *J. Org. Chem.* **1982**, *47*, 3557-3559.
- (51) Gibson, H. W.; Wang, H.; Bonrad, K.; Jones, J. W.; Slebodnick, C.; Zakharov, L. N.; Rheingold, A. L.; Habenicht, B.; Lobue, P.; Ratliff, A. E. *Org. Biomol. Chem.* **2005**, *3*, 2114-2121.
- (52) Lee, Y.-G.; Koyama, Y.; Yonekawa, M.; Takata, T. *Macromolecules* **2010**, *43*, 4070-4080.
- (53) Kohsaka, Y.; Konishi, G.-i.; Takata, T. *Polym. J* **2007**, *39*, 861-873.
- (54) Sato, T.; Takata, T. *Polym. J* **2009**, *41*, 470-476.
- (55) Takata, T. *Polym. J* **2006**, *38*, 1-20.
- (56) Sambrook, M. R.; Beer, P. D.; Wisner, J. A.; Paul, R. L.; Cowley, A. R. *J. Am. Chem. Soc.* **2004**, *126*, 15364-15365.
- (57) Weck, M.; Mohr, B.; Sauvage, J.-P.; Grubbs, R. H. *J. Org. Chem.* **1999**, *64*, 5463-5471.
- (58) Elizarov, A. M.; Chang, T.; Chiu, S.-H.; Stoddart, J. F. *Org. Lett.* **2002**, *4*, 3565-3568.
- (59) Raymo, F. M.; Houk, K. N.; Stoddart, J. F. *J. Am. Chem. Soc.* **1998**, *120*, 9318-9322.
- (60) Niu, Z.; Gibson, H. W. *Chem. Rev.* **2009**, *109*, 6024-6046.
- (61) Solov'ev, V. P.; Strakhova, N. N.; Raevsky, O. A.; Rudiger, V.; Schneider, H.-J. *J. Org. Chem.* **1996**, *61*, 5221-5226.
- (62) Huang, F.; Nagvekar, D. S.; Slebodnick, C.; Gibson, H. W. *J. Am. Chem. Soc.* **2004**, *127*, 484-485.
- (63) Naemura, K.; Nishioka, K.; Ogasahara, K.; Nishikawa, Y.; Hirose, K.; Tobe, Y. *Tetrahedron: Asymmetry* **1998**, *9*, 563-574.
- (64) De Greef, T. F. A.; Smulders, M. M. J.; Wolfs, M.; Schenning, A. P. H. J.; Sijbesma, R. P.; Meijer, E. W. *Chem. Rev.* **2009**, *109*, 5687-5754.
- (65) Brunsveld, L.; Folmer, B. J. B.; Meijer, E. W.; Sijbesma, R. P. *Chem. Rev.* **2001**, *101*, 4071-4098.
- (66) Niu, Z.; Slebodnick, C.; Huang, F.; Azurmendi, H.; Gibson, H. W. *Tetrahedron Lett.* **2011**, *52*, 6379-6382.
- (67) Yan, X.; Xu, D.; Chen, J.; Zhang, M.; Hu, B.; Yu, Y.; Huang, F. *Polym. Chem.* **2013**, *4*, 3312-3322.
- (68) Cram, D. J. In *Nobel Lecture, 8 December 1987*; Editor-in-Charge Tore Frängsmyr, E. B. G. M., Ed.; World Scientific Publishing Co: 1987.
- (69) Lehn, J.-M. In *Nobel Lecture, December 8, 1987*; Editor-in-Charge Tore Frängsmyr, E. B. G. M., Ed.; World Scientific Publishing Co.: 1987, p 48.
- (70) Pedersen, C. J. In *Nobel Lecture December 8, 1987*; Editor-in-Charge Tore Frängsmyr, E. B. G. M., Ed.; World Scientific Publishing Co.: 1987, p 17.
- (71) Lee, M.; Schoonover, D. V.; Gies, A. P.; Hercules, D. M.; Gibson, H. W. *Macromolecules* **2009**, *42*, 6483-6494.
- (72) Howáth, G.; Rusa, C.; Köntös, Z.; Gerencsér, J.; Huszthy, P. *Synth. Commun.* **1999**, *29*, 3719 - 3731.

CHAPTER 2

NEW HOSTS

INTRODUCTION

In the field of host-guest chemistry there is an ever-progressing race to find new higher binding systems, easier to synthesize systems, and or systems that bind differently. This opens the door to the production of new materials which may be accessed more easily than their predecessors and/or possess unique properties. As an example, work in our group began with a modest binding bis(*m*-phenylene)-24crown-8 / dialkylammonium system.¹ Due to ion pairing and higher association constants, the system was abandoned for the dibenzo-30-crown-10 / paraquat² and bis(*m*-phenylene)-32crown-10 / paraquat³ system and then these systems were eventually replaced by the higher binding cryptand / paraquat combination.^{2,4} With each change the system was simplified and/or higher binding was achieved, leading to more efficient host-guest combinations. As an illustration of the importance of this progression, if the goal is the production of supramolecular polymers or chain extension, with every increase in binding, higher molecular weights are achieved or a higher degree of chain extension is reached, respectively.⁵ Since the synthesis of the pyridyl dibenzo-30-crown-10 cryptands and the recent introduction of pseudocryptands achieving association constants close to those of the corresponding cryptands with paraquat,⁶ effort has been put into exploring pseudocryptands. Pseudocryptands are cyclic host compounds which contain one or two unconnected arms that can come together reversibly, by some driving force, to form a third arm to yield a cryptand-like structure; these compounds are an extension to the class of pseudomacrocyclic compounds.^{3,7-9}

Figure 2.1 provides cartoon examples of pseudocryptands.

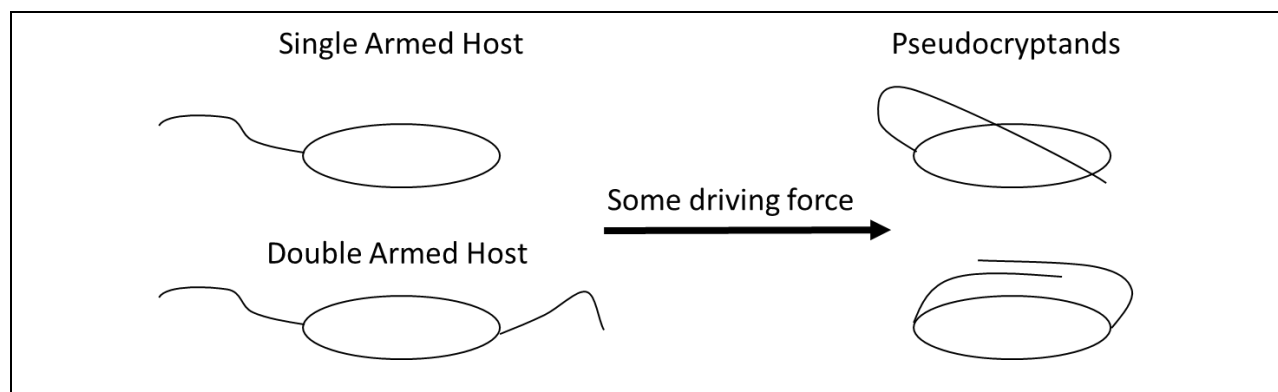
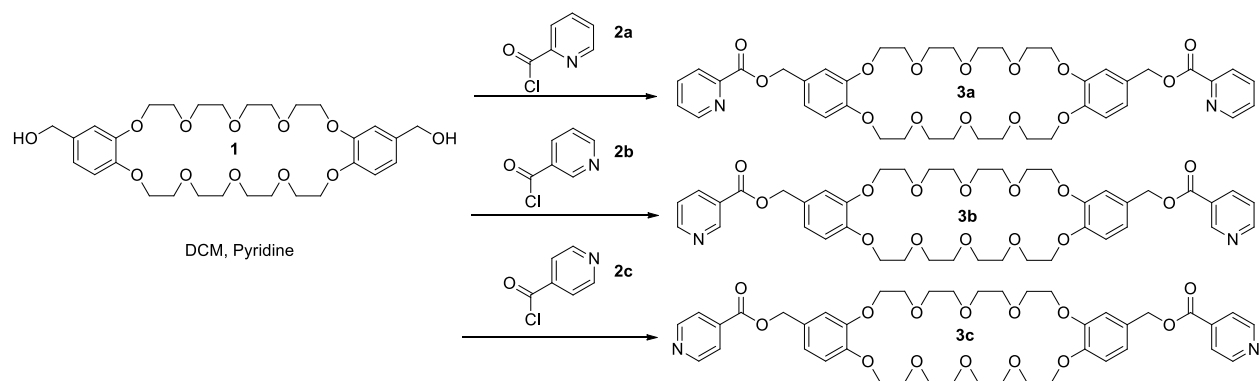


Figure 2.1. Cartoon depicting pseudocryptands.

Crown ether derivatives now offer an ease of synthesis and association constants competitive with their cryptand counterparts, as well as they can provide insight into the design of better cryptands. Here we explore the effects of the attachment of a pyridyl ester to *cis*-di(hydroxymethylbenzo)-30-crown-10. The variation of the point of attachment of the pyridyl group is expected to greatly affect the way in which the host interacts with either diquat or paraquat PF_6^- .

This leads to the conclusion that for pyridyl cryptands there must be an optimal pyridyl attachment to optimize binding for a given guest. Thus, a series containing three isomeric pyridyl esters was synthesized, **Scheme 2.1**. The underlying idea is that by changing the orientation in which the pyridyl ring could hydrogen interact with guests, we could better direct the synthesis of novel cryptands to allow for higher association constants with paraquat and diquat.



Scheme 2.1. Synthesis of pyridyl esters of dibenzo-30-crown-10: pseudocryptands **3a–3c**.

RESULTS AND DISCUSSION

A series of three pyridyl esters of dibenzo-30-crown-10 pseudocryptands, **3a–3c** (**Scheme 2.1**) was synthesized and association constants with paraquat and diquat were determined. As is the case with non-functionalized dibenzo-30-crown-10 and its cryptand counterpart,^{2,10} it was suspected that association constants with diquat would be higher than with paraquat. **Table 2.1** shows ITC data for titrations conducted in acetone at 25 °C.

Table 2.1. ITC results for **3a–3c** with diquat and paraquat obtained in acetone at 25 °C via ITC.

	Diquat		
	3a	3b	3c
$10^{-3} K_a (M^{-1})$	40.6 (±1.9)	4.36 (±0.10)	3.50 (±0.09)
$\Delta G (kcal mol^{-1})$	-6.28 (±0.29)	-4.96 (±0.11)	-4.83 (±0.13)
$\Delta H (kcal mol^{-1})$	-17.4 (±0.1)	-17.3 (±0.2)	-17.7 (±0.2)
$\Delta S (cal mol^{-1} K^{-1})$	-37.3 (±1.8)	-41.4 (±1.1)	-43.2 (±1.3)

	Paraquat		
	3a	3b	3c
K_a (M^{-1})	207 (± 5)	785 (± 12)	162 (± 11)
ΔG ($kcal\ mol^{-1}$)	-3.16 (± 0.08)	-3.95 (± 0.06)	-3.95 (± 0.20)
ΔH ($kcal\ mol^{-1}$)	-4.31 (± 0.04)	-10.2 (± 0.1)	-5.60 (± 0.08)
ΔS ($cal\ mol^{-1}\ K^{-1}$)	-3.86 (± 0.10)	-21.0 (± 0.35)	-8.66 (± 0.60)

As expected the ITC data confirmed that association constants for **3a**, **3b**, and **3c** were better with diquat PF_6^- than paraquat PF_6^- . Interestingly however, the ITC data reveals that attachment at the 2-position gives the highest association constant with diquat, while attachment at the 3-position is advantageous for binding paraquat. Looking first at the diquat series, as the pyridyl ring's attachment is moved from the 4- position to 2-, ΔH remains the same within experimental error, while ΔS becomes more negative. This is likely a result of the extent to which the cavity and pyridyl arms have to open to allow for optimal binding; thus as the attachment is moved, a larger volume is reached to obtain optimal placement of the pyridyl groups. Looking at the paraquat series, the interesting data point is the complex of paraquat with **3b**, although the ΔS term is significantly lower than for the other two complexes, its higher association constant can be attributed to it having a much larger enthalpy change.

Since ITC fits data to a given stoichiometric model, a Job Plot was constructed to confirm 1:1 complexation. In the 1H NMR titration experiment **3a** was titrated with diquat in varying ratios of crown:diquat from 9:1 to 1:9. **Figure 2.2** shows the Job Plot. The data indicates that the binding stoichiometry of **3a** with diquat is 1:1.

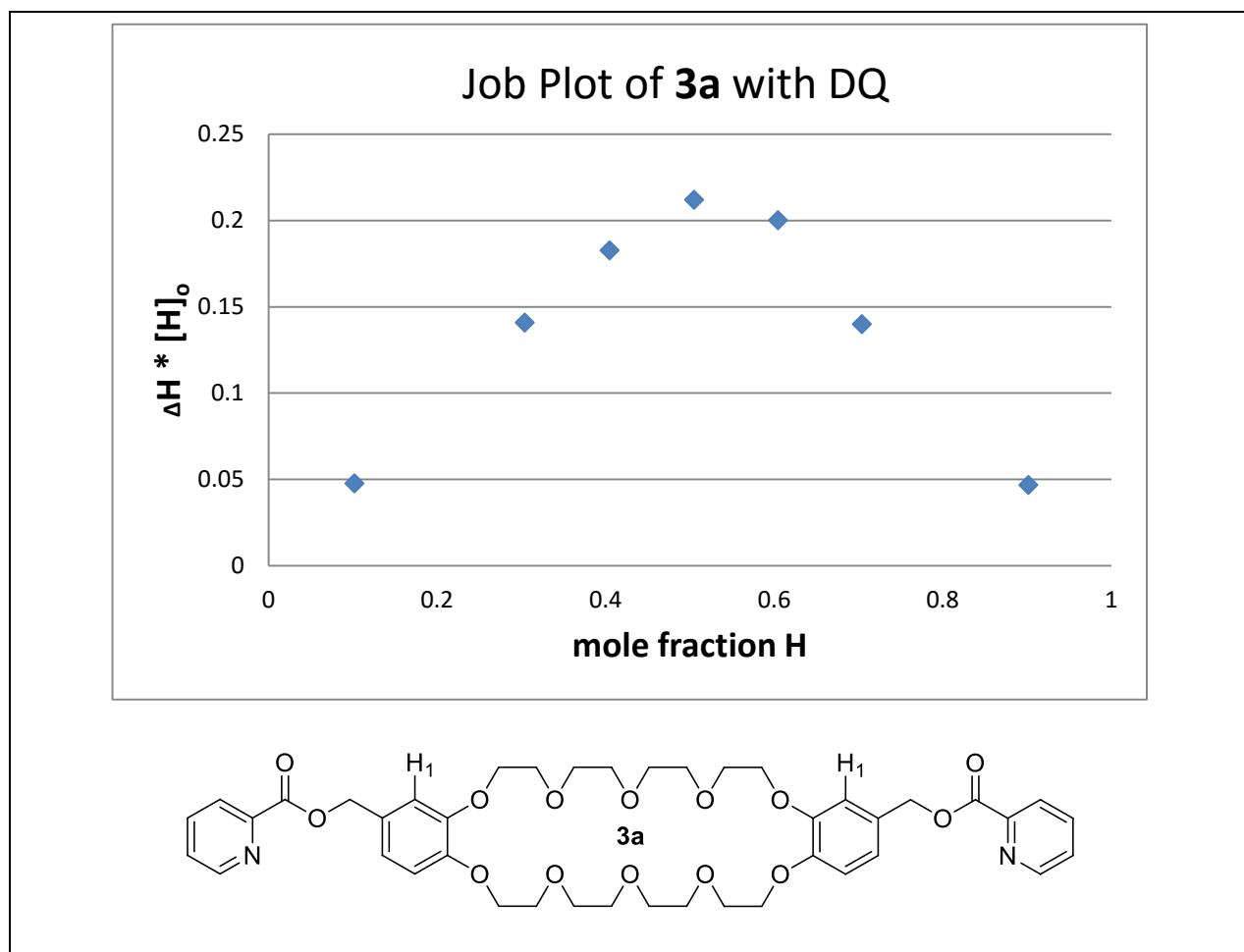


Figure 2.2. 500 MHz ^1H NMR Job Plot titration of **3a** with diquat in acetone- d_6 at room temperature; H_1 used for analysis.

Interestingly, using the obtained ΔH and ΔS values from **Table 2.1**, a linear relationship results when constructing a scatter plot of enthalpy vs. entropy for the complete series of **3a–3c**, seen in **Figure 2.3**. This type of correlation has been observed and described within peer reviewed literature in terms of enthalpy–entropy compensation.¹¹⁻¹³ Correlations such as those observed in **Figure 2.3** have recently driven arguments for a connection between entropy and internally stored energies,¹⁴ hidden term(s) connecting enthalpy and entropy,¹⁵ and the potential for a fourth law of thermodynamics that explains intermolecular binding processes.¹¹ However,

for this system and those found within literature sources,¹¹⁻¹³ the reason for this correlation is not yet apparent.

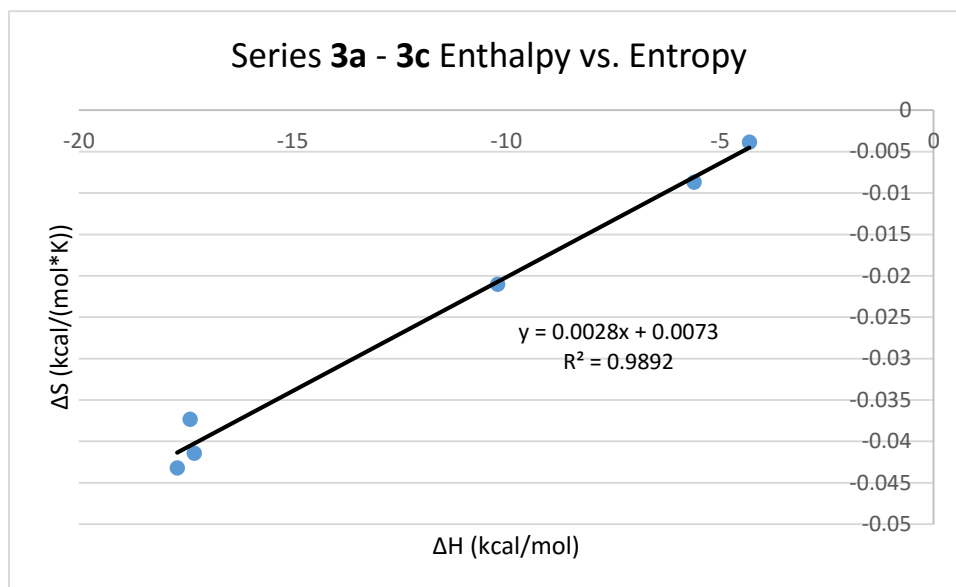
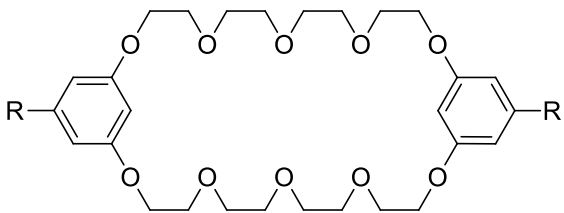


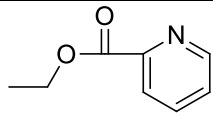
Figure 2.3. Scatter plot of enthalpies vs. entropies for **3a** – **3c** determined at 25 °C in acetone, values taken from **Table 2.1**.

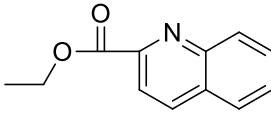
Table 2.2 provides association constants for similar bis(*m*-phenylene)-32-crown-10 pseudocryptands; compound **4a** is the analogous 32-crown-10 version of **3a**, while compounds **4b** and **4c** have been designed to increase binding with paraquat. Directly comparing **3a** to **4a**, it can be seen that the paraquat binding of **4a** is an order of magnitude higher than **3a**, but the diquat binding of **3a** is nearly two orders of magnitude higher than **4a**. It is worth pointing out that **3a** bound diquat better than the highly evolved host **4c**.

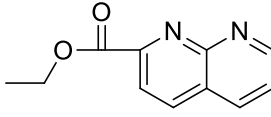
Table 2.2. K_a values for **4a** – **4c** with paraquat⁶ and diquat.⁹

Complex	$10^{-3} K_a (M^{-1})$
4a • paraquat	3.1 ^a
4b • paraquat	12.4 ^a
4c • paraquat	250 ^b
4a • diquat	0.77 ^c
4b • diquat	0.56 ^d
4c • diquat	32 ^d



4a. R = 

4b. R = 

4c. R = 

a. value obtained in CDCl₃/CDCN (1/1, v/v) via ¹H NMR.
b. value obtained in CHCl₃/CHCN (1/1, v/v) via ITC.
c. value obtained in acetone-*d*₆ at 25 °C via ¹H NMR.
d. value obtained in acetone at 25 °C via ITC.

From the ITC data it can be directly concluded that for diquat PF₆, **3a** is optimal. To identify the role of the pyridyl group at differing positions and gain insight into the design of better systems, structural information for the complex must be gathered. Both 2D NOESY and X-ray crystallography have been employed to provide 3D representations of the complexes. 2D NOESY spectra taken in acetone-*d*₆ at room temperature are as follows: **Figure 2.4 (3a • DQ PF₆)**, **Figure 2.5 (3b • DQ PF₆)** and **Figure 2.6 (3c • DQ PF₆)**. X-ray crystallography of **3b • DQ PF₆** grown by vapor diffusion of ether into acetone is shown in **Figure 2.7**.

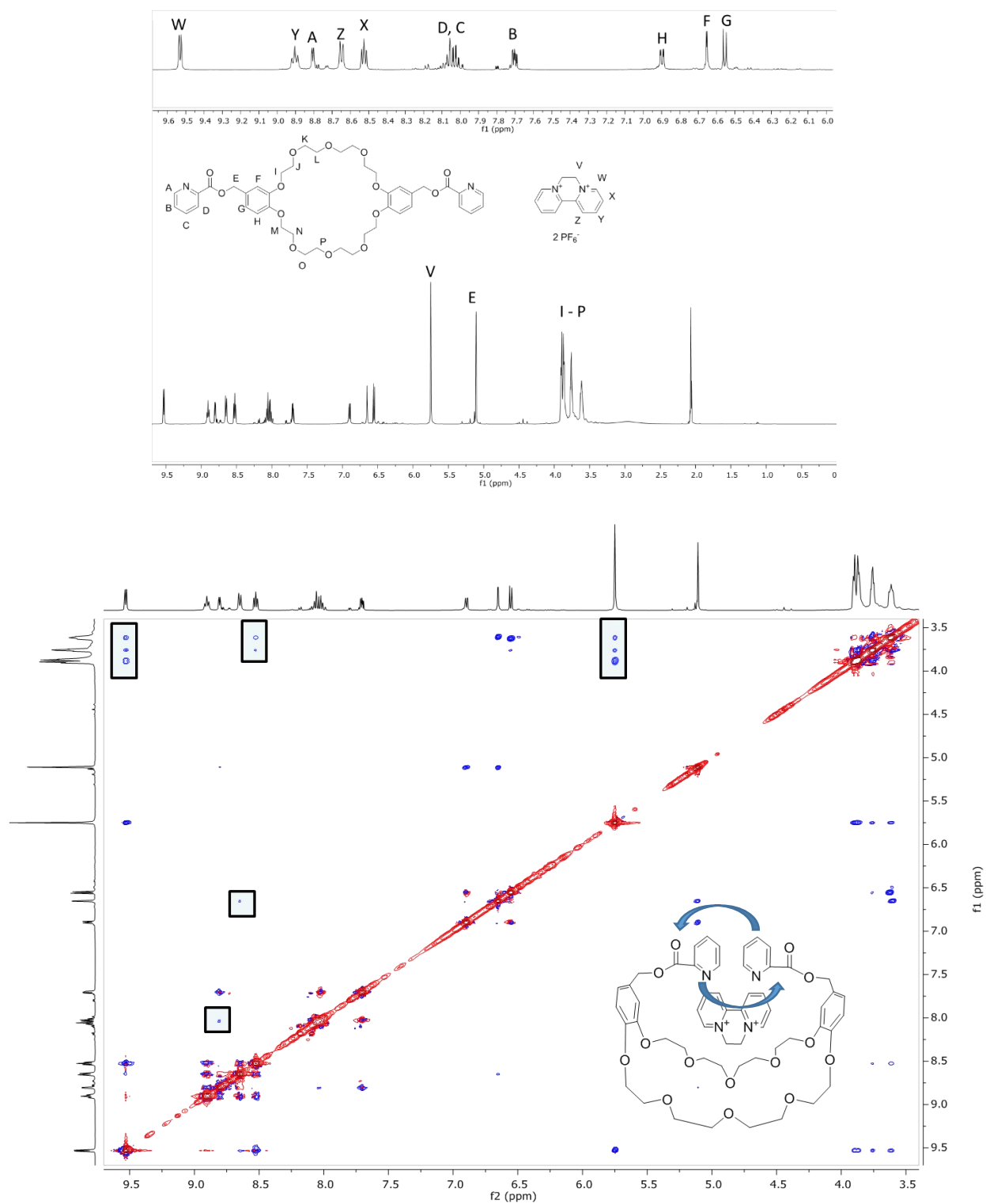


Figure 2.4. Top: 500 MHz ¹H NMR spectrum of a 1:1 mixture (15 mM) of **3a** and diquat PF₆ taken in acetone-*d*₆. Bottom: 2D NOESY of a 1:1 mixture of **3a** and diquat PF₆ taken in acetone-*d*₆; peaks of interest are highlighted and a possible 3D structure is shown.

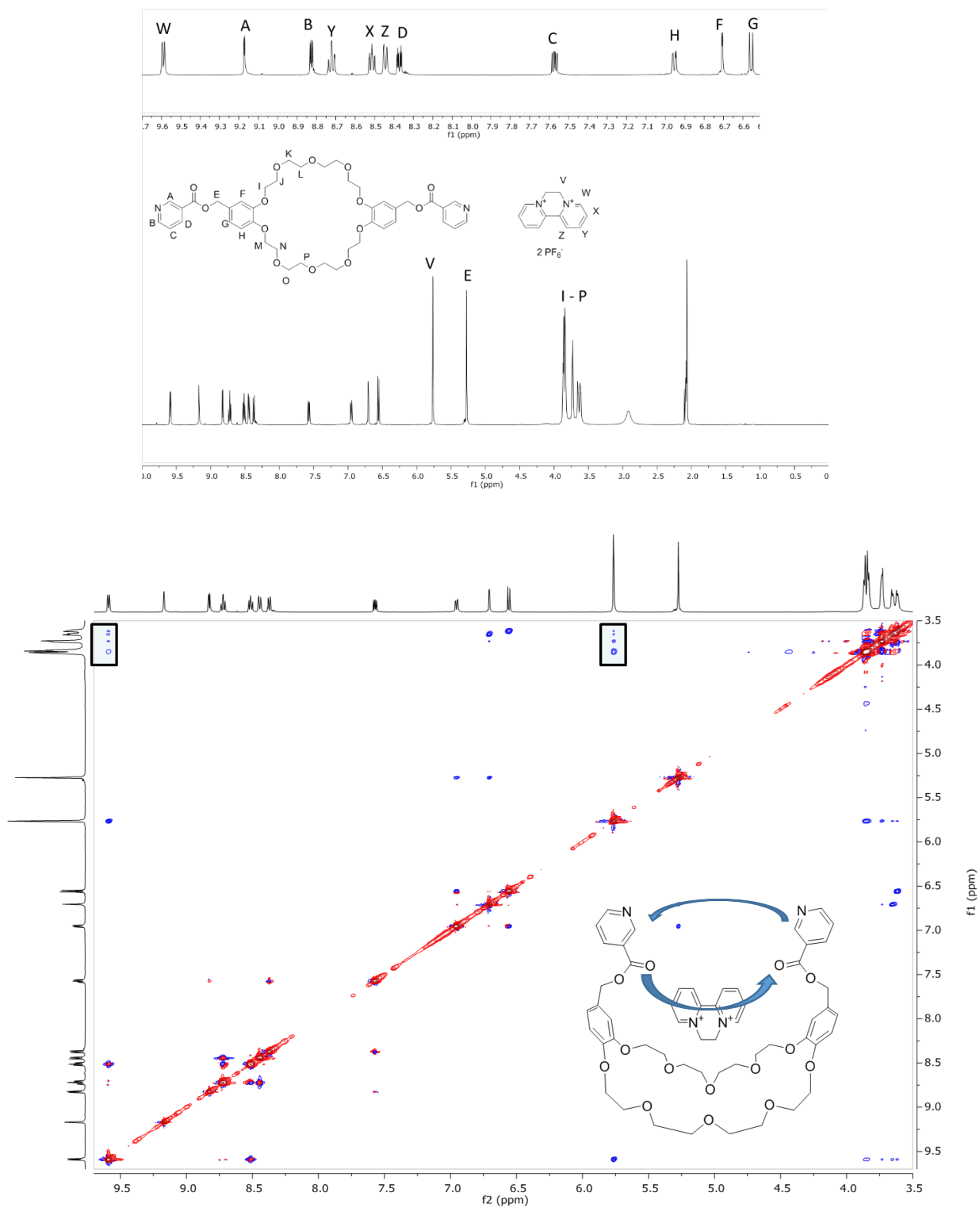


Figure 2.5. Top: 500 MHz ¹H NMR spectrum of a 1:1 mixture (15 mM) of **3b** and diquat PF₆ taken in acetone-*d*₆. Bottom: 2D NOESY of a 1:1 mixture of **3b** and diquat PF₆ taken in acetone-*d*₆; peaks of interest are highlighted and a possible 3D structure is shown.

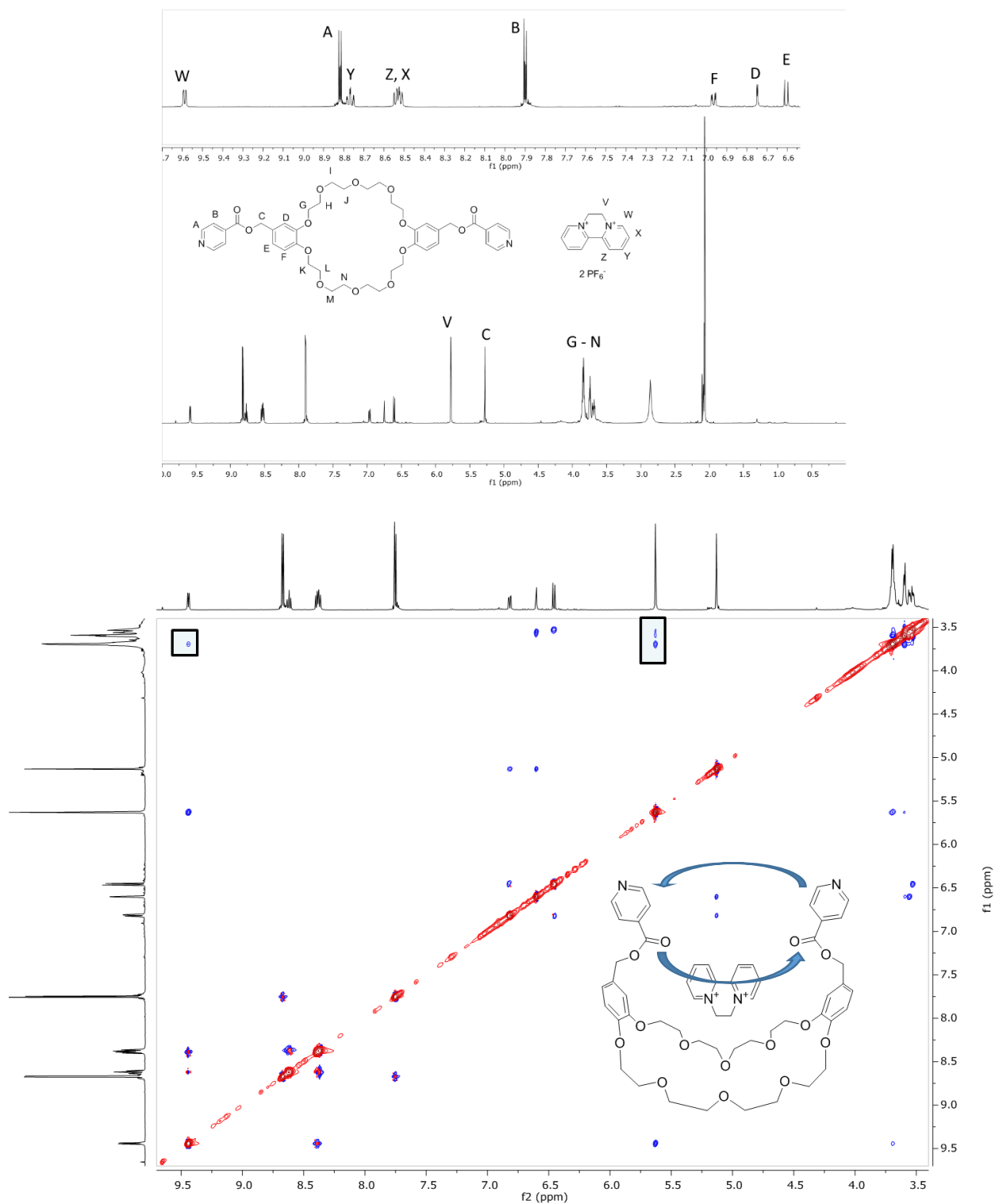


Figure 2.5. Top: 500 MHz ^1H NMR of a 1:1 mixture (15 mM) of **3c** and diquat PF_6^- taken in acetone- d_6 . Bottom: 2D NOESY of a 1:1 mixture of **3c** and diquat PF_6^- taken in acetone- d_6 , peaks of interest are highlighted and a possible 3D structure is shown.

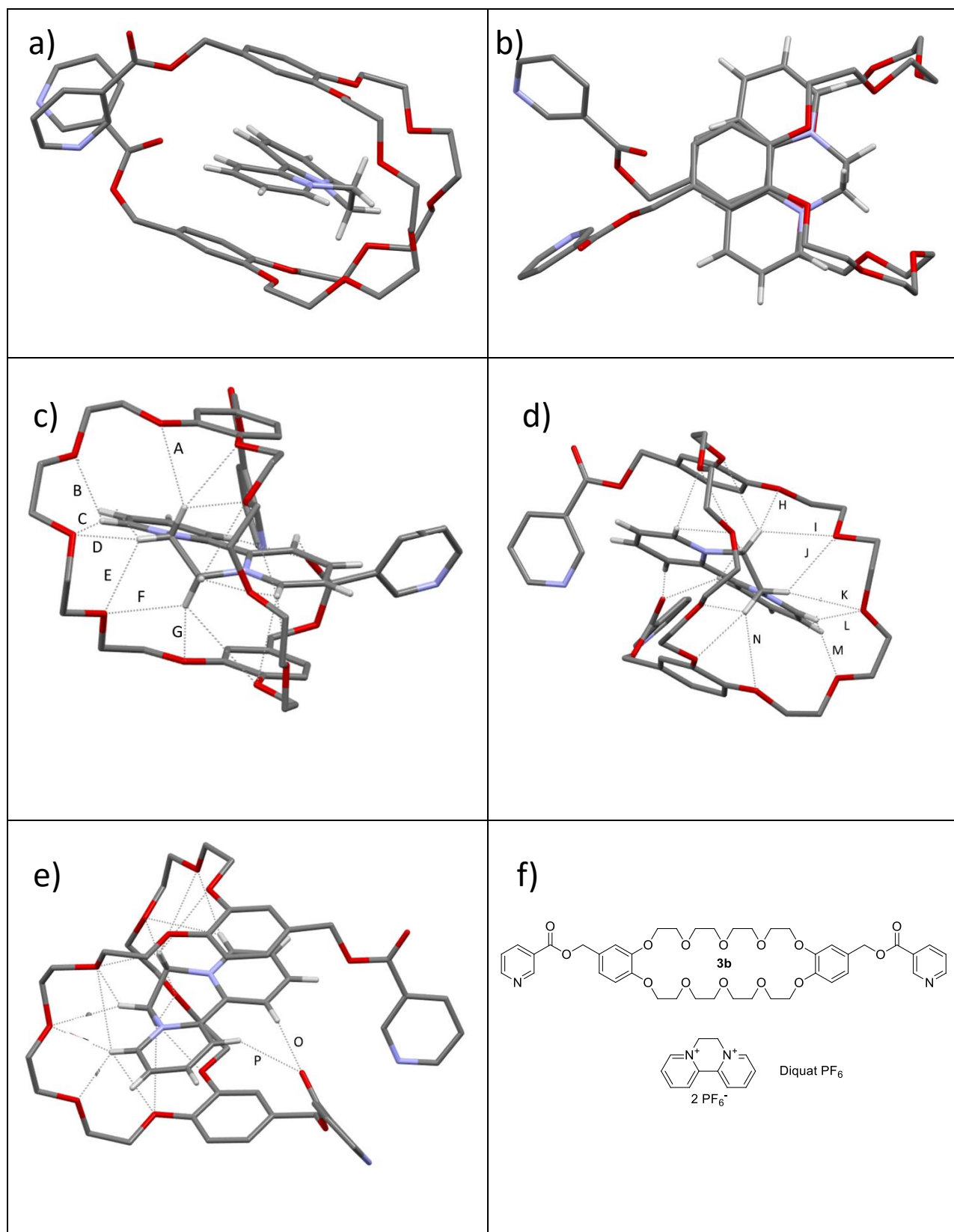


Figure 2.7. X-ray crystallography of $3b \cdot DQ PF_6$ grown by slow vapor diffusion of ether into acetone (crystal structure contains a reasonable amount of disorder, counter ions, solvent,

artifacts, and non-guest hydrogens have been removed for clarity): a) side view; b) top down view; c) hydrogen bonding to the *m*-ethyleneoxy chain; d) hydrogen bonding to the *p*-ethyleneoxy chain; e) hydrogen bonding at the ester; f) structures **3b** and diquat. Hydrogen-bond parameters: C---O distances (Å), C-H---O distances (Å), C-H ---O angles (deg) A: 3.455, 2.887, 117.29; B: 3.088, 2.405, 128.55; C: 3.605, 2.843, 137.98; D: 3.072, 2.093, 170.35; E: 3.031, 2.541, 110.42; F: 3.117, 2.458, 123.64; G: 3.320, 2.451, 146.20; H: 3.340, 2.447, 149.74; I: 3.421, 2.739, 126.35; J: 3.278, 2.808, 109.76; K: 3.619, 2.722, 150.96; L: 3.281, 2.399, 154.19; M: 2.954, 2.230, 132.31; N: 3.679, 3.170, 113.52; O: 3.445, 2.470, 173.75; P: 3.265, 2.470, 141.24. X-ray crystallography was performed and solved by Dr. Carla Slebodnick.

Complexes of **3a–c** with diquat, all contain roughly the same NOESY coupling, no interaction between the hydrogens of the substituted pyridine ring and those of the diquat cation and notable coupling between protons V and W of diquat with ethyleneoxy signals of the host. These results give support to the conclusion that diquat is likely sitting in a cupped pocket formed by the crown (similar to other taco structures observed for dibenzo-30-crown-10 systems^{2,10}). As to how the pyridyl groups are orientated in space, it is suspected that in the complex of **3a** • diquat, the pyridyl rings are sitting over one another as indicated by arrows in **Figure 2.4**, while in the complexes of **3b** and **3c**, the arms sit over one another, but the pyridyl units point outwards, **Figure 2.5** and **Figure 2.6**. In **Figure 2.4** a NOESY correlation is present between two protons that are on opposite sides of the pyridyl ring, protons A and D; the only logical conclusion for this is that the two pyridyl rings of **3a** are sitting on top of one another. Similar coupling was not observed in **3b** or **3c** with diquat. The lack of a distinguishable coupling between the pyridyl rings of **3b** and **3c** give rise to the speculation that π -stacking of the pyridyl groups is not occurring in either complex with diquat, as is likely the case with **3a** and has been observed in complexes of **4a**.^{6,9}

In the X-ray crystallographic structure of **3b** • diquat, **Figure 2.7**, most of the hydrogen bonding is occurring between the ethyleneoxy units and diquat, while the pyridyl nitrogen atoms sit too far away to play an active role. Additionally, it can be seen that only one carbonyl oxygen

is precipitating in hydrogen bonding. This gives rise to the conclusion that in the case of **3b** complexing with diquat the attached pyridyl arms are offering little benefit in the way of binding. As NOESY spectra are very similar among all three complexes, with the exception of **3a** • diquat, suggesting the pyridyl rings are stacked, it is suspected that all three complexes adopt an arrangement similar to that observed in **Figure 2.7**. Due to the association constant of **3a** with diquat being nearly an order of magnitude higher than **3b** or **3c**, it is concluded that for diquat, **3a** is the only compound with a significant benefit from the attached pyridyl groups.

Conclusion

Three pseudocryptands were successfully synthesized. The placement of the 2-pyridyl carboxylate group in the crown diol diester provided the best overall binding constant, **3a**•diquat in this series. However, all of these hosts (**3a–3c**) were worse in terms of the binding strength than the parent crown diol, $K_a = 5.0 \times 10^4 \text{ M}^{-1}$ with diquat and $1.1 \times 10^3 \text{ M}^{-1}$ with paraquat (acetone, 25 °C).¹⁰ Considering the association constants observed with **3a**•diquat ($4.06 \times 10^4 \text{ M}^{-1}$) and **3b**•paraquat (785 M^{-1}), the addition of the pyridyl ring resulted in a less receptive host pocket. Considering that the **3a**•diquat association constant was an order of magnitude higher than those of **3b** and **3c**, this was the only diquat or paraquat complex to show a NOESY correlation that suggested a pseudocryptand. The formation of a pseudocryptand is thus beneficial in terms of association constants.

EXPERIMENTAL

General Information: ^1H -NMR spectra were obtained on JEOL ECLIPSE-500, BRUKER-500, and AGILENT-NMR-vnmrs400 spectrometers. ^{13}C -NMR spectra were collected at 125 MHz and 101 MHz on these instruments, respectively. HR-MS were obtained using an Agilent LC-ESI-TOF system. Reagents were purchased and used as received without further purification, except for DCM, which was dried by distillation over CaH. Compound **1** was made in accordance with a literature procedure; similar yields were achieved.² ITC results were obtained using an instrument from Microcal, Inc. X-ray crystallography was performed at Virginia Tech and solved by Carla Slebodnick. Crystal structure of **3b** • DQ PF₆ was grown by slow vapor diffusion of ether into an acetone equimolar solution. X-ray crystallography tables can be found in the appendix of this dissertation.

Example of ITC Titration Method: Two different ITC titration methods were used for this work; in each the first data point was ignored to avoid error. Low gain titrations with paraquat PF₆ employed 25 aliquots using host in the cell (5 mM) and guest in the syringe (75 mM). High gain titrations with diquat PF₆ employed 100 aliquots using host in the cell (0.99 mM) and guest in the syringe (15 mM). For both methods acetone was used as the solvent and experiments were conducted at 25 °C. The following is a detailed description of titration of diquat PF₆ with **1a**; the other systems were done similarly with slightly different concentrations. Host **3a** was loaded into the cell of the instrument at a concentration of 0.994 mM, while a 250 μL ITC syringe was loaded with diquat PF₆ at a concentration of 15.00 mM. The instrument was set to high gain (high sensitivity). The titration was achieved through 100 injections of 2.50 μL every 180 s; a primary filter period of 2 s and a secondary filter period of 4 s were applied (filter period switch time was set to 120 s). A background titration used exactly the same titration conditions with the

exception that the solution of **3a** in the cell was replaced with acetone. The heats for the dilution experiment were subtracted from the heats for the titration of diquat PF₆ with **3a**. Analysis of the data was carried out using software provided by the manufacturer. A “One Set of Sites” model was used; stoichiometries other than 1:1 provided unsatisfactory fits and the “One Set of Sites” model was justified by an NMR-based Job Plot.

¹H NMR Job Plot Titration: A diquat solution was made at 0.968 mM and **3a** at 0.987 mM, both in deuterated acetone. NMR solutions were made at ratios of host/guest: 9.0/1.0, 7.0/3.0, 6.0/4.0, 5.0/5.0, 4.0/6.0, 3.0/7.0, and 1.0/9.0. Aromatic hydrogen H₁, **Figure 2.2**, of the crown was observed for the titration due to its large chemical shift.

General procedure 1, acid chlorides. Picolinoyl chloride (2a): Thionyl chloride (18.0 mL, 247 mmol) was added to a flask containing picolinic acid (4.35 g, 35.4 mmol) with magnetic stirring under nitrogen. The reaction mixture was allowed to stir at room temperature for 48 h, followed by removal of the excess thionyl chloride using evaporation to provide the desired product, 5.00 g (100%). No further purification was performed; the product was used directly.

General procedure 2. *Cis*-(4,4′)-Diyl((methylene)picolinate)-dibenzo-30-crown-10 (3a). Picolinoyl chloride (3.21 g, 22.7 mmol) was added to a flask with magnetic stirring, freshly distilled DCM (125 mL), and pyridine (2.9 mL, 36 mmol). The mixture was stirred briefly and **1** (0.38 g, 0.64 mmol) was added and the flask was placed under nitrogen to stir at room temperature for 48 h. Solvent was removed by rotary evaporation and the residue was dissolved in chloroform (50 mL). The mixture was washed with water (10 mL x 1), 2% NaHCO₃ (10 mL x 3), water (10 mL x 1), 1 M HCl (until the aqueous wash was clear) and water again until pH 7. The organic layer was dried over sodium sulfate and solvent was removed by rotary evaporation. The crude material was purified using column chromatography: neutral alumina eluting with

96:4 chloroform to methanol to give the desired product, white solid 0.45 g (87%), mp 97.1 - 99.2 °C. ¹H NMR (500 MHz, CDCl₃) δ 8.76 (m, 2H), 8.12 (m, 2H), 7.82 (m, 2H), 7.46 (m, 2H), 7.06–7.00 (m, 4H), 6.85 (d, *J* = 8 Hz, 2H), 5.36 (s, 4H), 4.14 (m, 8H), 3.89–3.82 (m, 8H), 3.78–3.72 (m, 8H), 3.69–3.64 (m, 9H). ¹³C NMR (101 MHz, CDCl₃) δ 165.07 (s), 149.91 (s), 149.17 (s), 148.90 (s), 148.08 (s), 136.97 (s), 128.73 (s), 126.90 (s), 125.26 (s), 122.36 (s), 115.10 (s), 113.97 (s), 70.90 (s), 70.70 (s), 69.69 (s), 69.15 (s), 67.52 (s) (21 peaks expected and 17 peaks found due to ethyleneoxy peak overlap). HR-MS: calc for C₄₂H₅₀N₂O₁₄ [M+NH₄]⁺: m/z 824.3600; found: m/z 824.3567 error (−4.1 ppm)

Nicotinoyl Chloride (2b). General procedure 1 was used to produce a solid (3.68 g, 100%) using thionyl chloride (15.0 mL, 206 mmol) and nicotinic acid (3.20 g, 26.0 mmol)

Isonicotinoyl Chloride (2c). General procedure 1 was used to produce a solid (3.69 g, 100%) using: thionyl chloride (10 mL, 138 mmol) and isonicotinic acid (3.21 g, 26.1 mmol)

***Cis*-(4,4′)-Diyl((methylene)nicotinate)-dibenzo-30-crown-10 (3b).** General procedure 2 was used with nicotinoyl chloride (3.00 g, 21.2 mmol), DCM (150 mL), pyridine (5.0 mL, 62 mmol), and **1** (0.51655 g, 0.86574 mmol) to produce a white crystalline solid (0.6655 g, 95%), mp 62.8 - 67.1 °C. ¹H NMR (500 MHz, CDCl₃) δ 9.24 (m, 2H), 8.77 (m, 2H), 8.30 (m, 2H), 7.38 (m, 2H), 6.98 (m, 4H), 6.87 (d, *J* = 8 Hz, 2H), 5.29 (s, 4H), 4.19–4.12 (m, 8H), 3.90–3.84 (m, 8H), 3.77 (m, 8H), 3.68 (m, 9H). ¹³C NMR (126 MHz, CDCl₃) δ 165.17 (s), 153.47 (s), 150.99 (s), 149.26 (s), 148.97 (s), 137.17 (s), 128.54 (s), 126.12 (s), 123.31 (s), 122.03 (s), 114.84 (s), 113.96 (s), 70.92 (s), 70.72 (s), 69.71 (s), 69.68 (s), 69.21 (s), 69.12 (s), 67.14 (s) (21 peaks expected and 19 peaks found due to ethyleneoxy peak overlap). HR-MS: calc for C₄₂H₅₀N₂O₁₄ [M + NH₄]⁺: m/z 824.3600; found: m/z 824.3584 error (−2.0 ppm)

Cis-(4,4')-Diyl((methylene)isonicotinate)-dibenzo-30-crown-10 (3c). General procedure 2 using: isonicotinoyl chloride (3.69 g, 26.1 mmol) DCM (125 mL), pyridine (2.8 mL, 34.8 mmol), and **1** (0.34 g, 0.570 mmol) produced a white solid (0.42 g, 91%), mp: 85.8–88.2 °C. ¹H NMR (500 MHz, CDCl₃) δ 8.76 (m, 4H), 7.84 (m, 4H), 7.00–6.95 (m, 4H), 6.86 (d, *J* = 8 Hz, 2H), 5.28 (s, 4H), 4.15 (m, 9H), 3.90–3.85 (m, 8H), 3.78 – 3.74 (m, 8H), 3.67 (m, 8H). ¹³C NMR (126 MHz, CDCl₃) δ 165.00 (s), 150.60 (s), 149.34 (s), 148.97 (s), 137.37 (s), 128.28 (s), 122.91 (s), 122.13 (s), 114.94 (s), 113.96 (s), 70.91 (s), 70.70 (s), 69.71 (s), 69.66 (s), 69.22 (s), 69.10 (s), 67.51 (s). (19 peaks expected and 17 peaks found due to ethyleneoxy peak overlap). HR–MS: calc for C₄₂H₅₀N₂O₁₄ [M + NH₄]⁺: m/z 824.3600; found: m/z 824.3615 error (1.7 ppm)

REFERENCES

- (1) Gibson, H. W.; Wang, H.; Bonrad, K.; Jones, J. W.; Slebodnick, C.; Zakharov, L. N.; Rheingold, A. L.; Habenicht, B.; Lobue, P.; Ratliff, A. E. *Org. Biomol. Chem.* **2005**, *3*, 2114-2121.
- (2) Pederson, A. M. P.; Ward, E. M.; Schoonover, D. V.; Slebodnick, C.; Gibson, H. W. *J. Org. Chem.* **2008**, *73*, 9094-9101.
- (3) Jones, J. W.; Zakharov, L. N.; Rheingold, A. L.; Gibson, H. W. *J. Amer. Chem. Soc.* **2002**, *124*, 13378-13379.
- (4) Bryant, W. S.; Jones, J. W.; Mason, P. E.; Guzei, I.; Rheingold, A. L.; Fronczek, F. R.; Nagvekar, D. S.; Gibson, H. W. *Org. Lett.* **1999**, *1*, 1001-1004.
- (5) Huang, F.; Nagvekar, D. S.; Zhou, X.; Gibson, H. W. *Macromolecules* **2007**, *40*, 3561-3567.
- (6) Niu, Z.; Slebodnick, C.; Schoonover, D.; Azurmendi, H.; Harich, K.; Gibson, H. W. *Org. Lett.* **2011**, *13*, 3992-3995.
- (7) Nabeshima, T. *Bull. Chem. Soc. Jpn.* **2010**, *83*, 969-991.
- (8) Huang, F.; Zakharov, L. N.; Rheingold, A. L.; Jones, J. W.; Gibson, H. W. *Chem. Commun.* **2003**, 2122-2123.
- (9) Niu, Z.; Price Jr, T. L.; Slebodnick, C.; Gibson, H. W. *Tetrahedron Lett.* **2016**, *57*, 60-63.
- (10) He, C.; Shi, Z.; Zhou, Q.; Li, S.; Li, N.; Huang, F. *J. Org. Chem.* **2008**, *73*, 5872-5880.
- (11) Piguet, C. *Dalton Trans.* **2011**, *40*, 8059-8071.
- (12) Gilli, P.; Ferretti, V.; Gilli, G.; Borea, P. A. *J. Phys. Chem.* **1994**, *98*, 1515-1518.
- (13) Pan, A.; Biswas, T.; Rakshit, A. K.; Moulik, S. P. *J. Phys. Chem. B* **2015**, *119*, 15876-15884.

- (14) Lambert, F. L.; Leff, H. S. *J. Chem. Educ* **2009**, 86, 94.
- (15) Starikov, E. B.; Nordén, B. *Chem. Phys. Lett.* **2012**, 538, 118-120.

Chapter 3

Cryptand Templatation

Introduction

Crown ethers are well known and have been greatly studied for their role as hosts in supramolecular chemistry. Although these hosts are capable of producing a wealth of supramolecular chemistries, the fact remains that their association constants with most guests is less than desirable and in many cases hinders the usage of the systems in certain supramolecular architectures. The typical association constant for 24-crown-8 to 32-crown-10 macrocycles paired with a variety of guests, such as dialkyl ammonium and paraquat, lie in the range of approximately $10^1 - 10^3$.^{1,2} The exceptions to this are the highly evolved pseudocryptand derivatives of bis(*m*-phenylene)-32crown-10, which have achieved association constants as high as 5×10^6 with paraquat.³ High association constants are important, because the production of polypseudorotaxanes suffer when an inadequate association constant is employed. As an example, the degree of polymerization for polypseudorotaxanes can be directly estimated from the association constant of the host and guest. Thus lower association constants require higher concentrations to achieve polymer formation. To illustrate this, consider *cis*(4,4')-di(hydroxymethylbenzo)-30-crown-10 with paraquat; the system has an association constant of $1.1 \times 10^3 \text{ M}^{-1}$ in acetone at 25 °C. Using the equation $DP = (K_a[H]_o)^{1/2}$ to estimate the degree of polymerization, it can be seen that if this system was used to produce polypseudorotaxanes at a 1 M concentration, only a DP of 33 would be achievable. Alternatively, the association constant of the cryptand **6** with paraquat has an association constant of $5.0 \times 10^6 \text{ M}^{-1}$ in acetone at room temperature. Using the previous equation $DP = (K_a[H]_o)^{1/2}$ with 5.0×10^6 , it can be seen that a

DP of 2,236 would be obtainable at a 1 M concentration with this system. Clearly high association constants are advantageous.

Since the widespread adoption of crown ethers such as dibenzo-30-crown-10 and bis(*m*-phenylene)-32crown-10 for paraquat and diquat complexes, research geared towards the production of a third arm of the macrocycles has significantly increased binding. Macrocycles containing a bridge are generally referred to as cryptands. **Figure 3.1** shows several cryptands that have significantly increased binding over their crown ether counterparts; **Table 3.1** gives the association constants of those compounds with dimethyl paraquat PF₆ (**7**).

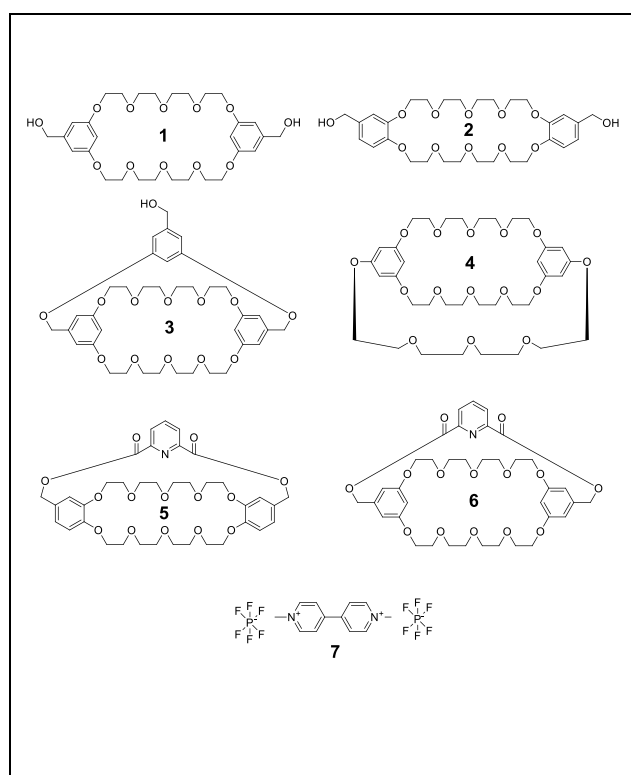


Table 3.1. Association constant summary of hosts **1** – **6** with **7**. Values were obtained from literature sources for **1•7**,¹ **2•7**,² **3•7**,⁴ **4•7**,⁵ **5•7**⁶ and **6•7**.⁴ Association constants obtained in acetone at room temperature.

Complex	K _a (M ⁻¹)
1•7	5.7 x 10 ²
2•7	1.1 x 10 ³
3•7	6.4 x 10 ³
4•7	6.1 x 10 ⁴
5•7	1.0 x 10 ⁵
6•7	5.0 x 10 ⁶

Figure 3.1. Sample host progression to cryptands.

From **Table 3.1** it can be seen that cryptands, when correctly designed, offer superior association constants to their crown ether counterparts. Pyridyl cryptands such as **5** and **6** are

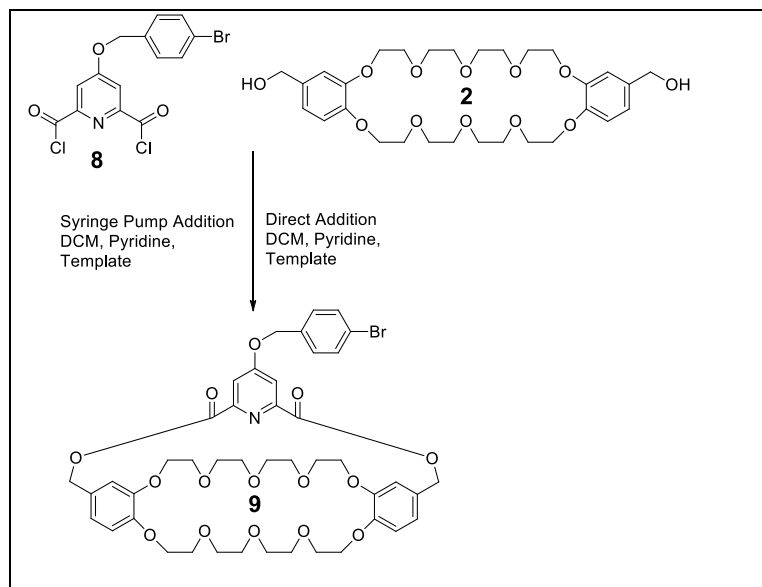
particularly noteworthy, affording association constants in the range of 10^5 to 10^6 M^{-1} ; their use, however, has been greatly hindered due to synthetic difficulties. The syntheses of **5** and **6** require cyclization reactions to form crown ethers first then second cyclization reactions to form the cryptands. The results of multiple cyclization reactions are lengthy reaction times, large volumes of solvent and low yields. To increase the deployment of **5**, **6** and similar derivatives, work was conducted to optimize the syntheses of these compounds, such that reaction times could be lowered and yields increased.

Results and Discussion

During routine work on the production of pyridyl cryptands **5**, general pseudo-high dilution conditions worked out by Pederson et al. were employed.⁶ As the procedure employed large volumes of the solvent DCM a shift was made to dry it via activated acidic alumina rather than distillation over CaH. Upon changing the drying method, significant yield increases in cryptand cyclization reactions were observed. It was determined that these yield increases were due to acidic alumina leaching into DCM and reacting with pyridine to form a pyridinium cation. The pyridinium cation was then suspected to act as a template for the cyclization reaction. This led to the examination of several pyridinium cations as potential templates: acidic alumina / pyridine, pyridinium acetate, pyridinium *p*-toluenesulfonate, pyridinium chloride, pyridinium PF₆, paraquat PF₆ and pyridinium TFSI.

The first templation experiments were carried out with acidic alumina / pyridine. At the time of this work, an aryl bromide derivative of **5** was sought after for its potential in coupling reactions; for this reason, initial optimizations focused on the synthesis of **9**, while later

optimizations focused on the synthesis of **5**. After the development of a procedure for the templation of **5**, it was tested on two other pyridyl cryptands, bis(*m*-phenylene)-32-crown-10 and dibenzo-24-crown-8. Emphasis was placed on the synthesis of **5**, because a high yield templated procedure already existed for its precursor, **2**.⁶ **Scheme 3.1** shows the synthesis of **9** with two different synthetic methodologies: syringe pump addition and direct addition. Syringe pump additions adhered to the procedure of Pederson et al., except in that a template was added to the reaction; both **8** and **2** were dissolved in separate solutions of DCM and loaded into syringes which were pumped into the reaction flask charged with DCM, pyridine and a template under nitrogen. For direct additions the reaction flask was charged with DCM, pyridine and **2**, mixed for 15 min and **8** was added all at once.



Scheme 3.1. Synthesis of **9**.

Table 3.2 provides the experimental results for **9** with templation. Experimentation focused heavily upon direct addition methods, given that syringe pump additions are time consuming and effective templation should negate the need for pseudo-high dilution conditions.

By simply filtering DCM through a column of acidic alumina and carrying out syringe pump addition, a yield of 78% was achievable.

Table 3.2 indicates yields of 30–40 % via direct addition using acidic alumina / pyridine, 4,4'-bipyridinium PF₆ or pyridinium *p*-toluenesulfonate. Poor results for pyridinium chloride reflected its poor solubility in DCM. Pyridinium *p*-toluenesulfonate was troublesome to remove and the acidic alumina / pyridine mixture seemed to be consuming **8** somehow. Inspection of multiple reaction mixtures employing the acidic alumina / pyridine and 4,4'-bipyridinium PF₆ template revealed large amounts of unreacted **2**; this could be remedied through three consecutive additions of **8**. It was suspected that consumption of **8** was likely due to residual water in the acidic alumina and 4,4'-bipyridinium PF₆. Additionally, it was determined that there was no reason to use 4,4'-bipyridinium PF₆ over pyridinium salt given that no significant yield increases were observed. 4,4'-Bipyridinium PF₆ in the presence of pyridine would yield pyridinium PF₆ as seen in **Figure 3.2**. Further inspection also reveals that the yield of the acidic alumina/pyridine system was inversely related to the amount of base added; typically, the more pyridine added to the reaction of **9**, the lower the yield.

Table 3.2. Initial templation experiments for the synthesis of **9**.

exp..	Addition	host (mmol)	guest (mmol)	Time (h)	DCM (L)	dried by	Base / vol (mL)	Additive	Yield
1	1.0 mL/h	0.71548	0.71722	97	2.7	acidic alumina	Pyridine / 2.4	N/A	78%
2	1.5 mL/h	1.211	1.214	240	2.7	acidic alumina	Pyridine / 3	N/A	46%
3	Direct 1.5 mL/h	0.5993	0.5997	48	0.700	acidic alumina	Pyridine/ 5	N/A	31%
4	1.5 mL/h	0.9003	0.9043	162.5	2.7	CaH	Pyridine / 15	N/A	20%
5	Direct	0.5868	1.184	41	0.600	acidic alumina	Pyridine / 5	N/A	30%
6	Direct	1.084	1.184	65	0.700	acidic alumina	Pyridine 5	acidic alumina 1 g	36%
7	Direct	0.6505	0.6532	62	0.300	CaH	Pyridine / 10.5	acetic acid 3.5 mL	0%
8	Direct	0.3989	0.4033	52	0.700	CaH	Pyridine / 5	neutral alumina 1g	0%
9*	Direct	0.4291	0.4437	67	0.600	CaH	Pyridine / 5	pyridinium p-toluenesulfonate 1.34 g	30%
10	Direct	0.3127	0.3187	242	0.700	CaH	Pyridine / 5	pyridinium chloride 1g	11%
11	Direct	0.4562	0.46205	116	0.750	CaH	Pyridine / 5	pyridium H ⁺ PF ₆	1%
12	Direct	0.4177	0.41943	70	0.750	CaH	Pyridine / 3	paraquat H ⁺ PF ₆	31%
13	Direct	0.4324	0.4388	24	0.750	CaH	4,4'-Bipyridyl / 1.4 g	paraquat H ⁺ PF ₆	23%
14	Direct	0.4086	0.41434	48	0.750	CaH	4,4'-Bipyridyl / 1.8 g	acidic alumina 1 g	1%
15	Direct	0.3915	0.428	60	0.200	CaH	Pyridine / 5	acidic alumina 1 g	23%
16	Direct	0.4049	0.4128	54	1.75	CaH	Pyridine / 10	acidic alumina 1 g	1%
17	Direct	0.5385	0.5416	18	0.700	CaH	Pyridine / 3.5	paraquat H ⁺ PF ₆	24%
18**	Direct	0.6516	1.9018	48	0.700	CaH	Pyridine / 4	paraquat H ⁺ PF ₆	85%

~Notes~
 * product would not decomplex from guest. Yield has been adjusted for by subtracting out a 1:1 complex of guest
 ** 3 additions of the acid chloride were made 12 h apart

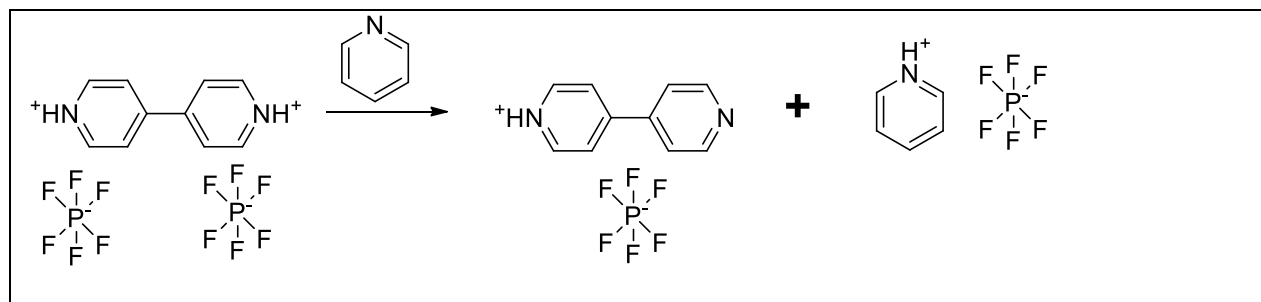
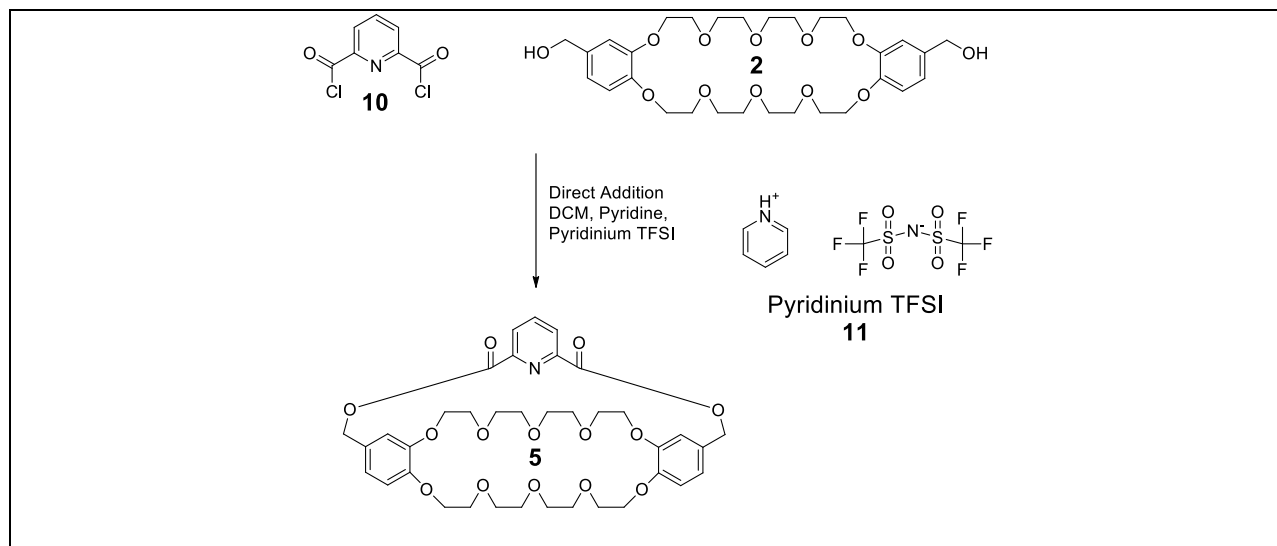


Figure 3.2. Paraquat H⁺PF₆ conversion to pyridinium PF₆ in the presence of pyridine.

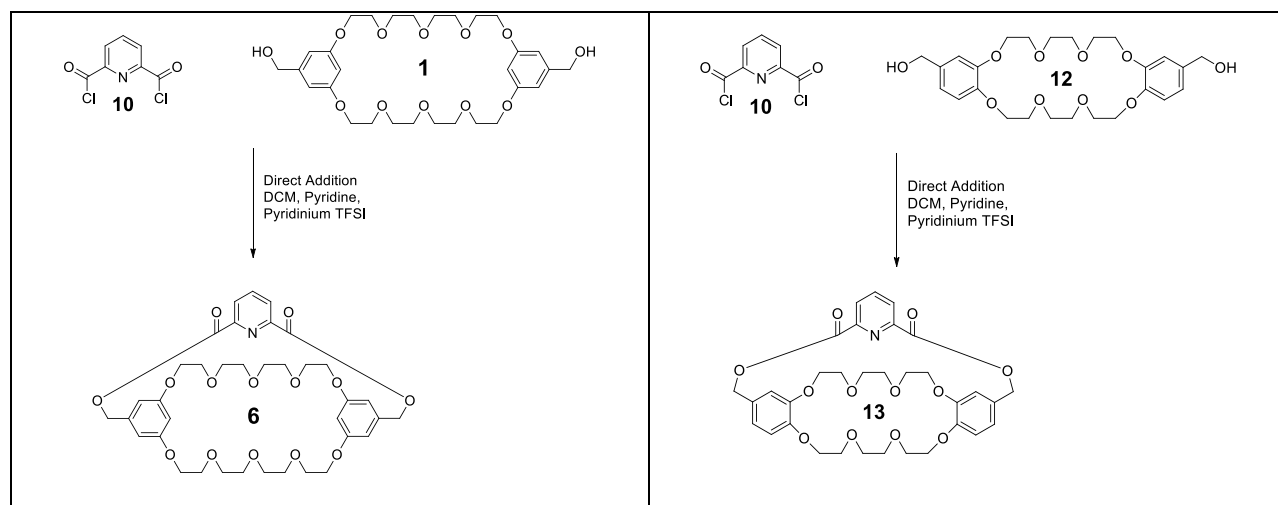
Although the acidic alumina/pyridine system could be made to work through multiple additions of **8**, optimizations would need to be made with every new purchase of acidic alumina, due to inconsistencies found between products. Thus the acidic alumina system was abandoned. Secondly, there was no reason to use 4,4'-bipyridinium PF₆ over a pyridinium salt. This led to the conclusion that a pyridinium salt should be investigated; it should be soluble in DCM and hydrophobic to prevent residual water from wrecking the reaction.

These guidelines led to the adoption of pyridinium TFSI, **11**, as a template; the salt is highly soluble in DCM, reasonably hydrophobic and can be easily dried via melting under vacuum. The template was optimized for the synthesis of **5**, **Scheme 3.2**, and emphasis was once again placed on a direct addition of reagents without the use of a syringe pump.



Scheme 3.2. Synthesis of **5**.

To provide a better understanding of the systems, the association constants of **1**, **2**, **5**, **6**, **12** and **13** were obtained with pyridinium TFSI in DCM at room temperature by ITC (**Table 3.3**).



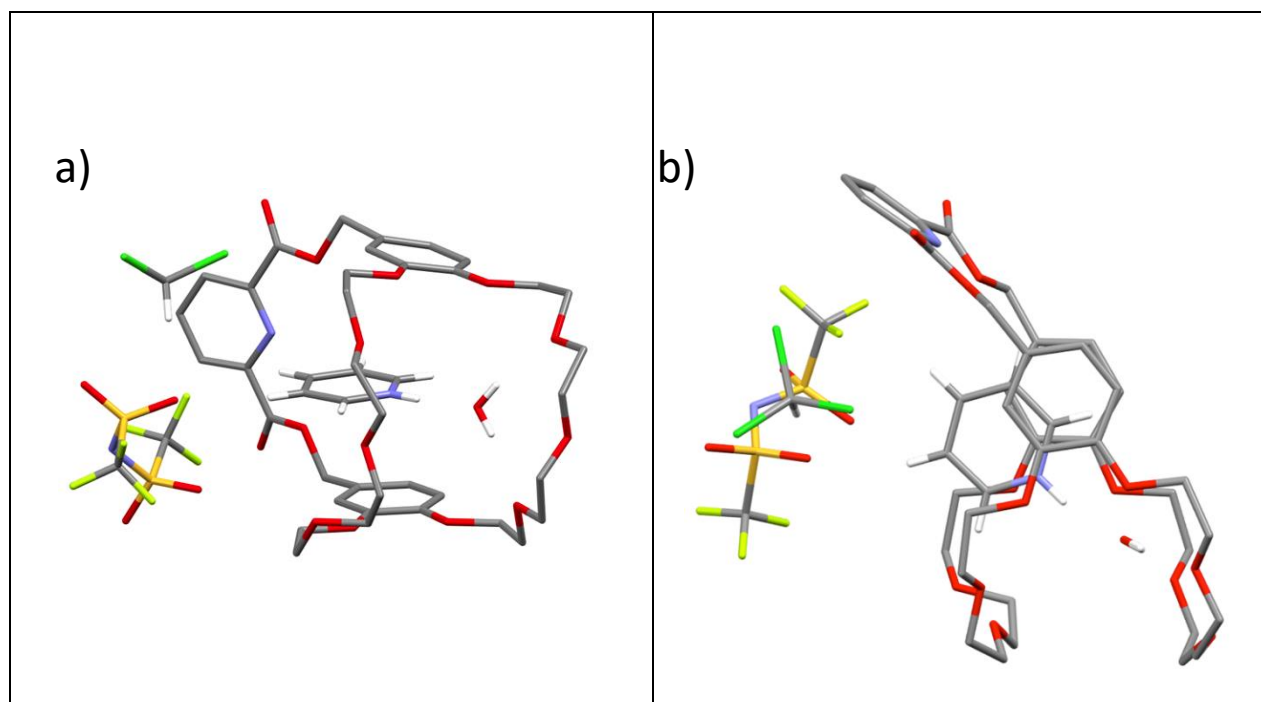
Scheme 3.3. Synthesis of **6** and **13**.

Table 3.3. Association constants of hosts **1**, **2**, **5**, **6**, **12** and **13** with guest **11** in DCM at 25 °C; error is indicated in parenthesis.

Complex	K_a (M⁻¹)	ΔG (kcal/mol)	ΔH (kcal/mol)	ΔS (cal/mol K)
1 • 11 crown	5.31 x 10 ² (±0.69 x 10 ²)	-3.72 (±0.48)	-4.14 (±0.24)	-1.42 (±0.20)
6 • 11 cryptand	1.37 x 10 ⁴ (±0.08 x 10 ⁴)	-5.64 (±0.33)	-11.6 (±0.1)	-20.0 (±1.2)
2 • 11 crown	7.46 x 10 ² (±0.57 x 10 ²)	-3.92 (±0.30)	-7.40 (±0.23)	-11.7 (±1.0)
5 • 11 cryptand	2.34 x 10 ⁴ (±0.11 x 10 ⁴)	-5.96 (±0.28)	-15.1 (±0.1)	-30.7 (±1.5)
12 • 11 crown	1.58 x 10 ³ (±0.21 x 10 ²)	-4.36 (±0.58)	-2.94 (±0.12)	4.78 (±0.67)
13 • 11 cryptand	8.69 x 10 ⁴ (±0.18 x 10 ⁴)	-6.74 (±0.14)	-11.5 (±0.1)	-16.0 (±0.3)

The cryptands (**5**, **6**, **13**) display higher association constants than their crown ether precursors (**1**, **2**, **12**). For **1** vs. **6** and **2** vs. **5** the increase is about 30-fold. For **12** vs. **13** the increase is only 5-fold. Additionally, it should be noted that the association constants of each cryptand (**5**, **6**, **13**) fell in the range of 10^4 , which is quite remarkable considering the association constant of **5** with dimethyl paraquat PF_6 in acetone at room temperature is 1.0×10^5 .⁶

Inspection of the crystal structure of **5** • **11** (**Figure 3.3**) shows hydrogen bondings and the shape of the complex. Water and chloroform have been incorporated into the crystal structure in a ratio of 1:1:1, for water:chloroform:**5**:**11**. The presence of water has been attributed to the usage of non-anhydrous solvents. Both water and chloroform play an active role in terms of intermolecular interactions; water acts as a hydrogen bonding bridge between the pyridinium N-H and ethyleneoxy oxygen atoms and chloroform hydrogen bonds with two of the TFSI oxygens (**Figure 3.3c**). Interestingly, the *p*-ethyleneoxy chain of **5** does not directly participate in hydrogen bonding with **11**.



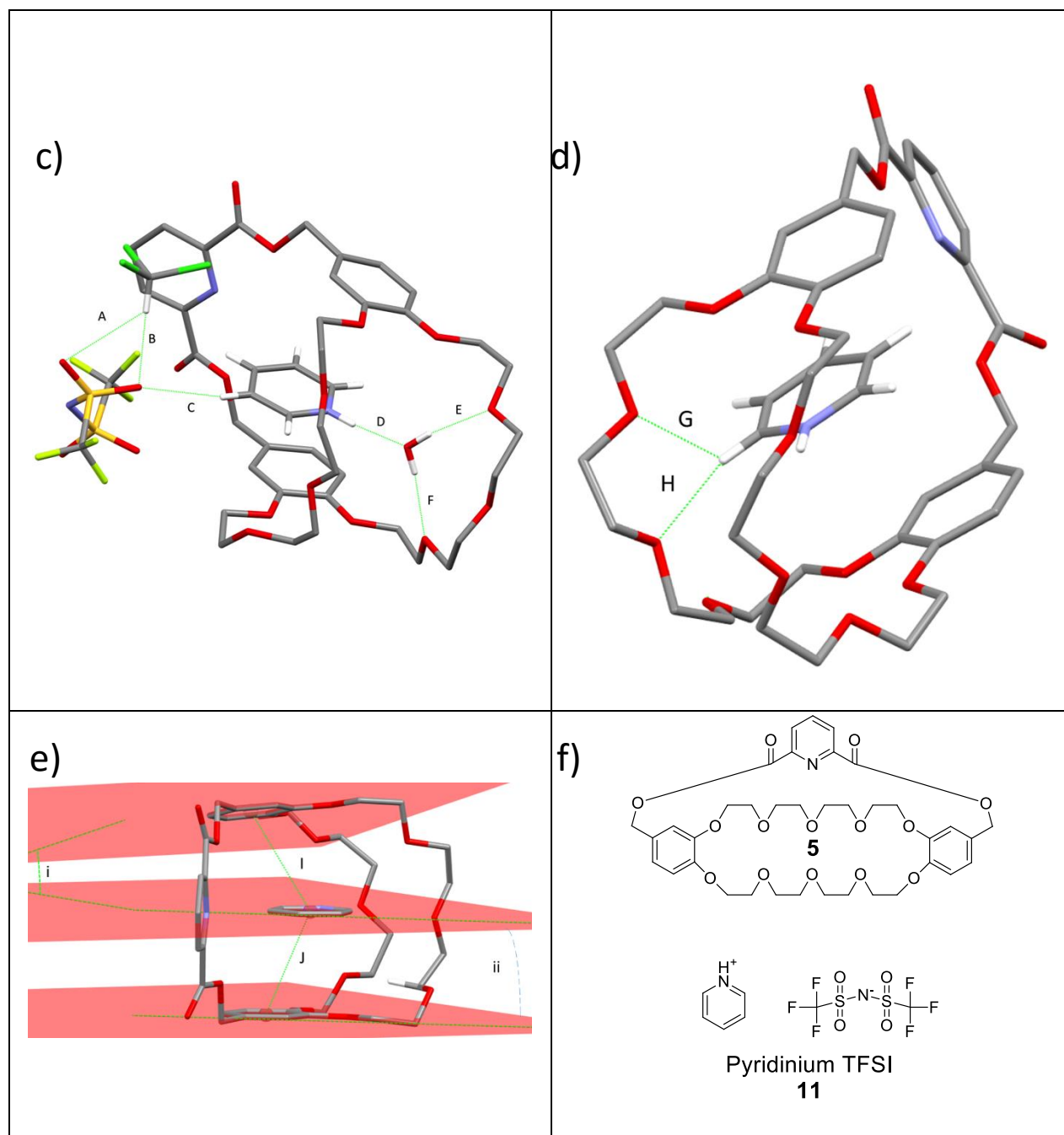


Figure 3.3. Crystal structure of **5** • **11** grown by slow solvent evaporation of an equimolar chloroform solution; hydrogens of **5** have been removed for clarity; a) side view; b) top view; c) hydrogen bonding involving chloroform, water and TFSI; d) hydrogen bonding involving the 3-substituted ethyleneoxy chain (chloroform, water, and TFSI removed for clarity); e) planes of stacked aromatic rings shown with centroids of stacked rings and plane inclinations indicated; f) structures **5** and **11**. Hydrogen-bond parameters: C---O distances (Å), C-H---O distances (Å), C-H---O angles (deg) A: 3.633, 2.969, 124.71; B: 3.282, 2.289, 172.28; C: 3.503, 2.589, 161.71; D: 2.660, 1.793, 167.73; E: 2.901, 2.097, 169.41; F: 2.861, 2.060, 170.62; G: 3.205, 2.663, 116.72; H: 3.315, 2.415, 157.98. Face-to-face π -stacking parameters: centroid-centroid distance

(Å): I: 3.972; J: 3.801; ring plane/ring plane inclinations (deg): i: 12.74°; ii: 0.18°. X-ray crystallography was performed and solved by Dr. Carla Slebodnick.

Although attempts to grow a crystal of **2** complexed with **11** were fruitless, there is literature precedence that when **2** complexes paraquats such as **7**, the host wraps around the paraquat in a taco fashion.⁶ Considering this and the previous ITC, X-ray crystallography, and templation results, it is reasonable to suspect that the pyridinium cation is templating the formation of the cryptand macrocycle by causing **2** to adopt a taco-like geometry (**Figure 3.4**).

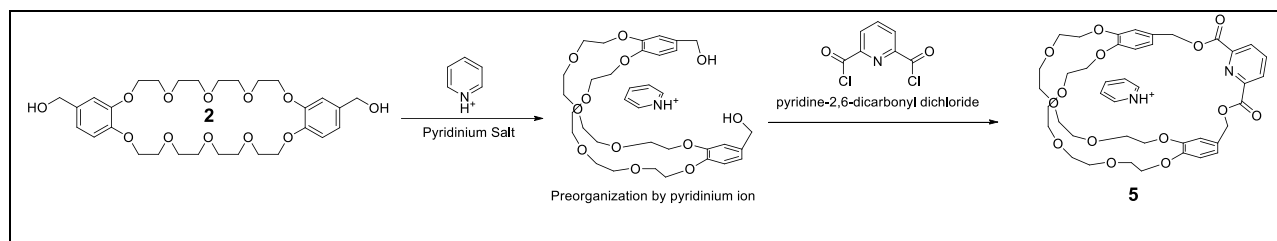


Figure 3.4. Proposed preorganization of diol **2** to a "taco complex" brought about by the pyridinium ion.

With these promising findings, optimization of a templated procedure using **11** for the synthesis of **5** was begun (**Scheme 3.2**). Emphasis was once again placed on directly combining the reagents by varying the following parameters: reagent concentrations, base concentration, pyridinium TFSI concentration, and solvent; results are summarized in **Table 3.4**. All reported yields are isolated yields. Optimizations used the following addition and mixing methodology. DCM, pyridine, **2** and **11** were allowed to mix for 15 min. followed by the complete addition of **10** into the reaction mixture. The reaction mixture was allowed to mix for 12 h; then workup was begun. The workup procedure followed Pederson et al., but with alterations as follows. The aqueous acidic wash step was removed. The column chromatography step was altered; instead of

loading and eluting the compound over neutral alumina, the compound was loaded onto basic alumina and eluted over neutral alumina. This allowed for the pyridinium cation to be deprotonated to pyridine, for a simplified isolation procedure.

Table 3.4. Templatation optimization of the synthesis of **5**; concentrations in mM.

Experiment number	[2] = [10]	[pyridine]	[11]	% Yield
1 non-templated	0.719	1.7	0	31
Variation: Reagent concentrations				
2	2.22	6.0	13.9	64
3	0.691	1.7	3.97	69
4	0.618	1.7	3.97	75
5	0.617	1.7	3.97	81
6	0.618	1.7	3.97	83
7	0.619	1.7	3.97	89
8	0.173	0.48	1.11	81
Variation: Pyridine				
9	0.619	35	3.97	76
Variation: Pyridinium TFSI concentration				
10	0.622	1.7	9.33	81
Variation: solvent change to chloroform				
11	0.630	1.7	3.97	49

The first parameter optimized was reagent concentration. Ideally at lower concentrations the reaction would benefit from high dilution conditions in addition to the templating agent, resulting in a yield increase. Acceptable yields were obtained over the entire starting material (**2** and **10**) range of 0.173 mM to 2.22 mM, but there appeared to be little practical reason to go below the concentration of ~0.6 mM. Experiment 8 at a reagent concentration of 0.173 mM gave a yield of 81% but required ~3.5 times the solvent. Repeating the ~0.6 mM reagent experiment five times gave a low yield of 69% and a high of 89%; the variation of 20% is attributed primarily to variations in quality and handling of the diacid chloride **10**, given that it was freshly synthesized for each experiment.

To determine the benefits of pyridinium TFSI as template, an experiment was run using parameters similar to the ~0.6 mM experiments except in that no pyridinium TFSI was added; a yield of 31% was obtained.

Using substrate concentrations of ~0.6 mM, the concentration of pyridine was varied. Although no significant yield change was observed by increasing the concentration of pyridine, the use of less was advantageous because it allowed for an easier workup of the product during column chromatography. Thus a pyridine concentration of 1.7 mM was adopted, ~2.5 equivalents.

Next, testing was conducted to determine if increased amounts of pyridinium TFSI (**11**) influenced yields; the concentration was increased from 1.1 to 9.33 mM (15 equivalents), but no significant yield change was observed. Thus, a pyridinium TFSI concentration of 3.97 mM, ~ 6 equivalents, was adopted.

Lastly, chloroform was tested as an alternative to DCM. A significant yield decrease was observed, attributed to the decreased solubility of **10** and **11** in chloroform.

alcohols of **12** hydrogen bonding with pyridinium TFSI. Occupying the alcohols of **12** in hydrogen bonding with pyridinium TFSI would inhibit the cyclization reaction and explain why templation did not occur.

Conclusion

A successful templation reaction has been developed for the production of pyridyl-based dibenzo-30-crown-10 and bis(*m*-phenylene)-32crown-10 cryptands. Using ~6 equivalents of template **11** and substrate concentrations of ~0.6 mM, and ~2.5 equivalents of pyridine in DCM, yields of 89 and 80% were obtained for **5** and **6**, respectively. Additionally, **11** complexed **5**, **6** and **13** all with association constants in the range of 10^4 M^{-1} .

Experimental

Measurements: ^1H -NMR spectra were obtained on JEOL ECLIPSE-500, BRUKER-500, and AGILENT-NMR-vnmrs400 spectrometers. ^{13}C -NMR spectra were collected at 125 MHz and 101 MHz on these instruments. HR-MS were obtained using an Agilent LC-ESI-TOF system. X-ray crystallography was performed at Virginia Tech and solved by Carla Slebodnick. Crystal structure of **5** • **11** was grown by slow solvent evaporation of an equimolar chloroform solution. X-ray crystallography tables can be found in the appendix of this dissertation. Reagents were purchased and used as received without further purification. Compounds **1**,⁷ **2**,⁶ **10**,⁸ **11**,⁹ and **12**¹⁰ were synthesized in accordance with literature procedures; similar yields were obtained. Compound **8** was prepared as described in chapter 6.

Example ITC titration: The association constants reported for **11** with **1**, **2**, **5**, **6**, **12** and **13** were obtained via ITC in DCM at 25 °C. The following is a detailed description of titration of **10** with **2**; the other systems were done similarly with slightly different concentrations. Host **2** was loaded into the cell of the instrument at a concentration of 1.46 mM, while a 250 μ L ITC syringe was loaded with **10** at a concentration of 22.4 mM. The instrument was set to high gain (high sensitivity). The titration was achieved through 50 injections of 5.00 μ L every 180 s; a primary filter period of 2 s and a secondary filter period of 4 s were applied (filter period switch time was set to 120 s). A background titration used exactly the same titration conditions with the exception that the solution of **2** was replaced with DCM. The heats for the dilution experiment were subtracted from the heats for the titration of **10** with **2**. Analysis of the data was carried out using software provided by the manufacturer. The first data point was ignored to avoid error. A “One Set of Sites” model was used; stoichiometries other than 1:1 provided unsatisfactory fits.

General procedure 1, syringe pump addition, dibenzo-30-crown-10 based pyridyl cryptand

5. To a round bottom flask containing DCM (2.5 L) was added acidic alumina (1.00 g) and pyridine (2.00 mL, 24.7 mmol). The contents were mixed for 15 min. **2** (0.2942 g, 0.4931 mmol) and **10** (0.1006, 0.4931 mmol) were each dissolved separately in DCM (25 mL) and loaded into syringes and additions were made at 1 mL / h. The reaction mixture was allowed to stir for 12 h and filtered. Following removal of solvent from the filtrate, the crude material was dissolved in DCM (50 mL) and washed with 1 M HCl (3 x 15 mL) and water (3 x 15 mL). Solvent was removed by rotary evaporation and the crude material was subjected to column chromatography using basic alumina eluting with DCM then DCM : MeOH (99:1 v:v). Isolated a white solid, 0.2773 g (77%); mp 160.8 – 162.9 °C (lit. mp 160.9–162.7 °C).⁶ ¹H NMR spectrum (400 MHz, CDCl₃): δ 8.33 (d, J = 8 Hz, 2H), 8.02 (t, J = 8 Hz, 1H), 6.94 (m, 4H), 6.77

(d, $J = 9$ Hz, 2H), 5.33 (s, 4H), 4.18–4.13 (m, 4H), 4.03–3.98 (m, 4H), 3.95–3.90 (m, 4H), 3.84–3.79 (m, 4H), 3.76–3.72 (m, 4H), 3.72–3.66 (m, 8H), 3.66–3.61 (m, 4H). ^{13}C NMR spectrum (101 MHz, CDCl_3): δ 164.80, 148.99, 148.89, 148.40, 138.14, 128.17, 127.98, 121.60, 114.21, 113.94, 70.98, 70.75, 70.72, 70.61, 69.68, 69.46, 68.97, 68.79, 67.60 (19 signals expected and 19 signals found). HR–MS: calc. for $\text{C}_{37}\text{H}_{45}\text{O}_{14}\text{N}$ [$\text{M} + \text{NH}_4$] $^+$: m/z 745.3178; found: m/z 745.3170 (error 1 ppm).

General procedure 2, direct addition, dibenzo-30-crown-10 based pyridyl cryptand 5. To a round bottom flask containing DCM (700 mL) was added **11** (1.00 g, 2.78 mmol), pyridine (2.00 mL, 24.7 mmol), and **2** (0.2587 g, 4336 μmol). The contents of flask were allowed to stir for 15 min. **10** (0.0885 g, 4.34 mmol) was then added directly to the reaction mixture. Stirring was continued for 12 h at which time solvent was removed by rotary evaporation and the crude material was subjected to column chromatography, basic alumina eluting with DCM and then DCM to MeOH (99:1 v:v); isolated white solid 0.2807 g, (89%); mp 160.4–162.6 °C (lit mp 160.9–162.7 °C).⁶ ^1H NMR spectrum (400 MHz, CDCl_3): δ 8.33 (d, $J = 8$ Hz, 2H), 8.02 (t, $J = 8$ Hz, 1H), 6.94 (m, 4H), 6.77 (d, $J = 9$ Hz, 2H), 5.33 (s, 4H), 4.18–4.13 (m, 4H), 4.03–3.98 (m, 4H), 3.95–3.90 (m, 4H), 3.84–3.79 (m, 4H), 3.76–3.72 (m, 4H), 3.72–3.66 (m, 8H), 3.66–3.61 (m, 4H). ^{13}C NMR spectrum (101 MHz, CDCl_3): δ 164.80, 148.99, 148.89, 148.40, 138.14, 128.17, 127.98, 121.60, 114.21, 113.94, 70.98, 70.75, 70.72, 70.61, 69.68, 69.46, 68.97, 68.79, 67.60 (19 signals expected and 19 signals found). HR–MS: calc. for $\text{C}_{37}\text{H}_{45}\text{O}_{14}\text{N}$ [$\text{M} + \text{NH}_4$] $^+$: m/z 745.3178; found: m/z 745.3170 (error 1 ppm).

Bis(*m*-phenylene)-32-crown-10 based pyridyl cryptand 6. General procedure 2 was used with: **11** (1.00 g, 2.78 mmol), **1** (0.2507 g, 0.4202 mmol), pyridine (0.10 mL, 1.2 mmol) **10** (0.0857 g, 0.420 mmol) and DCM (700 mL) to produce 0.2451 g, (80%) of a white solid; mp

147.9–151.2 °C, (lit mp 153.5–155.3 °C).⁴ Isolated via column chromatography on basic alumina eluting with DCM and then DCM:MeOH (99:1 v:v). ¹H NMR (400 MHz, CDCl₃) δ 8.34 (d, *J* = 8 Hz, 2H), 8.03 (t, *J* = 8 Hz, 1H), 6.54 (d, *J* = 2 Hz, 4H), 6.45 (t, *J* = 2 Hz, 2H), 5.31 (s, 4H), 3.96–3.88 (m, 8H), 3.76–3.71 (m, 8H), 3.67–3.59 (m, 16H). ¹³C NMR (101 MHz, CDCl₃) δ 165.10, 160.28, 148.50, 138.38, 137.51, 128.32, 106.51, 102.41, 71.18, 71.00, 69.87, 67.87, 67.71 (13 signals expected and 13 signals found). High res MS: calc. for C₃₇H₄₅O₁₄N [M + NH₄]⁺: m/z 745.3178; found: m/z 745.3195 (error –2.3 ppm).

Dibenzo-30-crown-10 based 4-(*p*-bromobenzyloxy)pyridyl cryptand 9. General procedure 1 was used with DCM (2.7 L), pyridine (2.4 mL), **3** (0.42690 g, 0.71548 mmol), **8** (0.27902 g, 0.71722 mmol) and acidic alumina as a template (1.00 g) to provide a solid which was purified by column chromatography using basic alumina eluting chloroform : methanol (99 : 1); 0.5064 g, (78%) of white solid, mp 188.8–192.7. ¹H NMR (400 MHz, CDCl₃) δ 7.88 (s, 2H), 7.55 (d, *J* = 8 Hz, 2H), 7.32 (d, *J* = 8 Hz, 2H), 6.94–6.92 (m, 4H), 6.77 (d, *J* = 9 Hz, 2H), 5.30 (s, 4H), 5.18 (s, 2H), 4.20–4.11 (m, 4H), 4.03–3.97 (m, 4H), 3.95–3.90 (m, 4H), 3.84–3.78 (m, 4H), 3.74 (m, 4H), 3.72–3.67 (m, 8H), 3.64 (m, 4H). ¹³C NMR (126 MHz, CDCl₃) δ 166.43 (s), 164.88 (s), 150.24 (s), 149.12 (s), 149.00 (s), 133.85 (s), 132.14 (s), 129.37 (s), 128.19 (s), 122.87 (s), 121.80 (s), 114.80 (s), 114.34 (s), 114.02 (s), 71.10 (s), 70.96 – 70.66 (m), 70.03 (s), 69.79 (s), 69.55 (s), 69.09 (s), 68.90 (s), 67.83 (s) (24 peaks expected and 24 peaks found). High res MS: calc. for C₄₄H₅₀NO₁₅Br [M + H]⁺: m/z 912.2437; found: m/z 912.2452 (error –1.6 ppm).

Bis(*m*-phenylene)-24crown-8 based pyridyl cryptand 13. General procedure 2 was used with: **12** (0.2491 g, 0.4898 mmol), **10** (0.0999 g, 0.490 mmol), pyridine (0.10 mL, 1.2 mmol), **11** (1.00 g, 2.78 mmol) and DCM (700 mL) to produce 0.0812 g, (26%); mp 160.0–163.3 °C, (lit mp 162.0–162.5 °C).¹¹ Isolation via column chromatography on basic alumina eluting with DCM

and then DCM:MeOH (99:1 v:v) to yield white solid. ^1H NMR (400 MHz, CDCl_3) δ 8.34 (d, $J = 8$ Hz, 2H), 8.03 (t, $J = 8$ Hz, 1H), 6.95 (d, $J = 2$ Hz, 2H), 6.92 (dd, $J = 2$ Hz, $J = 8$ Hz, 2H), 6.75 (d, $J = 8$ Hz, 2H), 5.28 (s, 4H), 4.18–4.14 (m, 4H), 4.04–4.00 (m, 4H), 3.95–3.91 (m, 4H), 3.86–3.82 (m, 4H), 3.79 (s, 4H), 3.73 (s, 4H). ^{13}C NMR (101 MHz, CDCl_3) δ 165.21, 149.50, 148.95, 148.65, 138.41, 128.28, 127.88, 122.37, 115.38, 113.55, 71.39, 70.99, 69.90, 69.83, 69.49, 68.98, 68.23 (17 signals expected and 17 signals found). High res MS: calc. for $\text{C}_{33}\text{H}_{37}\text{NO}_{12}$ [$\text{M} + \text{Na}$] $^{+1}$: m/z 662.2208; found: m/z 662.2203 (error 0.8 ppm).

References

- (1) Bryant, W. S.; Jones, J. W.; Mason, P. E.; Guzei, I.; Rheingold, A. L.; Fronczek, F. R.; Nagvekar, D. S.; Gibson, H. W. *Org. Lett.* **1999**, *1*, 1001-1004.
- (2) He, C.; Shi, Z.; Zhou, Q.; Li, S.; Li, N.; Huang, F. *J. Org. Chem.* **2008**, *73*, 5872-5880.
- (3) Niu, Z.; Slobodnick, C.; Schoonover, D.; Azurmendi, H.; Harich, K.; Gibson, H. W. *Org. Lett.* **2011**, *13*, 3992-3995.
- (4) Huang, F.; Switek, K. A.; Zakharov, L. N.; Fronczek, F. R.; Slobodnick, C.; Lam, M.; Golen, J. A.; Bryant, W. S.; Mason, P. E.; Rheingold, A. L.; Ashraf-Khorassani, M.; Gibson, H. W. *J. Org. Chem.* **2005**, *70*, 3231-3241.
- (5) Huang, F.; Gibson, H. W.; Bryant, W. S.; Nagvekar, D. S.; Fronczek, F. R. *J. Am. Chem. Soc.* **2003**, *125*, 9367-9371.
- (6) Pederson, A. M. P.; Ward, E. M.; Schoonover, D. V.; Slobodnick, C.; Gibson, H. W. *J. Org. Chem.* **2008**, *73*, 9094-9101.
- (7) Gibson, H. W.; Nagvekar, D. S. *Can. J. Chem.* **1997**, *75*, 1375-1384.
- (8) Jain, S. L.; Bhattacharyya, P.; Milton, H. L.; Slawin, A. M. Z.; Crayston, J. A.; Woollins, J. D. *Dalton Trans.* **2004**, 862-871.
- (9) Montavon, T. J.; Türkmen, Y. E.; Shamsi, N. A.; Miller, C.; Sumaria, C. S.; Rawal, V. H.; Kozmin, S. A. *Angew. Chem. Int. Ed.* **2013**, *52*, 13576-13579.
- (10) Gibson, H. W.; Wang, H.; Bonrad, K.; Jones, J. W.; Slobodnick, C.; Zakharov, L. N.; Rheingold, A. L.; Habenicht, B.; Lobue, P.; Ratliff, A. E. *Org. Biomol. Chem.* **2005**, *3*, 2114-2121.
- (11) Gibson, H. W.; Wang, H.; Slobodnick, C.; Merola, J.; Kassel, W. S.; Rheingold, A. L. *J. Org. Chem.* **2007**, *72*, 3381-3393.

Chapter 4

NEW GUESTS

INTRODUCTION

Association constants play a large role in supramolecular chemistry. Depending upon the application, either lower or high association constants may be desired. For many systems the desire is to have as much bound as possible, affording high molecular weight supramolecular polymers and systems capable of self-repair. Considering this, we seek host-guest systems that either lead to higher binding,¹⁻³ possess a unique responsive property⁴ or are easier to deploy.⁵ Of particular interest to our group are the dibenzo-30-crown-10 and bis(*m*-phenylene)-32-crown-10 hosts paired with paraquat guests, which have evolved into higher binding pyridyl cryptand / paraquat systems. Here, attempts are made to find better guests for the pyridyl cryptands **1a** and **1b** (Figure 4.1) from both the standpoint of being easier to synthesize as well as higher binding.

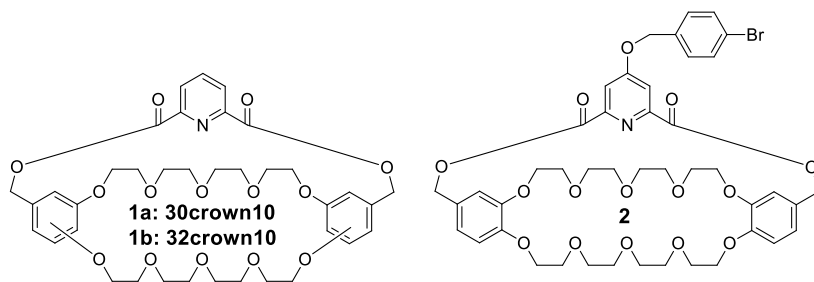


Figure 4.1. Pyridyl cryptands **1a** and **1b**, alongside functionalized pyridyl cryptand **2**.

RESULTS AND DISCUSSION

Currently the model guest most widely employed for **1a**, **1b**, and derivatives is dimethyl paraquat as the PF₆ salt (PQ PF₆). The widespread employment of this guest can be attributed to two things: first, the guest has a reasonable association constant with dibenzo-30-crown-10, bis(*m*-phenylene)-32crown-10 and analogous cryptands, extending to cryptands not containing a pyridyl group.^{1,6-8} Secondly, synthetically speaking, paraquats are relatively simple to synthesize and derivatize. The system however isn't without problems; due to the complexes being salts paired with neutral organic compounds, finding and choosing a solvent which allows for "good" solubility of both components, while not hindering binding can be challenging. Paraquat PF₆ salts are typically soluble in polar aprotic solvents, while crown ether / cryptand hosts generally exhibit lower solubilities in such solvents. Additionally, solvents with a high dielectric constant tend to drastically lower the association constants. To address this problem, variations in the paraquat salt were explored. Salt solubilities are highly influenced by the anion/cation combination. Thus a change from PF₆⁻ to a more appropriate anion, in terms of lower dielectric solvent solubility, has the effect of increasing the range of useable solvents and providing higher association constants.

Typically, the anion of choice for paraquat has been PF₆. Use of this salt pair generally leads to the adoption of one of the following solvent systems for solubility reasons: acetone, acetonitrile, or acetonitrile:chloroform mixtures. Considering that DCM has a dielectric constant much lower than acetonitrile or acetone, the goal became producing a paraquat salt with reasonable solubility in DCM. To achieve this goal two different paths were taken: first, different counterions were explored and, second, the N-methyl groups were changed to N-benzyl groups. The TFSI and large borate-containing counterions have been well documented in the

literature to increase the solubility of organic salts in low dielectric solvents.^{9,10} The choice of benzyl groups was made because a wide range of benzyl building blocks are commercially available. **Table 4.1** provides a listing of tested compounds, while **Table 4.2** gives their solubilities.

Table 4.1. Paraquat compounds.

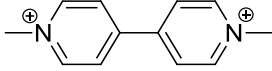
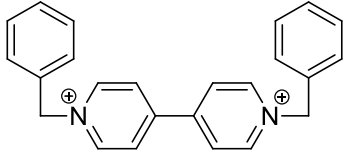
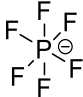
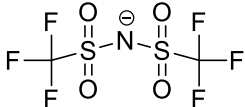
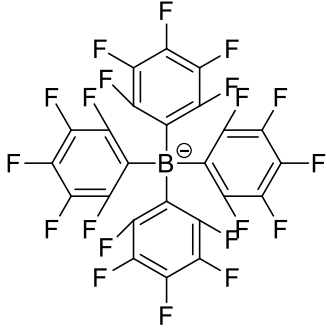
Counterion		
	3a	4a
	3b	4b
	3c	4c

Table 4.2. Paraquat solubilities (mM) at 25 °C.

Compound	Acetone	DCM
3a	56.2	Unobservable
3b	749	< 0.04
3c	Not taken	0.49
4a	261	Unobservable
4b	1,080	6.26
4c	Not taken	3.60

Using dimethyl paraquat PF₆ (**3a**) as a standard, improvement gains in solubility can be assessed. From **Table 4.1**, it can be seen that by changing from PF₆ to TFSI in **3b**, a 13-fold increase in its acetone solubility is achieved. In a similar fashion changing the methyl group to a benzyl group offers a solubility increase of over 4-fold in acetone. Due to the extremely high costs associated with **3c** and **4c**, only small quantities of these compounds were synthesized, resulting in too little to test the solubilities in acetone.

Tests of **3a** and **4a** in DCM resulted in no observable uptake. TFSI salts **3b** and **4b**, however, provided different results. With **3b**, although no measurable amount dissolved, a faint haze was observed. **4b** provided solubility in DCM. Tetrakis salts **3c** and **4c** also were soluble in DCM. It is noteworthy that the trend in solubility in DCM for **3b** and **3c** was inverse to that of **4b** and **4c**. For dimethyl paraquat, the tetrakis(perfluorophenyl)borate anion (**3c**) displayed higher solubility in DCM than the TFSI salt (**3b**), while for the dibenzyl paraquat, TFSI (**4b**) gave higher solubility in DCM than the borate (**4c**).

Solubility results showed three possibilities for using DCM as solvent for paraquat complexes with pyridyl cryptands **3c**, **4b**, and **4c**. Due to high synthetic costs associated with the synthesis of tetrakis(perfluorophenyl)borates **3c** and **4c**, these were not studied further. **Figure 4.2**, top, shows the ITC titration of **1a** with **4b**, while the bottom shows the ITC titration of **1b** with **4b**. **Table 4.3** compares association constants of **1a** / **1b** with **4b** in DCM to **1a** / **1b** with **3a** in acetone alongside **1a** with **3b** / **4a** / **4b** / in acetone.

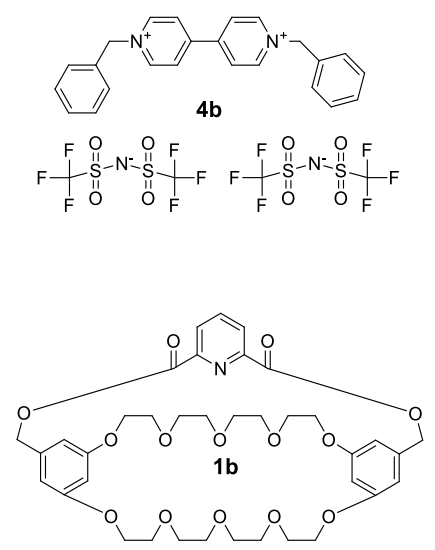
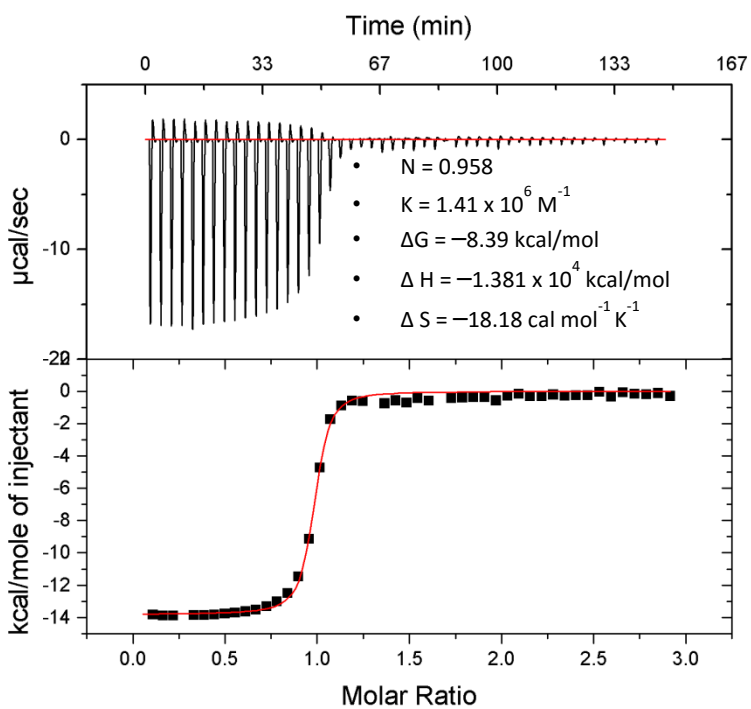
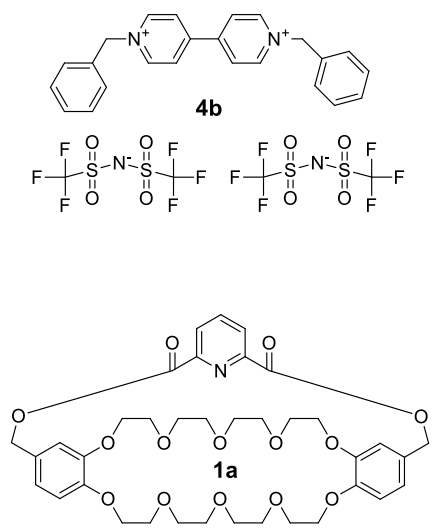
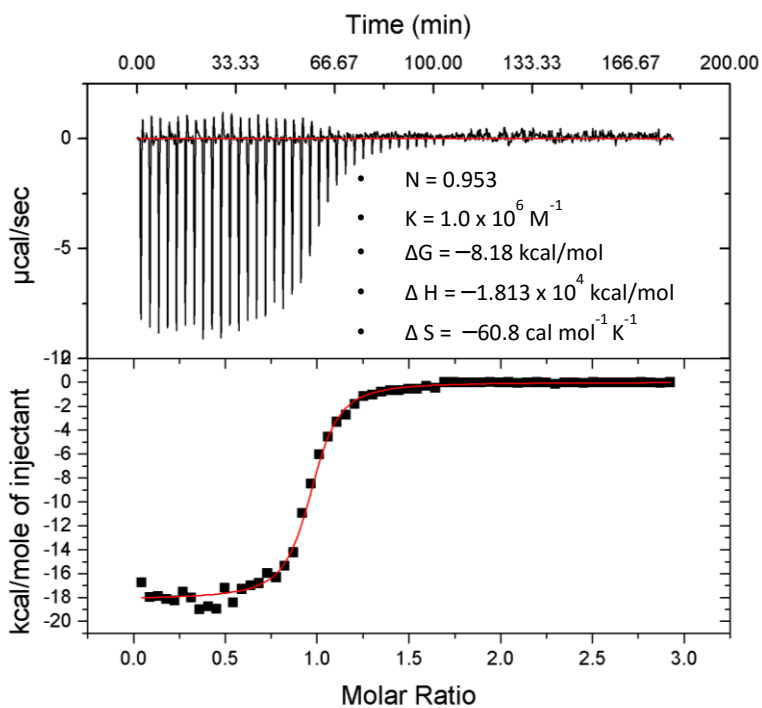


Figure 4.2. ITC titrations: top, **1a** • **4b** in DCM at 25 °C; bottom, **1b** • **4b** in DCM at 25 °C.

Table 4.3. Association constants ^a of hosts **1a** and **1b** with guests **3a**, **3b**, **4a** and **4b** at 25 °C; errors indicated in parenthesis. Values for **1a • 3a** (lit.) ¹ and **1b • 3a** (lit.) ⁸ were obtained from published sources.

	Solvent	K_a (M ⁻¹)	ΔG (kcal/mol)	ΔH (kcal/mol)	ΔS (cal/mol K)
1a • 3a (lit.)	acetone	1.00 x 10 ⁵	-6.82	-13.0	-20.7
1a • 3a	acetone	2.21 x 10 ⁵ (±0.22 x 10 ⁵)	-7.29 (±0.73)	-14.8 (±0.2)	-25.3 (±2.5)
1a • 3b	acetone	2.86 x 10 ⁵ (±0.17 x 10 ⁵)	-7.44 (±0.44)	-14.7 (±0.1)	-24.2 (±1.5)
1a • 4a	acetone	6.49 x 10 ⁵ (±0.54 x 10 ⁵)	-7.93 (±0.66)	-18.9 (±0.1)	-36.7 (±3.1)
1a • 4b	acetone	8.34 x 10 ⁵ (±0.49 x 10 ⁵)	-8.08 (±0.48)	-18.1 (±0.1)	-33.7 (±2.0)
1a • 4b	DCM	1.00 x 10 ⁶ (±0.13 x 10 ⁶)	-8.18 (±1.06)	-18.1 (±0.2)	-33.3 (±4.3)
1b • 3a (lit.)	acetone	5.0 x 10 ⁶ ^b	N/A	N/A	N/A
1b • 3a	acetone	1.12 x 10 ⁶ (±0.21 x 10 ⁶)	-8.25 (±1.55)	-18.8 (±0.4)	-35.4 (±6.7)
1b • 3b	acetone	2.22 x 10 ⁶ (±0.36 x 10 ⁶)	-8.66 (±1.40)	-17.5 (±0.201)	-29.7 (±4.8)
1b • 4b	DCM	1.41 x 10 ⁶ (±0.23 x 10 ⁶)	-8.39 (±1.37)	-13.8 (±0.1)	-18.2 (±3.0)

^a Association constant obtained by ITC.

^b Association constant obtained by NMR titration; ΔG , ΔH , and ΔS not reported.

The first noticeable item in **Table 4.3** is the differences observed for **1a • 3a** between the literature reported values and those obtained here. These differences likely result from differences in how the ITC experiments were run. The literature reported titration for **1a • 3a** was run using a 33 point titration, while values reported here were obtained using a 60 point titration. As the isotherm is fit to a mathematical construct, the more defined the curve, the better the fit; so it is reasonable to suspect that binding constants and thermal values would change as the curve becomes more defined. For comparisons the new **1a • 3a** titration will be used, since the parameters used for this experiment are those or close to those used for the remainder of the table.

The results were both remarkable and disheartening. As seen in **Table 4.3** changing from PF₆ to TFSI and methyl to benzyl groups, an association constant of $1.0 \times 10^6 \text{ M}^{-1}$ was obtained for **1a • 4b** in DCM at 25° C. By comparison, **1a • 3a** in acetone at 25° C has an association constant of $2.2 \times 10^5 \text{ M}^{-1}$; the changes led to nearly an order of magnitude increase in K_a , coming from the solvent DCM and a change from methyl to benzyl groups. Teasing out the effect of each change, we can see the effects of switching from acetone to DCM by looking at **1a • 4b** in **Table 4.3** for acetone and DCM. In the table it can be seen that K_a did not change within experimental error, and ΔH and ΔS also remained the same within experimental error. As for the effects of changing to N-benzyl groups, we see in the titration of **1a • 3b** compared to **1a • 4b**, K_a increased 2.9-fold. In terms of ΔH and ΔS , the benzyl group leads to a more favorable enthalpy term that offsets a less favorable entropy term. The change in ΔH for **1a • 3b** compared to **1a • 4b**, -14.7 vs. -18.1 , is likely attributable to the benzyl group increasing the

positive character of the benzylic protons relative to that of the methyl protons. Additionally, as in Chapter 2, a correlation was found between enthalpy and entropy values when graphed against one another. As in Chapter 2, the correlation is not apparent, a discussion of this may be found in Chapter 2.

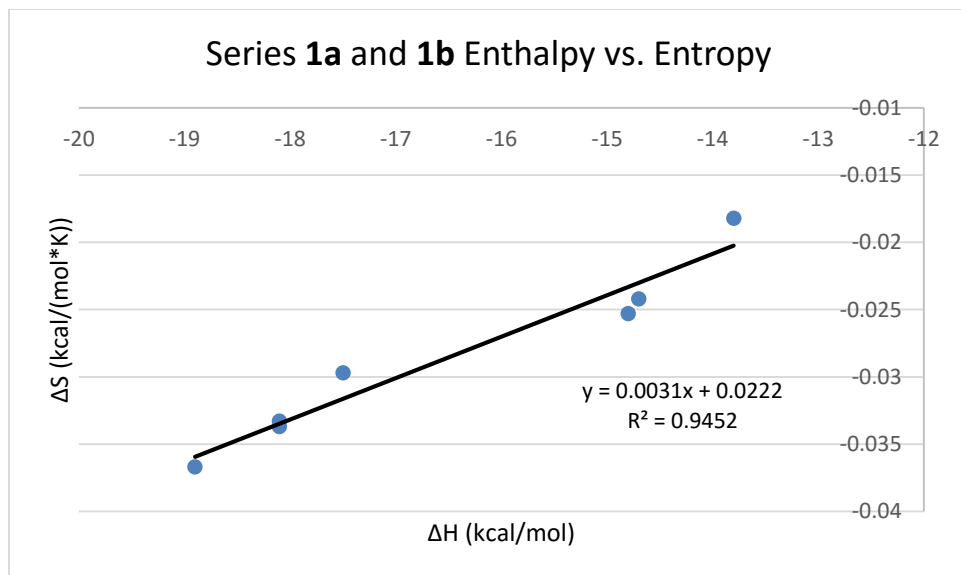
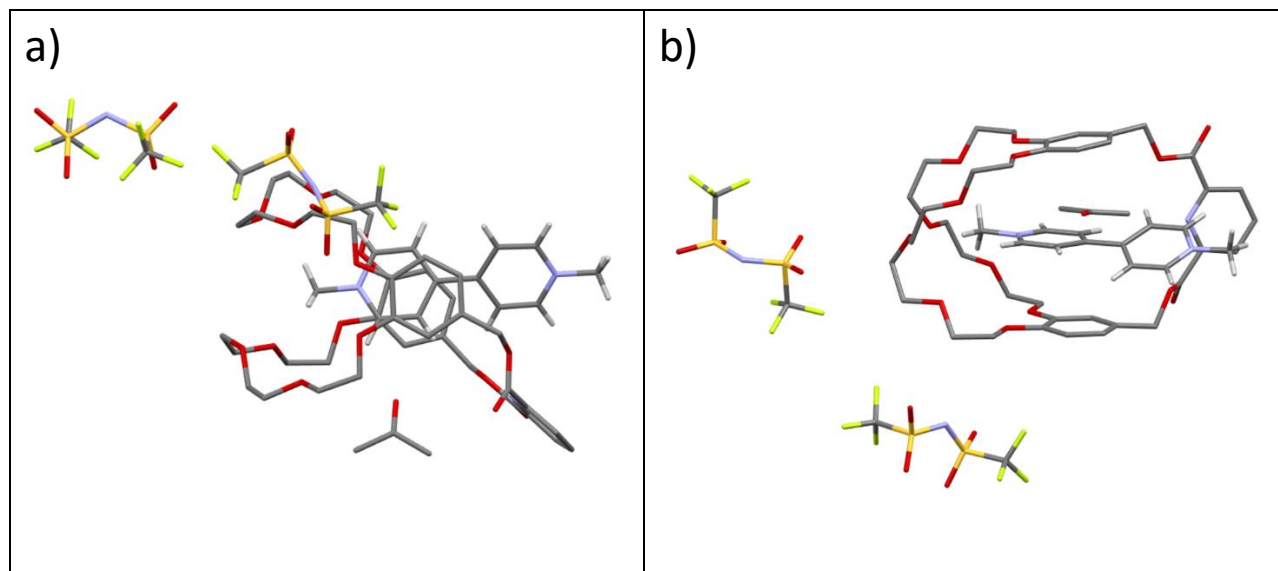


Figure 4.3. Scatter plot of enthalpies vs. entropies for **1a** and **1b** determined at 25 °C in acetone or DCM, values taken from **Table 4.3**.

Comparing PF₆ to TFSI reveals an interesting piece of information; TFSI counter ions consistently yield higher association constants in complexes with **1a** in **Table 4.4**. Dimethyl paraquat received a 32% boost in its association constant by switching to TFSI, while dibenzyl paraquat received a 28% boost. Additionally, it is noteworthy to point out that for these systems, in each instance, PF₆ had higher ΔH values than TFSI, ΔS was found to be the same within experimental error. Looking at the crystal structure of **1a** • **3b**, reveals why the association constant has increased. **Figure 4.4** shows that the paraquat cation seats directly in the cavity of the cryptand, as observed in other various difunctional paraquat PF₆ complexes with **1a** and

similar cryptands.^{1,8,11-13} In a direct comparison of crystal structures of **1a** • **3a** to **1a** • **3b**, there are several notable differences. First, instead of sitting between the pyridyl arm and crown ether portion of the cryptand, the paraquat has inserted itself in such a way that one methyl group sits directly inside the crown ether segment of the ring. This new orientation leads to five hydrogen bonds at less than 3 Å with the single methyl group; additionally, two protons on the paraquat ring provide four interactions that are less than 3 Å in spacing. The second methyl group of the complex sits directly outside of the cryptand's cavity and is hydrogen bonded to the oxygens of the TFSI counterion. In total the highly dispersed negative charge over the TFSI counter ion and multiple oxygen atoms, allow for the anion to play a greater role in interacting with the paraquat cation via hydrogen bonding. The result is a complex that contains more and stronger hydrogen bonds, leading to a higher association constant.



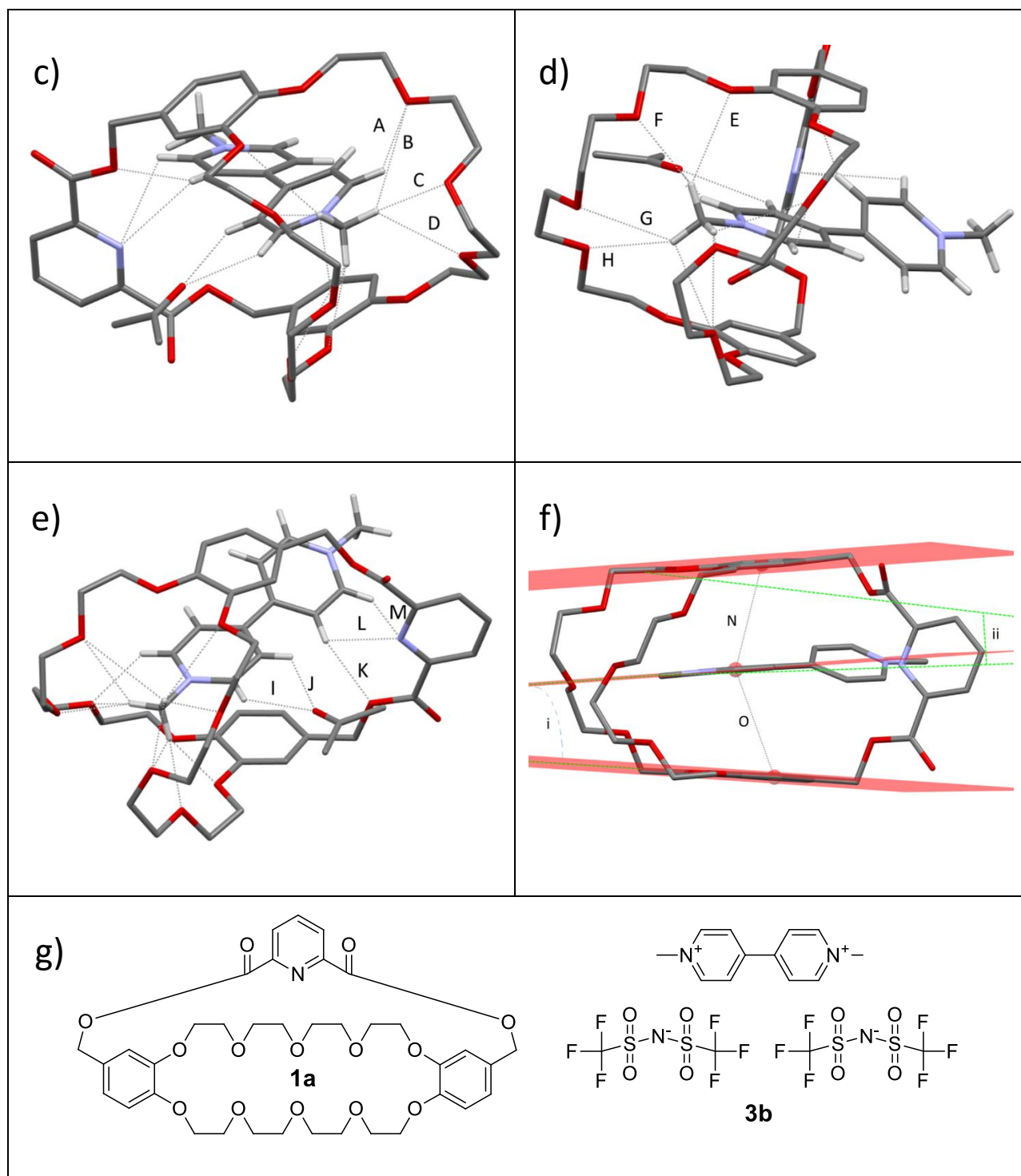


Figure 4.4. Crystal structure of **1a•3b** grown from a chloroform:acetone 1:1 (v:v) mixture by liquid-liquid diffusion of diethyl ether; non-paraquat hydrogen atoms and impurities have been removed for clarity; a) top view; b) side view; c) hydrogen bonding to the *p*-ethyleneoxy chain (counterions removed for clarity); d) hydrogen bonding to the *m*-ethyleneoxy chain (counter ions removed for clarity); e) hydrogen bonding to acetone (solvent), pyridine and ester group (counterions removed for clarity); f) planes of stacked aromatic rings shown with centroids of

stacked rings and plane inclinations indicated; g) structures **1a** and **3b**. Hydrogen-bond parameters: C---O distances (Å), C-H---O distances (Å), C-H---O angles (deg) A: 3.291, 2.560, 133.96; B: 3.818, 3.116, 129.64; C: 3.284, 2.339, 161.30; D: 3.403, 2.783, 121.72; E: 3.601, 2.826, 136.44; F: 3.264, 2.332, 156.38; G: 3.370, 2.828, 115.61; H: 3.866, 3.024, 144.66; I: 3.004, 2.327, 127.76; J: 3.140, 2.607, 115.86; K: 3.275, 2.426, 148.72; L: 3.248, 2.692, 117.95; M: 3.435, 3.066, 104.95. Face-to-face π -stacking parameters: centroid-centroid distance (Å): N) 3.586; O) 3.782; ring plane/ring plane inclinations (deg): i) 7.68°; ii) 1.63°. X-ray crystallography was performed and solved by Dr. Carla Slebodnick.

As literature reported results for **1b** • **3a** were obtained via NMR, to ensure a uniform comparison, the complexation of **1b** with **3a** was reassessed using ITC: $K_a = 1.12 \times 10^6$ in acetone at 25 °C. Although a small gain, using this value, it can be seen that switching to TFSI offers a near doubling of the association constant, **1b** • **3b** $K_a = 2.22 \times 10^6$. Additionally, considering **1b** • **3a** and **1b** • **3b** both ΔG and ΔS were found to be within experimental error, while ΔH values were very similar. The complex of **1b** with the benzyl paraquat **4b** gave a slight decrease in binding, but overall values were similar to one another. The association constant for **1b** • **4b** in DCM at 25° C, $1.41 \times 10^6 \text{ M}^{-1}$, was found to be less than the complex of **1b** • **3b** in acetone at 25 °C, 2.22×10^6

Encouraged by the results for **1a** • **4b** in DCM, it was speculated that the benzyl groups of **4b** could be used to further increase the association constant of a crypand which also contained a benzyl group, because there would be an increased opportunity for π -stacking. Thus the hypothesis was tested by ITC through the complexation of **2** • **4b**; **Figure 4.5** shows ITC results.

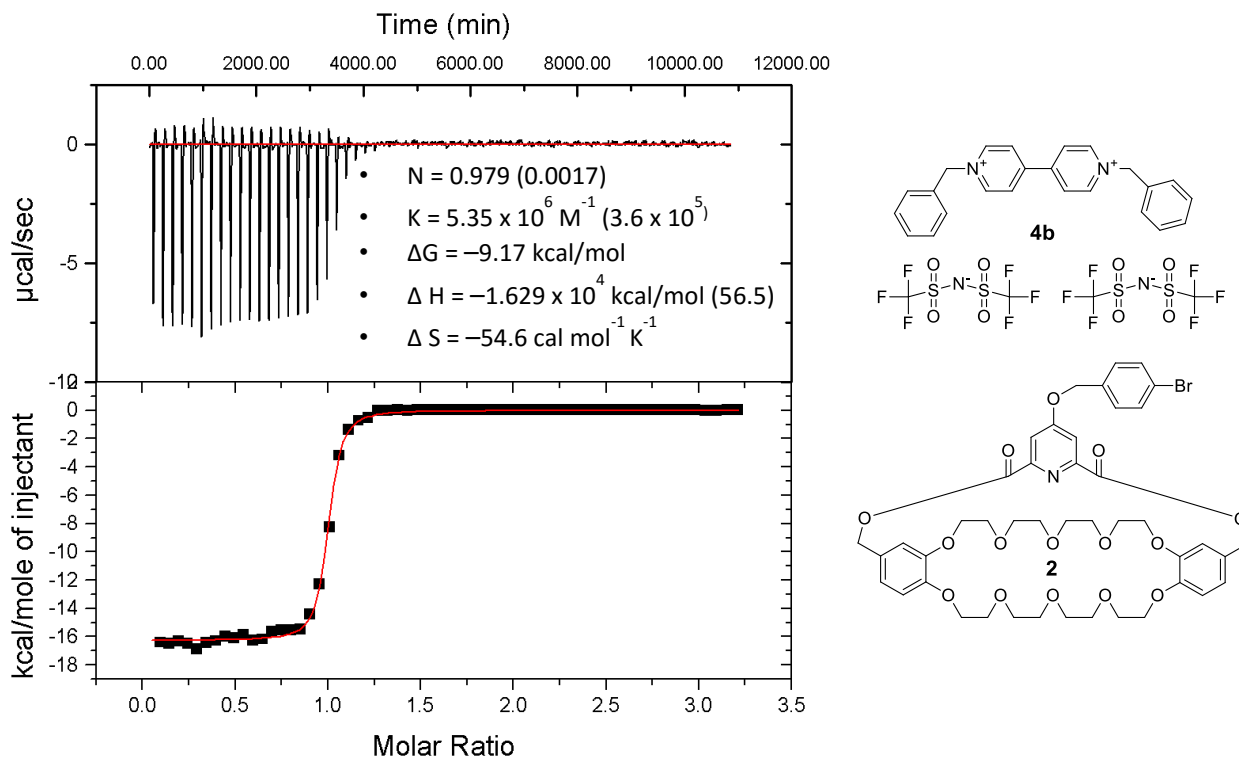
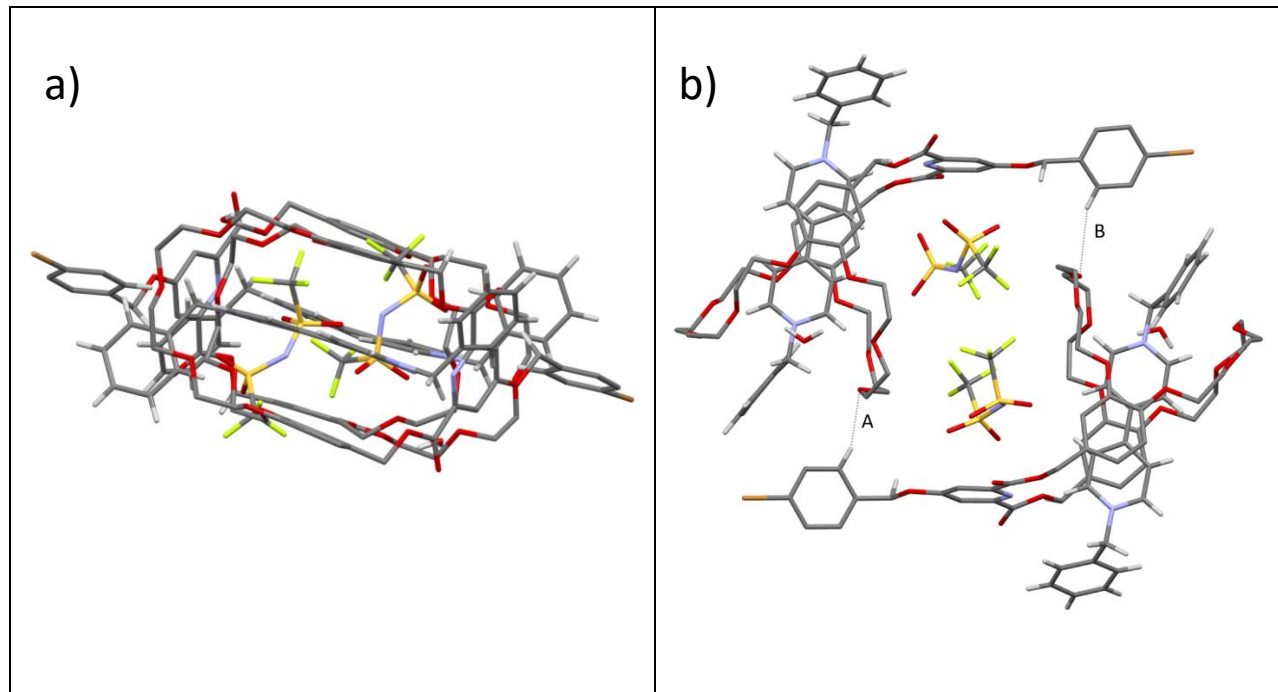


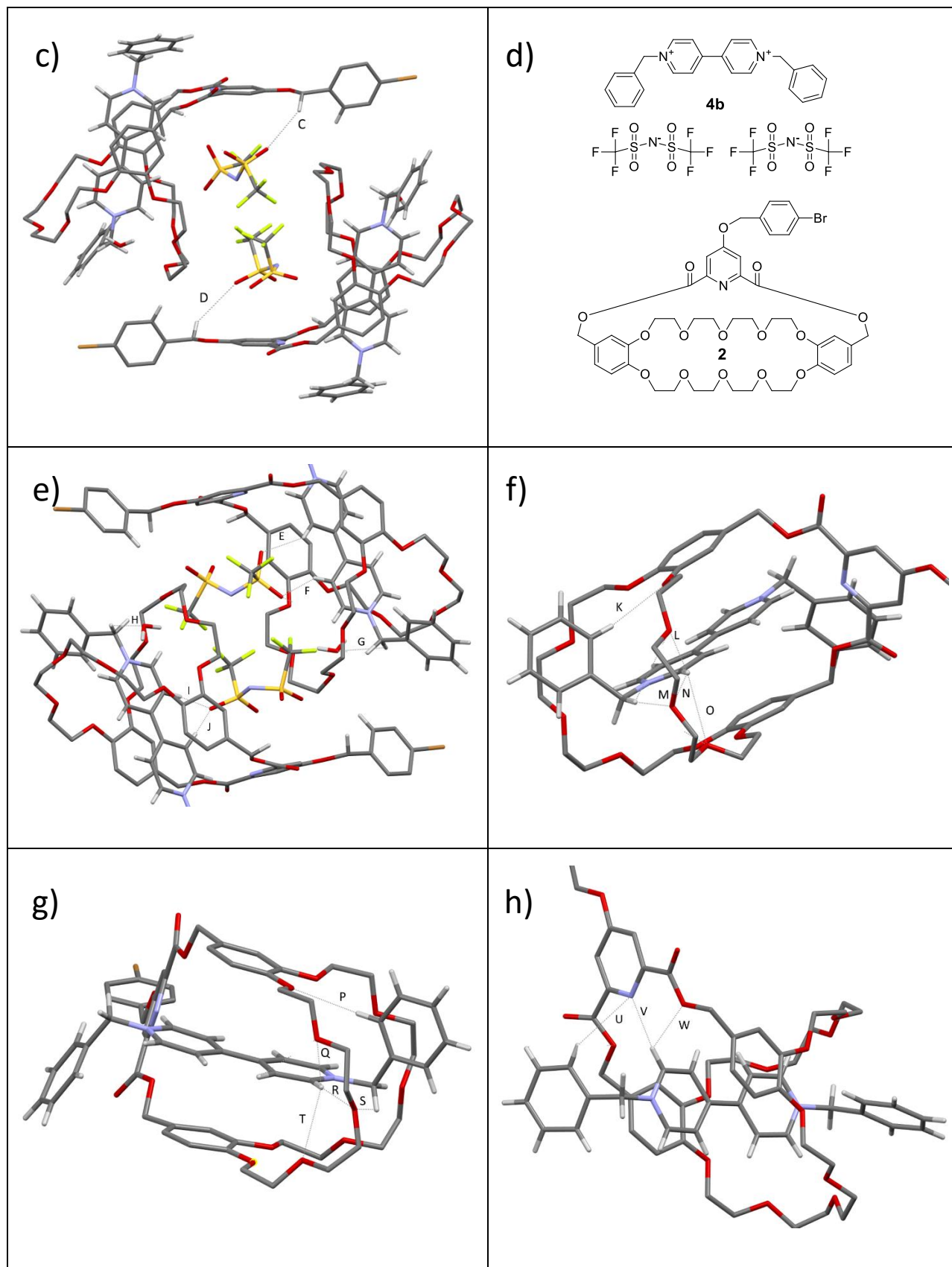
Figure 4.5. ITC titration of **2 • 4b** in DCM at 25 °C.

Figure 4.5 proved part of the hypothesis correct; by using a benzyl containing cryptand a 5-fold increase in the association constant was observed for **2 • 4b** ($K_a = 5.35 \times 10^6 \text{ M}^{-1}$), when compared to **1a • 4b**. The belief that this would be driven by π -stacking, however, was incorrect. **Figure 4.6** shows the crystal structure of **2 • 4b**. Sadly, due to the complexity of the complex and TFSI anion, a full structure containing the correct ratio of TFSI counter anions was not obtained; instead only one TFSI per paraquat could be solved for. The benzyl rings of the paraquat add extra points at which hydrogen bonding can occur. As an interesting note to the solid state and not necessarily relevant to solution complexation, the unit cell was found to be composed of two cryptand and two paraquat molecules. This is due to the 4-bromobenzyl ring attached to the cryptand offering a hydrogen in the 2-position that appears to be interacting with

an oxygen from the adjacent cryptand, **Figure 4.6b**. In **Figure 4.6b**, the hydrogen bonds labeled A and B have bond distances (angles) of 2.532 (154.80 °) and 2.855 (158.91 °), respectively.

Considering any interaction found in **2 • 4b** should likely be found in **1a • 4b**, the increase in association constant must be attributed to an interaction with the 4-bromobenzyl group. The one interaction which should be unique to **2 • 4b** over **1a • 4b** is the interaction of TFSI in these complexes with the host. **Figure 4.6c** shows hydrogen bonding between the TFSI counter ion and cryptand, two bonds at 3.020 and 2.717 Å. Although the listed hydrogen bonding is weak in nature, it only employs one of each of the TFSI oxygens while the other two oxygens moderately hydrogen bond to the paraquat, **Figure 4.6e**





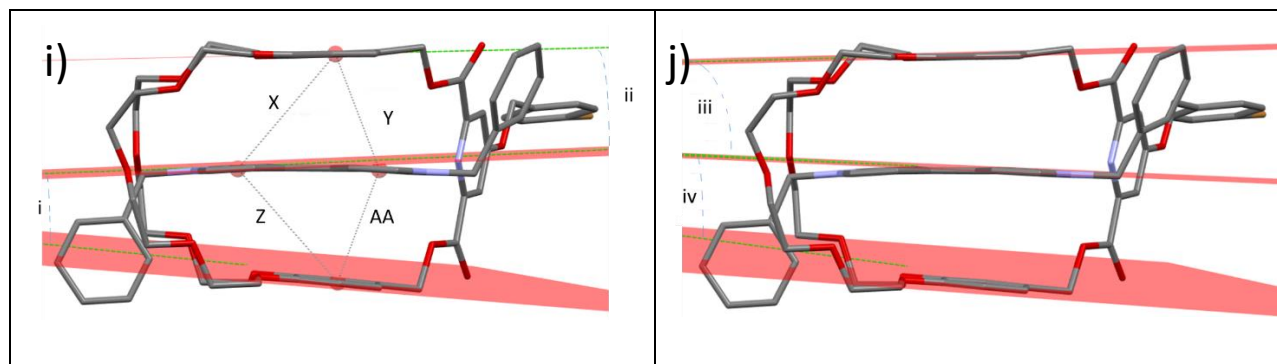
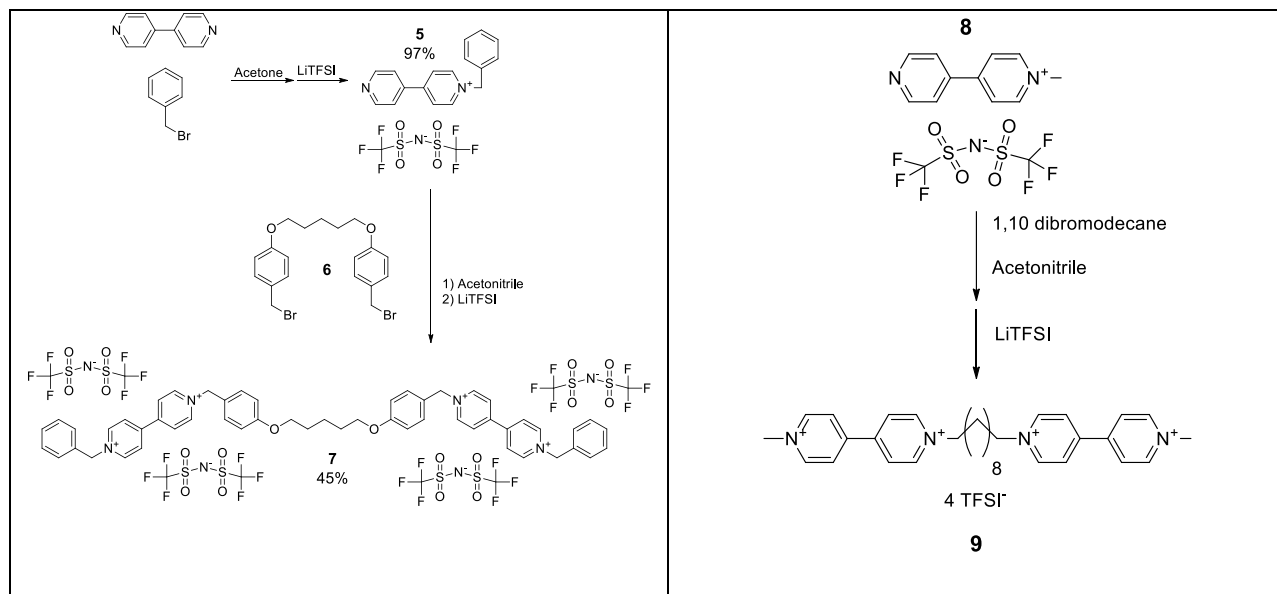


Figure 4.6. Incomplete crystal structure of **2 • 4b** grown by liquid-liquid diffusion of pentane into a 1:1 v:v mixture of dichloromethane : acetone (missing one two TFSI counter ions); hydrogens which do not belong to the guest or host hydrogens not believed to be hydrogen bonding are removed for clarity; a) side view; b) top view with cryptand–cryptand hydrogen bonding; c) zoom showing TFSI hydrogen bonding to cryptand; d) structures **4b** and **2**; e) zoom showing TFSI and water hydrogen bonding to paraquat; f) hydrogen bonding with *m*-ethyleneoxy chain (Second complex along with all non-guest hydrogens, TFSI, and water atoms removed for clarity); g) hydrogen bonding with *p*-ethyleneoxy chain (Second complex along with all non-guest hydrogens, TFSI, and water atoms removed for clarity); h) hydrogen bonding at the pyridyl arm (Second complex along with all non-guest hydrogens, TFSI, and water atoms removed for clarity); hydrogen-bond parameters: C---O distances (Å), C-H---O distances (Å), C-H---O angles (deg) A: 3.417, 2.532, 154.80; B: 3.758, 2.855, 158.91; C: 3.566, 2.717, 144.13; D: 3.793, 3.020, 135.71; E: 3.260, 2.428, 146.08; F: 3.414, 2.616, 141.89; G: 3.149, 2.745, 104.97; H: 3.295, 2.597, 127.53; I: 3.418, 2.515, 158.62; J: 3.368, 2.467, 158.21; K: 3.430, 2.529, 158.30; L: 3.104, 2.469, 124.18; M: 3.239, 2.261, 169.92; N: 3.502, 2.693, 143.32; O: 3.145, 2.803, 102.23; P: 3.493, 2.745, 136.13; Q: 3.110, 2.573, 115.97; R: 3.141, 2.208, 166.30; S: 3.554, 3.050, 112.89; T: 3.300, 2.833, 111.26; U: 3.790, 3.092, 131.53; V: 3.183, 2.276, 159.36; W: 3.059, 2.496, 117.87. Face-to-face π -stacking parameters: centroid-centroid distance (Å): X: 4.501; Y: 3.696; Z: 4.497; AA: 3.713; ring plane/ring plane inclinations (deg): i: 7.90°; ii: 1.10°; iii: 3.97°; iv: 3.65°. X-ray crystallography was performed and solved by Dr. Carla Slebodnick.

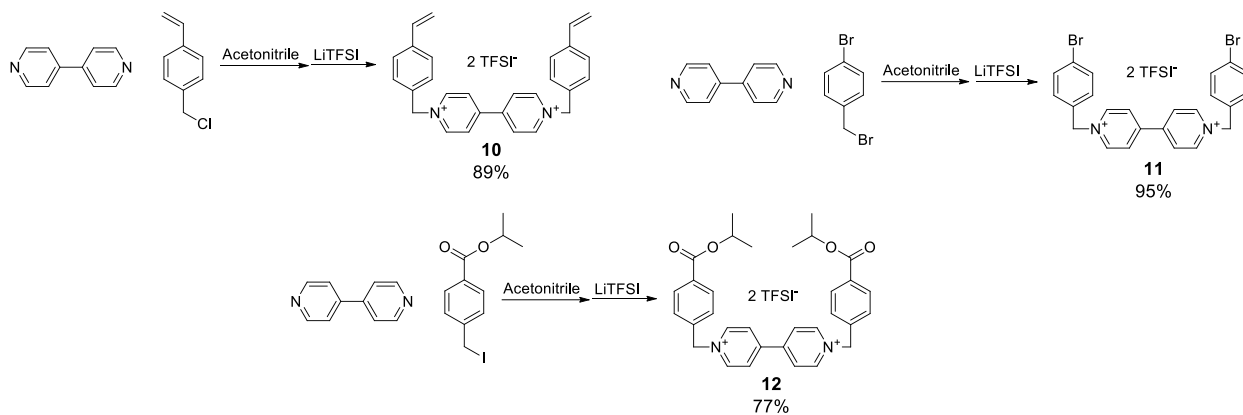
As previously stated, any interaction found in **2 • 4b** should likely be found in **1a • 4b**; with this in mind it can be reasoned why a significant increase in K_a was observed in **1a** but not **1b** when switching from dimethyl to dibenzyl paraquat. In **Figures 4.6f** and **4.6g**, it can be seen that a hydrogen of the benzyl group produced two hydrogen bonds of moderate strength, labeled K and U. It is reasonable to suspect that the placement of ethyleneoxy arms in **1b** would at best

net one hydrogen bond at this point, due to atom placement and the presence of a hydrogen at the 4-position in **1b**.

Several other derivatives of the benzyl paraquat TFSI were synthesized. **Scheme 4.1** shows the synthesis of useful bisparaquats **7** and **9**, which could be used for chain extensions,¹⁴ supramolecular polymers,^{2,15,16} or [3]pseudorotaxanes^{12,17} if combined with appropriate host compounds. Additionally, **Scheme 4.1** contains the most desirable feedstock molecules **5** and **8**; typically, [4,4'-bipyridin]-1-ium molecules (halfquats) are synthesized to break the symmetry and introduce functionality for more complex molecules. Both halfquats (**5** and **8**) and supramolecular guest monomers (**7** and **9**) were synthesized in acceptable yields, 97%, 41%, 91%, and 75%, respectively. In **Scheme 4.2**, the yields were 89% for **10**, 95% for **11**, and 77% for **12**, indicating halide and functionality can be altered while maintaining reasonable yields.



Scheme 4.1. Synthesis of benzylic bisparaquat TFSI monomer **7** and methyl bisparaquat TFSI monomer **9**.



Scheme 4.2. Variation of benzylic halide and functionality.

Typically, one of the forces that greatly drive complexation between a paraquat and cryptand are the relatively acidic protons of the carbon attached directly to the terminal nitrogen atoms of the 4,4'-bipyridinium moiety, **Figure 4.7**. These protons interact with lone pairs of electrons in the cryptands. It was anticipated that if these protons could be made more acidic, binding between the paraquat and cryptand could be further increased. To test this hypothesis a [4,4'-bipyridine]-1,1'-dium employing 2,3,4,5,6-pentafluorobenzyl rings was synthesized, **13**, **Scheme 4.3**.

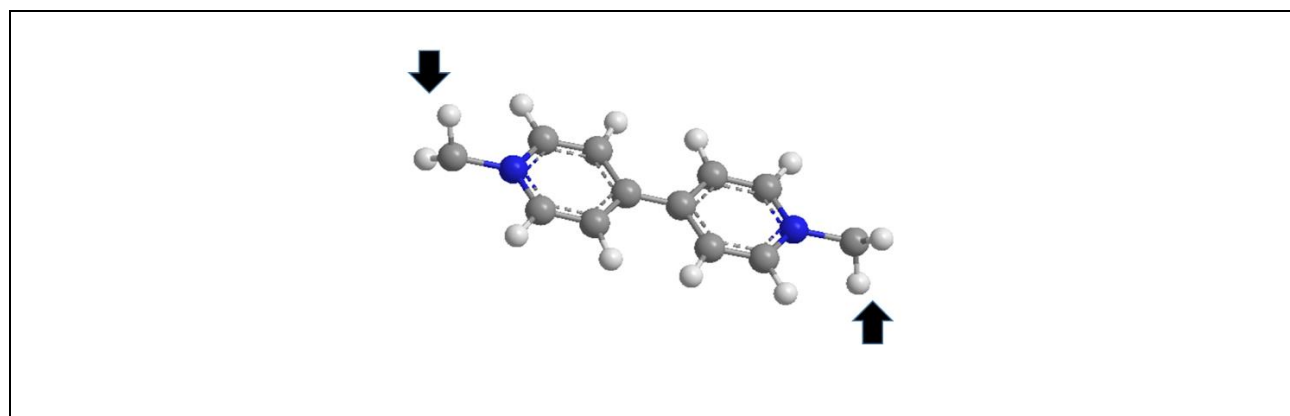
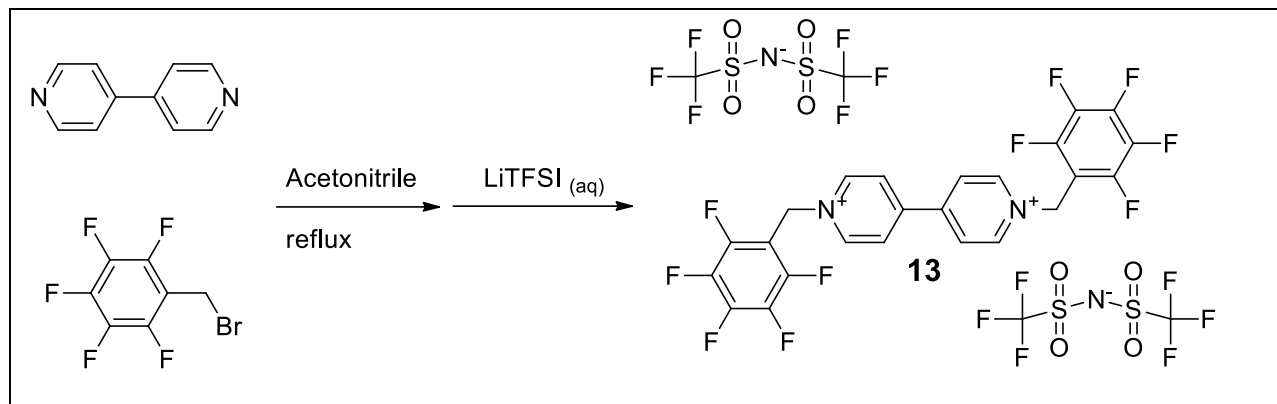


Figure 4.7. Paraquat acidic aliphatic protons.



Scheme 4.3. Synthesis of fluorinated guests: paraquat TFSI **13**.

It was anticipated that the electron deficient pentafluorophenyl rings of **13** could greatly increase the acidity of the benzylic protons and thereby ultimately drive the binding constant higher with **1a**. Comparing **13** to its hydrogen counterpart **4b**, the first notable item comes from the ^1H NMR spectrum; the benzylic protons of **13** are found 0.25 ppm downfield, indicating deshielding and more acidic protons. Secondly, by changing to fluorinated rings, the advantage of the salt being soluble in DCM was lost. From **Table 4.4** it can be seen that, despite the benzylic protons in **13** being more acidic, the binding constant decreased by an order of magnitude compared to **4b**. The ΔH value decreased markedly from -18.1 to -12.9 kcal/mol, even though the ΔS for **1a** • **4b** was -33.7 eu while ΔS for **1a** • **13** is -20.7 eu. In the case of dimethyl paraquat vs. dibenzyl paraquat, increased opportunities for intermolecular interactions yielded a net increase in binding constant with **1a** and analogous cryptands such as **2**. However, by changing the hydrogens atoms of the benzyl ring to fluorine atoms, a net loss was observed that was not outweighed by the increased acidity of the benzylic protons found in **13**.

Table 4.4. ITC results for **13** with **1a** obtained at 25 °C.

	Solvent	K_a (M⁻¹)	ΔG (kcal/ mol)	ΔH (kcal/mol)	ΔS (cal/molK)
1a • 13	acetone	8.47 x 10 ⁴ (±0.39 x 10 ⁴)	-6.72 (±0.31)	-12.9 (±0.2)	-20.7 (±1.0)

CONCLUSION

In conclusion, the original dimethyl paraquat PF₆ motif was successfully altered to a dibenzyl paraquat TFSI motif. This change resulted in increased solubility of the paraquat salt in less polar solvents. Taking advantage of the less polar solvent DCM, the association constant of dibenzo-30-crown-10-based pyridyl cryptand **1a** with dibenzyl paraquat TFSI (**4b**) increased by an order of magnitude over the analogous dimethyl paraquat PF₆ complex in acetone. However, the association constant of the 32-crown-10 counterpart did not increase similarly; K_a of cryptand **1b** with dibenzyl paraquat TFSI (**4b**) in DCM decreased slightly compared to dimethyl paraquat PF₆ in acetone. Although **1b** benefited from the change of PF₆ to TFSI with dimethyl paraquat, at best only a nearly doubling in K_a was observed. Inspection of several paraquat cryptand combinations revealed that TFSI-containing paraquats yielded higher association constants than their PF₆ counter parts, but gains were modest. A dibenzocrown ether based pyridyl cryptand containing a benzylic group led to a 5-fold increase in K_a with the dibenzyl paraquat as an apparent result of TFSI hydrogen bonding with the cryptand. Useful supramolecular guest monomers **7** and **9** were prepared and a number of functional dibenzyl

paraquat TFSI salts were synthesized. Lastly, 2,3,4,5,6-pentafluorobenzyl rings were installed on paraquat with the intent of increasing the acidity of the benzylic protons, in the hope of increasing association constants with **1a**; this attempt was fruitless. In total 10 new novel compounds were synthesized in this chapter.

EXPERIMENTAL

Measurements: ¹H-NMR spectra were obtained on JEOL ECLIPSE-500, BRUKER-500, and AGILENT-NMR-vnmrs400 spectrometers. ¹³C-NMR spectra were collected at 125 MHz and 101 MHz on these instruments. HR-MS were obtained using an Agilent LC-ESI-TOF system. Reagents were purchased and used as received without further purification. Compounds **3a**,¹⁸ **4a**,¹⁹ **6**,²⁰ and **8**²¹ were prepared as described by literature procedures; similar yields were achieved. Compound **1** was prepared as described in chapter 2 and compound **2** was prepared as described in chapter 7. X-ray crystallography was performed at Virginia Tech and solved by Dr. Carla Slebodnick. Crystal structure of **1a** • **3b** was grown from an equimolar solution of chloroform:acetone 1:1 (v:v) by liquid-liquid diffusion of diethyl ether. Crystal structure of **2** • **4b** was grown from an equimolar of dichloromethane:acetone 1:1 (v:v) by liquid-liquid diffusion of pentane. X-ray crystallography tables can be found in the appendix of this dissertation.

Solubility testing. All solubility testing was carried out at 25 °C. A mixture of solvent and excess paraquat salt was made and placed in a water bath at 25 °C for 8 h. A 5.00 mL aliquot was removed from the saturated solution using a volumetric pipette and placed in a cleaned tared vial. Solvent removal and determination of the mass of the solid residue allowed calculation of the molarity of the saturated solution.

Sample ITC titration. The following is an example using **1a** • **4b** in DCM at 25 °C. Host **1a** was loaded into the cell of the instrument at a concentration of 0.160 mM, while a 250 μ L ITC syringe was loaded with **4b** at a concentration of 2.291 mM. The instrument was set to high gain (high sensitivity). The titration was achieved through 60 injections of 4.167 μ L every 180 s; a primary filter period of 1 s and a secondary filter period of 3 s were applied (filter period switch time was set to 60 s). A background titration used exactly the same titration conditions with the exception that the solution of **1a** was replaced with DCM. The heats for the dilution experiment were subtracted from the heats for the titration of **4b** with **1a**. Analysis of the data was carried out using software provided by the manufacturer. A “One Set of Sites” model was used; stoichiometries other than 1:1 provided unsatisfactory fits; additionally, the first data point was ignored.

Dimethyl paraquat TFSI (3b). In 20 mL of water dimethyl paraquat iodide ²² (2.65 g, 6.02 mmol) was dissolved. This solution was then added to a second flask containing LiTFSI (4.10 g, 15.6 mmol) dissolved in 10 mL water. The resulting precipitate was filtered and allowed to air dry to provide a white solid: 4.32 g (96%), recrystallized from water and acetone three times 2.88 g (64%), mp 125.9–127.9 °C; lit. mp 130 °C.²¹ ¹H NMR (500 MHz, acetone-*d*₆) δ 9.42 (s, 4H), 8.87 (s, 4H), 4.77 (s, 6H). ¹³C NMR (126 MHz, acetone-*d*₆) δ 150.67 (s), 147.88 (s), 127.76 (s), 120.95 (q, J = 322 Hz), 49.46 (s) (5 signals expected and 5 signals found). High res MS: calc. for C₁₆H₁₄N₄O₈S₄F₁₂ [M+Na]⁺: m/z 768.9395; found: m/z 768.9405 (error 1.3 ppm).

Dimethyl paraquat TPFB (3c). In 3 mL of water dimethyl paraquat iodide ²² (63.1 mg, 0.143 mmol) was dissolved. This solution was added to a second flask containing tetrakis(pentafluorophenyl)borate ethyl etherate (310.4 mg, 0.3563 mmol) dissolved in 3 mL of water. The resulting precipitate was filtered and allowed to air dry to provide a white solid:

0.2171 g (98%), mp 204.6–208.5 °C. ¹H NMR (400 MHz, acetone-*d*₆) δ 9.51 (d, *J* = 7 Hz, 4H), 8.96 (d, *J* = 7 Hz, 4H), 4.79 (s, 6H). ¹³C NMR (101 MHz, acetone-*d*₆) δ 149.81 (s), 147.08 (s, overlap), 148.13 (br d, *J* = 237 Hz, overlap), 143.13 (br d, *J* = 773 Hz, overlap), 136.11 (br d, *J* = 253 Hz), 136.90 (s, overlap), 126.90 (s), 48.64 (s) (8 signals expected and 8 signals found). High res MS: calc. for C₃₆H₁₄F₂₀N₂B [M - TPFB]⁺: m/z 865.0925; found: m/z 865.0890 (error 4.0 ppm).

General Procedure 1: Dibenzyl paraquat TFSI (4b). To a round bottom flask containing acetonitrile (100 mL) was added 4,4'-dipyridyl (2.03 g, 13.0 mmol) and benzyl bromide (5.0 mL, 42 mmol) under nitrogen. The reaction mixture was held at reflux for 21 h, after which the solvent was removed by rotary evaporation. The crude material was triturated with acetonitrile and DCM, followed by collection on a fritted glass filter where it was washed with DCM and air dried: 6.45 g (99%), mp 260 (dec); lit. mp 260 (dec).²³ The precipitate (1.47 g, 2.95 mmol) was dissolved in 10 mL of water and after dissolving LiTFSI (2.11 g, 8.02 mmol) in 5 mL of water in a separate container, the two aqueous solutions were combined. The precipitate was filtered, washed with water and allowed to air dry; this provided a white solid: 2.6514 g (100%), recrystallized from water-acetone mixture (x3), mp 112.4–113.3 °C. ¹H NMR (500 MHz, DMSO-*d*₆) δ 9.52 (d, *J* = 7 Hz, 4H), 8.75 (d, *J* = 7 Hz, 4H), 7.62 (d, *J* = 7 Hz, 4H), 7.52–7.41 (m, 6H), 5.96 (s, 4H). ¹³C NMR (126 MHz, DMSO-*d*₆) δ 149.34 (s), 145.65 (s), 134.01 (s), 129.48 (s), 129.22 (s), 128.86 (s), 127.23 (s), 119.45 (q, *J* = 323 Hz), 63.54 (s) (9 peaks expected and 9 peaks found). High res MS: calc. for C₂₈H₂₂F₁₂N₄O₈S₄ [M+NH₄]⁺: m/z 916.0467; found: m/z 916.0503 (error –3.9 ppm).

General Procedure 2: 1,1'-bis(*p*-vinylbenzyl)-[4,4'-bipyridine]-1,1'-dium TFSI (10). To a round bottom flask containing acetonitrile (30 mL) was added 4,4'-dipyridyl (0.5071 g, 3.247

mmol) and *p*-vinylbenzyl chloride (1.2 mL, 8.5 mmol) under nitrogen. The reaction mixture was held at reflux for 21 h, after which time the solvent was removed by rotary evaporation. The crude material was triturated with DCM, collected on a filter, washed with DCM and air dried. The precipitate was dissolved in 10 mL water and after dissolving LiTFSI (2.35 g, 8.19 mmol) in 10 mL water in a separate container, the two aqueous solutions were combined. The precipitate was filtered, washed with water and allowed to air dry; this provided a white solid with a blueish tint: 2.74 g (89%), mp 261°C (dec). ¹H NMR (500 MHz, CD₂Cl₂) δ 8.93 (d, *J* = 7 Hz, 2H), 8.45 (d, *J* = 7 Hz, 2H), 7.57 (d, *J* = 8 Hz, 2H), 7.47 (d, *J* = 8 Hz, 2H), 6.78 (dd, *J* = 18, 11 Hz, 1H), 5.88 (d, *J* = 18 Hz, 1H), 5.82 (s, 2H), 5.40 (d, *J* = 11 Hz, 1H). ¹³C NMR (126 MHz, CD₂Cl₂) δ 150.81 (s), 145.54 (s), 140.55 (s), 135.85 (s), 130.41 (s), 130.08 (s), 128.07 (s), 120.08 (q, *J* = 323 Hz), 116.61 (s), 65.89 (s). High res MS +1 peak: calc. for C₃₂H₂₆O₈N₄S₄F₁₂ [M-TFSI]⁺: m/z 670.1264; found: m/z 670.1248 (error -2.4 ppm).

Dibenzyl paraquat TFSI (4b). General procedure 1 was used to produce a white solid: 2.6514 g (100%), mp 112.4-113.3°C, by using dibenzyl paraquat bromide (1.47 g, 2.95 mmol) and LiTFSI (2.11 g, 8.02 mmol) in 5 mL of water. ¹H NMR (500 MHz, DMSO-*d*₆) δ 9.52 (d, *J* = 7 Hz, 4H), 8.75 (d, *J* = 7 Hz, 4H), 7.62 (d, *J* = 7 Hz, 4H), 7.52-7.41 (m, 6H), 5.96 (s, 4H). ¹³C NMR (126 MHz, DMSO-*d*₆) δ 149.34 (s), 145.65 (s), 134.01 (s), 129.48 (s), 129.22 (s), 128.86 (s), 127.23 (s), 119.45 (q, *J* = 323 Hz), 63.54 (s) (9 peaks expected and 9 peaks found). High res MS: calc. for C₂₈H₂₂F₁₂N₄O₈S₄ [M+NH₄]⁺: m/z 916.0467; found: m/z 916.0503 (error -3.9 ppm).

Dibenzyl paraquat TPPB (4c). General procedure 1 was used to produce an off-white solid 162.3 mg (98%), mp 240.6-242.3 °C, by using dibenzyl paraquat dibromide (48.6 mg, 0.0975 mmol) and tetrakis(pentafluorophenyl)borate ethyl etherate (286.0 mg, 0.3283 mmol) dissolved

in 3 mL of water. ^1H NMR (400 MHz, acetone- d_6) δ 9.63 (d, $J = 7$ Hz, 4H), 8.96 (d, $J = 7$ Hz, 4H), 7.75–7.58 (m, 4H), 7.57–7.43 (m, 6H), 6.22 (s, 4H). ^{13}C NMR (101 MHz, acetone- d_6) δ 150.67 (s), 148.15 (br d, $J = 245$ Hz), 146.09 (s, overlap), 142.71 (br d, $J = 683$ Hz), 136.10 (br d, $J = 254$ Hz), 136.92 (s, overlap), 133.24 (s), 130.05 (s), 129.58 (s), 129.17 (s), 127.77 (s), 64.98 (s) (12 signals expected and 12 signals found). High res MS: calc. for $\text{C}_{72}\text{H}_{22}\text{F}_{40}\text{N}_2\text{B}_2$ $[\text{M}+\text{Na}]^+$: m/z 1719.1223; found: m/z 1719.1303 (error -4.7 ppm).

1-Benzyl-[4,4'-bipyridin]-1-ium TFSI (5). A solution of acetone (200 mL), 4,4'-dipyridyl (5.02 g, 32.1 mmol) and benzyl bromide (3.2 mL, 27 mmol) was held at reflux for 45 min and allowed to cool to room temperature. Half of the acetone was removed by rotary evaporation and the solution was diluted with ether and filtered. The solid was washed with ether, air dried and 3.01 g of the precipitate was dissolved in 30 mL water and a separate aqueous solution of LiTFSI (4.25 g, 14.0 mmol) in 10 mL of water was made. The two aqueous solutions were combined and after brief stirring extracted with DCM twice. The organic layers were combined and washed with water (x3). Removal of solvent provided the desired product as a white solid; 4.7063 g (97%), mp 90.8–92.5 °C. ^1H NMR (500 MHz, CDCl_3) δ 8.92 (d, $J = 7$ Hz, 2H), 8.83 (d, $J = 6$ Hz, 2H), 8.22 (d, $J = 7$ Hz, 2H), 7.63 (d, $J = 6$ Hz, 2H), 7.51–7.39 (m, 5H), 5.75 (s, 2H). ^{13}C NMR (126 MHz, CDCl_3) δ 154.89 (s), 151.48 (s), 144.80 (s), 140.83 (s), 131.52 (s), 130.59 (s), 130.01 (s), 129.45 (s), 126.16 (s), 121.46 (s), 119.80 (q, $J = 321$ Hz), 65.00 (s) (12 peaks expected and 12 peaks found). High res MS: calc. for $\text{C}_{19}\text{H}_{15}\text{O}_4\text{F}_6\text{N}_3\text{S}_2$ $[\text{M}-\text{TFSI}]^+$: m/z 247.1230; found: m/z 247.1223 (error -3 ppm).

1',1'''-(((Pentane-1,5-diylbis(oxy))bis(4,1-phenylene))bis(methylene))bis(1-benzyl-[4,4'-bipyridine]-1,1'-diium) TFSI (7). A solution of 1,5-bis[*p*-(bromomethyl)phenoxy]pentane,²⁰ (0.7450 g, 1.685 mmol), acetonitrile (100 mL) and 1-benzyl-[4,4'-bipyridin]-1-ium TFSI (1.8580

g, 3.5225 mmol) was held at reflux under nitrogen for 24 h. After it had cooled to room temperature, the mixture was filtered and the solid was washed with acetonitrile, DCM, and dried on the filter. The precipitate was dissolved in 30 mL of boiling water, while a separate aqueous solution of LiTFSI (1.1 g, 4.2 mmol) in 10 mL of water was made. The aqueous solution of the precipitate was filtered and the two solutions were combined and allowed to cool to room temperature. The water was decanted and the remaining material was triturated with water (x3) and collected. After complete removal of solvent in vacuum the material was collected as a yellow solid: 2.90 g (91%); the precipitate was purified via recrystallization from water-acetone three times (product remained a yellow solid) 1.43 g (45%), mp 116.4–118.8 °C. ^1H NMR (500 MHz, DMSO) δ 9.49 (m, 8H), 8.73 (m, 8H), 7.61 (m, 8H), 7.54–7.41 (m, 6H), 7.03 (d, $J = 9$ Hz, 4H), 5.96 (s, 4H), 5.86 (s, 4H), 4.00 (t, $J = 6$ Hz, 4H), 1.85–1.72 (m, 4H), 1.61–1.51 (m, 2H). ^{13}C NMR (126 MHz, DMSO) δ 160.11 (s), 149.85 (s), 149.66 (s), 146.13 (s), 145.85 (s), 134.51 (s), 131.26 (s), 129.98 (s), 129.73 (s), 129.36 (s), 127.70 (s), 127.63 (s), 126.19 (s), 119.94 (q, $J = 323$ Hz), 115.52 (s), 68.01 (s), 64.03 (s), 63.73 (s), 28.77 (s), 22.60 (s) (20 peaks expected and 19 peaks found, two peaks are believed to overlap at 126.19). High res MS: calc. for $\text{C}_{61}\text{H}_{52}\text{O}_{18}\text{F}_{24}\text{N}_8\text{S}_8$ $[\text{M}+\text{Na}]^+$: m/z 1919.0680; found: m/z 1919.0505 (error –9.12 ppm).

1',1'''-(decane-1,10-diyl)bis(1-methyl-[4,4'-bipyridine]-1,1'-dium) TFSI (9). 1-Methyl-[4,4'-bipyridin]-1-ium TFSI (6.10 g, 13.5 mmol) and 1,10 dibromodecane (1.64 g, 5.47 mmol) were combined in a round bottom flask, dissolved in acetonitrile (75 mL), and held at reflux under nitrogen for 12 h. The mixture was allowed to cool and the solid was collected on a glass frit and washed with cold acetonitrile followed by dichloromethane. The solid was dissolved in water and a separate solution of LiTFSI (4.01 g, 14.0 mmol) in water (10 mL) was made. The

two solutions were combined. The solid precipitate was collected and recrystallized from water to yield an off white product 6.53 g (75 %). Further purification was achieved via recrystallization from water-acetone, mp 93.2–94.4 °C. ¹H NMR (400 MHz, DMSO-*d*₆) δ 9.32 (d, *J* = 7 Hz, 4H), 9.24 (d, *J* = 7 Hz, 4H), 8.74 – 8.69 (m, 8H), 4.63 (t, *J* = 8 Hz, 4H), 4.40 (s, 6H), 1.94 (s, 4H), 1.40–1.18 (m, 12H). ¹³C NMR (101 MHz, DMSO-*d*₆) δ 149.03, 148.62, 147.04, 146.15, 126.95, 126.49, 119.89 (q, *J* = 323 Hz), 61.37, 48.46, 31.24, 29.28, 28.90, 25.98 (13 signals expected and 13 signals found). High res MS: calc. for C₄₀H₄₂N₈O₁₆S₈F₂₄ [M - TFSI]⁺: m/z 1322.0923; found: m/z 1322.0839 (error 6.4 ppm)

1,1'-Bis(*p*-bromobenzyl)-[4,4'-bipyridine]-1,1'-dium TFSI (11). General procedure 2 was used to produce a white solid, 4.2173 g (95%), mp 153.6–155.9 °C, using 4,4'-dipyridyl (0.6551 g, 4.19 mmol), *p*-bromobenzyl bromide (2.81 g, 11.2 mmol), acetonitrile (50 mL) and LiTFSI (3.00 g, 10.4 mmol) in 10 mL of water. ¹H NMR (400 MHz, DMSO-*d*₆) δ 9.44 (d, *J* = 7 Hz, 4H), 8.69 (d, *J* = 7 Hz, 4H), 7.66 (d, *J* = 8 Hz, 4H), 7.54 (d, *J* = 8 Hz, 4H), 5.88 (s, 4H). ¹³C NMR (101 MHz, DMSO-*d*₆) δ 149.74 (s), 146.17 (s), 133.70 (s), 132.62 (s), 131.65 (s), 127.64 (s), 123.52 (s), 119.89 (q, *J* = 323 Hz), 63.19 (s) (9 signals expected and 9 signals found). High res MS +1 peak: calc. for C₂₈H₂₀Br₂O₈N₄S₄F₁₂ [M+NH₄]⁺: m/z 1071.8677; found: m/z 1071.8676 (error 0.09 ppm).

1,1'-Bis(*p*-(isopropoxycarbonyl)benzyl)-[4,4'-bipyridine]-1,1'-dium TFSI (12). General procedure 2 was used to produce a white solid, 2.65 g (77%), mp 149.9–151.3 °C, using 4,4'-dipyridyl (0.50 g, 3.2 mmol), isopropyl *p*-(iodomethyl)benzoate (2.50 g, 8.22 mmol), acetonitrile (20 mL) and LiTFSI (2.39 g, 8.32 mmol) in 10 mL water. ¹H NMR (400 MHz, DMSO-*d*₆) δ 9.44 (d, *J* = 7 Hz, 4H), 8.71 (d, *J* = 7 Hz, 4H), 7.98 (d, *J* = 8 Hz, 4H), 7.67 (d, *J* = 8 Hz, 4H), 5.99 (s, 4H), 5.10 (hept, *J* = 6 Hz, 2H), 1.28 (d, *J* = 6 Hz, 12H). ¹³C NMR (101 MHz, DMSO-*d*₆) δ

165.05 (s), 149.75 (s), 146.37 (s), 139.15 (s), 131.57 (s), 130.28 (s), 129.60 (s), 127.66 (s), 119.9 (q, $J = 323$ Hz), 68.94 (s), 63.37 (s), 22.00 (s) (12 signals expected and 12 signals found). High res MS calc. for $C_{36}H_{34}O_{12}N_4S_4F_{12}$ $[M+NH_4]^+$: m/z 1088.1203; found: m/z 1088.1213 (error – 0.92 ppm).

1,1'-Bis((perfluorophenyl)methyl)-[4,4'-bipyridine]-1,1'-dium TFSI (13). General procedure 1 was used to produce a white solid, 4.88 g (99%), mp 166.5–167.9 °C, using 4,4'-dipyridyl (0.7161 g, 4.585 mmol), 2,3,4,5,6-pentafluorobenzylbromide (2.0 mL, 13 mmol), acetonitrile (20 mL), and LiTFSI (3.29 g, 11.5 mmol) in 10 mL water. 1H NMR (500 MHz, DMSO- d_6) δ 9.38 (d, $J = 6.9$ Hz, 4H), 8.75 (d, $J = 7.1$ Hz, 4H), 6.21 (s, 4H). ^{13}C NMR (126 MHz, DMSO- d_6) δ 150.13 (s), 146.70 (s), 146.09 (br d, $J = 255$ Hz), 142.25 (br d, $J = 255$ Hz), 137.71 (dt, $J = 252$, 13 Hz), 127.66 (s), 119.9 (q, $J = 323$ Hz), 107.87 (tt, $J = 8$, 4 Hz), 51.99 (s) (9 signals expected and 9 signals found). High res MS: calc. for $C_{14}H_7F_{11}N_2O_4S_2$ $[M - TFSI]^+$: m/z 260.0493; found: m/z 260.0492 (error 0.4 ppm).

REFERENCES

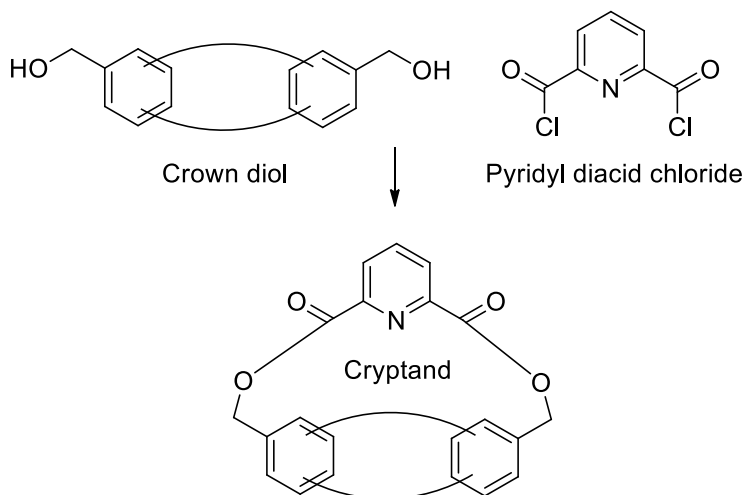
- (1) Pederson, A. M. P.; Ward, E. M.; Schoonover, D. V.; Slebodnick, C.; Gibson, H. W. *J. Org. Chem.* **2008**, *73*, 9094-9101.
- (2) Niu, Z.; Huang, F.; Gibson, H. W. *J. Am. Chem. Soc.* **2011**, *133*, 2836-2839.
- (3) Niu, Z.; Slebodnick, C.; Schoonover, D.; Azurmendi, H.; Harich, K.; Gibson, H. W. *Org. Lett.* **2011**, *13*, 3992-3995.
- (4) Niu, Z.; Slebodnick, C.; Huang, F.; Azurmendi, H.; Gibson, H. W. *Tetrahedron Lett.* **2011**, *52*, 6379-6382.
- (5) Niu, Z.; Slebodnick, C.; Bonrad, K.; Huang, F.; Gibson, H. W. *Org. Lett.* **2011**, *13*, 2872-2875.
- (6) He, C.; Shi, Z.; Zhou, Q.; Li, S.; Li, N.; Huang, F. *J. Org. Chem.* **2008**, *73*, 5872-5880.
- (7) Bryant, W. S.; Jones, J. W.; Mason, P. E.; Guzei, I.; Rheingold, A. L.; Fronczek, F. R.; Nagvekar, D. S.; Gibson, H. W. *Org. Lett.* **1999**, *1*, 1001-1004.

- (8) Huang, F.; Switek, K. A.; Zakharov, L. N.; Fronczek, F. R.; Slobodnick, C.; Lam, M.; Golen, J. A.; Bryant, W. S.; Mason, P. E.; Rheingold, A. L.; Ashraf-Khorassani, M.; Gibson, H. W. *J. Org. Chem.* **2005**, *70*, 3231-3241.
- (9) Greaves, T. L.; Drummond, C. J. *Chem. Rev.* **2015**, *115*, 11379-11448.
- (10) Greaves, T. L.; Drummond, C. J. *Chem. Soc. Rev.* **2013**, *42*, 1096-1120.
- (11) Gibson, H. W.; Wang, H.; Slobodnick, C.; Merola, J.; Kassel, W. S.; Rheingold, A. L. *J. Org. Chem.* **2007**, *72*, 3381-3393.
- (12) Huang, F.; Slobodnick, C.; Mahan, E. J.; Gibson, H. W. *Tetrahedron* **2007**, *63*, 2875-2881.
- (13) Pederson, A. M. P.; Vctor, R. C.; Rouser, M. A.; Huang, F.; Slobodnick, C.; Schoonover, D. V.; Gibson, H. W. *J. Org. Chem.* **2008**, *73*, 5570-5573.
- (14) Gibson, H. W.; Farcas, A.; Jones, J. W.; Ge, Z.; Huang, F.; Vergne, M.; Hercules, D. M. *J. Polym. Sci., Part A: Polym. Chem.* **2009**, *47*, 3518-3543.
- (15) Huang, F.; Nagvekar, D. S.; Zhou, X.; Gibson, H. W. *Macromolecules* **2007**, *40*, 3561-3567.
- (16) Huang, F.; Gibson, H. W. *Chem. Commun.* **2005**, 1696-1698.
- (17) Huang, F.; Guzei, I. A.; Jones, J. W.; Gibson, H. W. *Chem. Commun.* **2005**, 1693-1695.
- (18) Tang, B.; Yang, H.-M.; Hu, W.-J.; Ma, M.-L.; Liu, Y. A.; Li, J.-S.; Jiang, B.; Wen, K. *Eur. J. Org. Chem.* **2014**, *2014*, 6925-6934.
- (19) Xu, J.-F.; Huang, Z.; Chen, L.; Qin, B.; Song, Q.; Wang, Z.; Zhang, X. *ACS Macro Lett.* **2015**, *4*, 1410-1414.
- (20) Schalley, C. A.; Silva, G.; Nising, C. F.; Linnartz, P. *Helv. Chim. Acta* **2002**, *85*, 1578-1596.
- (21) Jordão, N.; Cabrita, L.; Pina, F.; Branco, L. C. *Chem. Eur. J.* **2014**, *20*, 3982-3988.
- (22) Pescatori, L.; Arduini, A.; Pochini, A.; Secchi, A.; Massera, C.; Ugozzoli, F. *Org. Biomol. Chem.* **2009**, *7*, 3698-3708.
- (23) Albrecht, M.; Yulikov, M.; Kohn, T.; Jeschke, G.; Adams, J.; Schmidt, A. *J. Mater. Chem.* **2010**, *20*, 3025-3034.

Chapter 5

CHELIDAMIC ACID DERIVATIVES

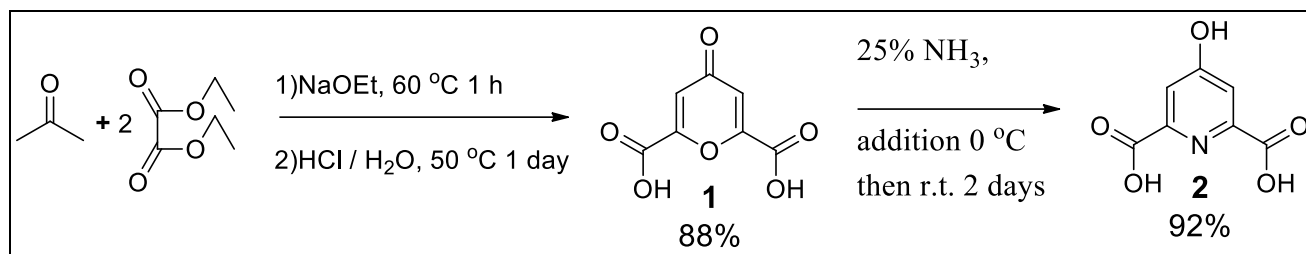
INTRODUCTION



Scheme 5.1. Typical route to pyridyl cryptands.

Although pyridyl cryptands are known and studied for their high binding constants with paraquats and diquats, without a synthetic “handle” on the molecules, this class of compounds is of little practical use. These compounds are typically produced via crown diols of varying size and a pyridine-2,6-diacid chloride. A functional group (“handle”) attached to the crown ether component leads to complications. However, if the functional group is placed on the pyridine component, some of these difficulties are removed. For this reason, chelidamic acid (**2**) and its derivatives have been studied in this chapter as presursors for functionalized cryptands. Compound **2** contains a hydroxyl group at the 4-position, which is ideal for functionalization, given the wide range of reactions available for hydroxyl moieties. Substitution at the 4-position provides a location that should have little effect on how the host and guest associate. Conveniently, a high yielding literature procedure exists for **2**; ¹ chelidonic acid (**1**) is

synthesized from acetone and diethyl oxalate via aldol condensations and converted to **2** by reaction with ammonia (**Scheme 5.2**).



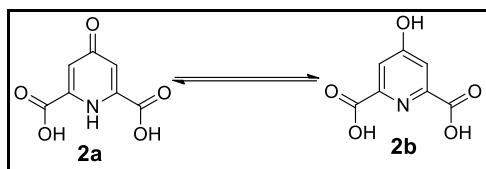
Scheme 5.2. Synthesis of Chelidamic Acid.

RESULTS AND DISCUSSION

Although **2** already contains the phenolic moiety, this would interfere with the esterification/cyclization step in the synthesis of cryptand. For this reason, other functionalities must be explored. **Scheme 5.3** shows the early directions explored using chelidamic acid.

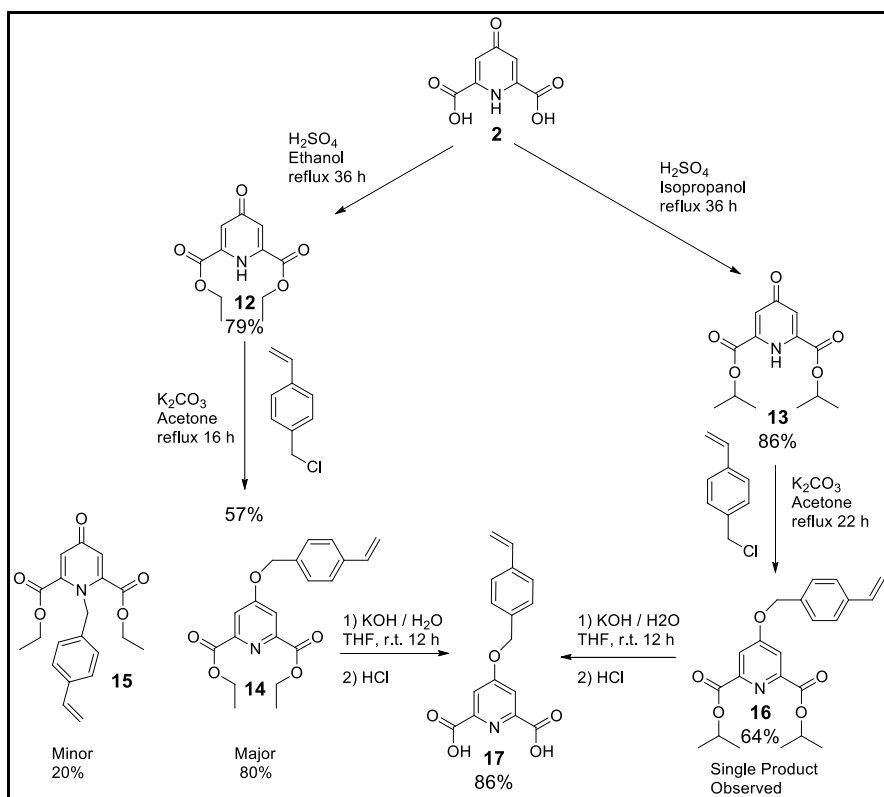
often lack the stability associated with their saturated counterparts. Therefore, attempts were made with palladium on carbon (10%) and hydrogen gas to reduce **5**; unfortunately, these attempts to produce **8** were unsuccessful. **5** could, however, be saponified by potassium hydroxide and water, but in doing so the alkyl halide was converted to an alcohol, i.e., **6** in a yield of 71%. Attempts to convert **6** to the diacid chloride **7** with thionyl chloride were, however, unsuccessful. It is hypothesized before the alcohol is converted to the chloride, the acid chloride is formed and reacts with the alcohol to form an ester. As acid chlorides are problematic to purify **7** was abandoned.

Alkylation of chelidamic was explored as an alternative to Heck coupling. **10** was synthesized via esterification of **2** with thionyl chloride and methanol to produce **9** in 82% yield. **9** was then alkylated using 5-bromopent-1-ene to provide **10** as a mixture of N and O alkylated products in a quantitative yield. Although **11** has been reported³ using a synthetic scheme slightly different than shown here, characterization and melting point of the compound were not provided. Instead a downstream product was characterized and reported after recrystallization; it is likely this was done because the synthesis resulted in a mixture of N and O alkylated products. The two different possibilities for alkylation arise from the tautomers **2a** and **2b** (Scheme 5.4). In **2a**, the ketone form, the nitrogen is available to react; in **2b**, the phenolic form, the oxygen is available to react. Although TLC indicated that the two isomeric compounds could be separated, inspection of the reaction showed an inefficiency in going from **9** to **10**, yield loss and increased effort in terms of purification. For these reasons, this synthetic methodology was abandoned.



Scheme 5.4. Tautomers of **2**.

To establish a synthetic route which would yield only the desired O-alkylated products, it was reasoned that if enough steric bulk could be placed around the nitrogen atom in chelidamic esters, N-alkylation could be stopped altogether. To test this theory, the ethyl ester **12** and isopropyl ester **13** were synthesized and reacted with *p*-vinylbenzyl chloride to determine if N alkylation could be halted, **Scheme 5.5**.



Scheme 5.5. N- vs. O-alkylation in the synthesis of styrene chelidamic acid derivative **17**.

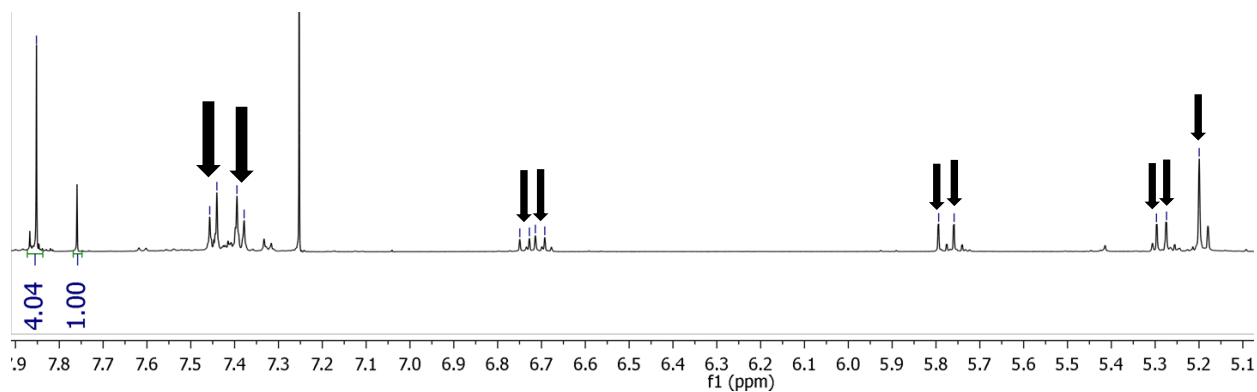


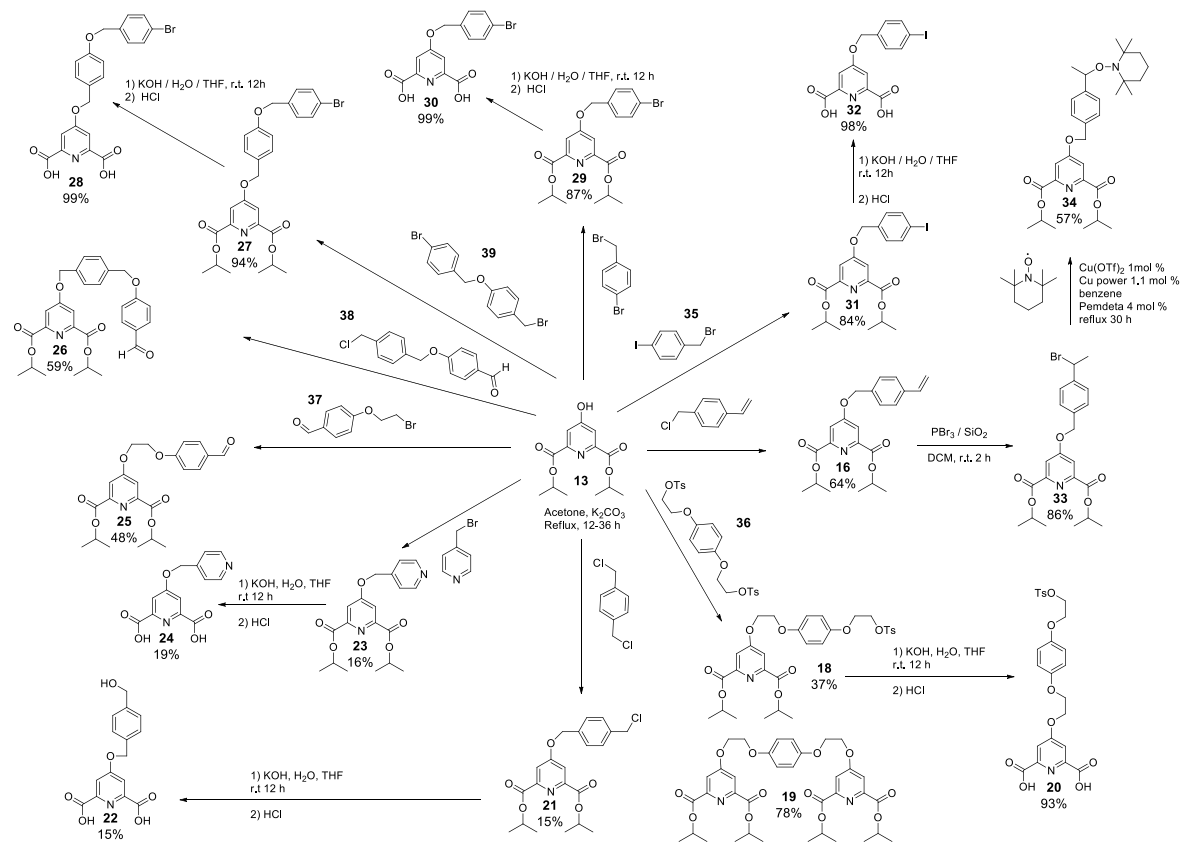
Figure 5.1. ^1H NMR spectrum (500 MHz, CDCl_3 , 23 $^\circ\text{C}$) of crude reaction mixture of **12** with *p*-vinylbenzyl chloride after removal of unreacted chloride. O-alkylated peaks contain an arrow and dash above them; approximately 80% O-alkylation (**14**) and 20% N-alkylation (**15**).

The reaction of ethyl ester **12** with *p*-vinylbenzyl chloride gave a mixture of **14** and **15** and as with **9**, O-alkylation was the major process (80:20, **Figure 5.1**). Use of isopropyl ester **13**, however, gave surprisingly different results; upon reaction with *p*-vinylbenzyl chloride: a single product, **16**, in a yield of 64%. Formation of a single product drastically reduces isolation time and difficulty, allowing for a simplified purification procedure. Purification of **16** was accomplished by filtering the reaction mixture through diatomaceous earth, solvent evaporation, and then titration with hexanes.

Additionally, the synthesis of **9**, **12**, and **13** provided an opportunity to pursue a second goal: develop a synthetic route to a diester which does not require the sometimes expensive and toxic chemical, thionyl chloride. It should be noted that acid catalyzed (sulfuric acid or *p*-toluenesulfonic acid) esterifications to produce **9** gave very low yields. Acid catalyzed esterification with sulfuric acid produced **12** and **13** in 79% and 86% yields, respectively. Yields for **9** using thionyl chloride were 87%.

To demonstrate the versatility of **13**, **Scheme 5.6** shows a wide range of products that have been synthesized from **13** with only O-alkylation being observed. These feedstock

molecules are capable of either directly undergoing saponification or reacted further to form more complicated precursors. Attempts were made to produce feedstock molecules (for the synthesis of cryptands) falling into the following categories: covalent monomers, initiators, chain terminators, leaving groups, aryl halides and Host-Guest monomer feedstocks.



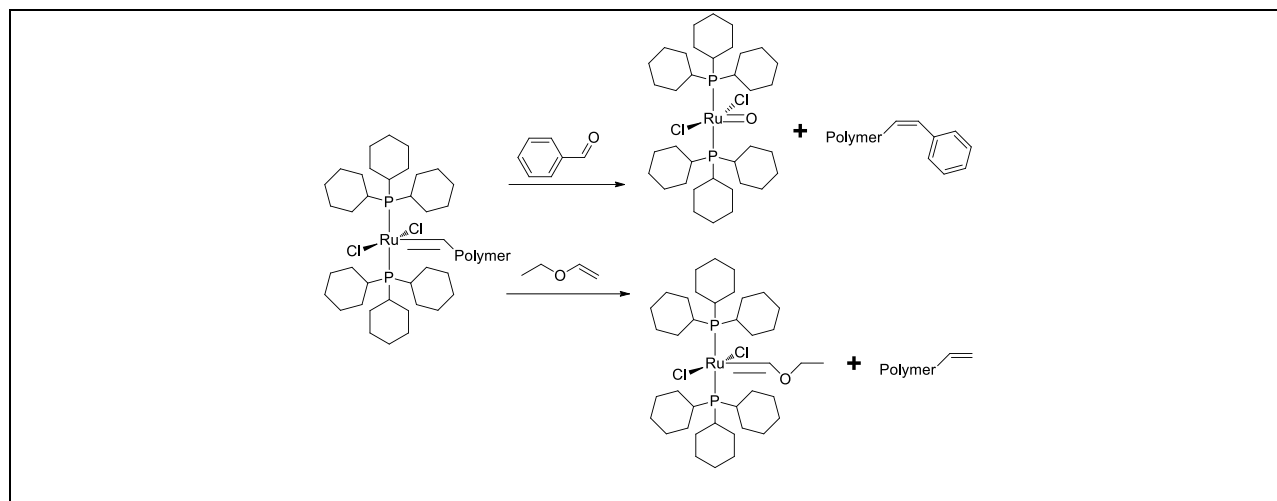
Scheme 5.6. Versatility of **13** as a feedstock chemical for chelidamic derivatives.

Beginning with the covalent monomer category, a single compound falls into this grouping, **16**, as seen in **Schemes 5.5** and **5.6**. It is anticipated that the styrene functionality of **16** would be capable of undergoing anionic, cationic, and free radical polymerizations, given that the resulting cryptand can survive the reaction conditions.

In addition to **16** serving as a feedstock molecule for a styrene cryptand, it also acts as the starting compound for the synthesis of an initiator. Olefins can be directly converted to either

secondary or tertiary bromides by reaction with PBr_3 in the presence of silica.⁴ Taking this into account, **16** was directly converted to **33** in 86% yield. Such secondary bromides are well known for their ability to initiate chain polymerizations.^{5,6} However, hydrolysis of the halide as observed in the synthesis of **6** and **22** would result in the conversion of the secondary bromide to a secondary alcohol. For this reason, **33** was converted to **34** in 57% yield using a procedure developed by Matyjaszewski et al. in which alkyl bromides can be directly converted to TEMPO derivatives in the presence of $\text{Cu}(\text{OTf})_2$.⁷ **34** provides an intermediate for a cryptand initiator which should not be affected by basic conditions during saponification.

Regarding polymerization, ROMP has advantages over cationic, anionic, and free radical polymerizations in that the conditions for these reactions are very mild; typically, DCM as a solvent at room temperature and Grubbs 1st generation catalyst.⁸⁻¹⁰ As cryptands contain ester functional groups, ROMP provides a mild reaction attachment to polymers. A ROMP polymerization can be quenched with either a vinyl ether or an aldehyde. Quenching with a vinyl ether terminates the polymer with a vinyl group, while adding the ethoxy group to the catalyst, thus rendering it incapable of continuing the polymerization. Quenching with an aldehyde terminates the polymer via substitution of the aldehyde while oxidizing the Grubbs catalyst, once again rendering it incapable of initiation.⁹⁻¹¹ The process of ROMP termination is shown in **Scheme 5.7**. Benzaldehydes **25** and **26** were synthesized from **13** with **37** and **38**, in 48% and 59% yields respectively, to provide ROMP chain terminators.



Scheme 5.7. ROMP quenching via aldehyde and ethylvinyl ether.

As previously mentioned the alkyl halide derivatives were incapable of standing up to the reaction conditions of saponification, which gave way to the isolation of **6** and **22** instead of the desired alkyl chlorides. To use these feedstock molecules for the synthesis of cryptands, saponification is required; thus an alternative approach was needed to produce a cryptand containing a leaving group. **18** was synthesized in 37% yield with a tosylate functionality, which was retained during saponification with potassium hydroxide to yield **20** in 93% yield. **20** provides a unique vantage point in that even if conversion of **20** to the acid chloride converts the tosylate group to a chloride, a leaving group will still be present in the molecule.

Initially the target molecule of the reaction between **13** and **36** at 2:1 stoichiometry was **19**, but **18** was isolated as a side product. The reaction of **13** (2 eq.) with **36** (1 eq.) in the presence of potassium carbonate was executed once using acetonitrile as the solvent and once using acetone. Acetone gave a 4:1 ratio of **18:19**, but with acetonitrile the product ratio was better than 1:99 **18:19**. Acetone provides a retarded reaction speed over acetonitrile, in which difunctional leaving groups such as **36** or 1,4-bis(chloromethyl)benzene may singly add to **13**, allowing control over mono- or di-additions. Without solvent control, introduction of leaving

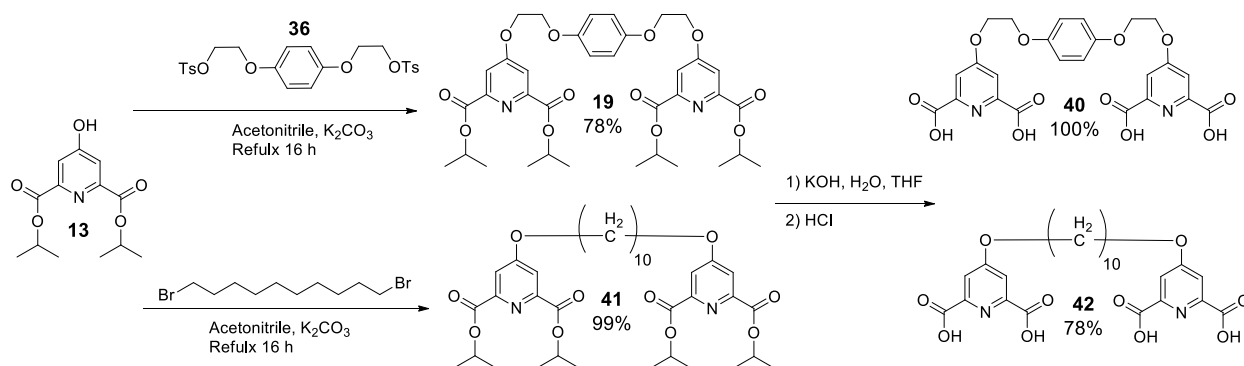
groups on **13** would require either a large excess of a difunctional component (such as **36**) or the use of unsymmetrical compounds with staged functionalities.

Aryl halides have a wide range of uses thanks to the recent development of coupling reactions, such as Heck, Suzuki, Ullman, and Sonogashira to just name a few. Given the versatility of aryl halides, several differing feedstocks were developed. **28** and **30** were prepared from aryl bromides. **30**, formed in a yield of 99%, was constructed to have the aryl bromide directly attached to the chelidamic acid portion of the molecule. It was envisioned that in some situations a spacer between the chelidamic acid portion of the molecule and aryl bromide could be advantageous; an example would be the formation of a supramolecular polymer. To satisfy this desire, **28** was synthesized with a linkage between the chelidamic acid portion of the molecule and aryl bromide. The last feedstock molecule for this grouping is **32**, which contains an aryl iodide. Although costlier than its bromide counterpart, the aryl iodide was synthesized to meet the demand of any problematic coupling reactions. Iodides are typically more reactive than bromides in palladium catalyzed coupling reactions.¹²⁻¹⁴

Host-guest monomers for supramolecular polymers fall into two separate types: A-B monomers and A-A/B-B monomers. A-B monomers involve tethering of the host to a guest; the monomer then self-associates to form a polymeric structure. A-A/B-B monomers are two separate difunctional monomers. Mixing A-A/B-B monomers at 1:1 stoichiometry is used to provide polymeric structures. Considering A-B monomers, cryptands associate very well with diquats, paraquats and to a lesser extent with pyridinium salts. Since diquats require an extensive synthetic scheme to build in functionality and both diquats and paraquats degrade in even weak bases, tethering either to **13** would be fruitless, since neither could survive the reaction conditions for saponification. The pyridinium cation, however, offers a reasonable

compromise. Although lower binding with cryptand systems, a direct synthesis can be formulated and the moiety will withstand saponification. **23** contains a pyridine ring that once reacted with acid will form a pyridinium cation capable of undergoing basic saponification.

Given the recent development of dibenzo-30-crown-10- and bis(*m*-phenylene)-32-crown-10-cryptand templation procedures (Chapter 3), the approach to a difunctional A–A monomer was to develop difunctional chelidamic acid derivatives for single pot, double cyclization. **Scheme 5.8** provides structures and synthetic schemes for **40** and **42**, each containing two chelidamic motifs tethered by different linkages.



Scheme 5.8. Difunctional A-A monomer precursors.

CONCLUSIONS

Here we have shown that chelidamic acid (**2**) is capable of producing a wealth of compounds to be used as feedstock molecules for cryptands. In this chapter, 27 new compounds were synthesized and fully characterized. The first obstacle overcome was N- vs. O-alkylation; it was found that by using the diisopropyl ester **13** as a precursor, N-alkylation could be stopped.

Additionally, **13** was made in high yield by acid catalysis, while avoiding the use of thionyl chloride. Next it was found that acetone could be used over acetonitrile to obtain compounds containing a leaving group in an economical fashion from difunctional electrophiles. From **13** a wide range of feedstock molecules were synthesized. Attempts made to produce feedstock molecules falling into the following categories were successful: covalent monomers (**16**), initiators (**34**), chain terminators (**25** and **26**), leaving groups (**16**, **18**, **20**, **21**), aryl halides (**27**, **28**, **29**, **30**, **31**, **32**), and A-B Host-Guest monomers (**19**, **23**, **40**, **41**, **42**).

EXPERIMENTAL

Measurements: ^1H -NMR spectra were obtained on JEOL ECLIPSE-500, BRUKER-500, and AGILENT-NMR-vnmrs400 spectrometers. ^{13}C -NMR spectra were collected at 125 MHz and 101 MHz on these instruments. HR-MS were obtained using an Agilent LC-ESI-TOF system. Reagents were purchased and used as received without further purification. Compounds **1**,¹ **2**,¹ **3**,² **9**,¹⁵ **10**,³ **12**,¹⁶ **35**,¹⁷ **36**,¹⁸ **37**,¹⁹ and **38**²⁰ were made in accordance with literature procedures; similar yields were achieved.

General procedure 1: (E)-4-(p-hydroxymethylstyryl)pyridine-2,6-dicarboxylic acid (6). **5** (187.8 mg, 0.5431 mmol) was dissolved in THF (50 mL) and a solution of 10 wt. % KOH (30 mL) in water was added to the solution while stirring. The solution was stirred for 12 h and THF was removed by rotary evaporation. The remaining aqueous solution was acidified to pH 1 and the solid precipitate was collected by filtration: 115.6 mg (71 %), mp 85.6–91.4 °C. ^1H NMR (500 MHz, DMSO- d_6) δ 8.40 (s, 2H), 7.78 (d, J = 16 Hz, 1H), 7.69 (d, J = 8 Hz, 2H), 7.46 (d, J = 16 Hz, 1H), 7.37 (d, J = 7 Hz, 2H), 4.53 (s, 2H). ^{13}C NMR (126 MHz, DMSO- d_6) δ 166.15 (s),

149.28 (s), 148.33 (s), 144.35 (s), 135.64 (s), 134.93 (s), 127.84 (s), 127.37 (s), 124.60 (d, $J = 8$ Hz), 63.18 (s). (11 peaks expected and 11 peaks found). HR MS: calc. for $C_{16}H_{13}O_5N$ $[M + H]^+$: m/z 300.0866; found: m/z 300.0872 (error -2 ppm).

(E)-Dimethyl 4-(2'-ethoxyvinyl)pyridine-2,6-dicarboxylate (4). To a flask containing DMF (100 mL) was added $Pd(OAc)_2$ (57.5 mg, 0.256 mmol), 4-bromocheilidamic methyl ester (2.16 g, 7.88 mmol), K_2CO_3 (1.30 g, 9.41 mmol), PPh_3 (156 mg, 0.595 mmol), and ethyl vinyl ether (1.0 mL, 10 mmol). The reaction mixture was stirred under nitrogen at 90 °C for 19 h. Solvent was removed by rotary evaporation and the crude material was dissolved in chloroform. The solution was washed with 1 M HCl (x 3) and water (x3), followed by drying over sodium sulfate. Filtration and removal of the solvent provided a material which was purified by passing through a silica column, eluting with hexanes:ethyl acetate 1:1 to give a mixture of *cis* and *trans* isomers; 0.74 g (35%), mp: 48.2–55.7 °C. 1H NMR (500 MHz, $CDCl_3$) δ 8.40 (s, 2H), 8.04 (s, 2H), 7.39 (d, $J = 13$ Hz, 1H), 6.54 (d, $J = 7$ Hz, 1H), 5.82 (d, $J = 13$ Hz, 1H), 5.31 (d, $J = 7$ Hz, 1H), 4.46 (qd, $J = 7, 1$ Hz, 8H), 4.11 (qd, $J = 7, 4$ Hz, 2H), 3.99 (q, $J = 7.0$ Hz, 2H), 1.45 (t, $J = 7$ Hz, 16H), 1.37 (t, $J = 7$ Hz, 3H). ^{13}C NMR (126 MHz, $CDCl_3$) δ 165.37 (s), 165.22 (s), 153.56 (s), 152.85 (s), 148.83 (s), 148.66 (s), 147.75 (s), 146.18 (s), 126.36 (s), 123.29 (s), 102.87 (s), 102.16 (s), 70.52 (s), 66.79 (s), 62.37 (s), 62.22 (s), 15.46 (s), 14.80 (s). (18 peaks expected and 18 found). HR MS: calc. for $C_{15}H_{19}NO_5$ $[2M + Na]^+$: m/z 609.2419; found: m/z 609.2364 (error -8.9 ppm). 1H NMR Cis- 1H NMR (500 MHz, $CDCl_3$) δ 8.04 (s, 2H), 5.82 (d, $J = 13$ Hz, 1H), 5.31 (d, $J = 6.9$ Hz, 1H), 4.46 (qd, $J = 7, 1$ Hz, 6H), 3.99 (q, $J = 7$ Hz, 2H), 1.37 (t, $J = 7$ Hz, 3H). 1H NMR Trans- 1H NMR (500 MHz, $CDCl_3$) δ 8.40 (s, 2H), 7.39 (d, $J = 13$ Hz, 1H), 6.54 (d, $J = 7$ Hz, 1H), 4.46 (qd, $J = 7, 1$ Hz, 6H), 4.11 (qd, $J = 7, 4$ Hz, 2H), 1.45 (t, $J = 7$ Hz, 3H).

(E)-Dimethyl 4-(*p*-chloromethylstyryl)pyridine-2,6-dicarboxylate (5). Dimethyl 4-bromopyridine-2,6-dicarboxylate (0.83g, 3.0 mmol), palladium acetate (22.2 mg, 0.0989 mmol), triphenylphosphine (63.5 mg, 0.242 mmol), and sodium carbonate (0.45 g, 4.2 mmol) were added to a small flask containing a magnetic stir bar. The solvent, DMF (80 mL), and *p*-vinylbenzyl chloride (0.60 mL, 4.3 mmol) was added to the flask once an oil bath had been prepared at 90 °C. The reaction mixture was allowed to stir under heat and nitrogen for 60 h. A portion of solvent was removed by rotary evaporation and the remaining mixture was dissolved in chloroform; the mixture was washed with 1M HCl (x2), water (x3), and dried over Na₂SO₄. After filtration and evaporation of the solvent, a minimal amount of chloroform was used to dissolve the product and it was precipitated into a small amount of ether (~100 times the volume of chloroform). The solution was filtered: a white yellow tinted solid, 146.5 mg (14%), mp 175.0–177.0 (dec). ¹H NMR (400 MHz, CDCl₃) δ 8.38 (s, 2H), 7.62 – 7.41 (m, 5H), 7.14 (d, *J* = 16 Hz, 1H), 4.62 (s, 2H), 4.05 (s, 6H). ¹³C NMR (126 MHz, CDCl₃) δ 165.38 (s), 148.85 (s), 147.59 (s), 138.78 (s), 135.68 (s), 135.11 (s), 129.34 (s), 128.98 (s), 127.77 (s), 125.05 (s), 53.38 (s), 45.83 (s). (12 peaks expected and 12 peaks found) HR MS: calc. for C₁₈H₁₆NO₄Cl [M + H]⁺: m/z 346.0841; found: m/z 346.0860 (error 5.7 ppm).

Attempted synthesis of (E)-4-(*p*-chloromethylstyryl)pyridine-2,6-dicarboxylic acid chloride (7). (E)-4-(*p*-hydroxymethylstyryl)pyridine-2,6-dicarboxylic acid (108.1 mg, 0.3612 mmol) and thionyl chloride (5 mL, 0.07 mol) in a round bottom flask under nitrogen were stirred at reflux for 21 h. Thionyl chloride was removed by evaporation. Product appeared as a dark discolored “gunk” which resisted being dissolved in the solvents DCM, chloroform and acetone.

Attempted synthesis of Dimethyl 4-(*p*-chloromethylphenethyl)pyridine-2,6-dicarboxylate (8). (E)-Dimethyl 4-(*p*-chloromethylstyryl)pyridine-2,6-dicarboxylate (55.3 mg 0.160 mmol)

was dissolved in chloroform (100 mL) and 10% Pd/C(10.0 mg 0.00940 mmol) was added. The mixture was placed under hydrogen gas (65 psi) and shaken for 24 h. The solution was filtered to remove the catalyst and solvent was removed by rotary evaporation (TLC and ^1H NMR revealed only starting materials).

Chelidamic Isopropyl ester (13). To a flask containing isopropanol (200 mL, 2.61 mol) was added sulfuric acid (0.20 mL, 3.8 mmol) and chelidamic acid (2.48 g, 13.5 mmol) with magnetic stirring. The solution was held at reflux under nitrogen for 36 h. Solvent was removed by rotary evaporation and the crude material was dissolved in chloroform, washed with 5% Na_2CO_3 once (1.1 eq. to sulfuric acid added), 2% NaHCO_3 (x4), water (x2), saturated NaCl (x1), and dried over sodium sulfate. Filtration and removal of the solvent provided the desired product: 3.11 g (86%), mp 128.7-129.8 °C; lit mp 145–146 °C.¹⁵ ^1H NMR (500 MHz, CDCl_3) δ 7.11 (s, 2H), 5.33–5.24 (m, 2H), 1.40 (d, $J = 6$ Hz, 12H). ^{13}C NMR (126 MHz, CDCl_3) δ 181.06 (s), 161.07 (s), 136.91 (s), 120.55 (s), 72.05 (s), 21.73 (s). (6 peaks expected and 6 peaks found). HR MS: calc. for $\text{C}_{13}\text{H}_{17}\text{O}_5\text{N}$ $[\text{M}+\text{H}]^+$: m/z 268.1179; found: m/z 268.1193 (error 5.2 ppm)

Diethyl 4-(*p*-vinylbenzyloxy)pyridine-2,6-dicarboxylate (14) and minor product diethyl 4-oxo-1-(*p*-vinylbenzyl)-1,4-dihydropyridine-2,6-dicarboxylate (15). To a flask containing acetone (100 mL) with a magnetic stir bar was added diethyl 4-hydroxypyridine-2,6-dicarboxylate (**12**, 1.64 g, 6.86 mmol), *p*-vinylbenzyl chloride (1.5 mL, 11 mmol) and potassium carbonate (1.44 g, 10.4 mmol). The mixture was held at reflux under nitrogen for 16 h, after which solvent was removed by rotary evaporation and the crude material dissolved in chloroform and washed with 1 M HCl (x3), saturated NaCl (x3), and dried over MgSO_4 . The solution was filtered and solvent removed by rotary evaporation to give the desired product; 2.18 g, (57 %), white solid, mp 64.2–70.6 °C. ^1H NMR (500 MHz, CDCl_3) δ 7.85 (s, 2H), 7.45 (d, $J = 8$ Hz,

2H), 7.39 (d, $J = 8$ Hz, 2H), 6.72 (dd, $J = 18, 11$ Hz, 1H), 5.78 (d, $J = 18$ Hz, 1H), 5.29 (d, $J = 11$ Hz, 1H), 5.20 (s, 2H), 4.46 (q, $J = 7$ Hz, 4H), 1.44 (t, $J = 7$ Hz, 6H). ^{13}C NMR (126 MHz, CDCl_3) δ 166.59 (s), 164.71 (s), 150.29 (s), 138.10 (s), 136.18 (s), 134.14 (s), 128.00 (s), 126.66 (s), 114.63 (s), 114.33 (s), 70.53 (s), 62.43 (s), 14.20 (s) (13 peaks expected and 26 peaks found total, 13 of which are attributed to O-alkylation and 13 to N-alkylation; only O-alkylated peaks are listed). HR MS: calc. for $\text{C}_{20}\text{H}_{21}\text{NO}_5$ $[\text{M}]^+$: m/z 356.1492; found: m/z 356.1463 (error 8.1 ppm)

Diisopropyl 4-(*p*-vinylbenzyloxy)pyridine-2,6-dicarboxylate (16). To a flask containing acetone (200 mL) was added *p*-vinylbenzyl chloride (7.0 mL, 50 mmol), chelidamic isopropyl ester (8.65 g, 32.4 mmol), and K_2CO_3 (7.4 g, 54 mmol). The mixture was held at reflux under nitrogen for 22 h with magnetic stirring. The mixture was filtered through celite p545 and solvent was removed by rotary evaporation. The crude material was triturated with hexanes and the remaining solid was collected: 7.98 g (64%), mp 96.2–98.1 °C. ^1H NMR (500 MHz, CDCl_3) δ 7.80 (s, 2H), 7.45 (d, $J = 8$ Hz, 2H), 7.39 (d, $J = 8$ Hz, 2H), 6.72 (dd, $J = 18, 11$ Hz, 1H), 5.78 (d, $J = 18$ Hz, 1H), 5.36–5.22 (m, 3H), 5.19 (s, 2H), 1.41 (d, $J = 6$ Hz, 12H). ^{13}C NMR (126 MHz, CDCl_3) δ 166.53 (s), 164.20 (s), 150.72 (s), 138.18 (s), 136.27 (s), 134.30 (s), 128.15 (s), 126.73 (s), 114.81 (s), 114.46 (s), 70.58 (s), 70.26 (s), 21.89 (s). (13 peaks expected and 13 peaks found). HR MS: calc. for $\text{C}_{22}\text{H}_{25}\text{NO}_5$ $[\text{M} + \text{H}]^+$: m/z 384.1805; found: m/z 384.1798 (error 2 ppm).

4-(*p*-vinylbenzyloxy)pyridine-2,6-dicarboxylic acid (17). General procedure 1 used with styrene chelidamic ester (**16**, 0.24 g, 0.63 mmol), THF (15 mL), and 10% wt. aqueous KOH (50 mL) to produce 0.16 g (86%), mp 140.2–144.2 °C. ^1H NMR (400 MHz, $\text{DMSO}-d_6$) δ 7.77 (s, 2H), 7.50 (d, $J = 8$ Hz, 2H), 7.44 (d, $J = 8$ Hz, 2H), 6.73 (dd, $J = 18, 11$ Hz, 1H), 5.84 (d, $J = 18$

Hz, 1H), 5.34 (s, 2H), 5.26 (d, $J = 11$ Hz, 1H). ^{13}C NMR (101 MHz, $\text{DMSO-}d_6$) δ 167.07 (s), 165.97 (s), 150.45 (s), 137.76 (s), 136.88 (s), 135.85 (s), 128.83 (s), 127.00 (s), 115.40 (s), 114.68 (s), 70.54 (s). HR MS: calc. for $\text{C}_{16}\text{H}_{13}\text{O}_5\text{N}$ $[\text{M} + \text{H}]^+$: m/z 300.0866; found: m/z 300.0864 (error 0.7 ppm).

Diisopropyl 4-(*p*-(2'-tosyloxyethoxy)phenoxyethoxy)pyridine-2,6-dicarboxylate (18). To a flask containing acetone (300 mL) was added the ditosylate (**36**, 3.33 g, 6.57 mmol), isopropyl ester chelidamic (**13**, 3.59 g, 13.4 mmol), and potassium carbonate (3.18 g, 23.0 mmol) with magnetic stirring under a stream of nitrogen. The reaction mixture was held at reflux for 24 h cooled to room temperature, filtered through Celite® p545 and the solvent was removed by rotary evaporation. The crude material was dissolved in DCM and washed with Na_2CO_3 (x2), saturated NaCl (x3), and dried over sodium sulfate. After filtration and removal of solvent, the material was purified by silica flash column chromatography eluting DCM to acetonitrile: 1.47 g (37%), a white solid **18:19** = 4:1, mp: 102.4–109.1 °C. ^1H NMR (500 MHz, CDCl_3) δ 7.84 (d, $J = 8$ Hz, 2H), 7.82 (s, 2H), 7.37 (d, $J = 8$ Hz, 2H), 6.86 (d, $J = 9$ Hz, 2H), 6.77 (d, $J = 9$ Hz, 2H), 5.32 (hept, $J = 6$ Hz, 2H), 4.53 – 4.46 (m, 2H), 4.39 – 4.35 (m, 2H), 4.35 – 4.32 (m, 2H), 4.16 – 4.10 (m, 2H), 2.48 (s, 3H), 1.45 (d, $J = 6$ Hz, 12H). ^{13}C NMR (126 MHz, CDCl_3) δ 166.50 (s), 164.11 (s), 152.97 (s), 152.76 (s), 150.68 (s), 144.92 (s), 132.96 (s), 129.85 (s), 128.03 (s), 115.84 (s), 115.69 (s), 114.14 (s), 70.17 (s), 68.17 (s), 67.29 (s), 66.70 (s), 66.25 (s), 21.81 (s), 21.66 (s) (19 peaks expected and 19 peaks found). HR MS: calc. for $\text{C}_{30}\text{H}_{35}\text{NO}_{10}\text{S}$ $[\text{M}+\text{H}]^+$: m/z 602.2055; found: m/z 602.2064 (error 1 ppm).

Tetraisopropyl 4,4'-(((1,4-phenylenebis(oxy))bis(ethane-2,1-diyl))bis(oxy))bis(pyridine-2,6-dicarboxylate) (19). To a flask containing acetonitrile (100 mL) was added the ditosylate (**36**, 5.78 g, 11.4 mmol), chelidamic isopropyl ester (**13**, 6.79 g, 25.4 mmol), and potassium carbonate

(5.85 g, 42.3 mmol) with magnetic stirring under a stream of nitrogen. The reaction mixture was held at reflux for 24 h. After cooling to room temperature the mixture was filtered through Celite® p545 and solvent was removed by rotary evaporation. The crude material was dissolved in DCM and washed with Na₂CO₃ (x2), saturated NaCl (x3), and dried over sodium sulfate. The product was obtained after filtration and removal of solvent: 6.21 g (78%), white solid, mp 193.1–195.4°C. ¹H NMR (500 MHz, CDCl₃) δ 7.81 (s, 4H), 6.89 (s, 4H), 5.30 (hept, *J* = 6 Hz, 4H), 4.52–4.46 (m, 4H), 4.37–4.32 (m, 4H), 1.43 (d, *J* = 6 Hz, 24H). ¹³C NMR (126 MHz, CDCl₃) δ 166.53 (s), 164.10 (s), 153.00 (s), 150.64 (s), 115.82 (s), 114.18 (s), 70.21 (s), 67.32 (s), 66.73 (s), 21.81 (s) (10 peaks expected and 10 peaks found). HR MS: calc. for C₃₆H₄₄N₂O₁₂ [M+H]⁺: m/z 697.2967; found: m/z 697.3000 (error 4.7 ppm).

4-(*p*-(2'-Tosyloxyethoxy)phenoxy)ethoxy)pyridine-2,6-dicarboxylic acid (20). General procedure 1 used with diisopropyl 4-(*p*-(2'-tosyloxyethoxy)phenoxyethoxy)pyridine-2,6-dicarboxylate (**18**, 0.2570 mg, 0.4271 mmol), 10% wt. KOH (20 mL), and THF (40 mL) to produce 0.2051 g (93%), mp: 103.8–107.3 °C. ¹H NMR (500 MHz, DMSO-*d*₆) δ 7.79 (d, *J* = 8 Hz, 2H), 7.76 (s, 2H), 7.47 (d, *J* = 8 Hz, 2H), 6.87 (d, *J* = 9 Hz, 2H), 6.77 (d, *J* = 9 Hz, 2H), 4.58 – 4.53 (m, 2H), 4.31 – 4.26 (m, 4H), 4.10 – 4.07 (m, 2H), 2.41 (s, 3H). ¹³C NMR (126 MHz, DMSO-*d*₆) δ 166.60 (s), 165.34 (s), 152.55 (s), 152.05 (s), 149.82 (s), 145.06 (s), 132.27 (s), 130.20 (s), 127.70 (s), 115.59 (s), 115.47 (s), 113.76 (s), 69.27 (s), 67.67 (s), 66.48 (s), 65.85 (s), 21.13 (s) (17 peaks expected and 17 peaks found). HR MS: calc. for C₂₄H₂₃NO₁₀S [M + H]⁺: m/z 518.1115; found: m/z 518.1077 (error 7.3 ppm).

Diisopropyl 4-(*p*-chloromethylbenzyloxy)pyridine-2,6-dicarboxylate (21). To a round bottom flask containing acetone (300 mL) was added α,α'-dichloro-*p*-xylene (3.57 g, 20.4 mmol) and K₂CO₃ (3.08 g, 22.3 mmol) with magnetic stirring. Chelidamic isopropyl ester (**13**, 0.91 g,

3.4 mmol) was dissolved in acetone and placed in an addition funnel attached to the reaction flask under nitrogen. The reaction flask was held at reflux and the chelidamic solution was added dropwise. After the chelidamic addition was complete, the mixture was kept at reflux for 36 h, filtered through Celite p545® and the solvent was removed by rotary evaporation. The crude material was triturated with hexanes and the solid was collected via filtration and purified on a silica column, eluting with dichloromethane: 0.21 g (15%), mp 141.1–143.7°C. ¹H NMR (400 MHz, CDCl₃) δ 7.80 (s, 2H), 7.43 (s, 4H), 5.33 – 5.22 (m, 2H), 5.20 (s, 2H), 4.59 (s, 2H), 1.41 (d, *J* = 6.3 Hz, 12H). ¹³C NMR (101 MHz, CDCl₃) δ 166.56 (s), 164.27 (s), 150.85 (s), 138.25 (s), 135.28 (s), 129.38 (s), 128.42 (s), 114.67 (s), 70.54 (s), 70.31 (s), 45.91 (s), 22.04 (s). (12 peaks expected and 12 peaks found). HR MS: calc. for C₂₁H₂₄NO₅Cl [M+H]⁺: *m/z* 406.1416; found: *m/z* 406.1405 (error 2.7 ppm).

4-(*p*-Hydroxymethylbenzyloxy)pyridine-2,6-dicarboxylic acid (22). General procedure 1 used with 4-(*p*-chloromethylbenzyloxy)pyridine-2,6-dicarboxylate (**21**, 214.1 mg, 0.5275 mmol), 10% wt. KOH (30 mL) and THF (30 mL) to produce 23.7 mg (15%), mp 127.0–134.3°C. ¹H NMR (500 MHz, DMSO-*d*₆) δ 7.81 (s, 2H), 7.50 (d, *J* = 1 Hz, 4H), 5.39 (s, 2H), 4.78 (s, 2H). ¹³C NMR (126 MHz, DMSO-*d*₆) δ 166.36 (s), 165.24 (s), 149.78 (s), 137.66 (s), 135.73 (s), 129.05 (s), 128.05 (s), 113.91 (s), 69.70 (s), 45.77 (s) (10 peaks expected and 10 peaks found). HR MS: calc. for C₁₅H₁₃O₆N [M - H]⁻: *m/z* 302.0670; found: *m/z* 302.0681 (error -3.6 ppm).

Diisopropyl 4-(pyridin-4'-ylmethoxy)pyridine-2,6-dicarboxylate (23). Chelidamic isopropyl ester (**13**, 1.80 g, 6.73 mmol), 4-bromomethylpyridine hydrobromide (2.00 g, 7.91 mmol), and potassium carbonate (2.50 g, 18.1 mmol) were combined in a round bottom flask with acetone (60 mL) under nitrogen and held at reflux for 4 days. After cooling, the mixture was filtered through Celite p545® and solvent was removed by rotary evaporation. The product was isolated

by flash column chromatography on silica, eluting with DCM to EA: 0.39 g (16%), mp 102.8–104.3 °C. ¹H NMR (400 MHz, CDCl₃) δ 8.68 (d, *J* = 6 Hz, 2H), 7.82 (s, 2H), 7.38 (d, *J* = 6 Hz, 2H), 5.30 (m, 2H), 5.25 (s, 2H), 1.43 (d, *J* = 6.3 Hz, 11H). ¹³C NMR (126 MHz, CDCl₃) δ 165.96 (s), 163.98 (s), 150.88 (s), 150.36 (s), 143.85 (s), 121.51 (s), 114.17 (s), 70.31 (s), 68.66 (s), 21.81 (s) (10 peaks expected and 10 peaks found). HR MS: calc. for C₁₉H₂₂N₂O₅ [M + H]⁺: m/z 359.1601; found: m/z 359.1616 (error –4.2 ppm).

4-(Pyridin-4-ylmethoxy)pyridine-2,6-dicarboxylic acid (24). General procedure 1 used with diisopropyl 4-(pyridin-4'-ylmethoxy)pyridine-2,6-dicarboxylate (**23**, 0.39 g, 1.1 mmol), 10% wt. KOH (20 mL), THF (20 mL) to produce a white solid, 56.6 mg (19%), mp: 205.1–207.3 °C (dec.). ¹H NMR (500 MHz, DMSO-*d*₆) δ 8.93 (br s, 2H), 8.09 (br s, 2H), 7.90 (br s, 2H), 5.74 (br s, 2H). ¹³C NMR (126 MHz, DMSO-*d*₆) δ 165.68, 165.19, 149.99, 143.07, 142.77, 123.85, 113.99, 67.77 (8 signals expected and 8 signals found). HR MS: calc. for C₁₃H₁₀N₂O₅ [M + H]⁺: m/z 275.0662; found: m/z 275.0674 (error –4.4 ppm).

Diisopropyl 4-(*p*-formylphenoxyethoxy)pyridine-2,6-dicarboxylate (25). To a round bottom flask containing acetone (125 mL) was added *p*-(2'-bromoethoxy)benzaldehyde (**37**, 4.77 g, 18.5 mmol), diisopropyl 4-hydroxypyridine-2,6-dicarboxylate (**13**, 4.14 g, 15.5 mmol), and potassium carbonate (3.82 g, 27.6 mmol) with magnetic stirring. The mixture was held at reflux under nitrogen for 31 h, filtered through Celite p545® and evaporated to provide a material which was purified by flash column chromatography (silica gel, eluting with DCM / EA). The product was found in the third fraction as a yellow tinted solid: 3.10 g (48%), mp: 111.8–112.9 °C. ¹H NMR (500 MHz, CDCl₃) δ 9.91 (s, 1H), 7.87 (d, *J* = 9 Hz, 2H), 7.81 (s, 2H), 7.06 (d, *J* = 9 Hz, 2H), 5.30 (hept, *J* = 6 Hz, 2H), 4.55 (dd, *J* = 6, 3 Hz, 2H), 4.48 (dd, *J* = 6, 3 Hz, 2H), 1.43 (d, *J* = 6 Hz, 12H). ¹³C NMR (126 MHz, CDCl₃) δ 190.69 (s), 166.31 (s), 164.04 (s), 163.16 (s), 150.74

(s), 132.03 (s), 130.54 (s), 114.83 (s), 114.07 (s), 70.23 (s), 66.88 (s), 66.25 (s), 21.80 (s) (13 peaks expected and 13 peaks found). HR MS: calc. for C₂₂H₂₅NO₇ [M+H]⁺: m/z 416.1704; found: m/z 416.1700 (error 1 ppm).

Diisopropyl 4-[*p*-(*p*'-formylphenoxy)methyl]benzyloxy]pyridine-2,6-dicarboxylate (26). To a flask containing acetone (60 mL) was added *p*-(*p*'-chloromethylbenzyloxy)benzaldehyde (**38**, 0.88 g, 3.4 mmol), chelidamic isopropyl ester (**13**, 0.87 g, 3.3 mmol), and potassium carbonate (0.90 g, 6.5 mmol) with magnetic stirring under nitrogen. The reaction mixture was held at reflux for 31 h, cooled to room temperature, passed through Celite p545® and evaporated. The desired product was obtained by triturating the crude material with hexanes: product is a yellow tinted solid, 0.9417 g (59%), mp 124.4–127.4 °C. ¹H NMR (500 MHz, CDCl₃) δ 9.90 (s, 1H), 7.85 (d, *J* = 9 Hz, 2H), 7.82 (s, 2H), 7.49 (s, 4H), 7.08 (d, *J* = 9 Hz, 2H), 5.29 (hept, *J* = 6 Hz, 2H), 5.23 (s, 2H), 5.18 (s, 2H), 1.42 (d, *J* = 6 Hz, 12H). ¹³C NMR (126 MHz, CDCl₃) δ 190.74 (s), 166.38 (s), 164.10 (s), 163.54 (s), 150.68 (s), 136.62 (s), 135.00 (s), 132.02 (s), 130.28 (s), 128.15 (s), 127.89 (s), 115.14 (s), 114.34 (s), 70.32 (s), 70.22 (s), 69.81 (s), 21.81 (s) (17 peaks expected and 17 peaks found). HR MS: calc. for C₂₈H₂₉NO₇ [M + H]⁺: m/z 492.2017; found: m/z 492.2029 (error 2.4 ppm).

Diisopropyl 4-[*p*-(*p*'-bromobenzyloxy)benzyloxy]pyridine-2,6-dicarboxylate (27). To a round bottom flask containing acetone (200 mL) was added diisopropyl ester chelidamic (**13**, 5.50 g, 20.6 mmol), K₂CO₃ (4.00 g, 28.9 mmol), and *p*-(*p*'-bromomethylphenoxy)methyl)bromobenzene (**39**, 7.91 g, 22 mmol) with magnetic stirring under nitrogen. The reaction was held at reflux for 19 h, followed by filtration through Celite p545® and removal of solvent via rotary evaporation. The remaining solid was triturated with boiling hexanes and filtered, product is a white solid: 10.51 g (94%), mp 90.4–92.6 °C. ¹H NMR (400

MHz, CDCl₃) δ 7.80 (s, 2H), 7.51 (d, *J* = 8 Hz, 2H), 7.36 (d, *J* = 9 Hz, 2H), 7.31 (d, *J* = 8 Hz, 2H), 6.98 (d, *J* = 9 Hz, 2H), 5.28 (hept, *J* = 6 Hz, 2H), 5.13 (s, 2H), 5.04 (s, 2H), 1.42 (d, *J* = 6 Hz, 12H). ¹³C NMR (101 MHz, CDCl₃) δ 166.68 (s), 164.35 (s), 159.09 (s), 150.82 (s), 135.95 (s), 132.02 (s), 129.94 (s), 129.25 (s), 127.58 (s), 122.20 (s), 115.37 (s), 114.63 (s), 70.71 (s), 70.42 (s), 69.52 (s), 22.04 (s) (16 peaks expected and 16 peaks found). HR MS: calc. for C₂₇H₂₈O₆NBr [M + Na]⁺: m/z 564.0992; found: m/z 564.0983 (error -2 ppm).

4-[*p*-(*p*'-Bromobenzyloxy)benzyloxy]pyridine-2,6-dicarboxylic acid (28). General procedure 1 used with diisopropyl 4-[*p*-(*p*'-bromobenzyloxy)benzyloxy]pyridine-2,6-dicarboxylate (**27**, 1.21 g, 2.23 mmol), 10% wt. KOH (20 mL) and THF (30 mL) to produce a white solid, 1.01 (99%), mp: 189.1–192.3 °C. ¹H NMR (500 MHz, DMSO-*d*₆) δ 7.77 (s, 2H), 7.58 (d, *J* = 8 Hz, 2H), 7.41 (dd, *J* = 8, 3 Hz, 4H), 7.03 (d, *J* = 8 Hz, 2H), 5.27 (s, 2H), 5.10 (s, 2H). ¹³C NMR (126 MHz, DMSO-*d*₆) δ 167.05 (s), 165.87 (s), 158.74 (s), 150.30 (s), 137.03 (s), 131.93 (s), 130.38 (d, *J* = 7.2 Hz), 128.37 (s), 121.51 (s), 115.44 (s), 114.49 (s), 70.51 (s), 68.95 (s) (14 peaks expected and 14 peaks found). HR MS: calc. for C₂₁H₁₆O₆NBr [M + H]⁺: m/z 458.0234; found: m/z 458.0238 (error -0.9 ppm).

Diisopropyl 4-(*p*-bromobenzyloxy)pyridine-2,6-dicarboxylate (29). To a flask containing acetone (125 mL) was added **13** (4.30 g, 16.1 mmol), *p*-bromobenzyl bromide (4.54 g, 18.2 mmol) and potassium carbonate (3.59 g, 26.0 mmol) with magnetic stirring. The mixture was held at reflux under nitrogen for 8 h, filtered through Celite p545® and the solvent was removed by rotary evaporation. The crude material was triturated with hexanes and the product was collected as a white solid: 6.14 g (87%), mp: 123.5–124.6 °C. ¹H NMR (500 MHz, CDCl₃) δ 7.80 (s, 2H), 7.55 (d, *J* = 8 Hz, 2H), 7.32 (d, *J* = 8 Hz, 2H), 5.29 (hept, *J* = 6 Hz, 2H), 5.17 (s, 2H), 1.43 (d, *J* = 6 Hz, 12H). ¹³C NMR (126 MHz, CDCl₃) δ 166.23 (s), 164.06 (s), 150.72 (s),

133.84 (s), 132.04 (s), 129.36 (s), 122.80 (s), 114.27 (s), 70.23 (s), 69.91 (s), 21.81 (s) (11 peaks expected and 11 peaks found); HR MS: calc. for C₂₀H₂₂O₅NBr [M + H]⁺: m/z 436.0754; found: m/z 436.0760 (error 1 ppm).

4-(*p*-Bromobenzyloxy)pyridine-2,6-dicarboxylic acid (30). General procedure 1 used with diisopropyl 4-(*p*-bromobenzyloxy)pyridine-2,6-dicarboxylate (**29**, 2.65 g, 6.07 mmol), 10% wt. KOH (50 mL) and THF (50 mL) to produce a white solid, 2.13 g (99%), mp: 185.7–187.7 °C. ¹H NMR (400 MHz, DMSO-*d*₆) δ 7.80 (s, 2H), 7.62 (s, 2H), 7.46 (d, *J* = 8 Hz, 2H), 5.36 (s, 2H). ¹³C NMR (101 MHz, DMSO-*d*₆) δ 163.17 (s), 162.12 (s), 146.66 (s), 131.94 (s), 128.36 (s), 126.81 (s), 118.32 (s), 110.75 (s), 66.17 (s) (9 peaks expected and 9 peaks found). HR MS: calc. for C₁₄H₁₀O₅NBr [M + H]⁺: m/z 351.9815; found: m/z 351.9827 (error –3.4 ppm).

Diisopropyl 4-(*p*-iodobenzyloxy)pyridine-2,6-dicarboxylate (31). To a round bottom flask containing acetone (75 mL) was added 1-bromomethyl-4-iodobenzene (**35**, 0.55 g, 1.9 mmol), chelidamic isopropyl diester (**13**, 0.59 g, 2.2 mmol), and potassium carbonate (0.52 g, 3.8 mmol). The flask was placed under nitrogen and held at reflux for 1 day, after which the flask was allowed to cool and filtered through Celite p545®. Solvent was removed by rotary evaporation and the crude material was purified via flash column chromatography (silica, eluting with 100% DCM to 100% EA; product elutes in 10% EA): 0.75 g (84%), white solid, mp 187.3–189.8 °C. ¹H NMR (500 MHz, CDCl₃) δ 7.79 (s, 2H), 7.76 (d, *J* = 8 Hz, 2H), 7.19 (d, *J* = 8 Hz, 2H), 5.29 (hept, *J* = 6 Hz, 2H), 5.15 (s, 2H), 1.43 (d, *J* = 6 Hz, 13H). ¹³C NMR (126 MHz, CDCl₃) δ 166.23 (s), 164.06 (s), 150.75 (s), 138.00 (s), 134.52 (s), 129.50 (s), 114.26 (s), 94.42 (s), 70.21 (s), 69.99 (s), 21.81 (s) (11 peaks expected and 11 peaks found). HR MS: calc. for C₂₀H₂₂O₅NI [M + H]⁺: m/z 484.0615; found: m/z 484.0586 (error 6.0 ppm).

4-(*p*-Iodobenzyloxy)pyridine-2,6-dicarboxylic acid (32). General procedure 1 used with diisopropyl 4-(*p*-iodobenzyloxy)pyridine-2,6-dicarboxylate (**31**, 0.75 g, 1.6 mmol), THF (50 mL), and 10% wt. potassium hydroxide (50 mL) to produce 0.61 g (98%), white solid, mp 187.3–189.8 °C. ¹H NMR (500 MHz, DMSO-*d*₆) δ 7.79 (m, 4H), 7.30 (d, *J* = 8 Hz, 2H), 5.34 (s, 2H). ¹³C NMR (126 MHz, DMSO-*d*₆) δ 166.27 (s), 165.23 (s), 149.78 (s), 137.34 (s), 135.41 (s), 129.96 (s), 113.91 (s), 94.44 (s), 69.40 (s) (9 peaks expected and 9 peaks found). HR MS: calc. for C₁₄H₁₀O₅NI [M + H]⁺: m/z 399.9676; found: m/z 399.9709 (error -8.3 ppm).

***p*-[*p*'-Bromomethylphenoxy]methyl]bromobenzene (39).** To a flask containing DCM (200 mL) was added *p*-(*p*'-bromobenzyloxy)benzyl alcohol (6.88 g, 23.5 mmol) and PBr₃ (1.4 mL, 15 mmol) with magnetic stirring under nitrogen. The solution was held at reflux for 39 h, after which it was poured into water, followed by washing the organic phase with water (x2), saturated NaCl (x2), and drying over sodium sulfate. Filtration and removal of the solvent provided the product as a lightly brown tinted solid: 8.21 g (98 %), mp: 76.4–78.8 °C. ¹H NMR (400 MHz, CDCl₃) δ 7.51 (d, *J* = 8 Hz, 2H), 7.31 (dd, *J* = 11, 8 Hz, 4H), 6.91 (d, *J* = 8 Hz, 2H), 5.01 (s, 2H), 4.49 (s, 2H). ¹³C NMR (101 MHz, CDCl₃) δ 158.77 (s), 135.96 (s), 131.96 (s), 130.74 (s), 130.69 (s), 129.27 (s), 122.20 (s), 115.27 (s), 69.51 (s), 34.00 (s) (10 peaks expected and 10 large peaks found, very small impurity signals; due to the product being an intermediate, it was used without further purification). HR MS: calc. for C₁₄H₁₂OBr₂ [M - Br]⁺: m/z 275.0066; found: m/z 275.0065 (error -0.4 ppm)

Diisopropyl 4-[*p*-(1'-bromoethyl)benzyloxy]pyridine-2,6-dicarboxylate (33). To a flask containing silica (2.20 g) was added 4-(*p*-vinylbenzyloxy)chelidamic isopropyl ester (**16**, 0.383 g, 0.998 mmol), and DCM (10 mL) with magnetic stirring under nitrogen. PBr₃ (0.08 mL, 0.85 mmol) was dissolved in DCM (1 mL) and added dropwise to the flask. After the addition was

complete, the flask was allowed to stir for 2 h. The mixture was filtered to remove solids and the filtrate was washed with NaHCO₃ (x3), saturated NaCl (x2), and dried over sodium sulfate. Filtration and rotary evaporation provided the product: 400 mg (86%), white solid, mp: 244.1–246.0 °C (dec). ¹H NMR (500 MHz, CDCl₃) δ 7.80 (s, 2H), 7.49 (d, *J* = 8 Hz, 2H), 7.42 (d, *J* = 4 Hz, 2H), 5.32–5.24 (m, 2H), 5.91 (s, 2H), 5.18 (q, *J* = 7 Hz, 1H), 2.05 (d, *J* = 7 Hz, 3H), 1.41 (d, *J* = 7 Hz, 12H). ¹³C NMR (126 MHz, CDCl₃) δ 166.38, 164.09, 150.67, 143.85, 143.85, 134.94, 129.38, 128.13, 127.35, 127.30, 114.34, 70.22, 48.67, 32.84, 26.74, 21.81 (13 peaks expected and 16 peaks found, 3 extra aromatic peaks founds, product believed to not be shelf stable at room temperature).

Diisopropyl 4-[*p*-[1'-(2'',2'',6'',6'')-tetramethylpiperidin-*N*-oxy]ethyl]benzyloxy]pyridine-2,6-dicarboxylate (34). To a round bottom flask containing benzene (10 mL) was added copper (II) trifluoromethanesulfonate (8.9 mg, 0.025 mmol), copper powder (48.2 mg, 0.758 mmol), TEMPO (0.149 g, 0.952 mmol), diisopropyl diisopropyl 4-[*p*-(1'-bromoethyl)benzyloxy]pyridine-2,6-dicarboxylate (**33**, 0.287 g, 0.618 mmol), and N,N,N',N'',N''-pentamethyldiethylenetriamine (0.02 mL, 0.1 mmol) with magnetic stirring under nitrogen. The mixture was held at reflux for 30 h, diluted with DCM, filtered through Celite p545®, and solvent was removed by rotary evaporation. The residue was purified using column chromatography (neutral alumina, eluting with DCM:MeOH 99:1); the product eluted as the first fraction: 0.1893 g (57%), white solid, mp 113.1–116.5 °C. ¹H NMR (500 MHz, CDCl₃) δ 7.81 (s, 2H), 7.40 – 7.35 (m, 4H), 5.34 – 5.24 (m, 2H), 5.20 (s, 2H), 4.80 (q, *J* = 6 Hz, 1H), 1.52 – 1.23 (m, 23H), 1.16 (s, 4H), 1.02 (s, 3H), 0.63 (s, 3H). ¹³C NMR (126 MHz, CDCl₃) δ 166.53 (s), 164.12 (s), 150.62 (s), 146.55 (s), 133.20 (s), 127.66 (s), 127.09 (s), 114.41 (s), 82.78 (s), 70.75 (s), 70.11 (s), 59.69 (s), 40.35 (s), 34.45 (s), 34.17 (s), 23.52 (s), 21.82 (s), 20.34 (s),

17.21 (s). (19 peaks expected and 19 peaks found). HR MS: calc. for C₃₁H₄₄O₆N₂ [M + H]⁺: m/z 541.3272; found: m/z 541.3283 (error -2.0 ppm)

4,4'-(((*p*-Phenylenebis(oxy))bis(ethane-2,1-diyl))bis(oxy))bis(pyridine-2,6-dicarboxylic acid)

(40). General procedure 1 used with tetraisopropyl 4,4'-(((*p*-phenylenebis(oxy))bis(ethane-2,1-diyl))bis(oxy))bis(pyridine-2,6-dicarboxylate) (**19**, 0.379 g, 0.544 mmol), THF (50 mL) and 10% aqueous potassium hydroxide (50 mL) to produce 0.287 g (100%), white solid, mp 260.0–265.0 °C (dec). ¹H NMR (500 MHz, DMSO-*d*₆) δ 7.78 (s, 4H), 6.93 (s, 4H), 4.57 (s, 4H), 4.30 (s, 4H). ¹³C NMR (126 MHz, DMSO-*d*₆) δ 166.53 (s), 165.26 (s), 152.42 (s), 149.76 (s), 115.49 (s), 113.69 (s), 67.61 (s), 66.43 (s) (8 peaks expected and 8 peaks found). HR MS: calc. for C₂₄H₂₀O₁₂N₂ [M + H]⁺: m/z 529.1089; found: m/z 529.1084 (error 0.9 ppm)

Tetraisopropyl 4,4'-(decane-1,10-diylbis(oxy))bis(pyridine-2,6-dicarboxylate) (41). To a

round bottom flask containing acetonitrile (200 mL) was added 1,10-dibromodecane (7.04 g, 23.5 mmol), chelidamic isopropyl ester (**13**, 12.8 g, 47.8 mmol), and potassium carbonate (8.50 g, 61.5 mmol) under nitrogen. The reaction was held at reflux for 4 days, after which it was filtered through Celite p 545® and the solvent was removed by rotary evaporation. The crude material was dissolved in DCM and washed with Na₂CO₃ (x2), saturated NaCl (x4), and dried over sodium sulfate. Filtration and removal of the solvent provided a white solid: 15.63 g (99%), mp 76.8 – 78.0 °C. ¹H NMR (500 MHz, CDCl₃) δ 7.72 (s, 4H), 5.29 (hept, *J* = 6 Hz, 4H), 4.12 (t, *J* = 6 Hz, 4H), 1.89–1.80 (m, 4H), 1.76 – 1.27 (m, 36H). ¹³C NMR (126 MHz, CDCl₃) δ 166.92 (s), 164.29 (s), 150.52 (s), 114.08 (s), 70.13 (s), 68.91 (s), 29.44 (s), 29.27 (s), 28.80 (s), 25.88 (s), 21.81 (s) (11 peaks expected and 11 peaks found). HR MS: calc. for C₃₆H₅₂N₂O₁₀ [M+H]⁺: m/z 673.3695; found: m/z 673.3707 (error 1.8 ppm).

4,4'-(Decane-1,10-diylbis(oxy))bis(pyridine-2,6-dicarboxylic acid) (42). General procedure 1 used with tetraisopropyl 4,4'-(decane-1,10-diylbis(oxy))bis(pyridine-2,6-dicarboxylate) (**41**, 1.86 g, 2.76 mmol), THF (50 mL) and 10% wt. potassium hydroxide (50 mL) to produce 1.08 g (78 %), white solid, mp 192.8–196.1 °C. ¹H NMR (500 MHz, DMSO-*d*₆) δ 7.69 (s, 4H), 4.21 (t, *J* = 6 Hz, 4H), 1.85 – 1.68 (m, 4H), 1.35 (m, 12H). ¹³C NMR (126 MHz, DMSO-*d*₆) δ 166.71 (s), 165.27 (s), 149.65 (s), 113.51 (s), 68.69 (s), 28.83 (s), 28.59 (s), 28.12 (s), 25.21 (s) (9 peaks expected and 9 peaks found). HR MS: calc. for C₂₄H₂₈O₁₀N₂ [M + H]⁺: m/z 505.1817; found: m/z 505.1840 (error –4.6 ppm).

REFERENCES

- (1) Howáth, G.; Rusa, C.; Köntös, Z.; Gerencsér, J.; Huszthy, P. *Synth. Commun.* **1999**, *29*, 3719-3731.
- (2) Picot, A.; Feuvrie, C.; Barsu, C.; Malvolti, F.; Le Guennic, B.; Le Bozec, H.; Andraud, C.; Toupet, L.; Maury, O. *Tetrahedron* **2008**, *64*, 399-411.
- (3) Seitz, M.; Milius, W.; Alt, H. G. *J. Mol. Catal. A: Chem.* **2007**, *261*, 246-253.
- (4) Sanseverino, A. M.; Mattos, M. C. S. d. *J. Braz. Chem. Soc.* **2001**, *12*, 685-687.
- (5) Matyjaszewski, K.; Xia, J. *Chem. Rev.* **2001**, *101*, 2921-2990.
- (6) Rosen, B. M.; Percec, V. *Chem. Rev.* **2009**, *109*, 5069-5119.
- (7) Matyjaszewski, K.; Woodworth, B. E.; Zhang, X.; Gaynor, S. G.; Metzner, Z. *Macromolecules* **1998**, *31*, 5955-5957.
- (8) Wiesener, E. F.; Edwards, J. P.; Scalfani, V. F.; Bailey, T. S.; Gin, D. L. *Macromolecules* **2011**, *44*, 5075-5078.
- (9) Grubbs, R. H. *Tetrahedron* **2004**, *60*, 7117-7140.
- (10) Bielawski, C. W.; Grubbs, R. H. *Prog. Polym. Sci.* **2007**, *32*, 1-29.
- (11) Choi, T.-L.; Grubbs, R. H. *Angew. Chem. Int. Ed.* **2003**, *42*, 1743-1746.
- (12) Yu, M.; Tang, R.-Y.; Li, J.-H. *Tetrahedron* **2009**, *65*, 3409-3416.
- (13) Wang, L.; Lu, W. *Org. Lett.* **2009**, *11*, 1079-1082.
- (14) Song, Y.; Jing, H.; Li, B.; Bai, D. *Chem. Eur. J.* **2011**, *17*, 8731-8738.
- (15) Lamture, J. B.; Zhou, Z. H.; Kumar, A. S.; Wensel, T. G. *Inorg. Chem.* **1995**, *34*, 864-869.
- (16) Froidevaux, P.; Harrowfield, J. M.; Sobolev, A. N. *Inorg. Chem.* **2000**, *39*, 4678-4687.
- (17) Vassiliou, S.; Xeilari, M.; Yiotakis, A.; Grembecka, J.; Pawełczak, M.; Kafarski, P.; Mucha, A. *Bioorg. Med. Chem.* **2007**, *15*, 3187-3200.
- (18) Wong, W. W. H.; Curiel, D.; Cowley, A. R.; Beer, P. D. *Dalton Trans.* **2005**, 359-364.

- (19) Biju, V.; Sudeep, P. K.; Thomas, K. G.; George, M. V.; Barazzouk, S.; Kamat, P. V. *Langmuir* **2002**, *18*, 1831-1839.
- (20) Pan, X.; Yi, F.; Zhang, X.; Chen, S. *Asian J. Chem.* **2012**, *24*, 3809-3813.

Chapter 6

Cryptand Functionalization

Introduction

In terms of complexation with paraquats, pyridyl cryptands far surpass the ability of crown ethers.¹⁻³ Adoption of pyridyl cryptands has however been slow at best, owing to problems in: lengthy syntheses, overall low yielding reactions for their production, and a lack of reasonable synthetic schemes to pyridyl feedstock molecules. The generally accepted method of synthesis involves syringe pump addition of substrates over several days into a large volume of solvent, to achieve pseudo-high dilution conditions. The result is a reaction that takes nearly a week to run and yields of about 45%; chapter 3, however, remedies this concern by introducing a templation method to accomplish the synthesis of dibenzo-30-crown-10- and bis(*m*-phenylene)-32crown-10-based pyridyl cryptands. The most direct route to functionalized 2,6-pyridinedicarboxylates makes use of the precursor chelidamic acid. Although commercially available, chelidamic acid has historically only been offered at relatively high prices, and published synthetic procedures for the compound were difficult or low yielding. These drawbacks have likely hindered the use of functionalized 2,6-pyridinedicarboxylates across many fields, resulting in fewer than expected published derivatives of chelidamic acid. Access to a high yielding, relatively easy synthesis, for chelidamic acid has recently been achieved by Horvath et al.⁴ and chapter 5 attempts to produce a more complete collection of chelidamic derivatives, while determining how to avoid N-alkylations during functionalization. Here we present functionalized cryptands with synthetic handles that can be further used to produce supramolecular assemblies of interest.

Results and Discussion

As some work of this chapter was completed before completion of chapter 3 (cryptand templation), some cryptands presented here were synthesized via syringe pump addition and others by templation. Pyridyl cryptands explored here are functionalized on the pyridine ring and formed using either dibenzo-30-crown-10 or bis(*m*-phenylene)-32crown-10 precursors. **Figure 6.1** shows a generic reaction scheme for the synthesis of functionalized cryptands. A chelidamic diacid chloride precursor is reacted with a crown diol in the presence of base to form the desired cryptand. These reactions are carried out through either templation or pseudo-high dilution.

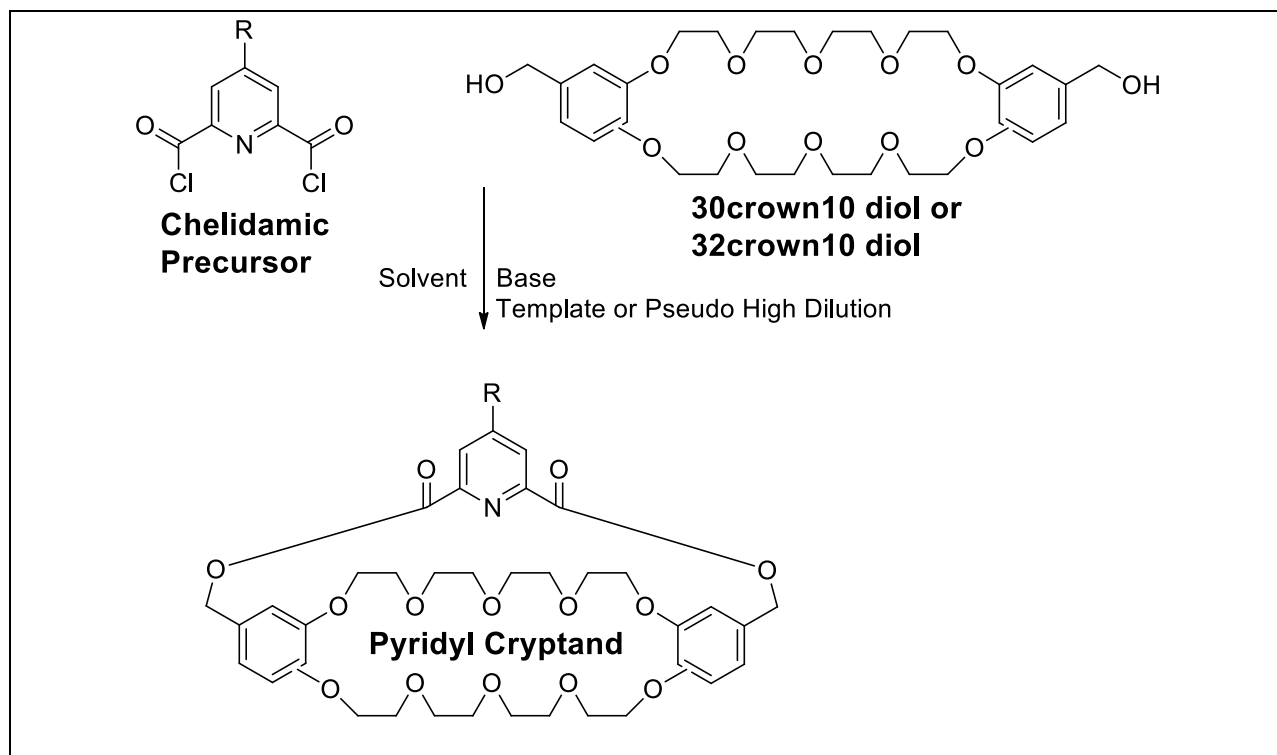
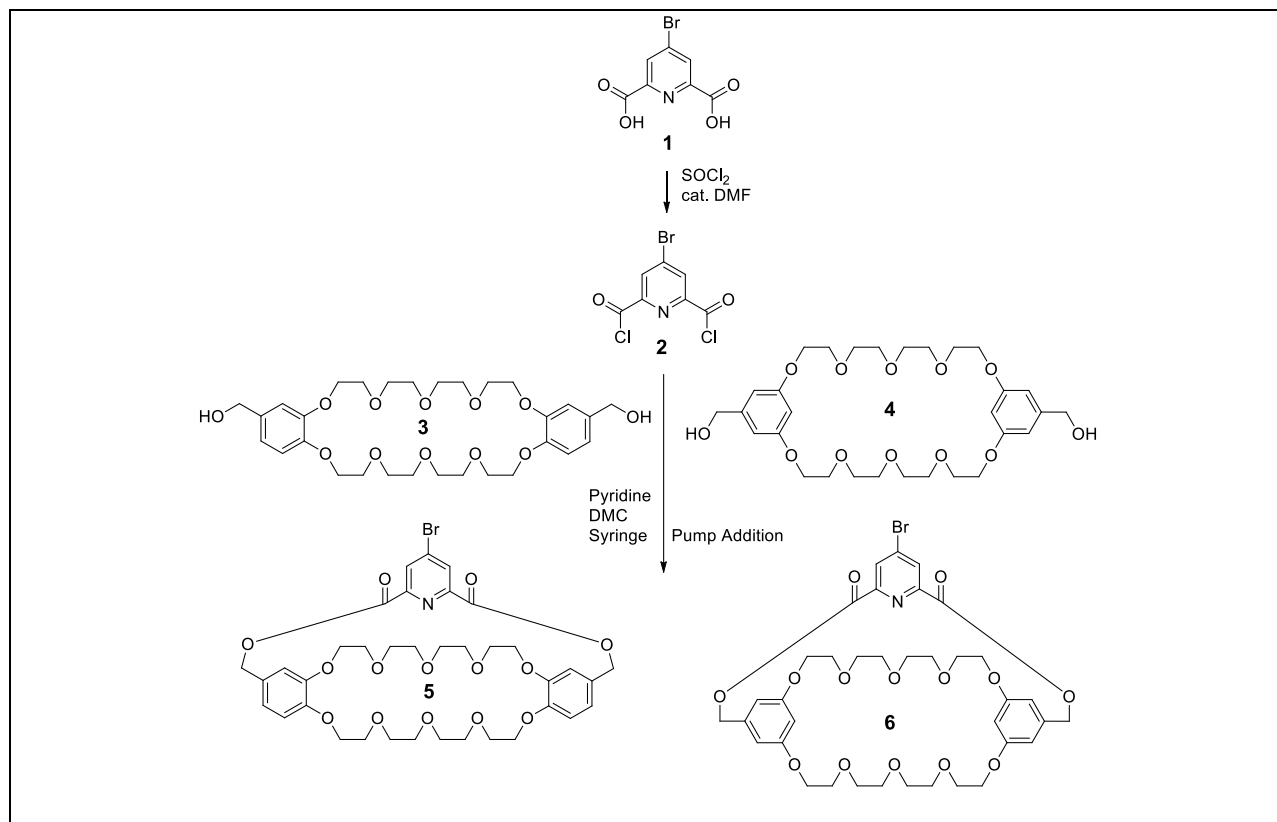


Figure 6.1. Generic reaction for dibenzo-30-crown-10- and bis(*m*-phenylene)-32crown-10 based-pyridyl cryptand synthesis.

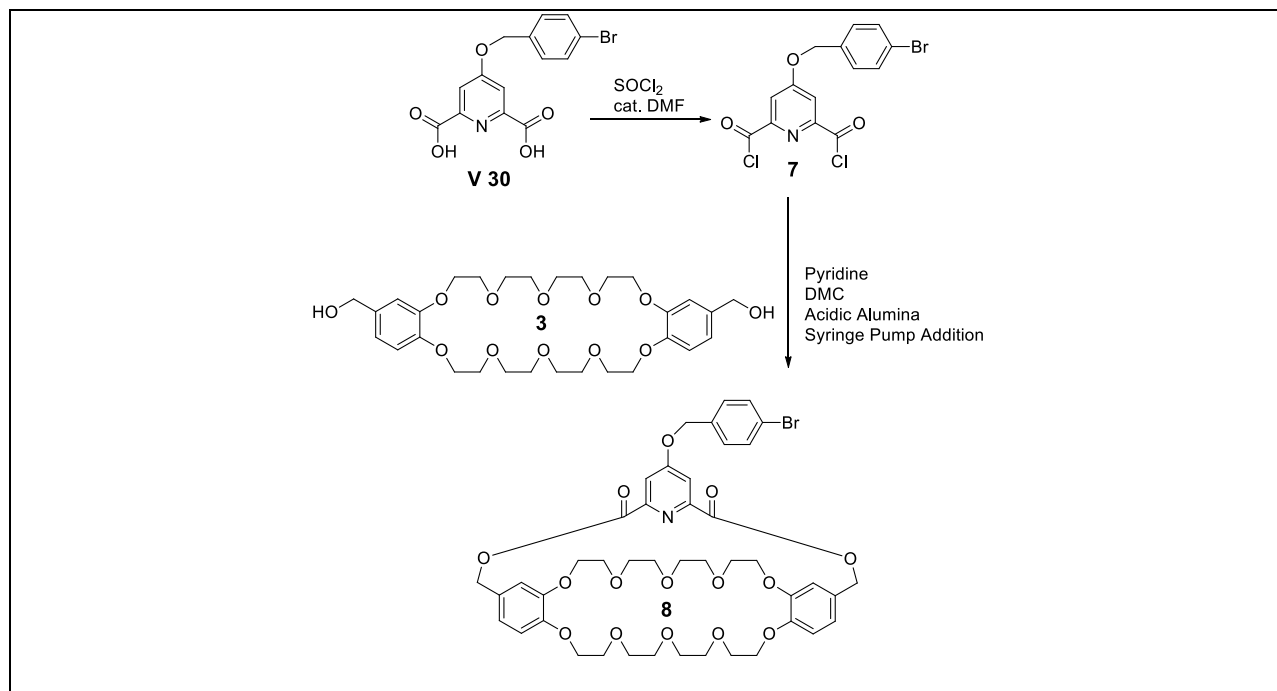
Because aryl halides are capable of withstanding harsh reaction conditions while being useful in a range of coupling reactions, such as: Hiyama coupling,⁵ Hiyama–Denmark coupling,⁶

Kumada coupling,⁷ Negishi coupling,⁸ Stille coupling,⁹ Suzuki coupling,¹⁰ and Heck coupling,¹¹ they were chosen for incorporation into the cryptands of **Figure 6.1**. It was reasoned that their inclusion could be used as a gateway to a wealth of supramolecular precursors. The first functionalized cryptands explored were the aryl bromide cryptands **5** and **6**, seen in **Scheme 6.1**. **5** and **6** were synthesized in 43 and 24% yields, respectively, by reacting **2** with either **3** or **4**, respectively, via syringe pump addition to achieve pseudo-high dilution conditions. These two cryptands were originally attempted by Adam M.-P. Pederson and determined to be unobtainable, as described in his dissertation.¹² The theory was that **2** was more sensitive to moisture than other chelidamic diacid chlorides and syringe pump use resulted in the hydrolysis of **2**. Syringe pump additions typically take place over 50 to 100 hours, making the seal between syringe and needle crucial to success. To address this problem, the air-tight glass syringes and metal needles were replaced with disposable plastic syringes and HPLC tubing. Through these changes, a tighter seal between the syringe and HPLC tubing was possible, and moisture could be better avoided. Employing this methodology resulted in the formation of **5** and **6**. Although **5** and **6** were successfully synthesized, exchange of the 4-bromo substituent to 4-chloro occurred with reaction times longer than 4 h to produce **2** from **1**. No noticeable exchange was observed with reaction times of less than 4 h; alternatively, thionyl bromide was used to avoid this problem.



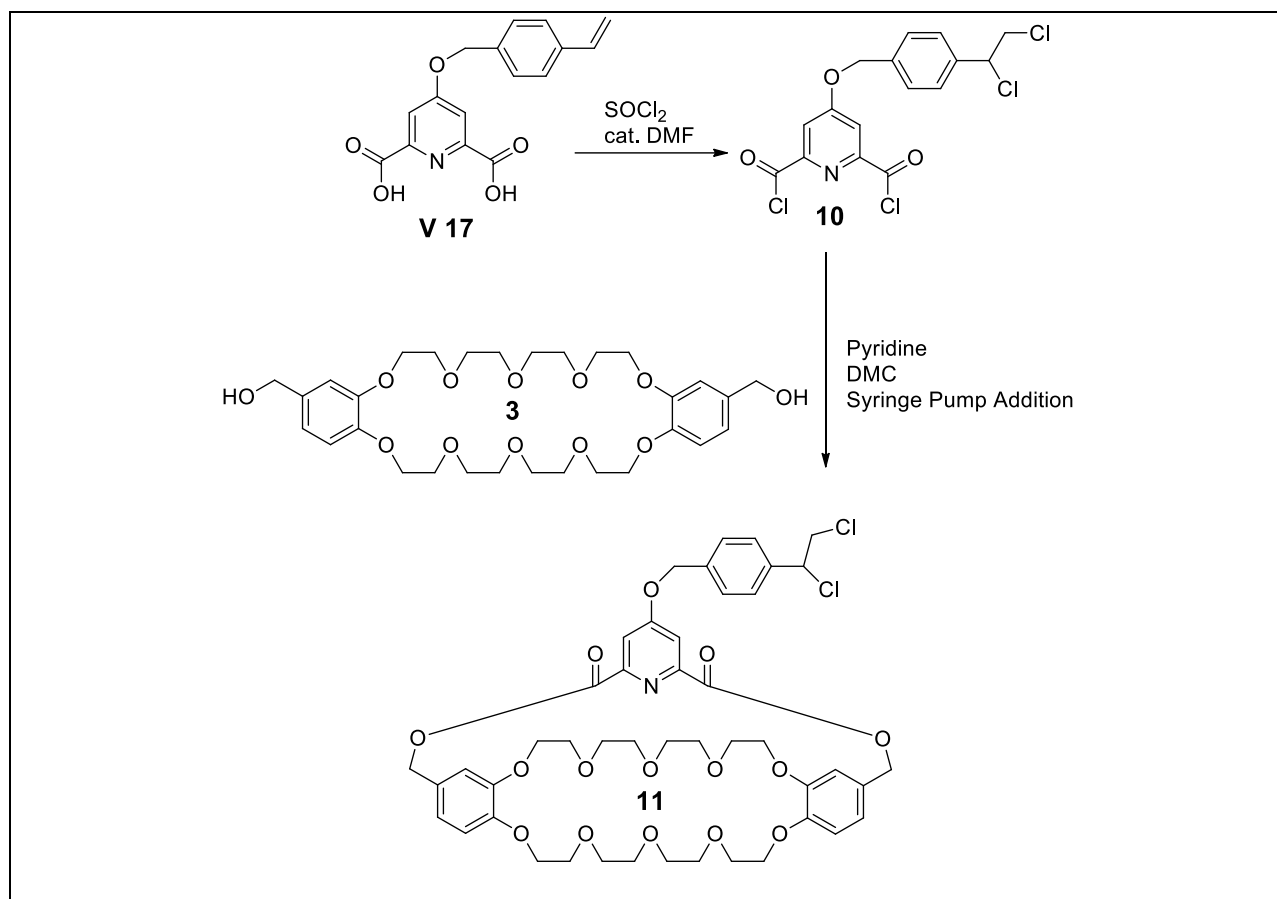
Scheme 6.1. Synthesis of functionalized cryptands **5** and **6**.

Anticipating several scenarios in which one may want a spacer between the cryptand and the aryl halide, **8** was prepared as seen in **Scheme 6.2**. As a special note, compounds discussed in other chapters will be named using that chapter's number in Roman numerals before the compound's number of that chapter; as an example compound **V 30** is found in chapter 5 as compound **30**. **8** contains the aryl bromide connected to the cryptand through an ether linkage as a 4-bromobenzyl attachment. Additionally, moving the bromide to a phenyl ring allows for reaction conditions to be better anticipated, as the bulk of published literature for coupling reactions focuses on halides attached to phenyl rings rather than pyridine rings.



Scheme 6.2. Synthesis of aryl bromide cryptand **8**.

In addition to the aryl bromide cryptands, attempts were made to synthesize a styrene-containing cryptand (**Scheme 6.3**). Multiple attempts yielded the same result, the olefin was consumed and dichloro product **10** was isolated. It was determined that the thionyl chloride was contaminated with sulfuryl chloride, which reacted with the double bond to **9**. Work conducted by a coworker, Dr. Arunachalam Murugan, showed that the desired styrene cryptand could be synthesized by either freshly distilling the thionyl chloride or by use of oxalyl chloride. Additionally, intentionally adding sulfuryl chloride to freshly distilled thionyl chloride resulted in the synthesis and isolation of **10**.



Scheme 6.3. Synthesis of cryptand **10**.

Conclusion

Several functionalized cryptands were successfully synthesized by incorporating the aryl bromide functionality into compounds **5**, **6** and **8**. Additionally, the isolation of dichloro cryptand **10** was achieved and its formation was determined to be due to the presence of the sulfuryl chloride in thionyl chloride. In total 4 new functionalized pyridyl cryptands and 2 new chelidamic derivatives were successfully synthesized.

Experimental

Measurements: ^1H -NMR spectra were obtained on JEOL ECLIPSE-500, BRUKER-500, and AGILENT-NMR-vnmrs400 spectrometers. ^{13}C -NMR spectra were collected at 125 MHz and 101 MHz on these instruments. HR-MS were obtained using an Agilent LC-ESI-TOF system. DCM was dried freshly distilling from CaH; other reagents were purchased and used as received without further purification. Compound **1**¹³ was made in accordance with literature procedures; similar yields were achieved. Compounds **V 17** and **V 30** were synthesized as described in chapter 5.

General procedure 1. 4-bromopyridine-2,6-dicarbonyl dichloride (2). 4-Bromopyridine-2,6-dicarboxylic acid ¹³ (0.7241 g, 2.943 mmol) and thionyl chloride (5 mL, 0.07 mol) was added to a round bottom flask under nitrogen. DMF (1 drop) was added to the reaction mixture and the mixture was brought to reflux and held there for 4 h with magnetic stirring. Excess thionyl chloride was removed by distillation and the material was used without further purification, an off-white solid with a yellow to pink tint 0.8325 g (100 %).

General procedure 2. Dibenzo-30-crown-10-based 4-bromopyridyl cryptand (5). 3 (0.25669 g, 0.43021 mmol) and 4-bromopyridine-2,6-dicarbonyl dichloride (0.121708 g, 0.43021 mmol) were freshly prepared and each dissolved in 50.0 mL of freshly distilled DCM. DCM (1.5 L) freshly distilled was added to a three-neck reaction flask along with pyridine (2.4 mL). Each of the two solutions was loaded into plastic syringes and metal needles were replaced with HPLC tubing sealed to the syringe. Additions from the syringes were made via syringe pump at 1 mL/h. After additions were complete, the reaction mixture was allowed to stir for 3 days, after which time solvent was removed by rotary evaporation and the resulting solid was dissolved into chloroform. The crude mixture was washed with 1M HCl (x 1), water (x 3),

followed by drying over Na₂SO₄. The mixture was filtered and solvent removed by rotary evaporation. The resulting residue was passed through a neutral alumina column, eluting with chloroform and methanol (97:3); the first eluting band contained the product; 81.05 mg (43%); mp 144.1–148.5 °C. ¹H NMR (400 MHz, CDCl₃) δ 8.48 (s, 2H), 6.94 (m, 2H), 6.93 (s, 2H), 6.78 (d, *J* = 9 Hz, 2H), 5.33 (s, 4H), 4.21–4.12 (m, 4H), 4.04–3.97 (m, 4H), 3.95–3.90 (m, 4H), 3.86–3.79 (m, 4H), 3.70 (m, 16H). ¹³C NMR (101 MHz, CDCl₃) δ 164.80, 148.99, 148.89, 148.40, 138.14, 128.17, 127.98, 121.60, 114.21, 113.94, 70.98, 70.75, 70.72, 70.61, 69.68, 69.46, 68.97, 68.79, 67.60 (19 signals expected and 19 signals found). High res MS: calc. for C₃₇H₄₄NO₁₄Br [M + NH₄]⁺: m/z 823.2283; found: m/z 823.2300 (error –2.1 ppm).

Bis(*m*-phenylene)-32crown-10-based 4-bromopyridyl cryptand (6). General procedure 2 was used with **2** (0.1532 g, 0.5414 mmol), **4** (0.3231 g, 0.5415 mmol) and pyridine (4.0 mL, 50 mmol) to produce a white solid that was purified by passing over neutral alumina, eluting with chloroform:methanol (98:2) to give the desired product; 0.1055 g (24%); mp 137.9–143.1 °C. ¹H NMR (500 MHz, CDCl₃) δ 8.48 (s, 2H), 6.52 (m, 4H), 6.45 (m, 2H), 5.30 (s, 4H), 3.93 (m, 8H), 3.76–3.72 (m, 8H), 3.65 (m, 8H), 3.61 (m, 8H). ¹³C NMR (126 MHz, CDCl₃) δ 163.92 (s), 160.11 (s), 149.25 (s), 137.07 (s), 134.97 (s), 131.42 (s), 106.49 (s), 102.27 (s), 71.03 (s), 70.84 (s), 69.69 (s), 67.94 (s), 67.71 (s) (13 signals expected and 13 signals found). High res MS: calc. for C₃₇H₄₄NO₁₄Br [M + NH₄]⁺: m/z 823.2283; found: m/z 823.2278 (error 0.6 ppm).

4-(*p*-Bromobenzyloxy)pyridine-2,6-dicarboxylic acid chloride (7). General procedure 1 was used with **V 30** (0.5177 g, 1.470 mmol), thionyl chloride (5 mL, 0.07 mol) and DMF (1 drop) to produce an off-white solid with a yellow tint 0.5719 g (100%). The product was used directly without characterization.

Dibenzo-30-crown-10-based 4-(*p*-bromobenzyloxy)pyridyl cryptand (8). General procedure 2 was used with DCM (2.7 L), pyridine (2.4 mL), **3** (0.42690 g, 0.71548 mmol), **7** (0.27902 g, 0.71722 mmol) and acidic alumina (1.00 g) as a template to provide a solid which was purified by column chromatography using neutral alumina, eluting with chloroform:methanol (99:1); 0.5064 g, (78%) of white solid, mp 188.8–192.7 °C. ¹H NMR (400 MHz, CDCl₃) δ 7.88 (s, 2H), 7.55 (d, *J* = 8 Hz, 2H), 7.32 (d, *J* = 8 Hz, 2H), 6.94–6.92 (m, 4H), 6.77 (d, *J* = 9 Hz, 2H), 5.30 (s, 4H), 5.18 (s, 2H), 4.20–4.11 (m, 4H), 4.03–3.97 (m, 4H), 3.95–3.90 (m, 4H), 3.84–3.78 (m, 4H), 3.74 (m, 4H), 3.72 – 3.67 (m, 8H), 3.64 (m, 4H). ¹³C NMR (126 MHz, CDCl₃) δ 166.43 (s), 164.88 (s), 150.24 (s), 149.12 (s), 149.00 (s), 133.85 (s), 132.14 (s), 129.37 (s), 128.19 (s), 122.87 (s), 121.80 (s), 114.80 (s), 114.34 (s), 114.02 (s), 71.10 (s), 70.86 (s), 70.83 (s), 70.73 (s), 70.03 (s), 69.79 (s), 69.55 (s), 69.09 (s), 68.90 (s), 67.83 (s) (24 peaks expected and 24 peaks found). High res MS: calc. for C₄₄H₅₀NO₁₅Br [M + H]⁺: m/z 912.2437; found: m/z 912.2452 (error –1.6 ppm).

4-(*p*-(1',2'-Dichloroethyl)benzyloxy)pyridine-2,6-dicarbonyl dichloride (9). General procedure 1 was used with **V 17** (0.16081 g, 0.53733 mmol), thionyl chloride (4.0 mL, 55 mmol), sulfonyl chloride (0.10 mL, 1.2 mmol) and DMF (1 drop) to produce an off-white solid 0.2187 g (100%). The product was used directly without characterization.

Dibenzo-30-crown-10-based 4-(*p*-(1,2-dichloroethyl)benzyloxy)pyridyl cryptand (10). General procedure 2 was used with **9** (0.1740 g, 0.4274 mmol), **3** (0.2551 g, 0.4275 mmol), and pyridine (3.0 mL, 37 mmol), to provide a solid which was purified via column chromatography, eluting with 98:2 (v:v) chloroform:methanol over neutral alumina; product isolated as fourth band, 29.1 mg (7%), mp 115.3–124.6 °C. ¹H NMR (500 MHz, CDCl₃) δ 7.90 (s, 2H), 7.49–7.45 (m, 2H), 7.39–7.37 (m, 2H), 6.94–6.92 (m, 4H), 6.76 (d, *J* = 8 Hz, 2H), 5.30 (s, 4H), 5.24 (s,

2H), 5.04–4.96 (m, 1H), 4.17–4.11 (m, 4H), 4.01–3.96 (m, 5H), 3.94–3.89 (m, 4H), 3.82–3.78 (m, 4H), 3.75–3.73 (m, 4H), 3.71–3.68 (m, 8H), 3.41–3.34 (m, 5H). High res MS: calc. for C₄₆H₅₃NO₁₅Cl₂ [M + NH₄]⁺: m/z 947.3131; found: m/z 947.3162 (error –3.3 ppm).

References

- (1) Huang, F.; Switek, K. A.; Zakharov, L. N.; Fronczek, F. R.; Slebodnick, C.; Lam, M.; Golen, J. A.; Bryant, W. S.; Mason, P. E.; Rheingold, A. L.; Ashraf-Khorassani, M.; Gibson, H. W. *J. Org. Chem.* **2005**, *70*, 3231-3241.
- (2) Pederson, A. M. P.; Vctor, R. C.; Rouser, M. A.; Huang, F.; Slebodnick, C.; Schoonover, D. V.; Gibson, H. W. *J. Org. Chem.* **2008**, *73*, 5570-5573.
- (3) Pederson, A. M. P.; Ward, E. M.; Schoonover, D. V.; Slebodnick, C.; Gibson, H. W. *J. Org. Chem.* **2008**, *73*, 9094-9101.
- (4) Howáth, G.; Rusa, C.; Köntös, Z.; Gerencsér, J.; Huszthy, P. *Synth. Commun.* **1999**, *29*, 3719-3731.
- (5) Monguchi, Y.; Yanase, T.; Mori, S.; Sajiki, H. *Synthesis* **2013**, *45*, 40-44.
- (6) Denmark, S. E.; Smith, R. C.; Chang, W.-T. T.; Muhuhi, J. M. *J. Am. Chem. Soc.* **2009**, *131*, 3104-3118.
- (7) Guo, W.-J.; Wang, Z.-X. *J. Org. Chem.* **2013**, *78*, 1054-1061.
- (8) Xi, Z.; Zhou, Y.; Chen, W. *J. Org. Chem.* **2008**, *73*, 8497-8501.
- (9) Mee, S. P. H.; Lee, V.; Baldwin, J. E. *Angew. Chem. Int. Ed.* **2004**, *43*, 1132-1136.
- (10) Kondolff, I.; Doucet, H.; Santelli, M. *Tetrahedron* **2004**, *60*, 3813-3818.
- (11) Kantam, M. L.; Srinivas, P.; Yadav, J.; Likhar, P. R.; Bhargava, S. *J. Org. Chem.* **2009**, *74*, 4882-4885.
- (12) Pederson, A. M.-P., Virginia Tech, 2009.
- (13) Pryor, K. E.; Shipps Jr, G. W.; Skyler, D. A.; Rebek Jr, J. *Tetrahedron* **1998**, *54*, 4107-4124.

Chapter 7

BISCRIPTANDS

Introduction

In supramolecular chemistry certain key molecules contain the potential to unlock a wealth of chemistry. Ditopic hosts can be used for supramolecular polymers, chain extensions, and crosslinking (**Figure 7.1**).

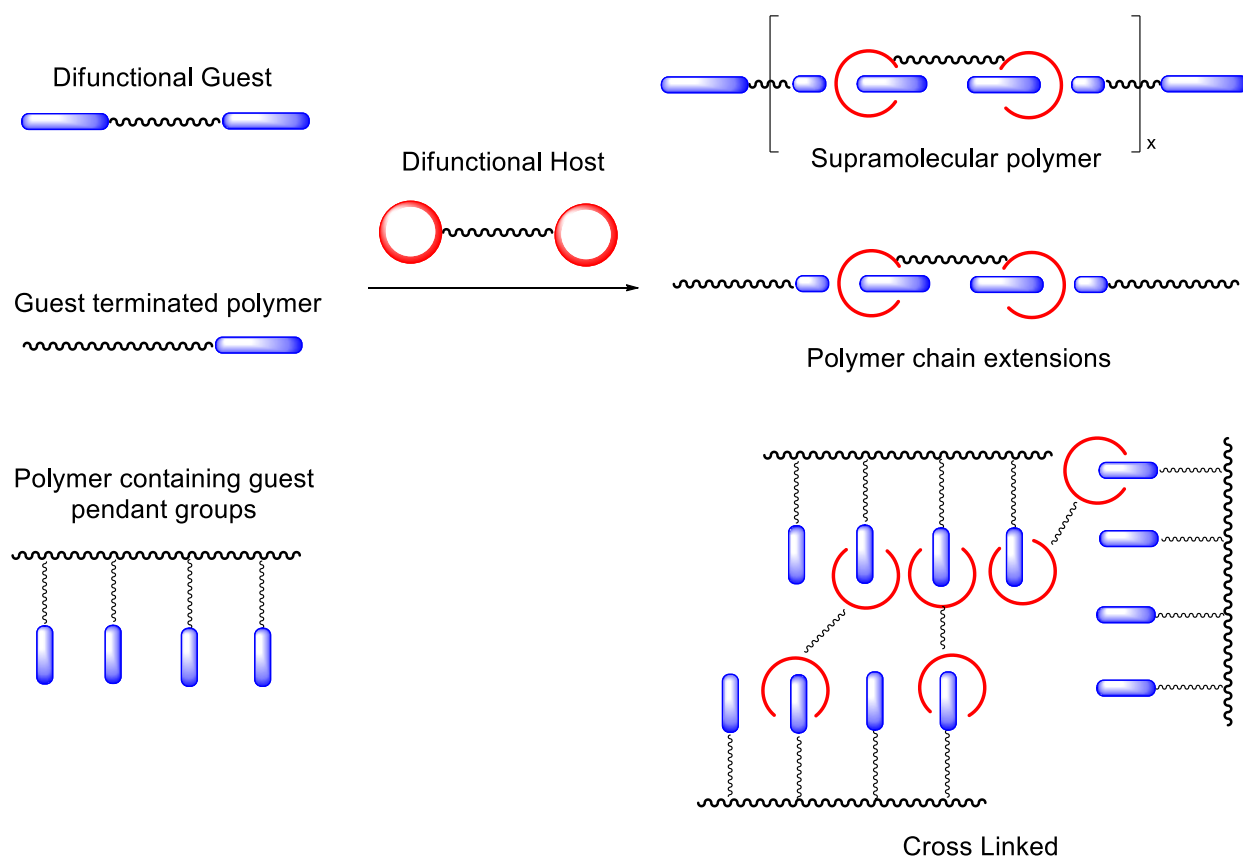


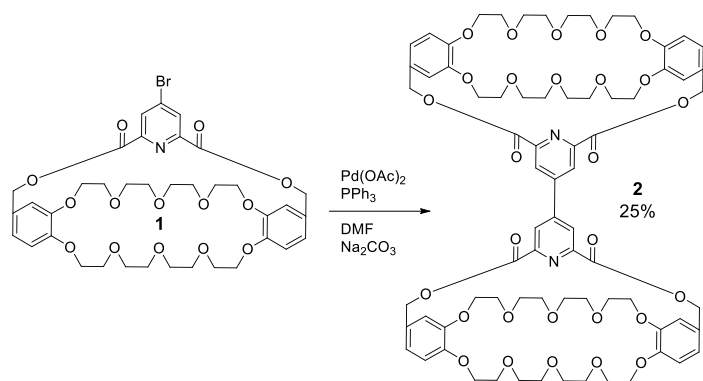
Figure 7.1. Uses for a Ditopic Host.

Supramolecular polymers and chain extensions have long been a focus within the Gibson group; formerly the host workhorses for these projects were ditopic crown ethers.¹⁻³ Host systems, however, have far surpassed simple crown ethers and evolved into cryptands.⁴⁻¹³

Specifically, pyridyl cryptands have demonstrated exceptionally high binding constants with paraquat guests.^{4,6,8,12} Up until recently, inadequate synthetic pathways existed for the synthesis of pyridyl cryptands, hindering their use and blocking the development of ditopic analogs. New synthetic pathways as well as correctly staged functional groups have removed many of the problems initially hindering the synthesis of cryptands and thereby now allow for the development of ditopic cryptands. Here synthetic strategies to produce biscryptands are reported and a suitable ditopic host compound is chosen to move forward with on supramolecular projects.

Results and Discussion

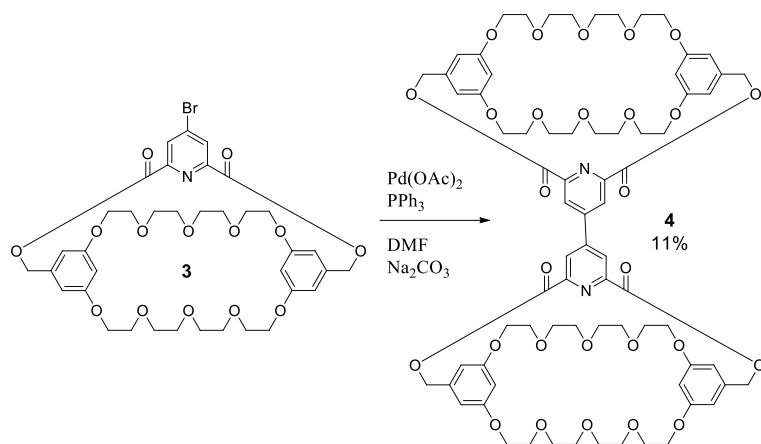
Initial attempts to synthesize a biscryptand employed the dibenzo-30-crown-10-based pyridyl cryptand **1** with the intent of Heck coupling the cryptand to a diolefin. These attempts were unsuccessful; coupling at the olefin was not observed. Instead Ullman coupling prevailed and **2** was formed as an unexpected product in 26% yield, with large quantities of **1** left unreacted after 36 h. Repeating the reaction, as shown in **Scheme 7.1**, without the diolefin and maintaining the previously used reagents with similar concentrations and reaction times, once again gave an Ullman coupled product as before in a yield of 25% with a large amount of **1** remaining unreacted. Similar conditions and reagents are known to give this Ullman coupling outcome.¹⁴



Scheme 7.1. Synthesis of Ullmann coupled cryptand **2**.

A similar reaction was carried out using the 32-crown-10 aryl bromide cryptand **3** to produce **4** in 11% yield; the yield reduction vs. **2** is primarily attributed to **4** being synthesized on a small scale (18 mg). Once again a large fraction of the aryl bromide was unreacted.

The desire to produce both dibenzo-30-crown-10 and bis(*m*-phenylene)-32crown-10 cryptands comes from the synthetic yields and the binding constants observed with dimethyl paraquat PF₆. The diol of dibenzo-30-crown-10, used to produce cryptand **1** is formed in high yield (93%)⁴ through a templation procedure, so large scale reactions are possible. The diol of bis(*m*-phenylene)-32-crown-10 cannot be synthesized through a templated reaction,^{4,15} but its pyridyl cryptand binds dimethyl paraquat PF₆ more than 10 times better than the dibenzo-30-crown-10 analog ($5 \times 10^6 \text{ M}^{-1}$ vs. $K_a = 1 \times 10^5 \text{ M}^{-1}$).^{4,6}



Scheme 7.2. Synthesis of **4** via Ullmann coupling.

Although **2** and **4** were the first biscryptands produced, their use was short lived. Complexation of **2** with dimethyl paraquat revealed that although a reasonable average binding constant was obtained, K_{a1} and K_{a2} varied significantly. **Figure 7.2** is an ITC plot of **2** with dimethyl paraquat PF₆ in acetone at 25 °C; analysis of the isotherm revealed that $K_{a1} = 4.50 \times 10^5 \text{ M}^{-1}$, while $K_{a2} = 1.78 \times 10^4 \text{ M}^{-1}$, with an average association constant of $2.33 \times 10^5 \text{ M}^{-1}$. For statistical complexation $K_{a2} = (1/4) K_{a1}$.¹⁶⁻¹⁸ This leads to the conclusion that the system is anti-cooperative ($K_{a2} = (3.96 \times 10^{-2}) K_{a1}$). The anti-cooperative behavior of **2** is attributed to the close proximity of the two host cavities, causing the complexation of the second paraquat to feel a repulsive electrostatic force from the first complexed paraquat. Due to the small scale on which **4** was synthesized and the binding constants obtained for **2**, no further effort was put into **4**. Instead, compounds **2** and **4** were abandoned for constructs that contain a linker between the two cryptand units.

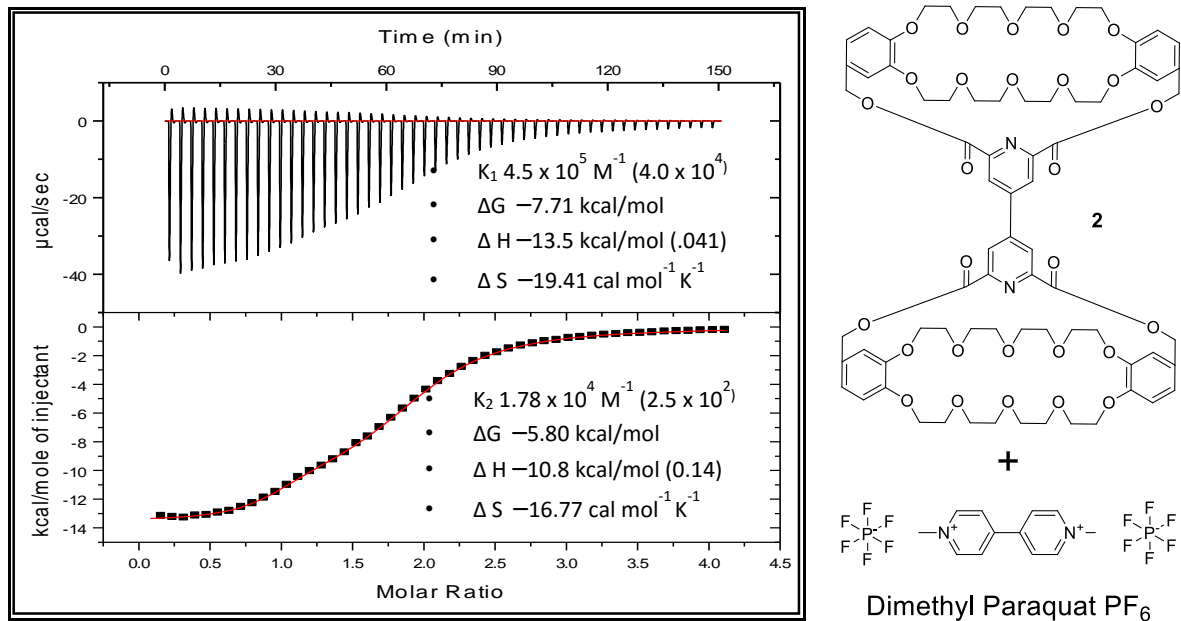
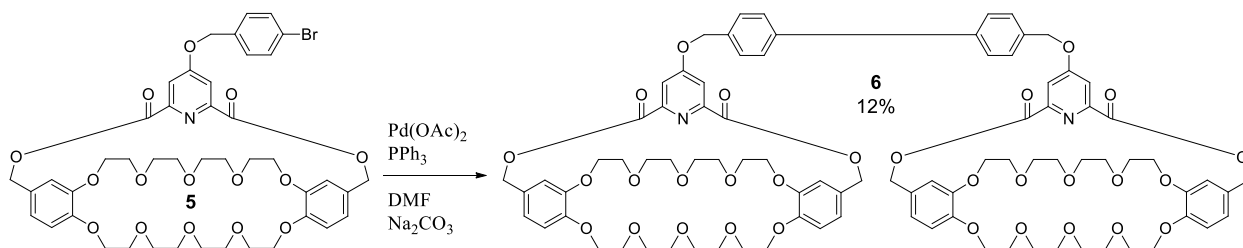


Figure 7.2. ITC titration of **2** with dimethyl paraquat PF₆ in acetone at 25 °C; error is indicated in parenthesis.

Since Ullman coupling proved to be possible using the aryl bromides **1** and **3**, aryl bromide **5** was developed such that coupling could be carried out to yield a biscryptand which contained a linker of moderate length, **6**. It was anticipated the longer linkage would overcome the anticooperativity observed with **4**.

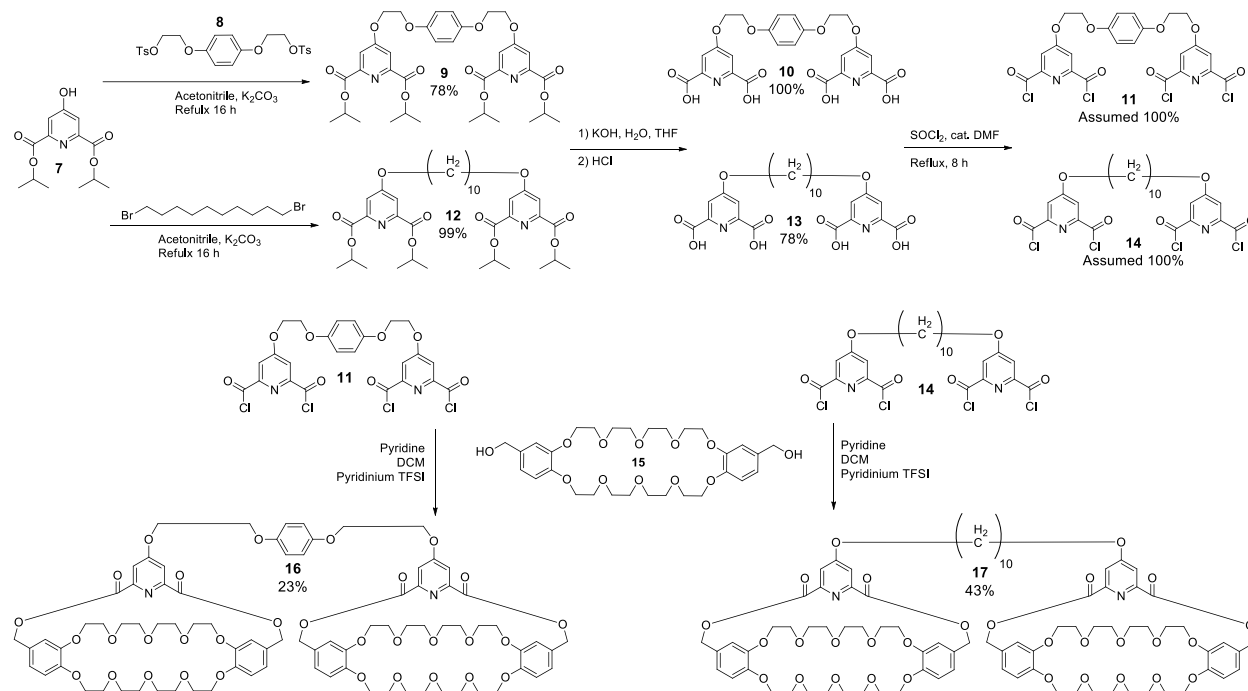


Scheme 7.3. Synthesis of biscryptand **6**.

Synthesis of **6** was achieved in a yield of 12% after 17 h. Chromatography provided recovery of the remaining starting material, providing a clear indication that the reaction had not

reached completion. At the same time progress was made on templation of the formation of cryptands and it became evident that biscryptands could be prepared more readily by these methods. For this reason, **6** was abandoned for the production of a new, easier overall synthesis.

Two biscryptands, **16** and **17**, were chosen for production based on the concept of carrying out a dual cyclization (**Scheme 7.4**).



Scheme 7.4. Synthesis of biscryptands **16** and **17**.

Linkages for **16** and **17** were chosen because the literature¹ indicates that if the linkage is long enough, the formation of cyclic species, a side reaction when producing supramolecular polymers, can be minimized. The suggested linkage length to avoid cyclics is a ten atom or greater linkage.¹

Syntheses of **16** and **17** were achieved via the previously developed templation reaction, whereby two cyclizations were carried out at the same time on double ended chelidamic acid

chlorides, **11** and **14**. Cyclization yields of 23% for **16** and 43% for **17** were achieved, resulting in a quicker and easier synthesis and isolation process compared to the halide coupling reactions.

As expected, ITC results revealed that the complexation process with dibenzyl paraquat TFSI was actually cooperative; this paraquat was chosen due to its solubility in DCM. **Figure 7.3** is the ITC plot of **17** with dibenzyl paraquat TFSI in DCM at 25 °C, yielding $K_{\text{avg}} = 4.36 \times 10^5 \text{ M}^{-1}$, $K_{\text{a1}} = 2.49 \times 10^5 \text{ M}^{-1}$ and $K_{\text{a2}} = 6.23 \times 10^5 \text{ M}^{-1}$; $K_{\text{a2}} = 2.5 K_{\text{a1}}$! Cooperative behavior found in other cryptand paraquat systems has been attributed to conformational changes and restrictions promoting the complexation of a second site and the first complexation bringing about a change in ion pairing and the local environment.¹⁹ Here we suggest a similar occurrence in which the first binding induces a conformational change that promotes the binding of the second paraquat. The crystal structures of complexes of 2,6-pyridyl cryptands of cis(4,4')-dibenzo-30-crown-10 with dimethyl paraquat PF₆ (and other paraquat PF₆ derivatives) typically reveal the guest π -stacked within the host in such a way that the paraquat methyl groups interact with the oxygen atoms of the host.⁴ It is likely that the electron poor benzyl moieties of the paraquat are capable of interacting via hydrogen bonding with the adjacent uncomplexed cryptand motif in **17**. This likely causes the second uncomplexed cryptand motif to adopt a conformation that assists in the complexation of the next paraquat guest.

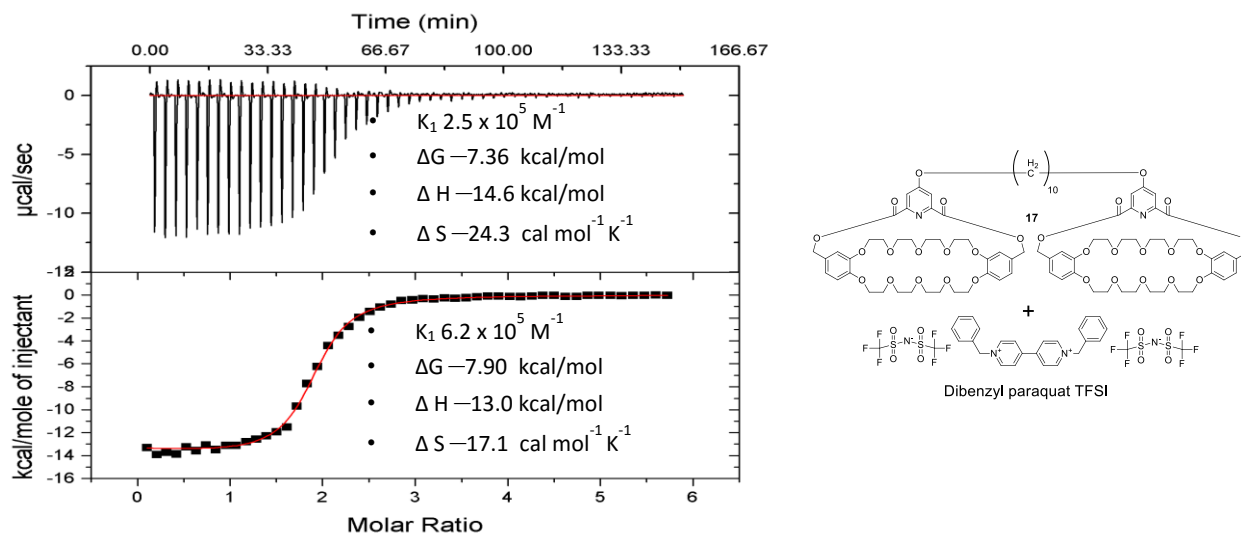


Figure 7.3. ITC titration of **17** with dibenzyl paraquat TFSI in DCM at 25 °C.

In a similar system, a ditopic paraquat guest was found to complex cooperatively with a monotopic crown ether host, by Niu and coworkers.²⁰ **Figure 7.4** shows Niu's cooperative system, host **18** and guest **19**.²⁰ The cooperative nature of Niu's system was determined via X-ray crystallography to be due to hydrogen bonding of a carbonyl oxygen of one macrocycle with an ethyleneoxy hydrogen of the other macrocycle in the [3]complex. Further analysis of the **18** • **19** complex suggested that once the [2]complex is formed, the conformational freedom of **19** is restricted through hydrogen and CH-- π bonds, thereby promoting the second addition of **18**.

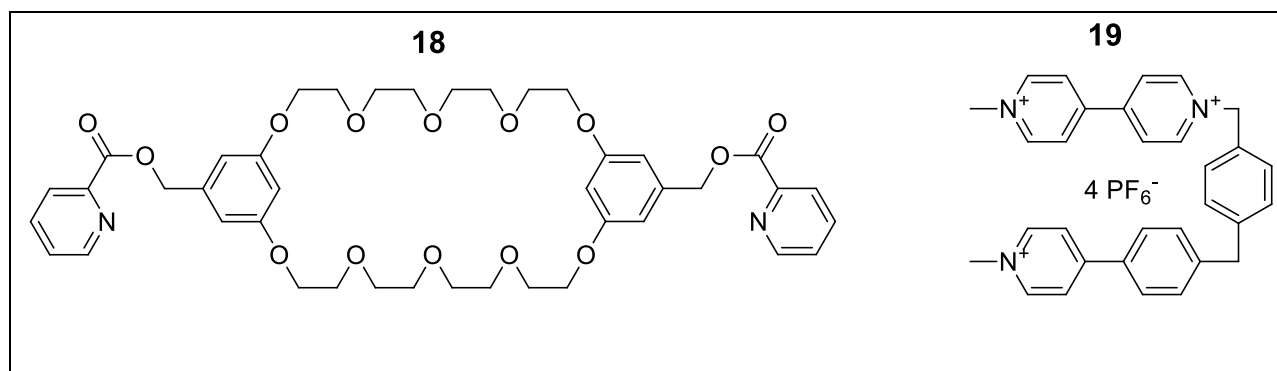


Figure 7.4. Niu's cooperative system: host **18** and guest **19**.²⁰

The successful synthesis of **16** and **17** led to the decision to begin self-assembly work. The weakness of this approach is that to vary the linker, new bispyridine precursors have to be prepared; that is, this synthesis is not modular. The precursor tetra(acid chloride)s **11** and **14** each required six synthetic steps, not counting those to make the linker. This is the same number of synthetic steps to reach the dibenzo-30-crown-10 diol precursor **15**, leading to a state of affairs where the chelidamic component is just as evolved, if not further evolved than **15**.

Conclusion

In total five novel biscryptands were successfully produced. Aryl bromide cryptands **1** and **3** were both used to successfully produce the respective biscryptands **2** and **4** through Ullmann reactions. Initial ITC results indicated that these ditopic hosts bind paraquats anticooperatively and we thus abandoned this approach to biscryptands. **6** was then synthesized to extend the linkage between the cryptand units. Continued improvements in template cyclization methods for the formation of the cryptands, however, resulted in **6** being abandoned in favor of **16** and **17**, which were produced directly from tetra(acid chloride)s. **16** and **17** offered shortened reaction times and reduced effort in purification when compared to **2**, **4**, and **6**. Importantly, the complexation of **16** with a paraquat derivative demonstrated highly positive cooperativity.

Experimental

Measurements: ^1H -NMR spectra were obtained on JEOL ECLIPSE-500, BRUKER-500, and AGILENT-NMR-vnmrs400 spectrometers. ^{13}C -NMR spectra were collected at 125 MHz and 101 MHz on these instruments. HR-MS were obtained using an Agilent LC-ESI-TOF system. Reagents were purchased and used as received without further purification. Compounds **7**,²¹ **8**,²² and **15**⁴ were made in accordance with literature procedures; similar yields were achieved. Compounds **1**, **3**, and **5** were synthesized as described in Chapter 6.

Biscryptand (dibenzo-30-crown-10-based pyridyl cryptand linked directly at the 4-pyridyl position) (2). **1** (34.67 mg, 0.0430 mmol), palladium acetate (2.1 mg, 0.0094 mmol), triphenylphosphine (18.9 mg, 0.072 mmol), and sodium carbonate (21.8 mg, 0.206 mmol) were added to a small flask containing a magnetic stir bar. DMF (20 mL) was added to the flask. The reaction mixture was stirred in an oil bath at 90 °C under nitrogen for 36 h. A small portion of solvent was removed by rotary evaporation and the remaining mixture was dissolved in chloroform; the mixture was washed with 1M HCl (2x), water (3x), and dried over Na_2SO_4 . After filtration and evaporation of the solvent, chromatography was used to isolate the coupled biscryptand product (neutral alumina, eluting with ethyl acetate/dichloromethane/methanol (30:30:2): 15.8 mg (25%), mp 107.8–114.5 °C. ^1H NMR (500 MHz, CDCl_3) δ 8.71 (s, 2H), 6.98 (d, $J = 8$ Hz, 4H), 6.80 (d, $J = 8$ Hz, 2H), 5.40 (s, 4H), 4.18 (t, $J = 4$, 4H), 4.03 (t, $J = 4$, 4H), 3.93 (t, $J = 4$, 4H), 3.84 (t, $J = 4$, 4H), 3.70 (m, 16H). ^{13}C NMR (126 MHz, CDCl_3) δ 164.47 (s), 150.02 (s), 149.20 (s), 149.04 (s), 146.54 (s), 128.06 (s), 125.60 (s), 121.94 (s), 114.41 (s), 114.01 (s), 71.08 (s), 70.80 (d, overlap of two singlets), 69.75 (s), 69.56 (s), 69.09 (s), 68.89 (s),

68.15 (s) (18 peaks expected and 18 peaks found). High res MS: calc. for $C_{74}H_{88}N_2O_{28}$ $[M+NH_4]^+$: m/z 1470.5862; found: m/z 1470.5845 (error -1.2 ppm)

Biscryptand (bis(*m*-phenylene)-32crown-10-based pyridyl cryptand linked directly at the 4-pyridyl position) (4). **3** (18.0 mg, 0.0223 mmol), Pd(OAc)₂ (2.2 mg, 9.8 μmol), PPh₃ (5.2 mg, 20 μmol), DMF (4 mL), and Na₂CO₃ (22 mg, 0.21 mmol) were combined in a round bottom flask with magnetic stirring and heated in an oil bath at 90 °C under nitrogen for 42 h, after which the mixture was diluted with chloroform and washed with 1 M HCl (2x), water (3x), and dried over Na₂SO₄. The solution was filtered, followed by solvent removal. Product isolation was achieved using preparative scale TLC (neutral alumina eluting with ethyl acetate:dichloromethane:methanol (30:30:1.5); 1.8 mg (11 %), mp: 96.1–105.4 °C. ¹H NMR (500 MHz, CDCl₃) δ 8.75 (s, 3H), 6.58 (m, 6H), 6.50–6.47 (m, 7H), 5.39 (s, 8H), 4.05–4.00 (m, 9H), 3.82 (s, 11H), 3.79–3.74 (m, 18H), 3.72–3.61 (m, 70H). Integration was very poor and indicated impurities, but further purification was not possible due to the small amount of material. High res MS: calc. for $C_{74}H_{88}N_2O_{28}$ $[M + NH_4]^+$: m/z 1470.5862; found: m/z 1470.5848 (error 0.95 ppm).

Biscryptand (dibenzo-30-crown-10-based pyridyl cryptand employing a biphenyl linkage) (6). To a flask containing DMF (5 mL) was added bromobenzyl 30-crown-10 cryptand **5** (37.0 mg, 40.5 μmol), palladium acetate (1.0 mg, 4.5 μmol), and potassium carbonate (31.7 mg, 229 μmol) under nitrogen with magnetic stirring. The mixture was held at reflux for 17 h and the solvent was removed by rotary evaporation. The crude material was dissolved in DCM, washed with 1 M HCl (7x), water (5x), and dried over sodium sulfate. The solution was filtered and rotary evaporation gave a material which was passed over neutral alumina, eluting with chloroform:methanol (97:3); 4.2 mg (12%), mp 113.4–120.1 °C. ¹H NMR (500 MHz, CDCl₃) δ

7.93 (s, 4H), 7.66 (d, $J = 8$ Hz, 4H), 7.54 (d, $J = 8$ Hz, 4H), 6.94 (d, $J = 8$ Hz, 8H), 6.77 (d, $J = 8$ Hz, 4H), 5.31 (s, 8H), 5.29 (s, 4H), 4.18–4.14 (m, 8H), 4.02 – 3.97 (m, 8H), 3.95–3.90 (m, 8H), 3.83–3.79 (m, 8H), 3.74 (m, 8H), 3.71–3.68 (m, 16H), 3.64 (m, 8H). Carbon NMR spectrum not obtained due to the small amount of material. High res MS: calc. for $C_{88}H_{100}N_2O_{30}$ $[M+NH_4]^+$: m/z 1683.6733; found: m/z 1683.6582 (error –8.97 ppm).

Tetraisopropyl 4,4'-(((*p*-phenylenebis(oxy))bis(ethane-2'',1''-diyl))bis(oxy))bis(pyridine-2''',6'''-dicarboxylate) (9). A mixture of acetonitrile (100 mL), **8** (5.78 g, 11.4 mmol), **7** (6.79 g, 25.4 mmol), and potassium carbonate (5.85 g, 42.3 mmol) was held at reflux for 24 h with magnetic stirring under nitrogen. After cooling to room temperature the mixture was filtered through Celite® p545 and solvent was removed by rotary evaporation. The crude material was dissolved in DCM and washed with Na_2CO_3 (x2), saturated NaCl (x3), and dried over sodium sulfate. The product was obtained after filtration and removal of solvent: 6.21 g (78%) of white solid, mp 193.1–195.4 °C. 1H NMR (500 MHz, $CDCl_3$) δ 7.81 (s, 4H), 6.89 (s, 4H), 5.30 (hept, $J = 6$ Hz, 4H), 4.52–4.46 (m, 4H), 4.37–4.32 (m, 4H), 1.43 (d, $J = 6$ Hz, 24H). ^{13}C NMR (126 MHz, $CDCl_3$) δ 166.53 (s), 164.10 (s), 153.00 (s), 150.64 (s), 115.82 (s), 114.18 (s), 70.21 (s), 67.32 (s), 66.73 (s), 21.81 (s) (10 peaks expected and 10 peaks found). High res MS: calc. for $C_{36}H_{44}N_2O_{12}$ $[M+H]^+$: m/z 697.2967; found: m/z 697.3000 (error 4.7 ppm)

4,4'-(((*p*-phenylenebis(oxy))bis(ethane-2'',1''-diyl))bis(oxy))bis(pyridine-2''',6'''-dicarboxylic acid) (10). **9** (0.3790 g, 0.5440 mmol) was dissolved in THF (50 mL) and 10% aqueous potassium hydroxide (50 mL) was added to the solution contained in a round bottom flask. The reaction mixture was then stirred at reflux for 27 h. THF was removed by rotary evaporation and concentrated HCl was added until pH=1. The precipitate was collected and washed with cool water and dried: 0.2871 g (100%) of a white solid, mp 260.0–265.0 °C (dec).

^1H NMR (500 MHz, DMSO- D_6) δ 7.78 (s, 4H), 6.93 (s, 4H), 4.57 (s, 4H), 4.30 (s, 4H). ^{13}C NMR (126 MHz, DMSO- D_6) δ 166.53 (s), 165.26 (s), 152.42 (s), 149.76 (s), 115.49 (s), 113.69 (s), 67.61 (s), 66.43 (s) (8 peaks expected and 8 peaks found). HR MS: calc. for $\text{C}_{24}\text{H}_{20}\text{O}_{12}\text{N}_2$ [$\text{M} + \text{H}$] $^+$: m/z 529.1089; found: m/z 529.1084 (error 0.9 ppm)

4,4'-(((*p*-phenylenebis(oxy))bis(ethane-2'',1''-diyl))bis(oxy))bis(pyridine-2''',6''')-dicarbonyl dichloride) (11). **10** (0.1120 g, 0.2120 mmol) was added to a round bottom flask followed by thionyl chloride (3 mL, 0.04 mol) and DMF (1 drop). The contents of the flask were held at reflux under nitrogen for 12 h and the solvent was removed by vacuum. The material was used directly without further purification; the yield was assumed to be quantitative.

Tetraisopropyl 4,4'-(decane-1'',10''-diylbis(oxy))bis(pyridine-2,6-dicarboxylate) (12). A round bottom flask containing acetonitrile (200 mL), 1,10-dibromodecane (7.04 g, 23.5 mmol), **7** (12.78 g, 47.82 mmol), and potassium carbonate (8.50 g, 61.5 mmol) under nitrogen was held at reflux for 4 days, after which it was filtered through Celite® p 545 and the solvent was removed by rotary evaporation. The crude material was dissolved in DCM and washed with Na_2CO_3 (2x), saturated NaCl (4x), and dried over sodium sulfate. Filtration and removal of the solvent provided the desired product as a white solid: 15.63 g (99%), mp 76.8–78.0 °C. ^1H NMR (500 MHz, CDCl_3) δ 7.72 (s, 4H), 5.29 (hept, $J = 6$ Hz, 4H), 4.12 (t, $J = 6$ Hz, 4H), 1.89–1.80 (m, 4H), 1.76–1.27 (m, 36H). ^{13}C NMR (126 MHz, CDCl_3) δ 166.92 (s), 164.29 (s), 150.52 (s), 114.08 (s), 70.13 (s), 68.91 (s), 29.44 (s), 29.27 (s), 28.80 (s), 25.88 (s), 21.81 (s) (11 peaks expected and 11 peaks found). High res MS: calc. for $\text{C}_{36}\text{H}_{52}\text{N}_2\text{O}_{10}$ [$\text{M} + \text{H}$] $^+$: m/z 673.3695; found: m/z 673.3707 (error 1.8 ppm)

4,4'-(Decane-1'',10''-diylbis(oxy))bis(pyridine-2,6-dicarboxylic acid) (13). **12** (1.86 g, 2.76 mmol) in THF (50 mL) and 10% wt. potassium hydroxide (50 mL) was held at reflux for 24 h,

followed by the removal of THF by rotary evaporation. The aqueous solution was acidified to pH 1 using concentrated HCl and the precipitate was collected via filtration: 1.0831 g (78 %) of a white solid, mp 192.8–196.1 °C. ¹H NMR (500 MHz, DMSO-*d*₆) δ 7.69 (s, 4H), 4.21 (t, *J* = 6 Hz, 4H), 1.85–1.68 (m, 4H), 1.35 (m, 12H). ¹³C NMR (126 MHz, DMSO-*D*₆) δ 166.71 (s), 165.27 (s), 149.65 (s), 113.51 (s), 68.69 (s), 28.83 (s), 28.59 (s), 28.12 (s), 25.21 (s) (9 peaks expected and 9 peaks found). HR MS: calc. for C₂₄H₂₈O₁₀N₂ [M + H]⁺: *m/z* 505.1817; found: *m/z* 505.1840 (error –4.6 ppm).

4,4'-(Decane-1'',10''-diylbis(oxy))bis(pyridine-2,6-dicarboxylic acid chloride) (14). 13 (0.2025 g, 0.4014 mmol), thionyl chloride (2.0 mL, 28 mmol) and DMF (1 drop) under nitrogen were held at reflux for 12 h and the solvent was removed by vacuum. The material was used directly without further purification, assuming the yield was quantitative.

Biscryptand (dibenzo-30-crown-10-based pyridyl cryptand containing a hydroquinone linkage) (16). A mixture of dry DCM (700 mL), **15** (0.52911 g, 0.88679 mmol), pyridine (2 mL), and acidic alumina (1.00 g) was stirred for 1 h. **11** (0.26701 g, 0.44340 mmol) dissolved in 20 mL of DCM then added. Stirring was continued for 32 h; the mixture was filtered through a small plug of neutral alumina. The solvent was removed by rotary evaporation and the crude material was taken up in DCM and washed with 1 M HCl (3x), water (3x) and dried over sodium sulfate. After filtration the solvent was removed by rotary evaporation and the material was purified using flash column chromatography, eluting with DCM to MeOH over neutral alumina: 0.1697 g (23%) of a white solid, mp 197.6–200.5 °C. ¹H NMR (500 MHz, CDCl₃) δ 7.91 (s, 4H), 6.99–6.93 (m, 8H), 6.90 (m, 4H), 6.79–6.77 (m, 4H), 5.31 (s, 8H), 4.53–4.48 (m, 4H), 4.36 (m, 4H), 4.20–4.14 (m, 8H), 4.03–3.99 (m, 8H), 3.96–3.92 (m, 8H), 3.85–3.80 (m, 8H), 3.75 (m, 8H), 3.73–3.68 (m, 16H), 3.65 (m, 12H). ¹³C NMR (126 MHz, CDCl₃) δ 166.66 (s), 164.84 (s),

153.04 (s), 150.10 (s), 149.05 (s), 148.94 (s), 128.16 (s), 121.73 (s), 115.89 (s), 114.61 (s), 114.32 (s), 114.00 (s), 71.02 (s), 70.79 (s), 70.76 (s), 70.65 (s), 69.72 (s), 69.49 (s), 69.03 (s), 68.84 (s), 67.74 (s), 67.46 (s), 66.74 (s) (23 signals expected and 23 signals found). High res MS: calc. for $C_{84}H_{100}N_2O_{32} [M + 2H]^{+2}$: m/z 825.3203; found: m/z 825.3223 (error 2.4 ppm).

Biscryptand (dibenzo-30-crown-10-based pyridyl cryptand containing a C₁₀ linkage) (17).

A mixture of dry DCM (700 mL), **15** (0.4789, 0.8026 mmol), pyridine (2 mL), and acidic alumina (1.0 g) was stirred for 1 h. **14** (0.2025 g, 0.4014 mmol) dissolved in 20 mL of DCM then added. Stirring was continued for 32 h; the mixture was filtered and the solvent was removed by rotary evaporation. The crude material was taken up in DCM and washed with 1 M HCl (3x), water (3x), then dried over sodium sulfate. After filtration the solvent was removed by rotary evaporation and the material was purified using flash column chromatography, eluting with DCM to MeOH over neutral alumina: 0.2828 g (43%) of a white solid, mp 103.9–106.2 °C. ¹H NMR (500 MHz, CDCl₃) δ 7.82 (s, 4H), 6.97–6.92 (m, 8H), 6.77 (d, *J* = 9 Hz, 4H), 5.31 (s, 8H), 4.16 (m, 12H), 4.01 (m, 8H), 3.93 (m, 8H), 3.81 (m, 8H), 3.75 (m, 8H), 3.71–3.68 (m, 16H), 3.64 (m, 8H), 1.86 (m, 4H), 1.49 (m, 4H), 1.41–1.32 (s, 8H). ¹³C NMR (126 MHz, CDCl₃) δ 167.03 (s), 165.00 (s), 149.95 (s), 149.04 (s), 148.94 (s), 128.19 (s), 121.70 (s), 114.52 (s), 114.32 (s), 114.02 (s), 71.04 (s), 70.81 (s), 70.76 (s), 70.66 (s), 69.73 (s), 69.49 (s), 69.05 (s), 68.86 (s), 67.67 (s), 29.43 (s), 29.25 (s), 28.76 (s), 25.86 (s) (24 peaks expected and 23 peaks found; it is believed that one peak overlaps another in the 71.04 to 70.66 region). MS: calc. for $C_{84}H_{108}N_2O_{30} [M+H]^+$: m/z 1625.7065; found m/z 1625.6921 (error –8.86 ppm)

References

- (1) Gibson, H. W.; Yamaguchi, N.; Jones, J. W. *J. Am. Chem. Soc.* **2003**, *125*, 3522-3533.
- (2) Niu, Z.; Huang, F.; Gibson, H. W. *J. Am. Chem. Soc.* **2011**, *133*, 2836-2839.

- (3) Huang, F.; Nagvekar, D. S.; Zhou, X.; Gibson, H. W. *Macromolecules* **2007**, *40*, 3561-3567.
- (4) Pederson, A. M. P.; Ward, E. M.; Schoonover, D. V.; Slebodnick, C.; Gibson, H. W. *J. Org. Chem.* **2008**, *73*, 9094-9101.
- (5) Pederson, A. M. P.; Vctor, R. C.; Rouser, M. A.; Huang, F.; Slebodnick, C.; Schoonover, D. V.; Gibson, H. W. *J. Org. Chem.* **2008**, *73*, 5570-5573.
- (6) Huang, F.; Switek, K. A.; Zakharov, L. N.; Fronczek, F. R.; Slebodnick, C.; Lam, M.; Golen, J. A.; Bryant, W. S.; Mason, P. E.; Rheingold, A. L.; Ashraf-Khorassani, M.; Gibson, H. W. *J. Org. Chem.* **2005**, *70*, 3231-3241.
- (7) Huang, F.; Lam, M.; Mahan, E. J.; Rheingold, A. L.; Gibson, H. W. *Chem. Commun.* **2005**, 3268-3270.
- (8) Huang, F.; Slebodnick, C.; Switek, K. A.; Gibson, H. W. *Chem. Commun.* **2006**, 1929-1931.
- (9) Huang, F.; Gibson, H. W.; Bryant, W. S.; Nagvekar, D. S.; Fronczek, F. R. *J. Am. Chem. Soc.* **2003**, *125*, 9367-9371.
- (10) Huang, F.; Zhou, L.; Jones, J. W.; Gibson, H. W.; Ashraf-Khorassani, M. *Chem. Commun.* **2004**, 2670-2671.
- (11) Niu, Z.; Gibson, H. W. *Org. Biomol. Chem.* **2011**, *9*, 6909-6912.
- (12) Gibson, H. W.; Wang, H.; Slebodnick, C.; Merola, J.; Kassel, W. S.; Rheingold, A. L. *J. Org. Chem.* **2007**, *72*, 3381-3393.
- (13) Huang, F.; Slebodnick, C.; Switek, K. A.; Gibson, H. W. *Tetrahedron* **2007**, *63*, 2829-2839.
- (14) Yu, M.; Tang, R.-Y.; Li, J.-H. *Tetrahedron* **2009**, *65*, 3409-3416.
- (15) Bryant, W. S.; Jones, J. W.; Mason, P. E.; Guzei, I.; Rheingold, A. L.; Fronczek, F. R.; Nagvekar, D. S.; Gibson, H. W. *Org. Lett.* **1999**, *1*, 1001-1004.
- (16) Perlmutter-Hayman, B. *Acc. Chem. Res.* **1986**, *19*, 90-96.
- (17) Marshall, A. G. *Biophysical Chemistry: Principles, Techniques and Applications*; John Wiley & Sons: New York: New York, 1978.
- (18) Connors, K. A. *Binding Constants: The Measurement of Molecular Complex Stability*; 1st edition ed.; Wiley-Interscience, 1987.
- (19) Huang, F.; Fronczek, F. R.; Gibson, H. W. *J. Am. Chem. Soc.* **2003**, *125*, 9272-9273.
- (20) Niu, Z.; Slebodnick, C.; Gibson, H. W. *Org. Lett.* **2011**, *13*, 4616-4619.
- (21) Howáth, G.; Rusa, C.; Köntös, Z.; Gerencsér, J.; Huszthy, P. *Synth. Commun.* **1999**, *29*, 3719-3731.
- (22) Wong, W. W. H.; Curiel, D.; Cowley, A. R.; Beer, P. D. *Dalton Trans.* **2005**, 359-364.

Chapter 8

Supramolecular Polymers

Introduction

Previous chapters focused upon the production of high yielding synthetic procedures for the production of cryptands and determined that the most efficient way to produce biscryptands was via dual cyclizations, which were made possible through templation. This chapter focuses on use of the previously produced biscryptands as monomers for supramolecular polymers by association with bisparaquats. Supramolecular polymers are of particular interest because of their dynamic character. This dynamic character allows for reversibility, since the linkages are constantly breaking apart and reforming. The extent of this process is defined in terms of an association constant, K_a ; **Figure 8.1** provides an example of this.

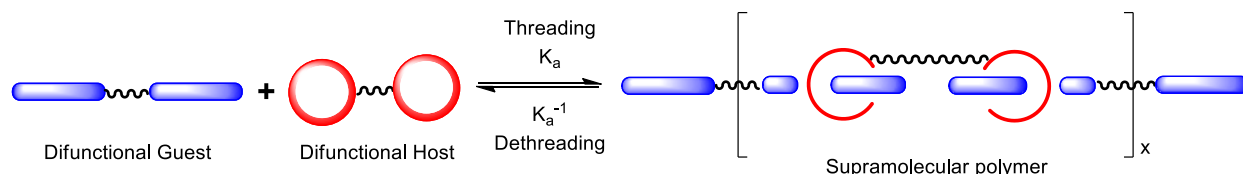
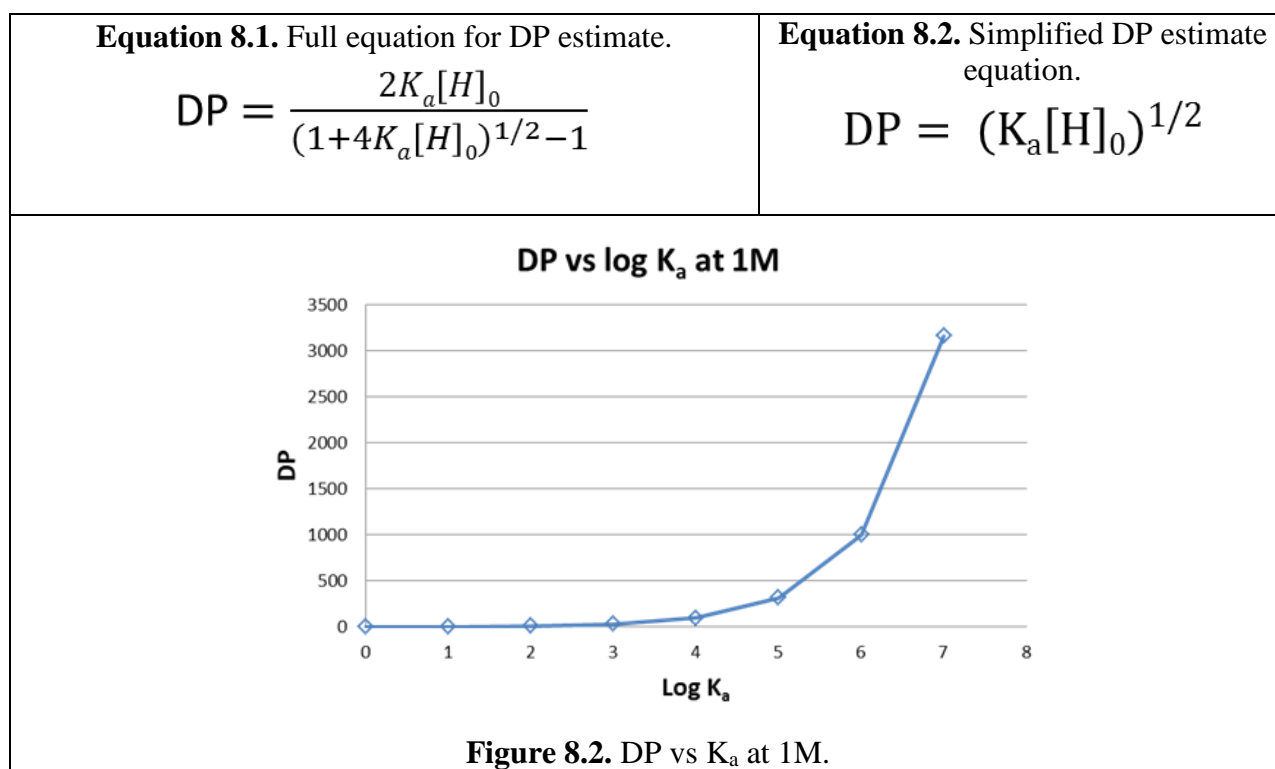


Figure 8.1. Association and disassociation of a supramolecular polymer.

Polymers of this type are thus unique in the sense that if the polymer sustains damage at the points of association, the polymer will be capable of repairing itself; thus these systems are sometimes marketed as being “self-healing”. A range of supramolecular polymers exist employing the crown ether motif to form polymeric structures. Additionally, it should be noted that some of these crown ether systems have displayed a strong tendency to thermally self-heal when deformed.¹ Stimuli have the ability to influence the association constant of the crown ether motif and to a certain extent the association constant can be controlled via stimuli such as

temperature, pH, electrochemistry, counter ion or light.² Recently supramolecular polymers have been reported using cryptand motifs of varying types.³ The extremely high binding pyridyl cryptand motif, however, has yet to be incorporated into a supramolecular polymer.

Although crown ethers have served the supramolecular community well, the focus of this work is on accessing and utilizing the higher binding cryptand motif. When considering supramolecular polymers, the association constant of the complex can be used to determine the degree of polymerization (DP) achievable for that system at a given concentration using **Equation 8.1**.⁴ When association constants are sufficiently high (i. e., $4K_a[H]_0 \gg 1$) the equation simplifies to **Equation 8.2**.



Equation 8.1 shows at a specific concentration of host the dependence of DP on the association constant. In **Figure 8.2** the DP for a hypothetical supramolecular polymer has been estimated at a concentration of 1 M while varying the K_a from 0 to 10 million. From **Figure 8.1**

it can be seen that the DP responds exponentially to the association constant; a DP of 100 is not achieved at a 1 M concentration until K_a is ten thousand. This becomes fairly problematic when considering most crown ethers have association constants below $1,000 \text{ M}^{-1}$ at $25 \text{ }^\circ\text{C}$; this translates into most crown ethers having a maximum DP of about 32. The normal workaround for this, to reach entanglement molecular weight, is to use amply high molecular weight monomers, since molecular weight actually dictates if polymeric properties are observed. A pyridyl cryptand system with paraquat would not need such a workaround to achieve a high molecular weight polymer. The pyridyl dibenzo-30-crown-10 cryptand with dimethyl paraquat PF_6 in acetone has an association constant of 1×10^5 , while the same cryptand with dibenzyl paraquat TFSI in DCM has an association constant of 1×10^6 . Using these association constants in **Equation 8.1** gives a DP of 316 for the acetone system and 1,000 for the DCM complex; either system is thus capable of producing a truly high molecular weight polymer.

In addition to the straight forward argument that higher association constants lead to higher molecular weight supramolecular polymers, it must also be acknowledged that association constants are highly depended on solvent and temperature; this adds a degree of control to DP. Moreover, the concentration of supramolecular monomers can be used to alter the DP of the polymeric system. As a last form of control over molecular weight, a monofunctional host or guest can be added to end cap the polymer. These items together highlight how the molecular weight of a supramolecular polymer is highly controllable and to what a great extent the molecular weight can be altered if sufficiently high association constants are employed. With a high association constant, using solvent, temperature, and concentration, a specific degree of polymerization can be “dialed in” by use of **Equation 8.1**.

Additionally, the previously stated points extend to supramolecular chain extensions as well, since the same biscryptands can be employed. For these reasons, an investigation was made into polymer chain extensions using one of the prepared biscryptands. Although several types of chain extensions exist, **Figure 8.3** displays a cartoon showing how a polymeric chain extension will be achieved here using a biscryptand. A polymer either terminated or initiated with a guest such as paraquat would allow for the doubling of its molecular weight through the addition of a biscryptand, via the linking of the two chains.

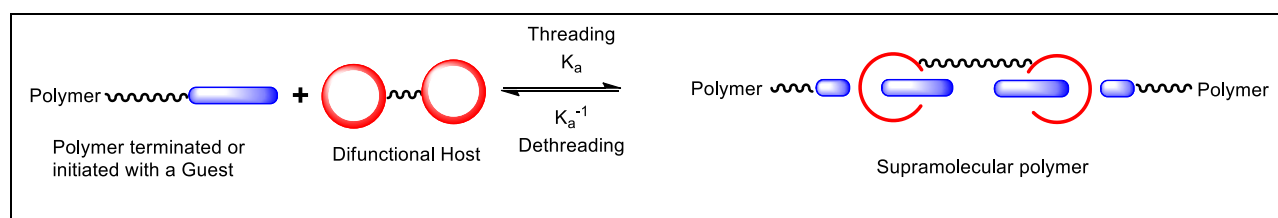


Figure 8.3. Cartoon depicting the intended chain extension technique employed within.

Results and Discussion

The biscryptands used in this work are those generated in chapter 7 via templation, **VII 16** and **VII 17** (**Figure 8.4**). To avoid confusion, compounds produced and described in other chapters will be labeled using that chapter's number as a Roman numeral followed by the compound's number in that chapter; as an example a compound found in chapter 7 and number in chapter 7 as 16 would be **VII 16**. The dibenzo-30-crown-10-based pyridyl cryptand motif was chosen over the bis(*m*-phenylene)-32-crown-10-based pyridyl cryptand for two reasons. First, a significantly higher total yield for the dibenzo-30-crown-10-based pyridyl cryptand was obtained. Second, work presented in previous chapters demonstrated that the dibenzo-30-crown-10-based pyridyl cryptand was capable of providing association constants similar to that of the

bis(*m*-phenylene)-32-crown-10-based pyridyl cryptand with dibenzyl paraquat TFSI in DCM at 25 °C.

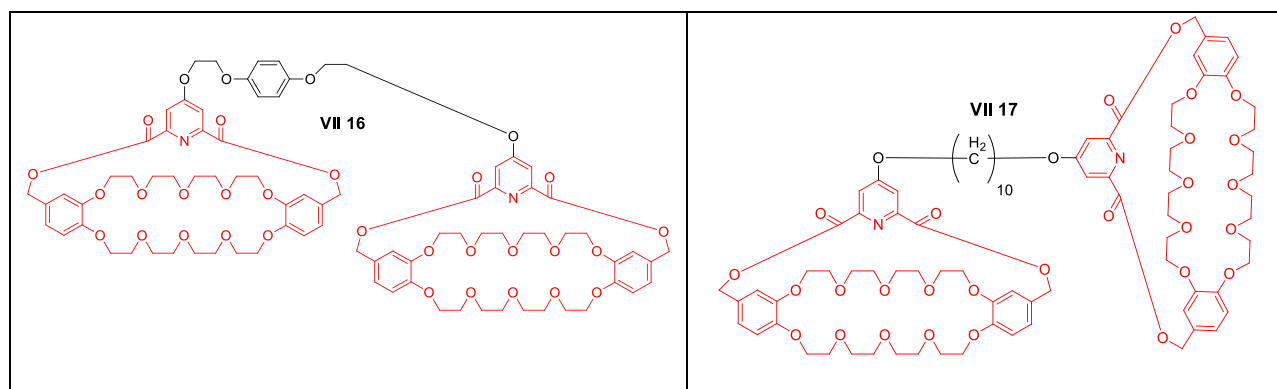
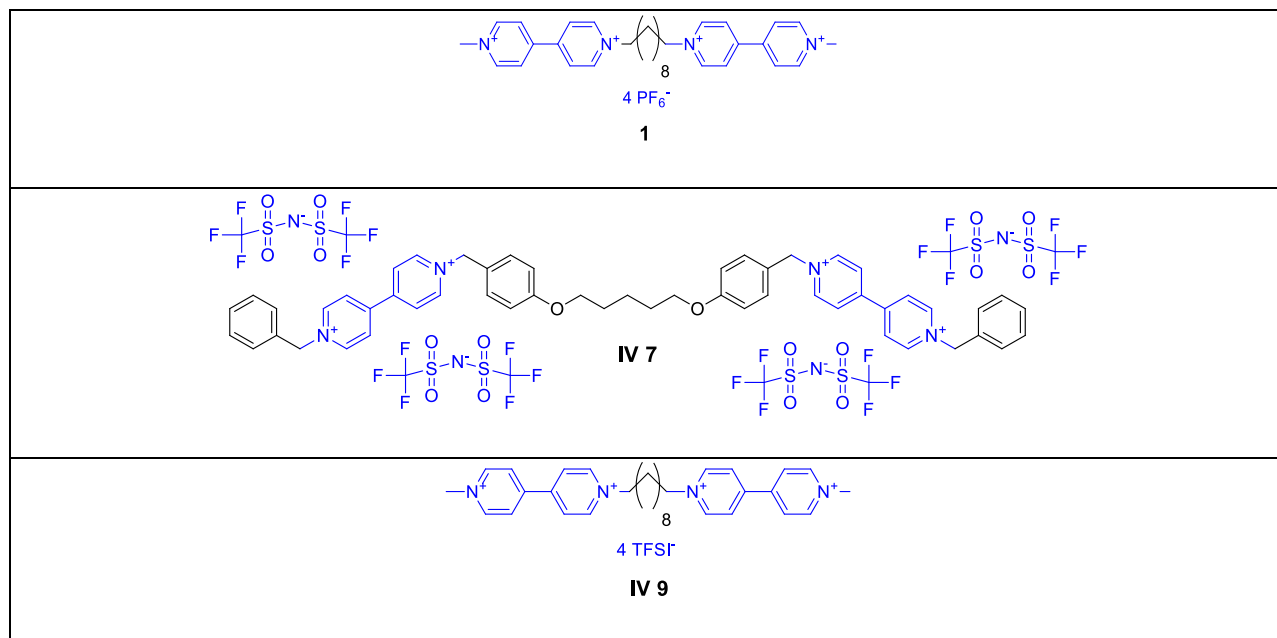


Figure 8.4. Biscriptands **VII 16** and **VII 17**.

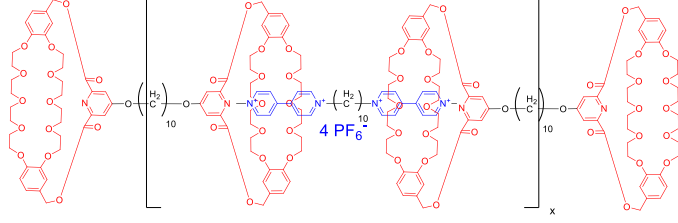
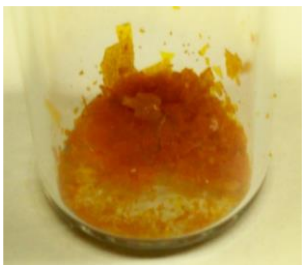
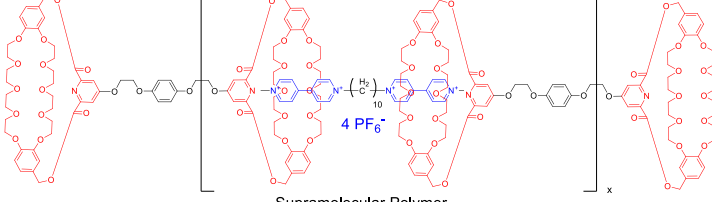

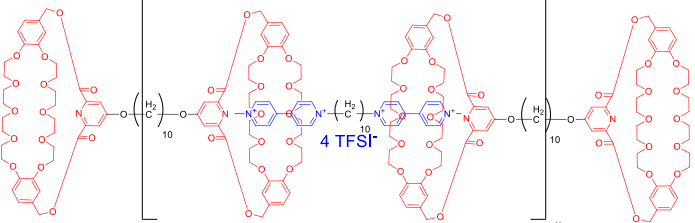

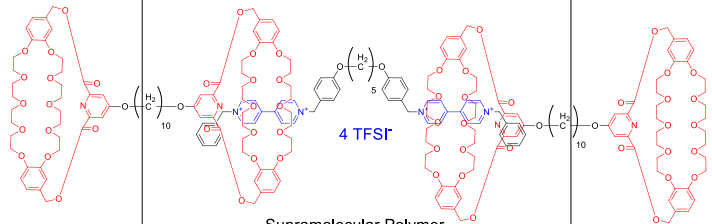

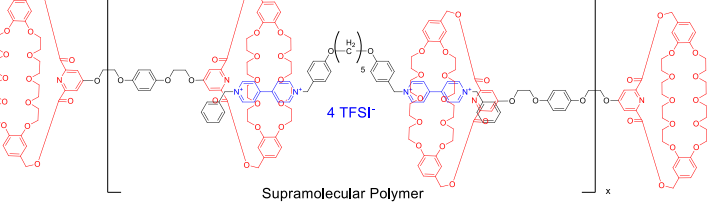

Bisparaquats used for this study are **1**, **IV 7**, and **IV 9** (**Scheme 8.1**). These bisparaquat were chosen for the following reasons. First, the literature⁵ dictates that to avoid the formation of cyclic species and promote the formation of linear supramolecular polymers, a linker of at least 10 atoms should be used.⁵ On an individual basis, **1** was chosen due to its high literature occurrence with crown ether and crown ether-like supramolecular polymer systems;^{3,6,7} this aids in assessing the newly developed biscriptands. **IV 9** was developed because of the drastic solubility increases observed in Chapter 4 using the TFSI counter ion instead of PF₆. Additionally, since the only difference between **IV 9** and **1** is a change from PF₆ to TFSI, direct conclusions about TFSI can be made. Model systems in Chapter 4 showed TFSI paraquats employing the N-benzyl group over N-methyl resulted in compounds soluble in DCM. **IV 7** contains two benzyl groups to insure maximum solubility in DCM. Additionally, benzylic groups provide increased molecular weight over their methyl counterparts. In theory, the increased solubility of **IV 9** and **IV 7** in less polar solvents should allow the polymers to be

formed in less polar solvents such as DCM, thereby achieving higher molecular weights than in more polar solvents such as acetone.



Scheme 8.1. Bisparaquats.

Using the host monomers **VII 16** and **VII 17** along with the guest monomers **1**, **IV 7**, and **IV 9**, five supramolecular polymers were synthesized by dissolving the host and guest separately and combining them. The monomers and polymers are as follows: **VII 17** + **1** for polymer **P1**, **VII 16** + **1** for polymer **P2**, **VII 17** + **IV 9** for polymer **P3**, **VII 17** + **IV 7** for polymer **P4**, and **VII 16** + **IV 7** for polymer **P5**. **P1–P5** are shown in **Scheme 8.2** along with a picture of a film of the supramolecular polymers cast from the indicated solvents.

<p>$\text{VII 17} + 1 \xrightleftharpoons{k_a}$</p>  <p>Supramolecular Polymer P1</p>	
<p>$\text{VII 16} + 1 \xrightleftharpoons{k_a}$</p>  <p>Supramolecular Polymer P2</p>	
<p>$\text{VII 17} + \text{IV 9} \xrightleftharpoons{k_a}$</p>  <p>Supramolecular Polymer P3</p>	
<p>$\text{VII 17} + \text{IV 7} \xrightleftharpoons{k_a}$</p>  <p>Supramolecular Polymer P4</p>	
<p>$\text{VII 16} + \text{IV 7} \xrightleftharpoons{k_a}$</p>  <p>Supramolecular Polymer P5</p>	

Scheme 8.2. Supramolecular polymers **P1** – **P5** along with their pictures. Films were cast via slow solvent evaporation using the following solvent systems and substrates: **P1** (chloroform / acetonitrile, 1/1 v/v on Teflon); **P2** (1,2-dichloroethane on silicon); **P3** (*o*-dichlorobenzene on glass); **P4** (1,2-dichloroethane on Teflon); **P5** (chloroform / acetonitrile, 1/1 v/v on glass).

The polymers were synthesized by dissolving the host monomer in chloroform and the guest monomer in acetone. The solutions of host and guest monomers independently were either colorless or slightly yellow. However, upon mixing the solutions instantly turned either a dark yellow or deep orange color, which persisted even after solvent evaporation. Color changes such as those observed are indicative of binding between cryptand hosts and paraquat guests due to charge transfer. Films cast by slow solvent evaporation were brittle. Casting was attempted with all polymers using the following solvent systems (as well as specifically indicated solvents in the text): DCM, chloroform / acetonitrile (1/1 v/v), and 1,2-dichloroethane.

P1 and **P2**, which employ a PF_6^- counter ion, resulted in very brittle films that could not be removed in their entirety or even pieces much larger than small flakes from glass, silicon, or Teflon. The picture shown for **P1** in **Scheme 8.2** is nothing more than flakes and the picture of **P2** is shown before removal from the casting mold. Polymers resulting from the TFSI⁻ counter ion (**P3–P5**) result in visually brittle polymers, but unlike their PF_6^- counter parts these polymers were removable from the surfaces of glass, silicon, and Teflon. Casting of **P5** was only carried out on a glass surface.

Castings of **P3** and **P4** were also carried out by redissolving the polymers in chloroform and allowing slow solvent evaporation. The results for all attempts were the same, a brittle material. Additionally, casting of **P3** was also carried out using *o*-dichlorobenzene (**Scheme 8.2**), which resulted in a material which was bendable for approximately one day while the material was plasticized. After this point, once an ample amount of *o*-dichlorobenzene had time to

evaporate, the film became brittle. It should also be noted that for polymers containing the TFSI⁻ counterion and cast from chloroform / acetone (50:50 v/v), it took 6 to 24 hours after casting for the film to reach its full brittleness. It was suspected that residual solvent was plasticizing the polymer and after 6 to 24 hours, the solvent had completely evaporated from the material. During this time slight deformations could be made to the material, again attributable to the material being slightly plasticized.

Visual inspection also shows that polymers **P1** to **P4** resulted in the formation of clear films, indicating amorphous polymers. To demonstrate the clarity of the films, **Figure 8.5** shows **P3** cast on glass and laying atop a sheet of paper containing text. Interestingly, **P5** was the only polymer of **P1–P5** which did not result in a clear material; films of **P5** were opaque as seen in **Scheme 8.2**.

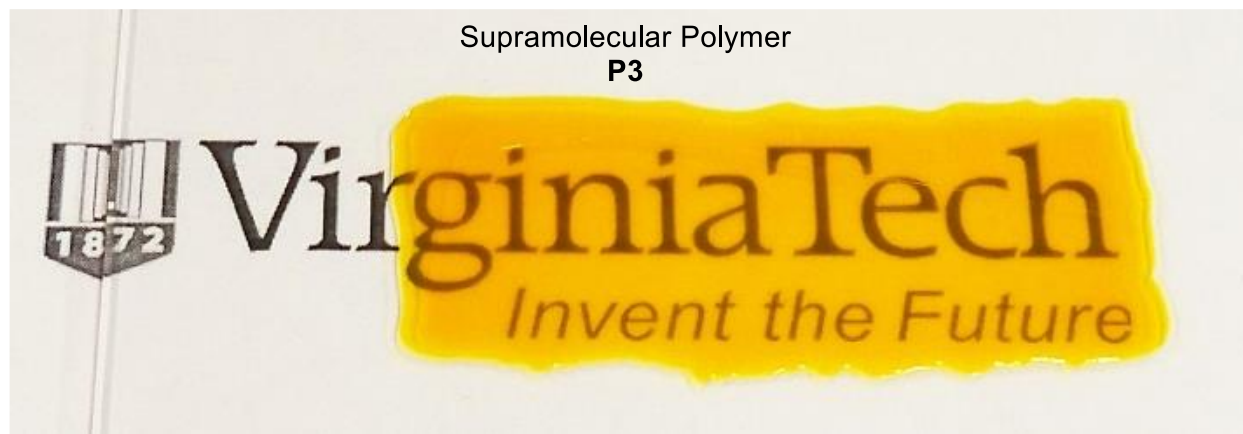


Figure 8.5. Supramolecular polymer **P3** cast on glass and laid on top of text to show clarity.

The last purely visual observation for **P1–P5** is that fibers could be pulled from high concentration solutions of all of the TFSI⁻ containing polymers (**P3** to **P5**). **Figure 8.6** shows images of a fiber pulled from **P3** made from a concentrated equimolar solution of **1** and **6**; in the figure, image A shows the flexible orange fibers pulled from **P3**, while images B, C, and D show

the fiber under light microscopy with increasing magnification (10x, 40x, and 60x respectively). It should be noted that fibers of **P3** were found to be flexible and strong enough to resist snapping while being bent, as seen in image A and B of **Figure 8.6**. A visual comparison of fibers and films from **P3** gave different observations; films were brittle and chipped upon applying mild force to the film, while fibers were capable of withstanding a mild amount of stress from bending and tugging.

One explanation for the drastically different behavior of films and fibers is how the solvent evaporates during polymer formation. It is suspected that as the films are cast via slow solvent evaporation, one of the monomers begin to precipitate before the other. Even when using TFSI paraquats, there is a large solubility difference between pyridyl cryptands and paraquats. Due to the ionic nature of paraquats, they are highly soluble in polar solvents such as acetone or acetonitrile, while cryptands tend to be highly soluble in mid-range polarity solvents such as DCM. This leads to a potential problem, due to the dynamic nature; if a linkage falls apart at sufficiently high concentrations, it is likely that one of the monomers precipitates out while the other stays in solution. However, as fibers are drawn, the solvent is flashed off as the polymer is pulled from solution, negating precipitation problems.

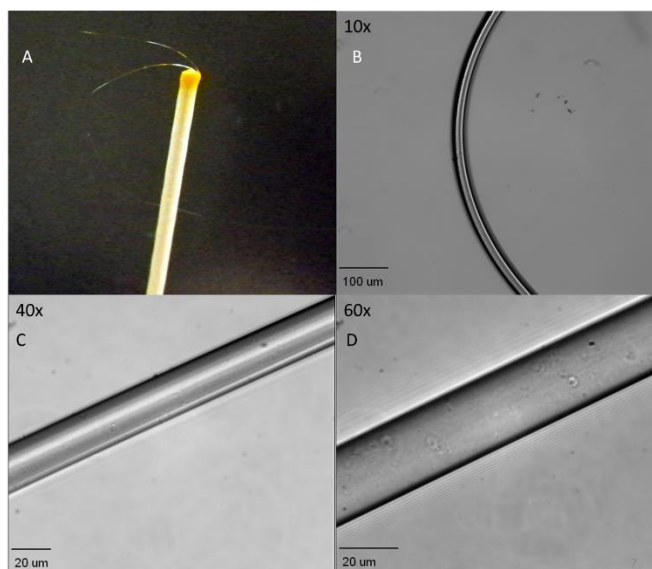


Figure 8.6. A) **P3** fiber color image taken on a black background, B) **P3** fiber differential interference contrast image at 10x magnification, C) **P3** fiber differential interference contrast image at 40x magnification, D) **P3** fiber differential interference contrast image at 60x magnification.

As supramolecular systems are dynamic and not covalent, it becomes a challenge to provide an exact molecular weight for polymers **P1–P5**. Looking at **Equation 8.1** and **Equation 8.2** it can be seen that the degrees of polymerization for **P1–P5** are dependent upon the concentration. To determine at what concentration high molecular weight polymers are achieved, we measured the viscosity. Due to the amount of material which is required to carry out a viscosity experiment over a range of dilutions, only the polymer **P3** was chosen for assessment. The solvent chosen for the viscosity experiment was DCM, to maximize the association constant and thus provide a best case scenario. **Figure 8.7** shows a log-log plot of specific viscosity vs. concentration of **P3** in DCM; the critical concentration where supramolecular polymer begins to form is where the two trend lines cross (log ~ -1.2 or 63 mM). The trend lines provide reasonable correlations. This plot indicates that for any equimolar concentration of monomers **VII 17** and **IV 9** in DCM above a concentration of 63 mM, a supramolecular polymer

is present in solution. Although dimethyl paraquat TFSI is not soluble enough in DCM to obtain an association constant with **VII 17**, using the association constant of dibenzyl paraquat TFSI with **VII 17** in DCM, $K_a \text{ average} = 4.36 \times 10^5$ (chapter 7), a reasonable estimate of DP may be made. Using **Equation 8.2** it is estimated that at a 63 mM concentration, the supramolecular polymer's DP = 166; with a repeat unit of 3,229 g / mol, this gives a theoretical molecular weight of 536 kDa.

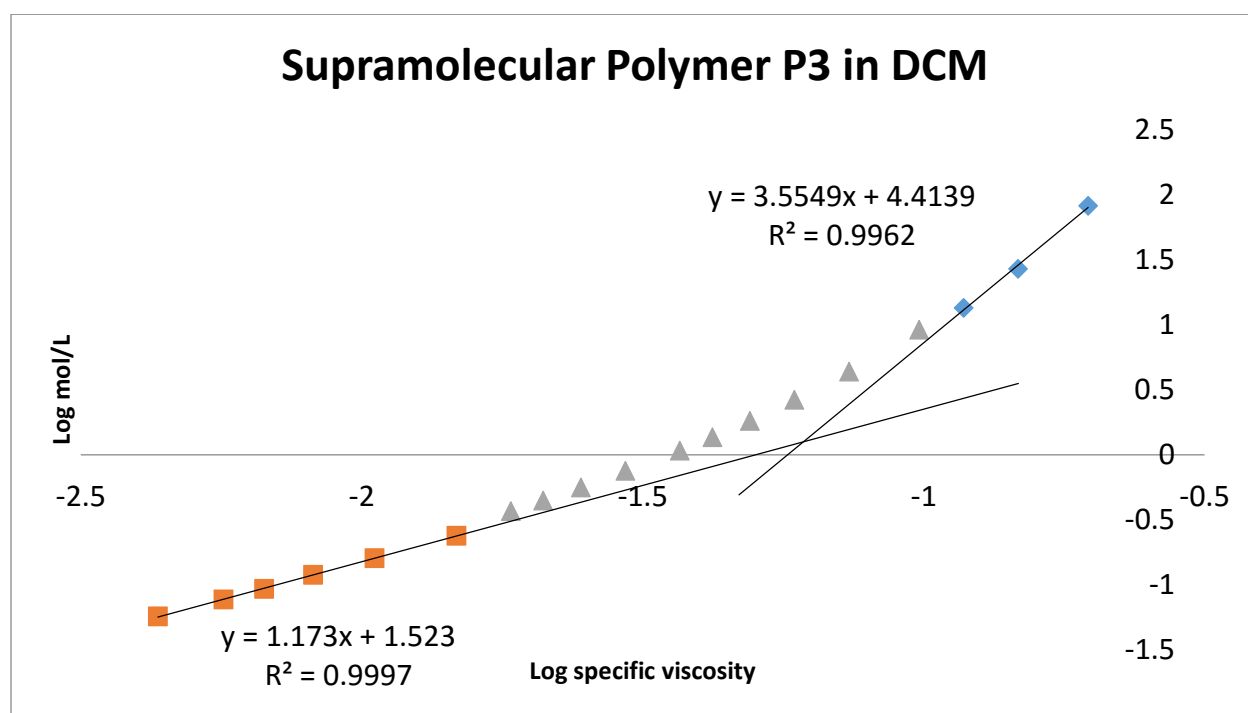


Figure 8.7. Viscosity plot of **P3**.

Despite 536 kDa being a large number, similar supramolecular cryptand / paraquat systems have been reported having critical monomer concentrations close to the observed 63 mM. Recent work from Niu et al. reported a supramolecular polymer made from a biscryptand/bisparaquat that displayed a critical monomer concentration of 53 mM.³ What is unique to the viscosity plot of **P3** however is the observed change in slopes for the two trend

lines along with the slope of the second line itself. The slope of the first trend line, which is attributed to cyclic dimeric species predominantly,^{4,5,8-10} is 1.17, while the slope of the second line, which is attributed to high molecular weight polymer is 3.55. Interestingly, the full span of the lower line is not linear; deviation from the first line begins at log conc = -1.6 or 30 mM, indicating that large oligomers are forming at low concentrations. It is noteworthy to point out that the slope of the second line, 3.55 is at the theoretical maximum.¹¹⁻¹³

In terms of the viscosity plot of **P3**, compared to a more notable supramolecular system of a differing type, the quadruple hydrogen bonding system of Meijer et. al. has been selected for comparison. Hydrogen bonding systems by Meijer et. al. has been found to contain association constants in excess of 10^6 M^{-1} and form supramolecular polymers.^{8,14,15} These systems have been found to contain critical monomer concentration around $\sim 130 \text{ mM}^8$ and contain slopes in the second lines of their log concentration vs. log viscosity plots of 3.76 and first lines of 1.¹⁴ By comparison, it can be seen that the newly developed polymer **P3** is on par with these systems.

Dynamic Light Scattering (DLS) was carried out on **P3** and **P4** at concentrations between 0.031 mM and 1.5 mM (1 mg/10 mL to 50 mg/10 mL and 1 mg/10 mL to 10 mg/10 mL, respectively) in DCM. As the highest of these values are well below the critical monomer concentration for **P3**, 63 mM, it was expected that only small oligomers or cyclic species would be present, displaying particle sizes less than 2 nm. **Figure 8.8**, however, shows that large particle sizes ($> 100 \text{ nm}$) were observed in DLS experiments, leading to the conclusion that the paraquat units are likely aggregated in the low dielectric solvent.

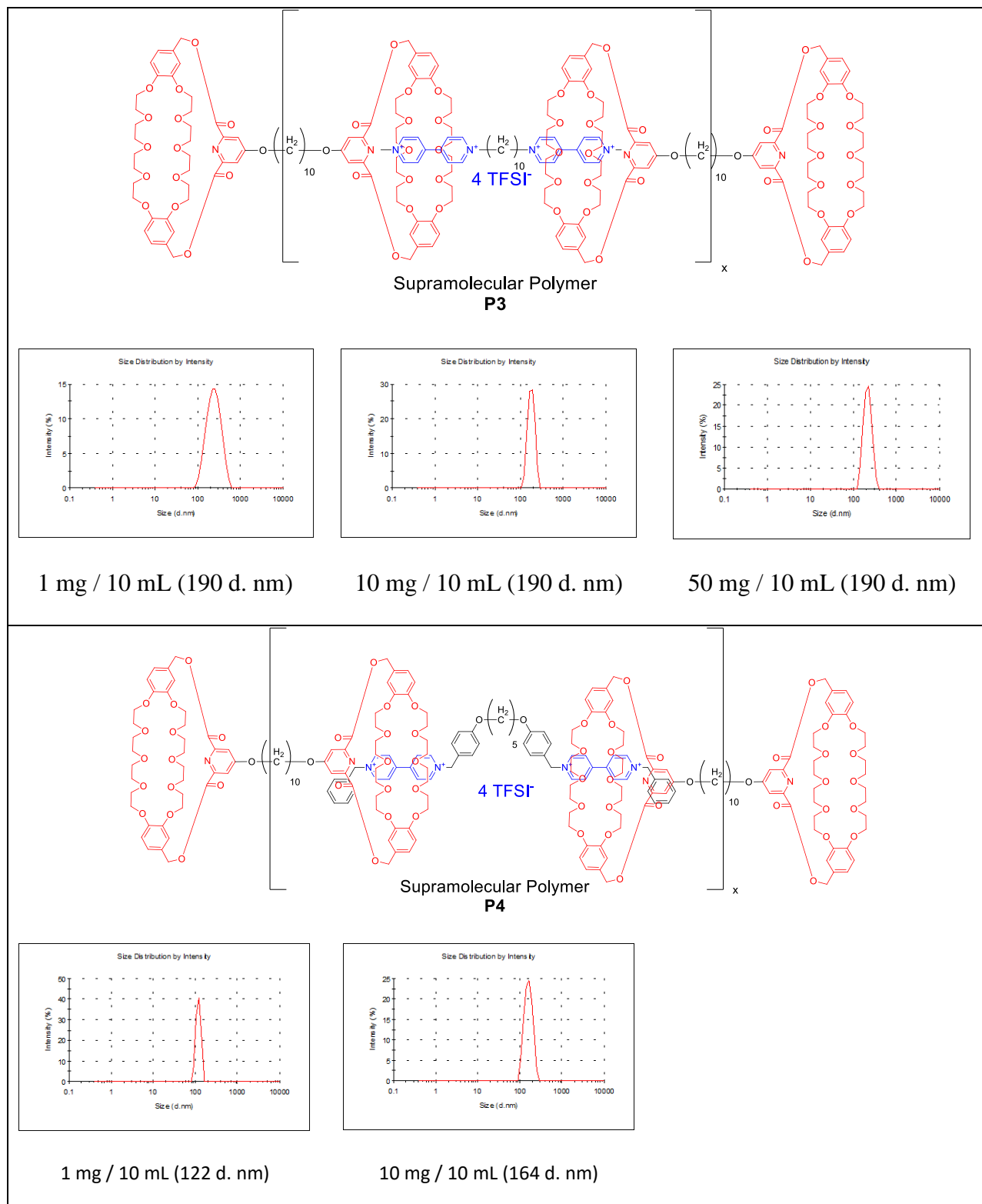


Figure 8.8. DLS data for **P3** and **P4**.

Thermal observations of T_g via DSC and 5% wt. loss by TGA for **P1** – **P5** are summarized in **Table 8.1**. T_g values for polymers **P1**–**P5** vary in the range of 44–103 °C and by direct comparison of polymers **P1** and **P3**, changing from a PF_6^- to a TFSI⁻ counter ion results in lowering the T_g of the material by 59 °C. **P2** produced from guest monomer **1** (PF_6^- counterion and ten carbon chain linkage) and host monomer **VII 16** (a hydroquinone linkage) provided the highest T_g value (112 °C). Comparing **P2** to **P1** we can see that the host hydroquinone linkage is responsible for a 9 °C increase in glass transition temperature over the use of a simple ten carbon alkyl straight chain. Additionally, it can be seen from **P2** and **P1** that there is no significant gain in thermal stability between the two host linkages, with weight loss values of 217 °C and 216 °C. It is interesting to note that **P2** has a higher T_g than **P1**, but upon changing the guest monomer to the benzylic TFSI paraquat **IV 7**, the T_g trends are inverted and **P5**, which contains host monomer **VII 16**, becomes the lower T_g by 2 °C, which is likely within experimental error. This inversion is attributed to the way in which binding occurs between the host and guest moieties and is supported by an increase in the association constants observed for benzylic paraquats over their methyl counter parts.

Table 8.1. T_g and 5% wt loss comparison of polymers **P1** - **P5**.

Host	Guest	Polymer	T_g	TGA 5% wt loss
VII 17 (c10)	1 (c10 PF_6^-)	P1	103 °C	217 °C
VII 16 (quinone)	1 (c10 PF_6^-)	P2	112 °C	216 °C
VII 17 (c10)	IV 9 (c10 TFSI)	P3	44 °C	223 °C
VII 17 (c10)	IV 7 (benzylic TFSI)	P4	78 °C	224 °C
VII 16 (quinone)	IV 7 (benzylic TFSI)	P5	76 °C	218 °C

An inspection of monomer DSC traces compared to resulting polymers show a clear loss of monomer crystallinity and the formation of an amorphous polymer. **Figure 8.9** shows an

overlay of DSC traces for monomers **VII 17** and **IV 9** along with the resulting polymer **P3** during the third heating cycle. As seen in **Figure 8.9**, the crystallinity of the guest monomer, **IV 9**, when combined with the host monomer, **VII 17**, has been lost and the presence of only a T_g indicates the formation of an amorphous polymer.

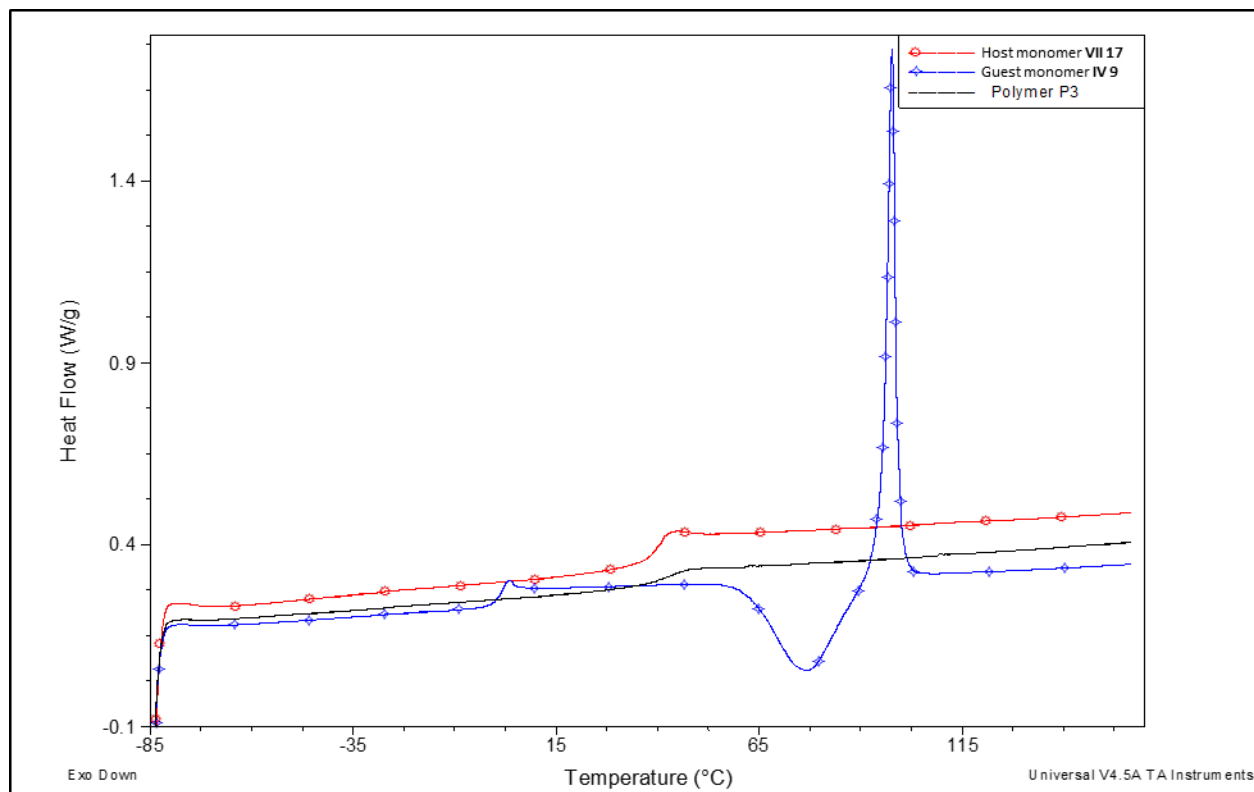


Figure 8.9. DSC overlay of monomer **VII 17**, monomer **IV 9**, and polymer **P3** using a scan rate of 5 °C / min, all traces are second heating.

Analysis via TGA showed a 5% wt. loss for polymers **P1–P5** closely grouped in the range of 216 °C to 224 °C. **Figure 8.10** shows an overlay of TGA data for polymers **P1–P5**; although 5% wt. loss values are similar for all five polymers, degradation patterns varied and were found to mostly depend upon the guest monomer. Degradation plots showed similar

patterns for a given counterion; this can be seen with **P1** and **P2** employing a PF_6^- counterion, and **P3–P5** employing a TFSI counterion.

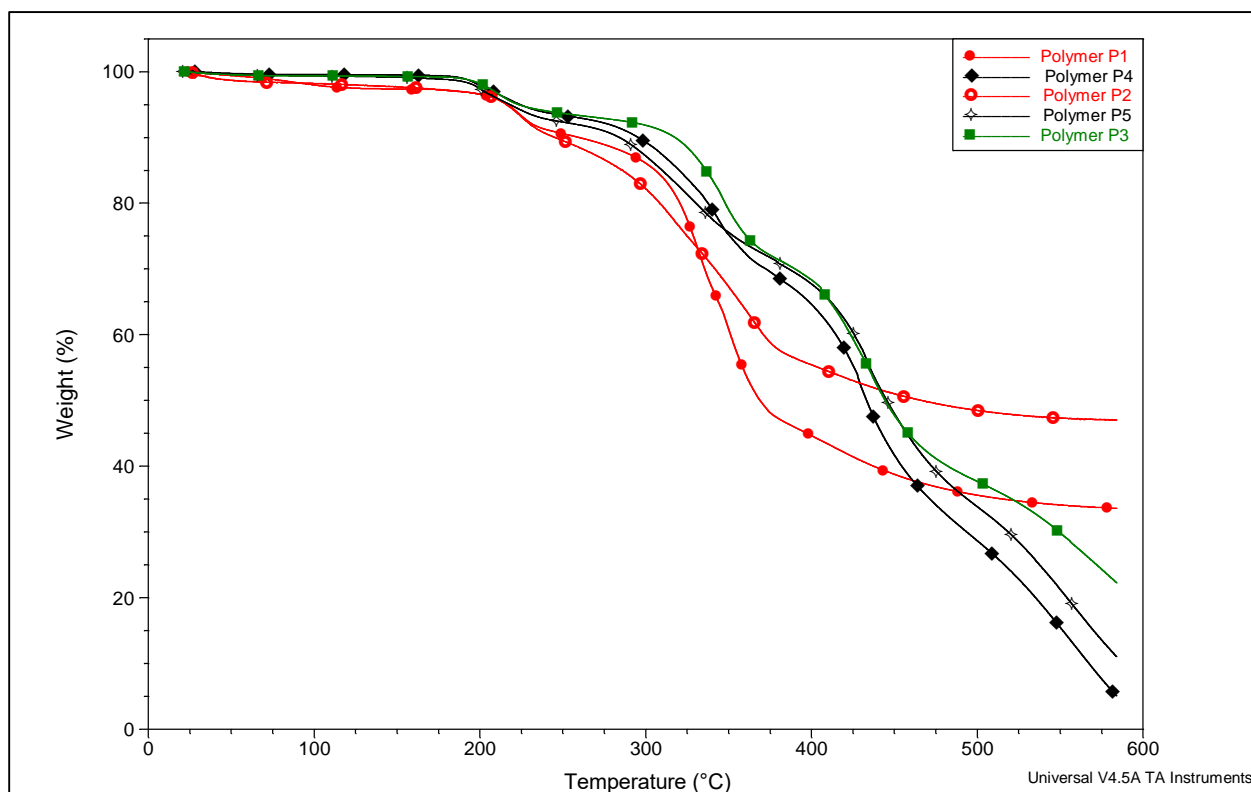
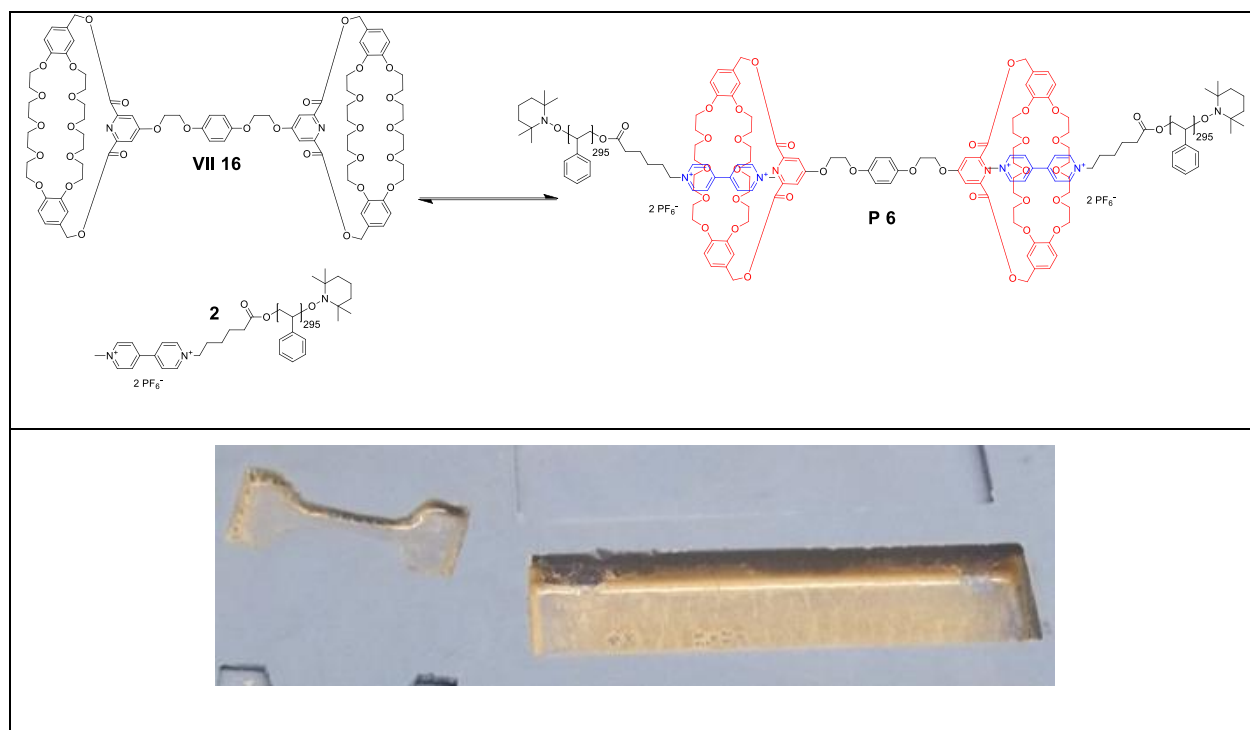


Figure 8.10. TGA overlay of polymers **P1–P5** using a heating rate of 20 °C / min under nitrogen.

By taking into account the theoretical degree of polymerization from association constants, demonstration of fiber formation, loss of crystallinity in the DSC trace, and viscosity experiments, it can be concluded that high molecular weight polymers have been achieved. Several attempts were made to correct the qualitative disparity between films and fibers by annealing films at elevated temperatures, melt pressing existing films for reannealing, casting from different solvents, and differing casting surfaces; however, no technique successfully changed the outcome. It is hypothesized that the reason for the poor behavior of the films is the drastic solubility difference between the two components. When a high dielectric solvent is used

such as acetone, the biscryptand has a much lower solubility than the paraquat, when a low dielectric solvent such as DCM is used, cryptands become the more soluble component. It is theorized that as solvent evaporates during casting the least soluble component falls out of solution first, skewing the stoichiometry and resulting in the formation of a film of relatively low molecular weight. When fibers are pulled from a concentrated solution, however, solvent evaporates rapidly from the polymer as it comes out of solution as a high molecular weight polymer. Further development of films will need to focus on processing techniques; one possible solution to this problem may be found in spin casting, as solvent would be removed relatively fast when compared to slow solvent evaporation.

As previously mentioned in the introduction, supramolecular chain extensions encompass many of the concepts and compounds found with supramolecular polymers. For these reasons an attempt was made to use biscryptand **VII 16** as a chain extender for a paraquat initiated polymer. **Scheme 8.3** shows the chain extension of polymer **2** using **VII 16**. Polystyrene paraquat was provided and prepared by Minjae Lee as described in his dissertation. **2** was determined to have a K_a of 1.66×10^5 in chloroform at 25 °C with the dibenzo-30-crown-10-based pyridyl cryptand, shown in red in **Scheme 8.3**. K_a results for the system were obtained via ITC by Daniel Schoonover; experimental conditions are described in his dissertation.¹⁶ Ideally due to the K_a of the system, nearly all the polymer should complex with **VII 16** to form the chain extended system **P6**.



Scheme 8.3. Synthesis of chain extended polystyrene paraquat.

Polymer **P6** was prepared by dissolving **VII 16** and **2** separately in chloroform and mixing the two solutions. Films cast from **P6** were pink, as seen in **Scheme 8.3**, and brittle. As with the previously synthesized supramolecular polymers containing the PF_6^- anion, **P1** and **P2**, films could not be removed from molds without chipping and breaking. In an attempt to validate that chain extension had occurred, solution viscosity was performed on **2** and **P6**. It was suspected that by doubling the molecular weight of the polymer via chain extension, the solution viscosity of **P6** would be noticeably higher than **2**. This however was not the case, as seen in **Figure 8.11**, the reduced and inherent viscosity of **P6** is lower than that of **2**. It is suspected that the paraquat units of **2** form aggregates in chloroform and when bis-cryptand **VII 16** is introduced, those aggregates are broken up. The net effect of breaking up the aggregates is a reduction in viscosity. As with polymers **P1–P5**, due to the brittle nature of **P6**, mechanical

testing was not possible. Future testing and experimenting will need to focus on casting techniques or a redesign.

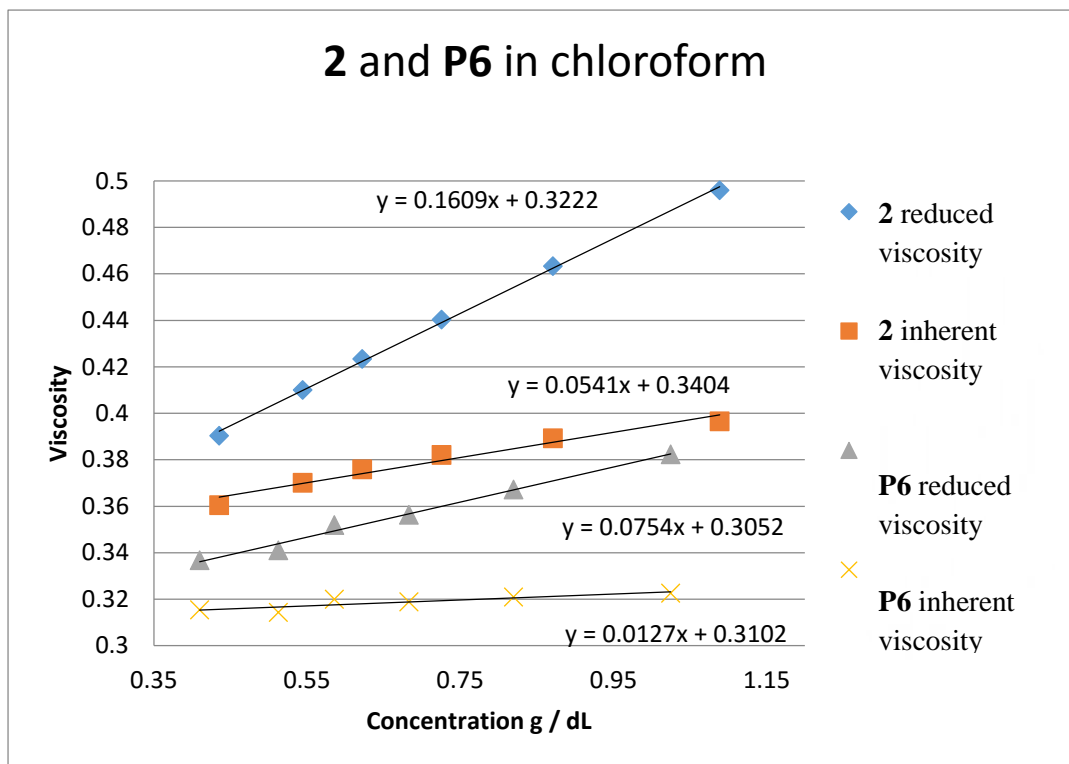


Figure 8.11. Viscosity plot of **2** and **P6** in chloroform at 25 °C.

Conclusions

Five supramolecular polymers, **P1–P5**, were been successfully synthesized in solution by taking advantage of the supramolecular cryptand / paraquat motifs. Fiber drawing was possible for TFSI ion containing polymers **P3–P5**. The glass transition temperature was reduced by 59 °C by changing from a PF₆ to TFSI counterion, P1 vs P3, respectively. T_gs ranged from 44 °C for **P3** to 112 °C for **P2**; all 5% wt. loss values were grouped in the range of 217 °C – 224 °C. **P3**

was found to have a critical monomer concentration at 63 mM and the slope at high concentration, 3.55, is the theoretical maximum and the highest reported for a pseudorotaxane supramolecular polymer. Additionally, chain extension was achieved using **VII 16** to form **P6**; due to the brittle nature of **P6**, however, mechanical data were not obtainable for this system.

Experimental

Measurements: ¹H-NMR spectra were obtained on a JEOL ECLIPSE-500 spectrometer, a BRUKER-500 spectrometer, and an AGILENT-NMR-vnmrs400 spectrometer. ¹³C-NMR spectra were collected on a JEOL ECLIPSE-500 spectrometer at 125 MHz, a BRUKER-500 spectrometer at 125 MHz, and an AGILENT-NMR-vnmrs 400 spectrometer at 101 MHz. HR-MS were obtained using an Agilent LC-ESI-TOF system. Reagents were purchased and used as received without further purification. Light microscopy was performed at Virginia Tech by Dr. Michelle B. Price using an Olympus IX81 Epifluorescence microscope. Fibers were water-mounted between two coverslips and imaged using differential interference contrast (DIC) microscopy at 10X magnification (with a water-immersion objective), 40X magnification (using an oil-immersion objective), or at 60X magnification (using an oil-immersion objective) depending on the size and shape of the fiber. Images were captured with an EMCCD Rolera-MGI FAST 1394 monochromatic camera (Olympus) and processed using Slidebook 3I software. Compounds **VII 16** and **VII 17** were prepared as described in Chapter 7; compounds **IV 7** and **IV 9** were prepared as described in Chapter 4. Compound **1**³ was prepared in accordance with literature procedures; similar yields were achieved. Polymer **2** was obtained from Minjae Lee and prepared as described in his dissertation.¹⁷

Supramolecular Polymer P1. **VII 17** (200.4 mg, 0.1233 mmol) was dissolved in 2 mL of chloroform and **1** (131.0 mg, 0.1233 mmol) was dissolved in 2 mL of acetone. The two solutions were mixed and a film was cast by slow evaporation of the mixed solvent system (331.4 mg). After mixing the solution was yellow, but as the solvent evaporated, the film became more orange in appearance.

Supramolecular Polymer P2. **VII 16** (199.7 mg, 0.1211 mmol) was dissolved in 2 mL of chloroform and **1** (128.7 mg, 0.1211 mmol) was dissolved into 2 mL of acetone. The two solutions were mixed and a film was cast by slow evaporation of the mixed solvent system (328.4 mg). After mixing the solution was yellow, but as the solvent evaporated, the film became more orange in appearance.

Supramolecular Polymer P3. **VII 17** (1.4052 g, 0.8643 mM) was dissolved in 2 mL of chloroform and **IV 9** (1.3857 g, 0.8643 mM) was dissolved in 2 mL of acetone. The two solutions were mixed and a film was cast by slow evaporation (2.7909 g). After mixing the solution was yellow, but as the solvent evaporated, the film became more orange in appearance.

Supramolecular Polymer P4. **VII 17** (203.1 mg, 0.1249 mM) was dissolved in 2 mL of chloroform and **IV 7** (237.1 mg, 0.1249 mM) was dissolved in 2 mL of acetone. The two solutions were mixed and a film was cast by slow evaporation of the mixed solvent system (440.2 mg). After mixing the solution was yellow, but as the solvent evaporated, the film became more orange in appearance.

Supramolecular Polymer P5. **VII 16** (203.9 mg, 0.1236 mmol) was dissolved in 2 mL of chloroform and **IV 7** (234.5 mg, 0.1236 mmol) was dissolved in 2 mL of acetone. The two solutions were mixed and a film was cast by slow evaporation of the mixed solvent system

(438.4 mg). After mixing the solution was yellow, but as the solvent evaporated, the film became more orange in appearance.

Supramolecular Polymer P6. **VII 16** (10.6 mg, 6.43 μmol) was dissolved in 1 mL of chloroform and **2** (399.4 mg, 12.68 μmol) was dissolved in 5 mL of chloroform. The two solutions were mixed and a film was cast by slow evaporation of the mixed solvent system (410 mg). After mixing the solution was yellow / pink, but as the solvent evaporated, the film became more pink in appearance.

References

- (1) Yan, X.; Xu, D.; Chen, J.; Zhang, M.; Hu, B.; Yu, Y.; Huang, F. *Polym. Chem.* **2013**, *4*, 3312-3322.
- (2) Ji, X.; Yao, Y.; Li, J.; Yan, X.; Huang, F. *J. Am. Chem. Soc.* **2013**, *135*, 74-77.
- (3) Niu, Z.; Huang, F.; Gibson, H. W. *J. Am. Chem. Soc.* **2011**, *133*, 2836-2839.
- (4) Huang, F.; Nagvekar, D. S.; Zhou, X.; Gibson, H. W. *Macromolecules* **2007**, *40*, 3561-3567.
- (5) Gibson, H. W.; Yamaguchi, N.; Jones, J. W. *J. Am. Chem. Soc.* **2003**, *125*, 3522-3533.
- (6) Veling, N.; Thomassen, P. J.; Thordarson, P.; Elemans, J. A. A. W.; Nolte, R. J. M.; Rowan, A. E. *Tetrahedron* **2008**, *64*, 8535-8542.
- (7) Zhang, M.; Yan, X.; Huang, F.; Niu, Z.; Gibson, H. W. *Acc. Chem. Res.* **2014**, *47*, 1995-2005.
- (8) de Greef, T. F. A.; Ercolani, G.; Ligthart, G. B. W. L.; Meijer, E. W.; Sijbesma, R. P. *J. Am. Chem. Soc.* **2008**, *130*, 13755-13764.
- (9) Yamaguchi, N.; Gibson, H. W. *Angew. Chem. Int. Ed.* **1999**, *38*, 143-147.
- (10) Zhou, Q.; Jiang, H.; Ding, L.; Wang, F.; Wu, T. *Sci. China Chem.* **2010**, *53*, 1081-1088.
- (11) van der Gucht, J.; Besseling, N. A. M.; Knoben, W.; Bouteiller, L.; Cohen Stuart, M. A. *Phys. Rev. E* **2003**, *67*, 051106.
- (12) Cates, M. E. *Macromolecules* **1987**, *20*, 2289-2296.
- (13) Cates, M. E.; Candau, S. J. *J. Phys.: Condens. Matter* **1990**, *2*, 6869 - 6892.
- (14) Sijbesma, R. P.; Beijer, F. H.; Brunsveld, L.; Folmer, B. J. B.; Hirschberg, J. H. K. K.; Lange, R. F. M.; Lowe, J. K. L.; Meijer, E. W. *Science* **1997**, *278*, 1601-1604.
- (15) De Greef, T. F. A.; Smulders, M. M. J.; Wolffs, M.; Schenning, A. P. H. J.; Sijbesma, R. P.; Meijer, E. W. *Chem. Rev.* **2009**, *109*, 5687-5754.
- (16) Schoonover, D. V., Virginia Tech, 2014.
- (17) Lee, M., Virginia Tech, 2010.

Chapter 9

Ionic Liquids and Mechanical Actuators

Recently ionic polymers have gained attention for their use in producing mechanical actuators, sensors and their potential use as artificial muscles.¹⁻³ Of particular interest to the author is mechanical actuation and upcoming chapters will focus on this. Mechanical actuators are produced when an ionic polymer containing mobile ions is placed between electrodes and a voltage is applied.^{4,5} Akle and Leo studied and modelled ionic polymers capable of mechanical actuation and proposed that actuation occurs due to a buildup of ions at the electrode, producing a volume change,⁶ which causes bending of the polymer film.

At the forefront of mechanical actuator research has been the marriage of ionic liquids and polymers from both the standpoint of swelling polymers with ionic liquids and the incorporation of ionic liquid motifs into polymers.⁷ This is a result of ionic liquids having remarkable conductivities,⁸ ultra-low vapor pressures and high thermal stabilities.^{9,10} The ionic liquid motifs of interest to the author are those that contain the imidazolium cation. Recent work has shown that when the imidazolium cation is paired with bis(trifluoromethanesulfonyl)imide (TFSI), outstanding conductivities can be achieved.¹¹⁻¹³ **Figure 9.1** shows a generic imidazolium cation alongside the TFSI counter ion. Additionally, work by Long and coworkers has shown that imidazolium cations may be used to produce mechanical actuators.^{5,14-16}

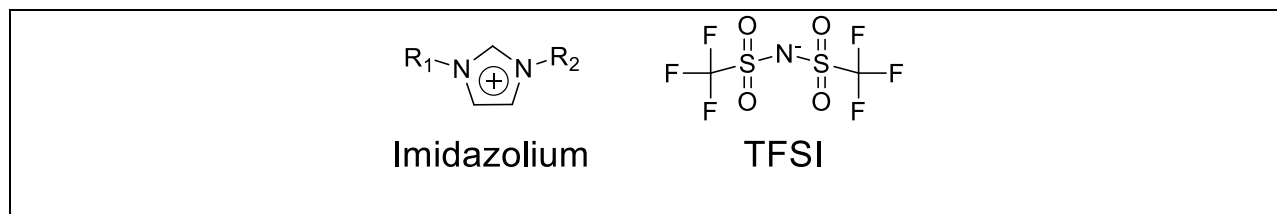


Figure 9.1. Generic structure of the imidazolium cation and TFSI counter ion.

The very first ionic liquid may have been a product isolated from a Friedel-Crafts reaction, called “red oil”,¹⁷ while others consider the first ionic liquid to be ethylammonium nitrate.¹⁸ As an all-encompassing broad definition, ionic liquid may be taken to mean a pure salt that at some temperature under normal pressure exhibits a liquid phase. Given that this definition could pertain to any salt that did not decompose before melting, an ionic liquid is generally taken to mean any salt which is a liquid at or below 100 °C at normal pressure. Additionally, those salts which are liquids at room temperature or below are referred to as room temperature ionic liquids.⁹

One of the initial and still used mechanical actuators makes use of the sulfonated fluoro polymer Nafion (produced by DuPont) swelled with an ionic liquid.^{6,14} The sustained use of Nafion is likely the result of a lack of commercially available ionic polymers; however, the swelling of polymers with ionic liquids has become a common practice to increase the concentration of charge carrying ions in the material. Despite the swelling of ionic polymers with ionic liquids providing better mechanical actuation, cationic and anionic charged species lead to dual direction actuation; that is after the mechanical actuator has bent towards one electrode, it will begin to bend towards the other.^{5,14} The reason this occurs is because when a polymer is swollen with an ionic liquid, both the anions and cations from the additive are free to migrate. The goal of upcoming work is to produce single direction actuation and the only way to achieve this is to have a single mobile ion.

Figure 9.2 shows a cartoon depicting an ionic liquid swollen polymer and a polymer that contains the cation incorporated into the polymer, undergoing actuation via an electrical potential. In the top picture it can be seen that both the cation and anion are capable of movement and thus actuation occurs towards both electrodes. Smaller more mobile ions move

more quickly through the material to produce actuation in the first direction. After the migration of several small ions, the film will bow in the opposite direction as larger less mobile ions of the opposite charge arrive at the opposite electrode. The size and volume of the ion moving determines the quantity of actuation. Smaller ions yield a smaller volume change and thus provide a smaller effect on actuation. At the bottom of **Figure 9.2** an actuator is shown with the cation incorporated into the polymer. In this depiction only the anion is free to move. Prohibiting the cation from movement allows for actuation in only one direction, when an electrical potential is applied. It should also be noted that single direction actuation can alternatively be achieved by incorporating the anion into a polymer and leaving the cation free to migrate through the material.

Given that actuation is a result of the migration of an ionic component through a polymer, measuring a material's conductivity becomes a convenient way to assess a material's potential as an actuator. Thus a high conductivity is desirable for actuation. Additionally, it has been observed that there is a correlation between T_g and conductivities. For both ionic monomers and polymers, lower T_g s tend to translate into higher conductivities.^{7,12} Conceptually this follows the same logic as the observation that conductivities are typically higher in the liquid phase than solid.¹⁹

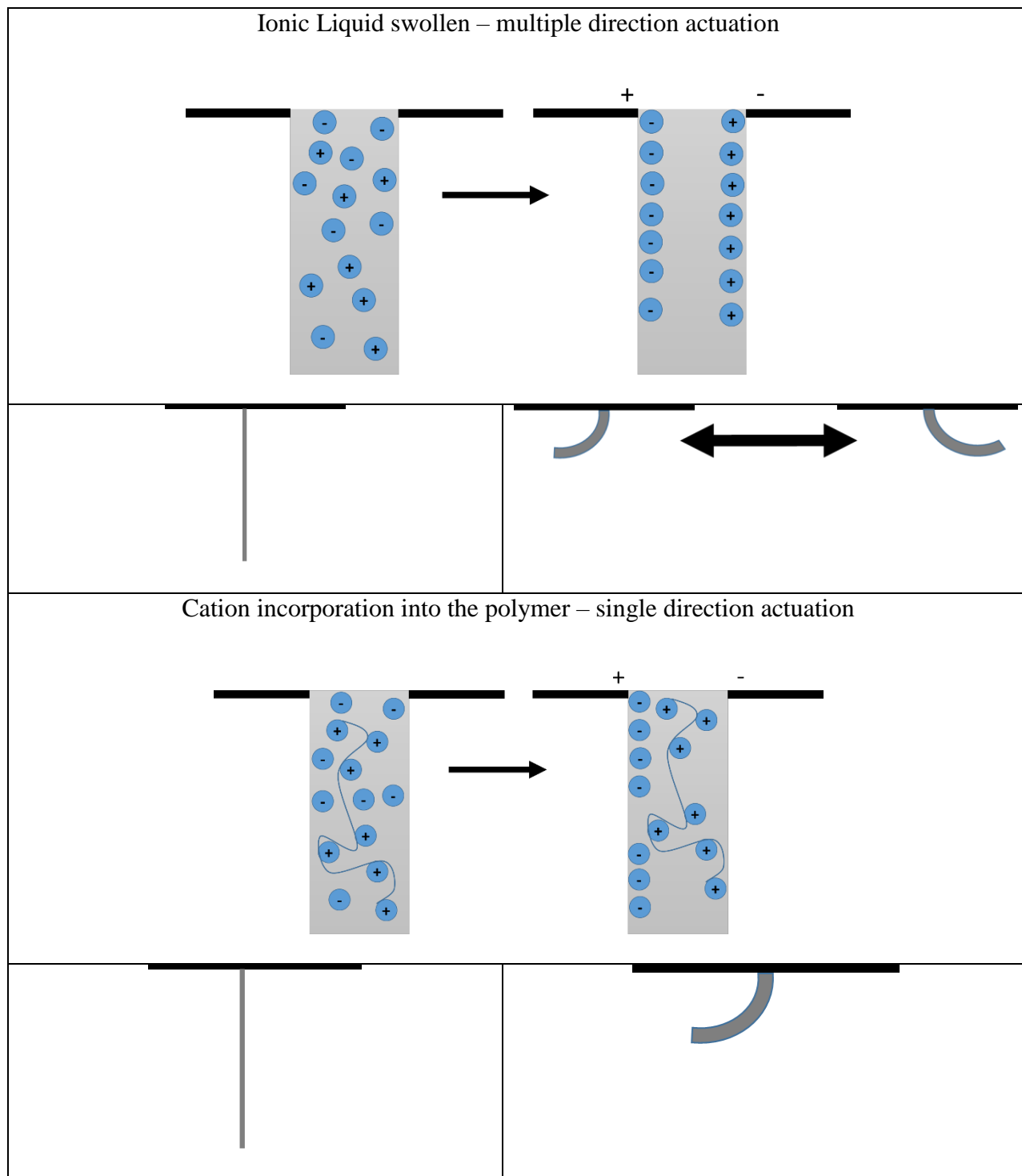


Figure 9.2. Multiple vs. single direction actuation. Top contains an ionic liquid swollen polymer, both cation and anion are mobile (dual direction actuation is observed); bottom contains the cation embedded into the polymer, only the anion is mobile (single direction actuation is observed).

Recent work within the Gibson group focused on imidazolium TFSI and hexafluorophosphate (PF₆) monomers and polymers in an attempt to develop mechanical actuators by way of (meth)acrylate monomers and corresponding polymers,^{11,20,21} polyesters,¹² and acyclic diene metathesis (ADMET) polymers.²² From the work it was determined that long side chain spacers, 10–22 atoms in length, and ethyleneoxy units were valuable in terms of high conductivity. Furthermore, it was determined that by attaching the imidazolium motif as a pendant group, conductivity could likewise be increased. The system was not without flaws; the acrylate monomers suffered from auto-polymerization. This increased the difficulty of using the acrylate system to the point that it was abandoned. Work to be discussed in upcoming chapters attempts to address the problem of auto-polymerization by changing the polymerizable group from an acrylate to a norbornene.

Work by Zheng et al. showed that a single armed norbornene monomer with an imidazolium PF₆ pendant group tethered by an ethyleneoxy chain was stable and underwent ring opening metathesis polymerizations (ROMP).²³ The system by Zheng et al. made use of Grubbs second generation catalyst. ROMP employing Grubbs catalysts usually makes use of gentle reaction conditions, the most common conditions being use of the solvent DCM at room temperature. This provided support for changing the polymerizable group from an acrylate to norbornene. It was determined that the system should contain two imidazolium arms to increase the amount of charge carrying species and take notice of previous work by adding the imidazolium as a pendant group with the TFSI anion and an ethyleneoxy tether. **Figure 9.3** shows the desired general imidazolium TFSI monomer structure.

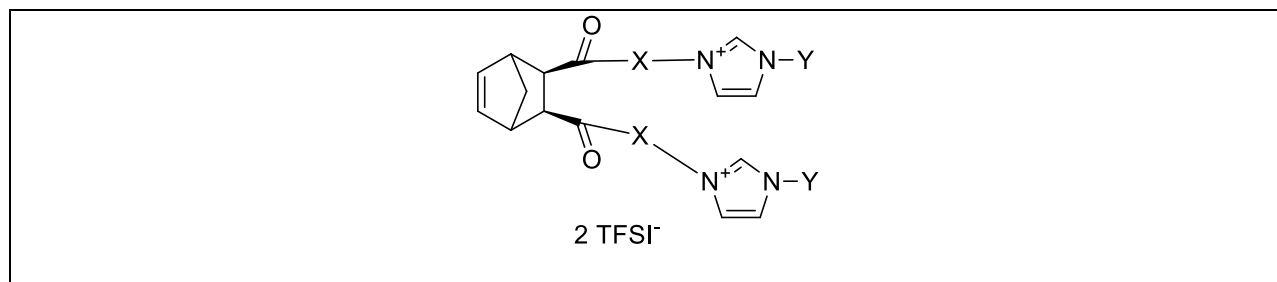


Figure 9.3. Target monomer architecture.

As seen in **Figure 9.3** by the presence of wedged bonds, the *exo* stereochemistry was chosen due to literature reports indicating that for ROMP of norbornene monomers via Grubbs catalyst, pure *exo* compounds are faster than their *endo* counterparts.²⁴

Monomers and homopolymers of the previously stated systems, which we are seeking to improve upon and replace, were all found to possess T_g s well below room temperature.^{11,12,20-22} Thus, the homopolymers possess a high conductivities, but have virtually no structural integrity as viscous oils. Needless to say, a mechanical actuator requires a film to produce a bending action. However, in order to do useful work as an actuator, the film must possess mechanical integrity. Therefore, a block copolymer must be produced to provide structural integrity to the material. Despite an AB diblock copolymer being capable of providing mechanical properties, the synthesis of an ABA triblock copolymer is preferred because the extra segment of A allows for a better entanglement and thereby typically results in better mechanical properties.²⁵ It should be noted that the material needs to have bicontinuous micro-separated phases to ensure the ions can move relatively unhindered through the soft phase of the polymer. **Figure 9.4** shows the various obtainable phase morphologies of AB and ABA block copolymers.²⁶⁻²⁸

AB diblock copolymer		ABA triblock copolymer	
Spheres	Hexagonal Cylinders	Gyroid	Lamellar
A: 0-21%	A: 21-33%	A: 33-37%	A: 37-63%
B: 79-100%	B: 67-79%	B: 63-67%	B: 37-63%
Increasing volume fraction of A			
Gyroid	Hexagonal Cylinders	Spheres	
A: 63-67%	A: 67-79%	A: 79-100%	
B: 33-37%	B: 21-33%	B: 0-21%	

Figure 9.4. Phase morphologies for AB and ABA block copolymers. A monomers are shown as orange ovals while B monomers are shown as light blue ovals. Figure has been adapted from literature sources.²⁶⁻²⁸

Norbornene polymers prepared via ROMP have a clear advantage for block copolymer formation: the ROMP reaction is “living”. For living polymerizations, after the consumption of

one monomer, a second can be added and this process can then be repeated until the reaction is quenched.

References

- (1) Shahinpoor, M.; Bar-Cohen, Y.; Simpson, J. O.; Smith, J. *Smart Mater. Struct.* **1998**, *7*, R15.
- (2) Oguro, K.; Kawami, Y.; Takenaka, H. *J. Micromachine Soc.* **1992**, *5*, 27 - 30.
- (3) Sadeghipour, K.; Salomon, R.; Neogi, S. *Smart Mater. Struct.* **1992**, *1*, 172 - 179.
- (4) Pelrine, R.; Kornbluh, R.; Pei, Q.; Joseph, J. *Science* **2000**, *287*, 836-839.
- (5) Wu, T.; Wang, D.; Zhang, M.; Heflin, J. R.; Moore, R. B.; Long, T. E. *ACS Appl. Mater. Interfaces* **2012**, *4*, 6552-6559.
- (6) Barbar, J. A.; Donald, J. L. *Smart Mater. Struct.* **2007**, *16*, 1348.
- (7) Green, M. D.; Long, T. E. *Polym. Rev.* **2009**, *49*, 291-314.
- (8) Hapiot, P.; Lagrost, C. *Chem. Rev.* **2008**, *108*, 2238-2264.
- (9) Welton, T. *Chem. Rev.* **1999**, *99*, 2071-2084.
- (10) Hallett, J. P.; Welton, T. *Chem. Rev.* **2011**, *111*, 3508-3576.
- (11) Choi, U. H.; Lee, M.; Wang, S.; Liu, W.; Winey, K. I.; Gibson, H. W.; Colby, R. H. *Macromolecules* **2012**, *45*, 3974-3985.
- (12) Lee, M.; Choi, U. H.; Salas-de la Cruz, D.; Mittal, A.; Winey, K. I.; Colby, R. H.; Gibson, H. W. *Adv. Funct. Mater.* **2011**, *21*, 708-717.
- (13) Shaplov, A. S.; Marcilla, R.; Mecerreyes, D. *Electrochim. Acta* **2015**, *175*, 18-34.
- (14) Jangu, C.; Wang, J.-H. H.; Wang, D.; Sharick, S.; Heflin, J. R.; Winey, K. I.; Colby, R. H.; Long, T. E. *Macromol. Chem. Phys.* **2014**, *215*, 1319-1331.
- (15) Green, M. D.; Wang, D.; Hemp, S. T.; Choi, J.-H.; Winey, K. I.; Heflin, J. R.; Long, T. E. *Polymer* **2012**, *53*, 3677-3686.
- (16) Gao, R.; Wang, D.; Heflin, J. R.; Long, T. E. *J. Mater. Chem.* **2012**, *22*, 13473-13476.
- (17) Wilkes, J. S. In *Ionic Liquids in Synthesis*; Wiley-VCH Verlag GmbH & Co. KGaA: 2003, p 1-6.
- (18) Walden, P. *Bull. Imp. Acad. Sci.* **1914**, *1800*, 405 - 422.
- (19) Ohno, H. *Electrochemical Aspects of Ionic Liquids, 2nd Edition*, 2011.
- (20) Lee, M.; Choi, U. H.; Colby, R. H.; Gibson, H. W. *Chem. Mater.* **2010**, *22*, 5814-5822.
- (21) Choi, U. H.; Mittal, A.; Price, T. L.; Gibson, H. W.; Runt, J.; Colby, R. H. *Macromolecules* **2013**, *46*, 1175-1186.
- (22) Aitken, B. S.; Buitrago, C. F.; Heffley, J. D.; Lee, M.; Gibson, H. W.; Winey, K. I.; Wagener, K. B. *Macromolecules* **2012**, *45*, 681-687.
- (23) Zheng, L.; Chen, F.; Xie, M.; Han, H.; Dai, Q.; Zhang, Y.; Song, C. *React. Funct. Polym.* **2007**, *67*, 19-24.
- (24) Moatsou, D.; Hansell, C. F.; O'Reilly, R. K. *Chem. Sci.* **2014**, *5*, 2246-2250.
- (25) Odian, G. *Principles of Polymerization*; 4th edition ed.; Wiley-Interscience, 2004.
- (26) Posocco, P.; Fermeglia, M.; Pricl, S. *J. Mater. Chem.* **2010**, *20*, 7742-7753.

- (27) Greaves, T. L.; Drummond, C. J. *Chem. Soc. Rev.* **2013**, *42*, 1096-1120.
- (28) Swann, J. M. G.; Topham, P. D. *Polymers* **2010**, *2*, 454-469.

Chapter 10

Norbornene TFSI Monomers

Introduction

The goal of the work described in this chapter was to synthesize monomers capable of producing block co-polymers and the attribute sought was single ion movement. Materials capable of single ion movement provide a starting point for the development of single direction actuators. For this work, ion movement was characterized and quantified via conductivity measurements. In our prior experience conductivity values correlate inversely with T_g values.¹⁻³ Higher conductivity values often result from lower T_g 's. Adhering to these previously learned trends within our lab, it was desired that the monomers and corresponding polymers would possess low T_g s for incorporation into block co-polymers as soft segments.

The end objective for these monomers is the production of ABA block co-polymers containing a Hard–Soft–Hard architecture, while having ions capable of moving throughout the soft material. Fundamental work on this topic within our group provided the framework for this project by establishing a polymer design that placed the cation in the pendant moiety of a polymer while leaving the anion free to move throughout the material.¹ The original work also provided information as to how the monomers should be designed in terms of the mobile ions and architecture. Ionic liquids provided inspiration for this work. Traditional ionic compounds (salts) are known for high melting points and their ability to act as electrolytes. These are undesirable, since high melting points would be problematic. Ionic liquids (salts with a melting point below 100 °C), conversely, provide a wide range of cation/anion combinations with melting points well below room temperature, making them ideal for providing mobile phases for

ions.⁴ The system chosen by initial work within our group was the imidazolium cation and PF_6^- anion. Employing the imidazolium cation with a PF_6^- anion gave acceptable conductivity values, but soon it was discovered that by switching the PF_6^- anion to TFSI^- , conductivities could be drastically improved.¹ In addition, this original work provided a layout for monomer design. It was found that conductivity could be maximized by placing the imidazolium cation as a pendant group on the monomer and that ethyleneoxy spacer units could be employed to lower the T_g of the monomer and thus increase the conductivity.³ It was further found that T_g values could be lowered and conductivities could be increased by placing ethyleneoxy units both before and after the imidazolium cationic pendant group.^{2,3}

Original work by our group was, however, not without a flaw. The polymerizable groups first investigated were acrylates and methacrylates (**Figure 10.1**).^{1,3,5} Monomers produced using the acrylate and methacrylate groups were found to have sufficiently high conductivities, but suffered from auto-polymerization at room temperature. This lack of shelf stability drastically hindered the use of these monomers and therefore a second generation of monomers was needed. In redesigning the monomers, norbornene was chosen as the polymerizable group by ROMP. Based on available literature for norbornene monomers, it was anticipated that such monomers should be shelf stable. As an additional note, ROMP reactions are typically gentle, being carried out at room temperature with a Grubbs catalyst in an easy to remove solvent such as DCM.

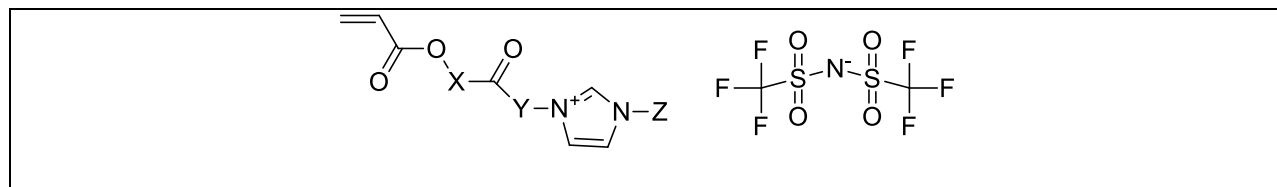


Figure 10.1. General structure of last generation imidazolium acrylate monomers (not shelf stable).

Results and Discussion

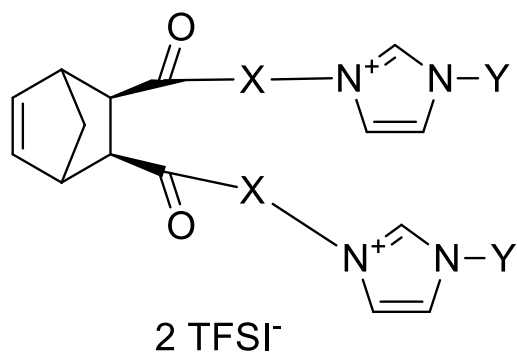
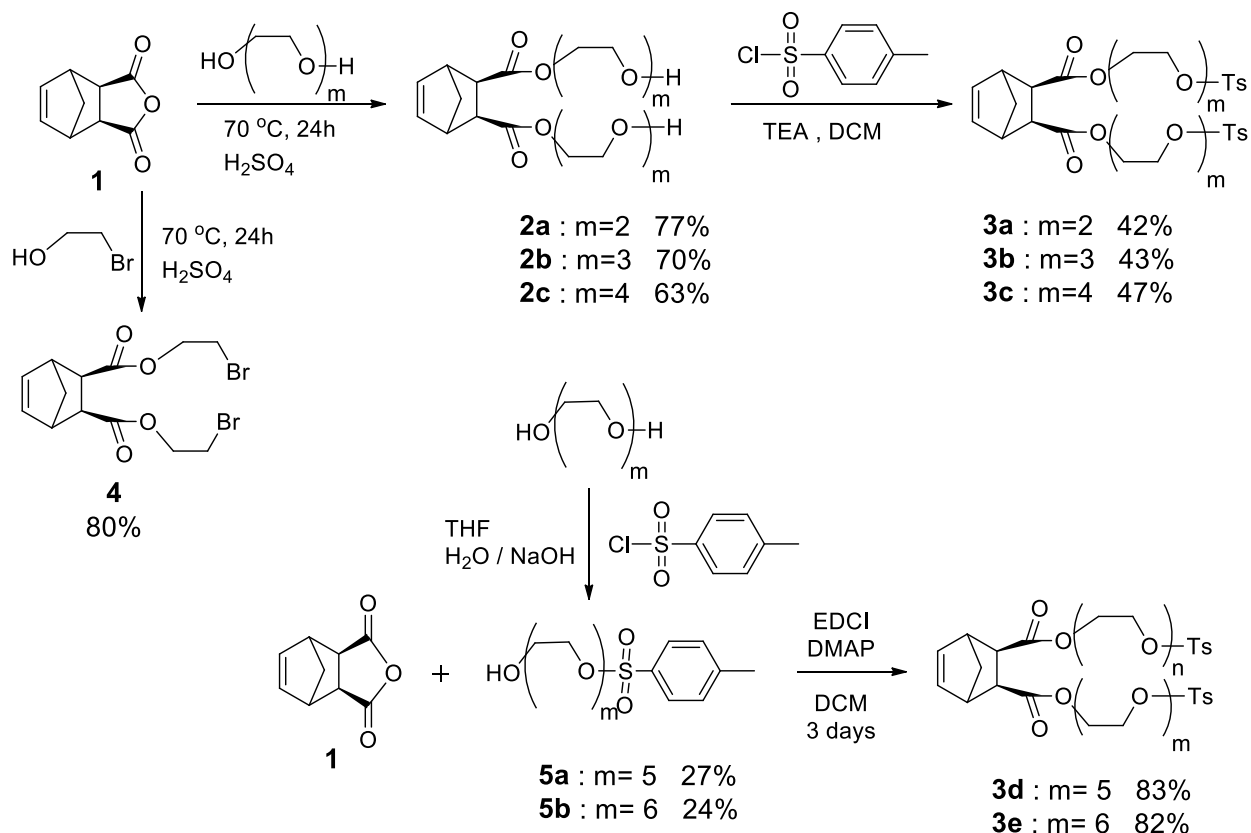


Figure 10.2. General imidazolium TFSI monomer structure.

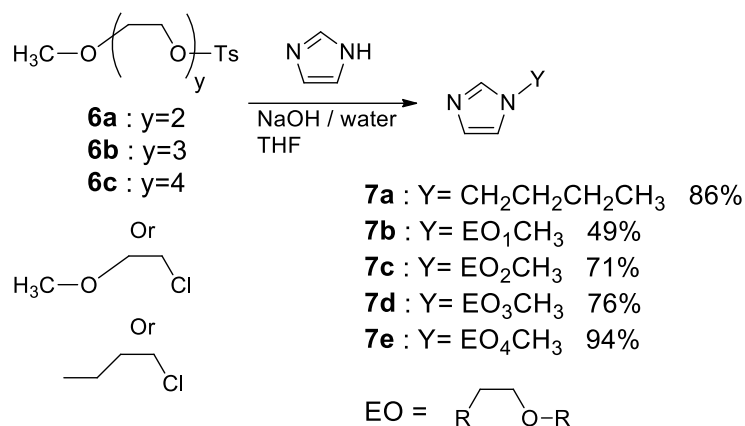
Figure 10.2 shows the chosen architecture for the imidazolium monomers developed here. The polymerizable group, norbornene, is tethered to the imidazolium cation by a linkage X and after the imidazolium group is a tail labeled Y. Linkages X and Y have both been designated as ethyleneoxy linkages, but Y also includes a straight chain C₄ linkage for comparison. The monomers contain the TFSI counter ion and are double armed to increase the overall ion content. Additionally, the *exo*-norbornene monomer was specifically selected over *endo* for its ability to more readily undergo ROMP.⁶



Scheme 10.1. Synthesis of norbornene monomers.

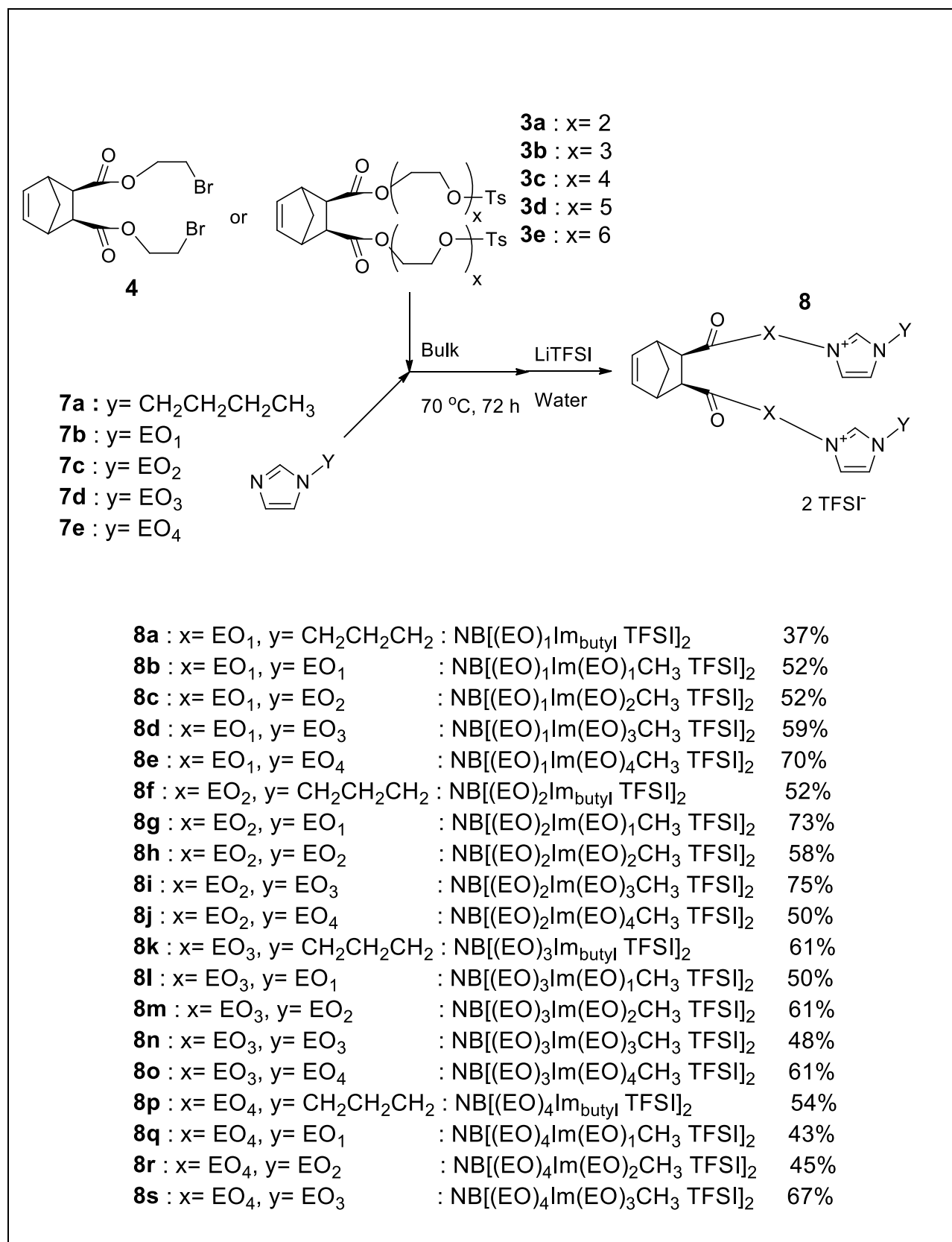
Taking into consideration the previous observations that ethyleneoxy units result in higher ionic conductivity than alkylene spacers, a synthetic scheme was developed to include various oligo(ethylene glycol) units (**Scheme 10.1**). As previously stated, *exo* norbornenes are advantageous in their polymerization rate; stereo purity of **1** was achieved through repeated recrystallizations and maintained throughout the synthetic pathways of **Scheme 10.1**. Although results indicated longer ethyleneoxy chains would be advantageous, how long the chains should be, was not easily predicted. With the addition of every ethyleneoxy unit, 88 amus of mass is added, mass which does not contain a charge of any type. Therefore, with the addition of each ethyleneoxy unit, the overall charge density of the molecule is diluted. Additionally, there is a difference between the X and Y chains, both perhaps playing their own unique roles. As a note, a uniform synthetic path was not chosen in **Scheme 10.1** due to difficulty, availability and cost

associated with ethyleneoxy precursors. **Scheme 10.2** shows the synthesis of imidazole precursors and yields.



Scheme 10.2. Synthesis of imidazole precursors.

In an attempt to find the optimal lengths of the ethyleneoxy chains for x and y (**Figure 10.1**), a matrix of monomers was synthesized (**Scheme 10.3**). Chain lengths for X were varied from one to six ethyleneoxy units, while Y was varied from one to four, with a butyl chain for comparison. Three routes have been established for the syntheses of these norbornene monomers and each has its own unique advantage for a specific subset of monomers.



Scheme 10.3. Imidazolium monomer synthesis.

The first synthetic method (used for monomers **8a–8e**) involved reaction of the norbornene precursor **1** with 2-bromoethanol in an esterification reaction to provide **4** (**Scheme 10.1**, 80%). **4** was then quaternized with one of the imidazoles **7a–7e** to provide monomers **8a–8e** (**Scheme 10.3**). This method offers the shortest and simplest synthetic route to the desired norbornene monomers, but the X linkage is limited to one ether oxygen and carbon chains.

The second synthetic method (for monomers **8f–8t**) used the oligo(ethylene glycol) of the desired length X in an esterification reaction with **1** to produce the diols **2a–2c** (**Scheme 10.1**). In this synthetic step the glycol was used both as reagent and solvent for the reaction to minimize the formation of side products; product isolation was carried out via aqueous washings. Observed yields for the reaction decreased as the ethyleneoxy chain increased in length and increased the solubility of the product in water. These compounds were then tosylated to give compounds **3a–3c**. Monomers **8f–8t** were produced by quaternization of **3a–3c** with the imidazoles **7a–7e**. This method is straightforward and contains purification steps that minimize the use of column chromatography; this method was found to be advantageous when dealing with ethylene glycols that were inexpensive.

The third synthetic method (**Scheme 10.1**), for the synthesis of monomers **8u** and **8v**, was utilized due to the costs associated with penta(ethylene glycol) (**5a**) and hexa(ethylene glycol) (**5b**). As these two compounds are obtained through either multi-step synthesis or large financial costs, a reaction scheme was generated to conserve them. The monotosylates were synthesized with tosyl chloride at a stoichiometry of 1:1 in an attempt to obtain a statistical product distribution (25% ethylene glycol, 50% monotosylate, and 25% ditosylate). Chromatography was used on the resulting mixtures and all products were isolated so that the ditosylate could be reconverted to the glycol and the reaction repeated. **5a** or **5b** once synthesized was then reacted

with **1** via EDCI coupling, to give the ditosylate **3d** or **3e** (purification by column chromatography). **3d** and **3e** were then quaternized with the imidazole **7c** to give compounds **8u** and **8v**, respectively.

Quaternizations for the production of monomers **8a–8v** were achieved by solventless reactions of either **4** or **3a–3e** with the desired imidazole at no more than 70 °C for 3 days. It was found that the use of solvent and or higher temperatures resulted in the formation of undesirable side products, both retro Diels–Alder and *exo* to *endo* inversion. Synthesis of these monomers began with the stereo pure *exo* compound **1**, which was synthesized and recrystallized in accordance with literature procedures, and confirmed via melting point and NMR. Care was taken in **Schemes 10.1** and **10.3** to avoid inversions of *exo* to *endo*, with all products being carefully watched for changes in the ¹H NMR spectra which might suggest inversion. To safeguard against unsuspected inversions, NOESY was performed on a portion of the products to confirm the stereochemistry. *Exo* validation via NOESY was typically only carried out for one monomer per ethyleneoxy linkage size. **Figure 10.3** shows how NOESY was used to confirm the *exo* monomers. For *endo* products, a NOESY correlation is observable between H₁ and H₂, but is not present in *exo* products. **Figure 10.3b** shows a partial NOESY spectrum of **8s** taken in deuterated chloroform at room temperature, peak assignments have been carefully made using COSY (not shown). In the spectra it can be seen that no correlation exists between between H₁ and H₂, thus confirming the presence of an *exo* product.

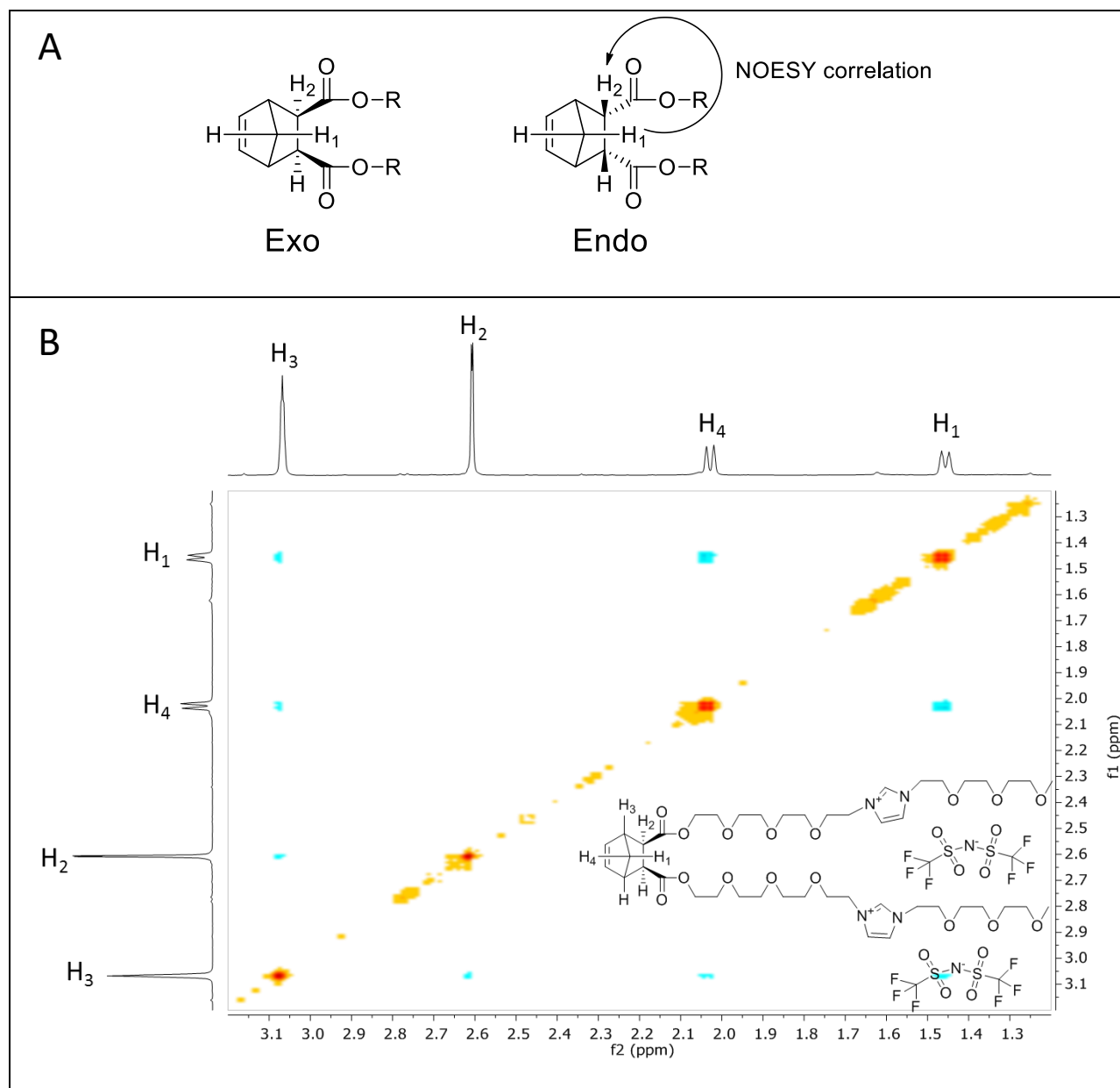


Figure 10.3. A) Observed *endo* vs *exo* NOESY correlations for norbornenes; B) partial NOESY spectrum of **8s** taken in CDCl₃ at room temperature.

Isolations of products **8a–8v** were carried out using a liquid–liquid extraction procedure in which the bulk material was taken up in water and extracted with DCM for 2 days before counter ion exchange. Since high purity was a concern for these monomers, the isolation method focused on the purity of the resulting product and not necessarily on the maximum yield. Yields

for **8a–8v** ranged from 27% to 81% with many of the monomers coming in near 50%. Chromatography for these products was avoided. It should be noted, however, that an alternative method for product isolation does exist; after the reaction, products can be washed with diethyl ether several times and then counter ion exchanged, followed by dissolving the product in DCM and washing with water. Although this method provides superior yields vs. the 2 day liquid–liquid extraction method, the material was not considered of high enough quality for conductivity measurements. For this reason, the alternative purification method was not carried out on the products reported here.

Monomers **8a–8t** comprises a systematic matrix in which the number of ethyleneoxy units in the linkages both before and after the imidazolium group was varied from one to four in an attempt to search out the optimal monomer. Additionally, butyl groups were positioned after the imidazolium group for comparison. Monomers **8u** and **8v** are stand-alone data points in the matrix. In addition to the numbering system within this text, the naming system $\text{NB}[(\text{EO})_x\text{Im}(\text{EO})_y\text{CH}_3]_2$ has been given to monomers **8a–8v**: NB indicates norbornene, EO ethyleneoxy and Im imidazolium, while subscripts x and y denote the number of ethyleneoxy units. Considering the linkage between the norbornene and imidazolium (6 possible units) and the linkage after the imidazolium group (5 possible units), the potential existed for a matrix of 30 monomers. Looking at monomers **8a–8v**, it can be seen that some monomers have been omitted; the reason for this will be discussed shortly. The synthesis of **8a–8v** offers a large array of monomers such that conclusions about the optimal number of ethyleneoxy units can be drawn and the “best” monomer in terms of conductivity can be found.

To assess the potential of each monomer, conductivity and T_g values (**Table 10.1**) were obtained. T_g values were evaluated because of the strong connectivity between T_g and

conductivity values; the general trend between T_g and conductivity is: lower T_g values tend to lead to higher conductivities. Conductivity values for monomers were measured at Penn State by U Hyeok Choi under the supervision of Prof. Ralph Colby.

Table 10.1. T_g ($^{\circ}\text{C}$) values of $\text{NB}[(\text{EO})_x\text{Im}(\text{EO})_y\text{CH}_3]_2$ TFSI.

		X					
		1	2	3	4	5	6
Y	Butyl	(8a) -44	(8f) -47	(8k) -47	(8p) -45		
	1	(8b) -39	(8g) -39	(8l) -43	(8q) -43		
	2	(8c) -45	(8h) -49	(8m) -47	(8r) -46	(8u) -46	(8v) -54
	3	(8d) -50	(8i) -54	(8n) -46	(8s) -45		
	4	(8e) -42	(8j) -57	(8o) -45	(8t) -47		

Table 10.2. $\text{NB}[(\text{EO})_x\text{Im}(\text{EO})_y\text{CH}_3]_2$ TFSI conductivity values (S/cm) at 25°C .

		X					
		1	2	3	4	5	6
Y	Butyl	(8a) 3.07E-05	(8f) 7.75E-05	(8k) N/A	(8p) 6.82E-05		
	1	(8b) 2.42E-05	(8g) 4.80E-05	(8l) 6.54E-05	(8q) 6.51E-05		
	2	(8c) 2.95E-05	(8h) 7.72E-05	(8m) 8.95E-05	(8r) 9.57E-05	(8u) N/A	(8v) N/A
	3	(8d) 7.10E-05	(8i) 5.39E-05	(8n) 8.93E-05	(8s) 7.90E-05		
	4	(8e) 3.88E-05	(8j) 6.26E-05	(8o) 7.94E-05	(8t) 6.99E-05		

T_g values range from a high of -39°C for compounds **8b** and **8g** to a low of -57°C for **8j**. Upon inspection of **Table 10.1** several conclusions can be drawn; first there are trends within

each row and column, but the correlation is not in the expected trend of more ethyleneoxy units resulting in lower T_g values. As we add more ethyleneoxy units to a monomer it is expected that the molecule would behave more and more like PEG. This, however, was not the case. In **Tables 10.1 and 10.2** columns correspond to the linkage between norbornene and imidazolium in the monomer (X) and rows correspond to the tail after imidazolium on the monomer (Y).

The change in **Table 10.1** for T_g values with respect to the linker X is relatively mild and could be seen as negligible or insignificant. As an example row $Y = 1$ has values of -39 , -39 , -43 , and -43 ; only two different values were observed and the separation was just 4 °C. It is worthwhile to note that there is an outlier in **Table 10.1, 8v** with a $T_g = -54$ °C, 9 °C lower than the grouping of values beside it; it is suspected that the six ethyleneoxy units of this molecule are beginning to behave like PEG.

Tail lengths, Y , play a much larger role in T_g than does the linkage X (**Table 10.1**); the effects are more pronounced in shorter linkages than longer ones. The general trend observed in the columns is a decrease in T_g until a minimum is achieved and then T_g increases. For short linkages where $X = 1$ or 2 the difference in T_g between the lowest and highest values is 11 °C or 18 °C, respectively. However, for $X = 3$ or 4 the difference in T_g between the lowest and highest value is only 4 °C; considering experimental error, there is little significant change.

Additionally, **Table 10.1** shows that the hydrocarbon butyl tail behaved, in terms of T_g , very similarly to a di(ethyleneoxy) tail. This is interesting in that the butyl tail is the same chain length as a single ethyleneoxy unit (the $Y = 1$ column), but T_g values for the single ethyleneoxy unit are higher. As this is uniform within the data set, we speculate that motion about the oxygen atom is either hindered or restricted, leading to a lower T_g value for the butyl group.

Since increasing the number of ethyleneoxy units should cause the resulting monomer to be more “PEG like”, it should drive the T_g downwards. Considering that the expected trend is not observed, the conclusion is reached that unexpected T_g trends must be attributed to the ethyleneoxy units not acting simply as PEG but instead behaving in a different manner, i. e., perhaps interacting with the imidazolium cation. As support for this concept, ^1H NMR was carried out in a solvent that greatly hinders hydrogen bonding, $\text{DMSO-}d_6$, and compared to results in a solvent which allows such interactions, CDCl_3 . **Figure 10.4** shows the ^1H NMR spectra of **8c** taken in six different deuterated solvents: CDCl_3 , CD_2Cl_2 , acetone- d_6 , acetonitrile- d_3 , methanol- d_4 , $\text{DMSO-}d_6$. Each solution was prepared at a concentration of 8.8 M.

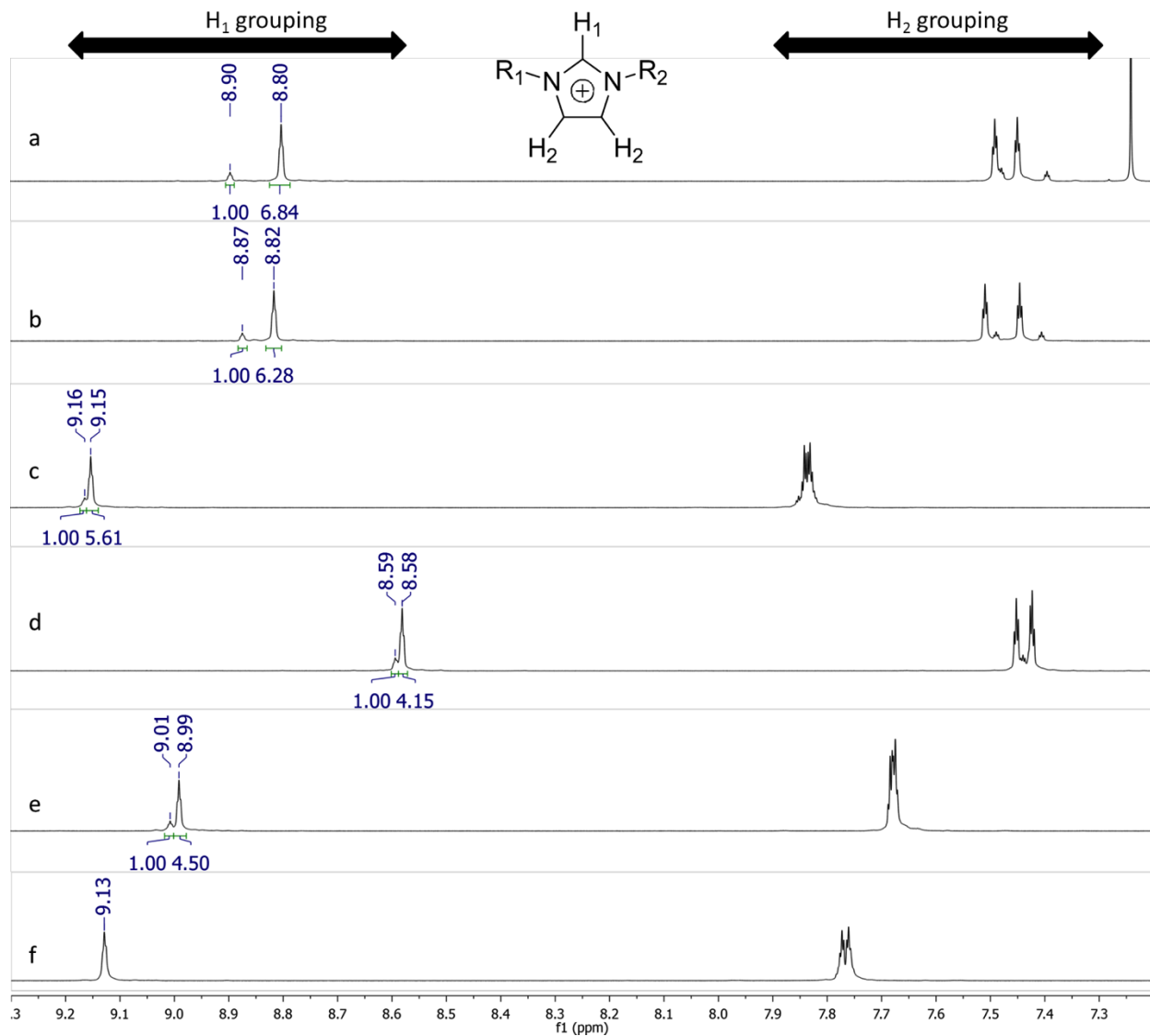


Figure 10.4. Partial ^1H NMR (500 MHz) spectra of **8c** at 8.8 mM taken in: a) CDCl_3 , b) CD_2Cl_2 , c) acetone- d_6 , d) acetonitrile- d_3 , e) methanol- d_4 , f) DMSO- d_6 .

8c was specifically selected for **Figure 10.4** due to its linkages: one ethyleneoxy unit between the norborene and imidazolium moieties and two after the imidazolium. This combination provides a situation in which only the tail moiety has the possibility of interacting with the imidazolium group. In **Figure 10.4** it can be seen that the protons of the imidazolium group in **8c** are clearly in different chemical environments in different solvents. As the solvent becomes more polar, the two signals for both H_1 and H_2 come closer together and the integration

difference between the two peaks shrinks. Two peaks are observed for H₁ with all solvents except DMSO-*d*₆. It is reasoned that the acidic hydrogens interact with the lone pairs of electrons of the ethyleneoxy chain, yielding the major set of signals, and also with the solvents via hydrogen bonding and other intermolecular solvation forces, leading to a separate minor set of signals. It is suspected that the single observed peak found within the DMSO-*d*₆ spectra is the result of peak overlapping; this is justified by the poor peak shapes of H₁ and H₂. Interestingly, if the peak ratios for a given proton are graphed vs the dielectric constants of the solvents, a linear relationship arises, **Figure 10.5**. Attempts were made to find correlations using E_T(30)⁷⁻¹⁰ but no connection could be found. In **Figure 10.5**, the proton H₁ was chosen for analysis because the two signals of this proton were better resolved than those for H₂. Reasoning that the higher the dielectric constant, the more competitive the solvent would be compared to the ethyleneoxy tail, **Figure 10.5** supports the theory that the smaller downfield peaks are due to solvent interactions, while the major signals arise from intramolecular hydrogen bonding of H₁ with the ether oxygens of the tail. As an additional note, studies have shown that the main component responsible for solvation of imidazolium containing compounds is the solvents ability to hydrogen bond with H₁, **Figure 10.4**.¹¹ One study using a pillararene based rotaxane with an imidazolium cation showed that the pillararene imidazolium interaction was limited when hydrogen-bonding solvents were used and maximized with solvents lacking a hydrogen-bond acceptor.¹² These studies along with the present data support the hypothesis that as the solvent becomes more nonpolar or contains less/weaker hydrogen-bond acceptors, the interaction of the imidazolium cation with intramolecular ethyleneoxy units should increase.

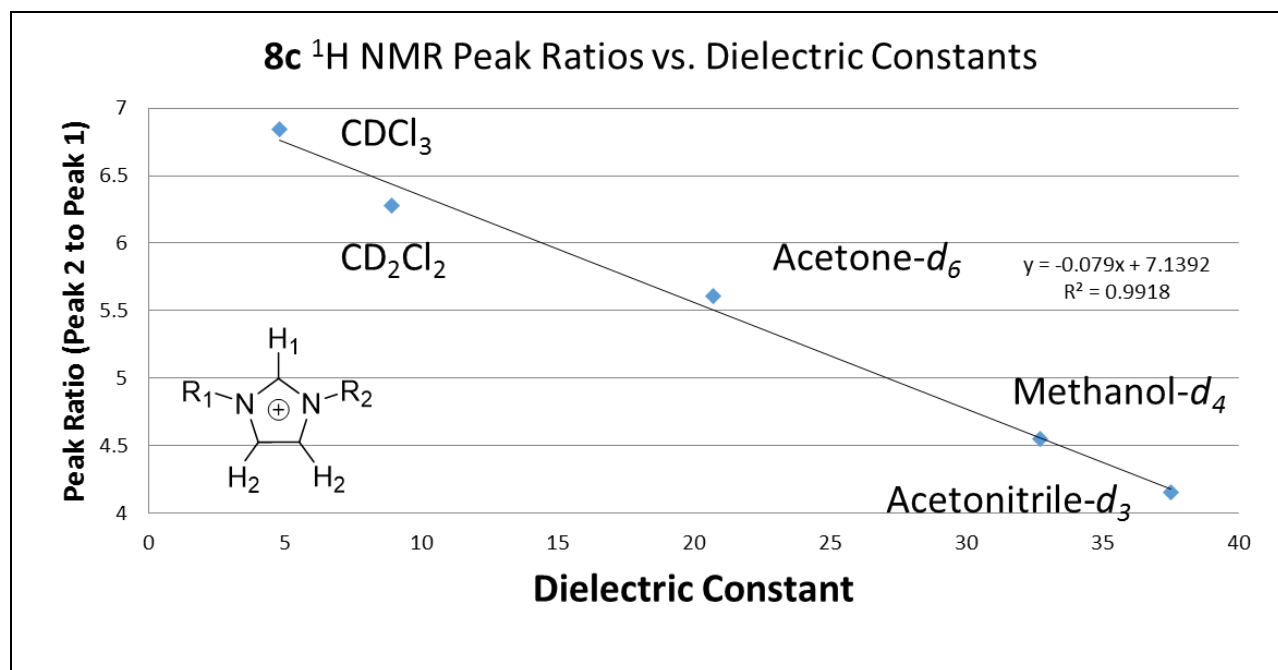


Figure 10.5. ¹H NMR peak ratios of H₁ for **8c** observed in **Figure 10.4** compared to corresponding solvent dielectric constants.

As a special note, some monomers in relatively nonpolar solvents such as CDCl₃ display only a single set of proton signals in their ¹H NMR spectra; no extra peaks are observed for the imidazolium protons. This is typically observed with moderate to large sized ethyleneoxy tail units Y. As an example **Figure 10.6a** shows the ¹H NMR spectrum of **8t** taken in CDCl₃. To explain this, we simply consider the two different possibilities for complexation: fast and slow exchange. When two peaks are present for a given hydrogen, slow exchange is occurring and the NMR experiment is capable of observing each chemical environment. When one single peak is present for a given hydrogen, fast exchange is occurring relative to the NMR time scale. Thus in **8t** and analogs, the longer ethyleneoxy tails allow for fast exchanging interactions with the imidazolium units. Note that the chemical shift of H₁ in **8t** lies between the two peaks observed in the same solvent for H₁ of **8c**. An attempt was made to test this hypothesis by using reduced temperature NMR; current capabilities within the Virginia Tech chemistry department allow for

samples to be run at a minimum of $-26\text{ }^{\circ}\text{C}$. **Figure 10.6b** shows the spectra of **8t** run at $-26\text{ }^{\circ}\text{C}$; no noticeable change was observed. This lack of change suggests that low enough temperatures were not achieved to isolate the individual interactions.

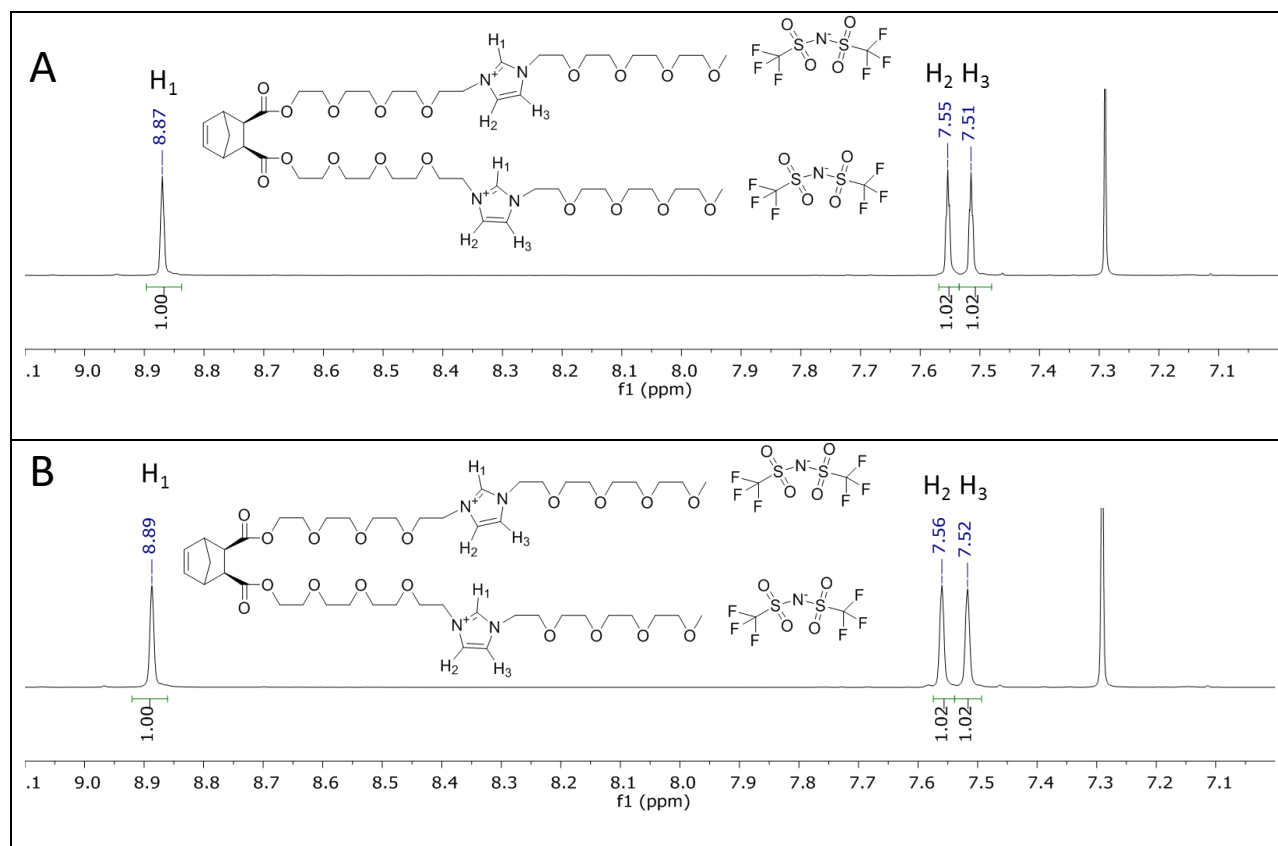


Figure 10.6. Partial ^1H NMR spectrum of **8t**, 600 MHz, CDCl_3 : A) $25\text{ }^{\circ}\text{C}$; B) $-26\text{ }^{\circ}\text{C}$.

The observation of extra peaks that disappear when a sufficiently polar solvent is used is not limited to ^1H NMR; this effect is also observed in the ^{13}C NMR. **Figure 10.7** contains partial ^{13}C NMR spectra of **8c** in CD_2Cl_2 and $\text{DMSO}-d_6$; in $\text{DMSO}-d_6$ a single set of ^{13}C signals is obtained, but in CD_2Cl_2 two distinct sets of signals are observed.

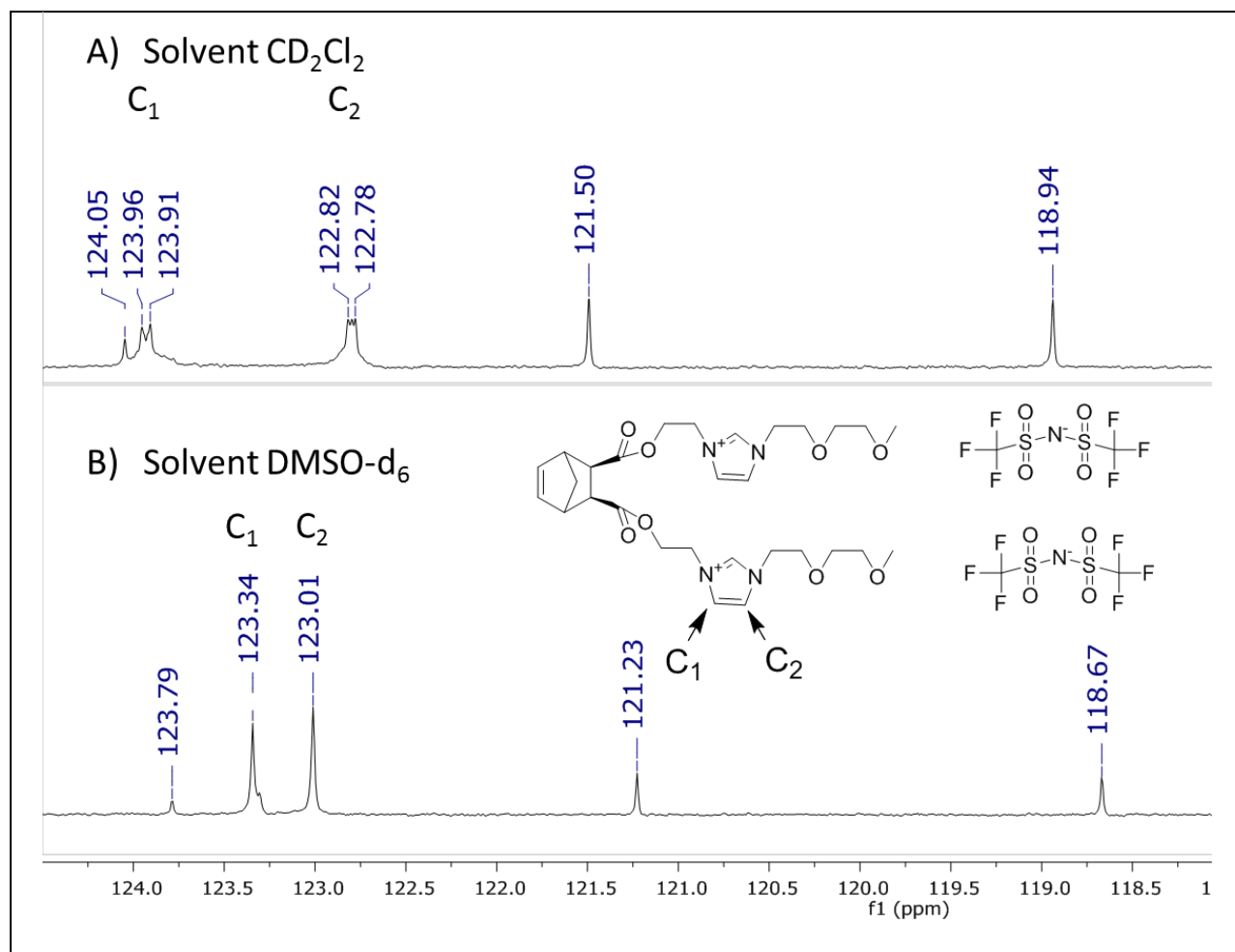


Figure 10.7. Partial ^{13}C NMR of **8c** at 126 MHz: A) solvent CD_2Cl_2 and B) solvent DMSO-d_6 .

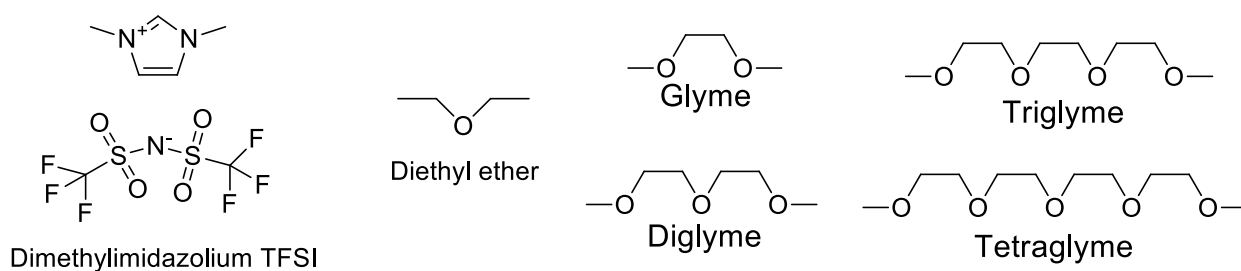


Figure 10.8. Compounds used to show intermolecular interactions between the imidazolium cation and ethyleneoxy units.

To aid in the understanding these results, dimethylimidazolium TFSI was studied by NMR in ether, glyme, diglyme, triglyme, and tetraglyme (**Figure 10.8**). The goal of the

experiments was to show interactions between the dimethylimidazolium cation and the ether oxygens. For the study, solvents and dimethylimidazolium TFSI were dried over molecular sieves for 2 days; then 0.200 g (0.530 mmol) of dimethylimidazolium TFSI was dissolved in 2 mL of each of the solvents to form 0.27 mM solutions. A sealed capillary containing chloroform-*d* in an NMR tube served as an external standard ($\delta = 7.26$ ppm) for chemical shifts. **Figure 10.9** shows ^1H NMR results from the experiments in the region of the imidazolium protons. It can be seen that as the number of oxygen atoms increases, the proton peaks of the imidazolium unit are steadily shifted upfield. H_1 was used for analysis over H_2 and the methyl groups because the chemical shift for this proton from its original location was greatest and because it should be the most acidic hydrogen. The shifting of imidazolium protons upfield likely indicates the degree to which hydrogen bonding is occurring with the acidic protons of the imidazolium ring. **Figure 10.10** shows the dependence of the chemical shift on the concentration of ether oxygen atoms; this graph supports the idea that the imidazolium protons are involved with interactions with the oxygen atoms of the ethereal solvents.

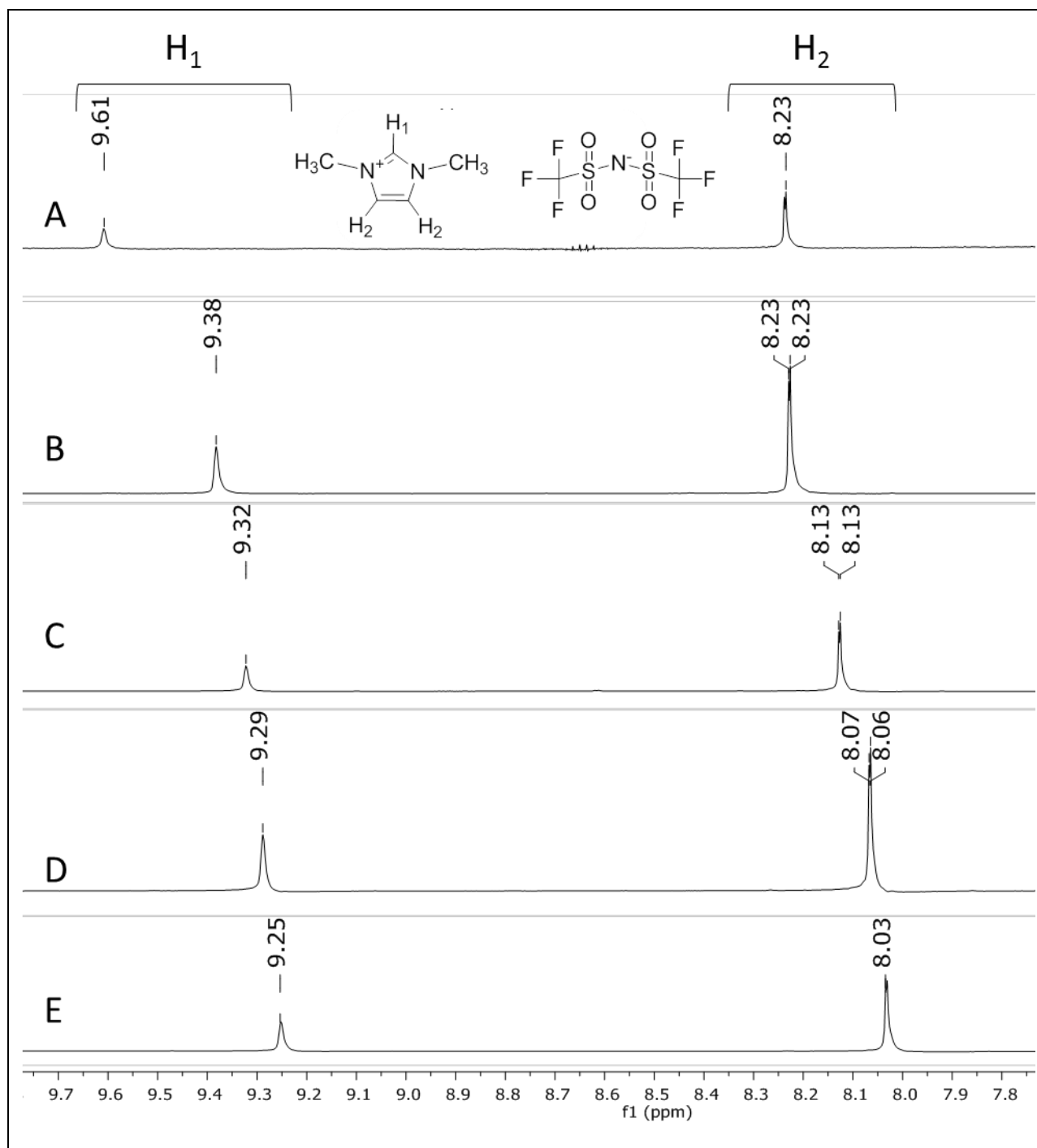


Figure 10.9. ¹H NMR (500 MHz) results from dimethyl imidazolium TFSI solvent experiments: A) ether, B) glyme, C) diglyme, D) triglyme, E) tetraglyme.

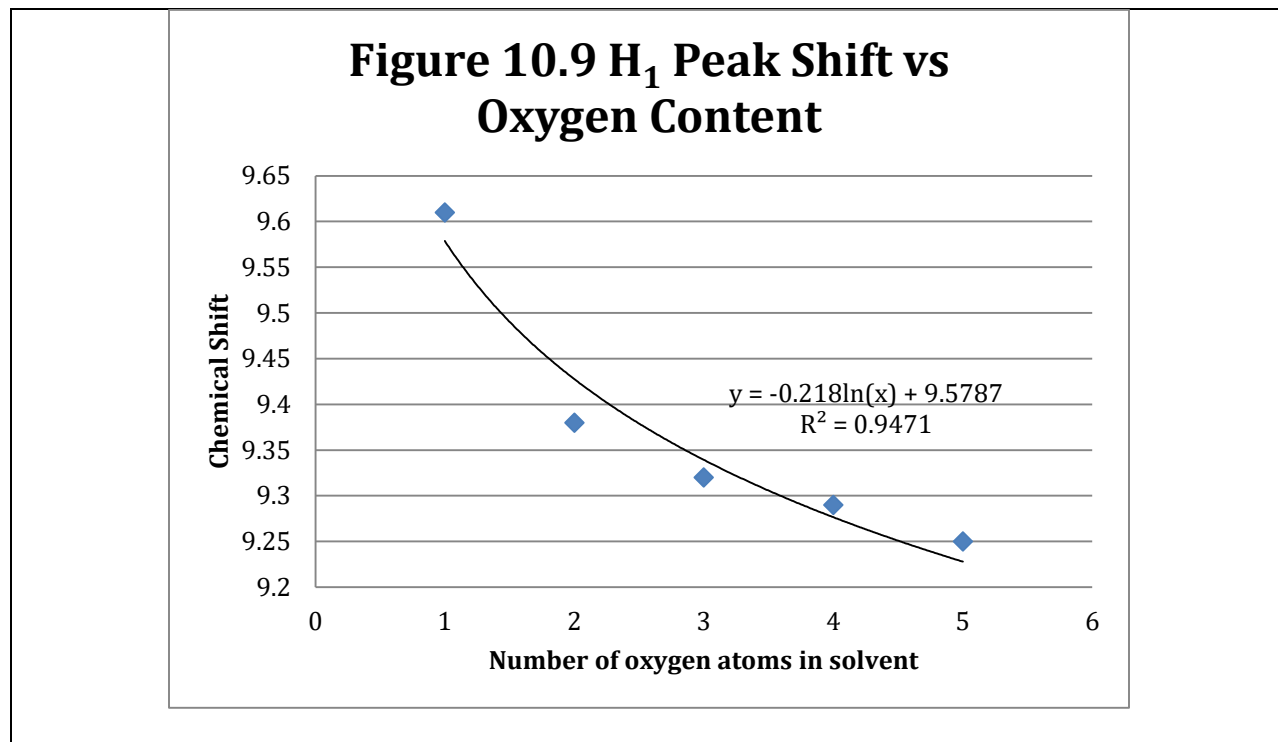


Figure 10.10. Figure 10.9 H₁ chemical peak shift vs oxygen content of solvent, fit to a logarithmic trend line.

To further explore the proposition that the monomers experience self-complexation, 2D NOESY was explored. For this experiment monomer **8d** was selected, because of its superior conductivity when compared to **8b** and **8e** (Table 10.2); all are similar monomers that contain a single ethyleneoxy unit linking the norbornene to the imidazolium units. **8d** exhibited a conductivity more than double those of **8b**, **8c**, or **8e**, perhaps due to interaction of its ethyleneoxy tail and imidazolium units and thus liberating a higher fraction of TFSI counterions. Figure 10.11 shows a partial 2D NOESY NMR of **8d** taken in acetone-*d*₆. Peak assignments were made by careful analysis of ¹H NMR and COSY data for **8d**, not shown.

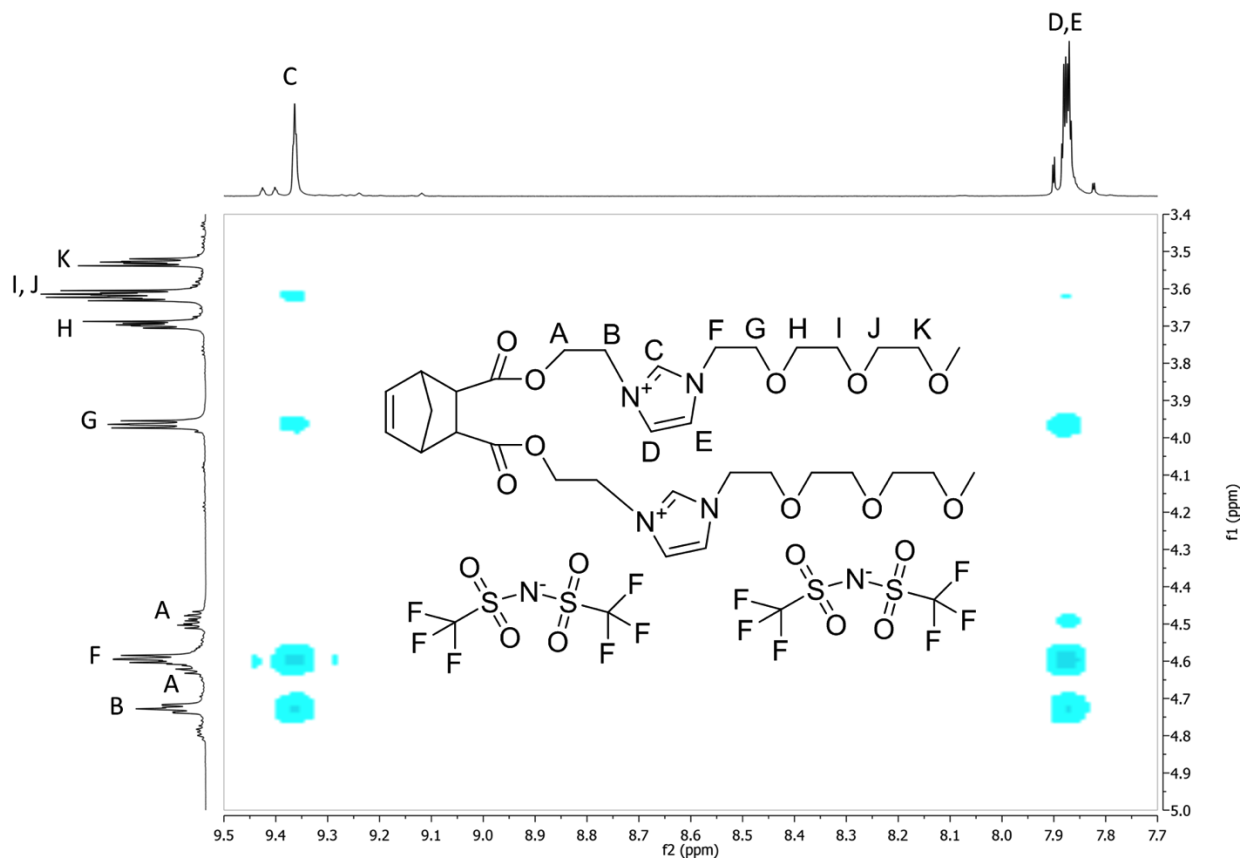


Figure 10.11. 2D NOESY NMR of **8d** taken in acetone- d_6 .

In **Figure 10.11** hydrogens A, B, F, and G of **8d** all show correlations with the imidazolium ring, as expected due to the close proximity of the atom connectivity. The following key points from the NOESY spectrum give insight into the geometry of the molecule: first, A is not coupled to C; second, G is coupled to C, D, and E; and third, I and/or J are/is coupled to C, D, and E while H and K are not. These correlations are shown in **Figure 10.12** with arrows indicating hydrogens that are close to one another. **Figure 10.12** also contains a suggested structure for the imidazolium tail group of **8d**. One possible explanation for hydrogens I and J being a considerable distance from the imidazolium ring but showing coupling while hydrogens H and K do not is that the ethyleneoxy tail group could be arching back on top of the imidazolium ring, as shown in **Figure 10.12**. This could account for the coupling

observed in the NOESY and allow one of the oxygens in the ethyleneoxy unit to be within the needed proximity for hydrogen bonding.

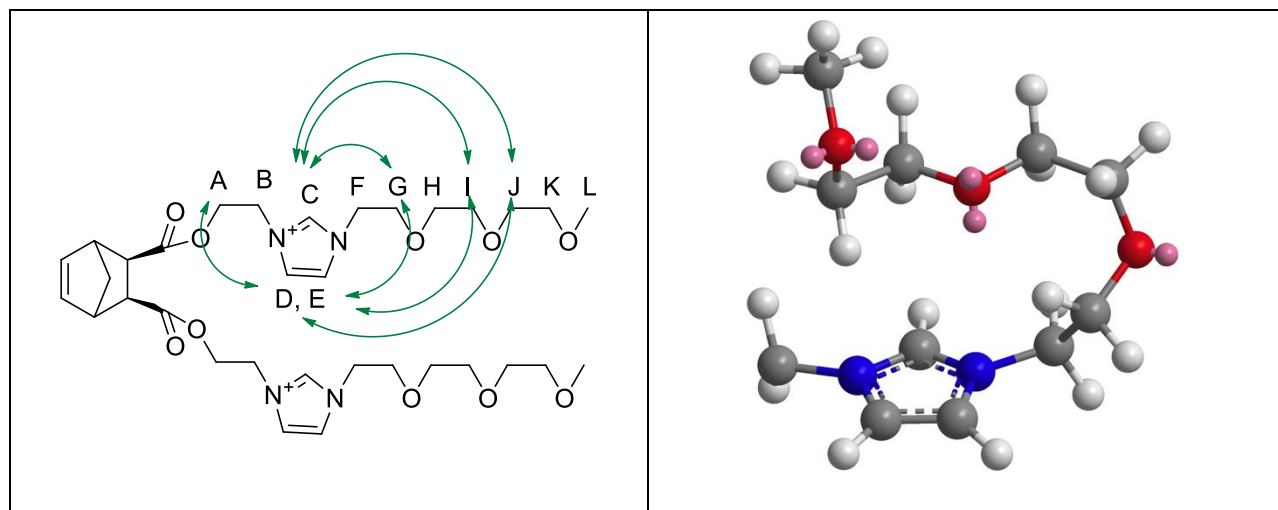


Figure 10.12. Imidazolium tail group 2-D NOESY correlation summary for **8d** in acetone- d_6 .

Conductivity values in **Table 10.2** range from a high of 9.57×10^{-5} S/cm for **8r**, down to a low of 2.42×10^{-5} S/cm for **8b**. The conductivity is influenced by several parameters such as T_g , charge density, and free (mobile) ion content. Much as with **Table 10.1** (T_g data) the data in **Table 10.2** trends in an up-down-up fashion. Interestingly though, the data suggest that the longer the spacer between the norbornene and imidazolium group (X), the better the conductivity. In addition to this, the data also shows that the Y row (tail length) plays a very large role. For the X = 1 column, a tail of three ethyleneoxy units proves to be optimal; however, for X= 2 to 4, a tail of two ethyleneoxy units was found to be superior. Although some values in this trend are close and could be disputed as experimentally indistinguishable, the overall general trend remains; for this reason, only Y tails of two ethyleneoxy units were synthesized for X = 5 and 6 ethyleneoxy units (**8u** and **8v**, respectively).

Comparison of ethyleneoxy tail groups units with the butyl tail shows a conductivity trend slightly different from that of T_g . At its best the butyl tail is a strong second place or roughly the same as the ethyleneoxy tails when the spacer (X) between the norbornene and imidazolium group are short. Once the ethyleneoxy spacer between the norbornene and imidazolium group (X) reach longer lengths, conductivity results for the butyl terminated monomers begin to fall off. In total, after $X = 3$ the butyl group loses competitiveness. This is likely due to the fact that the ethyleneoxy linker is able to wrap around the cation and free the anion. This indicates that for increased conductivities, the imidazolium unit should be well away from the norbornene group and contain a tail of two ethyleneoxy units. What is startling, however, is that conductivity values do not parallel T_g values; that is, the lowest T_g s do not correlate with the highest conductivities. In addition to this overall trend, the monomer with the lowest T_g was found to have a conductivity much lower than the monomer with the highest conductivity. **8j** had a T_g of -57 °C and a conductivity of $6.26E-05$ S/cm, while **8r** had a T_g of -46 °C and a conductivity of $9.57E-05$ S/cm, a T_g difference of 11 °C and a conductivity difference of $\sim 35\%$. This result indicates that conductivity is influenced by parameters other than T_g and as the ethyleneoxy unit becomes longer, it's not simply behaving more like PEG. One possibility for this observation could be that the oligo(ethyleneoxy) units in these monomers provide a differing level of interaction with the imidazolium cation. Monomers whose ethyleneoxy linkages interact less should behave more like PEG and have a lower T_g . Conversely ethyleneoxy linkages that strongly interact with the imidazolium cation would increase conductivity and due to ordering not reduce T_g .

Reasoning through the results, it is speculated that a long linkage between the imidazolium cation and the norbornene is desirable, so that steric crowding between the two

arms can be reduced and additional intermolecular interactions can be achieved. The tail after the imidazolium group then acts to wrap back around onto the cation for a stabilizing effect. This hypothesis can also serve as an explanation as to why in **Table 10.2**, the column of $X = 1$ seems to be inconsistent with $X = 2, 3,$ and 4 . In column $X = 1$, the Y value of 3 is the highest conducting material, but in $X = 2, 3$ and 4 , a Y value of 2 provides the best results. It is reasoned that when $X = 1$ the steric crowding at the cation is so intense that the terminal ethyleneoxy chain cannot interact effectively with the imidazolium unit. In a similar manner once at least a spacer of two ethyleneoxy units is employed, the terminal di(ethyleneoxy) tail can optimally arch back to stabilize the non-hindered cation. Any additional increase in ethyleneoxy units in the tail (more than two) simply dilutes the charge. But increases in the length of the chain tethering the imidazolium to norbornene increase the efficiency of the tail.

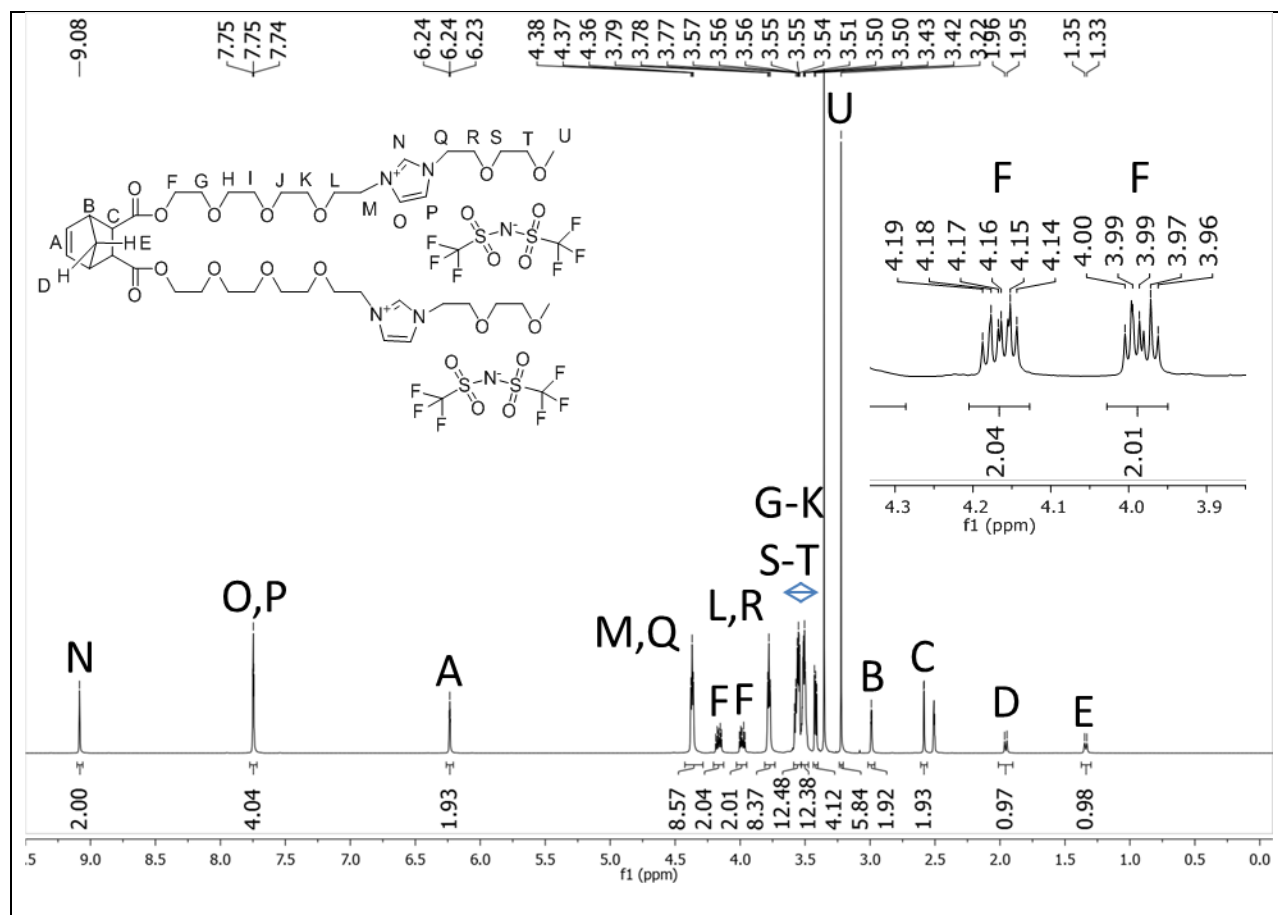


Figure 10.13. ^1H NMR spectrum (500 MHz) for **8r** in $\text{DMSO-}d_6$ at room temperature.

To understand what role the ethyleneoxy spacer in **8r** was playing (highest measured conducting monomer), NMR data were assessed (**Figure 10.13**). Assignments were made via careful analysis of the 2D COSY spectrum (not shown). The first distinguishing feature observed in all solvents explored with this product is the splitting of the proton F into two separate signals. Further inspection reveals that these two peaks, each appear to be overlapping triplets, which would give a classic ABX₂ multiplet. This suggests that each of the four hydrogens of F are in a unique chemical environment, likely a result of conformational effects. To probe this, three pieces of information must be considered: the ^{13}C NMR spectrum, computational data and the NOESY spectrum. Looking first at the ^{13}C NMR spectrum (**Figure**

10.14) no carbon signals are duplicated; 22 signals were expected and 21 signals were found; the peak located at 68.62 ppm is suspected to be two overlapping peaks. This provides evidence that only protons F are in question and not the attached carbons.

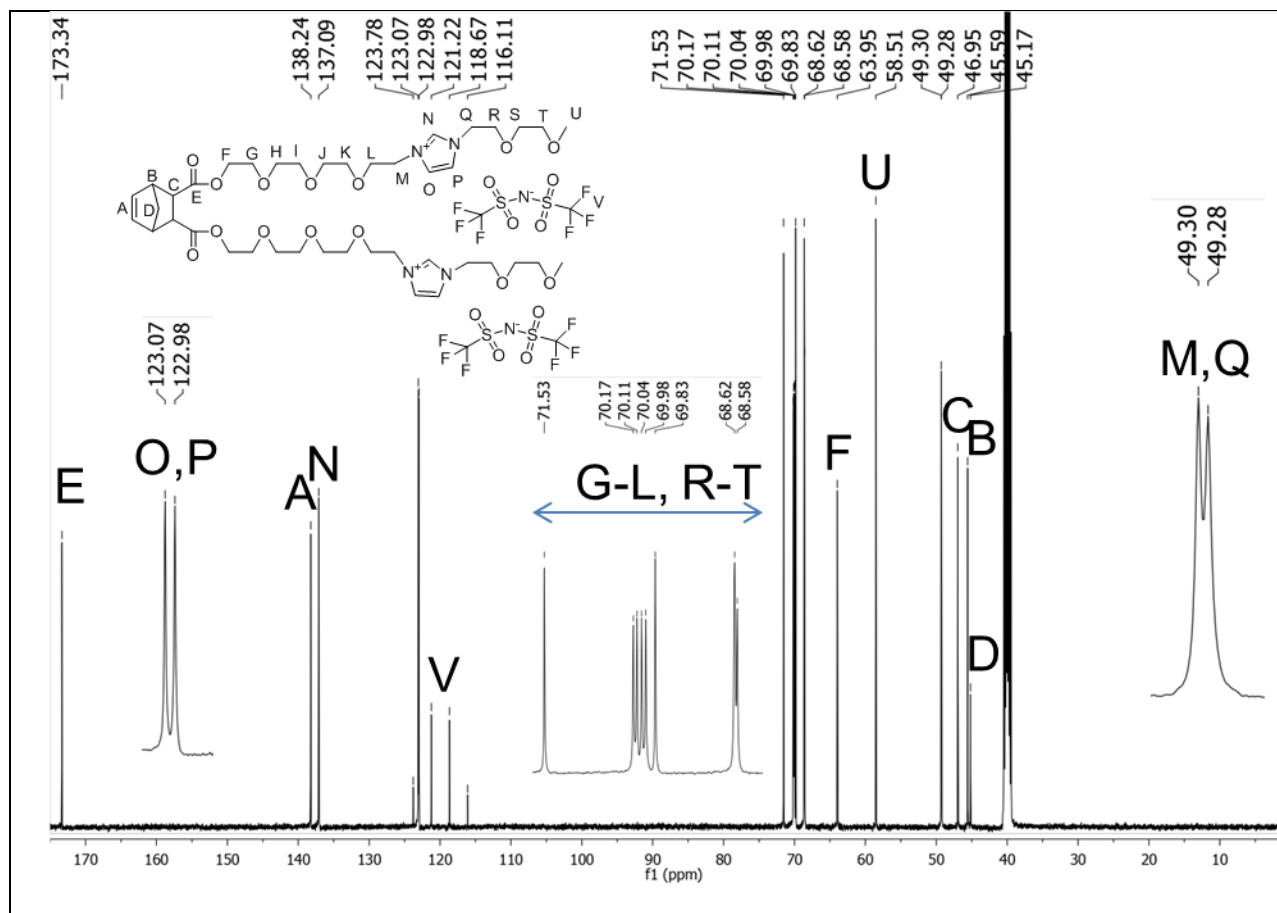


Figure 10.14. ^{13}C NMR spectrum (126 MHz) for **8r** in $\text{DMSO-}d_6$ at room temperature.

Secondly, a model system was explored through computational means to determine the spatial orientation of the ester group, opposite or aligned, **Figure 10.15**. The computational experiment employed both semiempirical and ab initio calculations; energy minimizations were tested using ten separate calculations. Nine out of ten energy minimizations indicated that an aligned orientation was preferred, while one indicated that the opposite configuration would be

avored. Additionally, the experiment suggested that at room temperature, bond rotation would be possible between the carbonyl and norbornene portion of the monomer.

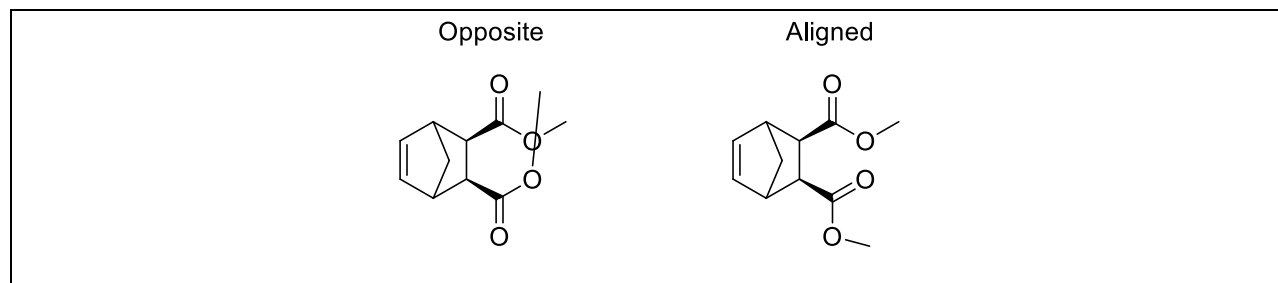


Figure 10.15. Molecules used for computational modeling to explore the optimal spatial orientation of ester groups in norbornene monomers.

Third, in the NOESY spectrum (**Figure 10.16**) one of the F proton signals is coupled to either or both of the L or R protons while the other is not. Given the lack of an additional carbon signal for either E or F and given the possibility of rotation between the carbonyl and norbornene, it is concluded that the two ester groups are geometrically the same and that once again only the two hydrogen signals are inequivalent.

Given that two signals are observed for the protons of F, computational results indicate free rotation between the carbonyl and norbornene is possible and NOESY shows a unique placement of each, it is reasoned that a conformational effect puts hydrogens of F in different environments.

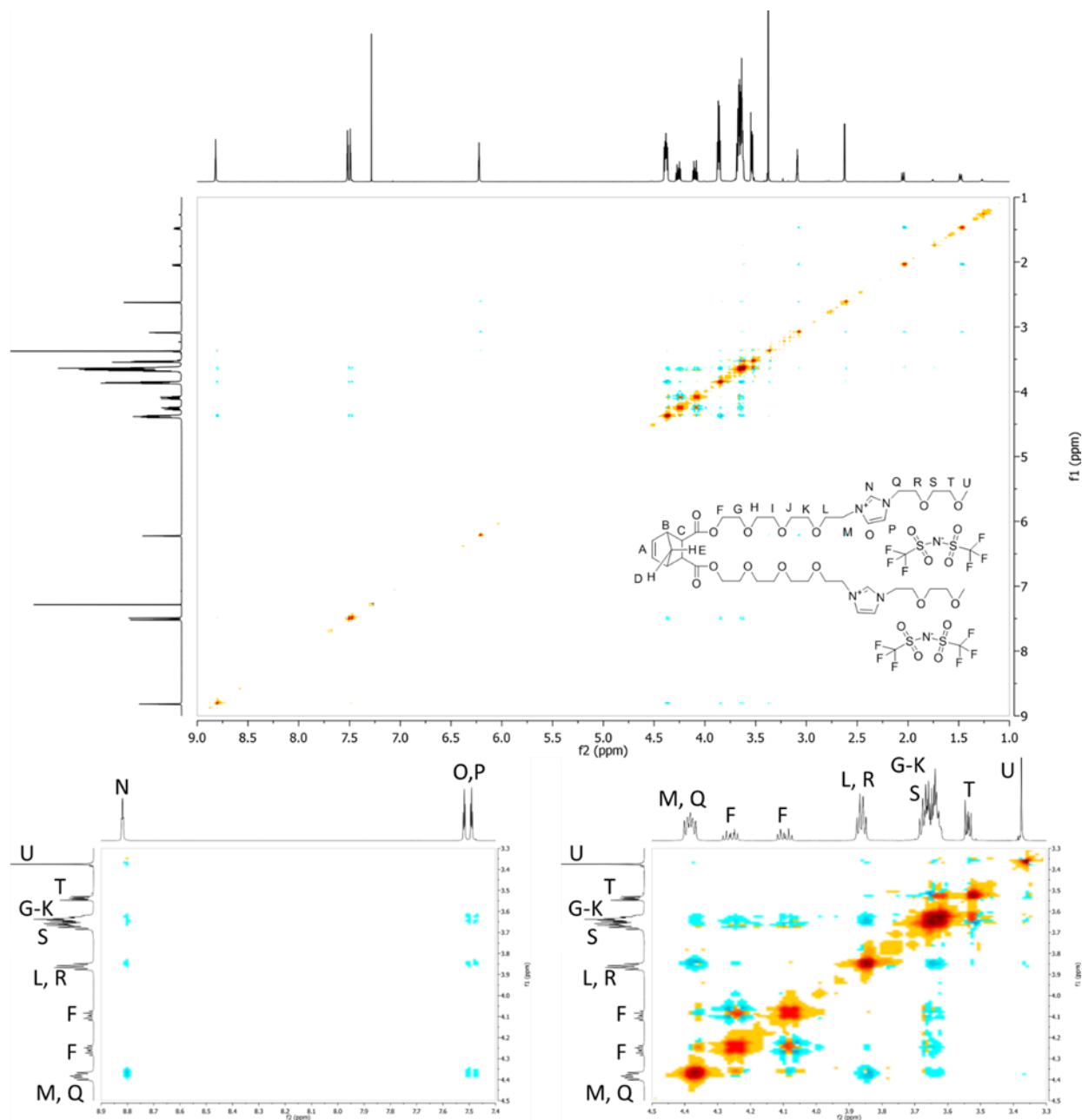


Figure 10.16. 2D NOESY (500 MHz) of **8r** in CDCl_3 at room temperature, degassed using argon.

Further analysis of **8r** using NOESY, both 2D (**Figure 10.16**) and 1D (**Figure 10.17**), proved that the ethyleneoxy units were within close proximity of the imidazolium cation. **Figure 10.18** provides a summary of notable interactions in both the 2D and 1D NOESY. In the summary it can be seen that the methyl group protons U couple to the imidazolium ring and the

norbornene proton C couples to the imidazolium proton P (and very weakly to O). One possibility is that the ethyleneoxy units wrap around the imidazolium ring; this would explain why proton P is through-space coupled to proton C. Given this result and considering the electron deficiency of the imidazolium cation, it is likely that the tether also coordinates with the imidazolium cation. Thus the tether plays two roles: allows the imidazolium to be far enough from the norbornene to provide optimal binding with the di(ethyleneoxy) tail and interacts with the cation.

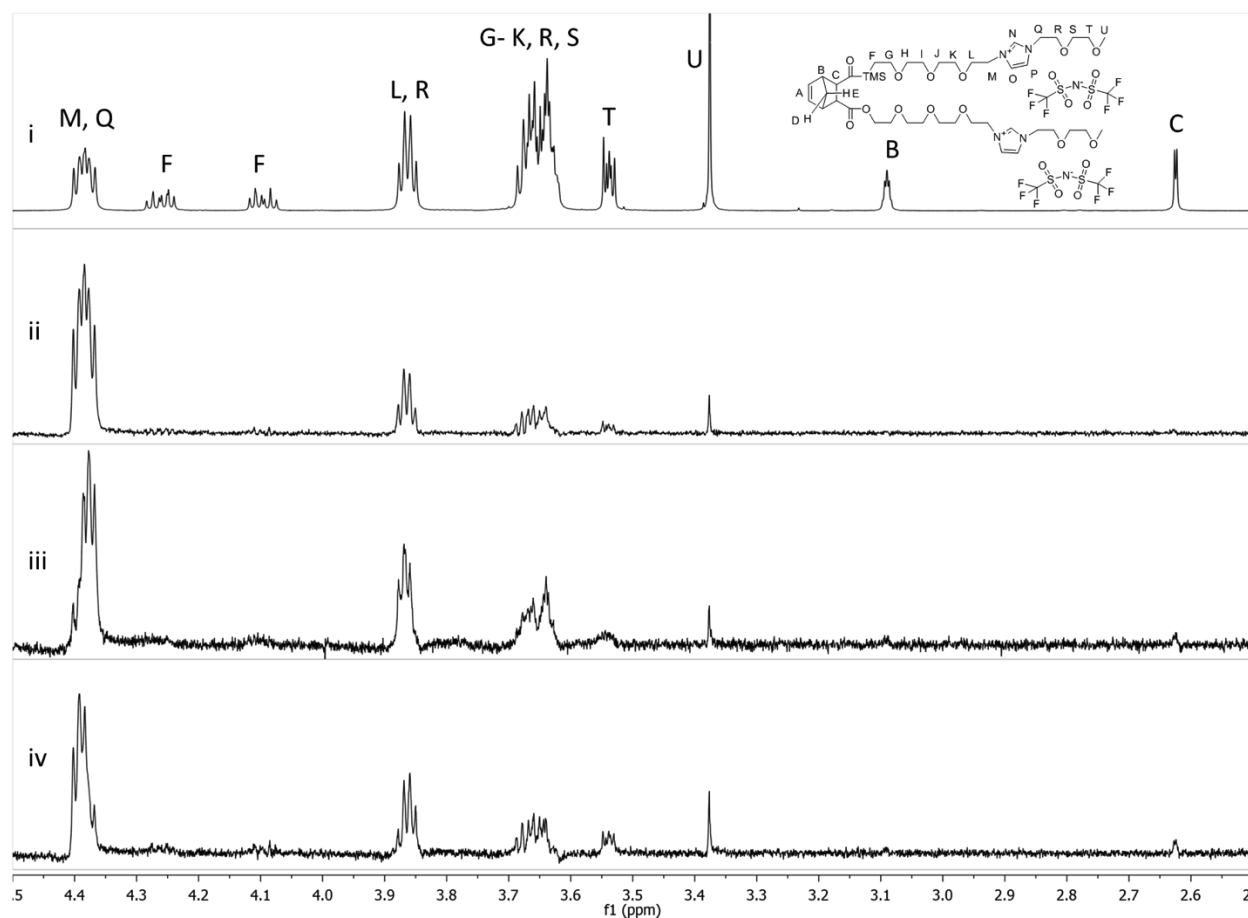


Figure 10.17. i) ^1H NMR (500 MHz) spectrum of **8r** in CDCl_3 at room temperature; ii) 1D NOESY *irradiated* peak N; iii) 1D NOESY *irradiated* peak O; iv) 1D NOESY *irradiated* peak P.

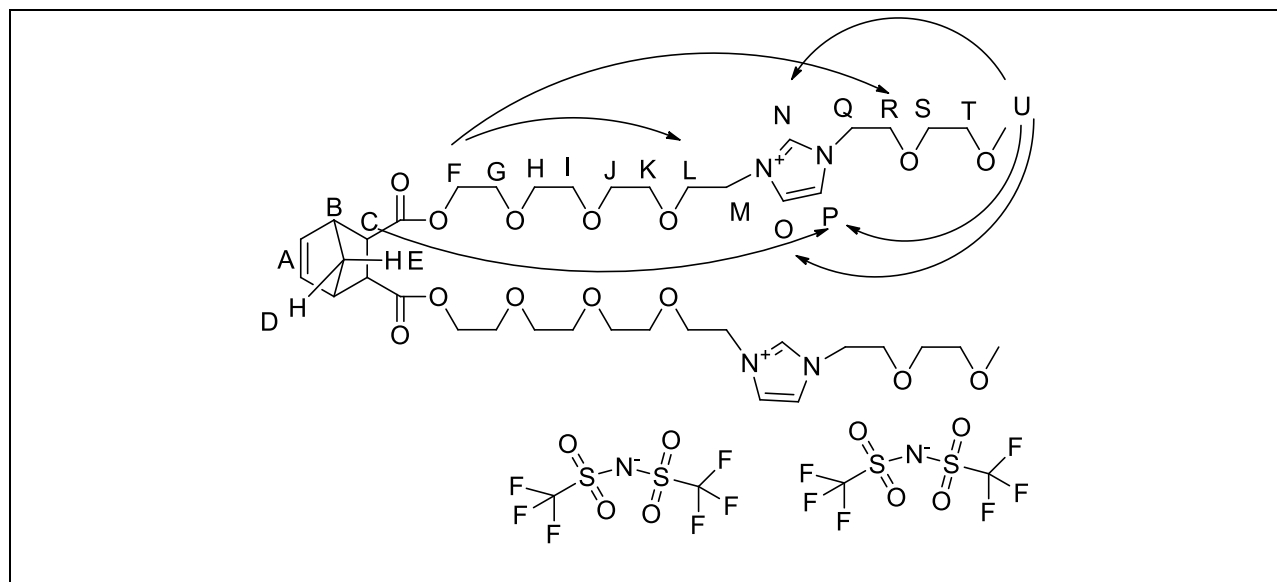


Figure 10.18. 1D and 2D NOESY summary of **8r**.

Although results indicate the greater the spacing of the imidazolium group from the norbornene monomer the higher the conductivity, it is unlikely that the remaining two pending monomers **8u** and **8v** will provide profoundly increased conductivity results. From the Y = 2 row of **Table 2** going from X = 1 to X = 2, a conductivity increase of 162% was observed, while for X = 2 to X = 3, an increase of 16% was seen and then finally X = 3 to X = 4 provided an increase of 7%. Clearly a diminishing return is observed. Taking into consideration the increased cost and synthesis time associated with penta(ethylene glycol) and hexa(ethylene glycol), it is clear that the optimal and practical monomer is **8r**, with four ethyleneoxy units between the imidazolium and norbornene rings and two terminal ethyleneoxy units.

As a final note it should be mentioned that the norbornene monomers developed here were shelf stable with no noticeable change to their ^1H NMR spectra over the course of several years. Additionally, monomers **8a–8v** were found to be generally stable up to 70 °C and no auto-polymerizations were observed within one year.

Conclusion

A matrix of monomers was synthesized to determine the optimal structure in terms of single ion conductivity to move forward with the production of polymeric systems. 37 new compounds were synthesized for this work, 22 of which were norbornene imidazolium TFSI monomers. It was found that a tail of two ethyleneoxy units was optimal. As for the chain tethering the imidazolium ring to the norbornene ring, it was generally found that the longer the oligo(ethyleneoxy) units, the better. But for practical reasons of cost and synthetic time, a tether of four ethyleneoxy units is optimal. NMR studies indicated that the ethyleneoxy units interact with the imidazolium cation, presumably via hydrogen bonding, provided the chain tethering the norbornene to the imidazolium unit was long enough. The optimal system exhibited a conductivity of 9.57×10^{-5} (S/cm) at 25 °C and a T_g of -46 °C. As a special note, within this matrix a decoupling of lower T_g values to higher conductivity values were observed. Additionally, observed shelf stability and reasonable conductivities for monomers **8a–8v** provided an acceptable platform to progress forward towards the synthesis of polymer systems.

Experimental

Measurements: ^1H -NMR spectra were obtained on JEOL ECLIPSE-500, BRUKER 500 and AGILENT NMR vnmrs400 spectrometers. ^{13}C -NMR spectra were collected on these instruments at 125 MHz, 125 MHz, and 101 MHz, respectively. HR-MS were obtained using an Agilent LC-ESI-TOF system. Reagents were purchased and used as received. DSC data were obtained from a TA Instrument Q2000 differential scanning calorimeter under N_2 ; heating

was carried out at a rate of 10 °C/min, while cooling used a quenching technique. The ionic conductivity measurements were performed by dielectric relaxation spectroscopy at Penn State by U Hyeok Choi using a sinusoidal voltage with amplitude 0.1 V and 10⁻¹–10⁷ Hz frequency range. Before each measurement was taken, the sample was held inside the instrument at 120 °C for 1 h to remove residual water. Data were collected in isothermal frequency sweeps every 5 K from 120 °C to –100 °C. For a detailed description of the method, please see work by U Hyeok Choi et al.¹ Compounds **1**,¹³ **6a**,¹⁴ **6b**,¹⁵ **6c**,¹⁴ and **7c**³ were prepared in accordance with literature procedures. ¹H NMR splitting abbreviations: s (singlet), d (doublet), t (triplet), q (quartet), quin (quintet), sex (sextet), h (heptet).

General procedure 1, norbornene esters. *Exo*-Bis(2-(2'-hydroxyethoxy)ethyl) bicyclo[2.2.1]hept-5-ene-2,3-dicarboxylate (2a). Norbornene anhydride (**1**) (19.63 g, 119.6 mmol) was added to a round bottom flask containing di(ethylene glycol) (500 mL, 3.74 mol) and the mixture was stirred briefly before adding sulfuric acid (0.5 mL, 9 mmol). The reaction mixture was heated at 70 °C with stirring for 20 h. After cooling to room temperature the reaction mixture was poured into water (1 L) and extracted with DCM (200 mL) 3x. The DCM extracts were combined and washed with 1 M HCl (100 mL x 3), saturated NaHCO₃ (100 mL x 2), water (100 mL x 3), and dried over sodium sulfate. Filtration and removal of solvent provided the desired product as a yellow tinted oil (32.98 g, 77 %). ¹H NMR (500 MHz, CDCl₃) δ: 6.22 (s, 2H), 4.24 (m, 4H), 3.77–3.65 (m, 8H), 3.59 (m, 4H), 3.18 (s, 2H), 3.13–3.08 (m, 2H), 2.68 (s, 2H), 2.12 (d, *J* = 9 Hz, 1H), 1.50 (d, *J* = 9 Hz, 1H). ¹³C NMR (126 MHz, CDCl₃) δ: 173.60 (s), 137.94 (s), 72.58 (s), 68.82 (s), 63.99 (s), 61.57 (s), 47.44 (s), 45.55 (s), 45.44 (s) (9 signals expected and 9 signals found). HR MS: calc. for C₁₇H₂₆O₈ [M + H]⁺: m/z 359.1700; found: m/z 359.1705 (error 1 ppm).

General procedure 2, norbornene tosylates. *Exo*-Bis(2-(2'-tosyloxyethoxy)ethyl)bicyclo[2.2.1]hept-5-ene-2,3-dicarboxylate (3a). *Exo*-Norbornene diol **2** (5.05 g, 14.1 mmol), TEA (33 mL, 0.24 mol), and DCM (20 mL) were combined in a round bottom flask and cooled to 0 °C. Tosyl chloride (41.97 g, 220.1 mmol) was dissolved in DCM (80 mL) and added dropwise via an addition funnel to the norbornene diol solution; once the tosyl chloride addition was complete, the reaction mixture was allowed to warm to room temperature and stir for 2 days. The reaction mixture was poured into water (100 mL) and the organic layer was washed with water (15 mL x 4), saturated NaCl (15 mL x 1), and dried over sodium sulfate. After filtration and removal of solvent the oil was washed with hexanes (100 mL x 2) and purified by flash column chromatography (silica eluting with DCM to acetonitrile) to yield a clear oil (3.97 g, 42%). ¹H NMR (500 MHz, CDCl₃) δ: 7.81 (d, *J* = 8 Hz, 4H), 7.36 (d, *J* = 8 Hz, 4H), 6.22 (m, 2H), 4.23–4.15 (m, 6H), 4.11–4.04 (m, 2H), 3.72–3.67 (m, 4H), 3.62 (m, 4H), 3.10 (s, 2H), 2.65 (d, *J* = 2 Hz, 2H), 2.46 (s, 6H), 2.07 (d, *J* = 9 Hz, 1H), 1.49 (d, *J* = 9 Hz, 1H). ¹³C NMR (126 MHz, CDCl₃) δ: 173.43, 144.89, 137.95, 132.98, 129.86, 127.95, 69.15, 69.14, 68.58, 63.60, 47.23, 45.74, 45.33, 21.64 (14 peaks expected and 14 peaks found). HR MS: calc. for C₃₁H₃₈O₁₂S₂ [M + H]⁺: m/z 667.1877; found: m/z 667.1842 (error –5.3 ppm).

General Procedure 3, Monotosylation of glycol. 14-hydroxy-3,6,9,12-tetraoxatetradecyl *p*-methylbenzenesulfonate (5a). Penta(ethylene glycol) (19.31 g, 81.04 mmol) and NaOH (3.21 g, 80.2 mmol) were dissolved in water (75 mL) and cooled to 0 °C with magnetic stirring. Tosyl chloride (15.51 g, 81.35 mmol) in THF (50 mL) was added dropwise to the reaction mixture via an addition funnel. After the tosyl chloride solution was completely added, the reaction mixture was stirred at room temperature for 24 h. THF was removed by rotary evaporation and the aqueous layer was extracted with DCM (3 x 50 mL). The organic mixture was washed with 10%

HCl (4 x 25 mL), water (3 x 25mL), and saturated NaCl (1 x 25 mL). DCM was removed by rotary evaporation and the resulting material was passed over silica; 100% DCM provided unreacted TsCl; 100% EA provided a ditosylated product (13.28 g) and lastly 100% acetonitrile provided the desired product as a clear oil, 8.74 g (27%). ¹H NMR (500 MHz, CDCl₃) δ 7.80 (d, *J* = 8 Hz, 2H), 7.34 (d, *J* = 8 Hz, 2H), 4.21–4.11 (m, 2H), 3.78–3.52 (m, 18H), 2.45 (s, 3H). ¹³C NMR (126 MHz, CDCl₃) δ 144.78, 133.01, 129.81, 127.98, 72.45, 70.75, 70.61, 70.60, 70.55, 70.53, 70.35, 69.24, 68.68, 61.75, 21.65 (15 signals expected and 15 signals found). HR MS: calc. for C₁₇H₂₈O₈S [M + NH₄]⁺: m/z 410.1843; found: m/z 410.1836 (error 2 ppm).

General Procedure 4, Esterification of *cis*-5-Norbornene-*exo*-2,3-dicarboxylic anhydride.

***Exo*-Bis(2-(2'-(2''-(2'''-(2''''-tosyloxyethoxy)ethoxy)ethoxy)ethyl)**

bicyclo[2.2.1]hept-5-ene-2,3-dicarboxylate (3d). *Cis*-5-Norbornene-*exo*-2,3-dicarboxylic anhydride (**1**) (0.88 g, 5.4 mmol) was combined in a round bottom flask with **5a** (4.06g, 10.3 mmol), EDCI (1.61 g, 10.4 mmol), DMAP (0.13 g, 1.1 mmol) and DCM (20 mL). The reaction mixture was stirred at room temperature for 3 days, after which 30 mL of DCM was added and the mixture was poured into water. The organic layer was collected and washed with water (3 x 10 mL). Solvent was then removed by rotary evaporation. Column chromatography using 100% DCM provided the desired product, 4.16 g (83%), as a viscous oil containing slight amounts of EDCI and DMAP. The product was used without further purification. ¹H NMR (400 MHz, CDCl₃) δ 7.71–7.69 (m, 4H), 7.17–7.15 (m, 4H), 6.17 (s, 2H), 4.29–4.27 (m, 4 H), 3.62–3.55 (m, 48H; overlaps with EDCI protons), 3.06 (s, 2H), 2.61 (s, 2H), 2.33 (s, 6H), 2.04 (d, *J* = 9 Hz, 1H), 1.45 (s, 1H). ¹³C NMR (101 MHz, CDCl₃) δ 173.47 (s), 144.79 (s), 137.90 (s), 132.88 (s), 129.02 (s), 126.08 (s), 70.65 (s), 70.50 (s), 70.48 (s), 70.36 (s), 70.21 (s), 70.13 (s), 68.80 (s), 67.03 (s), 47.18 (s), 45.70 (s), 45.28 (s), 21.36 (s) (20 signals expected and 18 signals found, 2

signals in the ethyleneoxy region are suspected to be overlapping). EDCI and DMAP NMR peaks were omitted for clarity. HR MS: calc. for $C_{43}H_{62}O_{18}S_2$ $[M + NH_4]^+$: m/z 948.3716; found: m/z 948.3649 (error 7.1 ppm).

General procedure 5, N-Alkylimidazoles 7. 1-Butylimidazole (7a). Imidazole (16.95 g, 249 mmol) and sodium hydroxide (9.40 g, 235 mmol) were added to a round bottom flask with water (10 mL) and stirred until the imidazole had completely dissolved. 1-Chlorobutane (21 mL, 0.26 mol) was diluted with THF (40 mL) and added to the reaction flask. Reflux was achieved and maintained for 12 h. THF was removed by rotary evaporation and the crude material was poured into water (50 mL). After extraction with DCM (3 x 100 mL), the organic layers were combined and washed with 10% sodium hydroxide (20 mL x 2), water (20 mL x 3), and dried over sodium sulfate. Filtration and removal of the solvent provided the desired product as a clear oil (21.27 g, 86%). 1H NMR (500 MHz, $CDCl_3$) δ : 7.45 (s, 1H), 7.05 (s, 1H), 6.90 (s, 1H), 3.93 (t, $J = 7$ Hz, 2H), 1.80–1.71 (m, 2H), 1.38–1.28 (m, 2H), 0.94 (t, $J = 7$ Hz, 3H). ^{13}C NMR (126 MHz, $CDCl_3$) δ : 137.09 (s), 129.40 (s), 118.78 (s), 46.73 (s), 33.10 (s), 19.74 (s), 13.51 (s) (7 signals expected and 7 signals found). HR MS: calc. for $C_7H_{12}N_2$ $[M + H]^+$: m/z 125.1073; found: m/z 125.1073 (error 0 ppm)

General procedure 6, Norbornene Imidazolium Salts. *Exo*-NB[(EO)₁Im(butyl) TFSI]₂, (8a). Norbornene **4** (3.32 g, 8.39 mmol) and imidazole **7a** (4.35 g, 35.0 mmol) were combined in a round bottom flask under nitrogen and heated at 70 °C with stirring for 3 days. After cooling to room temperature, the reaction mixture was taken up in water (50 mL) and extracted with DCM (200 mL) in a liquid-liquid apparatus for 2 days. LiTFSI (5.85 g, 20.4 mmol) was dissolved in water (10 mL) and added to the aqueous solution. The aqueous mixture was stirred for 4 h and allowed to sit overnight for the salt to “oil out”. The aqueous layer was decanted and extracted

twice with DCM (50 mL). The DCM extracts were combined with the remaining oil and washed with water (15 mL x 4). Solvent was removed by rotary evaporation and the product was dried under high vacuum for 12 h (3.29 g, 37%). ¹H NMR (500 MHz, DMSO-*d*₆) δ: 9.19 (s, 2H), 7.82 (s, 2H), 7.79 (s, 2H), 6.23 (s, 2H), 4.43 (m, 6H), 4.19 (m, 6H), 2.96–2.91 (m, 2H), 2.61 (m, 2H), 1.82–1.72 (m, 4H), 1.69 (d, *J* = 9 Hz, 1H), 1.34 – 1.18 (m, 5H), 0.90 (t, *J* = 7 Hz, 6H). ¹³C NMR (126 MHz, DMSO-*d*₆) δ: 172.45 (s), 137.71 (s), 136.48 (s), 122.76 (s), 122.50 (s), 119.44 (q, *J* = 323 Hz), 62.25 (s), 48.62 (s), 48.00 (s), 46.46 (s), 45.07 (s), 44.70 (s), 31.31 (s), 18.68 (s), 13.23 (s) (14 signals expected and 14 signals found). HR MS: calc. for C₃₁H₄₀O₁₂N₆S₄F₁₂ [M – TFSI]⁺: *m/z* 764.2217; found: *m/z* 764.2215 (error –0.2 ppm); calc. for C₃₁H₄₀O₁₂N₆S₄F₁₂ [M – 2 TFSI]⁺²: *m/z* 242.1525; found: *m/z* 242.1524 (error –0.4 ppm). *T_g* (DSC) = –44 °C. Conductivity at 25 °C = 3.07 X 10⁻⁵ S/cm.

***Exo*-Bis(2-(2'-(2''-hydroxyethoxy)ethoxy)ethyl) bicyclo[2.2.1]hept-5-ene-2,3-dicarboxylate (2b).** General procedure 1 was used to produce a clear oil (3.82 g, 70 %) by using: **1** (2.00 g, 12.2 mmol), tri(ethylene glycol) (50 mL, 374 mmol), and sulfuric acid (0.1 mL, 2 mmol). ¹H NMR (500 MHz, CDCl₃) δ: 6.21 (s, 2H), 4.23 (m, 4H), 3.79–3.57 (m, 20H), 3.11 (s, 2H), 2.66 (m, 2H), 2.10 (m, 1H), 1.49 (m, 1H). ¹³C NMR (126 MHz, CDCl₃) δ: 173.56 (s), 137.98 (s), 72.62 (s), 70.56 (s), 70.37 (s), 69.07 (s), 63.75 (s), 61.78 (s), 47.27 (s), 45.75 (s), 45.40 (s) (11 signals expected and 11 signals found). HR MS: calc. for C₂₁H₃₄O₁₀ [M + H]⁺: *m/z* 447.2225; found: *m/z* 447.2214 (error –2.3 ppm).

***Exo*-Bis(2-(2'-(2''-(2'''-hydroxyethoxy)ethoxy)ethoxy)ethyl) bicyclo[2.2.1]hept-5-ene-2,3-dicarboxylate (2c).** General procedure 1 was used to produce a clear oil (25.3 g, 63 %) by using: **1** (12.3 g, 74.8 mmol), tetra(ethylene glycol) (400 mL, 2.32 mol), and sulfuric acid (0.30 mL, 5.6 mmol). ¹H NMR (500 MHz, CDCl₃) δ: 6.21 (s, 2H), 4.27 (m, 2H), 4.15 (m, 2H), 3.77 –

3.55 (m, 28H), 3.10 (s, 2H), 2.65 (s, 2H), 2.09 (m, 1H), 1.49 (m, 1H). ¹³C NMR (126 MHz, CDCl₃) δ: 173.53 (s), 137.98 (s), 72.57 (s), 70.67 (s), 70.57 (s), 70.52 (s), 70.38 (s), 69.11 (s), 63.82 (s), 61.75 (s), 47.25 (s), 45.76 (s), 45.37 (s) (13 signals expected and 13 signals found). HR MS: calc. for C₂₅H₄₂O₁₂ [M + H]⁺: m/z 535.2749; found: m/z 535.2760 (error 2.1 ppm).

Exo-Bis(2-(2'-(2''-tosyloxyethoxy)ethoxy)ethyl) bicyclo[2.2.1]hept-5-ene-2,3-dicarboxylate (3b). General procedure 2 was used to produce a clear oil (4.13 g, 43%) by using: **2b** (5.68 g, 12.7 mmol), TEA (7.0 mL, 50 mmol), DCM (25 mL), and tosyl chloride (7.32 g, 38.4 mmol) in DCM (80 mL). ¹H NMR (400 MHz, CDCl₃) δ: 7.79 (d, *J* = 8 Hz, 4H), 7.34 (d, *J* = 8 Hz, 4H), 6.20 (m, 2H), 4.25 (m, 2H), 4.18–4.14 (m, 4H), 4.09 (m, 2H), 3.71 – 3.62 (m, 8H), 3.58 (s, 8H), 3.09 (m, 2H), 2.64 (s, 2H), 2.45 (s, 6H), 2.07 (d, *J* = 9 Hz, 1H), 1.47 (d, *J* = 9 Hz, 1H). ¹³C NMR (101 MHz, CDCl₃) δ: 173.47 (s), 144.82 (s), 137.94 (s), 133.03 (s), 129.84 (s), 127.97 (s), 70.73 (s), 70.45 (s), 69.22 (s), 69.10 (s), 68.74 (s), 63.73 (s), 47.25 (s), 45.76 (s), 45.34 (s), 21.64 (s) (16 peaks expected and 16 peaks found). High res MS: calc. for C₃₅H₄₆O₁₄S₂ [M + H]⁺: m/z 755.2402; found: m/z 755.2410 (error 1 ppm).

Exo-Bis(2-(2'-(2''-(2'''-tosyloxyethoxy)ethoxy)ethoxy)ethyl) bicyclo[2.2.1]hept-5-ene-2,3-dicarboxylate (3c). General procedure 2 was used to produce a clear oil (5.02 g, 47%) by using: **2c** (6.72 g, 12.6 mmol), TEA (7.00 mL, 50.2 mmol), DCM (20 mL) and tosyl chloride (7.06 g, 37.0 mmol) in DCM (80 mL). ¹H NMR (500 MHz, CDCl₃) δ: 7.80 (d, *J* = 8 Hz, 4H), 7.34 (d, *J* = 8 Hz, 4H), 6.22–6.18 (m, 2H), 4.27 (m, 2H), 4.18–4.14 (m, 4H), 4.10 (m, 2H), 3.71–3.57 (m, 24H), 3.09 (s, 2H), 2.64 (d, 2H), 2.45 (s, 6H), 2.08 (d, *J* = 9 Hz, 1H), 1.47 (d, *J* = 9 Hz, 1H). ¹³C NMR (126 MHz, CDCl₃) δ: 173.49 (s), 144.82 (s), 137.95 (s), 132.99 (s), 129.84 (s), 127.97 (s), 70.74 (s), 70.59 (s), 70.53 (s), 70.49 (s), 69.25 (s), 69.05 (s), 68.69 (s), 63.76 (s), 47.22 (s), 45.74

(s), 45.33 (s), 21.65 (s) (18 peaks expected and 18 peaks found). HR MS: calc. for $C_{39}H_{54}O_{16}S_2$ $[M + H]^+$: m/z 843.2926; found: m/z 843.2937 (error 1.4 ppm).

Exo-Bis(2-bromoethyl) bicyclo[2.2.1]hept-5-ene-2,3-dicarboxylate (4). **1** (3.58 g, 21.8 mmol) was added to a round bottom flask containing 2-bromoethanol (37.8 g, 302 mmol) and the mixture was stirred briefly before adding sulfuric acid (0.1 mL, 2 mmol). The reaction mixture was heated at 70 °C with stirring for 20 h. After cooling to room temperature the reaction mixture was poured into water and extracted with DCM three times. The DCM extracts were combined and washed with $NaHCO_3$ (x 4), water (x 3), and dried over sodium sulfate. Filtration and removal of solvent provided a material that was passed through a silica plug, eluted with DCM, to provide the desired product as an oil (6.87 g, 80%). 1H NMR (500 MHz, $CDCl_3$) δ : 6.24 (m, 2H), 4.38 (m, 4H), 3.54–3.48 (m, 4H), 3.17–3.13 (m, 2H), 2.68 (m, 2H), 2.07 (m, 1H), 1.52 (m, 1H). ^{13}C NMR (126 MHz, $CDCl_3$) δ : 173.07 (s), 137.94 (s), 64.10 (s), 47.13 (s), 45.93 (s), 45.27 (s), 28.81 (s) (7 signals expected and 7 signals found). HR MS: calc. for $C_{13}H_{16}Br_2O_4$ fragment $[M - C_2H_3Br_2]^+$: m/z 209.0814; found: m/z 209.0795 (error –9.1 ppm).

17-Hydroxy-3,6,9,12,15-pentaoxaheptadecyl p-methylbenzenesulfonate (5b). General Procedure 3 was used to produce a liquid (8.32 g, 24 %) by using; hexa(ethylene glycol) (22.47 g, 79.59 mmol), tosyl chloride (15.34 g, 80.46 mmol), NaOH (3.20 g, 80.0 mmol), water (10 mL), and THF (40 mL). 1H NMR (500 MHz, $CDCl_3$) δ 7.80 (d, $J = 8$ Hz, 2H), 7.35 (d, $J = 8$ Hz, 2H), 4.19–4.13 (m, 2H), 3.75–3.56 (m, 22H), 2.45 (s, 3H). ^{13}C NMR (126 MHz, $CDCl_3$) δ 144.77, 132.99, 129.81, 127.96, 72.48, 70.71, 70.59, 70.55, 70.53, 70.52, 70.50, 70.31, 69.26, 68.66, 61.71, 21.63 (17 signals expected and 16 signals found; peak @ 70.59 results from the overlapping of 2 peaks). HR MS: calc. for $C_{19}H_{32}O_9S$ $[M + Na]^+$: m/z 459.1659; found: m/z 459.1661 (error –0.4 ppm).

***Exo*-Bis(2-(2'-(2''-(2'''-(2''''-(2'''''-tosyloxyethoxy)ethoxy)ethoxy)ethoxy)ethoxy)ethyl)**

bicyclo[2.2.1]hept-5-ene-2,3-dicarboxylate (3e). General procedure 4 was used to produce a liquid (2.79 g, 82%) by using: **1** (0.37 g, 2.3 mmol), **5b** (2.04 g, 4.67 mmol), EDCI (0.87 g, 5.6 mmol), DMAP (0.14 g, 1.1 mmol), and DCM (50 mL). ¹H NMR (500 MHz, CDCl₃) δ 7.80 (d, *J* = 8 Hz, 4H), 7.35 (d, *J* = 8 Hz, 4H), 6.20 (s, 2H), 4.32–4.24 (m, 2H), 4.19–4.13 (m, 4H), 4.13–4.06 (m, 2H), 3.80–3.53 (m, 40H), 3.09 (s, 2H), 2.64 (d, *J* = 2 Hz, 2H), 2.45 (s, 6H), 2.08 (d, *J* = 9 Hz, 1H), 1.48 (d, *J* = 9 Hz, 1H). ¹³C NMR (126 MHz, CDCl₃) δ 173.47, 144.78, 137.95, 133.02, 129.82, 127.98, 72.49, 70.75, 70.61, 70.57, 70.52, 70.34, 69.24, 69.06, 68.68, 63.76, 61.75, 47.22, 45.75, 45.34, 42.73, 21.65 (22 signals expected and 22 found). HR MS: calc. for C₄₇H₇₀O₂₀S₂ [M + NH₄]⁺: *m/z* 1036.4240; found: *m/z* 1036.4303 (error –6.1 ppm).

1-(2'-Methoxyethyl)imidazole (7b). General procedure 5 was used to produce a yellow tinted liquid (43.5 g, 49 %) by using: imidazole (49.6 g, 729 mmol), sodium hydroxide (28.7 g, 718 mmol), water (30 mL), and 2-chloroethyl methyl ether (67.2 g, 711 mmol) in THF (120 mL). ¹H NMR (500 MHz, CDCl₃) δ: 7.52 (s, 1H), 7.05 (s, 1H), 6.97 (s, 1H), 4.09 (t, *J* = 5 Hz, 2H), 3.63 (t, *J* = 5 Hz, 2H), 3.34 (s, 3H). ¹³C NMR (126 MHz, CDCl₃) δ: 137.49 (s), 129.30 (s), 119.38 (s), 71.84 (s), 59.02 (s), 47.03 (s) (6 signals expected and 6 signals found). HR MS: calc. for C₆H₁₀N₂O [M + H]⁺: *m/z* 127.0866; found: *m/z* 127.0866 (error 0 ppm).

1-(2'-(2''-(2'''-methoxyethoxy)ethoxy)ethyl)imidazole (7d). General procedure 5 was used to produce a clear oil (6.76 g, 76 %) by using: imidazole (2.83 g, 41.6 mmol), sodium hydroxide (1.88 g, 47.0 mmol), water (3 mL), and **6b** (14.38 g, 45.17 mmol) in THF (20 mL). ¹H NMR (500 MHz, CDCl₃) δ: 7.53 (s, 1H), 7.04 (s, 1H), 6.99 (s, 1H), 4.11 (t, *J* = 5 Hz, 2H), 3.77–3.72 (m, 2H), 3.64–3.58 (m, 6H), 3.56–3.52 (m, 2H), 3.38 (s, 3H). ¹³C NMR (126 MHz, CDCl₃) δ: 137.56 (s), 129.27 (s), 119.41 (s), 71.94 (s), 70.72 (s), 70.61 (s), 70.59 (s), 70.56 (s), 59.05 (s),

47.05 (s) (10 signals expected and 10 signals found). HR MS: calc. for C₁₀H₁₈O₃N₂ [M + H]⁺: m/z 215.1390; found: m/z 215.1397 (error 3 ppm).

1-(2',5',8',11'-tetraoxatridecan-13'-yl)imidazole (7e). General procedure 5 was used to produce a clear oil (4.32 g, 94 %) by using: imidazole (2.76 g, 40.5 mmol), sodium hydroxide (1.53 g, 38.3 mmol), water (5 mL) and **6c** (6.46 g, 17.8 mmol) in THF (60 mL). ¹H NMR (500 MHz, CDCl₃) δ: 7.53 (s, 1H), 7.04 (s, 1H), 7.00 (s, 1H), 4.11 (t, *J* = 5 Hz, 2H), 3.74 (t, *J* = 5 Hz, 2H), 3.69–3.53 (m, 12H), 3.37 (s, 3H). ¹³C NMR (126 MHz, CDCl₃) δ: 137.52 (s), 129.24 (s), 119.40 (s), 71.93 (s), 70.70 (s), 70.61 (s), 70.56 (s), 70.54 (s), 70.52 (s), 59.00 (s), 47.03 (s) (12 signals expected and 11 signals found; it is believed that two peaks overlap at 70.61). HR MS: calc. for C₁₂H₂₂O₄N₂ [M + H]⁺: m/z 259.1652; found: m/z 259.1665 (error 5.0 ppm).

Exo-NB[(EO)₁Im(EO)₁CH₃ TFSI]₂ (8b). General procedure 6 was used to produce an oil (4.85 g, 52 %) by using: **4** (3.55g, 8.96 mmol), **7b** (4.42 g, 35.0 mmol) and LiTFSI (6.20 g, 21.6 mmol). ¹H NMR (400 MHz, DMSO-*d*₆) δ 9.12 (t, *J* = 2 Hz, 2H), 7.73 (dt, *J* = 4, 2 Hz, 4H), 6.19 (t, *J* = 2 Hz, 2H), 4.48–4.36 (m, 6H), 4.36–4.31 (m, 4H), 4.22–4.12 (m, 2H), 3.68–3.61 (m, 4H), 3.22 (s, 6H), 2.92–2.88 (m, 2H), 2.58 (d, *J* = 2 Hz, 2H), 1.67 (d, *J* = 9 Hz, 1H), 1.28 (dt, *J* = 9, 2 Hz, 1H). ¹³C NMR (101 MHz, DMSO-*d*₆) δ 172.90, 138.16, 137.27, 123.27, 123.00, 119.9 (q, *J* = 323 Hz), 69.97, 62.69, 58.49, 49.21, 48.41, 46.93, 45.53, 45.16. (14 signals expected and 14 signals found). HR MS: calc. for C₂₉H₃₆O₁₄N₆S₄F₁₂ [M – TFSI]⁺: m/z 768.1802; found: m/z 768.1792 (error –1.3 ppm). HR MS: calc. for C₂₉H₃₆O₁₄N₆S₄F₁₂ [M – 2TFSI]²⁺: m/z 244.1312; found: m/z 244.1288 (error –9.8 ppm). T_g (DSC) = –39 °C. Conductivity at 25 °C = 2.42 X 10^{–5} S/cm.

Exo-NB[(EO)₁Im(EO)₂CH₃ TFSI]₂ (8c). General procedure 6 was used to produce an oil (4.94 g, 52%) by using: **4** (3.30 g, 8.34 mmol), **7c** (5.00 g, 29.37 mmol), and LiTFSI (6.00 g, 20.9

mmol). ^1H NMR (500 MHz, CD_2Cl_2) δ : 8.82 (s, 2H), 7.54 (s, 2H), 7.50 (s, 2H), 6.25 (s, 2H), 4.46 (m, 8H), 4.41–4.36 (m, 4H), 3.90–3.83 (m, 4H), 3.65 (s, 4H), 3.55 (s, 4H), 3.36 (s, 6H), 3.08 (s, 2H), 2.72 (s, 2H), 1.82 (m, 1H), 1.49 (m, 1H). ^{13}C NMR (126 MHz, CD_2Cl_2) δ : 173.84 (s), 138.21 (s), 136.74 (s), 123.91 (s), 122.78 (s), 120.22 (q, $J = 323$ Hz), 71.92 (s), 70.57 (s), 68.68 (s), 62.80 (s), 58.89 (s), 50.40 (s), 49.23 (s), 47.80 (s), 45.92 (s), 45.49 (s) (16 signals expected and 16 major signals found; additionally, minor signals were observed for most carbon signals, this is due to an equilibrium between hydrogen bonded and non-hydrogen bonded ethyleneoxy-imidazolium moieties in CD_2Cl_2 ; see text for explanation). ^{13}C NMR (126 MHz, $\text{DMSO}-d_6$) δ 172.95, 138.17, 137.27, 123.31, 122.98, 119.91 (q, $J = 323$ Hz), 71.49, 69.77, 68.55, 62.78, 58.49, 49.34, 48.44, 46.94, 45.56, 45.17 (16 signals expected and 16 signals found). HR MS: calc. for $\text{C}_{33}\text{H}_{44}\text{O}_{16}\text{N}_6\text{S}_4\text{F}_{12}$ $[\text{M} - \text{TFSI}]^+$: m/z 856.2327; found: m/z 856.2312 (error -1.8 ppm). HR MS: calc. for $\text{C}_{33}\text{H}_{44}\text{O}_{16}\text{N}_6\text{S}_4\text{F}_{12}$ $(\text{M} - 2 \text{TFSI})^{+2}$: m/z 288.1580; found: m/z 288.1576 (error -1.4 ppm). T_g (DSC) = -45 °C. Conductivity at 25 °C = 2.95×10^{-5} S/cm.

Exo-NB[(EO)₁Im(EO)₃CH₃ TFSI]₂ (8d). General procedure 6 was used to produce an oil (7.57 g, 59%) by using: **4** (4.15 g, 10.5 mmol), **7d** (4.97 g, 23.12 mmol), and LiTFSI (6.50 g, 22.6 mmol). ^1H NMR (500 MHz, $\text{DMSO}-d_6$) δ : 9.16 (s, 2H), 7.79 (m, 4H), 6.29–6.19 (m, 2H), 4.54–4.41 (m, 6H), 4.41–4.33 (m, 4H), 4.22 (m, 2H), 3.81–3.75 (m, 4H), 3.59–3.53 (m, 4H), 3.53–3.46 (m, 8H), 3.43 (m, 4H), 3.24 (s, 6H), 2.98–2.92 (m, 2H), 2.63 (d, 2H), 1.72 (d, $J = 9$ Hz, 1H), 1.32 (d, $J = 9$ Hz, 1H). ^{13}C NMR (126 MHz, $\text{DMSO}-d_6$) δ : 172.99 (s), 138.21 (s), 137.28 (s), 123.41 (s), 122.96 (s), 119.94 ($J = 323$ Hz), 71.71 (s), 70.01 (s), 69.98 (s), 69.93 (s), 68.59 (s), 62.80 (s), 58.51 (s), 49.31 (s), 48.43 (s), 46.97 (s), 45.58 (s), 45.20 (s) (17 signals expected and 17 signals found). HR MS: calc. for $\text{C}_{37}\text{H}_{52}\text{O}_{18}\text{N}_6\text{S}_4\text{F}_{12}$ $[\text{M} - \text{TFSI}]^+$: m/z 944.2851; found: m/z 944.2840 (error -1.1 ppm). HR MS: calc. for $\text{C}_{37}\text{H}_{52}\text{O}_{18}\text{N}_6\text{S}_4\text{F}_{12}$ $[\text{M} - 2\text{TFSI}]^{+2}$: m/z 332.1836;

found: m/z 332.1840 (error 1 ppm). T_g (DSC) = -50 °C. Conductivity at 25 °C = 7.10×10^{-5} S/cm.

Exo-NB[(EO)₁Im(EO)₄CH₃ TFSI]₂ (8e). General procedure 6 was used to produce an oil (2.38 g, 70%) by using: **4** (1.03 g, 2.60 mmol), **7e** (1.90 g, 7.37 mmol) and LiTFSI (1.86 g, 6.48 mmol). ¹H NMR (500 MHz, DMSO-*d*₆) δ 9.14 (s, 2H), 7.78 (m, 4H), 6.23 (m, 2H), 4.46 (m, 6H), 4.41–4.35 (m, 4H), 4.22 (m, 2H), 3.79 (t, $J = 4$ Hz, 4H), 3.60–3.53 (m, 4H), 3.53–3.47 (m, 16H), 3.43 (t, $J = 4$ Hz, 4H), 3.24 (s, 3H), 3.23 (s, 3H), 2.95 (m, 2H), 2.63 (d, 2H), 1.72 (d, $J = 9$ Hz, 1H), 1.32 (d, $J = 9$ Hz, 1H). ¹³C NMR (126 MHz, DMSO-*d*₆) δ 172.98 (s), 138.22 (s), 137.30 (s), 123.41 (s), 122.97 (s), 119.95 (q, $J = 323$ Hz), 71.72 (s), 70.19 (s), 70.17 (s), 70.03 (s), 70.00 (s), 69.98 (s), 69.97 (s), 68.60 (s), 62.81 (s), 58.49 (s), 49.35 (s), 48.44 (s), 46.98 (s), 45.59 (s), 45.21 (s) (20 signals expected and 20 signals found). HR MS: calc. for C₄₁H₆₀O₂₀N₆S₄F₁₂ [M + Na]⁺: m/z 1335.2446; found: m/z 1335.2462 (error 1.2 ppm). HR MS: calc. for C₄₁H₆₀O₂₀N₆S₄F₁₂ [M – TFSI]⁺: m/z 1032.3375; found: m/z 1032.3392 (error 1.6 ppm). HR MS: calc. for C₄₁H₆₀O₂₀N₆S₄F₁₂ [M – 2TFSI]⁺²: m/z 376.2098; found: m/z 376.2111 (error 3.3 ppm). T_g (DSC) = -42 °C. Conductivity at 25 °C = 3.88×10^{-5} S/cm.

Exo-NB[(EO)₂Im_{butyl} TFSI]₂ (8f). General procedure 6 was used to produce an oil (1.28 g, 52%) by using **3a** (1.45 g, 2.18 mmol), **7a** (1.55 g, 12.5 mmol) and LiTFSI (2.36 g, 8.22 mmol). ¹H NMR (400 MHz, DMSO-*d*₆) δ 9.10 (s, 2H), 7.78 (t, $J = 2$ Hz, 2H), 7.71 (t, $J = 2$ Hz, 2H), 6.23 (t, $J = 2$ Hz, 1H), 4.36–4.29 (m, 4H), 4.20–4.07 (m, 6H), 3.95–3.90 (m, 2H), 3.78–3.71 (m, 4H), 3.57 (t, $J = 5$ Hz, 4H), 2.96–2.91 (m, 2H), 2.54 (d, $J = 2$ Hz, 2H), 1.89 (d, $J = 9$ Hz, 1H), 1.75 (p, $J = 8$ Hz, 4H), 1.32 (d, $J = 9$ Hz, 1H), 1.28–1.18 (m, 4H), 0.88 (t, $J = 8$ Hz, 6H). ¹³C NMR (101 MHz, DMSO-*d*₆) δ 173.21, 138.22, 136.74, 123.23, 122.66, 119.91 (q, $J = 323$ Hz), 68.45, 63.69, 49.20, 49.02, 46.99, 45.55, 45.22, 31.80, 19.20, 13.68 (16 signals expected and 16

signals found). HR MS: calc. for $C_{35}H_{48}O_{14}N_6S_4F_{12}$ $[M - TFSI]^+$: m/z 852.2741; found: m/z 852.2743 (error 0.2 ppm). HR MS: calc. for $C_{35}H_{48}O_{14}N_6S_4F_{12}$ $[M - 2TFSI]^{+2}$: m/z 286.1781; found: m/z 286.1791 (error 3.3 ppm). T_g (DSC) = -47 °C. Conductivity at 25 °C = 7.75×10^{-5} S/cm.

Exo-NB[(EO)₂Im(EO)₁CH₃ TFSI]₂ (8g). General procedure 6 was used to produce an oil (2.54 g, 73%) by using **3a** (2.03 g, 3.05 mmol), **7b** (1.53 g, 12.2 mmol) and LiTFSI (2.28 g, 7.94 mmol). 1H NMR (500 MHz, acetone- d_6) δ 9.04 (s, 2H), 7.78 (s, 4H), 6.27 (s, 2H), 4.62–4.54 (m, 8H), 4.27 (m, 2H), 4.12 (m, 2H), 3.97 (t, $J = 5$ Hz, 4H), 3.83 (t, $J = 5$ Hz, 4H), 3.74 (t, $J = 5$ Hz, 4H), 3.36 (s, 6H), 3.06 (s, 2H), 2.66 (d, $J = 2$ Hz, 2H), 2.08 (d, $J = 8$ Hz, 1H), 1.41 (d, $J = 8.5$ Hz, 1H). ^{13}C NMR (126 MHz, acetone- d_6) δ 174.01 (s), 138.80 (s), 137.70 (s), 123.95 (s), 123.77 (s), 121.07 (q, $J = 320$ Hz), 70.81 (s), 69.68 (s), 69.44 (s), 64.38 (s), 59.00 (s), 50.64 (s), 50.60 (s), 47.99 (s), 46.46 (s), 45.94 (s) (16 peaks expected and 16 peaks found). HR MS: calc. for $C_{33}H_{44}O_{16}N_6S_4F_{12}$ $[M - TFSI]^+$: m/z 856.2327; found: m/z 856.2356 (error 3.5 ppm). HR MS: calc. for $C_{33}H_{44}O_{16}N_6S_4F_{12}$ $[M - 2TFSI]^{+2}$: m/z 288.1574; found: m/z 288.1596 (error 7.5 ppm). T_g (DSC) = -39 °C. Conductivity at 25 °C = 4.80×10^{-5} S/cm.

Exo-NB[(EO)₂Im(EO)₂CH₃ TFSI]₂ (8h). General procedure 6 was used to produce an oil (1.54 g, 58%) by using **3a** (1.43 g, 2.15 mmol), **7c** (1.54 g, 12.2 mmol) and LiTFSI (1.75 g, 6.10 mmol). 1H NMR (500 MHz, DMSO- d_6) δ 9.08 (s, 2H), 7.76 (t, $J = 2$ Hz, 2H), 7.73 (t, $J = 2$ Hz, 2H), 6.26 (t, $J = 2$ Hz, 2H), 4.37 (m, 8H), 4.16 (m, 2H), 3.96 (m, 2H), 3.78 (t, $J = 4$ Hz, 8H), 3.59 (t, $J = 4$ Hz, 4H), 3.57–3.52 (m, 4H), 3.44–3.39 (m, 4H), 3.22 (s, 6H), 2.99–2.94 (m, 2H), 2.58 (d, $J = 2$ Hz, 2H), 1.91 (d, $J = 9$ Hz, 1H), 1.35 (d, $J = 9$ Hz, 1H). ^{13}C NMR (126 MHz, DMSO- d_6) δ 173.26 (s), 138.24 (s), 137.09 (s), 123.02 (s), 123.00 (s), 119.93 (q, $J = 323$ Hz), 71.52 (s), 69.82 (s), 68.56 (s), 68.53 (s), 68.47 (s), 63.70 (s), 58.52 (s), 49.30 (s), 49.21 (s), 47.01 (s), 45.57

(s), 45.24 (s) (18 signals expected and 18 signals found). HR MS: calc. for $C_{37}H_{52}O_{18}N_6S_4F_{12}$ [M – TFSI]⁺: m/z 944.2851; found: m/z 944.2863 (error 1.3 ppm). HR MS: calc. for $C_{37}H_{52}O_{18}N_6S_4F_{12}$ [M – 2TFSI]⁺²: m/z 332.1836; found: m/z 332.1838 (error 0.6 ppm). T_g (DSC) = –49 °C. Conductivity at 25 °C = 7.72 x 10⁻⁵ S/cm.

Exo-NB[(EO)₂Im(EO)₃CH₃ TFSI]₂ (8i). General procedure 6 was used to produce an oil (2.45 g, 75%) by using **3a** (1.67 g, 2.50 mmol), **7d** (1.85 g, 9.10 mmol) and LiTFSI (1.85 g, 6.46 mmol). ¹H NMR (500 MHz, CDCl₃) δ 8.81 (s, 2H), 7.52 (s, 2H), 7.42 (s, 2H), 6.29–6.16 (m, 2H), 4.37 (m, 8H), 4.20–4.15 (m, 3H), 3.84 (m, 8H), 3.67 (m, 8H), 3.64–3.60 (m, 8H), 3.55 (m, 4H), 3.36 (s, 6H), 3.08 (s, 2H), 2.65 (s, 2H), 2.03 (d, *J* = 9 Hz, 1H), 1.49 (d, *J* = 9 Hz, 1H). ¹³C NMR (126 MHz, CDCl₃) δ 173.55 (s), 137.95 (s), 136.33 (s), 123.18 (s), 122.76 (s), 119.80 (q, *J* = 321 Hz), 77.23 (s), 71.80 (s), 70.29 (s), 70.21 (s), 69.04 (s), 68.55 (s), 68.52 (s), 63.55 (s), 58.87 (s), 49.79 (s), 47.37 (s), 45.67 (s), 45.34 (s) (20 signals expected and 19 signals found; peak @ 70.21 is considered to be 2 overlapping peaks). HR MS: calc. for $C_{41}H_{60}O_{20}N_6S_4F_{12}$ [M – 2TFSI]⁺²: m/z 376.2098; found: m/z 376.2082 (error –4.4 ppm). T_g (DSC) = –54 °C. Conductivity at 25 °C = 5.39 x 10⁻⁵ S/cm.

Exo-NB[(EO)₂Im(EO)₄CH₃ TFSI]₂ (8j). General procedure 6 was used to produce an oil (3.43 g, 50%) by using **3a** (3.28 g, 4.92 mmol), **7e** (3.17 g, 12.3 mmol) and LiTFSI (4.70 g, 16.4 mmol). ¹H NMR (500 MHz, CDCl₃) δ 8.84 (s, 2H), 7.53 (s, 2H), 7.45 (s, 2H), 6.23 (s, 2H), 4.38 (s, 8H), 4.18 (s, 4H), 3.91–3.81 (m, 8H), 3.74–3.58 (m, 24H), 3.56–3.50 (m, 4H), 3.34 (s, 6H), 3.08 (s, 2H), 2.65 (s, 2H), 2.03 (d, *J* = 9 Hz, 1H), 1.49 (d, *J* = 9 Hz, 1H). ¹³C NMR (126 MHz, CDCl₃) δ 173.55 (s), 137.96 (s), 136.47 (s), 123.18 (s), 122.81 (s), 119.83 (q, *J* = 319 Hz), 71.85 (s), 70.43 (s), 70.36 (s), 70.32 (s), 70.27 (s), 70.23 (s), 69.04 (s), 68.58 (s), 68.55 (s), 63.56 (s), 58.86 (s), 49.84 (s), 49.81 (s), 47.38 (s), 45.67 (s), 45.35 (s) (22 signals expected and 22 signals

found). HR MS: calc. for $C_{45}H_{68}O_{22}N_6S_4F_{12}$ $[M - TFSI]^+$: m/z 1120.3899; found: m/z 1120.3860 (error -3.5 ppm). HR MS: calc. for $C_{45}H_{68}O_{22}N_6S_4F_{12}$ $[M - 2TFSI]^{+2}$: m/z 420.2361; found: m/z 420.2351 (error -2.4 ppm). T_g (DSC) = -57 °C. Conductivity at 25 °C = 6.26×10^{-5} S/cm.

Exo-NB[(EO)₃Im_{butyl} TFSI]₂ (8k). General procedure 6 was used to produce an oil (1.99 g, 61 %) by using **3b** (2.01 g, 2.66 mmol), **7a** (0.800 g, 6.44 mmol) and LiTFSI (1.91 g, 6.65 mmol). ¹H NMR (500 MHz, DMSO-*d*₆) δ 9.13 (s, 2H), 7.80 (t, $J = 2$ Hz, 2H), 7.75 (t, $J = 2$ Hz, 2H), 6.24 (t, $J = 2$ Hz, 2H), 4.38–4.31 (m, 4H), 4.22–4.12 (m, 6H), 3.99–3.94 (m, 2H), 3.81–3.74 (m, 4H), 3.55–3.50 (m, 12H), 2.99 (s, 2H), 2.58 (d, $J = 2$ Hz, 2H), 1.96–1.94 (m, 1H), 1.77 (quin, $J = 8$ Hz, 4H), 1.35–1.33 (m, 1H), 1.25 (h, $J = 8$ Hz, 4H), 0.91 (t, $J = 8$ Hz, 6H). ¹³C NMR (126 MHz, DMSO-*d*₆) δ 173.30, 138.22, 136.75, 123.25, 122.67, 119.93 (q, $J = 323$ Hz), 69.97, 69.92, 68.61, 68.56, 63.90, 49.27, 49.02, 46.96, 45.60, 45.18, 31.81, 19.21, 13.70 (19 signals expected and 19 found). HR MS: calc. for $C_{39}H_{56}O_{16}N_6S_4F_{12}$ $[M - TFSI]^+$: m/z 940.3266; found: m/z 940.3186 (error -8.5 ppm). T_g (DSC) = -47 °C.

Exo-NB[(EO)₃Im(EO)₁CH₃ TFSI]₂ (8l). General procedure 6 was used to produce an oil (0.86 g, 50 %) by using **3b** (1.06 g, 1.41 mmol), **7b** (0.712 g, 5.65 mmol) and LiTFSI (1.05 g, 3.66 mmol). ¹H NMR (500 MHz, acetone-*d*₆) δ 9.04 (s, 2H), 7.80 (s, 2H), 7.76 (s, 2H), 6.25 (s, 2H), 4.57 (s, 8H), 4.27 (m, 2H), 4.11 (m, 2H), 3.96 (m, 4H), 3.84 (m, 4H), 3.73–3.60 (m, 12H), 3.37 (s, 6H), 3.06 (s, 2H), 2.63 (s, 2H), 2.10 (m, 1H), 1.40 (m, 1H). ¹³C NMR (126 MHz, acetone-*d*₆) δ 173.07 (s), 137.84 (s), 136.73 (s), 123.04 (s), 122.81 (s), 120.13 (q, $J = 323$ Hz), 70.10 (s), 69.89 (s), 68.71 (s), 68.55 (s), 63.64 (s), 58.07 (s), 49.71 (s), 49.65 (s), 46.93 (s), 45.57 (s), 44.89 (s) (18 signals expected and 17 signals found; peak @ 70.10 ppm is considered to be two peaks overlapping). HR MS: calc. for $C_{37}H_{52}O_{18}N_6S_4F_{12}$ $[M - TFSI]^+$: m/z 944.2851; found: m/z 944.2853 (error 0.3 ppm). HR MS: calc. for $C_{37}H_{52}O_{18}N_6S_4F_{12}$ $[M - 2TFSI]^{+2}$: m/z 332.1836;

found: m/z 332.1849 (error 3.7 ppm). T_g (DSC) = -43 °C. Conductivity at 25 °C = 6.54×10^{-5} S/cm.

Exo-NB[(EO)₃Im(EO)₂CH₃ TFSI]₂ (8m). General procedure 6 was used to produce an oil (0.93 g, 61%) by using **3b** (0.884 g, 1.17 mmol), **7c** (0.898 g, 5.27 mmol) and LiTFSI (0.90 g, 3.1 mmol). ¹H NMR (500 MHz, acetone-*d*₆) δ 9.06 (s, 2H), 7.79 (s, 4H), 6.25 (s, 2H), 4.56 (s, 8H), 4.31–4.24 (m, 2H), 4.15–4.07 (m, 2H), 3.96 (m, 8H), 3.73–3.60 (m, 16H), 3.53–3.48 (m, 4H), 3.31 (s, 6H), 3.05 (s, 2H), 2.63 (s, 2H), 2.10 (d, $J = 9$ Hz, 1H), 1.40 (d, $J = 9$ Hz, 1H). ¹³C NMR (126 MHz, acetone-*d*₆) δ 173.06 (s), 137.84 (s), 136.82 (s), 122.92 (s), 122.88 (s), 120.12 (q, $J = 323$ Hz), 71.54 (s), 70.11 (s), 70.09 (s), 69.94 (s), 68.71 (s), 68.57 (s), 68.46 (s), 63.64 (s), 57.93 (s), 49.73 (s), 49.70 (s), 46.93 (s), 45.57 (s), 44.88 (s) (20 peaks expected and 20 peaks found). HR MS: calc. for C₄₁H₆₀O₂₀N₆S₄F₁₂ [M – TFSI]⁺: m/z 1032.3375; found: m/z 1032.3372 (error -0.3 ppm). HR MS: calc. for C₄₁H₆₀O₂₀N₆S₄F₁₂ [M – 2TFSI]⁺²: m/z 376.2098; found: m/z 376.2113 (error 3.9 ppm). T_g (DSC) = -47 °C. Conductivity at 25 °C = 8.95×10^{-5} S/cm.

Exo-NB[(EO)₃Im(EO)₃CH₃ TFSI]₂ (8n). General procedure 6 was used to produce an oil (1.27 g, 48%) by using **3b** (1.42 g, 1.88 mmol), **7d** (1.01 g, 4.70 mmol) and LiTFSI (1.35 g, 4.70 mmol). ¹H NMR (500 MHz, DMSO-*d*₆) δ 9.08 (s, 2H), 7.75 (dt, $J = 9, 2$ Hz, 4H), 6.24 (t, $J = 2$ Hz, 2H), 4.37 (t, $J = 4$ Hz, 8H), 4.16 (m, 2H), 3.97 (m, 2H), 3.81–3.75 (m, 8H), 3.55 (m, 12H), 3.53–3.48 (m, 12H), 3.43 (m, 4H), 3.24 (s, 6H), 3.02–2.96 (m, 2H), 2.59 (d, $J = 2$ Hz, 2H), 1.95 (d, $J = 9$ Hz, 1H), 1.35 (d, $J = 9$ Hz, 1H). ¹³C NMR (126 MHz, DMSO-*d*₆) δ 173.34 (s), 138.23 (s), 137.05 (s), 123.08 (s), 122.99 (s), 119.95 (q, $J = 323$ Hz), 71.71 (s), 70.03 (s), 69.99 (s), 69.97 (s), 69.94 (s), 68.64 (s), 68.62 (s), 68.65 (s), 63.92 (s), 58.50 (s), 49.26 (s), 46.97 (s), 45.60 (s), 45.18 (s) (22 signals expected and 20 found). HR MS: calc. for C₄₅H₆₈O₂₂N₆S₄F₁₂ [M – TFSI]⁺: m/z 1120.3899; found: m/z 1120.3946 (error 4.1 ppm). HR MS: calc. for

$C_{45}H_{68}O_{22}N_6S_4F_{12}$ [$M - 2TFSI$] $^{+2}$: m/z 420.2361; found: m/z 420.2381 (error 4.8 ppm). T_g (DSC) = -46 °C. Conductivity at 25 °C = 8.93×10^{-5} S/cm.

Exo-NB[(EO)₃Im(EO)₄CH₃ TFSI]₂ (8o). General procedure 6 was used to produce an oil (0.60 g, 61%) by using **3b** (0.503 g, 0.667 mmol), **7e** (0.430 g, 1.66 mmol) and LiTFSI (0.479 g, 1.67 mmol). 1H NMR (500 MHz, DMSO- d_6) δ 9.08 (s, 2H), 7.75 (m, 4H), 6.24 (t, $J = 2$ Hz, 2H), 4.37 (t, $J = 5$ Hz, 8H), 4.16 (m, 2H), 3.97 (m, 2H), 3.78 (m, 8H), 3.60–3.46 (m, 32H), 3.43 (m, 4H), 3.24 (s, 3H), 3.23 (s, 3H) 3.02–2.97 (m, 2H), 2.59 (d, $J = 2$ Hz, 2H), 1.95 (d, $J = 9$ Hz, 1H), 1.35 (d, $J = 9$ Hz, 1H). ^{13}C NMR (126 MHz, DMSO- d_6) δ 173.33 (s), 138.24 (s), 137.08 (s), 123.08 (s), 123.00 (s), 119.95 (q, $J = 323$ Hz), 71.72 (s), 70.21 (s), 70.18 (s), 70.06 (s), 70.04 (s), 70.01 (s), 69.99 (s), 69.94 (s), 68.65 (s), 68.62 (s), 68.59 (s), 63.92 (s), 58.51 (s), 58.49 (s), 49.30 (s), 49.26 (s), 46.97 (s), 45.61 (s), 45.19 (s) (24 signals expected and 25 signals found). HR MS: calc. for $C_{49}H_{76}O_{24}N_6S_4F_{12}$ [$M - TFSI$] $^+$: m/z 1208.4424; found: m/z 1208.4537 (error 9.4 ppm). HR MS: calc. for $C_{49}H_{76}O_{24}N_6S_4F_{12}$ [$M - 2TFSI$] $^{+2}$: m/z 464.2623; found: m/z 464.2667 (error 9.6 ppm). $T_g = -45$ °C. Conductivity at 25 °C = 7.94×10^{-5} S/cm.

Exo-NB[(EO)₄Im_{butyl} TFSI]₂ (8p). General procedure 6 was used to produce an oil (1.72 g, 54%) by using **3c** (2.04 g, 2.42 mmol), **7a** (0.751 g, 6.05 mmol) and LiTFSI (1.74 g, 6.05 mmol). 1H NMR (500 MHz, DMSO- d_6) δ 9.13 (s, 2H), 7.79 (t, $J = 2$ Hz, 2H), 7.76 (t, $J = 2$ Hz, 2H), 6.23 (t, $J = 2$ Hz, 2H), 4.38–4.32 (m, 4H), 4.22–4.13 (m, 6H), 3.98 (m, 2H), 3.80–3.74 (m, 4H), 3.61–3.53 (m, 8H), 3.50 (m, 12H), 3.00–2.97 (m, 2H), 2.58 (d, $J = 2$ Hz, 2H), 1.95 (m, 1H), 1.78 (quin, $J = 7$ Hz, 4H), 1.34 (m, 1H), 1.26 (sex, $J = 7$ Hz, 4H), 0.91 (t, $J = 7$ Hz, 6H). ^{13}C NMR (126 MHz, DMSO- d_6) δ 173.33 (s), 138.24 (s), 136.76 (s), 123.29 (s), 122.67 (s), 119.95 (q, $J = 323$ Hz), 70.17 (s), 70.12 (s), 70.04 (s), 69.97 (s), 68.63 (s), 68.54 (s), 63.94 (s), 49.27 (s), 49.03 (s), 46.96 (s), 45.59 (s), 45.17 (s), 31.81 (s), 19.21 (s), 13.70 (s) (21 signals expected and 21

signals found). HR MS: calc. for $C_{43}H_{64}O_{18}N_6S_4F_{12}$ $[M - TFSI]^+$: m/z 1028.3790; found: m/z 1028.3810 (error 1.9 ppm). HR MS: calc. for $C_{43}H_{64}O_{18}N_6S_4F_{12}$ $[M - 2 TFSI]^{+2}$: m/z 374.2306; found: m/z 374.2315 (error 2 ppm). T_g (DSC) = -45 °C. Conductivity at 25 °C = 6.82×10^{-5} S/cm.

Exo-NB[(EO)₄Im(EO)₁CH₃ TFSI]₂ (8q). General procedure 6 was used to produce an oil (1.25 g, 43%) by using **3c** (1.88 g, 2.23 mmol), **7b** (1.51 g, 12.0 mmol) and LiTFSI (2.09 g, 7.28 mmol). ¹H NMR (500 MHz, acetone-*d*₆) δ 9.02 (s, 2H), 7.77 (s, 2H), 7.72 (s, 2H), 6.24 (t, $J = 2$ Hz, 2H), 4.53 (m, 8H), 4.25 (m, 2H), 4.09 (m, 2H), 3.95–3.91 (m, 4H), 3.84–3.80 (m, 4H), 3.68 (m, 8H), 3.62 (m, 12H), 3.36 (s, 6H), 3.06 – 3.02 (m, 2H), 2.58 (d, $J = 2$ Hz, 2H), 2.08 (d, $J = 9$ Hz, 1H), 1.38 (d, $J = 9$ Hz, 1H). ¹³C NMR (126 MHz, acetone-*d*₆) δ 173.13 (s), 137.85 (s), 136.77 (s), 123.03 (s), 122.72 (s), 120.08 (q, $J = 323$ Hz), 70.25 (s), 70.13 (s), 70.12 (s), 70.09 (s), 69.88 (s), 68.67 (s), 68.46 (s), 63.69 (s), 58.08 (s), 49.66 (s), 49.59 (s), 46.89 (s), 45.53 (s), 44.86 (s) (20 peaks expected and 20 peaks found). HR MS: calc. for $C_{41}H_{60}O_{20}N_6S_4F_{12}$ $[M - TFSI]^+$: m/z 1032.3375; found: m/z 1032.3376 (error 0.08 ppm). HR MS: calc. for $C_{41}H_{60}O_{20}N_6S_4F_{12}$ $[M - 2TFSI]^{+2}$: m/z 376.2098; found: m/z 376.2116 (error 4.7 ppm). T_g (DSC) = -43 °C. Conductivity at 25 °C = 6.51×10^{-5} S/cm.

Exo-NB[(EO)₄Im(EO)₂CH₃ TFSI]₂ (8r). General procedure 6 was used to produce an oil (1.73 g, 45%) by using **3c** (2.29 g, 2.71 mmol), **7c** (0.856 g, 6.79 mmol) and LiTFSI (1.95 g, 6.79 mmol). ¹H NMR (500 MHz, DMSO-*d*₆) δ 9.08 (s, 2H), 7.75 (m, 4H), 6.24 (t, $J = 2$ Hz, 2H), 4.37 (t, $J = 5$ Hz, 8H), 4.17 (m, 2H), 4.03–3.95 (m, 2H), 3.78 (t, $J = 5$ Hz, 8H), 3.59–3.53 (m, 12H), 3.53–3.47 (m, 12H), 3.44–3.40 (m, 4H), 3.22 (s, 6H), 3.02–2.96 (m, 2H), 2.59 (d, $J = 2$ Hz, 2H), 1.96 (d, $J = 9$ Hz, 1H), 1.34 (d, $J = 9$ Hz, 1H). ¹³C NMR (126 MHz, DMSO-*d*₆) δ 173.34 (s), 138.24 (s), 137.09 (s), 123.07 (s), 122.98 (s), 119.95 (q, $J = 323$ Hz), 71.53 (s), 70.17

(s), 70.11 (s), 70.04 (s), 69.83 (s), 69.83 (s), 68.62 (s), 68.58 (s), 63.95 (s), 58.51 (s), 49.30 (s), 49.28 (s), 46.95 (s), 45.59 (s), 45.17 (s) (22 signals expected and 21 signals found). HR MS: calc. for $C_{45}H_{68}O_{22}N_6S_4F_{12}$ $[M - TFSI]^+$: m/z 1120.3899; found: m/z 1120.3891 (error -0.8 ppm). HR MS: calc. for $C_{45}H_{68}O_{22}N_6S_4F_{12}$ $[M - 2TFSI]^{+2}$: m/z 420.2361; found: m/z 420.2374 (error 3.2 ppm). T_g (DSC) = -46 °C. Conductivity at 25 °C = 9.57×10^{-5} S/cm.

Exo-NB[(EO)₄Im(EO)₃CH₃ TFSI]₂ (8s). General procedure 6 was used to produce an oil (2.07 g, 67%) by using **3c** (1.76 g, 2.09 mmol), **7d** (1.15 g, 5.39 mmol) and LiTFSI (1.58 g, 5.50 mmol). ¹H NMR (500 MHz, DMSO-*d*₆) δ 9.07 (s, 2H), 7.75 (m, 4H), 6.24 (t, *J* = 2 Hz, 2H), 4.37 (t, *J* = 5 Hz, 8H), 4.20–4.13 (m, 2H), 3.98 (m, 2H), 3.82–3.75 (m, 8H), 3.59–3.54 (m, 13H), 3.54–3.47 (m, 21H), 3.43 (m, 4H), 3.24 (s, 6H), 3.01–2.97 (m, 2H), 2.58 (d, *J* = 2 Hz, 2H), 1.95 (d, *J* = 9 Hz, 1H), 1.34 (d, *J* = 9 Hz, 1H). ¹³C NMR (126 MHz, DMSO-*d*₆) δ 173.33 (s), 138.24 (s), 137.06 (s), 123.06 (s), 123.03 (s), 119.95 (q, *J* = 323 Hz), 71.72 (s), 70.17 (s), 70.12 (s), 70.04 (s), 70.00 (s), 69.98 (s), 68.62 (s), 68.59 (s), 63.94 (s), 58.52 (s), 49.26 (s), 46.96 (s), 45.60 (s), 45.18 (s) (24 signals expected and 20 signals found). HR MS: calc. for $C_{49}H_{76}O_{24}N_6S_4F_{12}$ $[M - TFSI]^+$: m/z 1208.4424; found: m/z 1208.4441 (error 1.4 ppm). HR MS: calc. for $C_{49}H_{76}O_{24}N_6S_4F_{12}$ $[M - 2TFSI]^{+2}$: m/z 464.2623; found: m/z 464.2651 (error 6.0 ppm). T_g (DSC) = -45 °C. Conductivity at 25 °C = 7.90×10^{-5} S/cm.

Exo-NB[(EO)₄Im(EO)₄CH₃ TFSI]₂ (8t). General procedure 6 was used to produce an oil (1.08 g, 27%) by using **3c** (2.11 g, 2.50 mmol), **7e** (2.15 g, 8.31 mmol) and LiTFSI (1.79 g, 6.23 mmol). ¹H NMR (500 MHz, DMSO-*d*₆) δ 9.09 (s, 2H), 7.78–7.72 (m, 4H), 6.24 (m, 2H), 4.37 (m, 8H), 4.16 (m, 2H), 3.98 (m, 2H), 3.82–3.74 (m, 8H), 3.59–3.53 (m, 12H), 3.50 (m, 28H), 3.43 (m, 4H), 3.24 (s, 6H), 3.01 – 2.96 (m, 2H), 2.58 (m, 2H), 1.95 (d, *J* = 9 Hz, 1H), 1.34 (d, *J* = 9 Hz, 1H). ¹³C NMR (101 MHz, DMSO-*d*₆) δ 173.36, 138.20, 136.97, 122.99, 122.96, 119.88

(q, $J = 323$), 71.66, 70.14, 70.12, 70.06, 69.98, 69.97, 69.95, 69.94, 68.57, 68.52, 63.93, 58.47, 58.44, 49.22, 46.93, 45.55, 45.12 (26 signals expected and 23 signals found; peaks in the ethyleneoxy region suspected to be overlapping). HR MS: calc. for $C_{53}H_{84}O_{26}N_6S_4F_{12}$ $[M + Na]^+$: m/z 1599.4019; found: m/z 1599.3942 (error -4.8 ppm). HR MS: calc. for $C_{53}H_{84}O_{26}N_6S_4F_{12}$ $[M - TFSI]^+$: m/z 1296.4948; found: m/z 1296.4889 (error -4.6 ppm). HR MS: calc. for $C_{53}H_{84}O_{26}N_6S_4F_{12}$ $[M - 2TFSI]^{+2}$: m/z 508.2885; found: m/z 508.2869 (error -3.2 ppm). T_g (DSC) = -47 °C. Conductivity at 25 °C = 6.99×10^{-5} S/cm.

Exo-NB[(EO)₅Im(EO)₂CH₃ TFSI]₂ (8u). General procedure 6 was used to produce an oil (0.91 g, 35 %) by using **3d** (1.62 g, 1.73 mmol), **7c** (0.65 g, 5.2 mmol) and LiTFSI (1.25 g, 4.35 mmol). 1H NMR (500 MHz, DMSO- d_6) δ 9.08 (s, 2H), 7.76–7.75 (m, 4H), 6.24 (s, 2H), 4.37 (t, $J = 5$ Hz, 8H), 4.20–4.12 (m, 2H), 4.00–3.97 (m, 2H), 3.83–3.74 (m, 8H), 3.58–3.49 (m, 32 H), 3.43–3.40 (m, 4H), 3.22 (s, 6H), 3.02–2.94 (m, 2H), 2.60–2.59 (m, 2H), 1.97–1.95 (m, 1H), 1.35–1.33 (m, 1H). ^{13}C NMR (126 MHz, DMSO- d_6) δ 173.33, 138.23, 137.09, 123.06, 122.97, 119.93 (q, $J = 323$ Hz), 71.53, 70.22, 70.17, 70.14, 70.04, 69.98, 69.83, 68.61, 68.58, 63.95, 58.52, 49.29, 46.94, 45.59, 45.17 (24 signals expected and 21 signals found, 3 signals expected to be overlapping in ethyleneoxy region). HR MS: calc. for $C_{49}H_{76}O_{24}N_6S_4F_{12}$ $[M - 2TFSI]^{+2}$: m/z 464.2623; found: m/z 464.2609 (error -3.0 ppm). T_g (DSC) = -46 °C.

Exo-NB[(EO)₆Im(EO)₂CH₃ TFSI]₂ (8v). General procedure 6 was used to produce an oil (1.03 g, 81 %) by using **3e** (0.813 g, 0.798 mmol), **7c** (0.340 g, 2.00 mmol) and LiTFSI (0.580 g, 2.02 mmol). 1H NMR (500 MHz, DMSO- d_6) δ 9.08 (s, 2H), 7.76–7.74 (m, 4H), 6.24 (t, $J = 2$ Hz, 2H), 4.37 (t, $J = 5$ Hz, 8H), 4.18–4.14 (m, 2H), 4.01–3.96 (m, 2H), 3.82–3.73 (m, 8H), 3.58–3.54 (m, 12H), 3.51–3.48 (m, 28H), 3.43–3.41 (m, 4H), 3.22 (s, 6H), 3.02–2.98 (m, 2H), 2.61–2.60 (m, 2H), 1.97–1.95 (m, 1H), 1.35–1.33 (m, 1H). ^{13}C NMR (126 MHz, DMSO- d_6) δ 173.33,

138.23, 137.09, 123.07, 122.97, 119.93 (q, J = 323 Hz), 71.53, 70.24, 70.20, 70.17, 70.14, 70.04, 69.98, 69.83, 68.60, 63.96, 58.53, 49.29, 46.94, 45.58, 45.17 (26 signals expected and 21 signals found, 5 signals expected to be overlapping in ethyleneoxy region). HR MS: calc. for C₅₃H₈₄O₂₆N₆S₄F₁₂ [M + Na]⁺: m/z 1599.4024; found: m/z 1599.3987 (error 2.3 ppm). T_g (DSC) = -54 °C.

References

- (1) Choi, U. H.; Lee, M.; Wang, S.; Liu, W.; Winey, K. I.; Gibson, H. W.; Colby, R. H. *Macromolecules* **2012**, *45*, 3974-3985.
- (2) Lee, M.; Choi, U. H.; Salas-de la Cruz, D.; Mittal, A.; Winey, K. I.; Colby, R. H.; Gibson, H. W. *Adv. Funct. Mater.* **2011**, *21*, 708-717.
- (3) Lee, M.; Choi, U. H.; Colby, R. H.; Gibson, H. W. *Chem. Mater.* **2010**, *22*, 5814-5822.
- (4) Welton, T. *Chem. Rev.* **1999**, *99*, 2071-2084.
- (5) Choi, U. H.; Mittal, A.; Price, T. L.; Gibson, H. W.; Runt, J.; Colby, R. H. *Macromolecules* **2013**, *46*, 1175-1186.
- (6) Moatsou, D.; Hansell, C. F.; O'Reilly, R. K. *Chem. Sci.* **2014**, *5*, 2246-2250.
- (7) Reichardt, C. *Chem. Rev.* **1994**, *94*, 2319-2358.
- (8) Reichardt, C.; Schäfer, G. *Liebigs Ann.* **1995**, *1995*, 1579-1582.
- (9) Reichardt, C. *Green Chem.* **2005**, *7*, 339-351.
- (10) Machado, V. G.; Stock, R. I.; Reichardt, C. *Chem. Rev.* **2014**, *114*, 10429-10475.
- (11) Headley, A. D.; Kotti, S. R. S. S.; Ni, B. *Heterocycles* **2007**, *71*, 589-596.
- (12) Liu, Y.; Chipot, C.; Shao, X.; Cai, W. *J. Phys. Chem. C* **2016**, *120*, 6287-6293.
- (13) Matson, J. B.; Grubbs, R. H. *J. Am. Chem. Soc.* **2008**, *130*, 6731-6733.
- (14) Ouchi, M.; Inoue, Y.; Wada, K.; Iketani, S.; Hakushi, T.; Weber, E. *J. Org. Chem.* **1987**, *52*, 2420-2427.
- (15) Ouchi, M.; Inoue, Y.; Liu, Y.; Nagamune, S.; Nakamura, S.; Wada, K.; Hakushi, T. *Bull. Chem. Soc. Jpn.* **1990**, *63*, 1260-1262.

Chapter 11

NORBORNENE TFSI POLYMERS

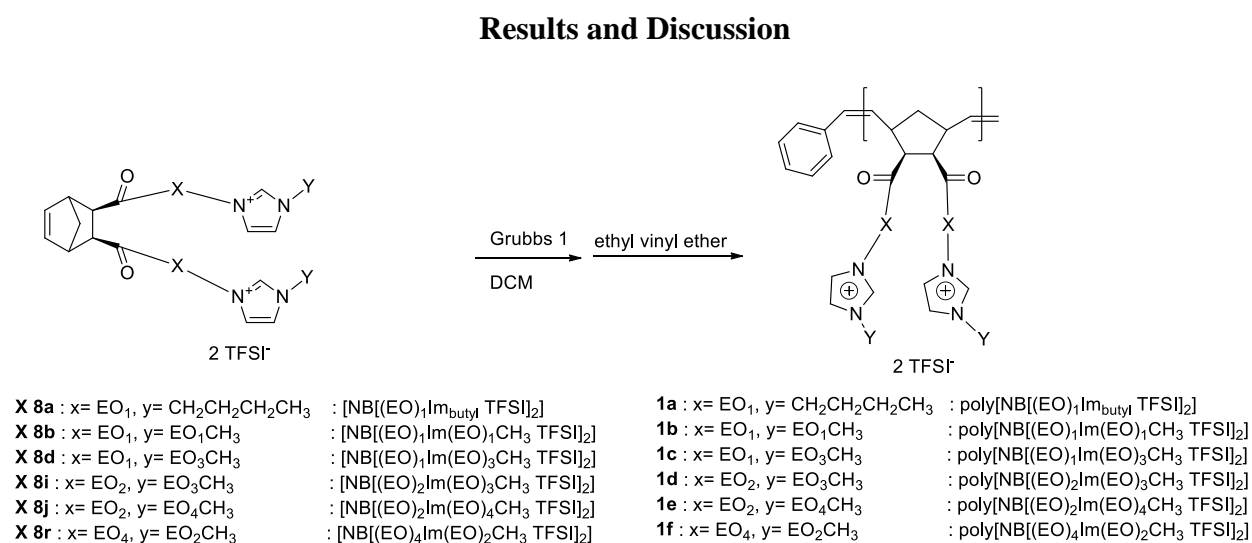
Introduction

The previous chapter, chapter 10, explored norbornene TFSI monomers employing ethyleneoxy units and sought to determine the ideal number of ethyleneoxy units to produce optimal conductivity. This chapter focuses on polymers made from the monomers in chapter 10 in an attempt to evaluate these monomers as polyelectrolytes suitable for incorporation as the soft phase in a triblock copolymer for electromechanical actuator applications. For ion transport low T_g polymers are considered highly desirable and typically lead to higher conductivities.¹ As in chapter 10, conductivity will be used as the final assessment of the electrolytes' suitability to move forward.

Due to the polymerizable group of these monomers being a norbornene, the polymerization method chosen was ROMP. ROMP was chosen over other methods such as the use of free radicals due to its livingness and mild reaction conditions.^{2,3} As the project progresses from being model systems into an ABA block copolymer, the living nature of ROMP makes it an attractive reaction for producing block copolymers.^{4,5} ROMP provides the advantage of incorporating different monomers in a controlled manner to allow easy access to block architectures. The monomers employed here in the presence of mild bases at temperatures just above 70 °C can undergo an inversion of stereochemistry from *exo* to *endo*. ROMP generally employs mild reaction conditions, quenching compounds and isolation techniques, making it the obvious choice for avoiding this isomerization and maintaining the stereochemistry of the monomers. Work by Zheng et al. optimized ROMP conditions for a set of norbornene monomers, containing imidazolium ethyleneoxy pendant groups, similar to those found in

chapter 10.⁶ Their work focused on a single armed monomer containing a PF₆ counterion and optimization was achieved using the second generation Grubbs catalyst. Due to increased costs associated with the Grubbs second generation catalyst and the widespread usage of Grubbs first generation catalyst with a range of norbornene monomers, we employed the Grubbs first generation catalyst.

The goal of the work is to produce polymers that have high conductivities based on one mobile ion, the anion. The objective of a single mobile ion is important because it is a requirement for single direction actuation.⁷⁻¹⁰ Additionally, as the end goal for these materials is incorporation into a triblock architecture, the T_g of the resulting material must be sufficiently low such that the polymer can be used as a soft segment in a multi-block polymer. To formulate an understanding of how structure correlates with glass transition temperature and conductivity, several monomers were chosen for polymerization in addition to the optimal monomer of chapter 10, **XI 8r**.



Scheme 11.1. Synthesis of imidazolium polymers **1a–1f**.

Scheme 11.1 shows the synthesis of polymers **1a–1f**. The monomers from chapter 10 have been renumbered to contain X in front of the number for clarity; monomers employed from chapter 10 are: **X 8a**, **X 8b**, **X 8d**, **X 8i**, **X 8j**, and **X 8r**. Polymerizations were carried out using ROMP via Grubbs 1st generation catalyst in DCM at room temperature at a concentration of 0.275 M for 13 h. Molecular weight was controlled via monomer to initiator ratios. Targeted degrees of polymerizations ranged from 29 to 50, while targeted molecular weights ranged from 38 to 61 kDa. Reaction termination was achieved by quenching with ethyl vinyl ether. Isolation of **1a–1f** was achieved by precipitation of the reaction mixture into a mixture of ether and methanol at $-70\text{ }^{\circ}\text{C}$; subsequent precipitations were carried out with identicality after dissolving the polymer in DCM. Molecular weight analysis was accomplished through ^1H NMR end group analysis of initiator to imidazolium signals. As an example **Figure 11.1** shows the end group analysis of **1d**; initiator phenyl signals used for analysis are shown in red and compared to imidazolium proton signals shown in blue. Integral 8.76 ppm = 29.96; integral 7.36 ppm = 1.20 H. $\text{DP} = (29.96 / 2) / (1.20 / 2) = 25.0$. For **1d** a DP of 25.0 gives an M_n of ~ 33 kDa.

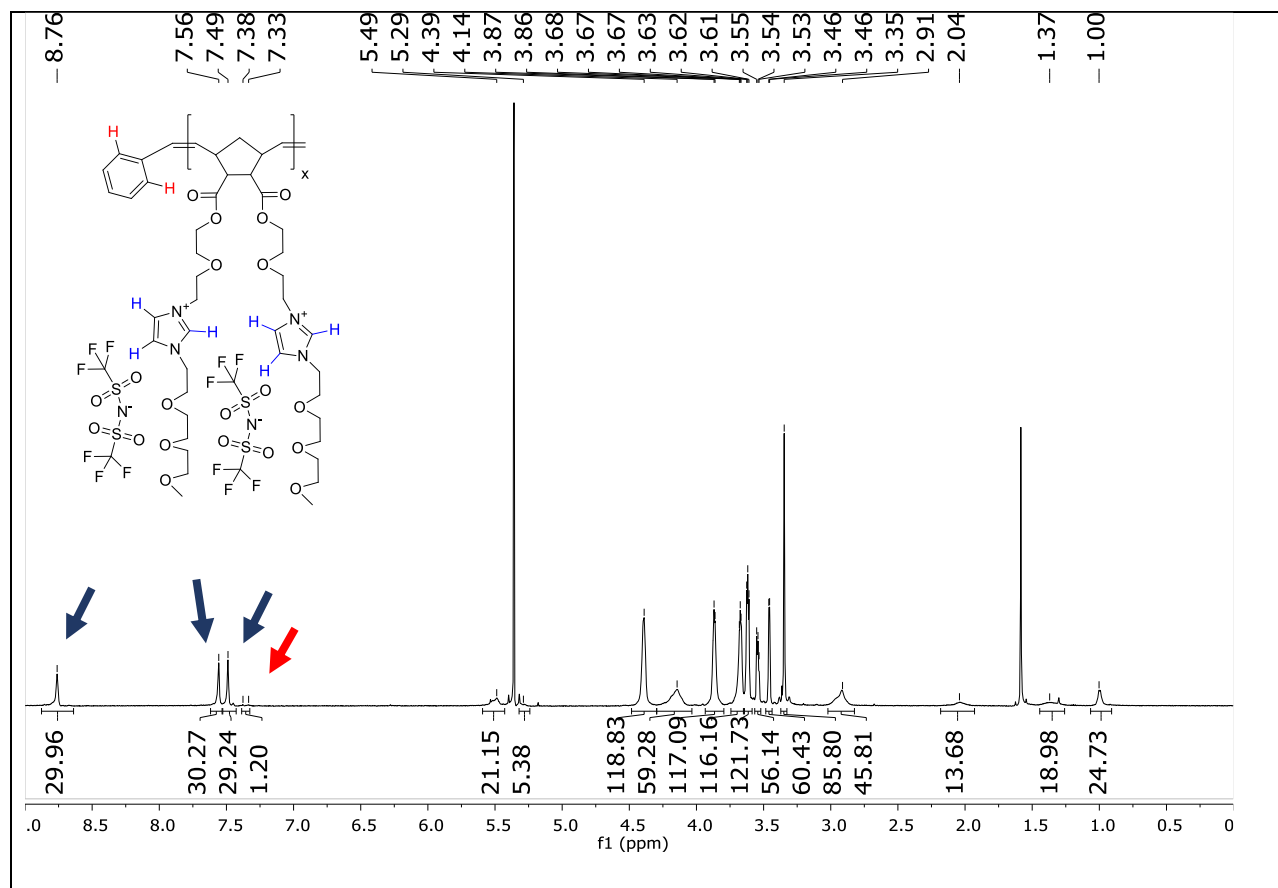


Figure 11.1. ^1H NMR spectrum (500 MHz, CD_2Cl_2 , room temp) of **1d** indicating DP = 25. Initiator hydrogens are indicated in red (integral 1.20) and imidazolium hydrogens are indicated in green and blue (integrals 29.96, 30.27 and 29.24).

Polymers originally selected for synthesis were **1b**, **1d** and **1f**; in an effort to fully establish trends, which will be discussed in the following text, polymerizations were extended to **1a**, **1c** and **1e**. The entire monomer set found in chapter 10 was not employed for the production of homopolymers, since monomer conductivities were all within the same order of magnitude.

Acceptable ROMP reaction times and concentrations were determined experimentally via ^1H NMR. ROMP reaction times at monomer concentrations of 0.275 M with 9.4 mM Grubbs catalyst in DCM were experimentally determined as 13 h to achieve 99% conversion as shown via the following ^1H NMR experiment. The polymerization of **X 8i** was carried out in CD_2Cl_2 in

an NMR tube and reaction progress at 25 °C was monitored via disappearance of the monomer's olefin signals (**Figure 11.2**). It should be noted for this reaction that the NMR tube remained within the NMR instrument for the duration of the experiment with constant spinning at 20 Hz. The target DP for this reaction was 29, $M_n = \sim 39$ kDa. A spectrum was taken every 10 minutes for the first hour then every 15 min until 99% of the monomer had been consumed. The monomer's olefinic proton signals, shown in red, were compared to the imidazolium protons, shown in blue, to determine the level of monomer consumption. **Figure 11.3** contains a plot of these results and a first order kinetic treatment of the data, showing that the polymerization is first order, implying the living nature of the reaction.

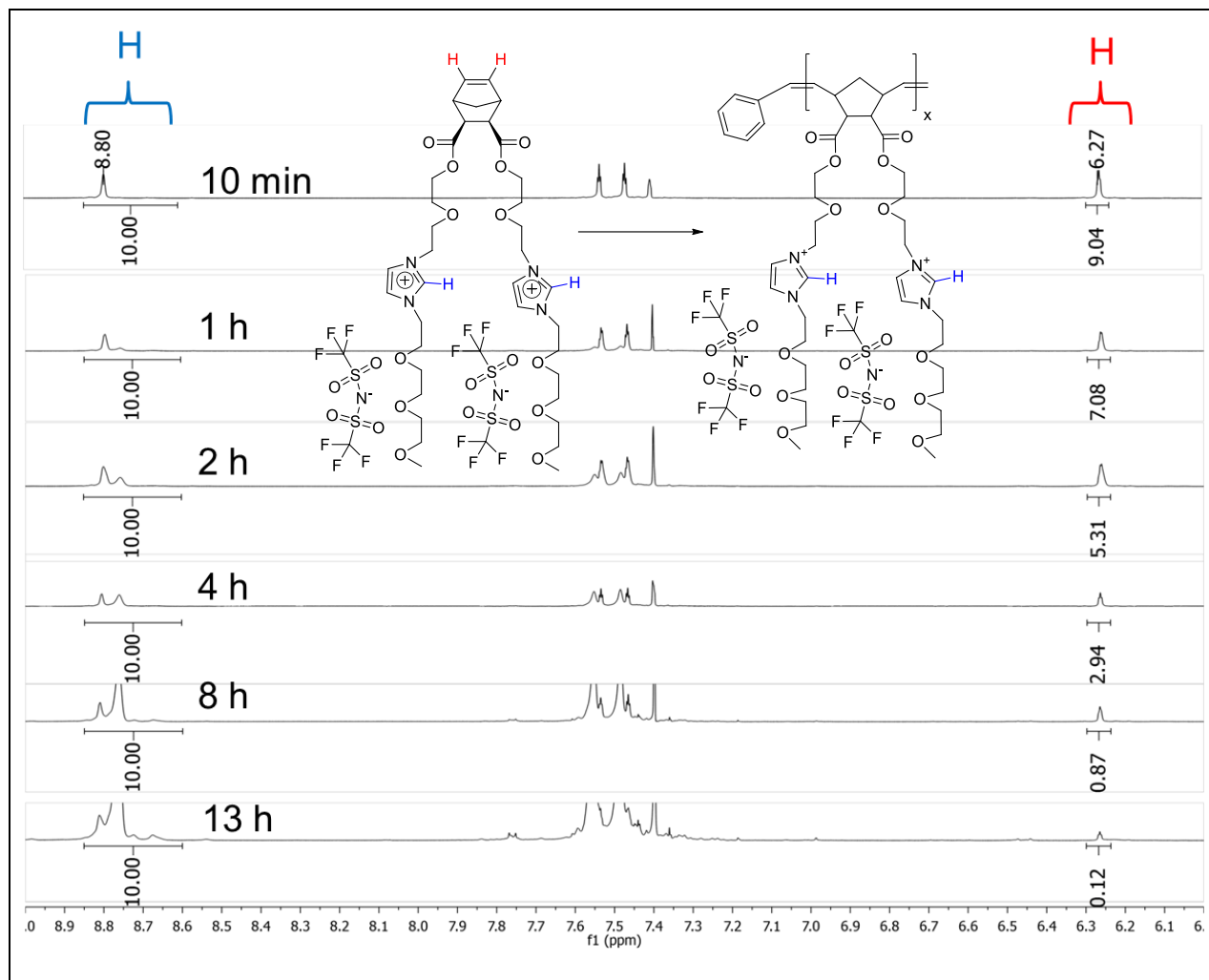


Figure 11.2. Partial ^1H NMR spectra (500 MHz) taken during the polymerization of monomer **X 8i** at 25 °C in CD_2Cl_2 .

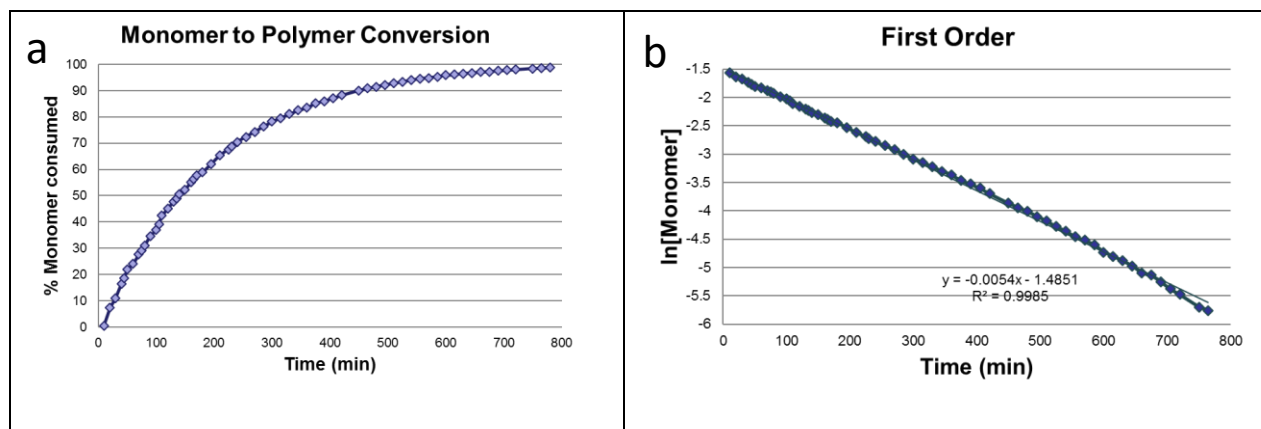


Figure 11.3. a) Consumption of monomer **X 8i** in the ROMP experiment of **Figure 11.2** as determined by ^1H NMR, b) graph of $\ln[\text{monomer}]$ vs time (pseudo-first order plot).

Figure 11.3a reveals that by 13 h, 99% of the monomer was consumed and converted to polymer, providing a guideline as to how long ROMP with Grubbs 1st should take with the stereo pure *exo* imidazolium monomers from chapter 10. The pure *exo* stereo chemistry has been chosen here because *exo* norbornene monomers polymerize quicker than their *endo* counterparts under ROMP conditions.¹¹ Polymers **1a–1f** were synthesized using this template of ~0.275 M monomer concentration in DCM with ~9 to 10 mM Grubbs 1st generation catalyst for 13 h. For each synthesized polymer, before quenching each polymerization was monitored for 99% + conversion via ¹H NMR.

Table 11.1 lists molecular weights determined via ¹H NMR for polymer **1a–1f** and their T_g values compared to their monomer counterparts. The target and determined molecular weights generally agree well with one another, except in cases where the reactions were quenched prematurely for one reason or another.

Viewing **Table 11.1**, the T_gs of most of the polymers are only 3–7 °C higher than those of the corresponding monomers. The major exceptions to this trend are **1a** which contains a butyl tail with an increase of 22 °C and **1e** which is 15 °C higher than its corresponding monomer. In regards to the previously developed acrylate and methacrylate monomers containing similar pendant groups and TFSI counterions, the differences in polymer and monomer T_gs ranged between 14–29 °C.^{1,12,13} Interestingly, the newly developed ROMP system narrows the gap between monomer and polymer T_g values, giving an additional advantage of the ROMP approach to ion conducting polymers.

In addition to the listed polymer **1d** in **Table 11.1** which has a M_n of 33 kDa and a T_g of –51 °C, a second sample of **1d** was prepared at a higher molecular weight to confirm consistency

in T_g values. The second sample was synthesized with a target M_n of 66 kDa and found to have a M_n of 60 kDa with a T_g of -49 °C. Considering the closeness of T_g values and associated error with the measurements, the results point to the T_g values being roughly the same and indicate for these polymers that molecular weights of approximately 30 kDa or higher are appropriate for assessing properties.

Table 11.1. Molecular weights (Da) and T_g values (°C) for Polymers **1a–1f** and Chapter 10 Monomers **X 8**.

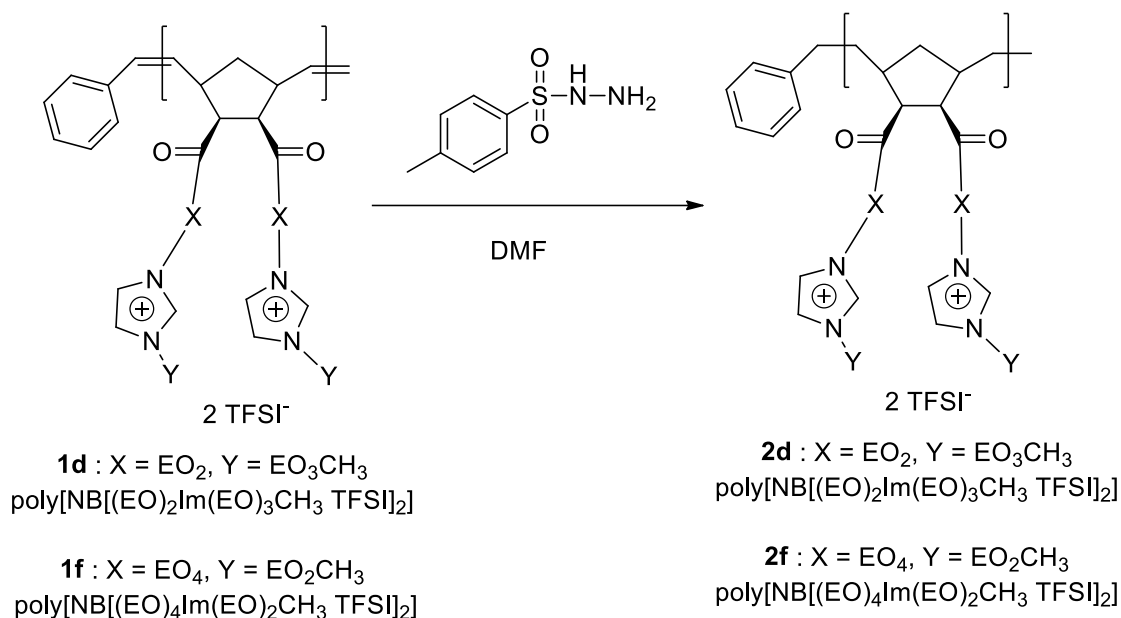
		X					
		EO ₁	EO ₂	EO ₃	EO ₄		
Y	Butyl	X 8a : -44 1a : Target $M_n = 44$ k $M_n = 35$ k, -22					
	EO ₁	X 8b = -39 1b : Target $M_n = 47$ k $M_n = 44$ k, -34					
	EO ₂					X 8r = -46 1f : Target $M_n = 45$ k $M_n = 45$ k, -39	
	EO ₃	X 8d = -50 1c : Target $M_n = 61$ k $M_n = 17$ k, -47				X 8i = -54 1d : Target $M_n = 39$ k $M_n = 33$ k, -51	
	EO ₄					X 8j = -57 °C 1e : Target $M_n = 56$ k $M_n = 26$ k, -42	

Table 11.2 includes conductivity values for polymers **1a–1f** along with their corresponding monomers. As in chapter 10, conductivity values shown in **Table 11.2** were determined at Penn State University by U Hyeok Choi under the supervision of Prof. Ralph Colby. In the X=1 column the polymers have conductivities more than an order of magnitude lower than their monomeric counterparts. However, for columns X>1, conductivities of the polymers drop less than an order of magnitude when compared to the monomer values. Thus,

we conclude that for optimal conductivities, a spacer of at least two ethyleneoxy units between the backbone of the polymer and imidazolium group must be used and that the N-terminal units should also be an oligo(ethylene glycol). Of the polymers examined to date the best system is **1f**, which has an EO₄ spacer and an EO₂ terminal group. This is not surprising given the monomer, **X 8r**, used for its synthesis displayed the highest conductivity in Chapter 10.

Table 11.2. Ionic Conductivities (S/cm) of **1a–1f** and Chapter 10 monomers **X 8** at 25 °C.

		X			
		EO ₁	EO ₂	EO ₃	EO ₄
Y	Butyl	X 8a: 3.07 x 10 ⁻⁵ 1a: 1.03 x 10 ⁻⁶			
	EO ₁	X 8b: 2.42 x 10 ⁻⁵ 1b: 8.10 x 10 ⁻⁷			
	EO ₂				X 8r: 9.57 x 10 ⁻⁵ 1f: 2.27 x 10 ⁻⁵
	EO ₃	X 8d: 7.10 x 10 ⁻⁵ 1c: 1.38 x 10 ⁻⁶	X 8i: 5.39 x 10 ⁻⁵ 1d: 1.37 x 10 ⁻⁵		
	EO ₄		X 8j: 6.26 x 10 ⁻⁵ 1e: 1.49 x 10 ⁻⁵		



Scheme 11.2. Synthesis of reduced polymers **2d** and **2f**.

In an attempt to further lower the T_g s of polymers **1** and thus increase conductivities, the olefinic backbones of **1d** and **1f** were reduced using p-toluenesulfonyl hydrazide (**Scheme 11.2**). According to the literature, by conversion of the double bonds to aliphatic, the T_g should be reduced by up to 30 °C.^{14,15} The polymer with the highest conductivity, **2f**, was chosen for reduction as well as polymer **2d**. Although a literature procedure¹⁴ was used, complete conversion could not be achieved by moderately increasing reaction times or through the addition of excess p-toluenesulfonyl hydrazide. By increasing reaction times to 24 h, it was possible to achieve a conversion of ~77% for **2d** and 83% for **2f**. Olefin reduction was monitored and determined by ¹H NMR as shown in **Figure 11.4**. For analysis, the integration of olefinic backbone hydrogens (red arrow) present in only the starting material was compared to the integration of the imidazolium 2-hydrogens (green arrow) found in both the starting material and product.

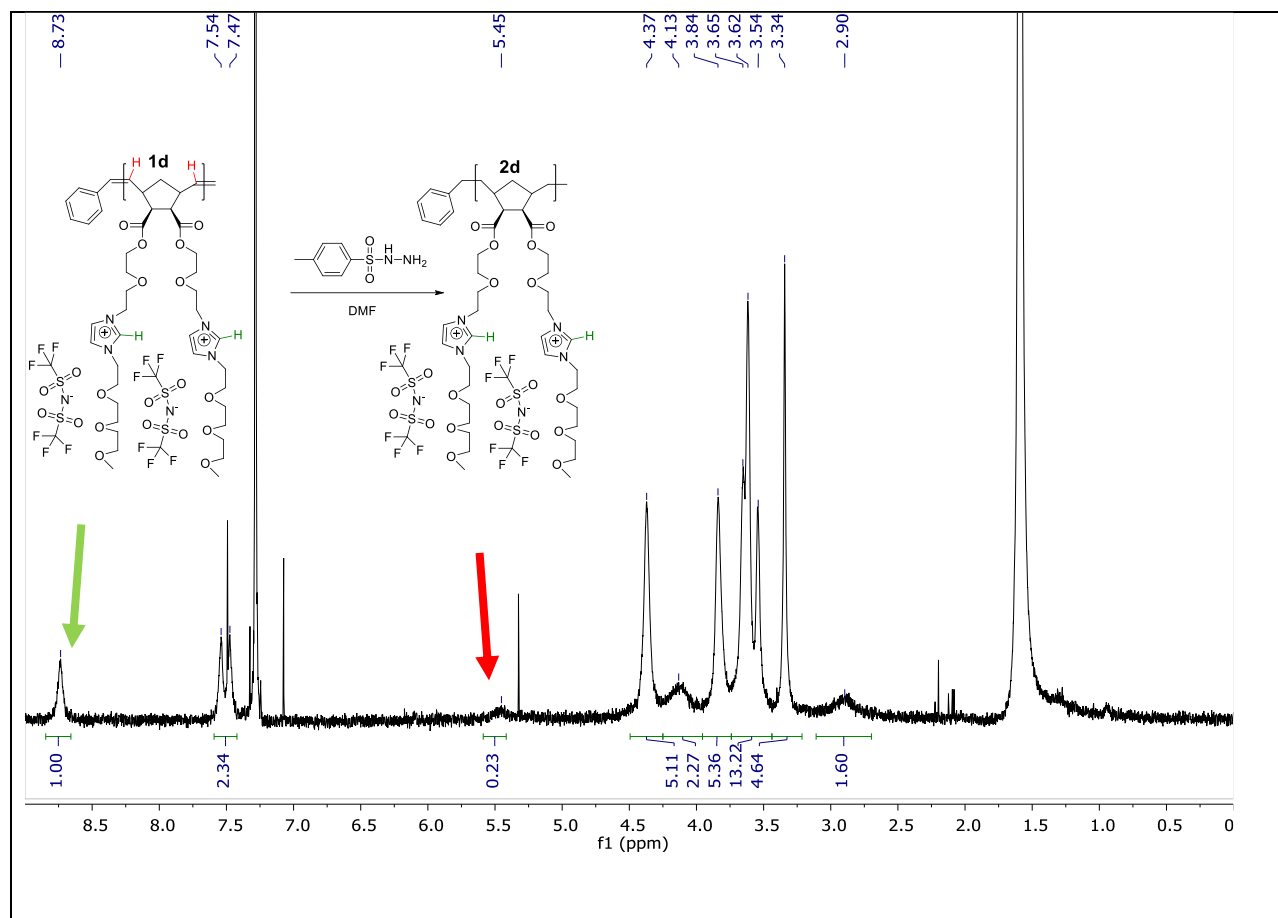


Figure 11.4. ^1H NMR spectrum (500 MHz, CDCl_3 , room temp) of **2d** indicating the loss of olefinic backbone hydrogens. Olefinic hydrogens are indicated in red (integral 0.23) and imidazolium hydrogens are indicated in green (integral 1.00).

Table 11.3 offers a comparison of the T_g and conductivity values for the reduced polymers vs. the unsaturated counterparts. Although a slight drop in T_g was observed for polymer **2f**, none was observed for polymer **2d** after hydrogenation. Furthermore, an increase in conductivity was not observed; in fact, the conductivities of both polymers decreased slightly upon reduction. These unexpected results suggest that perhaps the olefinic backbone is important in terms of conductivity.

The lack of an expected T_g reduction is credited to the absence of a complete

hydrogenation of the backbone. The drop in conductivity, however, must be attributed to the polymer fundamentally changing. It is reasonable to suspect from work carried out on other ROMP norbornene polymeric systems, that the polymers being produced here, **1a–1f**, adopt a helical structure due to the olefin backbone.^{16,17} Hydrogenation of the olefin backbone, **2d** and **2f**, would destroy any stereoregularity and lead to the polymer becoming a random coil. It is suspected that the original structures of **1a – 1f**, likely helical, as this would probably allow for better interactions between the ethyleneoxy units and imidazolium cation.

Table 11.3. T_g s and conductivities (25 °C) of hydrogenated polymers **2d** and **2f** compared to their unsaturated precursors **2d** and **2f**.

Polymer	T_g (°C)	Conductivity (S/cm)
1d	-51 °C	1.37×10^{-5}
2d	-51 °C	5.66×10^{-6}
1f	-39 °C	2.27×10^{-5}
2f	-46 °C	9.66×10^{-6}

Conclusions

In conclusion, Chapter 10 monomers **X 8a, 8b, 8d, 8i, 8j** and **8r** were converted to homopolymers **1a–1f** via ROMP. The glass transitions of the polymers are 3 to 20 °C higher than those of the monomers. The conductivities of the polymers are 4 to 30-fold lower than those of the monomers. Maximum conductivity was observed with the polymer with an ethyleneoxy linker equal to or greater than two units and a terminal diethyleneoxy unit. Only the TFSI anion is capable of movement throughout the bulk material and sets the stage for

proceeding forward with the production of ABA triblock polymers in the next chapter for use as electrochemical actuators with single direction movement.

Experimental

Measurements: ^1H -NMR spectra were obtained on JEOL ECLIPSE-500, BRUKER-500, and AGILENT-NMR-vnmrs400 spectrometers. ^{13}C -NMR spectra were collected at 125 MHz and 101 MHz on these instruments. HR-MS were obtained using an Agilent LC-ESI-TOF system. Reagents were purchased and used as received without further purification. DSC data were obtained on a TA Instrument Q2000 differential scanning calorimeter under N_2 ; heating was carried out at a rate of 10 $^\circ\text{C}/\text{min}$, while cooling used a quenching technique. TGA data were obtained on a TA Instrument under a N_2 : TGA Q500; heating was carried out at a rate of 20 $^\circ\text{C}/\text{min}$. The ionic conductivity measurements were performed by dielectric relaxation spectroscopy at Penn State University by U Hyeok Choi using a sinusoidal voltage with amplitude 0.1 V and 10^{-1} – 10^7 Hz frequency range for all experiments. Data were collected in isothermal frequency sweeps every 5 K from 120 $^\circ\text{C}$ to -100 $^\circ\text{C}$. Monomers **X 8a**, **8b**, **8d**, **8i**, **8j** and **8r** were prepared as described in chapter 10.

General procedure 1: Poly(nobornene imidazolium)s Poly(NB[(EO) $_1$ Im $_{\text{butyl}}$ TFSI] $_2$ (1a). Monomer **X 8a** (1.89 g, 1.80 mmol) was added to a reaction tube with dry DCM (4 mL) under nitrogen. Grubbs 1st generation catalyst (35.3 mg, 0.0429 mmol) was dissolved in a minimum amount of DCM (0.5 mL) and added. The solution was allowed to stir at room temperature until complete consumption of the monomer as determined by ^1H NMR. Ethyl vinyl ether (1.0 mL, 10 mmol) was added to quench the reaction. Volatile compounds were removed by vacuum.

The crude polymer was washed with ether (5 mL x 3), dissolved in methanol (40 mL) and added to 15% diethyl ether in methanol (6 mL) and the solution was cooled to dry ice temperature for 4 h to allow the polymer to “oil out”. Solvent was decanted and the process was repeated two additional times. The polymer was then placed under vacuum for 12 h; isolated: 1.04 g (55%). ¹H NMR (500 MHz, DMSO-*d*₆) δ 9.10 (s, 33.70H), 7.72 (m, 67H), 7.34 (s, 1.00H), 5.23 (m, 20H), 4.27 (m, 185H), 2.86 (br s, 23H), 2.69 (br s, 18H), 1.78 (br s, 74H), 1.26 (br s, 74H), 1.07 (m, 11H), 0.88 (br s, 99H). Target DP = 42; target M_n = 44 kDa. Measured by ¹H NMR DP = 33.7 and M_n = ~35 kDa by end group analysis of imidazolium proton signals compared to initiator phenyl signals. Integral 9.10 ppm = 32.32; integral 7.34 ppm = 1.00 H. DP = (33.70 / 2) / (1.00 / 2) = 33.7. T_g (DSC) = -22 °C. Conductivity at 25 °C = 1.03 x 10⁻⁶ S/cm.

General procedure 2: Reduced Poly(norbornene imidazolium)s Poly(NB[(EO)₂Im₃ TFSI]₂ (2d). Polymer **1d** (1.02 g, 0.0262 mmol) and *p*-toluenesulfonyl hydrazide (0.42 g, 2.3 mmol) were added to a reaction flask containing magnetically stirring DMF (20 mL). The reaction mixture was stirred at 140 °C for 24 h. Most of the DMF was removed by rotary evaporation and the material was precipitated into water. The bulk material was washed with water (15 mL x 5), toluene (15 mL x 5), water (15 mL x 3) and dried under vacuum for 1 day to give 1.01 g (99%) of reduced polymer. T_g (DSC) = -51 °C. Conductivity at 25 °C = 5.66 x 10⁻⁶ S/cm. ¹H NMR (500 MHz, CDCl₃) δ 8.73 (br s, 1H), 7.54–7.47 (m, 2H), 5.45 (br s, 0.23H), 4.37 (br s, 5H), 4.13 (br s, 2H), 3.84 (br s, 5H), 3.74–3.44 (m, 13H), 3.34 (br s, 5H), 2.90 (br s, 2H). ¹H NMR indicated reduction of ~77% of the olefinic units using the imidazolium signal at 8.73 ppm (1.00 H) compared to residual olefinic signal at 5.45 ppm (0.23 H)

Poly(NB[(EO)₁Im(EO)₁ TFSI]₂ (1b). General procedure 1 was used to produce 0.9475 g (78%) by using **X 8b** (1.215 g, 1.158 mmol) and Grubbs 1st generation catalyst (21.4 mg, 0.0260

mmol). ^1H NMR (500 MHz, $\text{DMSO-}d_6$) δ 9.09 (s, 41.78H), 7.70 (m, 82H), 7.35 (s, 1.00H), 5.25 (m, 20H), 4.28 (m, 224H), 3.69 (s, 80H), 3.26 (s, 123H), 2.87 (br s, 21H), 2.69 (br s, 16H), 1.79 (m, 16H), 1.24 (m, 17H). Target DP = 45; target M_n = 47 kDa. Measured by ^1H NMR DP = 41.8 and M_n = ~44 kDa by end group analysis of imidazolium proton signals compared to initiator phenyl signals. Integral 9.09 ppm = 41.78; Integral 7.35 ppm = 1.00 H. DP = (41.78 / 2) / (1.00 / 2) = 41.8. T_g (DSC) = -34 °C. Conductivity at 25 °C = 8.10×10^{-7} S/cm.

Poly(NB[(EO)₁Im(EO)₃CH₃ TFSI]₂) (1c). General procedure 1 was used to produce 1.871 g (96%) using **X 8d** (1.954 g, 1.595 mmol) and Grubbs 1st generation catalyst (26.0 mg, 0.0316 mmol). ^1H NMR (500 MHz, CD_2Cl_2) δ 9.02 – 8.73 (m, 13.41H), 7.70–7.42 (m, 27H), 7.39 (d, J = 16 Hz, 1.00H), 5.46 (br s, 7H), 4.59–4.29 (m, 76H), 3.96–3.84 (m, 33H), 3.73–3.52 (m, 133H), 3.41–3.31 (m, 49H), 2.93 (m, 14H), 2.01 (br s, 5H), 1.37 (br s, 9H). Target DP = 50; target M_n = 61 kDa. Measured by ^1H NMR DP = 13.4 and M_n = ~17 kDa by end group analysis of imidazolium proton signals compared to initiator phenyl signals. Integral 9.09–8.73 ppm = 13.4; integral 7.39 ppm = 1.00 H. DP = (13.4 / 2) / (1.00 / 2) = 13.4. T_g (DSC) = -47 °C. Conductivity at 25 °C = 1.38×10^{-6} S/cm.

Poly(NB[(EO)₂Im(EO)₃CH₃ TFSI]₂) (1d). General procedure 1 was used to produce 0.95 g (88%) by using **X 8i** (1.085 g, 0.8262 mmol) and Grubbs 1st generation catalyst (23.3 mg, 0.0283 mmol). ^1H NMR (500 MHz, CD_2Cl_2) δ 8.76 (br s, 30H), 7.56 (br s, 30 H), 7.49 (br s, 30 H), 7.36 (d, J = 21 Hz, 1.2 H), 5.49 (br s, 21 H), 5.29 (br s, 5 H), 4.39 (br s, 119 H), 4.14 (br s, 59 H), 3.87 (m, 117 H), 3.68–3.67 (m, 116 H), 3.63–3.61 (m, 122 H), 3.55–3.53 (m, 56 H), 3.46 (br d, J = 3.0 Hz, 60 H), 3.35 (br s, 86 H), 2.91 (br s, 46 H), 2.04 (br s, 14 H), 1.37 (br s, 19 H), 1.00 (br s, 25 H). Target DP = 29; target M_n = 39 kDa. Measured by ^1H NMR DP = 25 and M_n = ~33 kDa by end group analysis of imidazolium proton signals compared to initiator phenyl signals.

Integral 8.76 ppm = 29.96; integral 7.36 ppm = 1.20 H. DP = (29.96 / 2) / (1.20 / 2) = 25.0. T_g (DSC) = -51 °C. Conductivity at 25 °C = 1.37×10^{-5} S/cm.

Poly(NB[(EO)₂Im(EO)₄CH₃ TFSI]₂) (1e). General procedure 1 was used to produce 1.186 g (96%) by using **X 8j** (1.229 g, 0.8768 mmol) and Grubbs 1st generation catalyst (18.2 mg, 0.0221 mmol). ¹H NMR (500 MHz, CD₂Cl₂) δ 8.67 (m, 18.96H), 7.43–7.36 (m, 38.52H), 7.24 (d, J = 24 Hz, 1H), 5.36 (m, 11H), 5.20 (m, 5H), 4.27 (m, 75H), 4.03 (br s, 36H), 3.76 (m, 76H), 3.62 – 3.44 (m, 245H), 3.42–3.36 (m, 50H), 3.19 (s, 61H), 2.80 (br s, 29H), 1.92 (br s, 9H), 1.71 (br s, 7H), 1.25 (br s, 11H), 1.06 (q, J = 6.5 Hz, 30H). Target DP = 40; target M_n = 56 kDa. Measured by ¹H NMR DP = 18.7 and M_n = ~ 26 kDa by end group analysis of imidazolium proton signals compared to initiator phenyl signals. Integral 8.76 ppm = 18.69; Integral 7.24 ppm = 1.00 H. DP = (18.69 / 2) / (1.00 / 2) = 18.7. T_g (DSC) = -42 °C. Conductivity at 25 °C = 1.49×10^{-5} S/cm.

Poly(NB[(EO)₄Im(EO)₂CH₃ TFSI]₂) (1f). General procedure 1 was used to produce 1.301 g (97%) by using **X 8r** (1.338 g, 0.9550 mmol) and Grubbs 1st generation catalyst (24.6 mg, 0.0299 mmol). ¹H NMR (500 MHz, acetone-*d*₆) δ 9.06 (m, 32.39H), 7.78 (m, 64H), 7.38 (dd, J = 50, 8 Hz, 1H), 5.53 (m, 17H), 5.32 (m, 7H), 4.55 (m, 128H), 4.17 (m, 62H), 3.95 (m, 130H), 3.66 (m, 378H), 3.51 (m, 65H), 3.32 (s, 91H), 2.94 (s, 44H), 2.83 (m overlapping with HOD peak, 63H), 1.35 (m, 28H). Target DP = 32; target M_n = 45 kDa. Measured by ¹H NMR DP = 32.4 and M_n = ~45 kDa by end group analysis of imidazolium proton signals compared to initiator phenyl signals. Integral 9.06 ppm = 32.39; integral 7.38 ppm = 1.00 H. DP = (32.39 / 2) / (1.00 / 2) = 32.4. T_g = -39 °C. Conductivity at 25 °C = 2.27×10^{-5} S/cm.

Reduced Poly(NB[(EO)₄Im(EO)₂CH₃ TFSI]₂) (2f). General procedure 2 was used to produce 1.081 g (98%) by using **1f** (1.106 g, 0.02457 mmol) and *p*-toluenesulfonyl hydrazide (0.38 g, 2.0 mmol). ¹H NMR (500 MHz, CD₃CN) δ 8.66 (s, 1.00H), 7.48 (s, 2.08H), 5.40 – 5.21 (m, 0.17),

4.45 (br s, 0.25H), 4.32 (br s, 4H), 4.11 (m, 2H), 3.87–3.76 (m, 4H), 3.69 – 3.41 (m, 18H), 3.31 (s, 3H), 2.76 (m, 1H), 1.64–0.78 (m, 2H). ¹H NMR indicated reduction of ~83% of the olefinic units using the imidazolium signal at 8.66 ppm (1.00 H) compared to residual olefinic signal at 5.40–5.21 ppm (0.17 H). T_g = –46 °C. Conductivity at 25 °C = 9.66 x 10⁻⁶ S/cm.

References

- (1) Lee, M.; Choi, U. H.; Colby, R. H.; Gibson, H. W. *Chem. Mater.* **2010**, *22*, 5814-5822.
- (2) Naota, T.; Takaya, H.; Murahashi, S.-I. *Chem. Rev.* **1998**, *98*, 2599-2660.
- (3) Sutthasupa, S.; Shiotsuki, M.; Sanda, F. *Polym J* **2010**, *42*, 905-915.
- (4) Pitet, L. M.; Zhang, J.; Hillmyer, M. A. *Dalton Trans.* **2013**, *42*, 9079-9088.
- (5) Suga, T.; Sakata, M.; Aoki, K.; Nishide, H. *ACS Macro Lett.* **2014**, *3*, 703-707.
- (6) Zheng, L.; Chen, F.; Xie, M.; Han, H.; Dai, Q.; Zhang, Y.; Song, C. *React. Funct. Polym.* **2007**, *67*, 19-24.
- (7) Jangu, C.; Wang, J.-H. H.; Wang, D.; Sharick, S.; Heflin, J. R.; Winey, K. I.; Colby, R. H.; Long, T. E. *Macromol. Chem. Phys.* **2014**, *215*, 1319-1331.
- (8) Green, M. D.; Wang, D.; Hemp, S. T.; Choi, J.-H.; Winey, K. I.; Heflin, J. R.; Long, T. E. *Polymer* **2012**, *53*, 3677-3686.
- (9) Gao, R.; Wang, D.; Heflin, J. R.; Long, T. E. *J. Mater. Chem.* **2012**, *22*, 13473-13476.
- (10) Wu, T.; Wang, D.; Zhang, M.; Heflin, J. R.; Moore, R. B.; Long, T. E. *ACS Appl. Mater. Interfaces* **2012**, *4*, 6552-6559.
- (11) Moatsou, D.; Hansell, C. F.; O'Reilly, R. K. *Chem. Sci.* **2014**, *5*, 2246-2250.
- (12) Choi, U. H.; Lee, M.; Wang, S.; Liu, W.; Winey, K. I.; Gibson, H. W.; Colby, R. H. *Macromolecules* **2012**, *45*, 3974-3985.
- (13) Choi, U. H.; Mittal, A.; Price, T. L.; Gibson, H. W.; Runt, J.; Colby, R. H. *Macromolecules* **2013**, *46*, 1175-1186.
- (14) Yoon, K.-H.; Kim, K. O.; Schaefer, M.; Yoon, D. Y. *Polymer* **2012**, *53*, 2290-2297.
- (15) Yoon, K.-H.; Kim, K. O.; Wang, C.; Park, I.; Yoon, D. Y. *J. Polym. Sci., Part A: Polym. Chem.* **2012**, *50*, 3914-3921.
- (16) Rosebrugh, L. E.; Marx, V. M.; Keitz, B. K.; Grubbs, R. H. *J. Am. Chem. Soc.* **2013**, *135*, 10032-10035.
- (17) Hyvl, J.; Autenrieth, B.; Schrock, R. R. *Macromolecules* **2015**, *48*, 3148-3152.

Chapter 12

NORBORNENE TFSI TRIBLOCK POLYMERS

INTRODUCTION

The investigation of ionic liquids for use in mechanical actuators has steadily attracted attention over recent years.¹ At the forefront of this work has been the use of imidazolium ionic liquids,¹⁻⁶ because of their easy functionalization and excellent conductivities. Work towards mechanical actuators has ranged from simply swelling a polymer with an ionic liquid,⁶ to incorporation of the ionic liquid into polymers.² Swelling a polymer with an ionic liquid offers an easy approach, but since both the cation and anion are free to move, actuation occurs in both directions. Incorporation of either the cation or anion into the polymeric system restricts ion movement to a single component, thereby limiting actuation to a single direction, a desirable trait.

The previous two chapters assessed norbornene imidazolium TFSI monomers and their homopolymers (chapters 10 and 11, respectively). This chapter focuses on the incorporation of previously described systems into ABA triblock architectures via ROMP, through the use of the Grubbs 1st generation catalyst. The goal of this work was to produce an ABA triblock copolymer capable of mechanical actuation in a single direction and with sufficient mechanical strength to do work.

The ABA triblock design was chosen to be “hard--soft--hard” in which imidazolium monomers are incorporated as the soft B segment. Previous work (chapters 11 and 12) provided justification for the use of imidazolium monomers. The best of these monomers were found to have conductivities in the range of 10^{-4} S/cm and T_g values of approximately -39 °C. Additionally, it was observed that as long as an ethyleneoxy spacer of two or greater was used,

polymeric properties (T_g and conductivity) were found to be similar to those of the analogous monomers. For this reason, this chapter will focus on monomers that contain an ethyleneoxy linker of two or greater, bridging the imidazolium to norbornene.

RESULTS AND DISCUSSION

Before the synthesis of ABA triblock copolymers, an assessment of potential hard segments monomers was made; some candidates are shown in **Figure 12.1**. The choice was made to investigate monomers with aromatic and aliphatic pendant groups. By design the initial strategy was to focus on one monomer and progress to the next in the event of an impassable issue. For this reason, work with monomer **1** was completed before moving on to monomer **2**. As an initial assessment of the monomers, homopolymers were synthesized using ROMP conditions intended for triblock synthesis to determine the T_g . Ideally if the hard and soft phases of the ABA triblock do not mix, T_g values close to those of the individual homopolymers should be obtained.

The homopolymer of **1** synthesized using the Grubbs first generation catalyst at a molecular weight of 44 kDa formed brittle, light brown, translucent films having $T_g = 234$ °C. This value compared well to literature homopolymerization of **1** which has been reported at a molecular weight of 95 kDa to have T_g 226 °C.⁷ Homopolymers of **2**, synthesized using Grubbs first generation catalyst at a molecular weight of 49 kDa, formed brittle, dark brown, translucent films having T_g 128 °C. The homopolymer of **2** at a molecular weight of 68 kDa is reported to have T_g 135 °C.⁸ As with the soft segment monomers, pure *exo* norbornene hard segment

monomers were chosen here due to their ability to readily polymerize faster than their *endo* counterparts with ROMP conditions.⁹

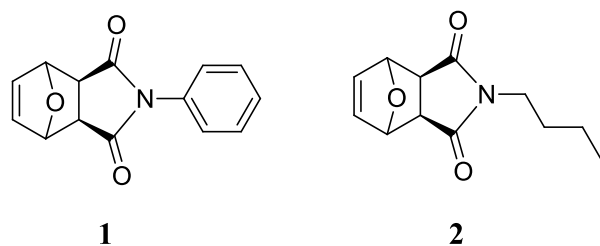
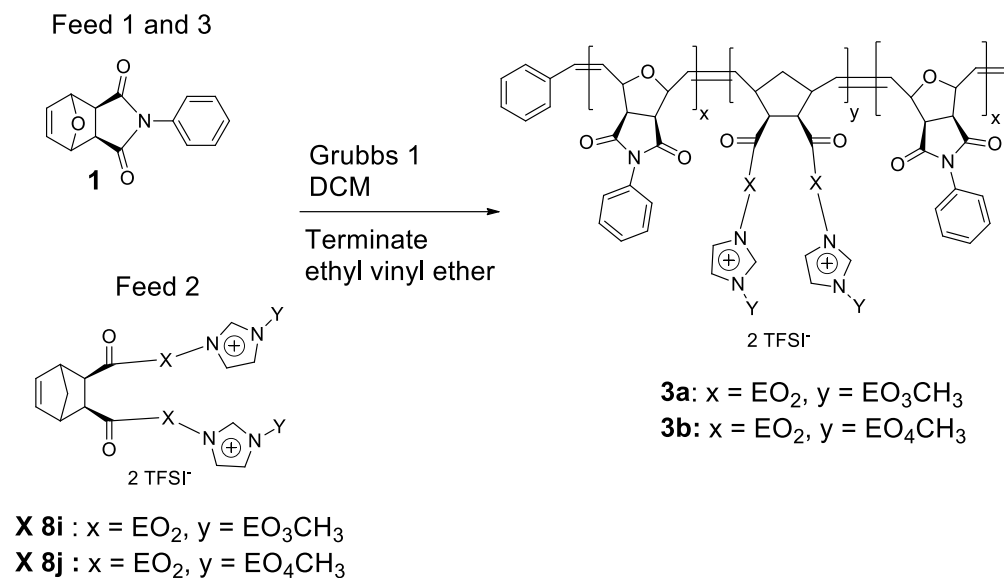


Figure 12.1. Hard segment monomers chosen for investigation.

Initial triblock studies began with the use of monomer **1**. The high T_g values obtained for the homopolymer of **1** indicated that the monomer would add much needed structural properties to the viscous liquid polymers of chapter 11. Using **1**, two separate ABA triblock copolymers were synthesized. Monomers used from chapter 10 have retained their previously used numbering and **X** has been placed before the number to indicate chapter 10 to avoid confusion. The soft segments **X 8i** and **X 8j** were chosen based solely on available material at the time, leading to triblocks **3a** and **3b** being intended to serve only as proof of concept and guidance in the development of future systems.

Scheme 12.1 shows the syntheses of triblock copolymers **3a** and **3b** carried out using ROMP with Grubbs 1st generation initiator. Conversions were monitored via ^1H NMR and sequential additions were not made until the previous monomer had been 99% consumed. Quenching of the reactions was achieved with ethyl vinyl ether.



Scheme 12.1. Synthesis of triblocks **3a** and **3b**.

Monomer feed ratios were chosen in an attempt to obtain the gyroid phase, one of the bicontinuous morphologies that is expected to yield good mechanical performance from the hard blocks and good ionic conductivity from the soft segments. From literature precedent the gyroid phases of ABA triblocks are expected to fall within the mole fraction constraints of an AB diblock copolymer, where the volume fraction of the B block is twice that of the of the A blocks.¹⁰ With this in mind the desired gyroid phase is expected to be close to the volume fraction region of 16:68:16 to 19:62:19, A:B:A.

Initially upon isolation, polymers **3a** and **3b** were cast using a slow solvent evaporation technique with DCM in a Teflon mold. Solvent evaporation was allowed for 24 h in the open and under vacuum for 2 days. These cast films were then cut and redissolved as needed to produce films which were cast from a range of solvents on substrates to be discussed later. Molecular weight, T_g, 5% wt. loss by TGA, conductivity and actuation parameters for **3a** and **3b** can be found in **Table 12.1**. **Figure 12.2** shows samples of **3a** and **3b** compared to their soft

segment monomers and homopolymer counterparts as well as the hard segment polymer. As seen in **Figure 12.2**, monomers and homopolymers of **X 8i** and **X 8j** were viscous oils while the homopolymer of **1** was brittle and had high T_g s. Films of **3a** and **3b** in **Figure 12.2** were non-brittle solids that demonstrated creasability, an indicator of mechanical strength.

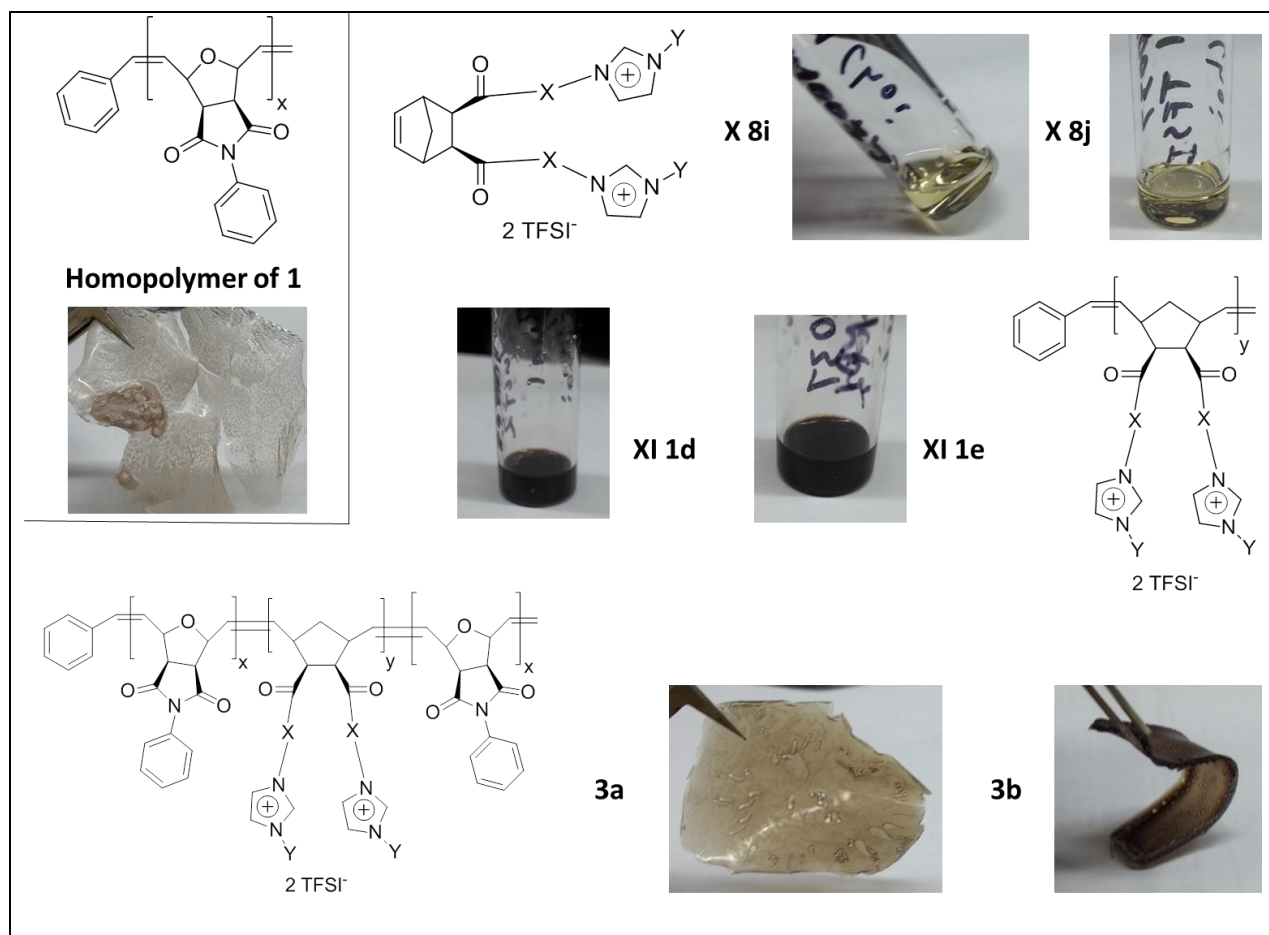


Figure 12.2. **3a** and **3b** visually compared to soft and hard segment homopolymers and monomers.

Table 12.1. Properties summary of ABA block copolymers **3a** and **3b**.

Polymer	Wt. ratios A:B:A	Target M_n (total) kDa	T_g ($^{\circ}\text{C}$)	5% wt. loss ($^{\circ}\text{C}$)	Conductivity (S/cm)	Actuation 63% curvature
3a	21:58:21	65.3	-38, 154	353	1.21×10^{-8}	20 s
3b	19.5:61:19.5	58.4	-11	353	N/A	50 s

Actuator testing was performed at Virginia Tech by Dong Wang under the supervision of Prof. James R. Heflin in the Department of Physics. Films were cast from 1,2-dichlorobenzene, 1,2-dichloroethane, chloroform and acetonitrile on glass, Teflon and silicon molds using slow solvent evaporation. Visual inspection and actuator testing led to the determination that for films of both **3a** and **3b**, chloroform casting on glass provided superior results.

Testing for actuation of **3a** and **3b** gave drastically different results. Films of **3a** were capable of reaching a maximum curvature of 0.14 mm^{-1} in 60 s and yielded a characteristic curvature time of 20 s. **3b** on the other hand was only capable of reaching a maximum curvature of 0.10 mm^{-1} in 176 s and had a characteristic curvature time of 50 s. Thus, triblock **3b** was abandoned and work focused on **3a**. **Figure 12.3** shows an overlay of starting and ending positions for **3a** when placed under a potential; the arrow on the figure indicates actuation. **Figure 12.4** shows the complete curvature diagram for **3a**.

In terms of “state of the art” actuation from imidazolium containing electromechanical actuators, systems have yielded a maximum curvature of as much as 4.00 mm^{-1} in 6.0 sec⁶ with a polymer swelled with 58 wt. % of an ionic liquid. As previously stated in the introduction, due to the system containing a free cation and anion, actuation occurred in both directions. However, **3a** produced only single direction actuation. Thus, to date actuation has generally only been reported for ionic liquid doped polymers and not the unswelled polymers.^{2,3,6}

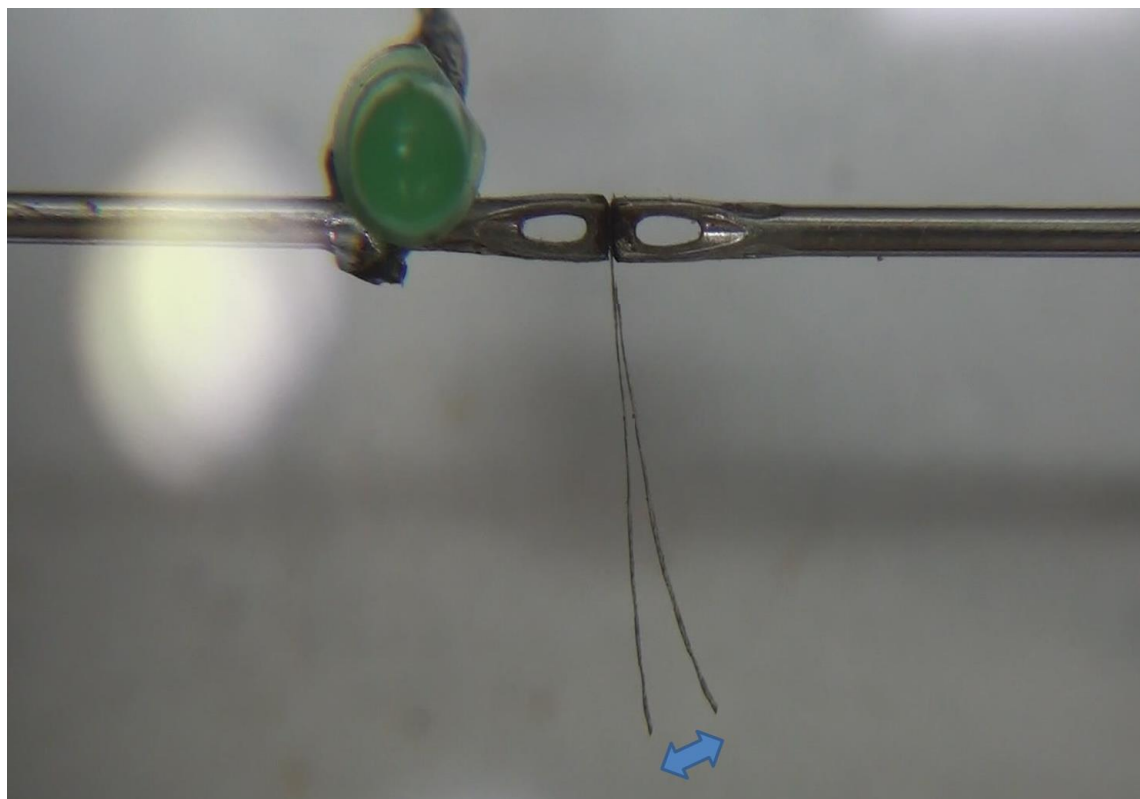


Figure 12.3. Overlay of **3a** starting and ending position with arrow showing actuation.

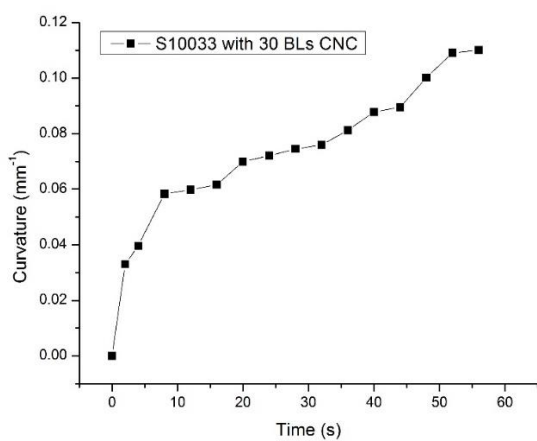


Figure 12.4. Curvature diagram for **3a** (actuation).

3a displayed T_g s at -38 and 154 °C, compared to the homopolymer of **XI 1d** ($T_g = -51$ °C) and the homopolymer of **1** ($T_g = 234$ °C). Clearly the phases of **3a** were mixed. To

determine the morphology of **3a**, SAXS was employed; **Figure 12.6** shows the resulting data. SAXS was conducted at Virginia Tech by Mingqiang Zhang under the direction of Prof. Robert Moore in the Chemistry Department. SAXS data indicated little ordering and confirmed the suspicion that a well-defined morphology was not achieved. An AB diblock copolymer of poly(norbornene dodecyl ester) and poly(norbornene imidazolium), **Figure 12.5**, by Scalfani et al. in which percent compositions were varied (sixteen compositions) displayed a range of morphologies from disordered to lamellae.¹¹ The SAXS of the triblock copolymer **3a** (**Figure 12.6**) is almost identical to SAXS data of Scalfani et al. on the morphology cusp of liquid-like packing (LLP) of spheres to a disordered state. Indeed these workers found no evidence of formation of the required bicontinuous gyroidal morphology even after annealing for two months. The authors conclude “*Ultimately, the strong degree of segregation inherent to the charged–uncharged architecture may limit the ability of the system to form the idealized gyroid network often sought for transport-related applications.*” and “*Failure to disorder even the lowest molecular weight symmetric sample with degree of polymerization of ~12 confirmed that accessible phase behavior for these BCPs is likely constrained to that of the strongly segregated regime.*”.

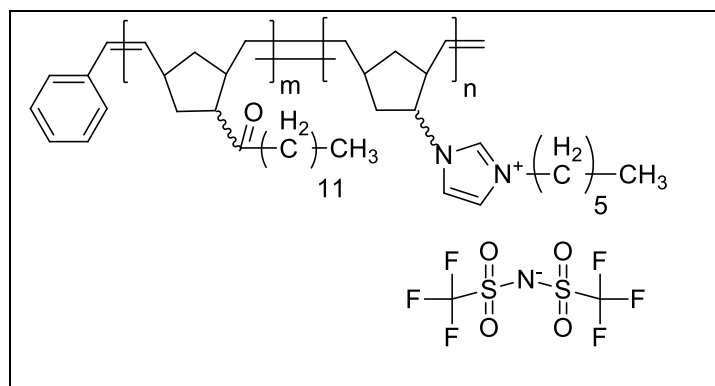


Figure 12.5. Imidazolium diblock copolymer by Scalfani et al.¹¹

As a last form of characterization, the conductivity of the system was determined to be 1.21×10^{-8} S/cm at 25 °C. Monomer **X 8i** and its homopolymer have conductivities in the range of 10^{-5} S/cm; the drop in conductivity to 10^{-8} S/cm for **3a** indicates a problematic hard segment choice that leads to phase mixing and low conductivity.

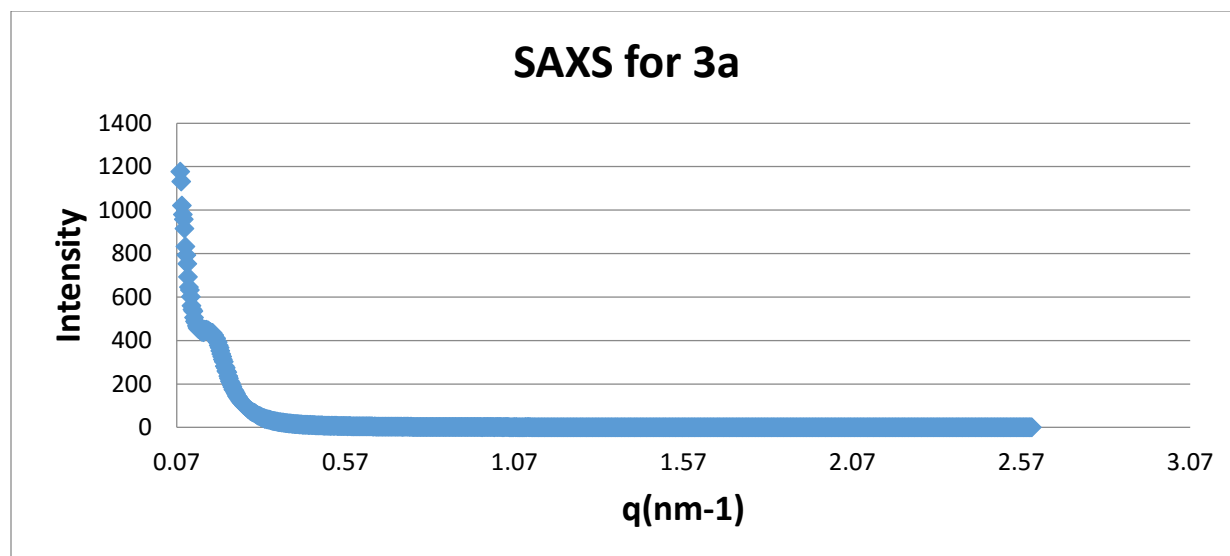


Figure 12.6. SAXS data for **3a**.

In an attempt to order the system, thermal annealing was conducted on **3a** in two different experiments (**Figure 12.7**). In the first experiment **3a** was thermally annealed at 170 °C for 12 h in nitrogen; this resulted in a slight stiffening and darkening of the material; the T_g s remained the same. In the second experiment **3a** was thermally annealed at 202 °C in nitrogen for 24 h; the material became brittle, dark, opaque and was determined to be degraded based on color and ^1H NMR changes. Both attempts at thermal annealing were unsuccessful and as seen in the higher temperature annealing, the T_g of the hard phase is too high to anneal without oxidative degradation. This leads to the conclusion that either better casting techniques are required to advance the material further or a lower T_g hard block could prove advantageous.

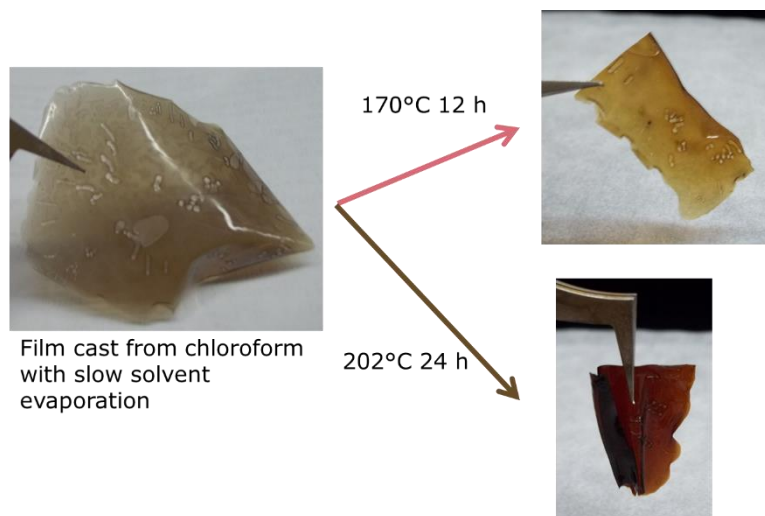
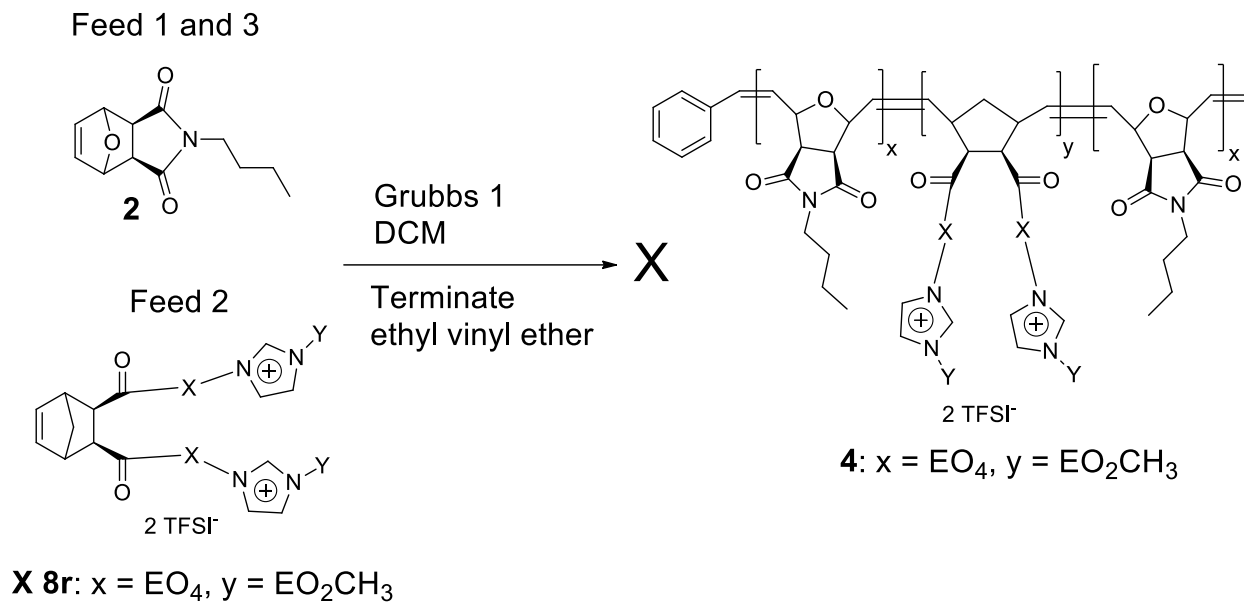


Figure 12.7. **3a** thermally annealed at 170 °C for 12h and 202 °C for 24 h in nitrogen.

Although single direction actuation was achieved with both **3a** and **3b**, problems existed. We speculated that the N-phenyl ring of the hard segment promoted phase mixing between segments; likely the driving force for this is $\pi - \pi$ stacking between the N-phenyl ring and imidazolium cation. In an attempt to lower the likelihood of phase mixing, the more aliphatic monomer **2** was chosen for investigation. **Scheme 12.2** shows the attempted synthesis of triblock copolymer **4**. As seen in **Scheme 12.2**, the soft segment monomer was changed from **X 8i** to **X 8r**, the optimal monomer from chapter 10. Additionally, the homopolymer of **2** has a T_g of 128 °C, which should allow for thermal annealing without degradation of the polymer.



Scheme 12.2. Attempted synthesis of triblock copolymer **4**.

Synthesis of **4** was attempted in an identical fashion to **3a** and **3b**, by use of ROMP employing the Grubbs 1st generation catalyst. During the attempted synthesis of **4**, however, upon > 99% consumption of **2** (which occurred rapidly) the polymerization showed signs of auto-termination. Several attempts were made, but the result was consistent, the soft segment monomer **X 8r** did not react and only a homopolymer of **2** was produced. This problem occurs sometimes in unhindered norbornenes and the general remedy for such problems is to retard the Grubbs catalyst and slow the reaction to a controllable point.¹² The solution was impractical for **4**, given the already sluggish uptake of **X 8r**, requiring approximately 13 h. For this reason, triblock copolymer **4** was abandoned.

CONCLUSIONS

In conclusion, ABA triblock copolymers capable of single direction actuation were successfully synthesized. Resulting materials **3a–3b** were found to give single direction actuation, but challenges in material design and processing remain if such triblock copolymers are to be optimized for functional electromechanical actuators. Attempts at the production of a triblock copolymer using hard segment monomer **2** were unsuccessful due to widely disparate rates of polymerizations.

EXPERIMENTAL

Measurements: ¹H–NMR spectra were obtained on JEOL ECLIPSE-500, BRUKER-500, and AGILENT-NMR-vnmrs400 spectrometers. ¹³C–NMR spectra were collected at 125 MHz and 101 MHz on these instruments. HR–MS were obtained using an Agilent LC-ESI-TOF system. Reagents were purchased and used as received without further purification. Compounds **1**¹³ and **2**¹⁴ were made in accordance with literature procedure. Compounds **X 8i**, **X 8j**, and **X 8r** were prepared as described in Chapter 10. DSC data were obtained on a TA Instrument Q2000 differential scanning calorimeter under N₂ at a rate of 10 °C/min, while cooling used a quenching technique. TGA data were obtained on a TA Instruments TGA Q500 at a rate of 20 °C / min under N₂. The ionic conductivity measurements were performed by dielectric relaxation spectroscopy at Penn State University by U Hyeok Choi, using a sinusoidal voltage with amplitude 0.1 V and 10⁻¹–10⁷ Hz frequency range for all experiments; data were collected in isothermal frequency sweeps every 5 K from 120 °C to –100 °C. The SAXS experiment was conducted at Virginia Tech by Mingqiang Zhang using a Rigaku S-Max 3000 SAXS system.

Actuation testing was conducted at Virginia Tech by Dong Wang on a custom-built probe station; the actuator made from the ABA triblock copolymer was powered by a Metroh Autolab μ AutoLab III/FRA 2 Impedance Analyzer, and monitored and recorded by a SONY HXR-MC1 CCD camera for further analysis.

General Procedure 1: ABA Triblock synthesis, A = poly((3aR,7aS)-2-phenyl-3a,4,7,7a-tetrahydro-1H-4,7-epoxyisoindole-1,3(2H)-dione), B = poly(NB[(EO)₂Im(EO)₃TFSI]₂) (3a).

Monomer **1** (0.3126 g, 1.296 mmol) was added to a reaction tube with dry DCM (4 mL) under nitrogen. Grubbs 1st generation catalyst (18.5 mg, 0.0225 mmol) was dissolved in a minimum amount of DCM (0.5 mL) and added. The solution was allowed to stir at room temperature and monitored by ¹H NMR until complete consumption of the monomer was observed. Monomer **X 8i** (0.8428 g, 0.6418 mmol) was added to the reaction mixture and monitored via ¹H NMR until complete consumption, at which time monomer **1** (0.3126 g, 1.296 mmol) was added. After consumption of the last monomer, ethyl vinyl ether (0.50 mL, 5.2 mmol) was added to quench the reaction. Volatile compounds were removed by vacuum. The crude polymer was washed with ether (5 mL x 3) then dissolved in a minimum amount of DCM (2 mL) and precipitated into a mixture of ether/DCM (v/v 85/15) (15 mL x 3) at dry ice temperature; this was repeated twice. The polymer was collected and dried under vacuum for 12 h: 1.38 g (94 %). Target DPs: initial block **1**: 58; center block **X 8i**: 29; terminal block **1**: 58. Total target M_n: 65.3k: initial block **1**: 13.9k (21 wt %); center block **X 8i**: 37.5k (58 wt %); terminal block **1**: 13.9k (21 wt %). ¹H NMR (500 MHz, CD₂Cl₂) δ 8.77 (br s, 1H), 7.61–7.36 (m, 10H), 7.29 (br s, 5H), 6.15 (br s, 3H), 5.90 (m, 1H), 5.48 (m, 0.65H), 5.32 (m, 0.25H), 5.19–5.11 (m, 1.32H), 4.69–4.64 (m, 3H), 4.39 (br s, 4H), 4.26–4.14 (m, 3H), 3.87 (br s, 4H), 3.67 (m, 4H), 3.62 (m, 5H), 3.56–3.41 (m, 7H),

3.35 (s, 3H), 2.91 (m, 2H), 2.03 (br s, 0.50H), 1.37 (br s, 0.68H). TGA (nitrogen) 5% wt. loss = 353 °C. $T_g = -25$ °C and +154. Conductivity at 25 °C = 1.1×10^{-8} S/cm.

ABA Triblock synthesis. **A** = poly((3aR,7aS)-2-phenyl-3a,4,7,7a-tetrahydro-1H-4,7-epoxyisoindole-1,3(2H)-dione), **B** = poly(NB[(EO)₂Im(EO)₄ TFSI]₂) (**3b**). General procedure 1 was used to produce 1.41 g (89%) of polymer using **1** (0.3730 g, 1.608 mmol), **X 8j** (1.1637 g, 0.83045 mmol), **1** (0.3730 g, 1.608 mmol) and Grubbs 1st generation catalyst (26.9 mg, 0.0327 mmol). Target DPs: initial block **1**: 49; center block **X 8j**: 25; terminal block **1**: 49. Total target M_n : 59.5 k: initial block **1**: 11.9 k (20 wt %); center block **X 8i**: 35.7 k (60 wt %); terminal block **1**: 11.9 k (20 wt %). ¹H NMR (500 MHz, CDCl₃) δ 8.75 (br s, 1H), 7.55–7.30 (m, 10H), 7.29–7.21 (m, overlap with chloroform peak, 10H), 6.07 (br s, 3H), 5.82 (br s, 1H), 5.42 (m, 1H), 5.16 (br s, 1H), 4.63–4.55 (m, 3H), 4.35 (br s, 4H), 4.09 (br s, 3H), 3.82 (br s, 5H), 3.62 (m, 14H), 3.52 (br s, 3H), 3.32 (m, 8H), 2.87 (br s, 2H), 2.01 (br s, 0.5H), 1.63 (m, overlap with HOD, 18H), 1.32 (s, 1H). TGA (nitrogen) 5% wt. loss = 346 °C. $T_g = -11$ °C.

Attempted synthesis: ABA Triblock, **A** = poly((3aR,7aS)-2-butyl-3a,4,7,7a-tetrahydro-1H-4,7-epoxyisoindole-1,3(2H)-dione), **B** = poly(NB[(EO)₂Im(EO)₃ TFSI]₂) (**4**). General procedure 1 was used with **2** (0.1817 g, 0.8212 mmol), **X 8r** (0.6467 g, 0.4615 mmol), **2** (0.1817 g, 0.8212 mmol) and Grubbs 1st generation catalyst (6.76 mg, 0.00821 mmol). Synthesis failed due to self-termination, homopolymer of **2** isolated, 0.15 g. ¹H NMR (500 MHz, CDCl₃) δ 6.08 (br s, 1.24H), 5.81 (br s, 0.42H), 5.03 (br s, 0.45H), 4.47 (br s, 1H), 3.48 (br s, 2H), 3.31 (br s, 2H), 1.31 (br s, 2H), 0.93 (t, $J = 7.3$ Hz, 3H).

REFERENCES

- (1) Green, M. D.; Long, T. E. *Polym. Rev.* **2009**, *49*, 291-314.

- (2) Margaretta, E.; Fahs, G. B.; Inglefield, D. L.; Jangu, C.; Wang, D.; Heflin, J. R.; Moore, R. B.; Long, T. E. *ACS Appl. Mater. Interfaces* **2016**, *8*, 1280-1288.
- (3) Jangu, C.; Wang, J.-H. H.; Wang, D.; Sharick, S.; Heflin, J. R.; Winey, K. I.; Colby, R. H.; Long, T. E. *Macromol. Chem. Phys.* **2014**, *215*, 1319-1331.
- (4) Green, M. D.; Wang, D.; Hemp, S. T.; Choi, J.-H.; Winey, K. I.; Heflin, J. R.; Long, T. E. *Polymer* **2012**, *53*, 3677-3686.
- (5) Gao, R.; Wang, D.; Heflin, J. R.; Long, T. E. *J. Mater. Chem.* **2012**, *22*, 13473-13476.
- (6) Wu, T.; Wang, D.; Zhang, M.; Heflin, J. R.; Moore, R. B.; Long, T. E. *ACS Appl. Mater. Interfaces* **2012**, *4*, 6552-6559.
- (7) Yoon, K.-H.; Kim, K. O.; Wang, C.; Park, I.; Yoon, D. Y. *J. Polym. Sci., Part A: Polym. Chem.* **2012**, *50*, 3914-3921.
- (8) Tuba, R.; Corrêa da Costa, R.; Bazzi, H. S.; Gladysz, J. A. *ACS Catal.* **2012**, *2*, 155-162.
- (9) Moatsou, D.; Hansell, C. F.; O'Reilly, R. K. *Chem. Sci.* **2014**, *5*, 2246-2250.
- (10) Posocco, P.; Fermeglia, M.; Pricl, S. *J. Mater. Chem.* **2010**, *20*, 7742-7753.
- (11) Scalfani, V. F.; Wiesenauer, E. F.; Ekblad, J. R.; Edwards, J. P.; Gin, D. L.; Bailey, T. S. *Macromolecules* **2012**, *45*, 4262-4276.
- (12) Schwab, P.; Grubbs, R. H.; Ziller, J. W. *J. Am. Chem. Soc.* **1996**, *118*, 100-110.
- (13) Deng, L.-P.; Liu, F.-M.; Wang, H.-Y. *J. Heterocycl. Chem.* **2005**, *42*, 13-18.
- (14) Liu, M.; van Hensbergen, J.; Burford, R. P.; Lowe, A. B. *polym. Chem.* **2012**, *3*, 1647-1658.

Chapter 13

OTHER NORBORNENE SALTS

Introduction

Original work in our lab on ion-conducting monomers and polymers begun with the PF_6 counter ion and migrated to the more desirable TFSI counter ion, to reap the benefits of lower glass transition temperatures (T_g) and higher conductivities, both of which result from the lower degree of ion pairing due to the highly delocalized TFSI anion.¹⁻⁴ In a similar manner, in this work, research was conducted on a variety of anions and cations in an attempt to find new cation/anion systems that could offer higher conductivities than the imidazolium TFSI combination. The norbornene architecture of chapter 10 (**Figure 13.1**) was employed; anions were tested in tandem with the development of the imidazolium/TFSI system by comparison of T_g s and conductivities. In regards to the development of a new cation system, the same philosophy was employed. The norbornene architecture was retained and employed, except the 4,4'-bipyridinium (paraquat) dication was substituted for the imidazolium moiety (**Figure 13.1**).

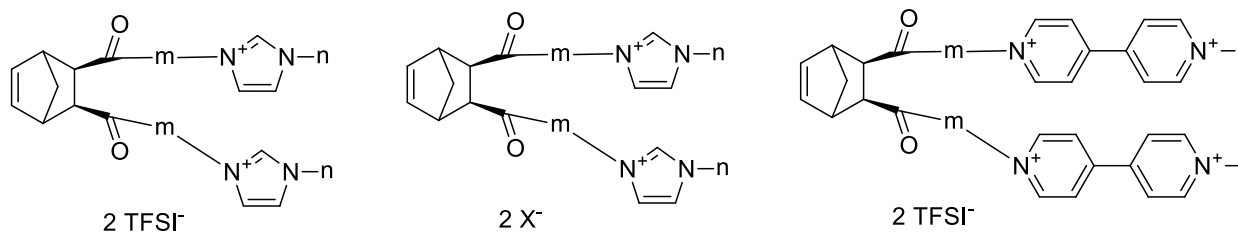
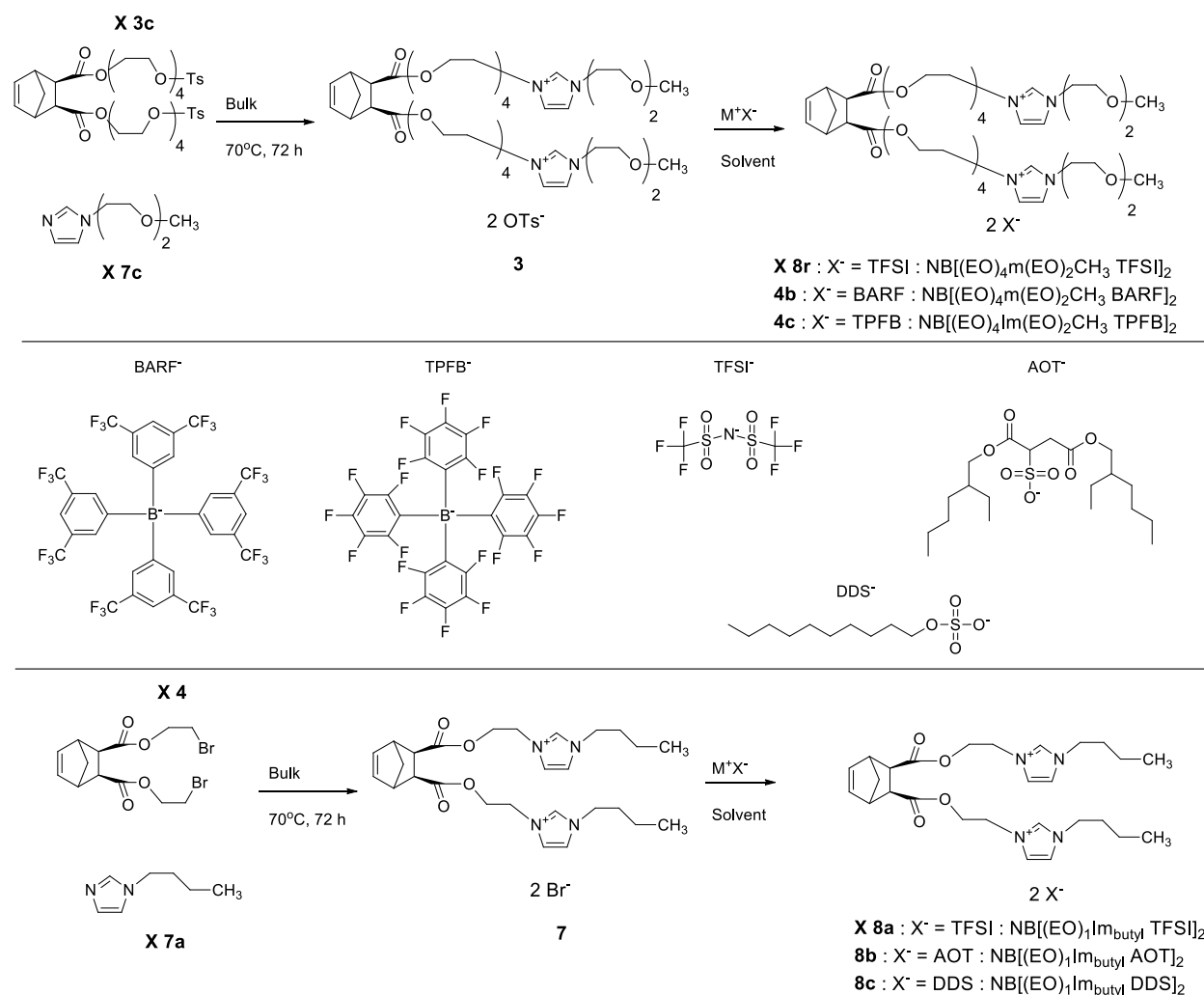


Figure 13.1. Imidazolium TFSI monomer architecture alongside two new systems: imidazolium/new anions and paraquat/TFSI.

Results and Discussion

The advantages of the TFSI counter ion over PF₆ are due to it being a much larger, bulkier ion and having the charge dispersed over a larger volume. This lowers the T_g and in turn results in higher conductivities.¹ PF₆ also undergoes hydrolysis to produce HF, which is undesirable for many reasons. For this reason, we chose to evaluate large bulky anions which have their negative charge highly dispersed as well as a few other anions which should have exceptionally low T_g values. Anions chosen for this evaluation were BARF, TPFB, AOT, and DDS (**Scheme 13.1**). For clarity, compounds from chapter 10 will maintain their previously used numbering and **X** will be placed in front of the number. Synthesis of **X 3c** and **X 7c** were carried out as described in chapter 10. Quaternization was also achieved as described in chapter 10; the procedure was as follows: **X 3c** and **X 7c** were mixed in bulk for 3 days at 70 °C after which liquid–liquid extraction with water and DCM was used for purification of **3**. **3** was counterion exchanged in water to form **X 8r**, **4b** and **4c** and purification was achieved as described in the experimental section. Starting materials **X 4** and **X 7a** were also synthesized as described in chapter 10; quaternization and purification for **7** mimicked those used for **3**. **7** was then counterion exchanged and purified as described in the experimental section to form **X 8a**, **8b** and **8c**.



Scheme 13.1. Synthesis of new monomers **4b**, **4c**, **8b** and **8c**.

Since TFSI is the currently employed anion of choice, compounds **X 8r** and **X 8a** were the reference point to which **4b**, **4c**, **8b** and **8c** were compared. BARF and TPFB, which were used to synthesize **4b** and **4c**, both take advantage of a negatively charged boron atom that has its charge highly dispersed over four aromatic rings. BARF disperses its negative charge over four phenyl rings substituted in the 3- and 5-positions with CF_3 groups, while TPFB employs four pentafluorophenyl rings. Both of these anions are highly attractive candidates due to their large size as well as the large area over which the negative charge is dispersed. The remaining anions,

AOT and DDS, differ greatly from BARF and TPFB in the sense that they have not been selected for their charge dispersion. Instead AOT, **8b**, was selected due to its non-symmetrical nature and because it is actually a mixture of eight stereoisomers at three chiral centers and hence was expected to lower T_g s and in turn raise conductivities. Lastly the DSS salt, **8c**, was synthesized to compare with **8b** and contrast sulfate and sulfonate groups.

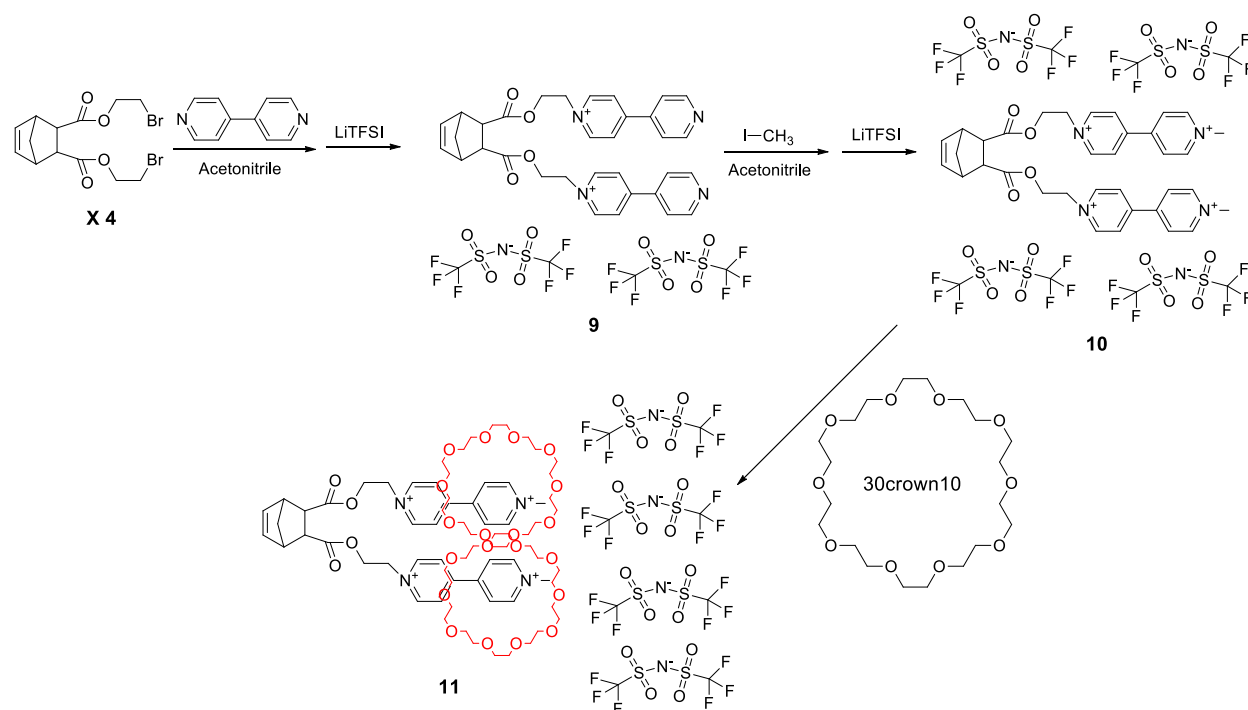
Table 13.1. T_g and Conductivity values for **4a** – **4c** and **8a** – **8c**.

Monomer	X	T_g (°C)	Conductivity (S/cm)
4a	TFSI	-46°C	9.57×10^{-5}
4b	BARF	-26°C & -6°C	3.19×10^{-8}
4c	TPFB	-27°C	N/A
8a	TFSI	-44°C	3.07×10^{-5}
8b	AOT	-25°C	2.57×10^{-9}
8c	DSS	5°C	1.24×10^{-10}

Table 13.1 provides T_g and conductivity values for these monomer salts. Looking first at the boron anions we can see that the T_g s of **4b** and **4c** are approximately 20 °C higher than their TFSI counterpart and conductivities are nearly three orders of magnitude lower. Despite the size of these anions, which allow for an abundant distribution of charge, the increased T_g values provide a medium which is less favorable to charge movement. Considering the similar T_g value of **4b** and **4c** alongside the low conductivity value of **4b** and the precursor of TPFB costing approximately \$1/2 mg, this was not pursued. Evaluating the sulfonate **8b** and sulfate **8c**, T_g values are nearly 20 °C higher and conductivities range from four to five orders of magnitude lower than their TFSI counterpart, **X 8a**. Once again the likely culprit for poor results is attributed greatly to increased T_g values. The T_g increase in **4b** and **4c** is likely in part due to the large and rigidly confined aromatic rings. **8b** and **8c**, however, contain flexible hydrocarbon chains, so the lower conductivity in these systems is partly attributed to the lack of charge

delocalization in the sulfonate and sulfate anions, leading to tighter ion pairs and fewer free anions.

Extrapolating to polymeric systems, it is suspected that, T_g s of polymers synthesized from BARF and TPFB would likely increase more than was observed in the TFSI system of chapter 10. The large size and rigidity of BARF and TPFB would likely slow their movement through a polymer in a greater way than was observed for TFSI. In comparison, TFSI is relatively compact and flexible, which would allow it to pass through polymeric medium much easier than BARF or TPFB.



Scheme 13.2. Synthesis of paraquat TFSI norbornene monomer **10** and proposed complexation with 30-crown-10.

The remaining item studied in this investigation was a paraquat TFSI complexed with a crown ether (**Scheme 13.2**). Synthesis of **10** was carried out by quaternization of **X 4** with 4,4-

bipyridyl, followed by counter ion exchange with LiTFSI to give **9**. **9** was then quaternized with methyl iodide and counter ion exchanged once again with LiTFSI to give **10**. The cation employed here, paraquat, is well known to complex with a variety of crown ether compounds;⁵⁻¹⁰ one of the primary driving forces for complexation is interaction between the electron rich oxygen atoms of the crown ethers and partially positively charged aromatic hydrogens of paraquat. The crown ether–paraquat complex, once formed, offers a reduction in the overall positive charge of the paraquat cation, via the previously mentioned interaction and other interactions, which allows the anion of the paraquat salt to become more dissociated from the cation. The net result is a larger fraction of non-paired anions,^{6,11} which should translate into higher conductivities. For this reason, **10** was mixed with 30-crown-10 to give complex **11**. It was anticipated that the conductivity would increase for this reason and because each paraquat cation is paired with two TFSI anions, while each imidazolium is paired with one. Ideally a paraquat such as **10** would be better suited to complexing dibenzo-30-crown-10,⁶ bis(*m*-phenylene)-32-crown-10⁵ or an analogous cryptand;^{5,6} these compounds were however, not chosen due to melting points as they are 80+ °C. It was believed that the use of these crowns would result in a complex in which the T_g of the material would be too elevated to allow for good conductivities.

Figure 13.2 shows partial NMR spectra of **10** and its mixture with 30-crown-10 to form complex **11**. In the time averaged spectrum of **Figure 13.2** it can be seen that the paraquat hydrogens have all shifted upfield approximately 0.02 ppm; typically, larger shifts are observed in similar systems as the stoichiometric amount of crown ether is increased and the fraction of complexed paraquat is increased. In **Figure 13.2** both the top and bottom ¹H NMR spectra were taken on 5.9 mM samples for comparison.

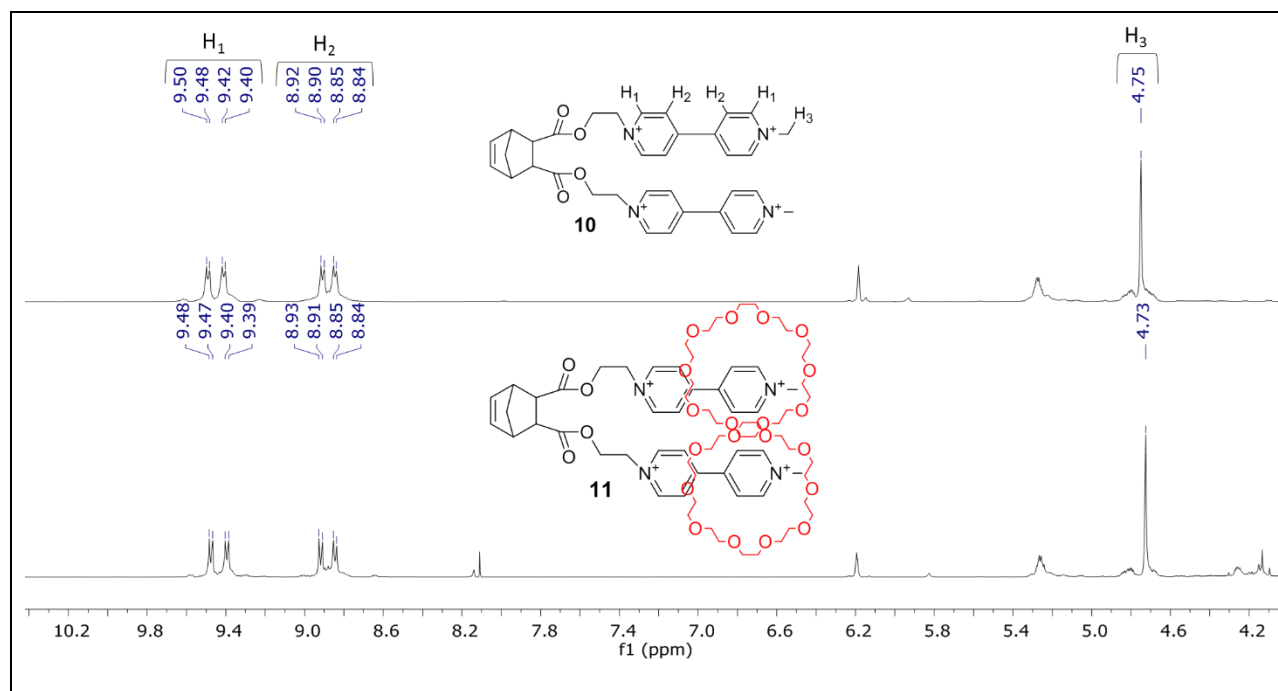


Figure 13.2. Partial ^1H NMR spectra taken in acetone- d_6 at room temperature of **10** (5.9 mM) and a mixture of **10** and 30-crown-10 (5.9 mM each component).

Table 13.2. Conductivity comparison of **8a and **11**.**

Monomer	X	Cation	Conductivity S/cm
8a	TFSI	Imidazolium	3.07×10^{-5}
11 (1:1 10 :30-crown-10 mol:mol)	TFSI	Paraquat	1.13×10^{-6}

As seen in **Table 13.2**, even with the aid of complexation with 30-crown-10, the conductivity of the paraquat TFSI was an order of magnitude lower than the corresponding imidazolium TFSI **X 8a**. A possible reason is that each paraquat contains two positive charges, leading to a situation where only the first anion is mobile and once separated from the paraquat cation, the buildup of positive charge restricts the movement of the second anion.

Conclusion

Four new imidazolium/anion combinations were tested for conductivity. Anions tested included BARF, TPFB, AOT, and DDS. Unfortunately, when compared to their TFSI counterpart, in terms of conductivity, the resulting materials were inferior. In further experimentation a new cation/TFSI combination was tested. The conductivity of the mixture of paraquat TFSI (**10**) with 30-crown-10 (to partially form complex **11**) was an order of magnitude lower than the corresponding imidazolium TFSI (**8a**).

Experimental

Measurements: ^1H -NMR spectra were obtained on JEOL ECLIPSE-500, BRUKER-500, and AGILENT-NMR-vnmrs400 spectrometers. ^{13}C -NMR spectra were collected at 125 MHz and 101 MHz on these instruments. HR-MS were obtained using an Agilent LC-ESI-TOF system. Reagents were purchased and used as received without further purification. DSC data were obtained on a TA Instrument Q2000 differential scanning calorimeter under N_2 ; heating was carried out at a rate of $10\text{ }^\circ\text{C}/\text{min}$, while cooling used a quenching technique. The ionic conductivity measurements were performed by dielectric relaxation spectroscopy at Penn State University by U Hyeok Choi under the direction of Prof. Ralph Colby using a sinusoidal voltage with amplitude 0.1 V and 10^{-1} – 10^7 Hz frequency range for all experiments; data were collected in isothermal frequency sweeps every 5 K from $120\text{ }^\circ\text{C}$ to $-100\text{ }^\circ\text{C}$. Compounds **X 3c**, **X 7c**, **3**, **X 8r**, **X 4**, **X 7a**, **7**, and **X 8a** were prepared as described in Chapter 10.

NB[(EO)₄Im(EO)₂CH₃ OTS]₂ (3). Norbornene **1** (1.89 g, 2.24 mmol) and imidazole **2** (0.708 g, 5.61 mmol) were combined in a round bottom flask under nitrogen and heated at $70\text{ }^\circ\text{C}$ with

stirring for 3 days. After cooling to room temperature, the reaction mixture was taken up in water (50 mL) and extracted with DCM (200 mL) in a liquid-liquid apparatus for 2 days. The aqueous layer was collected and water was removed by rotary evaporation. The resulting material was placed under a stream of nitrogen for one day and vacuum for two days (1.75 g, 80%, a viscous liquid). ^1H NMR (500 MHz, D_2O) δ 7.58 (d, $J = 8$ Hz, 4H), 7.48–7.43 (m, 4H), 7.26 (d, $J = 8$ Hz, 4H), 6.17 (t, $J = 2$ Hz, 2H), 4.33–4.28 (m, 8H), 4.25–4.17 (m, 2H), 4.06–3.99 (m, 2H), 3.80 (q, $J = 5$ Hz, 8H), 3.64 (t, $J = 5$ Hz, 4H), 3.60–3.52 (m, 20H), 3.49–3.45 (m, 4H), 3.24 (s, 6H), 3.03–2.98 (m, 2H), 2.66 (d, $J = 2$ Hz, 2H), 2.29 (s, 6H), 1.80 (d, $J = 9$ Hz, 1H), 1.37 (d, $J = 9$ Hz, 1H). ^{13}C NMR (126 MHz, D_2O) δ 175.87, 142.41, 139.42, 137.94, 129.40, 125.32, 122.62, 122.54, 70.88, 69.63, 69.51, 69.50, 69.47, 68.38, 68.31, 64.16, 58.01, 49.13, 49.11, 47.28, 45.47, 44.62, 20.44 (23 signals expected and 23 signals found). HR MS: calc. for $\text{C}_{55}\text{H}_{82}\text{N}_4\text{O}_{20}\text{S}_2$ [$\text{M} - 2 \text{ OTs}$] $^{+2}$: m/z 420.2361; found: m/z 420.2350 (error 2.6 ppm)

NB[(EO)₄Im(EO)₂CH₃ BARF]₂ (4b). To a flask containing acetone (10 mL) was added **3** (0.312 g, 0.264 mmol) and NaBARF (0.584 g, 0.649 mmol) with magnetic stirring under nitrogen. The reaction mixture was held at reflux for 20 h, after which solvent was removed by rotary evaporation. The remaining material was taken up in DCM and filtered. The solvent was removed by rotary evaporation and the desired product was collected as a viscous oil (0.676 g, 99%). ^1H NMR (500 MHz, $\text{DMSO-}d_6$) δ 9.09 (s, 2H), 7.76–7.75 (m, 4H), 7.67 (s, 8H), 7.62 (s, 16H), 6.21 (t, $J = 2$ Hz, 2H), 4.37 (t, $J = 5$ Hz, 8H), 4.20–4.14 (m, 2H), 4.00–3.96 (m, 2H), 3.81–3.75 (m, 8H), 3.59–3.46 (m, 24H), 3.42–3.38 (m, 4H), 3.20 (s, 6H), 3.00–2.96 (m, 2H), 2.58 (d, $J = 2$ Hz, 2H), 1.95 (d, $J = 9$ Hz, 1H), 1.33 (d, $J = 9$ Hz, 1H). ^{13}C NMR (126 MHz, $\text{DMSO-}d_6$) δ 173.32, 161.42 (q, $J = 50$ Hz), 138.19, 137.10, 134.50, 128.96 (qq, $J = 32, 3$ Hz), 127.69, 124.45 (d, $J = 273$ Hz), 123.03 (d, $J = 10$ Hz), 121.19, 118.05, 71.53, 70.17, 70.11, 70.05, 69.97, 69.82,

68.63, 68.59, 63.93, 58.46, 55.34, 49.30, 46.95, 45.58, 45.15, 31.08 (27 signals expected and 27 signals found). HR MS: calc. for $C_{105}H_{92}B_2N_4O_{14}F_{48}$ [M - BARF]⁺: m/z 1703.5375; found: m/z 1703.5376 (error -0.06 ppm)

NB[(EO)₄Im(EO)₂ TPFB]₂ (4c). To a flask containing acetone (10 mL) was added **3** (0.129 g, 0.109 mmol) and lithium tetrakis(pentafluorophenyl)boron (0.584 g, 0.670 mmol) with magnetic stirring under nitrogen. The reaction mixture was held at reflux for 20 h, after which solvent was removed by rotary evaporation. The remaining material was taken up in DCM and filtered. The solvent was removed by rotary evaporation and the desired product was collected as an oil (0.225 g, 95%). ¹H NMR (500 MHz, acetone-*d*₆) δ 9.14 (s, 2H), 7.83–7.81 (m, 4H), 6.21 (s, 2H), 4.59 (s, 8H), 4.33–4.22 (m, 2H), 4.12–4.10 (m, 2H), 3.96 (s, 8H), 3.74–3.57 (m, 28H), 3.29 (s, 6H), 3.04 (s, 2H), 2.60 (s, 2H), 1.38 (s, 1H), 1.23 (s, 1H). ¹³C NMR (126 MHz, acetone-*d*₆) δ 173.08 (s), 148.17 (d, *J* = 238 Hz), 137.75 (s), 137.18 (tt, *J* = 247, 14 Hz), 136.98 (s), 124.16 (bs), 122.95 (s), 122.80 (s), 71.55 (s), 70.26 (s), 70.16 (s), 70.13 (s), 70.10 (s), 69.95 (s), 68.69 (s), 68.52 (s), 68.50 (s), 63.62 (s), 57.83 (s), 49.74 (s), 49.72 (s), 46.91 (s), 45.54 (s), 44.84 (s) (25 signals expected and 24 signals found, two aromatic singlets overlapping due to splitting of aryl C-F signals). HR MS: calc. for $C_{89}H_{68}B_2F_{40}N_4O_{14}$ [M - TPFB]⁺: m/z 1519.4500; found: m/z 1519.4415 (error 5.6 ppm)

NB[(EO)₁Im_{butyl} AOT]₂ (8b). To a flask containing acetone (40 mL) was added **5** (1.21 g, 1.88 mmol) and dioctyl sulfosuccinate sodium salt (AOT) (2.10 g, 4.72 mmol) with magnetic stirring under nitrogen. The reaction mixture was held at reflux for 20 h, after which the solvent was removed by rotary evaporation. The remaining material was taken up in DCM and filtered. The solvent was removed by rotary evaporation and the desired product was collected as an oil (1.36 g, 55%). ¹H NMR (500 MHz, DMSO-*d*₆) δ 9.24–9.17 (m, 2H), 7.87–7.74 (m, 4H), 6.22 (m, 2H),

4.48–4.42 (m, 8H), 4.23–4.19 (m, 8H), 3.95–3.83 (m, 20H), 3.65 (dd, $J = 12, 4$ Hz, 4H), 2.96–2.91 (m, 6H), 2.89 (s, 2H), 2.82 (d, $J = 4$ Hz, 3H), 2.79 (d, $J = 4$ Hz, 2H), 2.62 (d, $J = 2$ Hz, 2H), 1.77 (p, $J = 8$ Hz, 6H), 1.70 (d, $J = 9$ Hz, 2H), 1.50 (bs, 10H), 1.41–1.13 (m, 30H), 0.94–0.79 (m, 22H). ^{13}C NMR (126 MHz, DMSO- d_6) δ 172.92, 171.48, 168.83, 138.18, 137.05, 136.78, 123.23, 122.99, 122.63, 66.65, 66.58, 66.55, 66.51, 62.78, 61.89, 59.74, 52.12, 49.08, 48.94, 48.46, 46.94, 45.56, 45.20, 38.64, 38.59, 38.56, 34.55, 31.86, 30.20, 30.08, 30.02, 28.80, 23.65, 23.62, 23.47, 23.44, 22.88, 22.85, 19.25, 19.19, 14.37, 14.35, 13.74, 11.27, 11.24, 11.20 (34 signals expected considering a single isomer of AOT, but AOT contains eight stereoisomers at three chiral centers, 46 signals found with many appearing to overlap). HR MS: calc. for $\text{C}_{67}\text{H}_{114}\text{N}_4\text{O}_{18}\text{S}_2$ $[\text{M} + \text{Na}]^+$: m/z 1349.7462; found: m/z 1349.7467 (error -0.4 ppm)

NB[(EO)₁Im_{butyl} DDS]₂ (8c). To a flask containing acetone (20 mL) was added **5** (0.78 g, 1.2 mmol) and dodecyl sodium sulfate (DDS) (0.88 g, 3.1 mmol) with magnetic stirring under nitrogen. The reaction mixture was held at reflux for 20 h, after which the solvent was removed by rotary evaporation. The remaining material was taken up in DCM and filtered. The solvent was removed by rotary evaporation and the desired product was collected as a viscous oil (0.96 g, 83%). ^1H NMR (400 MHz, DMSO- d_6) δ 9.28 (t, $J = 2$ Hz, 2H), 7.85–7.81 (m, 4H), 6.20 (t, $J = 2$ Hz, 2H), 4.42–4.40 (m, 4H), 4.21–4.17 (m, 8H), 3.65 (t, $J = 7$ Hz, 2H), 2.92–2.91 (m, 2H), 2.60 (d, $J = 1.8$ Hz, 2H), 1.82–1.64 (m, 8H), 1.50–1.39 (m, 4H), 1.22 (s, 30H), 0.93–0.80 (m, 24H). ^{13}C NMR (101 MHz, DMSO- d_6) δ 172.92, 138.16, 137.03, 123.21, 122.96, 65.95, 62.77, 59.70, 49.06, 48.45, 46.92, 45.54, 31.81, 31.74, 29.52, 29.51, 29.47, 29.23, 29.16, 25.97, 22.54, 19.16, 14.40, 13.74 (24 peaks expected and 24 peaks found). HR MS: calc. for $\text{C}_{47}\text{H}_{82}\text{N}_4\text{O}_{12}\text{S}_2$ $[\text{M} - 2 \text{ DDS}]^{+2}$: m/z 242.1520; found: m/z 242.1534 (error -5.8 ppm)

Bis(2-(1'-ethyl-[4',4'']-bipyridin)-1'-ium)) bicyclo[2.2.1]hept-5-ene-2,3-dicarboxylate (9). To a round bottom flask containing acetonitrile (40 mL) was added **5** (2.49 g, 6.27 mmol) and 4,4'-dipyridyl (6.57 g, 42.1 mmol) with magnetic stirring. The reaction mixture was held at reflux for 24 h. After cooling to room temperature the acetonitrile was decanted and the precipitate was washed with DCM (x 3) then dissolved in water. The aqueous solution was washed with DCM (x 3) and combined with an aqueous solution of TFSI (4.50 g, 15.7 mmol). The aqueous mixture was stirred briefly and allowed to sit until the product "oiled out" (approximately 7 h). The water was decanted and the oil was washed with water (x 3). The product was taken up in acetone and the solvent was removed after the product was isolated as a viscous oil: 2.34 g (34%). ¹H NMR (500 MHz, acetone-d₆) δ 9.37 (d, *J* = 7 Hz, 4H), 9.00 (d, 4H), 8.76 (d, *J* = 7 Hz, 4H), 8.17 (m, 4H), 6.20 (m, 2H), 5.31–5.16 (m, 4H), 4.86–4.75 (m, 2H), 4.72–4.63 (m, 2H), 3.05–3.01 (m, 2H), 2.73 (m, 2H), 1.78 (d, *J* = 9 Hz, 1H), 1.36 (d, *J* = 9 Hz, 1H). ¹³C NMR (126 MHz, acetone-d₆) δ 172.86 (s), 154.08 (s), 149.78 (s), 146.12 (s), 143.18 (s), 137.74 (s), 126.25 (s), 122.77 (s), 120.01 (q, *J* = 323 Hz), 62.92 (s), 60.38 (s), 47.06 (s), 45.48 (s), 44.93 (s) (13 signals expected and 13 major signals found). HR MS: calc. for C₃₇H₃₂N₆O₁₂S₄F₁₂ [M - TFSI]⁺: m/z 828.1591; found: m/z 828.1593 (error –0.2 ppm)

NB[(EO)₁PQCH₃ TFSI]₂ (10). To a flask containing acetonitrile (20 mL) was added **6** (2.34 g, 2.11 mmol) and methyl iodide (2.6 mL, 42 mmol) with magnetic stirring. The reaction mixture was heated to 35 °C where it was held for 3 days. The majority of solvent was removed by evaporation and the crude material was diluted with chloroform and filtered. The solid was washed with chloroform and added to a round bottom flask containing LiTFSI (1.50 g, 5.22 mmol) and acetone (40 mL). The mixture was refluxed for 3 days with magnetic stirring. The acetone was removed by rotary evaporation and the crude material was washed with water (x 4),

DCM (x 2), and then placed under vacuum to remove the remaining trace solvent; product was isolated as a viscous oil: 0.6762 g (19%). ^1H NMR (500 MHz, DMSO- d_6) δ 9.39 (d, $J = 7$ Hz, 4H), 9.31 (d, $J = 7$ Hz, 4H), 8.85 (d, $J = 7$ Hz, 4H), 8.78 (d, $J = 7$ Hz, 4H), 6.25–6.16 (m, 2H), 4.98 (s, 4H), 4.62 (m, 2H), 4.49–4.40 (m, 8H), 3.00–2.87 (m, 2H), 2.60 (m, 2H), 1.58 (m, $J = 9$ Hz, 1H), 1.28 (d, $J = 9$ Hz, 1H). ^{13}C NMR (126 MHz, DMSO- d_6) δ 172.91 (s), 149.67 (s), 148.43 (s), 147.17 (s), 146.83 (s), 138.17 (s), 126.87 (s), 126.59 (s), 119.93 (q, $J = 323$ Hz), 63.21 (s), 60.16 (s), 48.54 (s), 47.04 (s), 45.52 (s), 45.18 (s), 31.13 (s) (15 signals expected and 15 signals found). HR MS: calc. for $\text{C}_{43}\text{H}_{38}\text{N}_8\text{O}_{20}\text{S}_8\text{F}_{24}$ [$\text{M} - \text{TFSI}$] $^+$: m/z 1418.0406; found: m/z 1418.0426 (error -1.4 ppm)

NB[(EO) $_1$ PQCH $_3$ TFSI] $_2$ • 30crown10 (11). To a round bottom flask containing DCM (20 mL) were added **10** (0.6000 g, 0.3531 mmol) and 30-crown-10 (0.3111 g, 0.7062 mmol). The mixture was stirred at room temperature for 2 h followed by solvent removal via vacuum. The resulting material was collected as an oil (0.9111 g, 100%). Complexation was confirmed via ^1H NMR peak shifts (**Figure 13.2**). No complexation was observed via MS; this was attributed to a low binding constant and the dilute conditions of MS.

References

- (1) Lee, M.; Choi, U. H.; Salas-de la Cruz, D.; Mittal, A.; Winey, K. I.; Colby, R. H.; Gibson, H. W. *Adv. Funct. Mater.* **2011**, *21*, 708-717.
- (2) Choi, U. H.; Lee, M.; Wang, S.; Liu, W.; Winey, K. I.; Gibson, H. W.; Colby, R. H. *Macromolecules* **2012**, *45*, 3974-3985.
- (3) Choi, U. H.; Mittal, A.; Price Jr, T. L.; Lee, M.; Gibson, H. W.; Runt, J.; Colby, R. H. *Electrochim. Acta* **2015**, *175*, 55-61.
- (4) Kidd, B. E.; Lingwood, M. D.; Lee, M.; Gibson, H. W.; Madsen, L. A. *J. Phys. Chem. B* **2014**, *118*, 2176-2185.
- (5) Pederson, A. M. P.; Vctor, R. C.; Rouser, M. A.; Huang, F.; Slebodnick, C.; Schoonover, D. V.; Gibson, H. W. *J. Org. Chem.* **2008**, *73*, 5570-5573.
- (6) Pederson, A. M. P.; Ward, E. M.; Schoonover, D. V.; Slebodnick, C.; Gibson, H. W. *J. Org. Chem.* **2008**, *73*, 9094-9101.

- (7) Han, Y.; Cao, J.; Li, P.-F.; Zong, Q.-S.; Zhao, J.-M.; Guo, J.-B.; Xiang, J.-F.; Chen, C.-F. *J. Org. Chem.* **2013**, *78*, 3235-3242.
- (8) Han, Y.; Guo, J.; Cao, J.; Chen, C. *Chin. J. Chem.* **2013**, *31*, 607-611.
- (9) Chen, R.; Zhou, Q.; Zhang, B.; Wu, J.; Ye, Y.; Dai, G.; Jiang, H. *J. Polym. Sci., Part A: Polym. Chem.* **2015**, *53*, 1178-1181.
- (10) Ashton, P. R.; Ballardini, R.; Balzani, V.; Fyfe, M. C. T.; Gandolfi, M. T.; Martínez-Díaz, M. V.; Morosini, M.; Schiavo, C.; Shibata, K.; Stoddart, J. F.; White, A. J. P.; Williams, D. J. *Chem. Eur. J.* **1998**, *4*, 2332-2341.
- (11) Gibson, H. W.; Jones, J. W.; Zakharov, L. N.; Rheingold, A. L.; Slebodnick, C. *Chem. Eur. J.* **2011**, *17*, 3192-3206.

Chapter 14

Conclusions and Future Work

Given that this dissertation has focused in two major areas of work, cryptands and imidazolium monomers and polymers, the conclusions and future work chapter will be divided into two parts. Part 1 focuses on novel ideas revolving around cryptands, while part 2 concentrates on imidazolium monomers, polymers, and actuators.

Conclusions

Part 1:

Three new pseudo cryptands were successfully developed and characterized. The binding strength of these pseudocryptands was assessed with paraquat and diquat; results were modest.

Two major items have hindered the use of pyridyl cryptands: first a long synthesis that is moderate yielding and secondly a lack of functionalized precursors. A successful methodology was developed for the syntheses of pyridyl cryptands based on dibenzo-30-crown-10 and bis(*m*-phenylene)-32-crown-10. These syntheses took advantage of pyridinium TFSI to template the reaction. Optimal reaction conditions were determined to be ~6 equivalents of template with substrate concentrations of ~0.6 mM and ~2.5 equivalents of pyridine in DCM; yields as high as 89% were obtained for the pyridyl cryptand based on dibenzo-30-crown-10. Additionally, pyridinium TFSI was found to have association constants with pyridyl cryptands in the range of 10^4 , as determined by ITC in DCM at room temperature. Additionally, 27 new chelidamic feedstock molecules were developed to allow for functionality to be added to pyridyl cryptands.

Targeting the guest paraquat, binding with pyridyl cryptands was advanced through alterations of the paraquat salt, including changing the anion and nitrogen substituted group. Results revealed association constants in the range of 10^6 could be obtained with pyridyl cryptands based on dibenzo-30-crown-10 when the anion of paraquat was changed to TFSI, the nitrogen substituent changed to a benzyl group and the solvent changed to DCM.

Four (4) new monofunctionalized cryptands and five (5) new biscryptands were successfully synthesized and characterized. Using two biscryptands, chosen due to ease of synthesis, paired with three bisparaquat monomers, five (5) supramolecular polymers were synthesized. Characterization of the supramolecular polymers included DSC, TGA, light scattering and solution viscosity. T_g s ranged from 44 °C to 112 °C and all 5% wt. loss values were grouped in the range of 217°C - 224°C. Solution viscosity for one of the supramolecular polymers yielded a critical monomer concentration at 63 mM and the slope of a log concentration vs. log specific viscosity plot at higher concentration was found to be 3.55, the theoretical maximum.

Part 2:

A matrix of norbornene imidazolium TFSI monomers was developed. Monomers were designed to contain ethyleneoxy linkages both before and after the pendant imidazolium group. Evidence was found to suggest that the ethyleneoxy units aid in the stabilization of the imidazolium cation, thus producing a higher fraction of free anions. Ethyleneoxy unit lengths were varied both before and after the imidazolium group. It was determined the longer the linkage between the norbornene and imidazolium moieties, the better the conductivity, while a tail of two ethyleneoxy units was found to be optimal. The highest conductivity monomer tested

had a linkage of four ethyleneoxy units and a tail of two; this monomer was found to have a conductivity of 9.57×10^{-5} S/cm and a T_g of -46 °C.

Extending the norbornene imidazolium TFSI monomers, ROMP was used to produce several corresponding homopolymers, using the Grubbs first generation catalyst. It was determined that monomer conductivity and T_g ranges could be maintained in polymeric systems when monomers containing at least two ethyleneoxy units were used. The highest conducting homopolymer had a molecular weight of 45 kDa, T_g of -39 °C and a conductivity of 2.27×10^{-5} S/cm; the corresponding monomer contained a spacer of four ethyleneoxy units and a tail of two. Additionally, ROMP employing the Grubbs first generation catalyst was shown to be living.

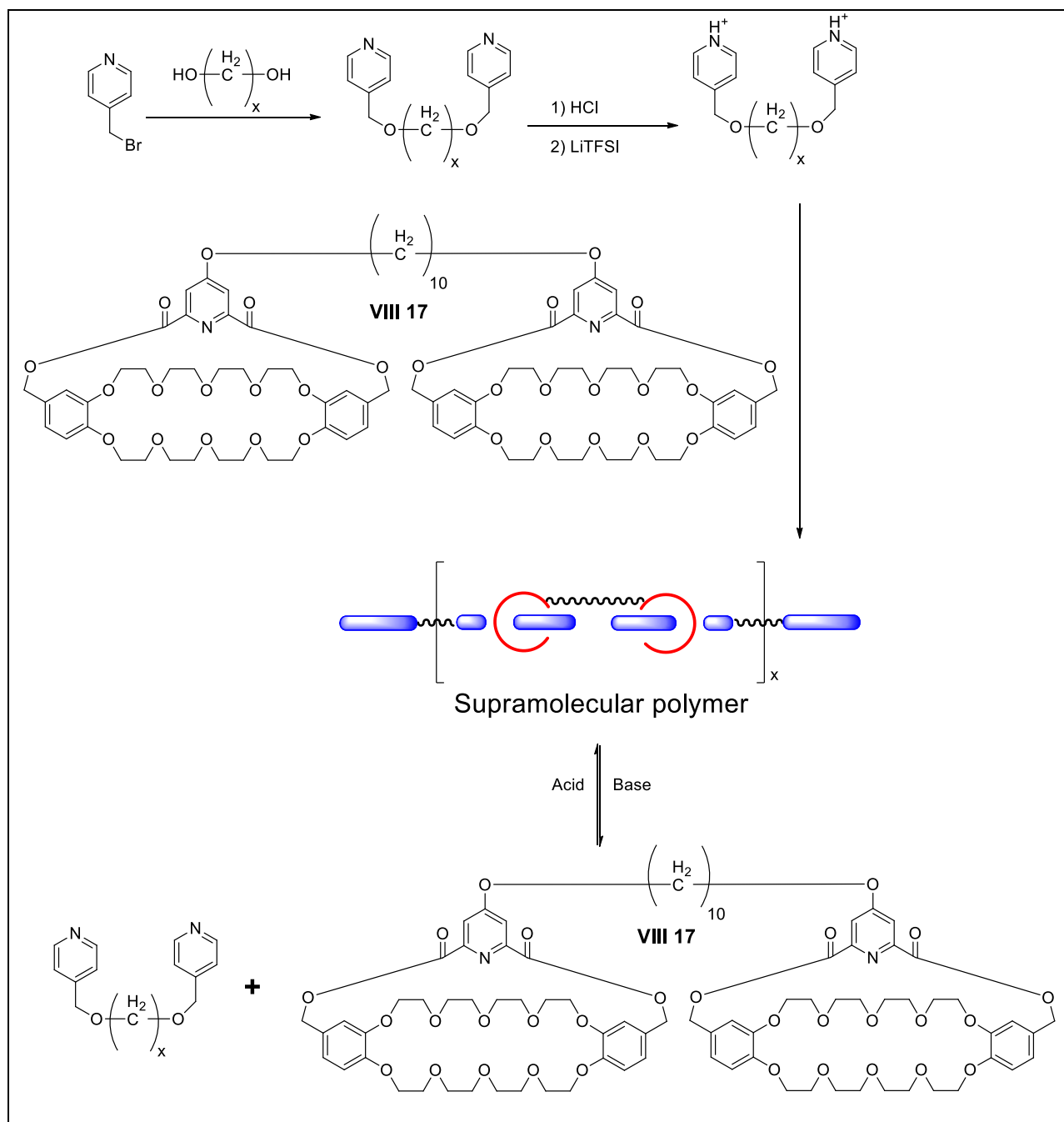
Using the norbornene imidazolium TFSI monomers, two ABA triblock copolymers were produced with a selected hard segment monomer as A and the norbornene imidazolium TFSI monomers as the soft segment monomer B. The copolymers were found to be creasable and capable of single direction actuation.

Future Work

Part 1:

Chapter 3 was fundamental in the development of an efficient method for the synthesis of pyridyl cryptands. Work made use of the pyridinium cation to form a template for the cyclization reaction and decent yield gains were achieved. Using ITC, binding constants for the cryptands were measured with the template pyridinium TFSI; all were found to be in the range of 10^4 at room temperature using DCM. Association constants in the range of 10^4 would be adequate for the production of supramolecular polymers. Given the range of commercially available pyridine derivatives and the ease with which a pyridinium cation may be deprotonated,

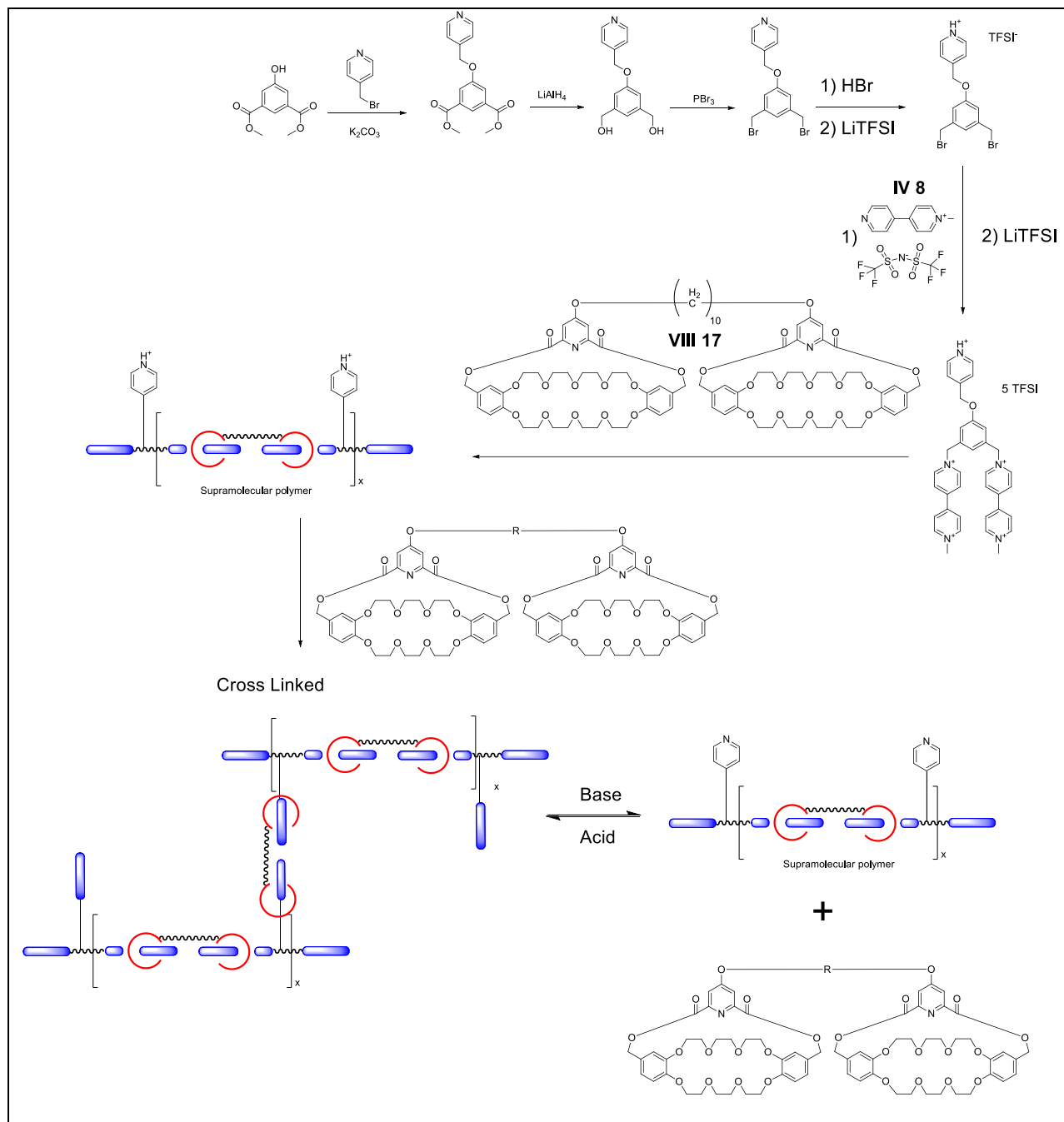
the production of difunctional pyridinium molecules could prove a reasonable direction to pursue. Bipyridinium cations (or higher) could be combined with the previously developed biscryptands of this dissertation to give switchable supramolecular polymers. That is, supramolecular polymers which can be easily turned back to monomers through the addition of a mild base or switched back to the polymeric system through the addition of acid. **Scheme 14.1** shows an example of a proposed switchable system using the pyridinium cation.



Scheme 14.1. Proposed switchable supramolecular polymer employing a difunctional pyridinium and biscryptand **VIII 17**.

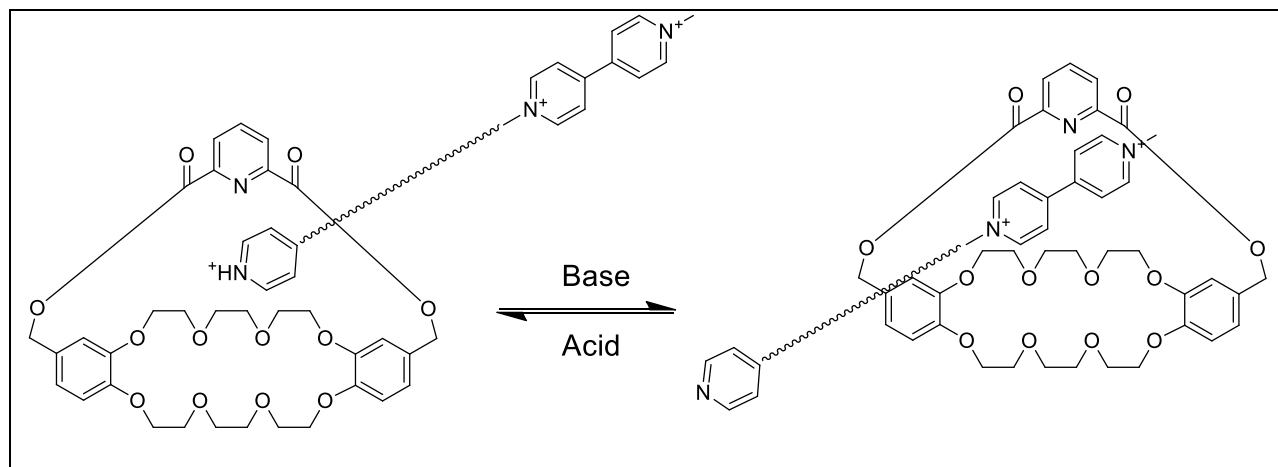
In a similar manner a bispyridinium salt could also allow for an intricate supramolecular polymer that contains a switchable crosslink. **Scheme 14.2** shows a simple example in which the biscryptand **VIII 17** is employed alongside a bis(24-crown-10-cryptand). **VIII 17** (as reported in

this dissertation) is higher binding with paraquat than the indicated 24-crown-10-cryptand, while the latter is higher binding with pyridinium salts than **VIII 17**. Stacking the motifs properly could allow for the crosslink to be switched back and forth from on to off with acid and base.



Scheme 14.2. Proposed switchable crosslink.

In chapter 3, the dibenzo-24-crown-8-based pyridyl cryptand was found to have an association constant in DCM of $8.69 \times 10^4 \text{ M}^{-1}$ with pyridinium TFSI. Additionally, chapter 4 showed that changing the solvent from acetone to DCM offered a ~20% increase in association constants (with tested systems). The literature reported association constant of dibenzo-24-crown-8-based pyridyl cryptand with paraquat is $1 \times 10^4 \text{ M}^{-1}$ in acetone at room temperature.¹ Given this, the association constant of the dibenzo-24-crown-8 pyridyl cryptand • pyridinium TFSI system should be assessed in acetone. If the association constant of the pyridinium TFSI system is higher than paraquat PF₆, a workable unit could be produced and controlled via acid-base treatments, as seen in **Scheme 14.3**. The system would work off the offset in association constants. Additionally, this system could be incorporated into a polymeric system and exploited to produce a material that could controllably move with external stimuli.



Scheme 14.3. Proposed workable unit.

Reviewing chapter 2 and referenced literature,^{2,3} it can be seen that pseudocryptands offer an ease of synthesis and when properly designed, significant increases in the association constants can be achieved. Given this and the development of a templated procedure for pyridyl

cryptands, found in chapter 3, alongside the functionalized cryptands found in chapters 6 and 7, an opportunity exists to be “first” to produce high binding cryptands assisted via a functionalized arm. If an arm could be tethered to a cryptand that could assist in binding, association constants could be increased even further. **Figure 14.1** shows what a cryptand with an arm assisting in binding might look like.

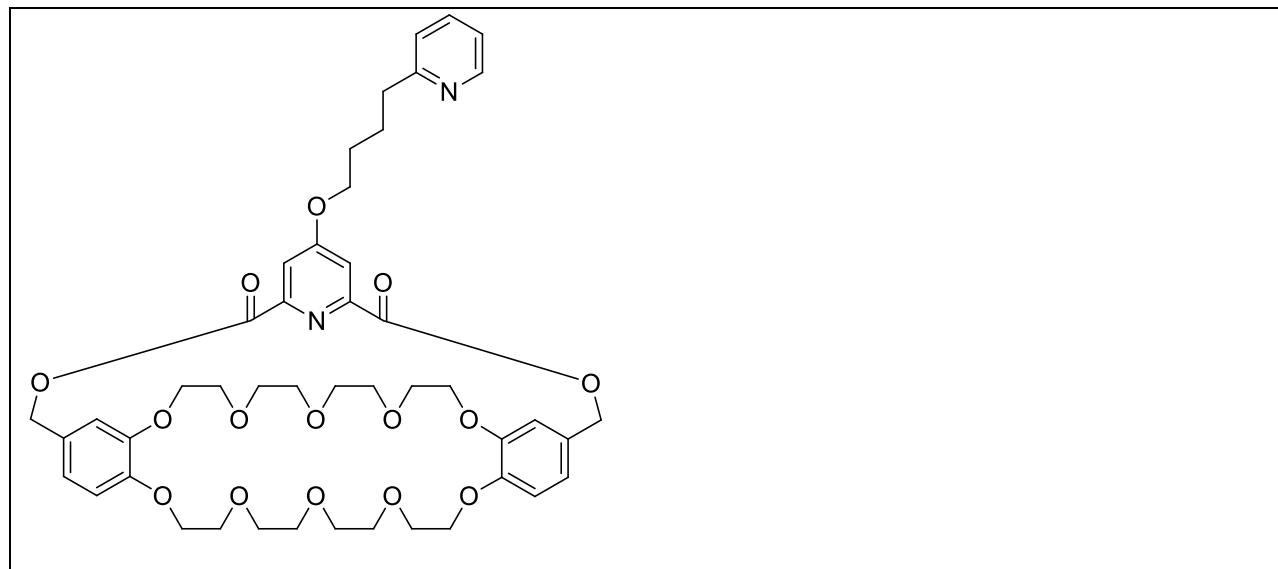
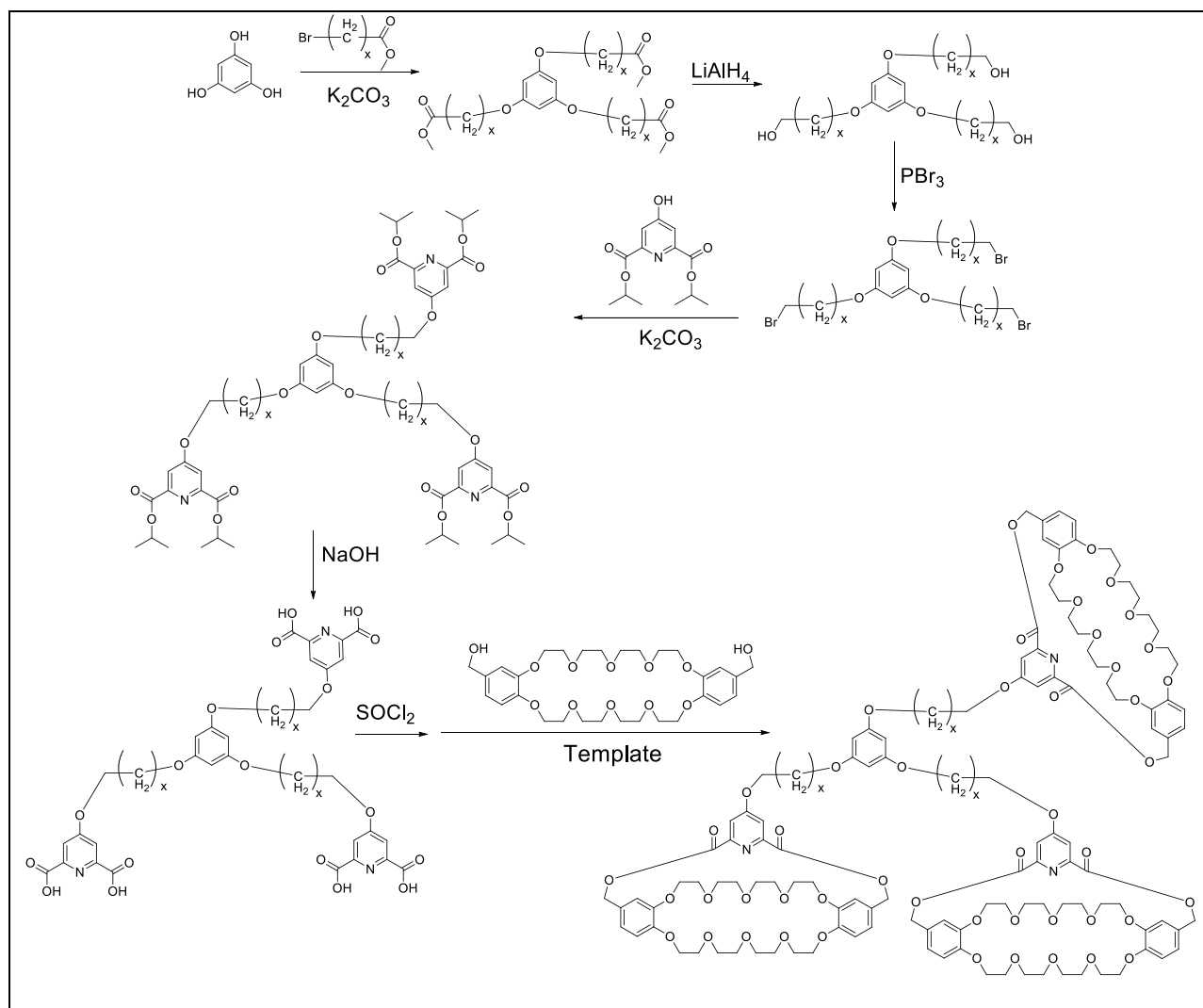


Figure 14.1. Generic structure of an arm that may assist in the binding of a guest.

Chapter 5 provided a wealth of functionalized chelidamic acid compounds, most of which were intended for the production of cryptands. A clear direction of future work would be to adopt these compounds and use the templated cryptand procedure found in chapter 3 to synthesize a range of highly desirable cryptands.

Chapter 7 ultimately focused on the production of biscryptands through a dual cyclization templated procedure. The next step for this work would be to attempt a tri- or tetra- cyclization, to produce either a three- or four bridge cryptand. Reviewing chapter 7 it can be seen that yields in the range of 40% were achievable for a dual cyclization; although likely to be much lower, a tri- or tetra- cyclization would provide valuable compounds. The increased functionality of a tri-

or tetracrypand could then be used to produce hyperbranched or star polymers. **Scheme 14.4** provides an example proposed synthesis for a tricryptand.



Scheme 14.4. Proposed synthesis for a tricryptand.

As indicated in chapter 8, the supramolecular polymers produced displayed a disparity between cast films and drawn fibers. It is suspected that this disparity is a result of one component precipitating before the other during film casting; see chapter 8 for a discussion. The logical next step for this work would be to pursue a casting technique which rapidly removes

solvent, such as spin casting. Employing such a casting technique could allow for less variance between films and fibers.

Additionally, chapter 8 showed a large variation in T_g values obtained from polymers containing PF_6 and TFSI salts. Work should be conducted to conclude whether mixed ratios of different anions (mixing bisparaquat PF_6 with bisparaquat TFSI) could net a system in which any T_g between the two values could be obtained. If successful, several other bisparaquats containing a range of counter ions could be synthesized. Such a semi-custom system could aid in the widespread adoption of these supramolecular polymers, given that an exactly desired T_g could be easily synthesized.

Part 2:

Considering the imidazolium actuators developed in this dissertation, if triblock copolymers are to be used further, advanced techniques in casting or a careful variation of hard to soft segment ratios will need to be explored to obtain well-defined phases. Additionally, although single direction actuation was sought, research could follow suit with the bulk of published literature and swell the triblock copolymers with an ionic liquid to develop a dual direction actuator.

Chapter 13 investigated variations to the imidazolium TFSI salt combination currently being employed. We concluded that the imidazolium TFSI combination was advantageous for conductivity, mainly because changing the TFSI counter anion resulted in significant increases in the T_g s. Given that actuation occurs due to the change in free volume, a potential direction for future work could be investigating extremely large counterions to maximize the observed volume change. **Figure 14.2** shows three extremely large counterions which are commercially available;

BARF and TPFB were explored in chapter 13. Although work from chapter 13 shows that these large ions increase the T_g of the resulting material significantly, thereby lowering conductivity, there is a question as to whether the larger volume change could offset the loss of conductivity in terms of actuation. Clearly a single molecule of HFPB with a molecular weight of 1760 g / mol would offer a greater volume change than TFSI with a molecular weight of 280 g / mol. A massive anion such as HFPB may provide remarkable results in terms of actuation. Thus it is suggested that an ABA triblock copolymer should be produced, as in chapter 12, using the larger anions shown in **Figure 14.2**.

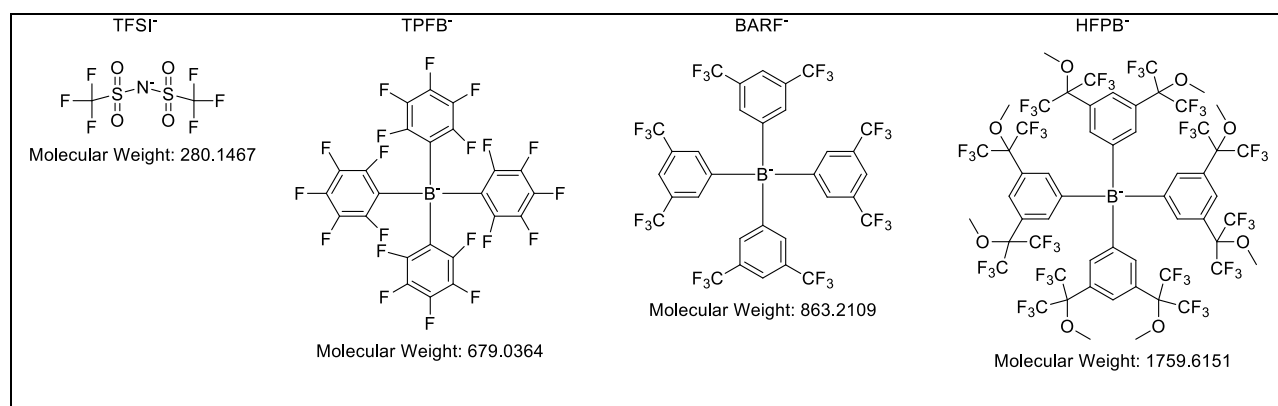


Figure 14.2. Large commercially available counterions.

References

- (1) Gibson, H. W.; Wang, H.; Slebodnick, C.; Merola, J.; Kassel, W. S.; Rheingold, A. L. *J. Org. Chem.* **2007**, *72*, 3381-3393.
- (2) Niu, Z.; Slebodnick, C.; Schoonover, D.; Azurmendi, H.; Harich, K.; Gibson, H. W. *Org. Lett.* **2011**, *13*, 3992-3995.
- (3) Niu, Z.; Price Jr, T. L.; Slebodnick, C.; Gibson, H. W. *Tetrahedron Lett.* **2016**, *57*, 60-63.

Appendix

X-ray crystallography

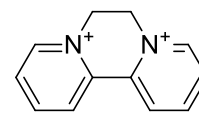
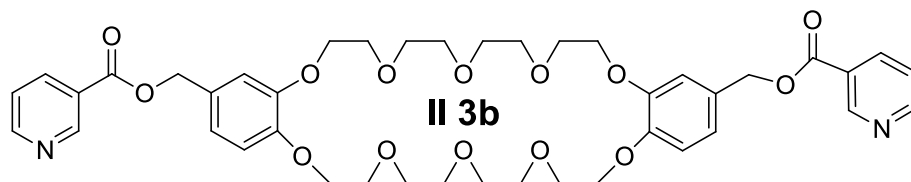
Procedure

An orange plate (0.02 x 0.25 x 0.49 mm³) was centered on the goniometer of a Rigaku Oxford Diffraction Nova diffractometer operating with CuK α radiation. The data collection routine, unit cell refinement, and data processing were carried out with the program CrysAlisPro.¹ The Laue symmetry was consistent with the triclinic space groups P1 and P-1. The centric space group P-1 was chosen. The structure was solved using SHELXT-2014² and refined using SHELXL-2014³ via Olex2.⁴ In the original structure model, the size and shape of the anisotropic displacement parameters and the presence of large residual electron density peaks suggested disorder in both polyether chains, both PF₆ anions, the acetone solvates. Attempts to model this disorder were only partially successful. A 2-position disorder model was used for the polyether chain and one PF₆ anion with relative occupancies refined to 0.508(12)/0.492(12) for polyether chain atoms C21 – C27, 0.506(16)/0.494(16) for polyether chain atoms C15 – C16, and 0.525(7)/0.475(7) for the PF₆ anion comprising P2 – F6. Further attempts to model disorder did not improve the model, presumably because the disorder is a both dynamic and static. The relatively large residual electron density peaks are attributed to incomplete modeling of the disorder. The final refinement model involved anisotropic displacement parameters for non-hydrogen atoms and a riding model for all hydrogen atoms. A rigid body displacement ellipsoid restraint (RIGU) was used for all atoms modeled with 2-position disorder.

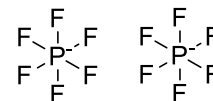
CrysAlisPro Software System, v1.171.37.35, Rigaku Oxford Diffraction, **2015**, Rigaku Corporation, Oxford, UK.
Sheldrick, G. M. "SHELXT – Integrated space-group and crystal structure determination." *Acta Cryst.* **2015**, A71, 3–8.
Sheldrick, G. M. "A short history of SHELX." *Acta Cryst.* **2008**, A64, 112-122.
Dolomanov, O.V.; Bourhis, L. J.; Gildea, R. J.; Howard, J. A. K.; Puschmann, H. *J. Appl. Cryst.* **2009**, **42**, 339–341.

X-ray crystallography tables

Chapter 2



Diquat PF₆



Crystal structure of **3b** • DQ PF₆ was grown by slow vapor diffusion of ether into an acetone equimolar solution.

Table A.1. Crystal data and structure refinement for cs2219.

Identification code	cs2219	
Empirical formula	[C ₄₂ H ₅₀ N ₂ O ₁₄ • C ₁₂ H ₁₂ N ₂][PF ₆] ₂ • 2(C ₃ H ₆ O)	
Formula weight	1397.17	
Temperature	100.00(10) K	
Wavelength	1.54184 Å	
Crystal system	Triclinic	
Space group	<i>P</i> -1	
Unit cell dimensions	<i>a</i> = 13.4306(4) Å	<i>α</i> = 100.240(2)°.
	<i>b</i> = 15.1390(5) Å	<i>β</i> = 110.402(3)°.
	<i>c</i> = 17.0352(4) Å	<i>γ</i> = 92.464(3)°.
Volume	3173.95(17) Å ³	
<i>Z</i>	2	
Density (calculated)	1.462 Mg/m ³	
Absorption coefficient	1.559 mm ⁻¹	
F(000)	1456	
Crystal size	0.488 x 0.247 x 0.022 mm ³	
Theta range for data collection	2.986 to 74.990°.	
Index ranges	-16 ≤ <i>h</i> ≤ 16, -18 ≤ <i>k</i> ≤ 18, -13 ≤ <i>l</i> ≤ 21	
Reflections collected	36146	
Independent reflections	12786 [R(int) = 0.0472]	
Completeness to theta = 67.000°	99.6 %	

Absorption correction	Gaussian
Max. and min. transmission	0.966 and 0.651
Refinement method	Full-matrix least-squares on F ²
Data / restraints / parameters	12786 / 261 / 1016
Goodness-of-fit on F ²	1.480
Final R indices [I>2sigma(I)]	R1 = 0.1165, wR2 = 0.3404
R indices (all data)	R1 = 0.1377, wR2 = 0.3822
Extinction coefficient	n/a
Largest diff. peak and hole	1.822 and -0.981 e.Å ⁻³

Table A.2. Bond lengths [Å] and angles [°] for cs2219.

O(1)-C(1)	1.369(5)	O(8B)-C(24B)	1.423(15)	C(7)-C(8)	1.417(5)
O(1)-C(13)	1.436(4)	O(8B)-C(25B)	1.359(17)	C(7)-C(12)	1.385(6)
O(2)-C(14)	1.403(10)	O(9B)-C(26B)	1.431(10)	C(8)-C(9)	1.382(5)
O(2)-C(15A)	1.533(9)	O(9B)-C(27B)	1.445(14)	C(9)-C(10)	1.389(5)
O(2)-C(15B)	1.488(10)	O(10)-C(8)	1.363(5)	C(10)-C(11)	1.383(5)
O(3)-C(16A)	1.549(13)	O(10)-C(28)	1.450(4)	C(10)-C(36)	1.516(5)
O(3)-C(16B)	1.351(14)	O(11)-C(29)	1.460(5)	C(11)-C(12)	1.397(6)
O(3)-C(17)	1.396(10)	O(11)-C(30)	1.334(5)	C(13)-C(14)	1.493(7)
O(4)-C(18)	1.429(7)	O(12)-C(30)	1.209(5)	C(15A)-C(16A)	1.456(18)
O(4)-C(19)	1.398(8)	O(13)-C(36)	1.458(5)	C(15B)-C(16B)	1.534(16)
O(5)-C(7)	1.371(5)	O(13)-C(37)	1.334(4)	C(17)-C(18)	1.466(12)
O(5)-C(20)	1.447(4)	O(14)-C(37)	1.205(4)	C(19)-C(20)	1.499(8)
O(6)-C(2)	1.372(5)	N(1)-C(32)	1.319(5)	C(21A)-C(22A)	1.41(2)
O(6)-C(21A)	1.41(2)	N(1)-C(33)	1.333(6)	C(23A)-C(24A)	1.458(17)
O(6)-C(21B)	1.465(14)	N(2)-C(39)	1.332(7)	C(25A)-C(26A)	1.482(17)
O(7A)-C(22A)	1.396(18)	N(2)-C(40)	1.313(10)	C(27A)-C(28)	1.639(13)
O(7A)-C(23A)	1.434(13)	C(1)-C(2)	1.413(5)	C(21B)-C(22B)	1.485(19)
O(8A)-C(24A)	1.434(11)	C(1)-C(6)	1.388(6)	C(23B)-C(24B)	1.44(2)
O(8A)-C(25A)	1.405(13)	C(2)-C(3)	1.387(6)	C(25B)-C(26B)	1.48(2)
O(9A)-C(26A)	1.448(14)	C(3)-C(4)	1.391(7)	C(27B)-C(28)	1.372(14)
O(9A)-C(27A)	1.433(15)	C(4)-C(5)	1.391(6)	C(30)-C(31)	1.488(5)
O(7B)-C(22B)	1.52(2)	C(4)-C(29)	1.497(7)	C(31)-C(32)	1.400(6)
O(7B)-C(23B)	1.460(17)	C(5)-C(6)	1.393(6)	C(31)-C(35)	1.379(5)

C(33)-C(34)	1.380(6)	C(46)-C(47)	1.386(5)	P(2A)-F(9A)	1.582(9)
C(34)-C(35)	1.376(6)	C(47)-C(48)	1.478(4)	P(2A)-F(10A)	1.573(6)
C(37)-C(38)	1.491(5)	C(48)-C(49)	1.372(5)	P(2A)-F(11A)	1.582(9)
C(38)-C(39)	1.381(7)	C(49)-C(50)	1.385(6)	P(2A)-F(12A)	1.585(10)
C(38)-C(42)	1.369(6)	C(50)-C(51)	1.370(7)	P(2B)-F(8B)	1.628(11)
C(40)-C(41)	1.350(11)	C(51)-C(52)	1.382(6)	P(2B)-F(9B)	1.795(14)
C(41)-C(42)	1.397(7)	C(53)-C(54)	1.509(6)	P(2B)-F(10B)	1.579(10)
N(3)-C(43)	1.353(5)	P(1)-F(1)	1.578(8)	P(2B)-F(11B)	1.532(12)
N(3)-C(47)	1.357(5)	P(1)-F(2)	1.635(9)	P(2B)-F(12B)	1.570(10)
N(3)-C(54)	1.481(5)	P(1)-F(3)	1.488(7)	O(16)-C(59)	1.200(7)
N(4)-C(48)	1.371(5)	P(1)-F(4)	1.690(8)	C(58)-C(59)	1.435(14)
N(4)-C(52)	1.334(5)	P(1)-F(5)	1.483(7)	C(59)-C(60)	1.487(12)
N(4)-C(53)	1.479(5)	P(1)-F(6)	1.571(7)	O(15)-C(56)	1.215(9)
C(43)-C(44)	1.390(7)	F(7)-P(2A)	1.593(5)	C(55)-C(56)	1.468(11)
C(44)-C(45)	1.372(8)	F(7)-P(2B)	1.534(7)	C(56)-C(57)	1.432(15)
C(45)-C(46)	1.391(6)	P(2A)-F(8A)	1.615(8)		

C(1)-O(1)-C(13)	116.2(3)	C(40)-N(2)-C(39)	116.6(6)
C(14)-O(2)-C(15A)	94.4(6)	O(1)-C(1)-C(2)	115.7(4)
C(14)-O(2)-C(15B)	129.2(6)	O(1)-C(1)-C(6)	124.9(3)
C(16B)-O(3)-C(17)	95.9(7)	C(6)-C(1)-C(2)	119.3(4)
C(17)-O(3)-C(16A)	127.6(7)	O(6)-C(2)-C(1)	115.4(4)
C(19)-O(4)-C(18)	114.7(4)	O(6)-C(2)-C(3)	125.3(3)
C(7)-O(5)-C(20)	115.5(3)	C(3)-C(2)-C(1)	119.3(4)
C(2)-O(6)-C(21A)	111.5(9)	C(2)-C(3)-C(4)	121.0(3)
C(2)-O(6)-C(21B)	120.4(7)	C(3)-C(4)-C(5)	119.6(4)
C(22A)-O(7A)-C(23A)	117.0(12)	C(3)-C(4)-C(29)	119.2(4)
C(25A)-O(8A)-C(24A)	114.7(8)	C(5)-C(4)-C(29)	121.2(5)
C(27A)-O(9A)-C(26A)	111.1(9)	C(4)-C(5)-C(6)	119.9(4)
C(23B)-O(7B)-C(22B)	115.7(9)	C(1)-C(6)-C(5)	120.7(3)
C(25B)-O(8B)-C(24B)	111.3(9)	O(5)-C(7)-C(8)	115.9(3)
C(26B)-O(9B)-C(27B)	111.3(9)	O(5)-C(7)-C(12)	125.2(3)
C(8)-O(10)-C(28)	116.4(3)	C(12)-C(7)-C(8)	118.8(4)
C(30)-O(11)-C(29)	114.1(3)	O(10)-C(8)-C(7)	115.8(3)
C(37)-O(13)-C(36)	115.3(3)	O(10)-C(8)-C(9)	124.1(3)
C(32)-N(1)-C(33)	117.0(3)	C(9)-C(8)-C(7)	120.1(3)

C(8)-C(9)-C(10)	120.7(3)	C(32)-C(31)-C(30)	122.3(4)
C(9)-C(10)-C(36)	118.2(3)	C(35)-C(31)-C(30)	118.9(3)
C(11)-C(10)-C(9)	119.4(4)	C(35)-C(31)-C(32)	118.7(4)
C(11)-C(10)-C(36)	122.3(4)	N(1)-C(32)-C(31)	123.3(4)
C(10)-C(11)-C(12)	120.7(4)	N(1)-C(33)-C(34)	124.1(4)
C(7)-C(12)-C(11)	120.3(3)	C(35)-C(34)-C(33)	118.6(4)
O(1)-C(13)-C(14)	108.3(3)	C(34)-C(35)-C(31)	118.4(3)
O(2)-C(14)-C(13)	110.6(4)	O(13)-C(36)-C(10)	111.7(3)
C(16A)-C(15A)-O(2)	98.6(8)	O(13)-C(37)-C(38)	111.8(3)
C(15A)-C(16A)-O(3)	114.7(9)	O(14)-C(37)-O(13)	124.7(3)
O(2)-C(15B)-C(16B)	107.3(7)	O(14)-C(37)-C(38)	123.5(3)
O(3)-C(16B)-C(15B)	100.5(7)	C(39)-C(38)-C(37)	122.6(4)
O(3)-C(17)-C(18)	108.4(5)	C(42)-C(38)-C(37)	119.4(4)
O(4)-C(18)-C(17)	109.8(5)	C(42)-C(38)-C(39)	118.0(4)
O(4)-C(19)-C(20)	108.9(4)	N(2)-C(39)-C(38)	124.2(5)
O(5)-C(20)-C(19)	109.2(4)	N(2)-C(40)-C(41)	124.1(5)
C(22A)-C(21A)-O(6)	102.2(15)	C(40)-C(41)-C(42)	119.4(6)
O(7A)-C(22A)-C(21A)	113.8(17)	C(38)-C(42)-C(41)	117.7(5)
O(7A)-C(23A)-C(24A)	109.7(10)	C(43)-N(3)-C(47)	121.3(4)
O(8A)-C(24A)-C(23A)	107.5(9)	C(43)-N(3)-C(54)	119.9(3)
O(8A)-C(25A)-C(26A)	113.2(10)	C(47)-N(3)-C(54)	118.7(3)
O(9A)-C(26A)-C(25A)	110.9(10)	C(48)-N(4)-C(53)	119.6(3)
O(9A)-C(27A)-C(28)	116.1(9)	C(52)-N(4)-C(48)	121.4(3)
O(6)-C(21B)-C(22B)	111.9(12)	C(52)-N(4)-C(53)	118.9(3)
C(21B)-C(22B)-O(7B)	108.0(10)	N(3)-C(43)-C(44)	120.1(4)
C(24B)-C(23B)-O(7B)	111.7(10)	C(45)-C(44)-C(43)	119.3(4)
O(8B)-C(24B)-C(23B)	108.6(10)	C(44)-C(45)-C(46)	120.1(4)
O(8B)-C(25B)-C(26B)	109.1(9)	C(47)-C(46)-C(45)	119.1(4)
O(9B)-C(26B)-C(25B)	110.2(9)	N(3)-C(47)-C(46)	119.9(3)
C(28)-C(27B)-O(9B)	103.6(8)	N(3)-C(47)-C(48)	119.1(3)
O(10)-C(28)-C(27A)	107.6(6)	C(46)-C(47)-C(48)	121.0(3)
C(27B)-C(28)-O(10)	108.6(6)	N(4)-C(48)-C(47)	117.9(3)
O(11)-C(29)-C(4)	107.9(4)	N(4)-C(48)-C(49)	118.8(3)
O(11)-C(30)-C(31)	111.5(3)	C(49)-C(48)-C(47)	123.3(3)
O(12)-C(30)-O(11)	125.0(4)	C(48)-C(49)-C(50)	120.1(4)
O(12)-C(30)-C(31)	123.5(4)	C(51)-C(50)-C(49)	119.8(4)

C(50)-C(51)-C(52)	119.0(3)	F(7)-P(2B)-F(10B)	78.5(5)
N(4)-C(52)-C(51)	120.8(4)	F(7)-P(2B)-F(12B)	163.2(7)
N(4)-C(53)-C(54)	108.3(3)	F(8B)-P(2B)-F(9B)	171.0(6)
N(3)-C(54)-C(53)	108.1(3)	F(10B)-P(2B)-F(8B)	90.1(6)
F(1)-P(1)-F(2)	85.5(4)	F(10B)-P(2B)-F(9B)	86.9(5)
F(1)-P(1)-F(4)	167.4(5)	F(11B)-P(2B)-F(7)	98.6(7)
F(2)-P(1)-F(4)	82.8(5)	F(11B)-P(2B)-F(8B)	92.2(8)
F(3)-P(1)-F(1)	90.5(5)	F(11B)-P(2B)-F(9B)	90.4(9)
F(3)-P(1)-F(2)	91.3(5)	F(11B)-P(2B)-F(10B)	176.2(10)
F(3)-P(1)-F(4)	85.2(4)	F(11B)-P(2B)-F(12B)	97.4(8)
F(3)-P(1)-F(6)	172.8(6)	F(12B)-P(2B)-F(8B)	88.1(6)
F(5)-P(1)-F(1)	111.0(6)	F(12B)-P(2B)-F(9B)	100.2(7)
F(5)-P(1)-F(2)	161.0(6)	F(12B)-P(2B)-F(10B)	85.7(7)
F(5)-P(1)-F(3)	97.7(4)	O(16)-C(59)-C(58)	121.6(8)
F(5)-P(1)-F(4)	81.4(6)	O(16)-C(59)-C(60)	122.6(9)
F(5)-P(1)-F(6)	85.3(4)	C(58)-C(59)-C(60)	115.2(8)
F(6)-P(1)-F(1)	94.6(5)	O(15)-C(56)-C(55)	120.7(9)
F(6)-P(1)-F(2)	84.0(5)	O(15)-C(56)-C(57)	123.8(8)
F(6)-P(1)-F(4)	88.7(5)	C(57)-C(56)-C(55)	115.5(7)
F(7)-P(2A)-F(8A)	87.7(4)		
F(9A)-P(2A)-F(7)	77.1(4)		
F(9A)-P(2A)-F(8A)	90.2(5)		
F(9A)-P(2A)-F(12A)	177.3(7)		
F(10A)-P(2A)-F(7)	168.1(5)		
F(10A)-P(2A)-F(8A)	90.4(4)		
F(10A)-P(2A)-F(9A)	91.2(4)		
F(10A)-P(2A)-F(11A)	89.2(4)		
F(10A)-P(2A)-F(12A)	90.6(5)		
F(11A)-P(2A)-F(7)	94.1(4)		
F(11A)-P(2A)-F(8A)	172.4(6)		
F(11A)-P(2A)-F(9A)	97.4(6)		
F(11A)-P(2A)-F(12A)	80.8(6)		
F(12A)-P(2A)-F(7)	101.1(6)		
F(12A)-P(2A)-F(8A)	91.7(6)		
F(7)-P(2B)-F(8B)	86.3(4)		
F(7)-P(2B)-F(9B)	84.8(6)		

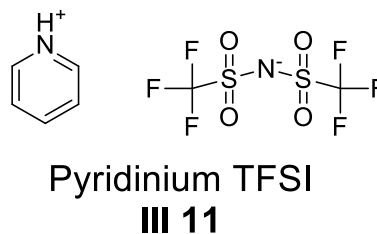
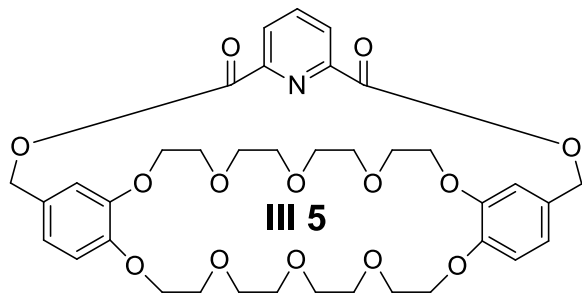
Table A.3. Hydrogen bonds for cs2219 [\AA and $^\circ$].

D-H...A	d(D-H)	d(H...A)	d(D...A)	\angle (DHA)
C(43)-H(43)...O(7A)	0.95	2.41	3.088(9)	128.5
C(52)-H(52)...O(4)	0.95	2.23	2.954(5)	132.3
C(54)-H(54A)...O(8A)	0.99	2.09	3.074(8)	170.4
C(55)-H(55A)...F(10B)#1	0.98	2.27	2.986(13)	129.3

Symmetry transformations used to generate equivalent atoms:

#1 x,y,z-1

Chapter 3



Crystal structure of **III 5** • **III 11** was grown by slow solvent evaporation of an equimolar chloroform solution.

Table A.4. Crystal data and structure refinement for cs2173.

Identification code	TP30CryPryTFS1 vial 02	
Empirical formula	[C ₃₇ H ₄₅ NO ₁₄ • C ₅ H ₆ N][C ₂ F ₆ NO ₄ S ₂] • H ₂ O • CHCl ₃	
Formula weight	1225.38	
Temperature	100.1(4) K	
Wavelength	1.54184 Å	
Crystal system	Triclinic	
Space group	<i>P</i> -1	
Unit cell dimensions	<i>a</i> = 10.85860(17) Å	<i>α</i> = 93.0710(11)°.
	<i>b</i> = 22.1145(4) Å	<i>β</i> = 90.2646(11)°.
	<i>c</i> = 22.6189(3) Å	<i>γ</i> = 93.6436(13)°.
Volume	5412.60(14) Å ³	
Z	4	
Density (calculated)	1.504 Mg/m ³	
Absorption coefficient	3.106 mm ⁻¹	
F(000)	2536	
Crystal size	0.3345 x 0.2398 x 0.0391 mm ³	
Theta range for data collection	2.876 to 74.900°.	
Index ranges	-11 ≤ <i>h</i> ≤ 13, -27 ≤ <i>k</i> ≤ 27, -28 ≤ <i>l</i> ≤ 28	
Reflections collected	88419	
Independent reflections	22093 [R(int) = 0.0528]	
Completeness to theta = 67.684°	100.0 %	

Absorption correction	Gaussian
Max. and min. transmission	0.886 and 0.544
Refinement method	Full-matrix least-squares on F ²
Data / restraints / parameters	22093 / 0 / 1417
Goodness-of-fit on F ²	1.043
Final R indices [I>2sigma(I)]	R1 = 0.0488, wR2 = 0.1290
R indices (all data)	R1 = 0.0587, wR2 = 0.1395
Extinction coefficient	n/a
Largest diff. peak and hole	1.709 and -1.490 e.Å ⁻³

Table A.5. Bond lengths [Å] and angles [°] for cs2173.

O(15)-C(38)	1.361(3)	O(28)-C(73)	1.336(2)	C(62)-C(63)	1.509(3)
O(15)-C(50)	1.433(3)	O(28)-C(74)	1.464(3)	C(64)-C(65)	1.502(3)
O(16)-C(51)	1.423(3)	N(2)-C(68)	1.339(3)	C(67)-C(68)	1.498(3)
O(16)-C(52)	1.425(3)	N(2)-C(72)	1.341(3)	C(68)-C(69)	1.395(3)
O(17)-C(53)	1.420(3)	C(38)-C(39)	1.417(3)	C(69)-C(70)	1.386(3)
O(17)-C(54)	1.424(3)	C(38)-C(43)	1.385(3)	C(70)-C(71)	1.386(3)
O(18)-C(55)	1.422(3)	C(39)-C(40)	1.382(3)	C(71)-C(72)	1.400(3)
O(18)-C(56)	1.423(3)	C(40)-C(41)	1.399(3)	C(72)-C(73)	1.502(3)
O(19)-C(44)	1.361(2)	C(41)-C(42)	1.380(3)	O(1)-C(1)	1.359(3)
O(19)-C(57)	1.433(2)	C(41)-C(66)	1.499(3)	O(1)-C(13)	1.433(2)
O(20)-C(39)	1.353(3)	C(42)-C(43)	1.397(3)	O(2)-C(14)	1.427(3)
O(20)-C(58)	1.432(3)	C(44)-C(45)	1.415(3)	O(2)-C(15)	1.412(3)
O(21)-C(59)	1.420(3)	C(44)-C(49)	1.388(3)	O(3)-C(16)	1.422(3)
O(21)-C(60)	1.431(3)	C(45)-C(46)	1.388(3)	O(3)-C(17)	1.421(3)
O(22)-C(61)	1.417(3)	C(46)-C(47)	1.399(3)	O(4)-C(18)	1.425(3)
O(22)-C(62)	1.422(3)	C(47)-C(48)	1.385(3)	O(4)-C(19)	1.423(3)
O(23)-C(63)	1.413(3)	C(47)-C(74)	1.501(3)	O(5)-C(7)	1.365(3)
O(23)-C(64)	1.420(3)	C(48)-C(49)	1.396(3)	O(5)-C(20)	1.431(2)
O(24)-C(45)	1.356(3)	C(50)-C(51)	1.497(3)	O(6)-C(2)	1.367(3)
O(24)-C(65)	1.429(2)	C(52)-C(53)	1.498(4)	O(6)-C(21)	1.429(2)
O(25)-C(66)	1.460(3)	C(54)-C(55)	1.503(4)	O(7)-C(22)	1.416(3)
O(25)-C(67)	1.337(3)	C(56)-C(57)	1.498(3)	O(7)-C(23)	1.421(3)
O(26)-C(67)	1.215(3)	C(58)-C(59)	1.507(3)	O(8)-C(24)	1.418(3)
O(27)-C(73)	1.208(3)	C(60)-C(61)	1.505(3)	O(8)-C(25)	1.415(3)

O(9)-C(26)	1.430(3)	C(32)-C(33)	1.385(4)	C(77)-C(78)	1.385(4)
O(9)-C(27)	1.420(3)	C(33)-C(34)	1.378(3)	C(78)-C(79)	1.375(4)
O(10)-C(8)	1.366(3)	C(34)-C(35)	1.389(3)	N(4)-C(80)	1.344(4)
O(10)-C(28)	1.431(2)	C(35)-C(36)	1.506(3)	N(4)-C(84)	1.327(3)
O(11)-C(29)	1.466(3)	S(3)-O(33)	1.4252(19)	C(80)-C(81)	1.366(4)
O(11)-C(30)	1.336(3)	S(3)-O(34)	1.4241(19)	C(81)-C(82)	1.369(4)
O(12)-C(30)	1.204(3)	S(3)-N(6)	1.581(2)	C(82)-C(83)	1.378(4)
O(13)-C(36)	1.208(3)	S(3)-C(87)	1.832(3)	C(83)-C(84)	1.384(4)
O(14)-C(36)	1.329(3)	S(4)-O(35)	1.4292(19)	Cl(1)-C(89)	1.766(3)
O(14)-C(37)	1.469(3)	S(4)-O(36)	1.4354(19)	Cl(2)-C(89)	1.763(3)
N(1)-C(31)	1.341(3)	S(4)-N(6)	1.568(2)	Cl(3)-C(89)	1.762(3)
N(1)-C(35)	1.337(3)	S(4)-C(88)	1.840(3)	Cl(4)-C(90)	1.769(3)
C(1)-C(2)	1.416(3)	F(7)-C(87)	1.326(3)	Cl(5)-C(90)	1.759(3)
C(1)-C(6)	1.384(3)	F(8)-C(87)	1.324(3)	Cl(6)-C(90)	1.759(3)
C(2)-C(3)	1.380(3)	F(9)-C(87)	1.331(3)	O(37)-H(37C)	0.77(4)
C(3)-C(4)	1.405(3)	F(10)-C(88)	1.321(3)	O(37)-H(37D)	0.79(4)
C(4)-C(5)	1.380(3)	F(11)-C(88)	1.325(3)	O(38)-H(38A)	0.82(5)
C(4)-C(29)	1.497(3)	F(12)-C(88)	1.329(3)	O(38)-H(38B)	0.81(5)
C(5)-C(6)	1.398(3)	S(1)-O(29)	1.4227(18)		
C(7)-C(8)	1.412(3)	S(1)-O(30)	1.4375(18)		
C(7)-C(12)	1.386(3)	S(1)-N(5)	1.568(2)		
C(8)-C(9)	1.380(3)	S(1)-C(85)	1.841(2)		
C(9)-C(10)	1.406(3)	S(2)-O(31)	1.4248(19)		
C(10)-C(11)	1.378(3)	S(2)-O(32)	1.4240(19)		
C(10)-C(37)	1.491(3)	S(2)-N(5)	1.586(2)		
C(11)-C(12)	1.399(3)	S(2)-C(86)	1.832(3)		
C(13)-C(14)	1.499(3)	F(1)-C(85)	1.329(3)		
C(15)-C(16)	1.502(3)	F(2)-C(85)	1.320(3)		
C(17)-C(18)	1.502(3)	F(3)-C(85)	1.321(3)		
C(19)-C(20)	1.502(3)	F(4)-C(86)	1.324(3)		
C(21)-C(22)	1.504(3)	F(5)-C(86)	1.332(3)		
C(23)-C(24)	1.493(4)	F(6)-C(86)	1.329(3)		
C(25)-C(26)	1.502(3)	N(3)-C(75)	1.341(3)		
C(27)-C(28)	1.508(3)	N(3)-C(79)	1.337(3)		
C(30)-C(31)	1.502(3)	C(75)-C(76)	1.373(4)		
C(31)-C(32)	1.396(3)	C(76)-C(77)	1.378(4)		

C(38)-O(15)-C(50)	116.52(18)
C(51)-O(16)-C(52)	111.45(18)
C(53)-O(17)-C(54)	112.15(19)
C(55)-O(18)-C(56)	111.32(17)
C(44)-O(19)-C(57)	116.77(16)
C(39)-O(20)-C(58)	119.12(17)
C(59)-O(21)-C(60)	115.09(18)
C(61)-O(22)-C(62)	112.49(17)
C(63)-O(23)-C(64)	111.62(17)
C(45)-O(24)-C(65)	117.50(16)
C(67)-O(25)-C(66)	113.09(16)
C(73)-O(28)-C(74)	112.56(16)
C(68)-N(2)-C(72)	116.24(18)
O(15)-C(38)-C(39)	114.75(19)
O(15)-C(38)-C(43)	125.82(19)
C(43)-C(38)-C(39)	119.4(2)
O(20)-C(39)-C(38)	113.84(18)
O(20)-C(39)-C(40)	125.83(19)
C(40)-C(39)-C(38)	120.3(2)
C(39)-C(40)-C(41)	119.8(2)
C(40)-C(41)-C(66)	119.8(2)
C(42)-C(41)-C(40)	119.8(2)
C(42)-C(41)-C(66)	120.3(2)
C(41)-C(42)-C(43)	121.0(2)
C(38)-C(43)-C(42)	119.7(2)
O(19)-C(44)-C(45)	114.78(18)
O(19)-C(44)-C(49)	125.34(19)
C(49)-C(44)-C(45)	119.84(19)
O(24)-C(45)-C(44)	114.98(17)
O(24)-C(45)-C(46)	125.33(19)
C(46)-C(45)-C(44)	119.68(19)
C(45)-C(46)-C(47)	120.25(19)
C(46)-C(47)-C(74)	119.4(2)
C(48)-C(47)-C(46)	119.62(19)
C(48)-C(47)-C(74)	120.9(2)

C(47)-C(48)-C(49)	120.9(2)
C(44)-C(49)-C(48)	119.7(2)
O(15)-C(50)-C(51)	108.62(19)
O(16)-C(51)-C(50)	109.56(19)
O(16)-C(52)-C(53)	109.77(19)
O(17)-C(53)-C(52)	109.2(2)
O(17)-C(54)-C(55)	109.5(2)
O(18)-C(55)-C(54)	108.96(19)
O(18)-C(56)-C(57)	109.24(18)
O(19)-C(57)-C(56)	107.26(18)
O(20)-C(58)-C(59)	106.35(17)
H(58A)-C(58)-H(58B)	108.6
C(59)-C(58)-H(58A)	110.5
C(59)-C(58)-H(58B)	110.5
O(21)-C(59)-C(58)	113.72(19)
O(21)-C(60)-C(61)	107.50(19)
O(22)-C(61)-C(60)	108.55(19)
O(22)-C(62)-C(63)	108.95(18)
O(23)-C(63)-C(62)	109.1(2)
O(23)-C(64)-C(65)	108.73(18)
O(24)-C(65)-C(64)	107.49(17)
O(25)-C(66)-C(41)	109.51(16)
O(25)-C(67)-C(68)	113.48(18)
O(26)-C(67)-O(25)	123.8(2)
O(26)-C(67)-C(68)	122.74(19)
N(2)-C(68)-C(67)	117.66(18)
N(2)-C(68)-C(69)	124.4(2)
C(69)-C(68)-C(67)	117.93(19)
C(70)-C(69)-C(68)	118.2(2)
C(69)-C(70)-C(71)	118.9(2)
C(70)-C(71)-C(72)	118.4(2)
N(2)-C(72)-C(71)	123.9(2)
N(2)-C(72)-C(73)	118.99(18)
C(71)-C(72)-C(73)	117.13(19)
O(27)-C(73)-O(28)	124.1(2)
O(27)-C(73)-C(72)	121.79(19)

O(28)-C(73)-C(72)	114.11(18)
O(28)-C(74)-C(47)	109.09(16)
C(1)-O(1)-C(13)	118.65(16)
C(15)-O(2)-C(14)	114.32(17)
C(17)-O(3)-C(16)	111.96(17)
C(19)-O(4)-C(18)	112.10(16)
C(7)-O(5)-C(20)	116.61(16)
C(2)-O(6)-C(21)	117.16(17)
C(22)-O(7)-C(23)	111.95(17)
C(25)-O(8)-C(24)	113.54(19)
C(27)-O(9)-C(26)	115.39(18)
C(8)-O(10)-C(28)	118.82(17)
C(30)-O(11)-C(29)	114.01(17)
C(36)-O(14)-C(37)	113.91(16)
C(35)-N(1)-C(31)	116.00(18)
O(1)-C(1)-C(2)	114.39(18)
O(1)-C(1)-C(6)	125.67(19)
C(6)-C(1)-C(2)	119.9(2)
O(6)-C(2)-C(1)	114.79(18)
O(6)-C(2)-C(3)	125.48(18)
C(3)-C(2)-C(1)	119.71(19)
C(2)-C(3)-C(4)	120.1(2)
C(3)-C(4)-C(29)	118.6(2)
C(5)-C(4)-C(3)	119.8(2)
C(5)-C(4)-C(29)	121.5(2)
C(4)-C(5)-C(6)	120.7(2)
C(1)-C(6)-C(5)	119.7(2)
O(5)-C(7)-C(8)	114.67(18)
O(5)-C(7)-C(12)	125.47(19)
C(12)-C(7)-C(8)	119.86(19)
O(10)-C(8)-C(7)	113.70(18)
O(10)-C(8)-C(9)	125.86(19)
C(9)-C(8)-C(7)	120.42(19)
C(8)-C(9)-C(10)	119.5(2)
C(9)-C(10)-C(37)	119.6(2)
C(11)-C(10)-C(9)	120.0(2)

C(11)-C(10)-C(37)	120.4(2)
C(10)-C(11)-C(12)	120.9(2)
C(7)-C(12)-C(11)	119.3(2)
O(1)-C(13)-C(14)	104.53(16)
O(2)-C(14)-C(13)	106.81(17)
O(2)-C(15)-C(16)	107.78(18)
O(3)-C(16)-C(15)	107.95(17)
O(3)-C(17)-C(18)	109.19(17)
O(4)-C(18)-C(17)	107.91(18)
O(4)-C(19)-C(20)	109.58(17)
O(5)-C(20)-C(19)	107.24(16)
O(6)-C(21)-C(22)	108.02(18)
O(7)-C(22)-C(21)	109.71(18)
O(7)-C(23)-C(24)	109.64(19)
O(8)-C(24)-C(23)	109.1(2)
O(8)-C(25)-C(26)	107.9(2)
O(9)-C(26)-C(25)	107.57(18)
O(9)-C(27)-C(28)	114.0(2)
O(10)-C(28)-C(27)	105.29(18)
O(11)-C(29)-C(4)	110.27(18)
O(11)-C(30)-C(31)	113.35(18)
O(12)-C(30)-O(11)	124.5(2)
O(12)-C(30)-C(31)	122.0(2)
N(1)-C(31)-C(30)	118.95(19)
N(1)-C(31)-C(32)	124.0(2)
C(32)-C(31)-C(30)	116.98(19)
C(33)-C(32)-C(31)	118.3(2)
C(34)-C(33)-C(32)	118.4(2)
C(33)-C(34)-C(35)	118.8(2)
N(1)-C(35)-C(34)	124.0(2)
N(1)-C(35)-C(36)	119.08(19)
C(34)-C(35)-C(36)	116.9(2)
O(13)-C(36)-O(14)	124.7(2)
O(13)-C(36)-C(35)	121.9(2)
O(14)-C(36)-C(35)	113.33(18)
O(14)-C(37)-C(10)	107.93(17)

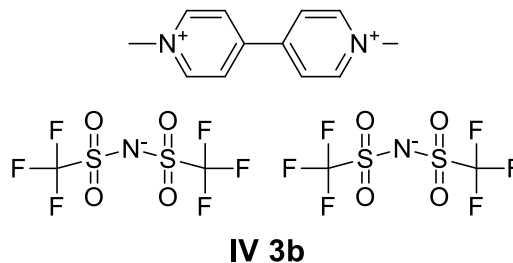
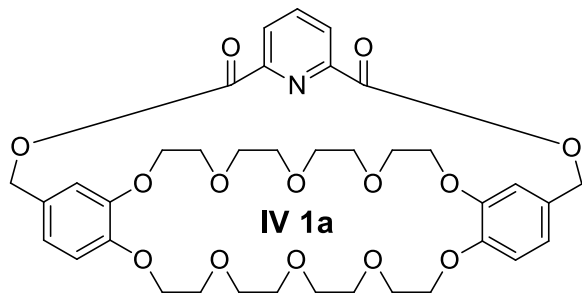
O(33)-S(3)-N(6)	108.57(11)
O(33)-S(3)-C(87)	102.98(13)
O(34)-S(3)-O(33)	118.81(13)
O(34)-S(3)-N(6)	116.89(12)
O(34)-S(3)-C(87)	104.75(14)
N(6)-S(3)-C(87)	102.38(12)
O(35)-S(4)-O(36)	117.97(12)
O(35)-S(4)-N(6)	108.76(11)
O(35)-S(4)-C(88)	103.26(12)
O(36)-S(4)-N(6)	116.47(11)
O(36)-S(4)-C(88)	104.98(11)
N(6)-S(4)-C(88)	103.34(12)
S(4)-N(6)-S(3)	124.61(12)
F(7)-C(87)-S(3)	109.10(18)
F(7)-C(87)-F(9)	108.8(2)
F(8)-C(87)-S(3)	111.14(19)
F(8)-C(87)-F(7)	108.3(2)
F(8)-C(87)-F(9)	108.6(2)
F(9)-C(87)-S(3)	110.8(2)
F(10)-C(88)-S(4)	110.10(18)
F(10)-C(88)-F(11)	108.6(2)
F(10)-C(88)-F(12)	108.7(2)
F(11)-C(88)-S(4)	111.35(19)
F(11)-C(88)-F(12)	108.3(2)
F(12)-C(88)-S(4)	109.73(17)
O(29)-S(1)-O(30)	118.18(12)
O(29)-S(1)-N(5)	108.67(11)
O(29)-S(1)-C(85)	103.52(11)
O(30)-S(1)-N(5)	116.91(11)
O(30)-S(1)-C(85)	104.00(11)
N(5)-S(1)-C(85)	103.38(12)
O(31)-S(2)-N(5)	116.84(11)
O(31)-S(2)-C(86)	104.90(13)
O(32)-S(2)-O(31)	118.99(12)
O(32)-S(2)-N(5)	108.49(11)
O(32)-S(2)-C(86)	103.15(12)

N(5)-S(2)-C(86)	101.96(12)
S(1)-N(5)-S(2)	124.22(13)
F(1)-C(85)-S(1)	109.41(17)
F(2)-C(85)-S(1)	111.62(17)
F(2)-C(85)-F(1)	108.5(2)
F(2)-C(85)-F(3)	109.0(2)
F(3)-C(85)-S(1)	110.23(18)
F(3)-C(85)-F(1)	108.1(2)
F(4)-C(86)-S(2)	111.06(19)
F(4)-C(86)-F(5)	109.0(2)
F(4)-C(86)-F(6)	109.0(2)
F(5)-C(86)-S(2)	108.54(19)
F(6)-C(86)-S(2)	111.34(18)
F(6)-C(86)-F(5)	107.7(2)
C(79)-N(3)-C(75)	122.4(2)
N(3)-C(75)-C(76)	119.3(2)
C(75)-C(76)-C(77)	119.7(2)
C(76)-C(77)-C(78)	119.7(2)
C(79)-C(78)-C(77)	118.8(2)
N(3)-C(79)-C(78)	120.0(2)
C(84)-N(4)-C(80)	122.2(2)
N(4)-C(80)-C(81)	120.2(2)
C(80)-C(81)-C(82)	118.8(2)
C(81)-C(82)-C(83)	120.6(2)
C(82)-C(83)-C(84)	118.7(2)
N(4)-C(84)-C(83)	119.6(2)
Cl(2)-C(89)-Cl(1)	110.18(16)
Cl(3)-C(89)-Cl(1)	110.57(14)
Cl(3)-C(89)-Cl(2)	108.42(17)
Cl(5)-C(90)-Cl(4)	109.40(16)
Cl(6)-C(90)-Cl(4)	110.26(14)
Cl(6)-C(90)-Cl(5)	110.50(15)
H(37C)-O(37)-H(37D)	112(4)
H(38A)-O(38)-H(38B)	109(4)

Table A.6. Hydrogen bonds for cs2173 [\AA and $^\circ$].

D-H...A	d(D-H)	d(H...A)	d(D...A)	$\angle(\text{DHA})$
N(4)-H(4)...O(38)	0.88	1.79	2.660(3)	167.6
O(37)-H(37C)...O(4)	0.77(4)	2.08(4)	2.850(2)	177(4)
O(37)-H(37D)...O(2)	0.79(4)	2.11(4)	2.894(2)	167(4)
O(38)-H(38A)...O(18)	0.82(5)	2.09(5)	2.901(3)	170(4)
O(38)-H(38B)...O(16)	0.81(5)	2.06(5)	2.861(3)	171(5)

Chapter 4



Crystal structure of **IV 1a** • **IV 3b** was grown from an equimolar solution of chloroform:acetone 1:1 (v:v) by liquid-liquid diffusion of diethyl ether.

Table A.7. Crystal data and structure refinement for cs2237.

Identification code	S1P7 with S100105P1	
Empirical formula	[C ₃₇ H ₄₅ NO ₁₄ •C ₁₂ H ₁₄ N ₂ ²⁺][C ₂ F ₆ NO ₄ S ₂ ⁻] ₂ •C ₃ H ₆ O	
Formula weight	1532.37	
Temperature	100.00(10) K	
Wavelength	0.71073 Å	
Crystal system	Monoclinic	
Space group	P 1 2 ₁ /c 1	
Unit cell dimensions	<i>a</i> = 13.9755(5) Å	<i>α</i> = 90°
	<i>b</i> = 23.6564(7) Å	<i>β</i> = 106.857(4)°
	<i>c</i> = 21.5448(9) Å	<i>γ</i> = 90°
Volume	6816.9(5) Å ³	
Z	4	
Density (calculated)	1.493 Mg/m ³	
Absorption coefficient	0.251 mm ⁻¹	
F(000)	3168	
Crystal size	0.649 x 0.493 x 0.309 mm ³	
Theta range for data collection	3.500 to 29.130°.	
Index ranges	-18<= <i>h</i> <=19, -32<= <i>k</i> <=32, -29<= <i>l</i> <=29	
Reflections collected	85870	
Independent reflections	18309 [R(int) = 0.0425]	
Completeness to theta = 25.242°	99.7 %	

Absorption correction	Gaussian
Max. and min. transmission	0.938 and 0.886
Refinement method	Full-matrix least-squares on F ²
Data / restraints / parameters	18309 / 5 / 934
Goodness-of-fit on F ²	1.028
Final R indices [I>2sigma(I)]	R1 = 0.1251, wR2 = 0.3347
R indices (all data)	R1 = 0.1577, wR2 = 0.3633
Extinction coefficient	n/a
Largest diff. peak and hole	2.523 and -1.246 e.Å ⁻³

Table A.8. Bond lengths [Å] and angles [°] for cs2237.

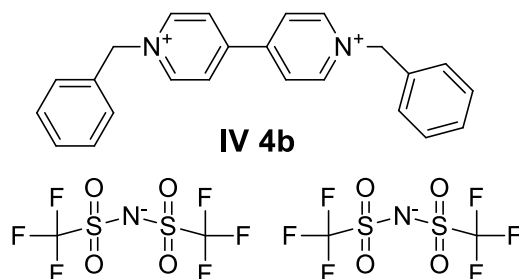
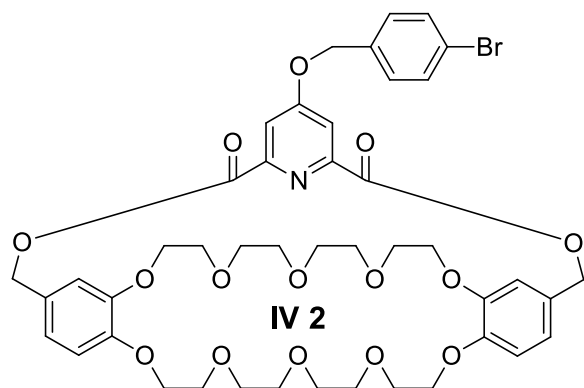
O(1)-C(1)	1.371(5)	O(13)-C(36)	1.222(6)	C(21)-C(22)	1.548(10)
O(1)-C(13)	1.444(7)	O(14)-C(36)	1.334(6)	C(23)-C(24)	1.461(11)
O(2)-C(14)	1.425(6)	O(14)-C(37)	1.476(7)	C(25)-C(26)	1.488(9)
O(2)-C(15)	1.429(6)	N(1)-C(31)	1.324(8)	C(27)-C(28)	1.486(7)
O(3)-C(16)	1.419(9)	N(1)-C(35)	1.355(6)	C(30)-C(31)	1.543(8)
O(3)-C(17)	1.422(8)	C(1)-C(2)	1.403(9)	C(31)-C(32)	1.400(9)
O(4)-C(18)	1.437(9)	C(1)-C(6)	1.382(9)	C(32)-C(33)	1.398(9)
O(4)-C(19)	1.397(9)	C(2)-C(3)	1.400(7)	C(33)-C(34)	1.356(10)
O(5)-C(7)	1.364(7)	C(3)-C(4)	1.432(11)	C(34)-C(35)	1.411(8)
O(5)-C(20)	1.448(6)	C(4)-C(5)	1.365(11)	C(35)-C(36)	1.483(8)
O(6)-C(2)	1.374(8)	C(4)-C(29)	1.513(7)	N(2)-C(38)	1.354(6)
O(6)-C(21)	1.440(8)	C(5)-C(6)	1.407(8)	N(2)-C(42)	1.336(6)
O(7)-C(22)	1.384(9)	C(7)-C(8)	1.435(6)	N(2)-C(43)	1.492(6)
O(7)-C(23)	1.458(9)	C(7)-C(12)	1.380(8)	N(3)-C(44)	1.349(7)
O(8)-C(24)	1.401(8)	C(8)-C(9)	1.378(7)	N(3)-C(48)	1.352(6)
O(8)-C(25)	1.423(7)	C(9)-C(10)	1.403(7)	N(3)-C(49)	1.488(7)
O(9)-C(26)	1.430(6)	C(10)-C(11)	1.397(8)	C(38)-C(39)	1.376(7)
O(9)-C(27)	1.416(6)	C(10)-C(37)	1.498(8)	C(39)-C(40)	1.404(6)
O(10)-C(8)	1.362(6)	C(11)-C(12)	1.384(9)	C(40)-C(41)	1.404(6)
O(10)-C(28)	1.447(6)	C(13)-C(14)	1.512(8)	C(40)-C(46)	1.487(7)
O(11)-C(29)	1.485(7)	C(15)-C(16)	1.516(7)	C(41)-C(42)	1.381(7)
O(11)-C(30)	1.303(10)	C(17)-C(18)	1.490(13)	C(44)-C(45)	1.381(7)
O(12)-C(30)	1.217(10)	C(19)-C(20)	1.493(11)	C(45)-C(46)	1.402(6)

C(46)-C(47)	1.401(7)	F(5)-C(51)	1.330(8)	S(4A)-O(21A)	1.478(8)
C(47)-C(48)	1.390(7)	F(6)-C(51)	1.331(7)	S(4A)-O(22A)	1.428(6)
S(1)-O(15)	1.465(5)	O(23)-C(55)	1.120(11)	S(4A)-C(53A)	1.805(10)
S(1)-O(16)	1.418(5)	C(54)-C(55)	1.474(14)	F(10A)-C(53A)	1.292(13)
S(1)-N(4)	1.579(4)	C(55)-C(56)	1.456(17)	F(11A)-C(53A)	1.343(11)
S(1)-C(50)	1.818(5)	S(3)-O(19)	1.432(6)	F(12A)-C(53A)	1.355(12)
S(2)-O(17)	1.416(4)	S(3)-O(20)	1.421(5)	S(4B)-O(21B)	1.407(17)
S(2)-O(18)	1.435(5)	S(3)-N(5)	1.605(5)	S(4B)-O(22B)	1.426(16)
S(2)-N(4)	1.566(4)	S(3)-C(52)	1.828(10)	S(4B)-C(53B)	1.60(3)
S(2)-C(51)	1.830(7)	F(7)-C(52)	1.281(10)	F(10B)-C(53B)	1.324(18)
F(1)-C(50)	1.341(7)	F(8)-C(52)	1.330(10)	F(11B)-C(53B)	1.363(18)
F(2)-C(50)	1.322(7)	F(9)-C(52)	1.342(8)	F(12B)-C(53B)	1.302(18)
F(3)-C(50)	1.332(7)	N(5)-S(4A)	1.634(5)		
F(4)-C(51)	1.316(8)	N(5)-S(4B)	1.548(7)		

C(1)-O(1)-C(13)	116.2(5)	C(5)-C(4)-C(3)	120.9(5)
C(14)-O(2)-C(15)	110.9(4)	C(5)-C(4)-C(29)	120.2(7)
C(16)-O(3)-C(17)	114.6(5)	C(4)-C(5)-C(6)	120.0(6)
C(19)-O(4)-C(18)	111.5(5)	C(1)-C(6)-C(5)	120.4(6)
C(7)-O(5)-C(20)	117.0(5)	O(5)-C(7)-C(8)	115.1(4)
C(2)-O(6)-C(21)	117.7(4)	O(5)-C(7)-C(12)	125.8(5)
C(22)-O(7)-C(23)	112.7(5)	C(12)-C(7)-C(8)	119.1(5)
C(24)-O(8)-C(25)	116.3(5)	O(10)-C(8)-C(7)	115.0(4)
C(27)-O(9)-C(26)	111.0(4)	O(10)-C(8)-C(9)	125.5(4)
C(8)-O(10)-C(28)	115.5(4)	C(9)-C(8)-C(7)	119.6(5)
C(30)-O(11)-C(29)	116.2(6)	C(8)-C(9)-C(10)	120.8(5)
C(36)-O(14)-C(37)	115.1(4)	C(9)-C(10)-C(37)	119.8(5)
C(31)-N(1)-C(35)	116.8(5)	C(11)-C(10)-C(9)	119.0(5)
O(1)-C(1)-C(2)	114.9(5)	C(11)-C(10)-C(37)	121.1(5)
O(1)-C(1)-C(6)	125.1(6)	C(12)-C(11)-C(10)	120.8(5)
C(6)-C(1)-C(2)	120.1(5)	C(7)-C(12)-C(11)	120.7(5)
O(6)-C(2)-C(1)	115.8(4)	O(1)-C(13)-C(14)	107.4(5)
O(6)-C(2)-C(3)	123.7(6)	O(2)-C(14)-C(13)	108.8(4)
C(3)-C(2)-C(1)	120.4(6)	O(2)-C(15)-C(16)	109.1(4)
C(2)-C(3)-C(4)	118.2(6)	O(3)-C(16)-C(15)	114.5(6)
C(3)-C(4)-C(29)	118.8(7)	O(3)-C(17)-C(18)	109.2(5)

O(4)-C(18)-C(17)	110.3(5)	C(39)-C(40)-C(46)	122.7(4)
O(4)-C(19)-C(20)	111.0(5)	C(41)-C(40)-C(39)	117.2(4)
O(5)-C(20)-C(19)	107.6(6)	C(41)-C(40)-C(46)	120.1(4)
O(6)-C(21)-C(22)	109.0(5)	C(42)-C(41)-C(40)	120.1(4)
O(7)-C(22)-C(21)	111.7(5)	N(2)-C(42)-C(41)	121.2(4)
O(7)-C(23)-C(24)	108.9(5)	N(3)-C(44)-C(45)	120.5(4)
O(8)-C(24)-C(23)	113.1(6)	C(44)-C(45)-C(46)	120.0(5)
O(8)-C(25)-C(26)	116.6(6)	C(45)-C(46)-C(40)	121.4(4)
O(9)-C(26)-C(25)	108.6(5)	C(47)-C(46)-C(40)	120.8(4)
O(9)-C(27)-C(28)	109.2(4)	C(47)-C(46)-C(45)	117.9(4)
O(10)-C(28)-C(27)	107.5(5)	C(48)-C(47)-C(46)	120.3(4)
O(11)-C(29)-C(4)	112.6(4)	N(3)-C(48)-C(47)	119.7(5)
O(11)-C(30)-C(31)	113.1(6)	O(15)-S(1)-N(4)	115.9(2)
O(12)-C(30)-O(11)	126.8(7)	O(15)-S(1)-C(50)	104.5(3)
O(12)-C(30)-C(31)	120.1(8)	O(16)-S(1)-O(15)	115.3(4)
N(1)-C(31)-C(30)	117.1(5)	O(16)-S(1)-N(4)	111.9(3)
N(1)-C(31)-C(32)	124.6(5)	O(16)-S(1)-C(50)	105.1(3)
C(32)-C(31)-C(30)	118.3(6)	N(4)-S(1)-C(50)	102.2(3)
C(33)-C(32)-C(31)	117.7(6)	O(17)-S(2)-O(18)	117.6(3)
C(34)-C(33)-C(32)	118.9(6)	O(17)-S(2)-N(4)	118.3(2)
C(33)-C(34)-C(35)	119.6(5)	O(17)-S(2)-C(51)	106.0(3)
N(1)-C(35)-C(34)	122.3(6)	O(18)-S(2)-N(4)	106.0(3)
N(1)-C(35)-C(36)	118.7(5)	O(18)-S(2)-C(51)	104.5(3)
C(34)-C(35)-C(36)	119.0(5)	N(4)-S(2)-C(51)	102.4(3)
O(13)-C(36)-O(14)	123.4(6)	S(2)-N(4)-S(1)	124.4(3)
O(13)-C(36)-C(35)	122.7(5)	F(1)-C(50)-S(1)	109.1(4)
O(14)-C(36)-C(35)	113.9(4)	F(2)-C(50)-S(1)	112.4(4)
O(14)-C(37)-C(10)	108.3(4)	F(2)-C(50)-F(1)	106.2(5)
C(38)-N(2)-C(43)	120.7(4)	F(2)-C(50)-F(3)	108.7(5)
C(42)-N(2)-C(38)	120.5(4)	F(3)-C(50)-S(1)	110.7(4)
C(42)-N(2)-C(43)	118.8(4)	F(3)-C(50)-F(1)	109.5(4)
C(44)-N(3)-C(48)	121.6(4)	F(4)-C(51)-S(2)	110.1(4)
C(44)-N(3)-C(49)	120.0(4)	F(4)-C(51)-F(5)	110.8(7)
C(48)-N(3)-C(49)	118.4(5)	F(4)-C(51)-F(6)	107.3(5)
N(2)-C(38)-C(39)	120.9(4)	F(5)-C(51)-S(2)	112.1(4)
C(38)-C(39)-C(40)	120.2(4)	F(5)-C(51)-F(6)	105.7(5)

F(6)-C(51)-S(2)	110.7(6)	F(10B)-C(53B)-S(4B)	124(2)
O(23)-C(55)-C(54)	119.7(12)	F(10B)-C(53B)-F(11B)	103(2)
O(23)-C(55)-C(56)	116.1(12)	F(11B)-C(53B)-S(4B)	115.4(17)
C(56)-C(55)-C(54)	124.2(10)	F(12B)-C(53B)-S(4B)	116.8(19)
O(19)-S(3)-N(5)	107.2(3)	F(12B)-C(53B)-F(10B)	90(2)
O(19)-S(3)-C(52)	103.9(4)	F(12B)-C(53B)-F(11B)	104(2)
O(20)-S(3)-O(19)	118.9(4)		
O(20)-S(3)-N(5)	117.8(3)		
O(20)-S(3)-C(52)	103.8(4)		
N(5)-S(3)-C(52)	102.8(3)		
S(3)-N(5)-S(4A)	124.2(3)		
S(4B)-N(5)-S(3)	110.4(3)		
F(7)-C(52)-S(3)	113.3(6)		
F(7)-C(52)-F(8)	106.9(9)		
F(7)-C(52)-F(9)	108.5(7)		
F(8)-C(52)-S(3)	111.6(6)		
F(8)-C(52)-F(9)	107.4(6)		
F(9)-C(52)-S(3)	108.9(6)		
N(5)-S(4A)-C(53A)	103.7(5)		
O(21A)-S(4A)-N(5)	106.2(4)		
O(21A)-S(4A)-C(53A)	100.7(5)		
O(22A)-S(4A)-N(5)	116.6(3)		
O(22A)-S(4A)-O(21A)	123.2(5)		
O(22A)-S(4A)-C(53A)	103.4(4)		
F(10A)-C(53A)-S(4A)	112.7(9)		
F(10A)-C(53A)-F(11A)	108.3(8)		
F(10A)-C(53A)-F(12A)	106.0(8)		
F(11A)-C(53A)-S(4A)	112.0(7)		
F(11A)-C(53A)-F(12A)	106.4(10)		
F(12A)-C(53A)-S(4A)	111.2(7)		
N(5)-S(4B)-C(53B)	92.8(8)		
O(21B)-S(4B)-N(5)	118.4(14)		
O(21B)-S(4B)-O(22B)	124.7(17)		
O(21B)-S(4B)-C(53B)	102.2(15)		
O(22B)-S(4B)-N(5)	104.1(11)		
O(22B)-S(4B)-C(53B)	109.8(13)		



Crystal structure of **IV 2 • IV 4b** was grown from an equimolar of dichloromethane:acetone 1:1 (v:v) by liquid-liquid diffusion of pentane.

Table A.9. Crystal data and structure refinement for cs2231.

Identification code	cs2231	
Empirical formula	[(C ₄₄ H ₅₀ BrNO ₁₅ •C ₂₄ H ₂₂ N ₂ ²⁺)[C ₂ F ₆ NO ₄ S ₂ ⁻] ₂ •H ₂ O•2CH ₂ Cl ₂	
Formula weight	1999.36	
Temperature	99.8(5) K	
Wavelength	1.54184 Å	
Crystal system	Monoclinic	
Space group	P 1 2 ₁ 1	
Unit cell dimensions	$a = 10.85497(19) \text{ \AA}$	$\alpha = 90^\circ$.
	$b = 51.7519(8) \text{ \AA}$	$\beta = 92.8891(17)^\circ$.
	$c = 14.4041(3) \text{ \AA}$	$\gamma = 90^\circ$.
Volume	8081.4(3) Å ³	
Z	4	
Density (calculated)	1.643 Mg/m ³	
Absorption coefficient	3.835 mm ⁻¹	
F(000)	4096	
Crystal size	0.334 x 0.105 x 0.011 mm ³	
Theta range for data collection	3.072 to 76.636°.	
Index ranges	-13<=h<=13, -64<=k<=64, -17<=l<=17	
Reflections collected	89317	

Independent reflections	32724 [R(int) = 0.0773]
Completeness to theta = 74.500°	99.6 %
Absorption correction	Gaussian
Max. and min. transmission	0.965 and 0.431
Refinement method	Full-matrix least-squares on F ²
Data / restraints / parameters	32724 / 1537 / 1862
Goodness-of-fit on F ²	1.095
Final R indices [I>2sigma(I)]	R1 = 0.0792, wR2 = 0.2148
R indices (all data)	R1 = 0.0877, wR2 = 0.2214
Absolute structure parameter	0.47(2)
Extinction coefficient	n/a
Largest diff. peak and hole	0.884 and -0.661 e.Å ⁻³

Table A.10. Bond lengths [Å] and angles [°] for cs2231.

Br(1)-C(42)	1.875(8)	O(11)-C(29)	1.450(9)	C(10)-C(11)	1.382(11)
O(1)-C(1)	1.329(10)	O(11)-C(30)	1.341(9)	C(10)-C(31)	1.488(11)
O(1)-C(13)	1.442(13)	O(12)-C(30)	1.206(10)	C(11)-C(12)	1.412(12)
O(2)-C(14)	1.436(16)	O(13)-C(31)	1.453(9)	C(13)-C(14)	1.455(16)
O(2)-C(15)	1.457(15)	O(13)-C(32)	1.341(9)	C(15)-C(16)	1.40(2)
O(3)-C(16)	1.381(16)	O(14)-C(32)	1.213(11)	C(17)-C(18)	1.472(18)
O(3)-C(17)	1.422(19)	O(15)-C(35)	1.360(10)	C(19)-C(20)	1.490(13)
O(4)-C(18)	1.444(12)	O(15)-C(38)	1.426(9)	C(21)-C(22)	1.553(13)
O(4)-C(19)	1.385(14)	N(1)-C(33)	1.327(10)	C(23)-C(24)	1.487(15)
O(5)-C(7)	1.367(9)	N(1)-C(37)	1.347(10)	C(25)-C(26)	1.500(14)
O(5)-C(20)	1.442(10)	C(1)-C(2)	1.418(12)	C(27)-C(28)	1.479(11)
O(6)-C(2)	1.370(10)	C(1)-C(6)	1.426(12)	C(30)-C(33)	1.487(10)
O(6)-C(21)	1.393(12)	C(2)-C(3)	1.372(11)	C(32)-C(37)	1.503(11)
O(7)-C(22)	1.400(13)	C(3)-C(4)	1.418(11)	C(33)-C(34)	1.395(11)
O(7)-C(23)	1.421(11)	C(4)-C(5)	1.368(11)	C(34)-C(35)	1.379(11)
O(8)-C(24)	1.450(12)	C(4)-C(29)	1.505(10)	C(35)-C(36)	1.388(11)
O(8)-C(25)	1.433(11)	C(5)-C(6)	1.390(12)	C(36)-C(37)	1.385(11)
O(9)-C(26)	1.432(10)	C(7)-C(8)	1.410(10)	C(38)-C(39)	1.501(11)
O(9)-C(27)	1.440(11)	C(7)-C(12)	1.364(12)	C(39)-C(40)	1.334(13)
O(10)-C(8)	1.371(10)	C(8)-C(9)	1.400(11)	C(39)-C(44)	1.404(13)
O(10)-C(28)	1.430(9)	C(9)-C(10)	1.409(11)	C(40)-C(41)	1.408(12)

C(41)-C(42)	1.386(13)	C(47)-C(48)	1.404(10)	N(4)-C(94)	1.335(12)
C(42)-C(43)	1.355(13)	C(48)-C(49)	1.399(11)	N(4)-C(98)	1.355(11)
C(43)-C(44)	1.399(13)	C(48)-C(73)	1.497(11)	N(4)-C(106)	1.502(12)
O(16)-C(45)	1.352(11)	C(49)-C(50)	1.377(11)	C(89)-C(90)	1.387(15)
O(16)-C(57)	1.437(10)	C(51)-C(52)	1.420(11)	C(90)-C(91)	1.399(12)
O(17)-C(58)	1.431(11)	C(51)-C(56)	1.410(11)	C(91)-C(92)	1.402(11)
O(17)-C(59)	1.436(10)	C(52)-C(53)	1.381(12)	C(91)-C(96)	1.454(12)
O(18)-C(60)	1.384(14)	C(53)-C(54)	1.408(11)	C(92)-C(93)	1.377(13)
O(18)-C(61)	1.446(13)	C(54)-C(55)	1.376(10)	C(94)-C(95)	1.372(14)
O(19)-C(62)	1.325(11)	C(54)-C(75)	1.493(11)	C(95)-C(96)	1.414(11)
O(19)-C(63)	1.388(13)	C(55)-C(56)	1.409(11)	C(96)-C(97)	1.374(12)
O(20)-C(51)	1.335(11)	C(65)-C(66)	1.503(12)	C(97)-C(98)	1.391(13)
O(20)-C(64)	1.445(10)	C(67)-C(68)	1.494(12)	C(99)-C(100)	1.467(15)
O(21)-C(46)	1.386(9)	C(69)-C(70)	1.490(14)	C(100)-C(101)	1.395(13)
O(21)-C(65)	1.437(10)	C(71)-C(72)	1.492(13)	C(100)-C(105)	1.412(15)
O(22)-C(66)	1.421(11)	C(57)-C(58)	1.537(12)	C(101)-C(102)	1.48(2)
O(22)-C(67)	1.429(10)	C(59)-C(60)	1.490(16)	C(102)-C(103)	1.29(2)
O(23)-C(68)	1.424(11)	C(61)-C(62)	1.53(2)	C(103)-C(104)	1.429(19)
O(23)-C(69)	1.397(12)	C(63)-C(64)	1.464(12)	C(104)-C(105)	1.352(16)
O(24)-C(70)	1.450(11)	C(74)-C(77)	1.508(10)	C(106)-C(107)	1.496(11)
O(24)-C(71)	1.441(11)	C(76)-C(81)	1.498(10)	C(107)-C(108)	1.391(12)
O(25)-C(52)	1.367(10)	C(77)-C(78)	1.383(12)	C(107)-C(112)	1.414(12)
O(25)-C(72)	1.449(10)	C(78)-C(79)	1.387(11)	C(108)-C(109)	1.365(14)
O(26)-C(73)	1.452(9)	C(79)-C(80)	1.406(10)	C(109)-C(110)	1.385(15)
O(26)-C(74)	1.316(10)	C(80)-C(81)	1.380(10)	C(110)-C(111)	1.385(15)
O(27)-C(74)	1.227(11)	C(82)-C(83)	1.494(12)	C(111)-C(112)	1.373(14)
O(28)-C(75)	1.451(8)	C(83)-C(84)	1.380(13)	N(5)-C(113)	1.372(11)
O(28)-C(76)	1.338(9)	C(83)-C(88)	1.399(12)	N(5)-C(117)	1.318(11)
O(29)-C(76)	1.212(9)	C(84)-C(85)	1.391(13)	N(5)-C(123)	1.491(11)
O(30)-C(79)	1.350(9)	C(85)-C(86)	1.368(13)	N(6)-C(118)	1.355(11)
O(30)-C(82)	1.437(10)	C(86)-C(87)	1.402(12)	N(6)-C(122)	1.347(10)
N(2)-C(77)	1.350(9)	C(86)-Br(2)	1.909(9)	N(6)-C(130)	1.503(11)
N(2)-C(81)	1.353(10)	C(87)-C(88)	1.391(11)	C(113)-C(114)	1.354(13)
C(45)-C(46)	1.434(10)	N(3)-C(89)	1.349(12)	C(114)-C(115)	1.396(11)
C(45)-C(50)	1.408(11)	N(3)-C(93)	1.371(11)	C(115)-C(116)	1.393(11)
C(46)-C(47)	1.378(11)	N(3)-C(99)	1.467(14)	C(115)-C(120)	1.496(11)

C(116)-C(117)	1.393(12)	C(133)-C(134)	1.413(17)	F(6)-C(138)	1.314(13)
C(118)-C(119)	1.374(12)	C(134)-C(135)	1.332(19)	S(3)-O(35)	1.431(8)
C(119)-C(120)	1.406(11)	C(135)-C(136)	1.372(17)	S(3)-O(36)	1.410(8)
C(120)-C(121)	1.374(11)	S(1)-O(31)	1.441(6)	S(3)-N(8)	1.561(8)
C(121)-C(122)	1.383(10)	S(1)-O(32)	1.430(7)	S(3)-C(139)	1.799(10)
C(123)-C(124)	1.524(11)	S(1)-N(7)	1.571(7)	S(4)-O(37)	1.439(6)
C(124)-C(125)	1.384(12)	S(1)-C(137)	1.844(9)	S(4)-O(38)	1.413(7)
C(124)-C(129)	1.386(12)	S(2)-O(33)	1.422(8)	S(4)-N(8)	1.563(8)
C(125)-C(126)	1.412(13)	S(2)-O(34)	1.433(7)	S(4)-C(140)	1.832(10)
C(126)-C(127)	1.358(15)	S(2)-N(7)	1.581(8)	F(7)-C(139)	1.327(12)
C(127)-C(128)	1.387(15)	S(2)-C(138)	1.819(10)	F(8)-C(139)	1.321(13)
C(128)-C(129)	1.395(13)	F(1)-C(137)	1.310(12)	F(9)-C(139)	1.360(13)
C(130)-C(131)	1.517(12)	F(2)-C(137)	1.343(12)	F(10)-C(140)	1.324(11)
C(131)-C(132)	1.375(12)	F(3)-C(137)	1.322(11)	F(11)-C(140)	1.349(11)
C(131)-C(136)	1.393(14)	F(4)-C(138)	1.325(12)	F(12)-C(140)	1.327(11)
C(132)-C(133)	1.432(12)	F(5)-C(138)	1.352(13)		

C(1)-O(1)-C(13)	115.2(8)	C(3)-C(2)-C(1)	121.9(7)
C(14)-O(2)-C(15)	113.0(10)	C(2)-C(3)-C(4)	119.2(7)
C(16)-O(3)-C(17)	119.7(12)	C(3)-C(4)-C(29)	119.0(7)
C(19)-O(4)-C(18)	112.8(8)	C(5)-C(4)-C(3)	120.2(7)
C(7)-O(5)-C(20)	116.1(6)	C(5)-C(4)-C(29)	120.7(7)
C(2)-O(6)-C(21)	116.2(7)	C(4)-C(5)-C(6)	121.1(8)
C(22)-O(7)-C(23)	113.4(8)	C(5)-C(6)-C(1)	120.2(7)
C(25)-O(8)-C(24)	111.6(7)	O(5)-C(7)-C(8)	114.5(7)
C(26)-O(9)-C(27)	112.9(6)	C(12)-C(7)-O(5)	125.5(7)
C(8)-O(10)-C(28)	116.3(6)	C(12)-C(7)-C(8)	120.0(7)
C(30)-O(11)-C(29)	115.2(6)	O(10)-C(8)-C(7)	117.0(7)
C(32)-O(13)-C(31)	116.2(6)	O(10)-C(8)-C(9)	124.1(7)
C(35)-O(15)-C(38)	118.4(6)	C(9)-C(8)-C(7)	118.9(7)
C(33)-N(1)-C(37)	115.9(6)	C(8)-C(9)-C(10)	121.2(7)
O(1)-C(1)-C(2)	117.7(8)	C(9)-C(10)-C(31)	119.9(7)
O(1)-C(1)-C(6)	125.0(8)	C(11)-C(10)-C(9)	118.5(7)
C(2)-C(1)-C(6)	117.3(7)	C(11)-C(10)-C(31)	121.5(7)
O(6)-C(2)-C(1)	113.9(7)	C(10)-C(11)-C(12)	120.3(7)
O(6)-C(2)-C(3)	124.2(7)	C(7)-C(12)-C(11)	120.9(7)

O(1)-C(13)-C(14)	110.7(11)	C(40)-C(39)-C(38)	120.1(8)
O(2)-C(14)-C(13)	110.3(10)	C(40)-C(39)-C(44)	120.1(8)
C(16)-C(15)-O(2)	110.4(12)	C(44)-C(39)-C(38)	119.8(8)
O(3)-C(16)-C(15)	120.2(13)	C(39)-C(40)-C(41)	119.9(8)
O(3)-C(17)-C(18)	111.6(11)	C(42)-C(41)-C(40)	119.7(8)
O(4)-C(18)-C(17)	109.4(10)	C(41)-C(42)-Br(1)	119.3(7)
O(4)-C(19)-C(20)	112.5(9)	C(43)-C(42)-Br(1)	119.1(7)
O(5)-C(20)-C(19)	109.5(7)	C(43)-C(42)-C(41)	121.2(8)
O(6)-C(21)-C(22)	106.4(8)	C(42)-C(43)-C(44)	118.5(8)
O(7)-C(22)-C(21)	108.6(8)	C(43)-C(44)-C(39)	120.6(8)
O(7)-C(23)-C(24)	112.0(8)	C(45)-O(16)-C(57)	113.7(6)
O(8)-C(24)-C(23)	105.4(8)	C(58)-O(17)-C(59)	111.2(7)
O(8)-C(25)-C(26)	107.6(7)	C(60)-O(18)-C(61)	112.9(9)
O(9)-C(26)-C(25)	108.4(7)	C(62)-O(19)-C(63)	117.2(9)
O(9)-C(27)-C(28)	109.1(7)	C(51)-O(20)-C(64)	116.5(7)
O(10)-C(28)-C(27)	108.7(6)	C(46)-O(21)-C(65)	114.9(6)
O(11)-C(29)-C(4)	109.7(6)	C(66)-O(22)-C(67)	112.7(6)
O(11)-C(30)-C(33)	112.0(6)	C(69)-O(23)-C(68)	114.5(7)
O(12)-C(30)-O(11)	124.6(7)	C(71)-O(24)-C(70)	110.3(7)
O(12)-C(30)-C(33)	123.4(7)	C(52)-O(25)-C(72)	116.3(7)
O(13)-C(31)-C(10)	108.2(6)	C(74)-O(26)-C(73)	116.6(6)
O(13)-C(32)-C(37)	113.2(7)	C(76)-O(28)-C(75)	116.1(5)
O(14)-C(32)-O(13)	123.2(7)	C(79)-O(30)-C(82)	117.3(6)
O(14)-C(32)-C(37)	123.5(7)	C(77)-N(2)-C(81)	114.3(6)
N(1)-C(33)-C(30)	120.1(7)	O(16)-C(45)-C(46)	117.1(7)
N(1)-C(33)-C(34)	123.7(7)	O(16)-C(45)-C(50)	126.3(7)
C(34)-C(33)-C(30)	116.1(7)	C(50)-C(45)-C(46)	116.6(7)
C(35)-C(34)-C(33)	119.4(7)	O(21)-C(46)-C(45)	113.6(7)
O(15)-C(35)-C(34)	125.1(7)	C(47)-C(46)-O(21)	124.8(7)
O(15)-C(35)-C(36)	116.9(7)	C(47)-C(46)-C(45)	121.6(7)
C(34)-C(35)-C(36)	117.9(7)	C(46)-C(47)-C(48)	120.1(7)
C(37)-C(36)-C(35)	118.3(8)	C(47)-C(48)-C(73)	119.3(7)
N(1)-C(37)-C(32)	119.5(7)	C(49)-C(48)-C(47)	119.3(7)
N(1)-C(37)-C(36)	124.7(7)	C(49)-C(48)-C(73)	121.4(7)
C(36)-C(37)-C(32)	115.8(7)	C(50)-C(49)-C(48)	120.7(7)
O(15)-C(38)-C(39)	109.2(6)	C(49)-C(50)-C(45)	121.8(7)

O(20)-C(51)-C(52)	116.7(7)	N(2)-C(77)-C(74)	118.0(7)
O(20)-C(51)-C(56)	126.1(7)	N(2)-C(77)-C(78)	125.3(7)
C(56)-C(51)-C(52)	117.2(7)	C(78)-C(77)-C(74)	116.7(7)
O(25)-C(52)-C(51)	114.3(8)	C(77)-C(78)-C(79)	118.6(7)
O(25)-C(52)-C(53)	124.4(7)	O(30)-C(79)-C(78)	116.6(6)
C(53)-C(52)-C(51)	121.3(8)	O(30)-C(79)-C(80)	125.2(7)
C(52)-C(53)-C(54)	120.3(7)	C(78)-C(79)-C(80)	118.2(7)
C(53)-C(54)-C(75)	119.9(7)	C(81)-C(80)-C(79)	118.0(7)
C(55)-C(54)-C(53)	119.9(7)	N(2)-C(81)-C(76)	118.0(6)
C(55)-C(54)-C(75)	120.1(7)	N(2)-C(81)-C(80)	125.5(7)
C(54)-C(55)-C(56)	120.0(7)	C(80)-C(81)-C(76)	116.5(6)
C(55)-C(56)-C(51)	121.3(7)	O(30)-C(82)-C(83)	107.4(7)
O(21)-C(65)-C(66)	109.1(7)	C(84)-C(83)-C(82)	122.3(9)
O(22)-C(66)-C(65)	110.8(7)	C(84)-C(83)-C(88)	118.5(8)
O(22)-C(67)-C(68)	111.2(7)	C(88)-C(83)-C(82)	119.1(8)
O(23)-C(68)-C(67)	108.8(7)	C(83)-C(84)-C(85)	121.4(9)
O(23)-C(69)-C(70)	116.2(9)	C(86)-C(85)-C(84)	118.6(9)
O(24)-C(70)-C(69)	107.2(7)	C(85)-C(86)-C(87)	122.5(8)
O(24)-C(71)-C(72)	109.8(8)	C(85)-C(86)-Br(2)	120.0(7)
O(25)-C(72)-C(71)	109.4(8)	C(87)-C(86)-Br(2)	117.6(6)
O(16)-C(57)-C(58)	107.0(7)	C(88)-C(87)-C(86)	117.2(8)
O(17)-C(58)-C(57)	108.1(7)	C(87)-C(88)-C(83)	121.6(8)
O(17)-C(59)-C(60)	110.5(9)	C(89)-N(3)-C(93)	118.7(8)
O(18)-C(60)-C(59)	111.1(9)	C(89)-N(3)-C(99)	119.9(8)
O(18)-C(61)-C(62)	106.3(9)	C(93)-N(3)-C(99)	121.4(8)
O(19)-C(62)-C(61)	113.8(12)	C(94)-N(4)-C(98)	120.7(8)
O(19)-C(63)-C(64)	112.3(8)	C(94)-N(4)-C(106)	119.2(7)
O(20)-C(64)-C(63)	110.0(8)	C(98)-N(4)-C(106)	120.1(7)
O(26)-C(73)-C(48)	109.2(6)	N(3)-C(89)-C(90)	119.9(8)
O(26)-C(74)-C(77)	113.9(7)	C(89)-C(90)-C(91)	123.2(8)
O(27)-C(74)-O(26)	125.2(7)	C(90)-C(91)-C(92)	115.1(8)
O(27)-C(74)-C(77)	120.8(7)	C(90)-C(91)-C(96)	124.3(7)
O(28)-C(75)-C(54)	108.8(6)	C(92)-C(91)-C(96)	120.6(7)
O(28)-C(76)-C(81)	113.1(6)	C(93)-C(92)-C(91)	120.6(7)
O(29)-C(76)-O(28)	124.4(7)	N(3)-C(93)-C(92)	122.3(7)
O(29)-C(76)-C(81)	122.5(7)	N(4)-C(94)-C(95)	122.3(8)

C(94)-C(95)-C(96)	118.4(8)	N(5)-C(117)-C(116)	120.4(7)
C(95)-C(96)-C(91)	119.9(7)	N(6)-C(118)-C(119)	120.3(7)
C(97)-C(96)-C(91)	121.9(7)	C(118)-C(119)-C(120)	119.7(8)
C(97)-C(96)-C(95)	118.2(8)	C(119)-C(120)-C(115)	119.4(7)
C(96)-C(97)-C(98)	121.0(8)	C(121)-C(120)-C(115)	121.8(7)
N(4)-C(98)-C(97)	119.3(8)	C(121)-C(120)-C(119)	118.6(7)
C(100)-C(99)-N(3)	113.9(8)	C(120)-C(121)-C(122)	120.0(7)
C(101)-C(100)-C(99)	116.9(10)	N(6)-C(122)-C(121)	120.5(7)
C(101)-C(100)-C(105)	120.5(10)	N(5)-C(123)-C(124)	112.3(7)
C(105)-C(100)-C(99)	122.6(9)	C(125)-C(124)-C(123)	121.2(8)
C(100)-C(101)-C(102)	116.6(12)	C(125)-C(124)-C(129)	120.1(8)
C(103)-C(102)-C(101)	121.8(11)	C(129)-C(124)-C(123)	118.6(8)
C(102)-C(103)-C(104)	120.4(12)	C(124)-C(125)-C(126)	117.9(8)
C(105)-C(104)-C(103)	120.7(12)	C(127)-C(126)-C(125)	121.5(9)
C(104)-C(105)-C(100)	119.9(11)	C(126)-C(127)-C(128)	121.0(9)
C(107)-C(106)-N(4)	112.8(7)	C(127)-C(128)-C(129)	118.0(9)
C(108)-C(107)-C(106)	124.1(8)	C(124)-C(129)-C(128)	121.5(9)
C(108)-C(107)-C(112)	117.9(8)	N(6)-C(130)-C(131)	111.5(7)
C(112)-C(107)-C(106)	117.9(7)	C(132)-C(131)-C(130)	119.5(8)
C(109)-C(108)-C(107)	120.1(9)	C(132)-C(131)-C(136)	119.5(8)
C(108)-C(109)-C(110)	121.7(9)	C(136)-C(131)-C(130)	121.0(8)
C(109)-C(110)-C(111)	119.6(9)	C(131)-C(132)-C(133)	119.8(9)
C(112)-C(111)-C(110)	119.2(9)	C(134)-C(133)-C(132)	117.9(10)
C(111)-C(112)-C(107)	121.5(8)	C(135)-C(134)-C(133)	120.6(11)
C(113)-N(5)-C(123)	119.0(7)	C(134)-C(135)-C(136)	121.5(12)
C(117)-N(5)-C(113)	121.8(7)	C(135)-C(136)-C(131)	120.6(10)
C(117)-N(5)-C(123)	119.1(7)	O(31)-S(1)-N(7)	107.6(4)
C(118)-N(6)-C(130)	119.0(7)	O(31)-S(1)-C(137)	102.9(4)
C(122)-N(6)-C(118)	120.9(7)	O(32)-S(1)-O(31)	119.3(4)
C(122)-N(6)-C(130)	120.1(7)	O(32)-S(1)-N(7)	118.5(4)
C(114)-C(113)-N(5)	119.1(8)	O(32)-S(1)-C(137)	103.3(4)
C(113)-C(114)-C(115)	121.6(8)	N(7)-S(1)-C(137)	102.3(4)
C(114)-C(115)-C(120)	122.8(7)	O(33)-S(2)-O(34)	119.1(5)
C(116)-C(115)-C(114)	117.4(8)	O(33)-S(2)-N(7)	116.4(4)
C(116)-C(115)-C(120)	119.7(7)	O(33)-S(2)-C(138)	102.4(5)
C(117)-C(116)-C(115)	119.7(8)	O(34)-S(2)-N(7)	108.9(4)

O(34)-S(2)-C(138)	103.0(5)	F(10)-C(140)-F(12)	109.4(7)
N(7)-S(2)-C(138)	104.8(5)	F(11)-C(140)-S(4)	111.2(6)
S(1)-N(7)-S(2)	126.7(5)	F(12)-C(140)-S(4)	109.4(6)
F(1)-C(137)-S(1)	108.4(6)	F(12)-C(140)-F(11)	107.5(8)
F(1)-C(137)-F(2)	107.1(8)		
F(1)-C(137)-F(3)	108.7(8)		
F(2)-C(137)-S(1)	111.6(6)		
F(3)-C(137)-S(1)	112.3(7)		
F(3)-C(137)-F(2)	108.6(8)		
F(4)-C(138)-S(2)	112.0(7)		
F(4)-C(138)-F(5)	106.2(9)		
F(5)-C(138)-S(2)	110.2(7)		
F(6)-C(138)-S(2)	110.7(7)		
F(6)-C(138)-F(4)	109.5(9)		
F(6)-C(138)-F(5)	108.0(9)		
O(35)-S(3)-N(8)	110.8(4)		
O(35)-S(3)-C(139)	103.8(5)		
O(36)-S(3)-O(35)	116.6(5)		
O(36)-S(3)-N(8)	114.1(4)		
O(36)-S(3)-C(139)	106.5(5)		
N(8)-S(3)-C(139)	103.6(5)		
O(37)-S(4)-N(8)	116.5(4)		
O(37)-S(4)-C(140)	104.7(4)		
O(38)-S(4)-O(37)	117.3(4)		
O(38)-S(4)-N(8)	113.5(4)		
O(38)-S(4)-C(140)	103.6(4)		
N(8)-S(4)-C(140)	97.8(4)		
S(3)-N(8)-S(4)	125.1(5)		
F(7)-C(139)-S(3)	110.6(7)		
F(7)-C(139)-F(9)	106.4(9)		
F(8)-C(139)-S(3)	112.6(7)		
F(8)-C(139)-F(7)	109.2(9)		
F(8)-C(139)-F(9)	107.4(8)		
F(9)-C(139)-S(3)	110.3(7)		
F(10)-C(140)-S(4)	111.9(7)		
F(10)-C(140)-F(11)	107.3(7)		

Table A.11. Hydrogen bonds for cs2231 [\AA and $^\circ$].

D-H...A	d(D-H)	d(H...A)	d(D...A)	\angle (DHA)
O(39)-H(39A)...O(7)	0.87	2.16	2.961(14)	153.5
O(39)-H(39B)...O(2)	0.87	2.24	2.909(14)	134.1
O(40)-H(40A)...O(19)	0.87	2.28	3.074(19)	152.4
O(40)-H(40A)...O(20)	0.87	2.63	3.196(12)	124.2
